

Wearable Robotics

Systems and Applications

Edited by

Jacob Rosen

Peter Walker Ferguson



Wearable Robotics Systems and Applications

Wearable Robotics Systems and Applications

Edited by

Jacob Rosen

*Bionics Lab, Department of Mechanical and Aerospace Engineering,
University of California, Los Angeles, CA, United States*

Peter Walker Ferguson

*Bionics Lab, Department of Mechanical and Aerospace Engineering,
University of California, Los Angeles, CA, United States*



ACADEMIC PRESS

An imprint of Elsevier

Academic Press is an imprint of Elsevier
125 London Wall, London EC2Y 5AS, United Kingdom
525 B Street, Suite 1650, San Diego, CA 92101, United States
50 Hampshire Street, 5th Floor, Cambridge, MA 02139, United States
The Boulevard, Langford Lane, Kidlington, Oxford OX5 1GB, United Kingdom

Copyright © 2020 Elsevier Inc. All rights reserved.

No part of this publication may be reproduced or transmitted in any form or by any means, electronic or mechanical, including photocopying, recording, or any information storage and retrieval system, without permission in writing from the publisher. Details on how to seek permission, further information about the Publisher's permissions policies and our arrangements with organizations such as the Copyright Clearance Center and the Copyright Licensing Agency, can be found at our website: www.elsevier.com/permissions.

This book and the individual contributions contained in it are protected under copyright by the Publisher (other than as may be noted herein).

Notices

Knowledge and best practice in this field are constantly changing. As new research and experience broaden our understanding, changes in research methods, professional practices, or medical treatment may become necessary.

Practitioners and researchers must always rely on their own experience and knowledge in evaluating and using any information, methods, compounds, or experiments described herein. In using such information or methods they should be mindful of their own safety and the safety of others, including parties for whom they have a professional responsibility.

To the fullest extent of the law, neither the Publisher nor the authors, contributors, or editors, assume any liability for any injury and/or damage to persons or property as a matter of products liability, negligence or otherwise, or from any use or operation of any methods, products, instructions, or ideas contained in the material herein.

British Library Cataloguing-in-Publication Data

A catalogue record for this book is available from the British Library

Library of Congress Cataloging-in-Publication Data

A catalog record for this book is available from the Library of Congress

ISBN: 978-0-12-814659-0

For Information on all Academic Press publications
visit our website at <https://www.elsevier.com/books-and-journals>

Publisher: Mara Conner

Acquisition Editor: Fiona Geraghty

Editorial Project Manager: Isabella Conti Silva

Production Project Manager: Sruthi Satheesh

Cover Designer: Mark Rogers

Typeset by MPS Limited, Chennai, India



Working together
to grow libraries in
developing countries

www.elsevier.com • www.bookaid.org

Contents

List of Contributors	xix
----------------------------	-----

CHAPTER 1 Upper Limb Exoskeleton Systems—Overview1

Yang Shen, Peter Walker Ferguson and Jacob Rosen

1.1	Introduction	1
1.2	Overview of Upper Limb Exoskeleton Systems	2
1.2.1	Mechanism	3
1.2.2	Actuation	4
1.3	Assistive Upper Limb Exoskeletons.....	8
1.3.1	AIST	9
1.3.2	SUEFUL-7	9
1.3.3	MULOS	9
1.3.4	HAL.....	9
1.3.5	ABLE	9
1.3.6	MyoPro.....	9
1.4	Rehabilitation Upper Limb Exoskeletons.....	10
1.4.1	MIT-MANUS.....	10
1.4.2	NeReBot.....	10
1.4.3	ARM Guide.....	10
1.4.4	ReoGo.....	11
1.4.5	GENTLE/s.....	11
1.4.6	ACT ^{3D}	11
1.4.7	iPAM	11
1.4.8	Bi-Manu-Track.....	11
1.4.9	MIME	11
1.4.10	KINARM.....	11
1.4.11	L-Exos	12
1.4.12	BONES.....	12
1.4.13	ARMin III	12
1.4.14	MGA.....	12
1.4.15	IntelliArm	12
1.4.16	MEDARM	13
1.4.17	Exorn	13
1.4.18	SRE.....	13
1.4.19	RUPERT IV	13
1.4.20	RehaBot.....	13
1.4.21	ETS-MARSE.....	13

1.4.22 Recupera-Reha	13
1.4.23 EXO-UL Series	14
1.5 Augmentation Upper Limb Exoskeletons.....	14
1.5.1 SARCOS Guardian XO	15
1.5.2 SARCOS Guardian GT.....	15
1.5.3 ShoulderX from SuitX	15
1.5.4 EksoVest from Ekso Bionics	15
1.6 Others	15
1.6.1 EXARM	15
1.6.2 X-Arm-2	16
1.6.3 SARCOS Master Arm.....	16
1.6.4 SAM	16
1.6.5 CAPIO	16
1.6.6 SARCOS Dextrous Arm	16
1.6.7 EMY	16
1.7 Conclusion	16
References.....	17

CHAPTER 2 Development and Control of an Upper Extremity Exoskeleton

Robot for Rehabilitation..... 23

*Brahim Brahmi, Maarouf Saad, M.H. Rahman, Cristobal Ochoa-Luna
and Islam Rasedul*

2.1 Introduction	23
2.2 Characterization of System Rehabilitation	25
2.2.1 Exoskeleton Robot Development	25
2.2.2 Dynamics of Ecole de Technologie Supérieure—Motion Assistive Robotic-exoskeleton for Superior Extremity Robot.....	25
2.2.3 Problem Statement	27
2.3 Control Design	28
2.3.1 Uncertain Estimation	28
2.3.2 Estimation of the State of the System	28
2.3.3 Design of Integral Second-Order Terminal Sliding Mode Controller.....	30
2.3.4 Active Assistive Motion	34
2.4 Experiment and Comparative Study	35
2.4.1 Experiment Setup.....	35
2.4.2 Results of Passive Assistive Motion.....	37
2.4.3 Comparative Study.....	37
2.4.4 Results of Active Assistive Motion.....	39
2.5 Conclusion	42
2.6 Ethics Statement.....	42
Acknowledgments	42
References.....	42

CHAPTER 3 Design of the Arm Exoskeleton ABLE Achieving Torque Control Using Ball Screw and Cable Mechanism.....	45
<i>Philippe Garrec</i>	
3.1 Introduction	45
3.2 The SCS Mechanism: A New Answer to the Challenge of Linear Torque Amplification.....	45
3.2.1 Mechanical Reversibility/Irreversibility—Backdrivability—Torque Transfer Linearity	46
3.2.2 Mechanical Torque Amplification on Servomanipulators	48
3.3 The First ABLE 4D.....	52
3.4 The Completion of ABLE 7D	54
3.4.1 Forearm—Wrist Design.....	54
3.4.2 A New Shoulder With Nonorthogonal Joints and Simple Bearing	60
3.5 Conclusion.....	62
Acknowledgments	64
References.....	65
CHAPTER 4 Rigid Versus Soft Exoskeletons: Interaction Strategies for Upper Limb Assistive Technology	67
<i>Domenico Chiaradia, Michele Xiloyannis, Massimiliano Solazzi, Lorenzo Masia and Antonio Frisoli</i>	
4.1 Introduction	67
4.2 Exoskeletons Descriptions	69
4.2.1 A Rigid Exoskeleton: The Rehab-Exos.....	70
4.2.2 Elbow Exosuit (Soft Exosuit)	71
4.3 Exoskeleton Models	73
4.3.1 Rehab-Exos (Rigid Exoskeleton).....	73
4.3.2 Exosuit (Soft Exosuit)	75
4.4 Controls Design.....	76
4.4.1 Direct Torque Control (Rigid Exoskeleton).....	76
4.4.2 Admittance Control (Soft Exosuit).....	77
4.5 Experimental Setup	79
4.5.1 Evaluation of the Direct Torque Control (Rigid Exoskeleton).....	79
4.5.2 Evaluation of the Admittance Control (Soft Exosuit)	80
4.6 Results	81
4.6.1 Evaluation of the Direct Torque Control (Rigid Exoskeleton).....	81
4.6.2 Evaluation of the Admittance Control (Soft Exosuit)	83
4.6.3 Assistive Performance: Rehab-Exos Versus Exosuit	84
4.7 Discussion.....	86
4.8 Conclusion	88
References.....	88

CHAPTER 5 EXO-UL Upper Limb Robotic Exoskeleton System Series: From 1 DOF Single-Arm to (7 + 1) DOFs Dual-Arm	91
<i>Yang Shen and Jacob Rosen</i>	
5.1 Introduction	91
5.2 Exoskeleton Systems	92
5.2.1 Prototype 1 (EXO-UL1)	92
5.2.2 Prototype 2 (EXO-UL3)	94
5.2.3 Prototype 3 (EXO-UL7)	95
5.2.4 Prototype 4 (EXO-UL8)	96
5.3 Related Research.....	99
5.3.1 Control Algorithms	99
5.3.2 Redundancy Resolution	99
5.3.3 Synergy Analysis	99
5.3.4 Dual-Arm Training	100
5.3.5 Virtual Reality	100
5.4 Summary.....	100
References.....	100
CHAPTER 6 PRISM: Development of a 2-DOF Dual-Four-Bar Exoskeleton Shoulder Mechanism to Support Elevation, Depression, Protraction, and Retraction	105
<i>Joel C. Perry, Chris K. Bitikofer, Parker W. Hill, Shawn T. Trimble and Eric T. Wolbrecht</i>	
6.1 Introduction	105
6.1.1 Rehabilitation Robotics: Exoskeleton Versus End-Effector	106
6.1.2 Exoskeleton Shoulder Background.....	106
6.1.3 Overview	111
6.2 Methods: PRISM Development	111
6.2.1 BLUE SABINO Concept.....	112
6.2.2 EXO-UL8 Design Approach.....	113
6.2.3 Shoulder Range of Motion Requirements Estimation	114
6.2.4 Conceptual Design of a Remote Biomimetic Shoulder Module	116
6.2.5 Gravity Compensation Methods	120
6.3 Results	120
6.3.1 Shoulder Range of Motion Requirements Estimation	122
6.3.2 Dual Four-Bar Mechanism Proof-of-Concept Mockup	122
6.3.3 Exoskeleton Clavicle Design and Assembly	124
6.3.4 Spring-Based Gravity Compensation	124
6.3.5 PRISM Final Design	126
6.4 Conclusion and Discussion	128

Acknowledgments	129
References.....	129
CHAPTER 7 Design and Modeling of Shoulder Exoskeleton Using Two Revolute Joints	133
<i>Carlos Parga and Wen Yu</i>	
7.1 Introduction	133
7.2 Shoulder Exoskeleton With 2 Degrees of Freedom.....	133
7.3 Shoulder Exoskeleton Design	135
7.4 Modeling the Shoulder Exoskeleton.....	139
7.5 Control for the Exoskeleton.....	141
7.5.1 Lyapunov Stability.....	141
7.5.2 Linear Control.....	142
7.5.3 Sliding Mode Controller	142
7.5.4 Neural Control.....	143
7.6 Electronic and Control System	143
7.7 Experimental Results.....	145
7.8 Conclusion.....	148
References.....	148
CHAPTER 8 Hand Exoskeleton Systems—Overview.....	149
<i>Peter Walker Ferguson, Yang Shen and Jacob Rosen</i>	
8.1 Introduction	149
8.2 Overview of Hand Exoskeleton Systems	150
8.2.1 Mechanism	150
8.2.2 Actuation	154
8.2.3 Transmission	155
8.2.4 Sensing Method.....	156
8.2.5 Control.....	157
8.3 Assistive Hand Exoskeletons	158
8.3.1 Brown et al	158
8.3.2 Lucas et al	159
8.3.3 In et al	159
8.3.4 Kadowaki et al	159
8.3.5 OFX	159
8.3.6 ExoGlove.....	159
8.3.7 Polygerinos et al.....	160
8.3.8 HX	160
8.3.9 Secciani et al	160

8.4	Rehabilitation Hand Exoskeletons.....	160
8.4.1	HWARD.....	161
8.4.2	Gentle/G	161
8.4.3	Wege et al	162
8.4.4	Kawasaki et al.....	162
8.4.5	HANDEXOS	162
8.4.6	Tong et al	162
8.4.7	HEXORR	163
8.4.8	ATX.....	163
8.4.9	iHandRehab.....	163
8.4.10	Rahman et al	163
8.4.11	Arata et al.....	163
8.4.12	IOTA	163
8.4.13	HEXOSYS-I	164
8.4.14	Zhang et al	164
8.4.15	BRAVO	164
8.4.16	Sinfonia	164
8.4.17	Agarwal et al.....	164
8.4.18	Abdallah et al	165
8.4.19	Ferguson et al.....	165
8.4.20	DexoHand.....	165
8.5	Augmentation Hand Exoskeletons.....	165
8.5.1	Shields et al.....	166
8.5.2	Skil Mate	166
8.5.3	Hasegawa et al	166
8.5.4	Tadano et al.....	167
8.5.5	Matheson et al.....	167
8.5.6	RoboGlove	167
8.6	Others	167
8.6.1	SKK Hand Master.....	168
8.6.2	Rutgers Master II-ND	168
8.6.3	Stergiopoulos et al	168
8.6.4	Fontana et al.....	168
8.6.5	Jo et al	168
8.7	Conclusion.....	169
	References.....	170
CHAPTER 9	A Portable Tailor-Made Exoskeleton for Hand Disabilities	177
	<i>Benedetto Allotta, Matteo Bianchi, Enrico Meli, Alessandro Ridolfi and Nicola Secciani</i>	
9.1	Introduction	177

9.2	Kinematic Analysis and Synthesis.....	177
9.3	Kinematic Chain Assessment: First Device	179
9.3.1	Mechanical Design.....	181
9.3.2	Electronics and Control Architecture	182
9.3.3	Testing and Discussion	182
9.4	Ergonomics Improvements: Second Device.....	183
9.4.1	Mechanical Design.....	183
9.4.2	Electronics and Control Architecture	184
9.4.3	Testing and Discussion	185
9.5	User-Based Actuation Strategy: Final Device.....	185
9.5.1	Mechanical Design.....	186
9.5.2	Electronic Components and Control Architecture	186
9.5.3	Testing and Discussion	190
9.6	Conclusions	190
	References.....	191
	Further Reading	191
CHAPTER 10 Optimal Kinematic Design of the Link Lengths of a Hand Exoskeleton.....		193
<i>Peter Walker Ferguson, Brando Dimapasoc and Jacob Rosen</i>		
10.1	Introduction	193
10.2	Method.....	194
10.2.1	Modeling the Human Digits	194
10.2.2	Exoskeleton Topology	195
10.2.3	Modeling the 3R Planar Mechanisms	197
10.2.4	The Optimization Algorithm	197
10.3	Results	200
10.3.1	Simulation Results	200
10.3.2	Physical Prototype Evaluation	201
10.4	Discussion.....	201
10.4.1	Link Length Evaluation	201
10.4.2	Prototype Workspace Evaluation	203
10.5	Conclusion	204
	Acknowledgement	204
	References.....	204
CHAPTER 11 Lower Limb Exoskeleton Systems—Overview		207
<i>Hao Lee, Peter Walker Ferguson and Jacob Rosen</i>		
11.1	Introduction	207
11.2	Assistive Exoskeletons.....	208

11.3	Rehabilitation Exoskeletons.....	215
11.3.1	Rehabilitation With Weight Support	215
11.3.2	Rehabilitation Without Weight Support.....	217
11.4	Augmentation Exoskeletons.....	217
11.4.1	Assistance Directly Applied to Tasks	218
11.4.2	Assistance Applied on Users	219
11.5	Actuation of Lower Limb Exoskeletons.....	221
11.6	Future for Lower Limb Exoskeletons.....	222
	References.....	223

CHAPTER 12 WalkON Suit: A Medalist in the Powered Exoskeleton

Race of Cybathlon 2016 **231**

Jungsu Choi and Kyoungchul Kong

12.1	Introduction	231
12.2	Design of WalkON Suit	232
12.2.1	Overall Configuration	232
12.2.2	Actuation Systems.....	232
12.2.3	Robotic Legs	234
12.2.4	Control Unit and Backpack	235
12.2.5	Crutches.....	235
12.2.6	User Display.....	235
12.3	Sensor System	235
12.4	Human Factors	236
12.4.1	Pilot	236
12.4.2	Knee—Ankle—Foot Orthosis	237
12.5	Control System.....	238
12.5.1	Processes of Overall Control System	238
12.5.2	Main Functions of the Control System	240
12.6	Evaluation.....	244
12.6.1	Training	244
12.6.2	Cybathlon 2016	246
12.6.3	Analysis of Cybathlon 2016	246
12.7	After the Cybathlon.....	247
	Acknowledgment	248
	References.....	248

CHAPTER 13 Design of Lower-Limb Exoskeletons and Emulator Systems **251**

Kirby Ann Witte and Steven H. Collins

13.1	Introduction	251
13.2	Exoskeleton Emulator Testbeds.....	251
13.2.1	Emulator Pros and Cons	252
13.2.2	Off-Board Components—Power, Actuation, and Control Hardware	254

13.3	Untethered Systems	254
13.4	Mechanical Design of Onboard Components.....	255
13.4.1	Loading Analysis—Free Body Diagrams.....	255
13.4.2	Safety Stops and Physical Interfaces.....	256
13.4.3	Frame and Joint Design	260
13.4.4	Sensing	264
13.4.5	Series Elasticity for Improved Torque Tracking.....	266
13.4.6	Materials and Manufacturing.....	267
13.5	Control.....	269
13.5.1	Case Study—Control of Any CMU Emulator	271
13.6	Making Strides in the Future	271
	References.....	272
CHAPTER 14 Physical Assistant Robot Safety		275
<i>Yoji Yamada and Yasuhiro Akiyama</i>		
14.1	Introduction	275
14.2	Contact Safety of the Physical Assistant Robot.....	275
14.2.1	Introduction	275
14.2.2	Verification and Validation Test Procedure.....	276
14.2.3	Verification Experiments for Obtaining an Inherently Safe Region Against Blister Generation	276
14.2.4	Validation Test Method for Wound Risk.....	280
14.2.5	Application of a Surrogate Skin for Safety Validation.....	285
14.2.6	Summary	286
14.3	Fall Risk During Gait Using a Wearable Robot	286
14.3.1	Introduction	286
14.3.2	Mismatch Between the Motion of the Wearable Robot and the Wearer	288
14.3.3	Contact With an Environmental Object	292
14.3.4	Curving Motion Under Limited Degree of Freedom	295
14.3.5	Summary	297
14.4	Conclusions	297
	References.....	298
CHAPTER 15 Current Evidence for Use of Robotic Exoskeletons in Rehabilitation		301
<i>Arun Jayaraman, Borislav Marinov, Yashna Singh, Sheila Burt and William Zev Rymer</i>		
15.1	Brief History of Exoskeletons.....	301
15.1.1	Early Designs	301

15.1.2	First Prototypes 1961–73	301
15.1.3	The Exoskeleton Awakening: 2001–08.....	302
15.1.4	The New Exoskeleton Renaissance: 2015–18 and Onwards.....	302
15.1.5	Exoskeletons in Development	302
15.1.6	Current Food and Drug Administration—Approved Devices	303
15.2	Overview of Clinical Evidence.....	305
15.2.1	Early-Stage Feasibility and Case Studies.....	307
15.2.2	Randomized Controlled Trials.....	308
15.3	A Look to the Future.....	309
	References.....	309

CHAPTER 16 Structural Exoskeletons and Soft Fabric Exosuits

for Assistive Walking..... 311

Lawrence J. Jasinski

16.1	Burden of Spinal Cord Injury	312
16.1.1	Demographics.....	312
16.1.2	Adverse Health Outcomes	312
16.2	Current Treatment Options	314
16.2.1	Wheelchairs.....	314
16.2.2	Leg Braces.....	315
16.2.3	Functional Electric Stimulation	315
16.2.4	Standing Frames and Standing Mobility Devices.....	316
16.3	Rationale for Exoskeletons	316
16.4	ReWalk Product Summary.....	317
16.4.1	ReWalk Components and Specifications	317
16.4.2	Communicator.....	317
16.4.3	Exoskeleton	318
16.4.4	Waist Pack.....	318
16.4.5	System Configuration	318
16.4.6	Video Links.....	318
16.4.7	Levels of Patient Training	320
16.5	Safety and Efficacy Profile	320
16.5.1	Patient Selection.....	320
16.5.2	Safe Ambulatory Function and Patient Tolerance	321
16.5.3	Exoskeleton-Assisted Walking Simulates Normal Physiological Effects	322
16.5.4	Impact on Quality of Life	325
16.6	Economic Impact.....	328
16.6.1	Challenges of Exoskeletons	329
16.6.2	Exosuits	329
16.6.3	Design of the ReStore Exosuit	330

16.7 Conclusion	331
References.....	331

CHAPTER 17 Hybrid Exoskeletons to Restore Gait in Individuals With Paralysis From Spinal Cord Injury..... 335

Sarah R. Chang, Rudi Kobetic and Ronald J. Triolo

17.1 Introduction	335
17.2 Technologies to Restore Walking.....	335
17.2.1 Functional Neuromuscular Stimulation Systems	335
17.2.2 Lower Limb Orthoses	336
17.2.3 Powered Exoskeletons	336
17.3 Current State-of-the-Art Systems for Restoration of Walking	337
17.3.1 Hybrid Neuroprosthesis	337
17.3.2 Powered Exoskeletons and Functional Neuromuscular Stimulation	339
17.3.3 Powered Exoskeletons and Implanted Functional Neuromuscular Stimulation	340
17.3.4 The Need for Speed	340
17.3.5 Ease of Use and Cosmesis	341
17.3.6 Other Applications of Hybrid Systems	342
17.4 Conclusions	342
References.....	343

CHAPTER 18 Hybrid Wearable Robotic Exoskeletons for Human Walking 347

Juan C. Moreno, Samer Mohammed, Nitin Sharma and Antonio J. del-Ama

18.1 Introduction	347
18.2 Advances in Hybrid Wearable Technologies	348
18.2.1 Modeling Approaches for Control.....	349
18.3 Potential Future Technologies	350
18.4 Clinical and Usability Factors.....	351
18.5 Case Study	352
18.5.1 Results	356
18.5.2 Discussion	358
18.5.3 Case Study Conclusion	360
18.6 Challenges and Future Directions.....	360
18.7 Conclusion	361
References.....	361
Further Reading	364

CHAPTER 19 Upper Limb Active Prosthetic Systems—Overview	365
<i>Claudio Castellini</i>	
19.1 Introduction/Motivation	365
19.2 The Past	367
19.3 The Present	368
19.3.1 Design of Prosthetic Devices.....	368
19.3.2 Control.....	370
19.3.3 Amputations and Patients	372
19.4 The Future: A Short Note	373
References.....	374
CHAPTER 20 Design Principles of a Light, Wearable Upper Limb Interface for Prosthetics and Teleoperation.....	377
<i>Claudio Castellini</i>	
20.1 Wearable Interfaces for Wearable Robots.....	377
20.2 Current Problems.....	378
20.2.1 Sensors and Bodily Signals	379
20.2.2 The Physical Interface: Properly Housing the Sensors.....	381
20.2.3 Signal Processing, Machine Learning, Adaptation	382
20.3 Design Guidelines for a Wearable Upper Limb Interface	383
20.3.1 Current Pitfalls	383
20.3.2 Implementation and Testing	384
20.3.3 Final Remark: Not Just Prosthetics	385
Acknowledgment	387
References.....	387
CHAPTER 21 The Modular Prosthetic Limb	393
<i>Matthew S. Johannes, Eric L. Faulring, Kapil D. Katyal, Matthew P. Para, John B. Helder, Alexander Makhlin, Tom Moyer, Daniel Wahl, James Solberg, Steve Clark, Robert S. Armiger, Travis Lontz, Kathryn Geberth, Courtney W. Moran, Brock A. Wester, Thomas Van Doren and Julio J. Santos-Munne</i>	
21.1 Introduction and Overview	393
21.1.1 Background	393
21.1.2 Early Development: Prototypes and Phases	394
21.1.3 MPL Architecture Overview, Capabilities, and Features	399
21.2 MPL Detailed Description	400
21.2.1 Upper Arm and Wrist Design.....	401
21.2.2 Hand Design.....	413
21.2.3 Fingers	413
21.2.4 Auxiliary Subsystems	430

21.3	High-Level Controls and System Interfacing	433
21.3.1	High-Level Controls	433
21.3.2	VulcanX and the OCU.....	434
21.3.3	The VIE and the vMPL	435
21.3.4	Web Interface.....	435
21.4	Select MPL Applications and Uses	438
21.4.1	Cortical Control and Feedback.....	438
21.4.2	Amputees.....	439
21.4.3	Robo Sally.....	440
21.5	Conclusion	441
	Acknowledgments	441
	References.....	441

CHAPTER 22 Sensing and Control for Prosthetic Hands in Clinical and Research Applications..... 445

Luke E. Osborn, Mark M. Iskarous and Nitish V. Thakor

22.1	Introduction	445
22.2	Prosthesis Control.....	446
22.2.1	Movement Signals.....	447
22.2.2	Movement Decoding.....	448
22.2.3	Targeted Muscle Reinnervation and Osseointegration	449
22.2.4	State of the Art.....	450
22.3	Sensors for Prosthetic Hands	450
22.3.1	Sensing in Biology.....	450
22.3.2	Sensing Devices	451
22.3.3	State of the Art.....	453
22.4	Sensory Feedback.....	454
22.4.1	Tactile.....	454
22.4.2	Pain.....	457
22.4.3	Proprioception	457
22.4.4	State of the Art.....	458
22.5	Future Directions	459
22.5.1	Prosthetic Sockets	460
22.5.2	Prosthesis Control	460
22.5.3	Augmented Reality Training	460
22.5.4	Sensors and e-Skins	460
22.5.5	Sensory Feedback	461
22.6	Conclusion	461
	Acknowledgment	461
	Abbreviations.....	461
	References.....	462

CHAPTER 23 Lower Limb Active Prosthetic Systems—Overview	469
<i>Alexandra S. Voloshina and Steven H. Collins</i>	
23.1 Introduction	469
23.2 Background.....	470
23.3 Systems.....	472
23.3.1 Mechanical Configuration and Actuation Approaches	472
23.3.2 Control Approaches	476
23.4 Conclusions and Future Directions.....	479
References.....	480
CHAPTER 24 Controlling a Powered Transfemoral Prosthetic Leg Using a Unified Phase Variable	487
<i>Dario J. Villarreal and Robert D. Gregg</i>	
24.1 Background.....	488
24.2 Phase Variable Algorithm.....	490
24.2.1 Real-Time Phase Variable Algorithm for Control Applications	490
24.3 Controlling a Transfemoral Powered Prosthetic Leg Using a Phase Variable....	493
24.3.1 Control Law	493
24.3.2 Hardware Setup.....	494
24.3.3 Experimental Protocol	495
24.3.4 Results From Amputee Experiments.....	496
24.3.5 Discussion of Amputee Experiments	500
References.....	505
Index	507

List of Contributors

Yasuhiro Akiyama

Nagoya University, Nagoya, Japan

Benedetto Allotta

Department of Industrial Engineering (DIEF), University of Florence, Florence, Italy

Robert S. Armiger

The Johns Hopkins University Applied Physics Laboratory, Laurel, MD, United States

Matteo Bianchi

Department of Industrial Engineering (DIEF), University of Florence, Florence, Italy

Chris K. Bitikofer

Mechanical Engineering Department, University of Idaho, Moscow, ID, United States

Brahim Brahmi

University of Quebec in Montreal (School of Higher Technology), Montreal, QC, Canada

Sheila Burt

Shirley Ryan AbilityLab, Center for Bionic Medicine & The Max Näder Lab for Rehabilitation Technologies and Outcomes Research, Chicago, IL, United States

Claudio Castellini

Institute of Robotics and Mechatronics, DLR – German Aerospace Center, Wessling, Germany

Sarah R. Chang

Orthocare Innovations, LLC, Edmonds, WA, United States

Domenico Chiaradia

PERCRO Laboratory, TeCIP Institute, Scuola Superiore Sant'Anna, Pisa, Italy

Jungsu Choi

The Department of Robotics Engineering, Yeungnam University, Gyeongbuk, Korea

Steve Clark

HDT Global, Solon, OH, United States

Steven H. Collins

Department of Mechanical Engineering, Stanford University, Stanford, CA, United States

Antonio J. del-Ama

National Hospital for Paraplegics (SESCAM), Toledo, Spain

Brando Dimapasoc

Bionics Lab, Department of Mechanical and Aerospace Engineering, University of California, Los Angeles, CA, United States

Eric L. Faulring

HDT Global, Solon, OH, United States

Peter Walker Ferguson

Bionics Lab, Department of Mechanical and Aerospace Engineering, University of California, Los Angeles, CA, United States

Antonio Frisoli

PERCRO Laboratory, TeCIP Institute, Scuola Superiore Sant'Anna, Pisa, Italy

Philippe Garrec

CEA-DRT-LIST-DIASI, Interactive Robotics Service, Saclay, France

Kathryn Geberth

HDT Global, Solon, OH, United States

Robert D. Gregg

Electrical Engineering and Computer Science, University of Michigan, Ann Arbor, MI, United States

John B. Helder

The Johns Hopkins University Applied Physics Laboratory, Laurel, MD, United States

Parker W. Hill

Mechanical Engineering Department, University of Idaho, Moscow, ID, United States

Mark M. Iskarous

Department of Biomedical Engineering, Johns Hopkins School of Medicine, Baltimore, MD, United States

Lawrence J. Jasinski

ReWalk Robotics, Southborough, MA, United States

Arun Jayaraman

Shirley Ryan AbilityLab, Center for Bionic Medicine & The Max Näder Lab for Rehabilitation Technologies and Outcomes Research, Chicago, IL, United States; Department of Physical Medicine & Rehabilitation, Northwestern University, Chicago, IL, United States; Department of Medical Social Sciences, Northwestern University, Chicago, IL, United States; Department of Physical Therapy & Human Movement Sciences, Northwestern University, Chicago, IL, United States

Matthew S. Johannes

The Johns Hopkins University Applied Physics Laboratory, Laurel, MD, United States

Kapil D. Katyal

The Johns Hopkins University Applied Physics Laboratory, Laurel, MD, United States

Rudi Kobetic

Department of Veterans Affairs, Advanced Platform Technology Center, Louis Stokes Cleveland Department of Veterans Affairs Medical Center, Cleveland, OH, United States

Kyoungchul Kong

The Department of Mechanical Engineering, Korea Advanced Institute of Science and Technology, Daejeon, Korea

Hao Lee

Bionics Lab, Department of Mechanical and Aerospace Engineering, University of California, Los Angeles, CA, United States

Travis Lontz

HDT Global, Solon, OH, United States

Alexander Makhlin

The Johns Hopkins University Applied Physics Laboratory, Laurel, MD, United States

Borislav Marinov

Exoskeleton Report LLC, San Jose, CA, United States

Lorenzo Masia

Department of Physics and Astronomy, Institute of Technical Informatics ZITI, Heidelberg University, Heidelberg, Germany

Enrico Meli

Department of Industrial Engineering (DIEF), University of Florence, Florence, Italy

Samer Mohammed

University of Paris-Est, Créteil (UPEC), Paris, France

Courtney W. Moran

The Johns Hopkins University Applied Physics Laboratory, Laurel, MD, United States

Juan C. Moreno

Cajal Institute (CSIC), Madrid, Spain

Tom Moyer

HDT Global, Solon, OH, United States

Cristobal Ochoa-Luna

University of Quebec in Montreal (School of Higher Technology), Montreal, QC, Canada

Luke E. Osborn

Department of Biomedical Engineering, Johns Hopkins School of Medicine, Baltimore, MD, United States

Matthew P. Para

The Johns Hopkins University Applied Physics Laboratory, Laurel, MD, United States

Carlos Parga

Center for Research and Advanced Studies of the National Polytechnic Institute, Mexico City, Mexico

Joel C. Perry

Mechanical Engineering Department, University of Idaho, Moscow, ID, United States

M.H. Rahman

University of Wisconsin—Milwaukee, Milwaukee, WI, United States

Islam Rasedul

University of Wisconsin—Milwaukee, Milwaukee, WI, United States

Alessandro Ridolfi

Department of Industrial Engineering (DIEF), University of Florence, Florence, Italy

Jacob Rosen

Bionics Lab, Department of Mechanical and Aerospace Engineering, University of California, Los Angeles, CA, United States

William Zev Rymer

Department of Physical Medicine & Rehabilitation, Northwestern University, Chicago, IL, United States; Shirley Ryan AbilityLab, Single Motor Unit Laboratory, Chicago, IL, United States; Department of Physiology, Northwestern University, Chicago, IL, United States

Maarouf Saad

University of Quebec in Montreal (School of Higher Technology), Montreal, QC, Canada

Julio J. Santos-Munne

HDT Global, Solon, OH, United States

Nicola Secciani

Department of Industrial Engineering (DIEF), University of Florence, Florence, Italy

Nitin Sharma

University of Pittsburgh, Pittsburgh, PA, United States

Yang Shen

Bionics Lab, Department of Mechanical and Aerospace Engineering, University of California, Los Angeles, CA, United States

Yashna Singh

Shirley Ryan AbilityLab, Single Motor Unit Laboratory, Chicago, IL, United States

Massimiliano Solazzi

PERCRO Laboratory, TeCIP Institute, Scuola Superiore Sant'Anna, Pisa, Italy

James Solberg

HDT Global, Solon, OH, United States

Nitish V. Thakor

Department of Biomedical Engineering, Johns Hopkins School of Medicine, Baltimore, MD, United States; Department of Electrical and Computer Engineering, Johns Hopkins University, Baltimore, MD, United States; Singapore Institute for Neurotechnology, National University of Singapore, Singapore, Singapore

Shawn T. Trimble

Mechanical Engineering Department, University of Idaho, Moscow, ID, United States

Ronald J. Triolo

Department of Veterans Affairs, Advanced Platform Technology Center, Louis Stokes Cleveland Department of Veterans Affairs Medical Center, Cleveland, OH, United States; Department of Biomedical Engineering, Case Western Reserve University, Cleveland, OH, United States

Thomas Van Doren

HDT Global, Solon, OH, United States

Dario J. Villarreal

Electrical and Computer Engineering Department, Mechanical Engineering Department, Southern Methodist University, University Park, TX, United States

Alexandra S. Voloshina

Department of Mechanical Engineering, Stanford University, Stanford, CA, United States

Daniel Wahl

HDT Global, Solon, OH, United States

Brock A. Wester

The Johns Hopkins University Applied Physics Laboratory, Laurel, MD, United States

Kirby Ann Witte

Department of Mechanical Engineering, Carnegie Mellon University, Pittsburgh, PA, United States

Eric T. Wolbrecht

Mechanical Engineering Department, University of Idaho, Moscow, ID, United States

Michele Xiloyannis

Sensory-Motor Systems (SMS) Lab, ETH Zurich, Zurich, Switzerland

Yoji Yamada

Nagoya University, Nagoya, Japan

Wen Yu

Center for Research and Advanced Studies of the National Polytechnic Institute, Mexico City, Mexico

UPPER LIMB EXOSKELETON SYSTEMS—OVERVIEW

1

Yang Shen, Peter Walker Ferguson and Jacob Rosen

Bionics Lab, Department of Mechanical and Aerospace Engineering, University of California, Los Angeles, CA, United States

1.1 INTRODUCTION

Exoskeletons have been developed for several decades. During the physical human–robot interaction (pHRI), exoskeleton systems are at a very special position. Unlike serial robotic manipulators which interact with human operators at the end-effector, exoskeletons cover the human limb in one or more joints, and synchronously moves with the human's joints. This design, on the one hand, enables more application potentials, like strength augmentation, movement correction akin to an orthosis, or natural teleoperation, yet on the other hand, brings challenges in mechanism design, actuation and power transmission, manufacturing, sensing, and control algorithms development, which require a deep understanding of human anatomy, motor control, biomechanics, etc.

There exists a considerable difference between exoskeleton techniques in upper limb and lower limb applications, based on the motivation as well as the technical difficulties. The authors focus on upper limb exoskeleton systems in this chapter and provide an overview of their applications as assistive, rehabilitative, augmentative, and other devices. Both “rigid” exoskeletons and “soft” exosuits are reviewed. This study works as a review of state-of-the-art techniques and development on upper limb exoskeleton-like devices excluding systems worn on the trunk (e.g., spine injury prevention exoskeletons). An additional notable class of rehabilitation robot that can be used for the upper limbs is the dynamometer. Dynamometers such as the Biomed System 4 Pro and the HUMAC NORM feature a single motor that can be repositioned and connected to various attachments to target specific motions. These are not covered in this chapter. Although conceptual designs are helpful as guidance for research, they are generally not included in this review if no working prototypes have been presented in the literature (e.g., 6-Rexos [1]).

The first powered upper limb exoskeleton is generally considered to be the Hardiman, developed in the 1960s by General Electric and the US armed forces [2]. Initial designs were frequently targeted at augmenting capabilities for soldiers, and this remains an active area of research (e.g., the SARCOS series, which is detailed later in this chapter). Later, in order to alleviate the lack of experienced physical therapists, the applications extended to rehabilitation, which requires better human-in-the-loop understanding, like intention detection and motion control. These systems

branched out to become much of rehabilitative robotics. Additionally, as the world population has aged, increased focus has shifted toward exoskeletons designed for assisting the elderly or disabled without expectation of recovery, such as those MyoPro systems developed based on the Myomo e100 NeuroRobotic System [3]. Due to the cost of human labor in labor-intensive industries such as construction and manufacturing, and employer desire to reduce injuries due to moving heavy objects, numerous exoskeletons began to be developed to augment wearers in industry. Lastly, numerous upper limb exoskeletons have been developed for other purposes such as teleoperation and as haptic devices in virtual reality (VR) environments. For all these systems, the historical trend has been for the need for active systems due to the inadequacy of purely passive ones. Before diving into a discussion of applications on assistive, rehabilitation, augmentation/industry, and others, the rest of the chapter is divided into the following parts: mechanism, actuation, transmission, sensing method, control strategies, and other related research. Readers will find a similar organization in the sister chapter (Chapter 8: Hand Exoskeleton Systems—Overview) [4].

1.2 OVERVIEW OF UPPER LIMB EXOSKELETON SYSTEMS

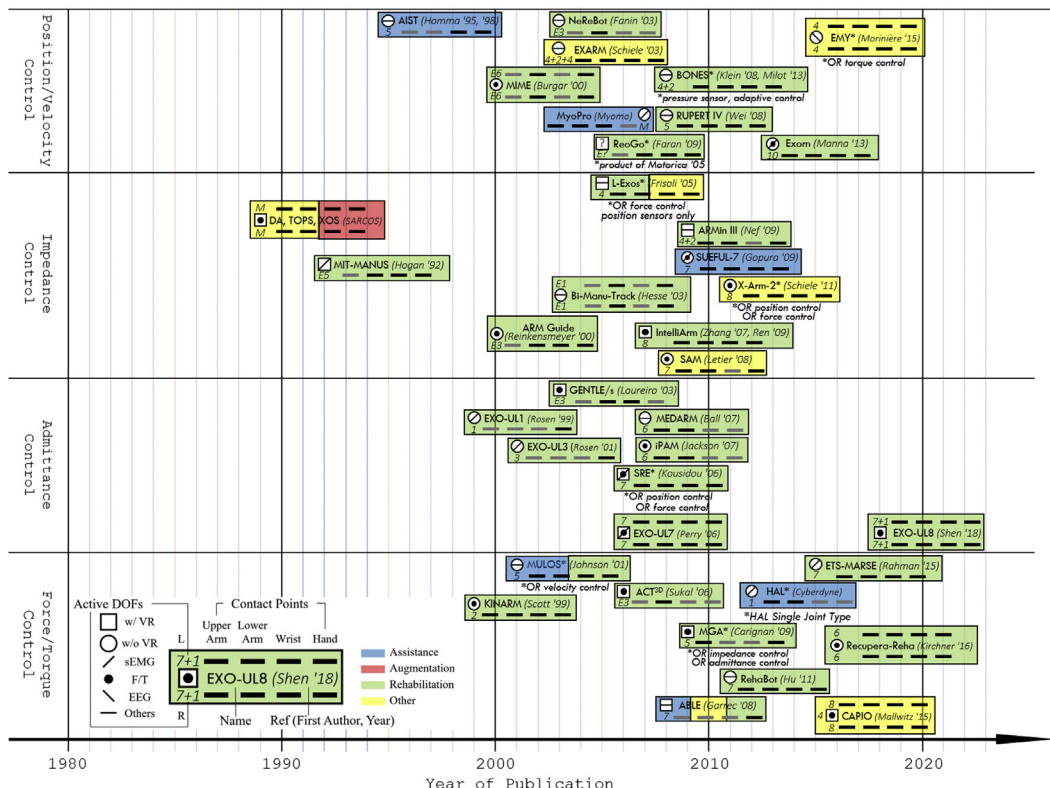
With no standard in designing and developing upper limb exoskeleton systems, one may categorize them in different ways—but some perspectives can always stand out more. The high-dimensional categorization approach may contain elements of:

- Mechanism: active and passive degrees of freedom (DoFs); where the pMRI occurs (upper arm, lower arm, wrist, hand); single or dual arm.
- Actuation method: electric motors, pneumatic, hydraulic, series elastic actuator (SEA), etc.
- Transmission: direct drive, cable-driven, etc.
- Sensing method: surface electromyography (sEMG) signals, force/torque sensors, electroencephalography (EEG) signals, etc.
- Control approach: position/velocity, force/torque, admittance, impedance, etc.
- Applications: assistive, rehabilitation, augmentation/industry, etc.

Therefore the authors have created two figures in order to give the audience an illustrative and informative overview of upper limb exoskeleton systems from different view angles.

[Fig. 1.1](#) provides a chronological overview of the development of around 40 exoskeleton systems. Some well-known end-effector devices are also covered. The horizontal axis ranges from 1980 to 2020, while the vertical axis generally categorizes the upper limb exoskeleton systems in their control methods: position/velocity control, impedance control, admittance control, and force/torque control. Readers may notice that multiple systems, due to their functionalities, could switch between several control modalities, which have been marked in the figures. Systems are marked in different colors to indicate the applications. The actuation mechanism and whether or not it has VR are also annotated.

[Fig. 1.2](#) utilizes the same annotation but provides an active-DoF-based table of existing upper limb exoskeleton systems. The horizontal axis ranges from DoF = 1 to DoF = 10 + . Interestingly, no systems are designed to have nine DoFs.

**FIGURE 1.1**

A chronological overview of existing upper limb exoskeleton systems.

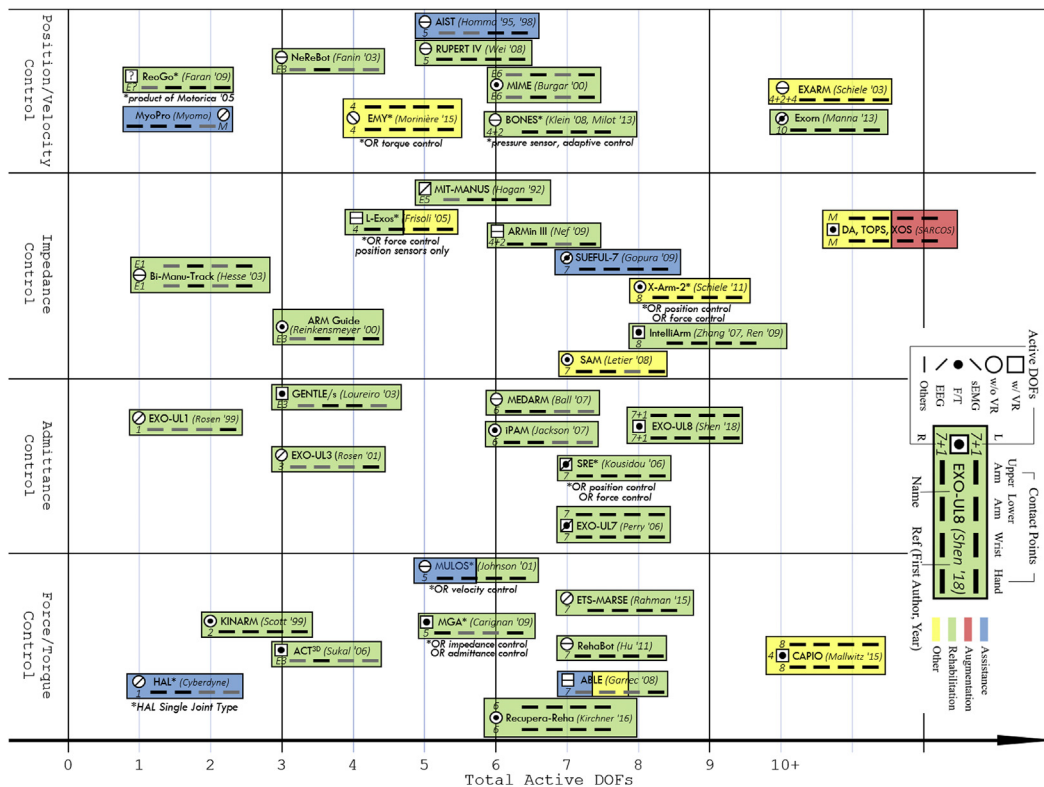
1.2.1 MECHANISM

This section discusses how the human arm moves and thus how upper limb exoskeleton systems are designed.

One approach to understanding the functionalities of an exoskeleton system is to look into the number of active and passive DoFs the system has. This directly tells which joints are capable of moving—the rough idea of the whole workspace; and which human arm joints are supposed to be assisted, trained, or augmented.

An upper limb exoskeleton is supposed to interact with a human arm. Thus we have two entities in this complex human-in-the-loop system to discuss: the exoskeleton and the human arm.

Although surrounded by muscles and other tissues, the human upper extremity, anatomically, is often simplified to have seven DoFs: shoulder extension/flexion, shoulder adduction/abduction, shoulder internal/external rotation, elbow extension/flexion, forearm pronation/supination, wrist extension/flexion, and wrist radial/ulnar deviation. However, the extra DoF in its joint space brings us challenging complexity since the maximum DoFs in the task space is six—three position DoFs and three orientation

**FIGURE 1.2**

An overview of existing upper limb exoskeleton systems based on the number of active DoFs.

DoFs. This does not only require us to understand how a human does the redundancy resolution (e.g., under gravitational loads [5]) or some natural coupling among joints (i.e., synergistic movements [6,7]), but also to take into consideration when designing exoskeleton mechanisms.

The DoFs of an exoskeleton can be used to categorize the systems. The number of arms is also an important consideration because additional movement protocols can be utilized if multiple arms are available (e.g., mirror-image symmetric training).

Another factor that needs consideration is where the human–machine contact occurs. More contact sites may indicate better controllability of the human, but may also introduce unwanted resistance or synergistic movement.

1.2.2 ACTUATION

1.2.2.1 Electric motors

Many exoskeletons use this category of actuators to achieve high control precision and quick response. However, due to its generally low power-to-mass ratio, the upper limb exoskeletons

developed, especially with high DoFs/complexity—which requires more actuators—usually need to compromise either power or portability. “Portable” is not used in this context as an equivalent to “wearable.” The latter focuses more on how to achieve a better physical human–machine interaction, rather than purely lighter weight to enable transportation by the user. However, there is a trend in the field that exoskeletons/exosuits are becoming lightweight to introduce more application scenarios (e.g., labor-intensive assembly lines), rather than staying in the laboratory settings. Another disadvantage of electric motors is their high cost.

1.2.2.1.1 Pneumatic actuators

Using a pneumatic actuator could save significant self-weight, while keeping a relatively high torque output. However, two major factors should be considered when developing exoskeletons using this kind of actuator. On the one hand, it brings more complexities and challenges to the controller’s design—delay and/or hysteresis could happen—and to resolve these issues proportional regulators and valves are needed, but with additional costs and complexity. On the other hand, heavy pumps and/or compressed gas containers may sacrifice the system’s portability, oil/lubricant might also contaminate the system, and downtime/maintenance is increased.

1.2.2.1.2 Hydraulic actuators

Hydraulic actuators could satisfy requirements for even higher torque output, especially for augmenting human capability. Similar to pneumatic actuators, control is less precise than electric motors, and incompressible liquid from a pump could contaminate the whole system and safety might be compromised. Additional devices like a fluid reservoir, motors, pumps, valves, heat exchangers, and noise-reduction equipment make this category of actuator more suitable in human capability augmentation than providing assistance or robotic physical therapy to elderly people and patients.

1.2.2.1.3 Series elastic actuators

SEAs are known for their advantages in achieving stable force control, as well as safety in pHRI. There are different approaches to achieve a specific level of compliance: to tune the stiffness of the transmission systems and physical links connecting the actuator to the end effector, to change the energy storage capacity of that transmission/linkage pair, and to modify the damping ratio of the transmission/linkage, etc. [8].

1.2.2.2 Transmission

1.2.2.2.1 Direct drive, gear, or linkage

To straightforwardly realize power transmission from a rotary or linear actuator, one may choose to position the actuator right next to the anatomical arm joint and fix the links with human arm linkages. The strategy works well with elbow flexion/extension, which is usually the first joint an exoskeleton prototype builds on. However, when the DoF becomes higher, for example, shoulder complex, ingenious mechanisms are needed to realize the movement while avoiding bulky design and possible singularities to maximize the reachable workspace (not only in task space, but also in joint space). In addition, a straightforward solution like direct drive, gear, or linkage is highly

possible to bring in heavy self-weight (which requires active gravity compensation later in the controller) and reduces the safety level in pHRI.

1.2.2.2.2 Cable-driven

This transmission method could enable a lightweight design since all actuators, even if they are heavy or bulky, could be positioned at the back/end of the exoskeleton systems. The part directly in contact with the human upper extremity could be reduced in both size and weight. However, control could be an issue. Sometimes the torque output is also compromised, or a stronger cable is used.

1.2.2.2.3 Other transmissions

Other power transmission approaches have also been proposed: hydraulic transmission [9], Bowden cables [10], tendon drive [11], etc.

1.2.2.3 Sensing method

An upper limb exoskeleton's movement could be generally categorized in the following modes, with the order of increasing “assistive” torque output:

- As a resistive trainer, the exoskeleton exerts resistance force/torque on the human arm so that muscle strength could be exercised.
- As an orthosis, the exoskeleton corrects the user's abnormal movement by applying force fields in multiple directions.
- As a pure follower, the exoskeleton detects human's intention and follows the human's movement with little or no resistance applied to the human arm.
- As an assistive device, the exoskeleton provides assistive force fields to help the user to accomplish a task.
- Following a predefined trajectory, the exoskeleton fully controls the user's movement with position control.
- As a capability augmentation device, the exoskeleton provides force/torque to compensate not only for the weight of the user's arm but also that of the object to be moved.

To properly guide the exoskeleton's movement as discussed above, the system normally needs at least one of the following sensing methods as input signals.

1.2.2.3.1 Position sensors

As one essential information in understanding the exoskeleton's spatial configuration and thus analyzing its kinematics and dynamics, position is commonly measured, either directly or indirectly, by a variety of sensors. These include but are not limited to encoders, potentiometers, flex sensors, and transducers. Footprint, measurement accuracy, data transmission rate and reliability, and cost are common factors taken into consideration when one type is chosen over another.

1.2.2.3.2 Force/torque sensors

For features with force information involved, for example, providing assistance, force/torque sensors are needed to tell the exoskeleton when to move and to stop. These sensors are also necessary

for haptic applications like teleoperation and rehabilitation/training in VR. Sometimes redundant force/torque sensors are mounted to the system to bring in additional safety layers.

1.2.2.3.3 Electromyogram

Electromyogram (EMG), normally measured in a noninvasive way—by placing electrodes on the surface of arm skin to detect the upcoming muscle activities (e.g., elbow flexion)—could help the exoskeleton decide which joints to move in order to accommodate the human arm movement in the very near future. If the signal is well filtered and analyzed, this surface EMG approach could be very helpful in controlling the exoskeleton's movement as theoretically no force interaction between the human arm and exoskeleton is needed. However, in practice it is difficult to make use of this sensing strategy due to some long-standing problems: setting up and calibration are time-consuming; signals are often noisy; a high-DoF exoskeleton system may need a very complex and expensive multichannel sEMG measurement device.

1.2.2.3.4 Electroencephalogram

Similar to sEMG, an EEG is also measured using a noninvasive cap with electrodes detecting electrical activities in the human brain. It has the same advantages as sEMG and even works with stroke patients with no arm movement capability. However, the signal could be as noisy as sEMG and requires additional processing.

Sensor fusion using multiple sensing methods may make the system's intention detection more stable and safer. Lobo-Prat et al. [12] provided a good review of noninvasive intention detection in active movement-assistive devices.

1.2.2.4 Control

To command the upper limb exoskeleton to accomplish a task together with a human in the loop, the system needs to transmit the sensed signals via a controller to actuators. Shown in Figs. 1.1 and 1.2, upper limb exoskeleton systems are categorized into different control strategies, which sometimes may in reverse tell what functionalities the system has. Based on the difference in applications, researchers utilized control strategies including but not limited to the following.

1.2.2.4.1 Position/velocity control

Often used in passive motion like predefined trajectory following or teleoperation, position/velocity control aims to achieve a desired joint position/velocity in order to track a trajectory.

1.2.2.4.2 Force/torque control

To provide assistance or even further augment the user's capability, a controller may estimate how much force/torque is needed and send the command to the actuators. Force/torque control is also often combined with biosignal control discussed below.

1.2.2.4.3 Impedance control

First introduced in Ref. [13], impedance control is used to modulate the system's dynamic behavior. It accepts flow (e.g., position/velocity) as inputs and yield effort (e.g., force/torque).

1.2.2.4.4 Admittance control

A reversed version of impedance control, the admittance controller accepts effort (e.g., force/torque signals) as inputs and yield flow (e.g., desired position commands) to actuators. If force/torque sensors are equipped on the human–machine interface, the user’s movement would produce an interaction force which directly results in exoskeleton movement. Tuning the “stiffness” makes the user feel that the exoskeleton is difficult or easy to move. The user always feels some “resistance,” which sacrifices as input to the controller—overtuning the sensitivity may make the system unstable and oscillate with tiny unwanted movements.

1.2.2.4.5 Master/slave system

As in Ref. [14], exoskeleton users could build interconnections using teleoperation: one wears an exoskeleton as the master side and teleoperates the slave side—another exoskeleton worn by another user. The communication could be unilateral or bilateral, and position control or force control could be used based on the functionality needed. This framework could also be expanded to scenarios with different types of slave side: to teleoperate an industrial manipulator in hazardous materials handling, underwater or extraterrestrial exploration; to teleoperate an avatar in VR in poststroke rehabilitation training; the healthy side teleoperates the affected side in poststroke upper extremity rehabilitation training (bimanual mode) [15].

1.2.2.4.6 Biosignal control

As mentioned in Section 1.2.2.3, this control approach does not rely on force or position information measured from the human–machine interface, but more on biosignals like sEMG and EEG which could directly tell which joints should move. Mapping from the measured signals to control signals, however, needs to be determined based on the system’s complexity (e.g., number of DoFs) in kinematics and dynamics.

One may also find hybrid control strategies with other names like AAN (assist-as-needed) control, adaptive control, etc.

1.3 ASSISTIVE UPPER LIMB EXOSKELETONS

To differentiate “assistive” upper limb exoskeletons from “rehabilitation” and “augmenting” devices, here we define them as systems providing *necessary* assistance to the human operator to accomplish activities of daily living (ADLs). Like many lower limb exoskeleton systems which usually provide predefined gait trajectories, upper limb exoskeleton systems help to finish the rest of the trajectories if the human operators are not capable of accomplishing them, for example, reaching out to grab a coffee mug. Due to high-DoF joint and task space and intention detection requirement, not many systems are developed under this category, compared with rehabilitative and augmentative upper limb exoskeletons.

Upper limb exoskeletons in this category include but are not limited to the following.

1.3.1 AIST

Upper limb motion assist system by AIST [16,17]: this research was first proposed and developed in the mid-1990s; the system consists of two such orthoses placed on the forearm near the elbow and the wrist. By changing the positions of both orthoses, two rotations and three translations of the forearm can be controlled. The system's power transmission is based on a cable-driven mechanism, and position/velocity control is implemented.

1.3.2 SUEFUL-7

Published in 2009, SUEFUL-7 [18] features offset centers of rotation at the wrist to match the slightly offset joint axes of the wrist and a moving center of rotation at the shoulder joint to more accurately match movements of the shoulder. In this seven-DoF system, impedance control is used with both sEMG and F/T signals as inputs.

1.3.3 MULOS

MULOS (motorized upper limb orthotic system) [19] uses cable transmissions at the shoulder joints, a bevel gearbox at the elbow, and a timing belt at the forearm. The five-DoF system has three DoFs at the shoulder, one DoF at the elbow, and one to provide pronation/supination. It utilizes force/torque control or velocity control, and also comes with applications in rehabilitation as.

1.3.4 HAL

The hybrid assistive limb (HAL) is a serial cyborg-type robot developed by Cyberdyne Inc [20]. It has a single-joint prototype that could be used to assist or even train upper limb movement. It utilizes sEMG signals to actuate the movements.

1.3.5 ABLE

ABLE [21] features screw-and-cable transmission systems that enable the motor to be placed along the limb parallel to the cable. This permits ABLE to have a highly compact design compared with systems with transversal motors or beveled gearboxes. Readers should note that ABLE also has applications in rehabilitation and other areas. It contains seven DoFs.

1.3.6 MYOPRO

As mentioned previously in this chapter, MyoPro [22] by Myomo, Inc. (Cambridge, Massachusetts, United States), utilizes EMG signals to realize a one-DoF elbow flexion/extension movement. It aims to assist arm movement, when paralyzed by a stroke, injury, or disease.

1.4 REHABILITATION UPPER LIMB EXOSKELETONS

Stroke is one of the leading causes of disability. Every year there are approximately 800,000 new stroke patients in the United States, with many of them suffering from various disabilities—over 50% of survivors have mild to severe weakness of the affected upper extremity that is managed by physical therapies to try to improve skillful arm and hand movements, strength, speed, and coordination [23,24]. As a result of brain lesions, stroke victims often lose some of their upper limb motor capabilities, such as the ability to lift their arms up, spasticity, and abnormal synergy [25]. Patients usually have the potential to rehabilitate (to some extent) based on neuroplasticity, and physical therapy intervention helps accelerate recovery.

Automating rehabilitation training for the affected upper extremity by employing robotic systems has been proposed to increase the number of repetitions of exercise with more normal kinematics. For decades, engineers and physical therapists have been developing robots to automate the poststroke training process, resulting in a shift in research trends from low-dimensional, end-effector style *manipulanda* to high-dimensional, fully covered *exoskeletons*, which can simultaneously manipulate the multiple DoFs of the human arm as well as provide additional features, such as tunnel-like force fields and gravity compensation [26].

A few end-effector-based systems are discussed next.

1.4.1 MIT-MANUS

The MIT-MANUS [27–30], commercialized as the InMotionArm (Interactive Motion Technologies, Inc., Cambridge, Massachusetts, United States), is a direct-drive five-bar linkage SCARA robot. The robot is attached to the patient’s forearm and produces horizontal planar translations. Additional attachments have been developed to enable active control of forearm pronation/supination, wrist flexion/extension, and wrist abduction/adduction. The system is used with robotic therapy games to motivate and coordinate therapeutic tasks, a strategy adopted by the majority of upper limb robotic rehabilitation systems.

1.4.2 NEREBOT

NeReBot [31–33] maneuvers the patient’s arm by changing the lengths of three cables suspending orthoses/splints worn by the patient. It is a cable-driven robot featuring a single splint attached to the entire forearm actuated by three motors.

1.4.3 ARM GUIDE

ARM Guide (Assisted Rehabilitation and Measurement Guide) [34] contains three DoFs, and works a diagnostic tool to provide a basis for evaluation of abnormal tone, incoordination, and weakness.

1.4.4 REOGO

The ReoGo Therapy System [35] is designed to provide exercises including elbow flexion/extension, reach forward waist level, reach forward shoulder level, and horizontal abduction.

1.4.5 GENTLE/S

The GENTLE/s [36] and ACT^{3D} [37,38] both feature a HapticMASTER robot (FCS Control Systems, The Netherlands) [39] connected to a forearm orthosis. The HapticMASTER enables each device with three active translational DoFs of the forearm.

The GENTLE/s system also features a passive elbow orthosis suspended from above by cables for gravity compensation.

1.4.6 ACT^{3D}

The ACT^{3D} (Arm Coordination Training 3-D) robotic system [37,38] provides adjustable active gravity compensation, to provide shoulder abduction torque.

1.4.7 iPAM

The iPAM system [40,41] features two rigid 3D robot arms connected to the patient at the upper arm and wrist. The system can therefore actively control the positions of the upper arm and forearm, but both connection points passively permit all orientation DoFs.

1.4.8 BI-MANU-TRACK

Bi-Manu-Track [42], MIME [43], and KINARM [44,45] are dual-arm robotic systems and are thus capable of bimanual therapy, a desirable feature that is not achievable with a single-arm system.

Bi-Manu-Track is a portable reconfigurable device limited to one active and one passive DoF between forearm pronation/supination and wrist flexion/extension.

1.4.9 MIME

MIME [43] consists of six-DoF Puma-560 robots and position digitizers attached at each forearm.

1.4.10 KINARM

KINARM [44,45] is a planar device that mechanically supports the weight of the arm while actuating two-DoF horizontal motions.

End-effector robots have been shown to be effective in rehabilitation, and several have even found commercial success. However, these robots suffer from several critical limitations.

End-effector robots typically have significantly reduced ranges of motion when compared to the human arm. For the workspace of an end-effector robot to encompass the workspace of the human arm, the robot must be very large because the base of the robot must be outside of the reach of the

arm to prevent collisions. In addition, the robot would need to reach each part of the workspace of the human arm without physically overlapping with the user.

End effectors move individual points of the human arm. The human arm is a redundant manipulator with seven DoFs, so controlling position and/or orientation of a point on the arm does not control the configuration of the entire arm. Consequently, it is challenging for an end-effector rehabilitation robot to target a specific joint motion for therapy. To the best of the authors' knowledge, there is no end-effector rehabilitation robot that can determine and control all of the DoFs of the human arm.

To circumvent these and other limitations, a large number of upper limb exoskeleton robots have been developed. Upper limb exoskeletons are structured in an anthropometric fashion that supports the partial/full range of motion of the human arm. They are designed to be worn by the user, and are attached at multiple locations. Although this can significantly complicate the design of the robot, it enables much larger ranges of motion and the ability to target specific joint motions for therapy.

1.4.11 L-EXOS

L-Exos [46–48] has a passive forearm DoF, but an attachment makes it active and adds two hand DoFs (thumb and forefinger). L-Exos can apply a 100 N force on the palm in any direction enabling its use as a haptic feedback device for VR.

1.4.12 BONES

BONES [49–51] uses a parallel mechanism for a spherical joint at the shoulder and a serially placed actuator for the elbow DoF. An attachment can add the forearm DoF and wrist flexion/extension.

In order to account for the human shoulder not being a perfect spherical joint, several exoskeletons have been designed with additional or offset shoulder DoFs.

1.4.13 ARMIN III

ARMin III [52] couples the shoulder elevation angle with a vertical translation of the shoulder, and has an attachable active forearm pronation/supination and wrist flexion/extension module.

1.4.14 MGA

The MGA (Maryland-Georgetown-Army) exoskeleton [53] has an extra vertical translation shoulder DoF, thus totaling six DoFs, and force/torque sensors mounted on both the upper arm and handle. It can be used for either orthopedic rehabilitation or neurorehabilitation via functional training.

1.4.15 INTELLIARM

IntelliArm [54,55] has not only the added active vertical translation and but also two passive horizontal translation shoulder DoFs. All together it has eight (active) and two (passive) DoFs.

1.4.16 MEDARM

MEDARM (Motorized Exoskeleton Device for Advanced Rehabilitation of Motor function) [56] replaces the standard three-DoF shoulder mechanism with two rotational DoFs at the sternoclavicular joint and three rotational DoFs at the glenohumeral joint.

1.4.17 EXORN

Exorn [57,58] is a portable exoskeleton designed to have all the DoFs of the human arm, including two at the shoulder girdle and four at the glenohumeral joint.

1.4.18 SRE

SRE (Salford Rehabilitation Exoskeleton) [59] is a seven-DoF rehabilitation exoskeleton that has a singularity when the arm is parallel to the ground due to the shoulder joint design.

1.4.19 RUPERT IV

RUPERT (Robotic Upper Extremity Repetitive Trainer) IV [60,61] is a five-DoF portable exoskeleton. PID + ILC control is implemented.

1.4.20 REHABOT

RehaBot [62] is a commercially developed upper limb exoskeleton that is part of a larger rehabilitation system. Three series elastic actuators (SEAs) and four low-inertia direct drives are responsible for its seven DoFs.

1.4.21 ETS-MARSE

ETS-MARSE [63,64] is a rehabilitation exoskeleton designed for use with EMG-based control. The earlier single-arm exoskeletons feature a wide range of designs with varying complexities targeting various joints. However, single-arm exoskeletons are inherently incapable of performing tasks requiring coordination between both arms. More importantly, bilateral movement training has been shown to be more effective in specific aspects of stroke rehabilitation than unilateral movement training [65]. To perform bilateral actions, it is, therefore, necessary to use a dual-arm exoskeleton. Due in part to the complexity of dual-arm systems, they tend to be more recently developed, and there are far fewer, compared to single-arm exoskeletons.

1.4.22 RECUPERA-REHA

The modular upper limb portion of the full-body Recupera-Reha [66] system is a recent dual-arm exoskeleton designed for stroke rehabilitation. It has six active DoFs, including one for hand grasp, and one passive DoF for wrist flexion/extension for each arm. The shoulder mechanism uses

brushless DC motors, while the elbow and forearm DOFs are actuated by two different custom serial elastic actuators.

1.4.23 EXO-UL SERIES

EXO-UL series [67] of rehabilitative upper limb exoskeleton systems started from Rosen's work known as EXO-UL1 [68–70] and EXO-UL3 [71], which contains one DoF (elbow) and three DoFs (shoulder and elbow), respectively. Later the third generation, EXO-UL7, was developed to enable dual-arm training. This generation of anthropometric seven-DoF powered exoskeleton system was initially called the “Cable-Actuated Dexterous Exoskeleton for Neuro-rehabilitation” (CADEN-7) [72], but later the authors decided to include its name under the “EXO-UL” series [73].

The latest generation, EXO-UL8 [5,15,74–76], contains an extra DoF in the hand gripper, and utilizes a direct gear-drive mechanism and is thus stronger than EXO-UL7.

The goal of hand rehabilitation exoskeletons is to restore, or at least improve, the ability of the patient to use the hand without the exoskeleton. This is done to enable the patient to resume normal ADLs without the need to constantly wear an assistive device. Many ADLs involving the hand are reach-and-grasp tasks that also require movement of the arms. As it is not uncommon for patients with hand impairments to also have impairments in the arm, it is a logical step to design a single exoskeleton combining both a multi-DoF hand exoskeleton and a full arm exoskeleton. However, there are relatively few examples of this in the literature. Instead, many upper limb exoskeletons with hand modules actuate just one DoF to permit a single simple grasp. EXO-UL8 is an example.

In Ref. [77], Ferguson et al. created a three-finger hand exoskeleton with reconfigurable mechanical coupling to actuate all five digits. Each exoskeleton finger independently controlled two DoF F/E motions using a motor and Bowden cable transmission system. The device was designed to be further integrated with the EXO-UL8 [76] and BLUE SABINO [78] upper limb exoskeletons. For details, the readers should refer to Chapter 8, Hand Exoskeleton Systems—Overview [4].

1.5 AUGMENTATION UPPER LIMB EXOSKELETONS

Unlike those with applications in providing necessary assistance in ADLs or training in rehabilitation, augmentation upper limb exoskeletons “increase” human users’ strength by compensating for the gravitational weights of the human arm or even external loads, or amplifying the force applied to the environment via teleoperation. These devices are used in heavy-duty industrial tasks like moving objects, long-time assembly, etc.

For safety reasons, passive (with no or small powered actuators) exoskeletons are more commonly used, although active (equipped with multiple powered actuators) ones can bring much more capability augmentation.

1.5.1 SARCOS GUARDIAN XO

As a spin-off from the University of Utah in the early 1980s, several series of exoskeletons with different applications were produced. The SARCOS Guardian XO is a full-body exoskeleton that can augment the user's capability in moving and transporting heavy objects.

1.5.2 SARCOS GUARDIAN GT

The SARCOS Guardian GT system contains a dual-arm exoskeleton, as well as a dual-arm mobile robot. It has the capabilities to carry out hazardous jobs such as welding and heavy-duty assembly work.

1.5.3 SHOULDERX FROM SUITX

ShoulderX from SuitX (US Bionics, Inc., Emeryville, California, United States) augments its wearer by reducing forces at the shoulder complex, reducing the risk of shoulder injuries and increasing workplace productivity. It weighs 7 lb (3.17 kg) and does not come with actuators and computers.

1.5.4 EKSOVEST FROM EKSO BIONICS

Similar to ShoulderX, EksoVest (Ekso Bionics, Richmond, California, United States) is also an upper body exoskeleton that elevates and supports the worker's arms to assist with tasks ranging from chest height to overhead. The unit weighs 9.5 lb (4.3 kg) and provides 5–15 lb (2.2–6.8 kg) adjustable lift assistance to each arm.

1.6 OTHERS

In addition to exoskeletons for assistance, rehabilitation, and augmentation, there exist a number of systems in the literature/industry that are classified in this chapter as “other” exoskeletons. Applications for these exoskeletons vary, but a significant subset of them is used as haptic devices or for teleoperation (hazardous materials or extraterrestrial exploration). A particular interest over the past two decades has been exoskeletons for use in VR applications. Since the systems used in industries normally do not have publications illustrating their specifications, some are not included in Figs. 1.1 and 1.2. Here we mention some interesting and seemingly successful prototypes.

1.6.1 EXARM

Developed by the European Space Agency (ESA/ESTEC), EXARM [79] allows astronauts inside the International Space Station (ISS) to remote-control EUROBOT.

1.6.2 X-ARM-2

X-Arm-2 [80], as a descendant of EXARM, incorporates four Bowden cables and four direct-drive actuators for haptic feedback, as well as six passive joints.

1.6.3 SARCOS MASTER ARM

The SARCOS Master Arm [81] and SAM (Sensoric Arm Master) [82,83] are single-arm exoskeletons designed for teleoperation. The SARCOS Master Arm and SAM have the seven main DoFs of the human arm: shoulder flexion/extension, shoulder abduction/adduction, shoulder internal/external rotation, elbow flexion/extension, forearm pronation/supination, wrist flexion/extension, and wrist abduction/adduction.

1.6.4 SAM

SAM [82,83] is a wearable and portable system, weighing just 7 kg. A hybrid controller is implemented locally on each joint of the exoskeleton.

1.6.5 CAPIO

CAPIO [84] is a dual-arm exoskeleton with 20 active DoFs, including four on the back and an extra translational DoF at each elbow. CAPIO uses serial elastic actuators and is designed for use as a haptic feedback device and teleoperation.

1.6.6 SARCOS DEXTROUS ARM

SARCOS Dextrous Arm (DA) [85] is a master–slave system with 10 DoFs, for research and operation in hazardous environments.

1.6.7 EMY

EMY [86] is a dual-arm exoskeleton with active DoFs of shoulder internal/external rotation, shoulder flexion/extension, elbow flexion/extension, and forearm pronation/supination. It features the same screw-cable system for actuation that ABLE [21] uses. The forearm DoF is achieved by a parallel structure of three rods on ball-joints connecting a rotating arch to a fixed arch. EMY is designed specifically for the evaluation of the brain–machine interface.

1.7 CONCLUSION

This chapter summarizes current upper limb exoskeleton systems for a variety of applications, and categorizes them based on two main perspectives: chronologically and DoF-based. Although systems have been developed to be applied in assistive, rehabilitative, augmentative, and other tasks, the most common application of the systems surveyed is for rehabilitation.

Multiple aspects of an upper limb exoskeleton system are discussed: mechanism, actuation, transmission, sensing method, and control. How to effectively improve the heuristic power-to-weight ratio of a system, especially a high-DoF one, still remains an open question. As lighter and more powerful actuators are invented and adopted, and innovative mechanisms are designed and utilized, we expect truly wearable and portable systems to be developed.

REFERENCES

- [1] M. Gunasekara, R. Gopura, S. Jayawardena, 6-REXOS: upper limb exoskeleton robot with improved pHRI, *Int. J. Adv. Robot. Syst.* 12 (2015). Available from: <https://doi.org/10.5772/60440>.
- [2] R.S. Mosher, From Handiman to Hardiman, *Soc. Automot. Eng. Trans.* 76 (1967) 588–597. Available from: <https://doi.org/10.4271/670088>.
- [3] J. Stein, e100 NeuroRobotic system, *Expert. Rev. Med. Devices.* 6 (2009) 15–19. Available from: <https://doi.org/10.1586/17434440.6.1.15>.
- [4] P.W. Ferguson, Y. Shen, J. Rosen, *Hand exoskeleton systems - overview*, in: J. Rosen, P.W. Ferguson (Eds.), *Wearable Robotics: Systems and Applications*, Elsevier, 2019.
- [5] Y. Shen, B.P. Hsiao, J. Ma, J. Rosen, Upper limb redundancy resolution under gravitational loading conditions: arm postural stability index based on dynamic manipulability analysis, in: 2017 IEEE-RAS 17th International Conference on Humanoid Robotics (Humanoids), IEEE, 2017, pp. 332–338. <<http://dx.doi.org/10.1109/HUMANOIDS.2017.8246894>>.
- [6] M. Simkins, A. Burleigh Jacobs, J. Rosen, Rhythmic affects on stroke-induced joint synergies across a range of speeds, *Exp. Brain Res.* 229 (2013) 517–524. Available from: <https://doi.org/10.1007/s00221-013-3613-2>.
- [7] A. Feldman, Y. Shen, J. Rosen, Modeling of joint synergy and spasticity in stroke patients to solve arm reach tasks, in: 2017 IEEE Signal Processing in Medicine and Biology Symposium (SPMB), 2017 IEEE, 2017, pp. 1–3. <<http://dx.doi.org/10.1109/SPMB.2017.8257046>>.
- [8] J. Hurst, A. Rizzi, D. Hobbelin, Series elastic actuation: potential and pitfalls, *Int. Conf. Climbing Walk. Robot.* 2004. http://mime.oregonstate.edu/research/drl/publications/_documents/hurst_2004a.pdf.
- [9] K. Xu, D. Qiu, N. Simaan, A pilot investigation of continuum robots as a design alternative for upper extremity exoskeletons, in: 2011 IEEE International Conference on Robotics and Biomimetics, 2011, 656–662. <<http://dx.doi.org/10.1109/ROBIO.2011.6181361>>.
- [10] F. Martinez, I. Retolaza, A. Pujana-Arrese, A. Cenitagoza, J. Basurko, J. Landaluze, Design of a five actuated DOF upper limb exoskeleton oriented to workplace help, in: Proceedings of the 2nd Biennial IEEE/RAS-EMBS International Conference on Biomedical Robotics and Biomechatronics, Bio Rob 2008, 2008, pp. 169–174. <<http://dx.doi.org/10.1109/BIOROB.2008.4762788>>.
- [11] A. Frisoli, L. Borelli, A. Montagner, S. Marcheschi, C. Procopio, F. Salsedo, et al., Arm rehabilitation with a robotic exoskeleton in Virtual Reality, in: 2007 IEEE 10th International Conference on Rehabilitation Robotics ICORR'07, 2007, pp. 631–642. <<http://dx.doi.org/10.1109/ICORR.2007.4428491>>.
- [12] J. Lobo-Prat, P.N. Kooren, A.H. Stienen, J.L. Herder, B.F.J.M. Koopman, P.H. Veltink, Non-invasive control interfaces for intention detection in active movement-assistive devices, *J. Neuroeng. Rehabil.* 11 (2014). Available from: <https://doi.org/10.1186/1743-0003-11-168>.
- [13] N. Hogan, Impedance control: an approach to manipulation, in: 1984 American Control Conference, IEEE, 1984, pp. 304–313. <<https://doi.org/10.23919/ACC.1984.4788393>>.

- [14] J. Lanini, T. Tsuji, P. Wolf, R. Riener, D. Novak, Teleoperation of two six-degree-of-freedom arm rehabilitation exoskeletons, in: IEEE International Conference on Rehabilitation Robotics, 2015, pp. 514–519. <<https://doi.org/10.1109/ICORR.2015.7281251>>.
- [15] Y. Shen, J. Ma, B. Dobkin, J. Rosen, Asymmetric dual arm approach for post stroke recovery of motor functions utilizing the EXO-UL8 Exoskeleton System: a pilot study, in: 2018 40th Annual International Conference of the IEEE Engineering in Medicine and Biology Society (EMBC), IEEE, 2018, pp. 1701–1707. <<https://doi.org/10.1109/EMBC.2018.8512665>>.
- [16] K. Homma, T. Arai, Design of an upper limb motion assist system with parallel mechanism, in: Proceedings of the 1995 IEEE International Conference on Robotics and Automation, 1995, pp. 1302–1307. <<https://doi.org/10.1109/ROBOT.1995.525460>>.
- [17] K. Homma, S. Hashino, T. Arai, An upper limb motion assist system: experiments with arm models, in: Proceedings of the 1998 IEEE/RSJ International Conference on Intelligent Robots and Systems. Innovations in Theory, Practice and Applications (Cat. No.98CH36190), vol. 2, 1998, pp. 758–763. <<https://doi.org/10.1109/IROS.1998.727285>>.
- [18] R.A.R.C. Gopura, K. Kiguchi, Y. Li, SUEFUL-7: a 7DOF upper-limb exoskeleton robot with muscle-model-oriented EMG-based control, in: 2009 IEEE/RSJ International Conference on Intelligent Robotics and Systems, IEEE, 2009, pp. 1126–1131. <<https://doi.org/10.1109/IROS.2009.5353935>>.
- [19] G.R. Johnson, D.A. Carus, G. Parrini, S.S. Marchese, R. Valeggi, The design of a five-degree-of-freedom powered orthosis for the upper limb, Proc. Inst. Mech. Eng. Part H J. Eng. Med. 215 (2001) 275–284. Available from: <http://dx.doi.org/10.1243/0954411011535867>.
- [20] Cyberdyne Inc., H.A.L., 2019. <https://www.cyberdyne.jp/english/> (accessed 11.08.19).
- [21] P. Garrec, J.P. Friconneau, Y. Méasson, Y. Perrot, ABLE, an innovative transparent exoskeleton for the upper-limb, in: 2008 IEEE/RSJ International Conference on Intelligent Robotics and Systems IROS, 2008, pp. 1483–1488. <<https://doi.org/10.1109/IROS.2008.4651012>>.
- [22] J.M. McBean, K. Narendran, Powered orthotic device and method of using same, US8,585,620 B2, 2013.
- [23] E.J. Benjamin, M.J. Blaha, S.E. Chiuve, M. Cushman, S.R. Das, R. Deo, et al., Heart disease and stroke statistics-2017 update: a report from the American Heart Association, Circulation 135 (2017) e146–e603. Available from: <https://doi.org/10.1161/CIR.0000000000000485>.
- [24] B.H. Dobkin, Rehabilitation after stroke, N. Engl. J. Med. 352 (2005) 1677–1684. Available from: <https://doi.org/10.1056/NEJMcp043511>.
- [25] P. Langhorne, J. Bernhardt, G. Kwakkel, Stroke rehabilitation, Lancet 377 (2011) 1693–1702. Available from: [https://doi.org/10.1016/S0140-6736\(11\)60325-5](https://doi.org/10.1016/S0140-6736(11)60325-5).
- [26] H.S. Lo, S.Q. Xie, Exoskeleton robots for upper-limb rehabilitation: state of the art and future prospects, Med. Eng. Phys. 34 (2012) 261–268. Available from: <https://doi.org/10.1016/j.medengphy.2011.10.004>.
- [27] N. Hogan, H.I. Krebs, J. Charnnarong, P. Srikrishna, A. Sharon, MIT-MANUS: a workstation for manual therapy and training. I, in: Proceedings of the IEEE International Symposium on Robot and Human Communication, IEEE, 1992, pp. 161–165. <https://doi.org/10.1109/ROMAN.1992.253895>.
- [28] H.I. Krebs, M. Ferraro, S.P. Buerger, M.J. Newberry, A. Makiyama, M. Sandmann, et al., Rehabilitation robotics: pilot trial of a spatial extension for MIT-Manus, J. Neuroeng. Rehabil. 1 (2004) 1–15. Available from: <https://doi.org/10.1186/1743-0003-1-5>.
- [29] S.K. Charles, H.I. Krebs, B.T. Volpe, D. Lynch, N. Hogan, Wrist rehabilitation following stroke: initial clinical results, in: 9th International Conference on Rehabilitation Robotics 2005. ICORR 2005, 2005, pp. 13–16. <<https://doi.org/10.1109/ICORR.2005.1501040>>.
- [30] L. Dipietro, H.I. Krebs, S.E. Fasoli, B.T. Volpe, J. Stein, C. Bever, et al., Changing motor synergies in chronic stroke, J. Neurophysiol. 98 (2007) 757–768. Available from: <https://doi.org/10.1152/jn.01295.2006>.

- [31] C. Fanin, P. Gallina, A. Rossi, U. Zanatta, S. Masiero, NeRebot: a wire-based robot for neurorehabilitation, in: International Conference on Rehabilitation Robotics, 2003, pp. 23–26.
- [32] G. Rosati, P. Gallina, S. Masiero, A. Rossi, Design of a new 5 d.o.f. wire-based robot for rehabilitation, in: Proceedings of the 2005 IEEE 9th International Conference on Rehabilitation Robotics, 2005, pp. 430–433. <<https://doi.org/10.1109/ICORR.2005.1501135>>.
- [33] G. Rosati, M. Andreolli, A. Biondi, P. Gallina, Performance of cable suspended robots for upper limb rehabilitation, in: Proceedings of the 2007 IEEE 10th International Conference on Rehabilitation Robotics, Noordwijk, 2007, pp. 385–392. <<https://doi.org/10.1109/ICORR.2007.4428454>>.
- [34] D.J. Reinkensmeyer, L.E. Kahn, M. Averbuch, A. McKenna-Cole, B.D. Schmit, W.Z. Rymer, Understanding and treating arm movement impairment after chronic brain injury: progress with the ARM guide, *J. Rehabil. Res. Dev.* 37 (2000) 653–662. Available from: <http://www.ncbi.nlm.nih.gov/pubmed/11321001>.
- [35] S. Faran, O. Einav, D. Yoeli, M. Kerzhner, D. Geva, G. Magnazi, et al., Reo assessment to guide the ReoGo therapy: reliability and validity of novel robotic scores, in: 2009 Virtual Rehabilitation International Conference VR 2009, 2009, p. 209. <<https://doi.org/10.1109/ICVR.2009.5174247>>.
- [36] R.U.I. Loureiro, F. Amirabdollahian, M. Topping, B. Driessens, Upper limb robot mediated stroke therapy—GENTLE/s approach, *Auton. Robots* 15 (2003) 35–51. Available from: <https://doi.org/10.1023/A:1024436732030>.
- [37] T.M. Sukal, M.D. Ellis, J.P.A. Dewald, Source of work area reduction following hemiparetic stroke and preliminary intervention using the ACT3Dsystem, in: Annual International Conference on IEEE Engineering in Medicine and Biology Proceedings, 2006, pp. 177–180. <<https://doi.org/10.1109/IEMBS.2006.259311>>.
- [38] M.D. Ellis, T.M. Sukal-moulton, S. Member, J.P.A. Dewald, Impairment-based 3-D robotic intervention improves upper extremity work area in chronic stroke: targeting abnormal joint torque coupling with progressive shoulder abduction loading, *IEEE Trans. Robot.* 25 (2009) 549–555. Available from: <https://doi.org/10.1109/TRO.2009.2017111>.
- [39] R.Q. Van Der Linde, P. Lammertse, HapticMaster – a generic force controlled robot for human interaction, *Ind. Robot. Int. J.* 30 (2003) 515–524. Available from: <https://doi.org/10.1108/01439910310506783>.
- [40] A. Jackson, P. Culmer, S. Makower, M. Levesley, R. Richardson, A. Cozens, et al., Initial patient testing of iPAM - a robotic system for Stroke rehabilitation, in: 2007 IEEE 10th International Conference on Rehabilitation Robotics ICORR'07, 2007, pp. 250–256. <<https://doi.org/10.1109/ICORR.2007.4428435>>.
- [41] P.R. Culmer, A.E. Jackson, S. Makower, R. Richardson, J.A. Cozens, M.C. Levesley, et al., A control strategy for upper limb robotic rehabilitation with a dual robot system, *IEEE/ASME Trans. Mechatron.* 15 (2010) 575–585. Available from: <https://doi.org/10.1109/TMECH.2009.2030796>.
- [42] S. Hesse, G. Schulte-Tigges, M. Konrad, A. Bardeleben, C. Werner, Robot-assisted arm trainer for the passive and active practice of bilateral forearm and wrist movements in hemiparetic subjects, *Arch. Phys. Med. Rehabil.* 84 (2003) 915–920. Available from: [https://doi.org/10.1016/S0003-9993\(02\)04954-7](https://doi.org/10.1016/S0003-9993(02)04954-7).
- [43] C.G. Burgar, P.S. Lum, P.C. Shor, H.F. Machiel Van der Loos, Development of robots for rehabilitation therapy: the Palo Alto VA/Stanford experience, *J. Rehabil. Res. Dev.* 37 (2000) 663–673.
- [44] S.H. Scott, Apparatus for measuring and perturbing shoulder and elbow joint positions and torques during reaching, *J. Neurosci. Methods* 89 (1999) 119–127. Available from: [https://doi.org/10.1016/S0165-0270\(99\)00053-9](https://doi.org/10.1016/S0165-0270(99)00053-9).
- [45] A.M. Coderre, A.A. Zeid, S.P. Dukelow, M.J. Demmer, K.D. Moore, M.J. Demers, et al., Assessment of upper-limb sensorimotor function of subacute stroke patients using visually guided reaching, *Neurorehabil. Neural. Repair.* 24 (2010) 528–541. Available from: <https://doi.org/10.1177/1545968309356091>.
- [46] A. Frisoli, F. Rocchi, S. Marcheschi, A. Dettori, F. Salsedo, M. Bergamasco, et al. Arm exoskeleton for haptic interaction in virtual environments, in: Proceedings of the 1st Joint Eurohaptics Conference and

- Symposium in. Haptic Interfaces Virtual Environment and Teleoperator Systems, 2005, pp. 195–201. <<https://doi.org/10.1109/WHC.2005.15>>.
- [47] S. Marcheschi, A. Frisoli, C.A. Avizzano, M. Bergamasco, A method for modeling and control complex tendon transmissions in haptic interfaces, in: Proceedings of the 2005 IEEE International Conference on Robotics and Automation, Barcelona, Spain, 2005, pp. 1773–1778. <<https://doi.org/10.1109/ROBOT.2005.1570370>>.
- [48] A. Frisoli, M. Bergamasco, L. Borelli, A. Montagner, G. Greco, C. Procopio, et al., Robotic assisted rehabilitation in virtual reality with the L-EXOS, in: Proceedings of the 7th International Conference on Disability, Virtual Reality and Associated Technology With ArtAbilitation (ICDVRAT 2008), 2008, pp. 253–260.
- [49] J. Klein, S.J. Spencer, J. Allington, K. Minakata, E.T. Wolbrecht, R. Smith, et al., Biomimetic orthosis for the neurorehabilitation of the elbow and shoulder (BONES), in: Proceedings of the 2nd Biennial IEEE/RAS-EMBS International Conference on Biomedical Robotics and Biomechatronics, BioRob 2008, 2008, pp. 535–541. <<https://doi.org/10.1109/BIOROB.2008.4762866>>.
- [50] E.T. Wolbrecht, V. Chan, D.J. Reinkensmeyer, J.E. Bobrow, Optimizing compliant, model-based robotic assistance to promote neurorehabilitation, IEEE Trans. Neural. Syst. Rehabil. Eng. 16 (2008) 286–297. Available from: <https://doi.org/10.1109/TNSRE.2008.918389>.
- [51] M.-H. Milot, S.J. Spencer, V. Chan, J.P. Allington, J. Klein, C. Chou, et al., A crossover pilot study evaluating the functional outcomes of two different types of robotic movement training in chronic stroke survivors using the arm exoskeleton BONES, J. Neuroeng. Rehabil. 10 (2013) 112. Available from: <https://doi.org/10.1186/1743-0003-10-112>.
- [52] T. Nef, M. Guidali, R. Riener, ARMin III – arm therapy exoskeleton with an ergonomic shoulder actuation, Appl. Bionics Biomech. 6 (2009) 127–142. Available from: <https://doi.org/10.1080/11762320902840179>.
- [53] C. Carignan, J. Tang, S. Roderick, Development of an exoskeleton haptic interface for virtual task training, in: Proceedings of the 2009 IEEE/RSJ International Conference on Intelligent Robotics and Systems, 2009, pp. 3697–3702. <<https://doi.org/10.1109/IROS.2009.5354834>>.
- [54] L.Q. Zhang, H.S. Park, Y. Ren, Developing an intelligent robotic arm for stroke rehabilitation, in: Proceedings of the 2007 IEEE 10th International Conference on Rehabilitation Robotics, 2007, pp. 984–993. <<https://doi.org/10.1109/ICORR.2007.4428543>>.
- [55] Y. Ren, H.S. Park, L.Q. Zhang, Developing a whole-arm exoskeleton robot with hand opening and closing mechanism for upper limb stroke rehabilitation, in: Proceedings of the 2009 IEEE International Conference on Rehabilitation Robotics, 2009, pp. 761–765. <<https://doi.org/10.1109/ICORR.2009.5209482>>.
- [56] S.J. Ball, I.E. Brown, S.H. Scott, MEDARM: a rehabilitation robot with 5DOF at the shoulder complex, in: Proceedings of the 2007 IEEE/ASME International Conference on Advanced Intelligent Mechatronics, 2007, pp. 1–6. <<https://doi.org/10.1109/AIM.2007.4412446>>.
- [57] S.K. Manna, S. Bhaumik, A bioinspired 10 DOF wearable powered arm exoskeleton for rehabilitation, J. Robot. 2013 (2013) 1–15. Available from: <https://doi.org/10.1155/2013/741359>.
- [58] S.K. Manna, D. Kumar, S. Bhaumik, Design & analysis of a portable exoskeleton structure for rehabilitation – a mechatronic approach, in: Proceedings of IEEE International Conference on Research and Development Prospects on Engineering and Technology-2013 (ICRDPE'13), IEEE, 2013, pp. 214–220.
- [59] S. Kousidou, N. Tsagarakis, D.G. Caldwell, C. Smith, Assistive exoskeleton for task based physiotherapy in 3-dimensional space, in: Proceedings of the 1st IEEE/RAS-EMBS International Conference on Biomedical Robotics and Biomechatronics, BioRob 2006, 2006, pp. 266–271. <<https://doi.org/10.1109/BIOROB.2006.1639097>>.

- [60] S. Balasubramanian, H.R. Wei, M. Perez, B. Shepard, E. Koeneman, J. Koeneman, et al., RUPERT: an exoskeleton robot for assisting rehabilitation of arm functions, in: Proceedings of the 2008 Virtual Rehabilitation, 2008, pp. 163–167. <<https://doi.org/10.1109/ICVR.2008.4625154>>.
- [61] R. Wei, S. Balasubramanian, L. Xu, J. He, Adaptive iterative learning control design for RUPERT IV, in: Proceedings of the 2nd Biennial IEEE/RAS-EMBS International Conference on Biomedical Robotics and Biomechatronics, BioRob 2008, 2008, pp. 647–652. <<https://doi.org/10.1109/BIOROB.2008.4762841>>.
- [62] J. Hu, Y.J. Lim, Y. Ding, D. Paluska, A. Solocheck, D. Laffery, et al., An advanced rehabilitation robotic system for augmenting healthcare, in: International Conference on IEEE Engineering Medicine and Biology Society EMBS, 2011, pp. 2073–2076. <<https://doi.org/10.1109/IEMBS.2011.6090384>>.
- [63] M.H. Rahman, M.J. Rahman, O.L. Cristobal, M. Saad, J.P. Kenné, P.S. Archambault, Development of a whole arm wearable robotic exoskeleton for rehabilitation and to assist upper limb movements, Robotica. 33 (2015) 19–39. Available from: <https://doi.org/10.1017/s0263574714000034>.
- [64] M.H. Rahman, C. Ochoa-Luna, M. Saad, EMG based control of a robotic exoskeleton for shoulder and elbow motion assist, J. Autom. Control Eng. 3 (2015) 270–276. Available from: <https://doi.org/10.12720/joace.3.4.270-276>.
- [65] H. Kim, L.M. Miller, I. Fedulow, M. Simkins, G.M. Abrams, N. Byl, et al., Kinematic data analysis for post-stroke patients following bilateral versus unilateral rehabilitation with an upper limb wearable robotic system, IEEE Trans. Neural. Syst. Rehabil. Eng. 21 (2013) 153–164. Available from: <https://doi.org/10.1109/TNSRE.2012.2207462>.
- [66] E.A. Kirchner, N. Will, M. Simnofske, L.M.V. Benitez, B. Bongardt, M.M. Krell, et al., Recupera-reha: exoskeleton technology with integrated biosignal analysis for sensorimotor rehabilitation, 2. Transdisziplinäre Konf December 12–13 “Technische Unterstützungssysteme, Die Menschen Wirklich Wollen”. Transdisziplinäre Konf. “Technische Unterstützungssysteme, Die Menschen Wirklich Wollen”, Hamburg, 2016pp. 504–517.
- [67] Y. Shen, J. Rosen, EXO-UL upper limb exoskeleton system, in: J. Rosen, P.W. Ferguson (Eds.), Wearable Robotics: Systems and Application, Elsevier, 2019.
- [68] J. Rosen, Natural Integration of a Human Arm/Exoskeleton System, Tel-Aviv University, 1997.
- [69] J. Rosen, M.B. Fuchs, M. Arcan, Performances of hill-type and neural network muscle models-toward a myosignal-based exoskeleton, Comput. Biomed. Res. 32 (1999) 415–439. Available from: <https://doi.org/10.1006/cbmr.1999.1524>.
- [70] J. Rosen, M. Brand, M.B. Fuchs, M. Arcan, A myosignal-based powered exoskeleton system, IEEE Trans. Syst. Man, Cybern. Part A Syst. Humans. 31 (2001) 210–222. Available from: <https://doi.org/10.1109/3468.925661>.
- [71] J.C. Perry, J. Rosen, Case study: an upper limb powered exoskeleton, in: J.L. Pons (Ed.), Wearable Robot. Biomechatronic Exoskeletons, John Wiley & Sons, 2008.
- [72] J.C. Perry, J. Rosen, S. Burns, Upper-limb powered exoskeleton design, IEEE/ASME Trans. Mechatron. 12 (2007) 408–417. Available from: <https://doi.org/10.1109/TMECH.2007.901934>.
- [73] J.C. Perry, J.M. Powell, J. Rosen, Isotropy of an upper limb exoskeleton and the kinematics and dynamics of the human arm, Appl. Bionics Biomech. 6 (2009) 175–191. Available from: <https://doi.org/10.1080/11762320902920575>.
- [74] Y. Shen, P.W. Ferguson, J. Ma, J. Rosen, Upper limb wearable exoskeleton systems for rehabilitation: state of the art review and a case study of the EXO-UL8 - dual-arm exoskeleton system, in: Wearable Technology in Medicine and Health Care, 2018, pp. 71–90. doi:10.1016/B978-0-12-811810-8.00004-X.
- [75] Y. Shen, Control and Dynamic Manipulability of a Dual-Arm/Hand Robotic Exoskeleton System (EXO-UL8) for Rehabilitation Training in Virtual Reality, UCLA, 2019. Available from: <https://escholarship.org/uc/item/12k313g8>.

- [76] Y. Shen, J. Sun, J. Ma, J. Rosen, Admittance control scheme comparison of EXO-UL8: a dual-arm exoskeleton robotic system, in: 2019 IEEE 16th International Conference on Rehabilitation Robotics (ICORR), IEEE, 2019, pp. 611–617. <<https://doi.org/10.1109/ICORR.2019.8779545>>.
- [77] P.W. Ferguson, B. Dimapasoc, Y. Shen, J. Rosen, Design of a hand exoskeleton for use with upper limb exoskeletons, in: M.C. Carrozza, S. Micera, J.L. Pons (Eds.), Wearable Robot. Challenges Trends. WeRob 2018. Biosyst. Biorobotics, Springer International Publishing, Pisa, 2019, pp. 276–280. Available from: <http://dx.doi.org/10.1007/978-3-030-01887-0-53>.
- [78] J.C. Perry, R. Maura, C.K. Bitikofer, E.T. Wolbrecht, BLUE SABINO: development of a bilateral exoskeleton instrument for comprehensive upper-extremity neuromuscular assessment, in: L. Masia, S. Micera, M. Akay, J.L. Pons (Eds.), Converging Clinical and Engineering Research on Neurorehabilitation III, Springer International Publishing, Cham, 2019, pp. 493–497.
- [79] A. Schiele, G. Visentin, The ESA human arm exoskeleton for space robotics telepresence, in: Proceedings of the 7th International Symposium on Artificial Intelligent Robotics and Automation in Space, 2003, pp. 19–23.
- [80] A. Schiele, G. Hirzinger, A new generation of ergonomic exoskeletons - the high-performance X-Arm-2 for space robotics telepresence, in: IEEE International Conference on Intelligent Robotics and Systems, 2011, pp. 2158–2165. <<https://doi.org/10.1109/IROS.2011.6048553>>.
- [81] M. Mistry, P. Mohajerian, S. Schaal, An exoskeleton robot for human arm movement study, in: Proceedings of the 2005 IEEE/RSJ International Conference on Intelligent Robotics and Systems, 2005, pp. 4071–4076. <<https://doi.org/10.1109/IROS.2005.1545450>>.
- [82] P. Letier, M. Avraam, S. Veillerette, M. Horodinca, M. De Bartolomei, A. Schiele, et al., SAM: a 7-DOF portable arm exoskeleton with local joint control, in: Proceedings of the 2008 IEEE/RSJ International Conference on Intelligent Robotics and Systems IROS, 2008, pp. 3501–3506. <<https://doi.org/10.1109/IROS.2008.4650889>>.
- [83] J. Rebelo, T. Sednaoui, E.B. Den Exter, T. Krueger, A. Schiele, Bilateral robot teleoperation: a wearable arm exoskeleton featuring an intuitive user interface, IEEE Robot. Autom. Mag. 21 (2014) 62–69. Available from: <https://doi.org/10.1109/MRA.2014.2360308>.
- [84] M. Mallwitz, N. Will, J. Teiwes, E.A. Kirchner, The CAPIO active upper body exoskeleton and its application for teleoperation, in: Proceedings of the 13th Symposium on Advanced Space Technologies in Robotics and Automation. ESA/Estec Symposium on Advanced Space Technologies in Robotics and Automation (ASTRA-2015), ESA, 2015, pp. 1–8.
- [85] D. McMonagle, Robotic Hands and Arms Developed by Raytheon SARCOS and SARCOS (Sterling), 2010. <https://sspd.gsfc.nasa.gov/workshop_2010/day2/Don_McMonagle/100325_SatServ_Workshop_Raytheon_w-markings-B.pdf>.
- [86] B. Morinière, A. Verney, N. Abroug, P. Garrec, Y. Perrot, EMY: a dual arm exoskeleton dedicated to the evaluation of Brain Machine Interface in clinical trials, in: Proceedings of the 2015 IEEE/RSJ International Conference on Intelligent Robotics and Systems IROS, Hamburg, 2015, pp. 5333–5338. <http://dx.doi.org/10.1109/IROS.2015.7354130>.

DEVELOPMENT AND CONTROL OF AN UPPER EXTREMITY EXOSKELETON ROBOT FOR REHABILITATION

2

Brahim Brahmi¹, Maarouf Saad¹, M.H. Rahman², Cristobal Ochoa-Luna¹ and Islam Rasedul²

¹*University of Quebec in Montreal (School of Higher Technology), Montreal, QC, Canada* ²*University of Wisconsin—Milwaukee, Milwaukee, WI, United States*

2.1 INTRODUCTION

Unfortunately the human nervous system can be affected by many diseases. Many types of injury, such as structural defects, cerebral palsy, brain tumors, spinal injury, multiple sclerosis, or other neurological diseases, can damage the nervous system, which means the loss of functional capacity [1,2]. In patients who have been paralyzed, maximum capacity can be restored through physical therapy applications and robotic instrumentation [3]. The aim of the physical therapy and neural rehabilitation program is to help the patient to reach the best possible condition and gain independence of their functions. Thus preventing the emergence, minimization, or eventual elimination of problems that may subsequently develop from the disease. Recently new physiotherapy rehabilitation robots have been developed to complete the physiotherapy treatment. These kinds of robots have shown a high potential in limiting the patient's disability, increasing their functional movements, ensuring their return to normal life, and helping them in daily living activities [4,5]. By employing these devices, physical therapy can be increased and can be profitable. In addition, they can conserve the time and energy of therapists, motivate the patient, and may develop the overall rehabilitation process.

There are different levels of robotic assistance strategies used after neurological accidents to provide a fitting physical therapy. The extremely urgent care after the accident—usually the first 6 weeks after the incident—is passive physical therapy [6]. In this type of therapy the robot carries the limb of the subject, which is completely passive, to realize a therapy task. Its advantage is based on the capability of the robot to provide intensive therapy for a long time period [7,8]. The active assisted and active modes permit the patient to initiate the movement voluntarily. Then the exoskeleton's wearer can realize a free motion (active mode) or the robot can correct or guide this movement (active assisted mode), for example, they limit the tremors or correct the trajectory. After detecting the initiation of a motion, usually predetermined, the robot will guide the achievement of the activity, often utilizing an impedance and/or admittance control [9]. Additionally, these strategies can be utilized for the evaluation or study of a subject's movements. In these modes,

theoretically, the patient should not feel the presence of the exoskeleton robot—this is known as robot transparency. Therefore the subject is completely active, and the exoskeleton robot should not affect the movement. However, these devices are still an emerging area and suffer from many challenges. These kinds of robots present additional complexity beyond the control of conventional robotic manipulators due to the complex mechanical structure designed for human use, the types of assistive motion, and the sensibility of the interaction with a large diversity of human wearers [10]. As a result these conditions make the robot system vulnerable to the uncertainties of dynamics and external disturbances, such as saturation, friction forces, backlash, and payload. The main challenge addressed in this chapter is to develop a robust control system allowing the exoskeleton robot to achieve the desired physiotherapy treatment in the presence of the mentioned uncertainties and external disturbances.

Control of uncertain nonlinear dynamics is one of the challenging topics of nonlinear control engineering problems. Numerous nonlinear control techniques have been designed to overcome the effect of the uncertain nonlinear dynamics and the bounded unexpected external disturbances that influence the exoskeleton's performance, for example, conventional adaptive control [11], sliding mode H_∞ control [12], and backstepping control [13,14]. Actually, sliding mode control (SMC) is considered one of the most robust nonlinear controllers developed to control uncertain nonlinear dynamics [15]. However, conventional SMC suffers from two major shortcomings. The first one is that SMC ensures an asymptotic convergence to the equilibrium without finite-time convergence. Many control techniques have been developed to overcome this problem, such as terminal sliding mode control (TSMC) [16]. TSMC utilizes a nonlinear switching surface to guarantee the finite-time convergence by including a fractional order, which allows the states' trajectories to converge to equilibrium faster. In the literature the accuracy performance of TSMC is improved by proposing a new approach, for instance, fast TSMC [17] and nonsingular TSMC [18]. A second major problem is that SMC is fundamentally based on a larger high-gain switching controller which pushes the system states to converge to the equilibrium. Nevertheless, the high-activity switching gain causes an undesirable chattering dilemma which can damage the actuators of the exoskeleton robot [19]. Many conventional approaches were developed to avoid the undesirable chattering problem, for example, by exchanging the discontinuous function by a continuous function (as a saturation function) [11], exponential reaching law [20]. Second-order sliding mode controller (SOSMC) is considered to be one of the more efficient approaches dedicated to eliminating the chattering problem and providing a high-performance precision [21]. Additionally, various approaches have been developed to improve the performance of SOSMC, such as twisting control and supertwisting control [22,23]. The main idea of SOSMC is to allow a sliding surface and its consecutive derivatives to go to zero and to maintain the discontinuous control under an integral function, which can eliminate the undesirable chattering. Nevertheless, the second-time derivative of the sliding surface might produce instability of the system, a risk that the nonlinear uncertainties and external disturbances amplify. Recently, second-order terminal sliding mode control (SOTSMC) was introduced to provide a great control performance to deal with a chattering phenomenon and provide a finite-time convergence [24,25]. So to the best of our knowledge, no SOTSMC with integral action has been proposed before to solve the mentioned problems.

Motivated to deal with the mentioned problem, and based on our previous works [26,27], we proposed a new integral second-order terminal sliding mode controller (ISOTSMC) combined with quasi-time delay estimation (TDE) to provide a good approximation of the uncertainties and the

bounded external disturbances of an exoskeleton robot and achieve a different rehabilitation protocols. Unlike conventional TDE [26,27], quasi-TDE uses time-delayed knowledge only about the previous control input without time-delayed information about the system's state to provide an accurate estimation of unknown dynamics. The time-delayed information only of the control input due to its ability to bring the necessary quantity of information of the system. The incorporation of integral control relies on its attractive characteristics—it has delivered good performance with conventional SMC [28]. The control scheme aims to keep the high precision of the SOSMC, eliminate the chattering problem, and provide a finite-time convergence to equilibrium without velocity measurement. The proposed control is evaluated with healthy subjects using passive and active rehabilitation modes. The active assistive motion is achieved by estimating the desired motion intention (DMI) of the exoskeleton's user. This mode is evaluated under a virtual environment (VE) as an interface [29]. This VE is a highly attractive tool contributing numerous benefits; it allows the creation of immersive and interactive scenes where the oriented task can be introduced in the form of serious games. This interface helps also in stimulation of the subjects and visualizes the performed tasks.

The rest of the chapter is organized as follows. The dynamics of the robot is presented in the next section. The control scheme is described in [Section 2.3](#). Experimental results and some comparisons are given in [Section 2.4](#). Finally, the conclusion is presented in [Section 2.5](#).

2.2 CHARACTERIZATION OF SYSTEM REHABILITATION

2.2.1 EXOSKELETON ROBOT DEVELOPMENT

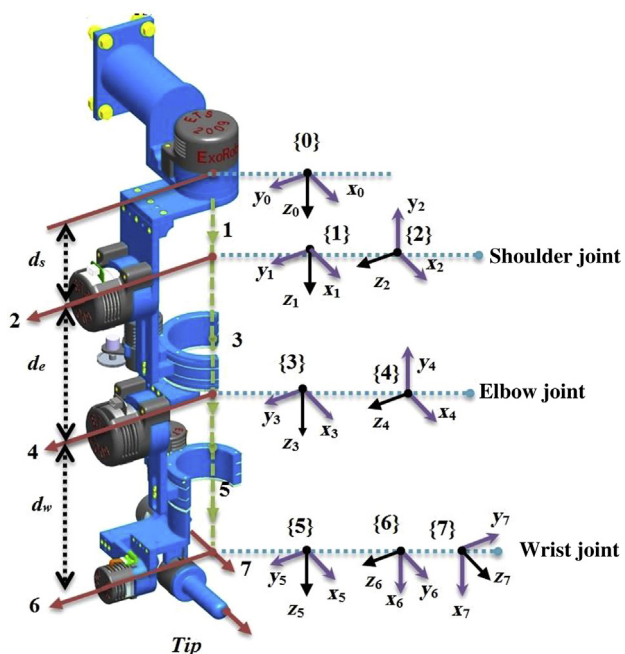
The developed exoskeleton robot ETS-MARSE (Ecole de Technologie Suprieure—Motion Assistive Robotic-exoskeleton for Superior Extremity) is a redundant robot consisting of seven degrees of freedom, as shown in [Fig. 2.1](#). It is created to provide an assistive physical therapy motion to the injured upper limbs. The idea of the designed exoskeleton is basically extracted from the anatomy of the upper limb of the human to be ergonomic for the wearer during the physical therapy session. The shoulder part consists of three joints, the elbow part comprises one joint, and the wrist part consists of three joints. Each of these parts and joints is responsible for performing a variety of upper limb motions, as shown in [Table 2.1](#). The design of the ETS-MARSE has special features compared with the existing exoskeleton robots. All of the special characteristics of the ETS-MARSE and comparisons with similar existing exoskeleton robots are summarized in [30,31]. The modified Denavit–Hartenberg parameters are given in [Table 2.2](#). These parameters are obtained from frames of reference, as shown in [Fig. 2.1](#), and are used to obtain the homogeneous transformation matrices.

2.2.2 DYNAMICS OF ECOLE DE TECHNOLOGIE SUPRIEURE—MOTION ASSISTIVE ROBOTIC-EXOSKELETON FOR SUPERIOR EXTREMITY ROBOT

The dynamics of the ETS-MARSE robot is expressed in joint space as follows:

$$M(\theta)\ddot{\theta} + C(\theta, \dot{\theta})\dot{\theta} + G(\theta) + f_{dis} = \tau \quad (2.1)$$

where θ , $\dot{\theta}$, and $\ddot{\theta} \in \Re^7$ are, respectively, the joint's position, velocity, and acceleration vectors, $M(\theta) \in \Re^{7 \times 7}$, $C(\theta, \dot{\theta})\dot{\theta} \in \Re^7$, and $G(\theta) \in \Re^7$ are, respectively, the symmetric positive definite inertia

**FIGURE 2.1**

Reference frames of ETS-MARSE.

Table 2.1 Workspace of ETS-MARSE Exoskeleton Robot

Joint (<i>i</i>)	Motion	Workspace (degrees)
1	Shoulder joint horizontal flexion/extension	0/140
2	Shoulder joint vertical flexion/extension	140/0
3	Shoulder joint internal/external rotation	-85/75
4	Elbow joint flexion/extension	120/0
5	Forearm joint pronation/supination	-85/85
6	Wrist joint ulnar/radial deviation	-30/20
7	Wrist joint flexion/extension	-50/60

matrix, the Coriolis, and centrifugal vector, and the gravitational vector including the users arm and the exoskeleton arm. $\tau \in \Re^7$ is the torque vector, $f_{dis} \in \Re^7$ is the external disturbances vector. Without loss of generality, the matrices of the dynamics model (Eq. 2.1) can be rewritten as follows:

$$\begin{cases} M(\theta) = M_0(\theta) + \Delta M(\theta) \\ C(\theta, \dot{\theta}) = C_0(\theta, \dot{\theta}) + \Delta C(\theta, \dot{\theta}) \\ G(\theta) = G_0(\theta) + \Delta G(\theta) \end{cases} \quad (2.2)$$

Table 2.2 Modified Denavit–Hartenberg Parameters

Joint (i)	α_{i-1}	a_{i-1}	a_{i-1}	θ_b
1	0	0	d_s	θ_1
2	$-\frac{\pi}{2}$	0	0	θ_2
3	$\frac{\pi}{2}$	0	d_e	θ_3
4	$-\frac{\pi}{2}$	0	0	θ_4
5	$\frac{\pi}{2}$	0	d_w	θ_5
6	$-\frac{\pi}{2}$	0	0	$\theta_6 - \frac{\pi}{2}$
7	$-\frac{\pi}{2}$	0	0	θ_7

where $M_0(\theta)$, $C_0(\theta, \dot{\theta})$ and $G_0(\theta)$ are respectively the known inertia matrix, the Coriolis/centrifugal matrix, and the gravity vector. $\Delta M(\theta)$, $\Delta C(\theta)$, and $\Delta G(\theta)$ are the uncertain parts. Let us introduce new variables such that $z_1 = \theta$ and $z_2 = \dot{\theta}$; hence the dynamics model expressed in Eq. (2.1) can be rewritten as follows:

$$\begin{cases} \dot{z}_1 = z_2 \\ \dot{z}_2 = U(t) + f(z_1 z_2) + H(z_1, z_2, \dot{z}_2) \end{cases} \quad (2.3)$$

with:

- $U(t) = U(z_1) = M_0^{-1}(\theta)\tau$
- $f(z_1, z_2) = M_0^{-1}(\theta)[-C_0(\theta, \dot{\theta})\dot{\theta} - G_0(\theta)]$
- $H(z_1, z_2, \dot{z}_2) = M_0^{-1}(\theta)[-f_{dis} - \Delta M(\theta)\dot{\theta} - \Delta C(\theta, \dot{\theta})\dot{\theta} - \Delta G(\theta)]$

2.2.3 PROBLEM STATEMENT

The developed approach aims to create a new integral second-order terminal sliding mode control (ISOTSMC) to enhance the performance of conventional second-order SMC and to guarantee the finite-time convergence of the sliding surface. Since the dynamic parameters of the exoskeleton robot are unknown, the integration of quasi-TDE to estimate them ensures a desirable rehabilitation performance. The control strategy is developed to be suitable to complete the passive and active rehabilitation movement by obtaining a control input that drives the measured trajectory to follow the reference trajectory even if the exoskeleton robot performs with uncertain dynamics and unforeseen bounded external disturbances and without velocity measurement.

Property 1: [11] *The inertia matrix $M_0(\theta)$ is symmetric and positive definite for all $\theta \in \mathbb{R}^7$.*

Assumption 1: *The function $H(z_1, z_2, \dot{z}_2)$ is a global Lipschitz function.*

Assumption 2: *The desired trajectory is bounded.*

Assumption 3: *The external disturbance f_{dis} is supposed to be continuous, has finite energy, and satisfies $\|f_{dis}\| < \epsilon$ with ϵ an unknown positive disturbance boundary.*

2.3 CONTROL DESIGN

2.3.1 UNCERTAIN ESTIMATION

According to the dynamics model of the exoskeleton robot (Eq. 2.3) the uncertainties part can be written as follows:

$$H(z_1, z_2, \dot{z}_2) = \dot{z}_2 - U(t) - f(z_1, z_2) \quad (2.4)$$

Practically, none of the dynamic parameters of the exoskeleton robot are easily obtained due to the uncertainties and their variation during the exoskeleton's tasks. As established, if $H(z_1, z_2, \dot{z}_2)$ is uncertain it might influence the control proposition. If Assumption 1 is verified, we can use quasi-TDE to estimate $H(z_1, z_2, \dot{z}_2)$ as follows:

$$\bar{H}(z_1, z_2, \dot{z}_2) \simeq H_{t_d}(z_1, z_2, \dot{z}_2) = \dot{z}_2 - f(z_1, z_2) - U(t - t_d) \quad (2.5)$$

where t_d is a very small time delay constant. Practically, the smallest constant that can be achieved in real time is the sampling period. Based on Eq. (2.5), the dynamics model (Eq. 2.3) of the exoskeleton robot can be rewritten as:

$$\dot{z}_2 = U(t) + f(z_1, z_2) + \tilde{H}(z_1, z_2, \dot{z}_2) + \tilde{H}(z_1, z_2, \dot{z}_2) \quad (2.6)$$

where $\tilde{H}(z_1, z_2, \dot{z}_2) = H(z_1, z_2, \dot{z}_2) - \bar{H}(z_1, z_2, \dot{z}_2)$ denotes the estimation error of the uncertain part.

Remark 1: Based on Assumption 1, the uncertain part $H(z_1, z_2, \dot{z}_2)$ fulfills Lipschitz condition where:

$$\tilde{H}(z_1, z_2, \dot{z}_2) = H(z_1, z_2, \dot{z}_2) - H_{t_d}(z_1, z_2, \dot{z}_2) \leq Q t_d \quad (2.7)$$

where Q is the Lipschitz constant.

To facilitate the control design, let us accept the following assumption:

Assumption 4: Based on the bounded of the estimation error of the uncertainties $\tilde{H}(z_1, z_2, \dot{z}_2)$, we assume that the first-time derivative of this error is bounded as:

$$|\dot{\tilde{H}}(z_1, z_2, \dot{z}_2)| \leq \nu$$

where ν is unknown positive definite.

2.3.2 ESTIMATION OF THE STATE OF THE SYSTEM

It is clear from Eq. (2.5) that the estimation implementation required the first and the second derivative (\dot{z}_2, \ddot{z}_2) of the measured position z_1 . In fact the measured position is the only feedback obtained from the exoskeleton robot using the Hall sensor [32]. Many estimation approaches are employed to estimate the velocity and acceleration variables of the exoskeleton robot such as high-gain observer, filter second order, and sliding mode observer [33]. Nevertheless, the conventional approaches can provide only asymptotic convergence of the state estimation, while we need a

finite-time convergence of these states. To achieve this purpose, we used the robust exact differentiator [34]. Particularly, acknowledging that the n th-order differentiator is ready to give the real-time robust exact differentiation reach to the order n , a second-order robust exact differentiator is sketched as follows:

$$\begin{cases} \dot{\psi}_0 = -\Sigma_1 |\psi_0 - z_1|^{\frac{2}{3}} sign(\psi_0 - z_1) + \psi_1 \\ \dot{\psi}_1 = -\Sigma_2 |\psi_1 - \dot{\psi}_0|^{\frac{1}{3}} sign(\psi_1 - \dot{\psi}_0) + \psi_2 \\ \dot{\psi}_2 = -\Sigma_3 sign(\psi_2 - \dot{\psi}_1) \end{cases} \quad (2.8)$$

where $\Sigma_1 = 3\Sigma^{1/3}$, $\Sigma_2 = 1.5\Sigma^{1/3}$, and $\Sigma_3 = 1.1\Sigma$ with $\Sigma \geq |\ddot{z}_2|$. The outputs of the differentiator ψ_0 , ψ_1 , and ψ_2 are, respectively, the estimated values of z_1 , z_2 , and \dot{z}_2 . Then the estimated values are produced in finite time:

$$\psi_0 = \hat{z}_1, \psi_1 = \hat{z}_2, \psi_2 = \dot{\hat{z}}_2 \quad (2.9)$$

Let us determine the errors of the state's estimation as follows:

$$e_1 = z_1 - \hat{z}_1, e_2 = z_2 - \hat{z}_2, e_3 = \dot{z}_2 - \dot{\hat{z}}_2 \quad (2.10)$$

The estimator (Eq. 2.8) can be rewritten in the following form:

$$\begin{cases} \dot{e}_1 = -\Sigma_1 |e_1|^{\frac{2}{3}} sign(e_1) + e_2 \\ \dot{e}_2 = -\Sigma_2 |e_2|^{\frac{1}{3}} sign(e_2) + e_3 \\ \dot{e}_3 = -\Sigma_3 sign(e_3) \end{cases} \quad (2.11)$$

where $e_1 = e_2 = e_3 = 0$ is realized in finite time. Based on the state's estimator (Eq. 2.8), the proposed uncertain estimator Eq. (2.5) becomes as follows:

$$\tilde{H}(z_1, z_2, \dot{z}_2) = \hat{H}(\hat{z}_1, \hat{z}_2, \dot{\hat{z}}_2) + \chi \quad (2.12)$$

where:

$$\hat{H}(z_1, z_2, \dot{z}_2) = \dot{\hat{z}}_2 - f(\hat{z}_1, \hat{z}_2) - U(t - t_d) \quad (2.13)$$

$$\chi = e_3 + f(e_1, e_2) \quad (2.14)$$

Remark 2: Based on Eq. (2.11), we can conclude that $\dot{\chi}$ is bounded, where $|\dot{\chi}| \leq \varphi$ with φ is unknown positive definite. Through the estimator of the uncertainties Eq. (2.13), we can conclude the estimator error as: $\tilde{\dot{H}} = \tilde{H} + \chi = H - \hat{H}$. Taking into consideration Assumption 4, we can obtain: $|\tilde{\dot{H}}| \leq \varphi + \nu$.

Remark 3: The stability analysis of the second-order robust exact differentiator is provided in Ref. [34]. Practically, the state estimator is designed to have a speedier dynamics than the controller by tuning its gains Σ_1 , Σ_2 , and Σ_3 , where the errors of the state estimation e_1 , e_2 , and e_3 will converge faster than the tracking error of the exoskeleton system.

For the obtained dynamic model (Eq. 2.3) with state estimation (Eq. 2.9) and uncertain dynamic estimation (Eq. 2.13), the objective of the designed control is to drive the measured trajectory to track the desired trajectory accurately, in the presence of the errors of the estimation e_1 , e_2 , e_3 , and \tilde{H} .

2.3.3 DESIGN OF INTEGRAL SECOND-ORDER TERMINAL SLIDING MODE CONTROLLER

The first step in the control development is to define the surface S in terms of position error. Then select the integral terminal type of the sliding surface, where the latter must be stable and ensure the finite-time convergence. Let us select the integral terminal surface as follows:

$$S = \lambda_1 e + \lambda_2 \int_0^t |e|^\beta \text{sign}(e) dy \quad (2.15)$$

where $e = z_1 - z^d$ is the position error and $z_1, z^d \in \Re^7$ is the measured and desired trajectory, respectively, and $\lambda_1 = \text{diag}(\lambda_{1ii}) > 0$, $\lambda_2 = \text{diag}(\lambda_{2ii}) > 0$, where $i = 1, \dots, 7$ and $1/2 < \beta < 1$. Taking the first-time derivative of S , we obtain:

$$\dot{S} = \lambda_1 \dot{e} + \lambda_2 |e|^\beta \text{sign}(e) \quad (2.16)$$

Theorem 2.1: Considering the exoskeleton robot system (Eq. 2.3) that satisfies the mentioned properties and assumptions, and the selected surface (Eq. 2.15) is stable and finite-time independent of the initial state.

Proof 1: Let us consider the following Lyapunov function:

$$V_e = \frac{1}{2} \sum_{i=1}^7 e_i^2 \quad (2.17)$$

where $V_e(e_0)$ is the initial value of the selected Lyapunov function. The time derivative of the Lyapunov function Eq. (2.17) can be obtained by

$$\dot{V}_e = \sum_{i=1}^7 e_i \dot{e}_i \quad (2.18)$$

Let us assume that $\dot{S} = 0$ is provided, from Eq. (2.16) we can obtain the following expression using scalar form:

$$\dot{e}_i = -\frac{\lambda_{2i}}{\lambda_{1i}} |e_i|^\beta \text{sign}(e_i); \text{ with, } i = 1, \dots, 7. \quad (2.19)$$

Substituting Eq. (2.19) into Eq. (2.18) we obtain:

$$\begin{aligned} \dot{V}_e &= -\sum_{i=1}^7 \frac{\lambda_{2i}}{\lambda_{1i}} |e_i|^\beta e_i \text{sign}(e_i) \\ &= -\sum_{i=1}^7 \frac{\lambda_{2i}}{\lambda_{1i}} (e_i^2)^{\frac{\beta+1}{2}} \\ &= -\sum_{i=1}^7 \frac{2^{\frac{\beta+1}{2}} \lambda_{2i}}{\lambda_{1i}} (V_e)^{\frac{\beta+1}{2}} \end{aligned} \quad (2.20)$$

where $|e_i| = e_i \text{sign}(e_i)$, Therefore $\dot{V}_e \leq 0$ is verified. We can rewrite Eq. (2.20) as follows:

$$\dot{V}_e + \sum_{i=1}^7 u_i V_e^\mu \leq 0 \quad (2.21)$$

where $v_i = \left(2^{\frac{\beta+1}{2}}\lambda_{2i}\right)/\lambda_{1i}$ and $\mu = (\beta + 1)/2$, taking into consideration $1/2 < \beta < 1$ and $3/4 < \mu < 1$.

So, according to Ref. [35], the convergence of the finite time t_s can be given by:

$$t_s = \frac{V_e^{1-\mu}(e_0)}{v(1-\mu)} \quad (2.22)$$

where $V_e(e_0)$ is the Lyapunov function's initial value.

Remark 4: It is obvious from Eq. (2.22) that the initial value of the Lyapunov function $V_e(e_0)$ and the ratio $\lambda_{2i}/\lambda_{1i}$ manage the finite-time convergence t_s of the selected sliding surface (Eq. 2.15). A large value of $\lambda_{2i}/\lambda_{1i}$ can ensure a short convergence time. Likewise, a too large gain ratio may produce an overshoot influence. Therefore the trade-off between fast convergence and control performance is required to choose λ_{1i} and λ_{2i} .

Since the selected surface is chosen, the incorporation of ISOTSMC with quasi-TDE can be easily set up now. Taking the second-time derivative of Eq. (2.16) as:

$$\ddot{S} = \lambda_1 \ddot{e} + \sum_{i=1}^7 \beta \lambda_{2i} |e|^{\beta-1} \dot{e}_i \quad (2.23)$$

where $\ddot{e} = \dot{z}_2 - \ddot{z}^d$. However, the state \dot{z}_2 is not available. By using the state estimator, from Eq. (2.10) we have:

$$\dot{\hat{z}}_2 = \dot{z}_2 - e_3 \quad (2.24)$$

By utilizing Eqs. (2.6) and (2.12); Eq. (2.24) becomes:

$$\dot{\hat{z}}_2 = U(t) + f(z_1, z_2) + \tilde{H}(z_1, z_2, \dot{z}_2) + \bar{H}(z_1, z_2, \dot{z}_2) - e_3 = U(t) + f(z_1, z_2) + \tilde{H}(z_1, z_2, \dot{z}_2) + \hat{H}(\hat{z}_i, \hat{z}_2, \dot{\hat{z}}_2) + \chi - e_3 \quad (2.25)$$

Substituting Eq. (2.13) into Eq. (2.25) and considering Eq. (2.10), we find:

$$\dot{\hat{z}}_2 = U(t) - U(t - t_d) + \tilde{H}(z_1, z_2, \dot{z}_2) + \dot{\hat{z}}_2 \quad (2.26)$$

Substituting Eq. (2.26) into Eq. (2.23), and using Eq. (2.19), we obtain:

$$\ddot{S} = \lambda_1(U(t) - U(t - t_d) + \tilde{H}(z_1, z_2, \dot{z}_2) + \dot{\hat{z}}_2 - \ddot{z}^d) - \sum_{i=1}^7 \beta \frac{\lambda_{2i}^2}{\lambda_{1i}^2} |e|^{2\beta-1} \text{sign}(e_i) \quad (2.27)$$

Theorem 2.2: Considering the exoskeleton robot system (Eq. 2.3) which satisfies the mentioned properties and assumptions, the control law of Integral second-order terminal SMC incorporating quasi-TDE ensures the convergence of the sliding surface and its first and second derivative to zero in finite-time given by:

$$U(t) = U(t - t_d) - K_1 |\dot{S}|^{\frac{1}{2}} \text{sign}(S) - \dot{\hat{z}}_2 + \ddot{z}^d + \sum_{i=1}^7 \beta \frac{\lambda_{2i}^2}{\lambda_{1i}^2} |e|^{2\beta-1} \text{sign}(e_i) - \int_0^t K_2 \text{sign}(S) \quad (2.28)$$

where $K_1 = k_1 \lambda_1 = \text{diag}(K_{1ii}) > 0$ and $K_2 = k_2 \lambda_1 = \text{diag}(K_{2ii}) > 0$ with $k_1 > 0$, $k_2 > 0$ are constants positive definite and $i = 1, \dots, 7$, whenever the following conditions are verified:

$$K_{1i} > 2\varrho t_d, K_{2i} > \frac{\varrho t_d(K_{1i})^2 - (K_{1i})^3}{2(3K_{1i} - 2\varrho t_d K_{1i})} \quad (2.29)$$

Proof 2: Before starting to proof the stability of the exoskeleton system and choosing the Lyapunov function candidate, let us substitute the control law Eq. (2.28) into Eq. (2.27). We obtain:

$$\begin{cases} \ddot{s} = -K_1 |\dot{S}|^{\frac{1}{2}} \text{sign}(S) + \lambda_1 \tilde{H}(z_1, z_2, \dot{z}_2) + w \\ \dot{w} = -K_2 \text{sign}(S) \end{cases} \quad (2.30)$$

It can be seen that Eq. (2.30) has the same structure as the supertwisting control [22,23]. Let us now introduce new variables such that: $\eta_1 = S$ and $\eta_2 = \dot{S}$. The system (Eq. 2.30) becomes as follows:

$$\begin{cases} \dot{\eta}_1 = \eta_2 \\ \eta_2 = -K_1 |\eta_2|^{\frac{1}{2}} \text{sign}(\eta_1) + \lambda_1 \tilde{H}(z_1, z_2, \dot{z}_2) + w \\ \dot{w} = -K_2 \text{sign}(\eta_1) \end{cases} \quad (2.31)$$

To ensure the convergence of the robot system (Eq. 2.3), we will assume the following quadratic Lyapunov function candidate:

$$V = \gamma^T R_\gamma \quad (2.32)$$

where $\gamma = [\gamma_{1i}, \gamma_{2i}]$, $\gamma_{1i} = |\eta_{2i}|^{\frac{1}{2}} \text{sign}(\eta_{1i})$,

$\gamma_{2i} = w_i$. The Lyapunov function (Eq. 2.32) is chosen to be continuous and nondifferentiable at $S_i = 0$ [36]. It is positive definite and radially bounded by choosing an appropriate matrix $R \in \mathbb{R}^{2 \times 2}$ such that:

$$R = \frac{1}{2} \begin{bmatrix} K_{1i}^2 + 4K_{2i} & -K_{1i} \\ -K_{1i} & 2 \end{bmatrix}$$

with

$$\alpha_{\min}\{R\} \|\gamma\|^2 \leq V \leq \alpha_{\max}\{R\} \|\gamma\|^2 \quad (2.33)$$

where $\alpha_{\min}\{R\}$ and $\alpha_{\max}\{R\}$ are the minimum and maximum eigenvalues of $\{R\}$, respectively, and $\|\gamma\|$ is s the Euclidean norm of γ . Taking the derivative of the Lyapunov function Eq. (2.32):

$$\dot{V} = \dot{\gamma}^T R_\gamma + \gamma^T R_{\dot{\gamma}} \quad (2.34)$$

The time derivative of γ can be defined as follows:

$$\begin{cases} \dot{\gamma}_{1i} = \frac{1}{2|\eta_{2i}|^{\frac{1}{2}}} \dot{\eta}_{2i} \\ \dot{\gamma}_{1i} = \dot{w}_i; i = 1, \dots, 7 \end{cases} \quad (2.35)$$

Using Eqs. (2.31) and (2.35), we can rewrite $\dot{\gamma}$ in matrix form, where $|\eta_{1i}| \leq |\eta_{2i}|^{1/2}$:

$$\dot{\gamma} = \frac{1}{|\gamma_{1i}|} \begin{bmatrix} K_{1i} & 1 \\ \frac{1}{2} & \frac{1}{2} \\ -K_{2i} & 0 \end{bmatrix} \begin{bmatrix} \gamma_{1i} \\ \gamma_{2i} \end{bmatrix} + \frac{1}{|\gamma_{1i}|} \begin{bmatrix} \lambda_1 \\ \frac{1}{2} \\ 0 \end{bmatrix} \tilde{H}(z_1, z_2, \dot{z}_2) \quad (2.36)$$

The above equation can be written in the form:

$$\dot{\gamma} = \frac{1}{|\gamma_{1i}|} [A_s \gamma + B_s \tilde{H}(z_1, z_2, \dot{z}_2)] \quad (2.37)$$

where $A_s = \begin{bmatrix} K_{1i} & 1 \\ \frac{1}{2} & \frac{1}{2} \\ -K_{2i} & 0 \end{bmatrix}$; $B_s = \begin{bmatrix} \lambda_1 \\ \frac{1}{2} \\ 0 \end{bmatrix}$. Substituting Eq. (2.37) into Eq. (2.34), we obtain:

$$\dot{V} = \frac{1}{|\gamma_{1i}|} \gamma^T [A_s^T R + R A_s] \gamma + \frac{2}{|\gamma_{1i}|} \tilde{H}(z_1, z_2, \dot{z}_2) B_s^T R \gamma \quad (2.38)$$

From Remark 1, we have $\tilde{H}(z_1, z_2, \dot{z}_2) \leq \varrho t_d$. So the following inequality can be established: $2\tilde{H}(z_1, z_2, \dot{z}_2) B_s^T R \gamma \leq \varrho t_d \gamma^T M \gamma$, where:

$$M = \frac{1}{2} \begin{bmatrix} K_{1i}^2 + 4K_{2i} & -\frac{1}{2} K_{1i} \\ -\frac{1}{2} K_{1i} & 0 \end{bmatrix}$$

Therefore Eq. (2.38) becomes:

$$\dot{V} \leq \frac{1}{|\gamma_{1i}|} \gamma^T [A_s^T R + R A_s + \varrho t_d M] \gamma \quad (2.39)$$

Eq. (2.39) can be rewritten as follows:

$$\dot{V} \leq \frac{1}{|\gamma_{1i}|} \gamma^T \Omega \gamma \quad (2.40)$$

where Ω is expressed such that: $\Omega = -[A_s^T R + R A_s + \varrho t_d M]$ and Ω is computed as follows:

$$\Omega = \frac{-K_{1i}}{2} \begin{bmatrix} K_{1i}^2 + 6K_{2i} - \varrho t_d \left(K_{1i} + 4 \frac{K_{2i}}{K_{1i}} \right) & -\frac{\varrho t_d}{2} - K_{1i} \\ -\frac{\varrho t_d}{2} - K_{1i} & 1 \end{bmatrix}$$

The derivative of the Lyapunov function \dot{V} is negative definite if the conditions given in the Eq. (2.29) function are verified. This selection will ensure that the $\det(\Omega) > 0$, while Ω is positive and symmetric. In such cases, we can rewrite Eq. (2.40) as:

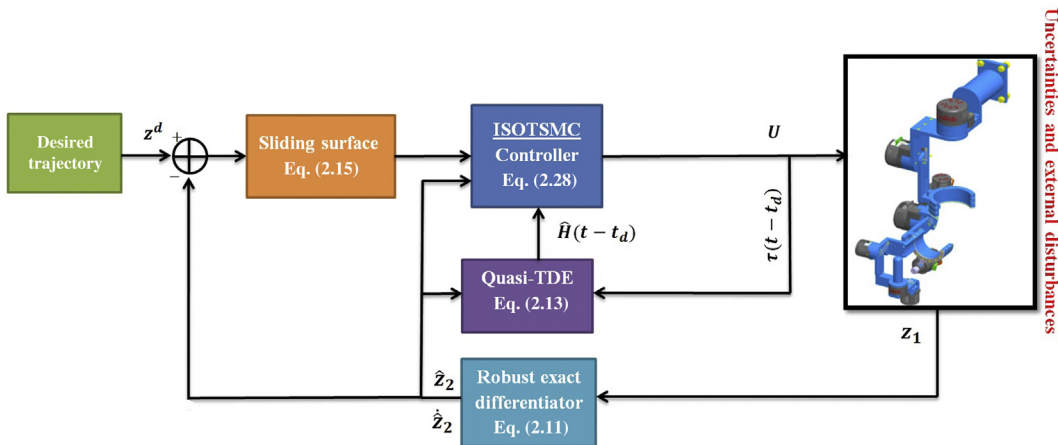
$$\dot{V} \leq \frac{-1}{|\gamma_{1i}|} \alpha_{\min}\{\Omega\} \|\gamma\|^2 \quad (2.41)$$

where $\alpha_{\min}\{\Omega\}$ is the minimum eigenvalue of Ω . Eq. (2.41) proves that the Lyapunov function is seminegative definite. Now let us prove the finite-time convergence of the system. From Eq. (2.33), we have:

$$\frac{V^{1/2}}{\alpha_{\max}^{1/2}\{R\}} \leq \|\gamma\|^2 \leq \frac{V^{1/2}}{\alpha_{\min}^{1/2}\{R\}} \quad (2.42)$$

We can easily conclude that: $|\gamma_{1i}| \leq \|\gamma\|$ and from Eqs. (2.41) and (2.42), we have:

$$\begin{aligned} \dot{V} &\leq \frac{-1}{|\gamma_{1i}|} \alpha_{\min}\{\Omega\} \|\gamma\|^2 \\ &\leq \frac{\alpha_{\min}\{\Omega\}}{\alpha_{\max}^{1/2}\{R\}} V^{1/2} \end{aligned} \quad (2.43)$$

**FIGURE 2.2**

General schematic of the proposed control.

According to this equation, the finite-time convergence of the sliding surface can be obtained such that:

$$T_s = \frac{2\alpha_{\max}^{1/2}\{R\}}{\alpha_{\min}^{1/2}\{\Omega\}} V^{1/2}(\gamma(0)) \quad (2.44)$$

The structure of the control scheme is shown in Fig. 2.2.

2.3.4 ACTIVE ASSISTIVE MOTION

In this section let us define the desired trajectory in the active rehabilitation mode. In this protocol the desired trajectory will be defined by the exoskeleton's wearer. With the help of the sensor force which is mounted on the tip of the exoskeleton robot, we can transform the exercising force by the user to their DMI. In this case, the desired trajectory is updated as follows [37]:

$$z^d = z_1 + \Delta z^d \quad (2.45)$$

where $\Delta z^d \in \Re^7$ is the DMI of the subject. If $\Delta z^d \rightarrow 0$, this means that the exoskeleton's wearer stops exercising forces on the force sensor, making the exoskeleton decrease its motion, and whenever $z^d = z_1$ the exoskeleton rests in its most recent position. To estimate the DMI from the user's force, we can use the following equation [38]:

$$F_m = J(z_1) \Delta z^d \quad (2.46)$$

where $F_m \in \Re^7$ is the measured user's force, $J(z_1) \in \Re^{6 \times 7}$ is the Jacobian matrix of the exoskeleton robot. To solve Eq. (2.46) we used damped least squares (DLS) or Levenberg–Marquardt stabilization [39]. This approach was employed firstly to avoid the singularity of the inverse kinematics

solution [40]. Rather than merely obtaining the minimum vector Δz^d that provides a best solution to Eq. (2.46), we determine the value of Δz^d that minimizes the quantity:

$$\min_{\Delta z^d} \|J(z_1) - F_m\|^2 + \gamma \|\Delta z^d\|^2 \quad (2.47)$$

where $0 < \gamma < 1$ is the damping factor and can be determined to be positive depending upon the accurate estimation specifications. The sum of Eq. (2.47) can be written as:

$$\left\| \begin{bmatrix} J(z_1) \\ \gamma I_{6 \times 6} \end{bmatrix} \Delta z^d - \begin{bmatrix} F_m \\ 0 \end{bmatrix} \right\|^2 \quad (2.48)$$

Consequently, the DLS solution is:

$$\Delta z^d = J^T (JJ^T + \gamma^2 I_{6 \times 6})^{-1} F_m \quad (2.49)$$

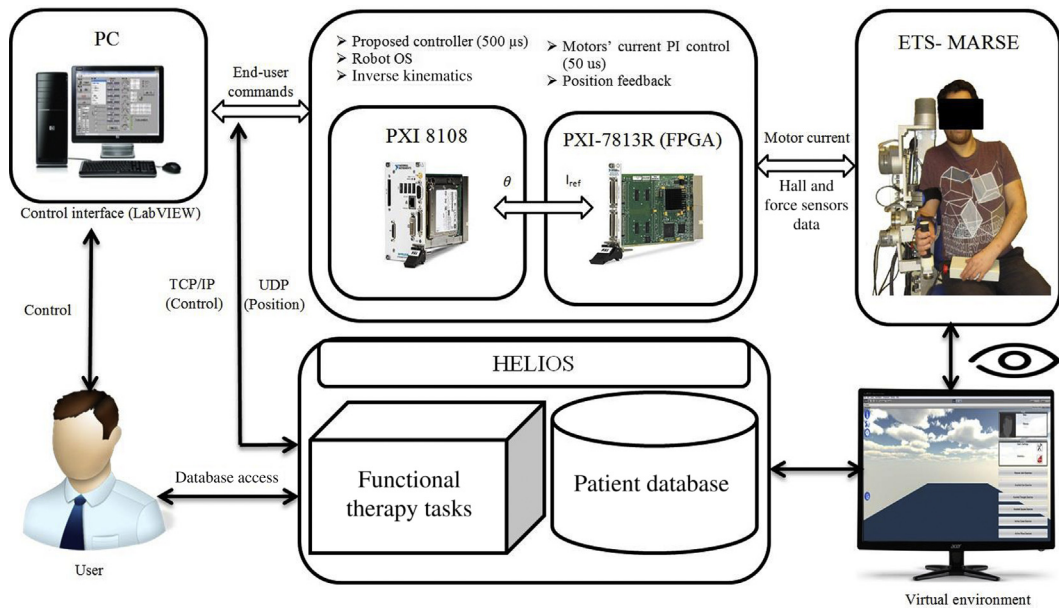
Remark 5: By helping the DLS algorithm, the exoskeleton robot is able to catch the user's DMI which permits the achievement of the active rehabilitation treatment.

Remark 6: The reference trajectories that are used in this chapter are planned on Cartesian space by using the pseudoinverse of the Jacobian matrix since the exoskeleton robot is redundant ($J(z_1) \in \Re^{6 \times 7}$), where all singularity states are avoided [40].

2.4 EXPERIMENT AND COMPARATIVE STUDY

2.4.1 EXPERIMENT SETUP

Implementation was carried out on the ETS-MARSE system described below. The system consists of three processing units; the first is a PC where the top-level commands are sent to the robot using the *LabVIEW* interface, that is, the control scheme selection, joint or Cartesian space trajectory, gain adjustments, etc. This PC also receives the data after the robot task is executed to analyze its performance. The other two processing units are part of a National Instruments PXI platform. Firstly, a NI-PXI 8081 controller card with an Intel Core Duo processor; in this card the main operating system of the robot and the top-level control scheme are executed; in our case the ISOTSMC as well as the estimation based on quasi-TDE approach, at a sampling time of 500 μ s. Finally, at input–output level a NI-PXI-7813R remote input–output card with an FPGA (field programmable gate array) executes the low-level control, that is, a PI current control loop (sampling time of 50 μ s) to maintain the current of the motors required by the main controller. Also in this FPGA the position feedback via Hall sensors (joint position), and basic input–output tasks are executed. Force sensor feedback is important to accurately control the movement of the exoskeleton. A high linearity six-axis force sensor (NANO17-R-1.8-M2-M1PCI, ATI Industrial Automation) is so chosen to obtain accurate real-time force measurements. This sensor is mounted on the tip of the exoskeleton robot. The joint of the ETS-MARSE is powered by brushless DC motors (Maxon EC-45, EC-90) combined with harmonic drives (gear ratio 120:1 for motor-1, motor-2, and motor-4 and

**FIGURE 2.3**

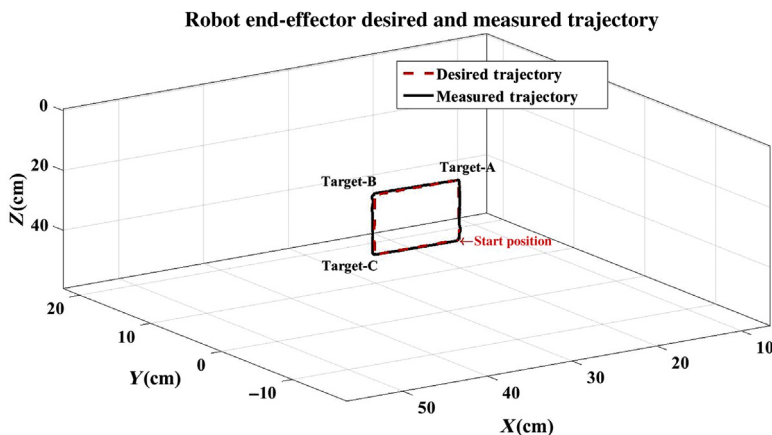
General schematic of the experimental architecture with humans.

gear ratio 100:1 for motor-3 and motors-5–7 [30,31]. The virtual environment (HELIOS) software is created in the open source Unity platform. This interface consists of a collection of functional movement tasks defined by a therapist [29]. The diagram of the architecture and the overview of the ETS-MARSE system with a human subject is shown in Fig. 2.3.

An experimental session was created to show the effectiveness of the designed control system. The physical therapy tasks were performed by two different healthy subjects (average age: 27 ± 4.6 years; average height: 170 ± 8.75 cm; average weight: 75 ± 18 kg). Every subject engaged in a full session under the supervision of a therapist and a control engineer. The role of the therapist was the description of the range of motion of each subject and the attribution of the proper tasks. In the session, the subject was comfortably seated in a chair in front of the virtual interface, as shown in Fig. 2.3. The experimental session was separated into two scenarios. In the first scenario, each subject performed the designed task with a rectangular form as shown in Fig. 2.4. This task (Initial position–Target-A–Target-B–Target-C–Initial position) is expressed in Cartesian space to evaluate the proposed control. The initial position of the exoskeleton robot is given where the elbow joint position is at 90 degrees. This part is followed directly by a comparison study with a conventional approach [22] to show the benefits of the proposed control algorithm. In the second scenario, each subject has interacted with the VE and tried to follow the reference trajectory. It is important to notice that the external disturbances here are represented by different physiological conditions of the subjects, such as nonlinear biomechanical characteristics of the musculoskeletal system and the different payload of the upper limb for each subject. The control gains were chosen manually, as shown in Table 2.3.

Table 2.3 Controller Parameters

Gains	Value $i = 7$
λ_{1i}	2.5
λ_{1i}	1.8
k_1	18
k_2	10
β	0.6
Υ	0.86; $i = 1$
Σ	42; $i = 1$

**FIGURE 2.4**

Workspace trajectories of the robot in Cartesian space using the proposed controller, performed by Subject-1 (age: 28 years; height: 177 cm; weight: 83 kg).

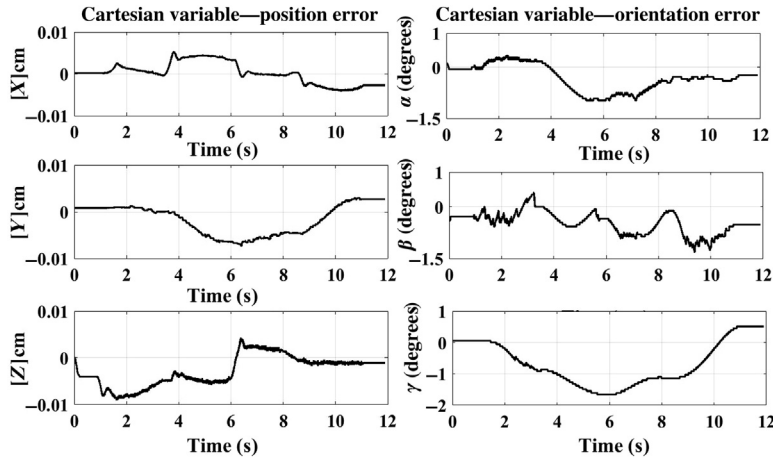
2.4.2 RESULTS OF PASSIVE ASSISTIVE MOTION

The experimental results with the ETS-MARSE robot in Cartesian space conducted by Subject-1 (age: 28 years; height: 177 cm; weight: 83 kg) using the proposed control strategy are shown in Figs. 2.4–2.6. From Fig. 2.4, we notice that the reference trajectory (red line) nearly interlocked with the measured trajectory (black line). In this case, we can say that these results are reasonably good.

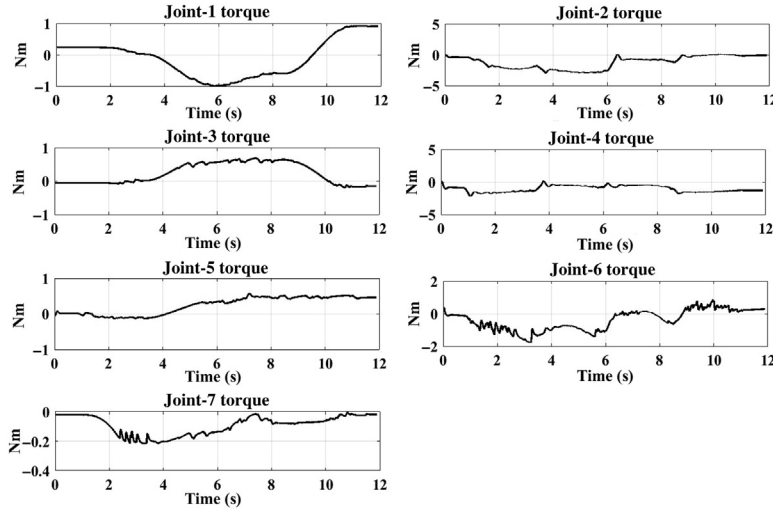
Fig. 2.5 exhibits the Cartesian tracking errors as functions of time, where they are clearly converging and smaller along the reference trajectory. Fig. 2.6 shows that the control input is bounded without any remarkable chattering. So these results confirm that the proposed control algorithm is proper to accomplish the desired rehabilitation performance even when the nonlinear dynamics of the exoskeleton robot are uncertain and without velocity measurement.

2.4.3 COMPARATIVE STUDY

In order to prove the feasibility and efficiency of the proposed control algorithm, we compared it experimentally with the conventional approach [22]. In the latter the authors proposed a

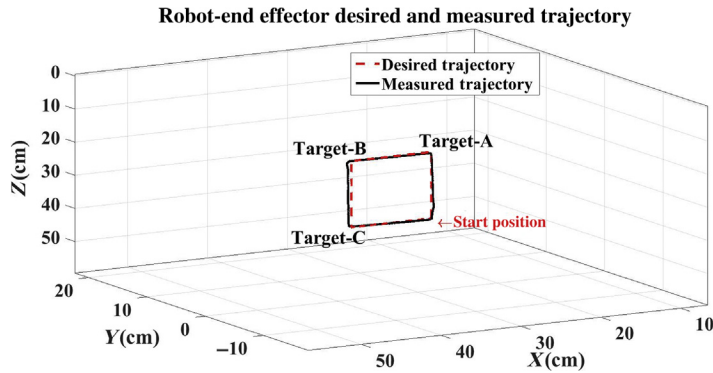
**FIGURE 2.5**

Cartesian errors.

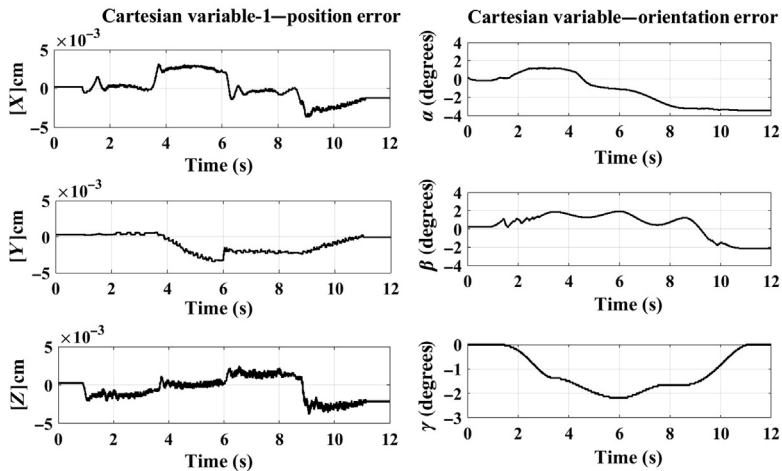
**FIGURE 2.6**

Control inputs of the proposed controller.

supertwisting controller with a known dynamics model of the system. Fig. 2.7 presents the Cartesian tracking (red is the reference trajectory, black is real trajectory) performed by Subject-1 (age: 28 years; height: 177 cm; weight: 83 kg) using the conventional control algorithm. In fact, as seen from Figs. 2.7–2.9, the conventional control shows a good performance. It ensures that the Cartesian error is getting smaller with time. However, the control inputs of the conventional control presented in Fig. 2.9 illustrate a noisy signal with a chattering phenomenon, while the proposed

**FIGURE 2.7**

Workspace trajectories of the robot in Cartesian space using conventional controller, performed by Subject-1 (age: 28 years; height: 177 cm; weight: 83 kg).

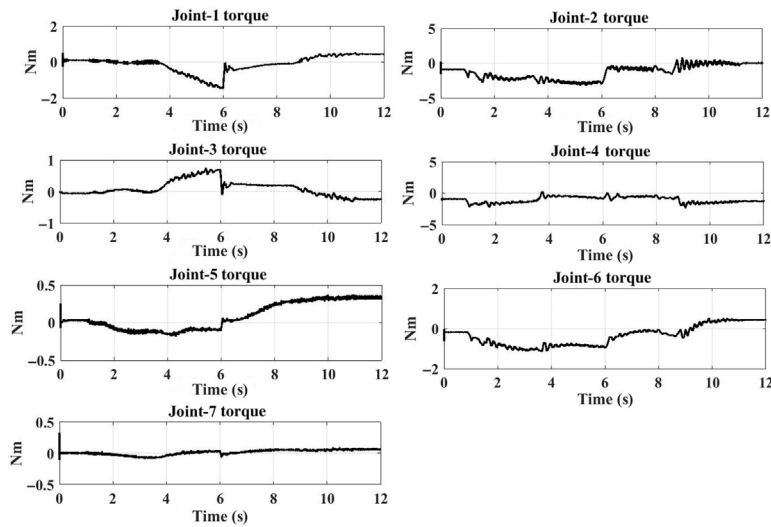
**FIGURE 2.8**

Cartesian error of performance's conventional control.

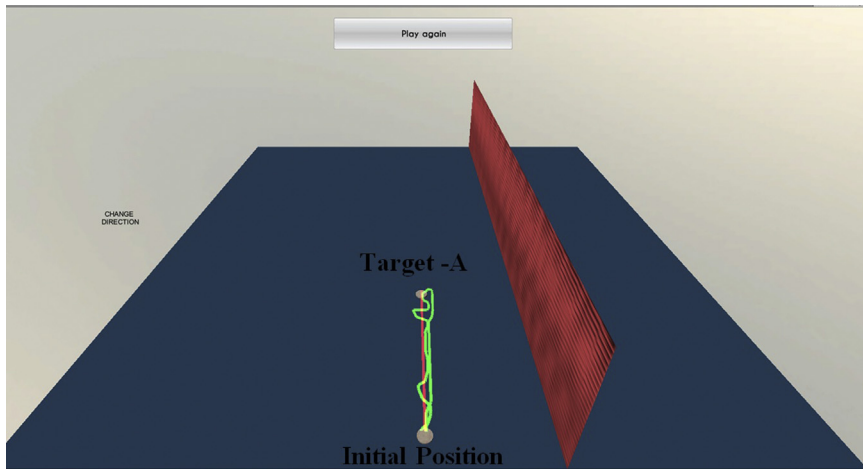
controller provides a smooth control input (Fig. 2.6). It is important to mention that we employed the same gains values that we employed in the proposed approach. From the comparison of the two experimental results, we can conclude that the proposed control algorithm strategy without velocity measurement provides a high level of precision and robustness to the nonlinear uncertain dynamics and unknown disturbances without remarkable chattering, compared with the conventional control.

2.4.4 RESULTS OF ACTIVE ASSISTIVE MOTION

Fig. 2.10 presents the performance of the Subject-2 (age: 31 years; height: 183 cm; weight: 83.5 kg) in the virtual interface with the help of the ETS-MARSE exoskeleton robot (red line is the

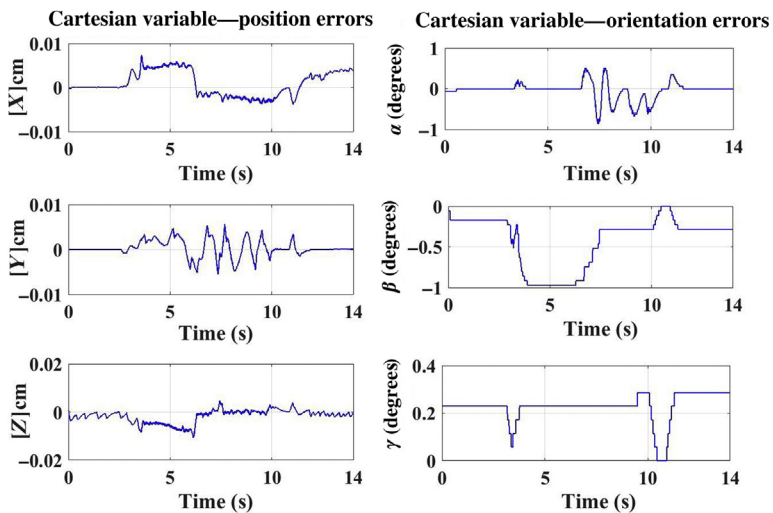
**FIGURE 2.9**

Control inputs of the conventional controller.

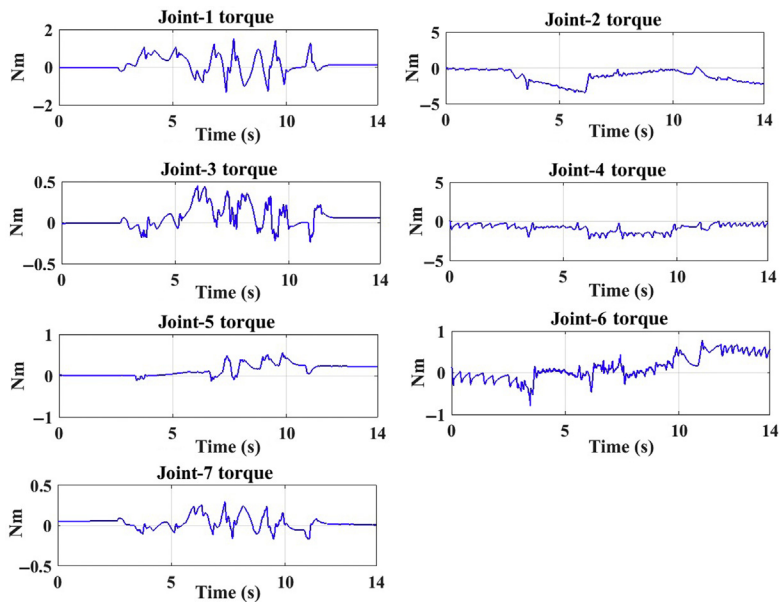
**FIGURE 2.10**

Workspace tracking of the robot using the proposed controller performed by Subject-2 (age: 31 years; height: 183 cm; weight: 83.5 kg).

desired and the green line is the real trajectory). Fig. 2.11 shows the workspace of error tracking of the exoskeleton robot in Cartesian space. It is clear from these plots (Figs. 2.10–2.12) that the designed control algorithm achieved the desired rehabilitation performance with small tracking errors and acceptable control input.

**FIGURE 2.11**

Cartesian errors.

**FIGURE 2.12**

Torque input of active rehabilitation task.

2.5 CONCLUSION

In this chapter we investigated the control applied to passive and active rehabilitation protocols of an exoskeleton robot without velocity measurement by presenting a new integral second-order terminal sliding mode incorporating TDE. We used second-order sliding mode due to its attractive characteristics of fast convergence, accuracy, and attenuation of chattering. However, its problem is that the unknown dynamics of the exoskeleton robot and external disturbances can be amplified by the second derivative of the sliding surface, which leads to the instability of the robot system. Applying quasi-TDE to estimate the unknown dynamics and external disturbances permits a reduction of chattering. The controller is dedicated to improving the robustness of the SOSMC while overcoming its main limitation. The stability analysis is formulated and demonstrated based on the Lyapunov function. An experimental physiotherapy session with healthy subjects was created to examine the utility and feasibility of the proposed control algorithm, which was proved experimentally. In future work, we aim to develop sophisticated force control able to achieve a collaborative human–exoskeleton robot.

2.6 ETHICS STATEMENT

In this research ethics approval was not required as per Ecole de Technologie Supérieure, Montreal, Canada and national regulations since the subjects were healthy (not real neurological patients) and no subjects were recruited other than the researchers working in this project. Also written and informed consent was obtained from the research participants.

ACKNOWLEDGMENTS

This research was supported by The Power Electrics and Industrial Control Research Group (GREPCI), Ecole de Technologie Supérieure, Montreal, Canada.

REFERENCES

- [1] E. Lundström, A. Terént, J. Borg, Prevalence of disabling spasticity 1 year after first-ever stroke, *Europ. J. Neurol.* 15 (6) (2008) 533–539.
- [2] D.S. Nichols-Larsen, P. Clark, A. Zeringue, A. Greenspan, S. Blanton, Factors influencing stroke survivors quality of life during subacute recovery, *Stroke* 36 (7) (2005) 1480–1484.
- [3] U. Keller, S. Schölich, U. Albisser, C. Rudhe, A. Curt, R. Riener, et al., Robot-assisted arm assessments in spinal cord injured patients: A consideration of concept study, *PLoS One* 10 (5) (2015) e0126948.
- [4] A.-M. Hughes, S.B. Bouças, J.H. Burridge, M.A. Murphy, J. Buurke, P. Feys, et al., Evaluation of upper extremity neurorehabilitation using technology: a European Delphi consensus study within the EU cost action network on robotics for neurorehabilitation, *J. Neuroeng. Rehabil.* 13 (1) (2016) 86.
- [5] U. Keller, H.J. van Hedel, V. Klamroth-Marganska, R. Riener, Charmin: the first actuated exoskeleton robot for pediatric arm rehabilitation, *IEEE/ASME Trans. Mech.* 21 (5) (2016) 2201–2213.

- [6] A. De Morand, *Pratique de la rééducation neurologique*, Elsevier Masson, 2014.
- [7] B. Brahim, S. Maarouf, C.O. Luna, B. Abdelkrim, M. Rahman, Adaptive iterative observer based on integral backstepping control for upper extremity exoskeleton robot, in: Modelling, Identification and Control (ICMIC), 2016 8th International Conference on, IEEE, 2016, pp. 886–891.
- [8] B. Brahim, M.H. Rahman, M. Saad, C.O. Luna, Iterative estimator-based nonlinear backstepping control of a robotic exoskeleton, *World Acad. Sci. Eng. Technol. Int. J. Mech. Aerospace Ind. Mech. Manuf. Eng.* 10 (8) (2016) 1361–1367.
- [9] Z. Li, Z. Huang, W. He, C.-Y. Su, Adaptive impedance control for an upper limb robotic exoskeleton using biological signals, *IEEE Trans. Ind. Electr.* 64 (2) (2017) 1664–1674.
- [10] S. Xie, et al., Advanced robotics for medical rehabilitation, *Springer Tracts Adv. Robot.* 108 (2016) 1–357.
- [11] J.-J.E. Slotine, W. Li, et al., *Applied Nonlinear Control*, vol. 199, Prentice hall, Englewood Cliffs, NJ, 1991.
- [12] G. Rigatos, P. Siano, M. Abbaszadeh, Nonlinear h-infinity control for 4-dof underactuated overhead cranes, *Trans. Inst. Meas. Control* (2017).
- [13] B. Brahma, M. Saad, M.H. Rahman, C. Ochoa-Luna, Cartesian trajectory tracking of a 7-dof exoskeleton robot based on human inverse kinematics, *IEEE Trans. Syst. Man Cybern. Syst.* 99 (2017) 1–12.
- [14] J. Zhou, C. Wen, *Adaptive Backstepping Control of Uncertain Systems: Non-Smooth Nonlinearities, Interactions or Time-Variations*, Springer, Berlin, 2008.
- [15] K.D. Young, V.I. Utkin, U. Ozguner, A control engineer’s guide to sliding mode control, in: Variable Structure Systems, 1996. VSS’96. Proceedings, 1996 IEEE International Workshop on, IEEE, 1996, pp. 1–14.
- [16] Y. Wu, X. Yu, Z. Man, Terminal sliding mode control design for uncertain dynamic systems, *Syst. Control Lett.* 34 (5) (1998) 281–287.
- [17] X. Yu, M. Zhihong, Fast terminal sliding-mode control design for nonlinear dynamical systems, *IEEE Trans. Circuits Syst. I: Fund. Theory Applicat.* 49 (2) (2002) 261–264.
- [18] Y. Feng, X. Yu, Z. Man, Non-singular terminal sliding mode control of rigid manipulators, *Automatica* 38 (12) (2002) 2159–2167.
- [19] L.M. Fridman, An averaging approach to chattering, *IEEE Trans. Auto. Control* 46 (8) (2001) 1260–1265.
- [20] C.J. Fallaha, M. Saad, H.Y. Kanaan, K. Al-Haddad, Sliding-mode robot control with exponential reaching law, *IEEE Trans. Ind. Electr.* 58 (2) (2011) 600–610.
- [21] A. Levant, Principles of 2-sliding mode design, *Automatica* 43 (4) (2007).
- [22] T. Gonzalez, J.A. Moreno, L. Fridman, Variable gain super-twisting sliding mode control, *IEEE Trans. Auto. Control* 57 (8) (2012) 2100–2105.
- [23] G. Tenoch, J. A. Moreno, L. Fridman, Variable gain super-twisting sliding mode control. *IEEE Trans. Auto. Control* 57 (8) (2011) 2100–2105.
- [24] S. Ding, J. Wang, W.X. Zheng, Second-order sliding mode control for non-linear uncertain systems bounded by positive functions, *IEEE Trans. Ind. Electr.* 62 (9) (2015) 5899–5909.
- [25] L. Zhao, J. Huang, H. Liu, B. Li, W. Kong, Second-order sliding-mode observer with online parameter identification for sensorless induction motor drives, *IEEE Trans. Ind. Electr.* 61 (10) (2014) 5280–5289.
- [26] B. Brahma, M. Saad, C. Ochoa-Luna, M.H. Rahman, Adaptive control of an exoskeleton robot with uncertainties on kinematics and dynamics, in: Rehabilitation Robotics (ICORR), 2017 International Conference on, IEEE, 2017, pp. 1369–1374.
- [27] B. Brahma, M. Saad, C.O. Luna, P. Archambault, M. Rahman, Sliding mode control of an exoskeleton robot based on time delay estimation, in: Virtual Rehabilitation (ICVR), 2017 International Conference on, IEEE, 2017, pp. 1–2.

- [28] A.M. Shotorbani, A. Ajami, S.G. Zadeh, M.P. Aghababa, B. Mahboubi, Robust terminal sliding mode power flow controller using unified power flow controller with adaptive observer and local measurement, *IET Gen. Trans. Distrib.* 8 (10) (2014) 1712–1723.
- [29] S. Ferrer, C. Ochoa-Luna, M. Rahman, M. Saad, P. Archambault, Helios: the human machine interface for MARSE robot, in: *Human System Interaction (HSI), 2013 The 6th International Conference on*, IEEE, 2013, pp. 177–122.
- [30] M.H. Rahman, M.J. Rahman, O. Cristobal, M. Saad, J.-P. Kenné, P.S. Archambault, Development of a whole arm wearable robotic exoskeleton for rehabilitation and to assist upper limb movements, *Robotica* 33 (1) (2015) 19–39.
- [31] M.H. Rahman, M. Saad, J.-P. Kenné, P.S. Archambault, Control of an exoskeleton robot arm with sliding mode exponential reaching law, *Int. J. Control Auto. Syst.* 11 (1) (2013) 92–104.
- [32] C.O. Luna, M.H. Rahman, M. Saad, P. Archambault, W.-H. Zhu, Virtual decomposition control of an exoskeleton robot arm, *Robotica* 34 (7) (2016) 1587–1609.
- [33] J.M. Ali, N.H. Hoang, M.A. Hussain, D. Dochain, Review and classification of recent observers applied in chemical process systems, *Comput. Chem. Eng.* 76 (2015) 27–41.
- [34] A. Levant, Higher-order sliding modes, differentiation and output-feedback control, *Int. J. Control* 76 (9–10) (2003) 924–941.
- [35] H. Wang, Z.-Z. Han, Q.-Y. Xie, W. Zhang, Finite-time chaos synchronization of unified chaotic system with uncertain parameters, *Commun. Nonlinear Sci. Num. Simulat.* 14 (5) (2009) 2239–2247.
- [36] J.A. Moreno, M. Osorio, A Lyapunov approach to second-order sliding mode controllers and observers, in: *Decision and Control, 2008. CDC 2008. 47th IEEE Conference on*, IEEE, 2008, pp. 2856–2861.
- [37] C. Ochoa Luna, M. Habibur Rahman, M. Saad, P.S. Archambault, S. Bruce Ferrer, Admittance-based upper limb robotic active and active-assistive movements, *Int. J. Adv. Robot Syst.* 12 (9) (2015) 117.
- [38] A.M. Khan, D.-W. Yun, M.A. Ali, K.M. Zuhair, C. Yuan, J. Iqbal, et al., Passivity based adaptive control for upper extremity assist exoskeleton, *Int. J. Control Auto. Syst.* 14 (1) (2016) 291–300.
- [39] C.L. Lawson, R.J. Hanson, *Solving Least Squares Problems*, SIAM, 1995.
- [40] C.W. Wampler, Manipulator inverse kinematic solutions based on vector formulations and damped least-squares methods, *IEEE Trans. Syst. Man Cybern.* 16 (1) (1986) 93–101.

3

DESIGN OF THE ARM EXOSKELETON ABLE ACHIEVING TORQUE CONTROL USING BALL SCREW AND CABLE MECHANISM

Philippe Garrec

CEA-DRT-LIST-DIASI, Interactive Robotics Service, Saclay, France

3.1 INTRODUCTION

By the end of the 1990s, our laboratory initiated the development of the master arm Virtuose 6D intended to succeed the MA23 for the needs of force feedback teleoperation. The MA23 is a well-known electric servomanipulator designed in 1974 by a team led by Jean Vertut which had been the first in the world where motor torque amplification (speed reduction) was achieved without gears [1,2]. Later, this innovation was acknowledged by J.K. Salisbury at MIT, who proposed a new solution—the capstan drive—an equivalent of a gear without teeth to drive the Force Reflecting Hand Controller, a 6-DOF desktop master arm implemented at the JPL [3]. This principle was proved successful especially in sensitive torque-controlled haptic devices such as the 3-DOF Phantom from Sensable [4] and on the first four joints of the 7-DOF WAM manipulator from Barrett Inc. [5]. The design of the 6-DOF Virtuose 6D master arm (Fig. 3.1), (today marketed by Haption under the name MAT6D) led to the invention of the Screw-and-Cable-System (SCS) [6–8] in combining the advantages of a high-potential industrial component (the ball screw) and the preexisting cable joint transmissions using an innovative flexible attachment.

Shortly after this first achievement, the potential of the SCS as a new actuator for torque-controlled applications and its unique ease of integration into serial articulated structures was fully realized. We then decided to leverage this capital by launching the design of an exoskeleton arm as a rehabilitation device.

3.2 THE SCS MECHANISM: A NEW ANSWER TO THE CHALLENGE OF LINEAR TORQUE AMPLIFICATION

Limiting or controlling the torque in a machine using the current seems a logical, somewhat trivial principle. It was actually used early in general industry, for example, in regulating the traction on a rolling mill sheet, on textile wire tensile, or the traction effort of an electric locomotive. It was used as early as 1954 by R. Goertz at Argonne National Laboratory laboratories to achieve the

**FIGURE 3.1**

The Virtuose 6D CEA prototype: first master arm driven by ball screw and cable system (SCS).

transmission of force between two distant manipulators allowing remote manipulation of radioactive materials. With this first electrical master slave manipulator, mechanical transmissions were emulated using an elastic coupling law involving a proportional joint control. Given the poor unit torque per mass available with an electrical motor, early designers of these manipulators were facing the necessity to amplify the torque with the least amount of perturbative forces (friction and inertia). They were using accurate reversible gears and multiple small electric motors. We will come back to this notion a little further into this chapter. Since then the concept of closed-loop joint torque using torque sensors has been continually discussed and often proposed as a best compromise between transparency and rigidity. However, today the open-loop mechanical amplification associated with current measurement is still widely used because of its simplicity, reliability, and performance, in particular for highly sensitive devices such as haptic arms or haptic teleoperators. The pioneering period, roughly spanning from 1954 to 1974 [9–13], ended with the invention, by a team led by J. Vertut at CEA, of the MA23, where for the first time, torque amplification was performed exclusively by cables using block-and-tackles. The SCS actuator came as a new response to the same challenge of the linear torque amplification [14,15]. However, it also possessed a distinctive property over its predecessors: the capacity to drive a transversal joint with a longitudinal motor, thus achieving the function of a bevel gear without its well-known inconveniences: weight, volume, torque ripple, and cost.

3.2.1 MECHANICAL REVERSIBILITY/IRREVERSIBILITY—BACKDRIVABILITY—TORQUE TRANSFER LINEARITY

For clarity, the important concept of mechanical reversibility should be explained in more detail. It is defined in the theory of mechanism as the reciprocal property of irreversibility (or self-locking). This is demonstrated using the theory of a contact point sliding on an incline in the presence of dry

friction (Coulomb). Both properties can be synthetically understood using the input–output torque transfer law of any mechanism (Fig. 3.2).

These notional diagrams represent the torque transfer law for each sense of movement (speed is the independent parameter) under the form of two bold boundaries. The light straight line corresponds to the speed reduction ratio characteristic, that is, the torque transfer in the absence of friction. Consequently the friction losses under any torque transfer conditions can be estimated as the difference between the boundaries and the speed ratio characteristics.

The left figure shows that a reversible mechanism submitted to an output torque only (vertical axis) will transmit a torque at its input as soon as its magnitude is superior to a certain threshold value. On the contrary, the right figure shows that an irreversible mechanism submitted to the same output torque only, does not transmit any torque at its input, whatever its intensity (the mechanism is self-locked).

This allows the clear expression of the desired goal as the concept of linear amplification, independently from the motion. A similar diagram could be plotted using both the speed and the acceleration as independent parameters: it would then express both the friction and the inertial forces responsible for the nonlinearity of the force transfer law. A transparent mechanism has therefore a strictly linear torque transfer characteristic, independent of the speed and acceleration.

When using a torque sensor at the output of the actuator, it is possible to close the loop on the input torque controlled by the motor. For an irreversible mechanism, this creates the possibility of virtually suppressing the nonlinearity of the torque transfer law, making the mechanism eventually backdrivable. With this terminology, we see that the terms “artificial reversibility” and “reversibilization,” which are sometimes used, are both confusing. Table 3.1 was presented in Ref. [16]

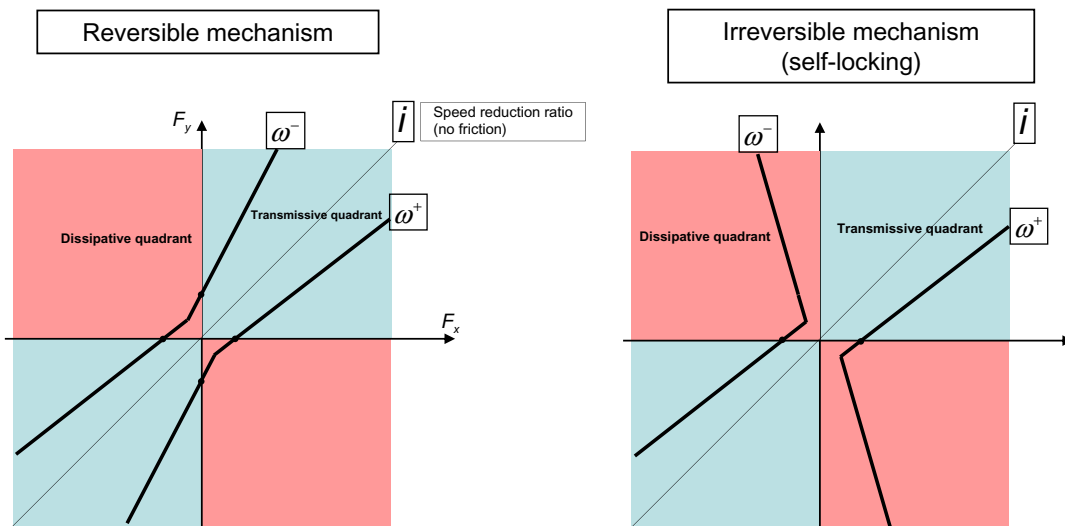


FIGURE 3.2

Comparative torque transfer diagram for a reversible and irreversible mechanism.

Table 3.1 Suggested Terminology for Reversibility Versus Backdrivability in Mechanical Transmission

Mechanical Type (Constructive Property)	Behavior	
Reversible	Backdrivable	
Irreversible	Self-locking	Backdrivable if assisted (force closed loop)

together with the proposition of a merit index for transparency. It synthesizes the various concepts and suggested terminology:

3.2.2 MECHANICAL TORQUE AMPLIFICATION ON SERVOMANIPULATORS

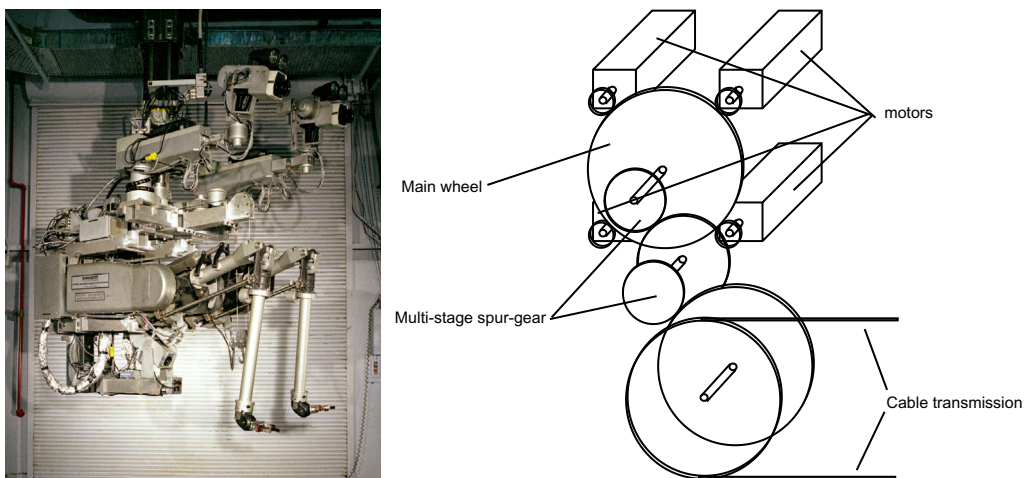
The first principle has been used by R. Goertz on all his designs from the E1 model (the first servo-manipulator) to the M2 model (Fig. 3.3). Motor torque is amplified using spur gears installed at the base of the arm and driving the joints either directly for the local first movements or, like the scheme shows, through transmission cables for remote joints (Fig. 3.3).

The second principle is due to J. Vertut and his team for the design of the MA23 electrical master slave manipulator. The motor torque is amplified using a cable that drives a transmission cable. Alternatively, a metallic tape was used instead of the cable, a choice that was also common on mechanical master slave manipulators. It was the first mechanical transmission for robotic arms where the motor torque was amplified without gears (Fig. 3.4).

The last principle introduced by J.K. Salisbury, the capstan, has been used on the Model C and on the Force Reflecting Hand Controller. A preloaded transmission cable connects to pulleys of different diameters. The cable is crossed in order to allow cables to be as short as possible and almost tangential to the pulleys. Frequently, the cable transmits its effort on the small diameter only by adherence (using the exponential adherence law like on a winch). This results in a low preload and friction created by the cable tension on the bearings is negligible. It is arguably the most linear (or transparent) principle to linearly amplify the torque of an electrical motor and it is most commonly found on haptic devices with the notable exception of the slave arm WAM Arm from Barrett Technology (Fig. 3.5).

With the SCS (Fig. 3.6), the articulated segment is driven by a preloaded cable transmission loop. The screw linearly moves one side of the loop, causing the segment to rotate. The nut rotates in a bearing and can be driven by a timing belt or by a direct-drive motor according to the needs [17]. The innovation lies in the absence of linear guidance and its replacement by a flexible antirotative locking device and a special attachment. This is typically achieved using a pair of coupled rollers attached to the screw thanks to a flexible coupling. Complementing this, the cable is attached in the middle of the screw thanks to a bore providing enough play to accept the unavoidable misalignment of the cable as well as the kinematic oscillations generated by the ball screw–nut system in the absence of a linear guide.

This solution virtually suppresses undesirable constraints and reduces the hyperstaticity of the mounting, in particular the reaction of the flexure moment applied on the nut. The friction, depending on fewer parameters, is reduced and becomes both regular and reproducible over the full stroke.

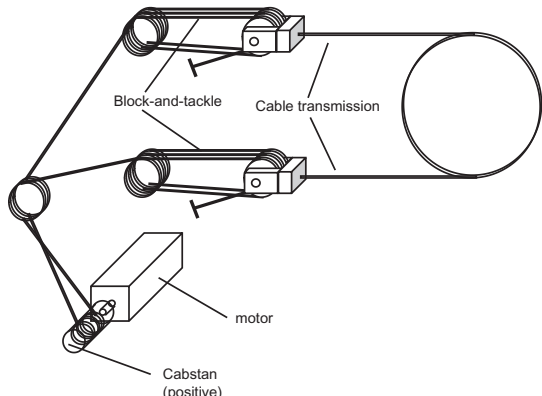
**FIGURE 3.3**

The spur gear torque amplifier originally used in the servomanipulator Model E1 (1954, ANL/CRL) and up to the M2 servomanipulator system (ORNL/CRL).

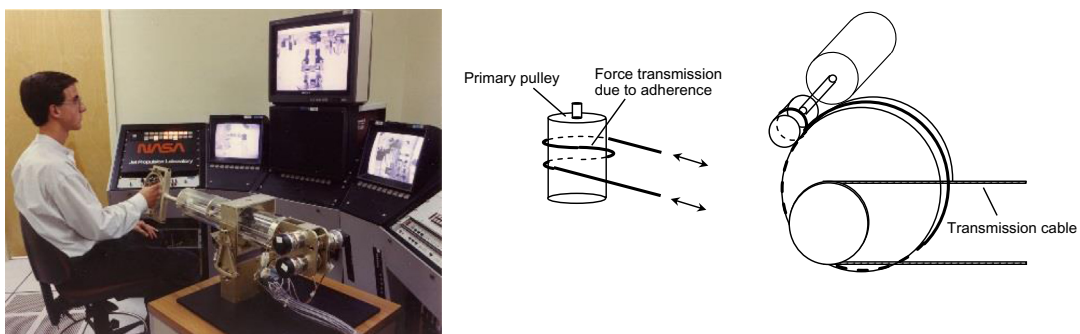
Courtesy of Oak Ridge National Laboratory, U.S. Dept. of Energy.

**FIGURE 3.4**

The block-and-tackle torque amplifier mechanism used in the servomanipulator MA23 (CEA/La Calhène).

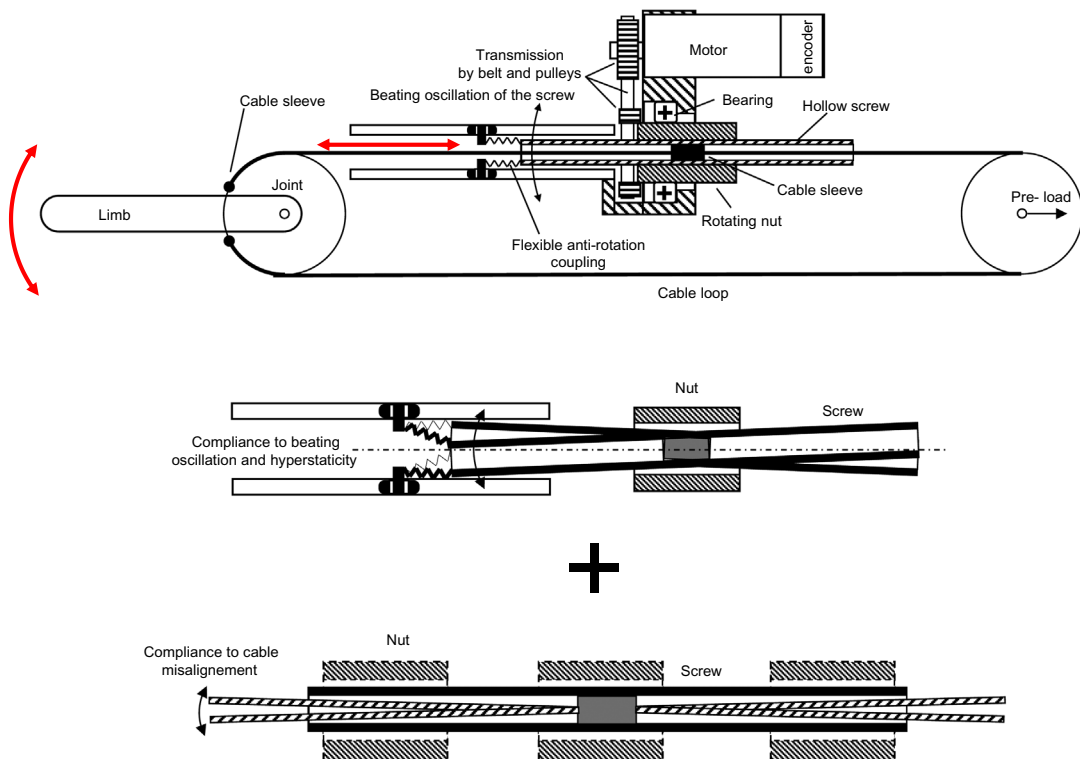


The diagram Fig. 3.7 presents an experimental torque-force transfer diagram obtained with a THK BNK 1010 ball screw (Dia: 10 mm ; Lead: 10 mm) on a test rig. The diagram below obtained with a model, expresses the theoretical filtering effect on the flexure moment and therefore on the torque ripple, obtained with the original attachment. The typical friction threshold represents

**FIGURE 3.5**

The capstan drive torque amplifier used in the model C master arm (NASA/JPL).

Courtesy of NASA/JPL.

**FIGURE 3.6**

SCS actuator basic principle.

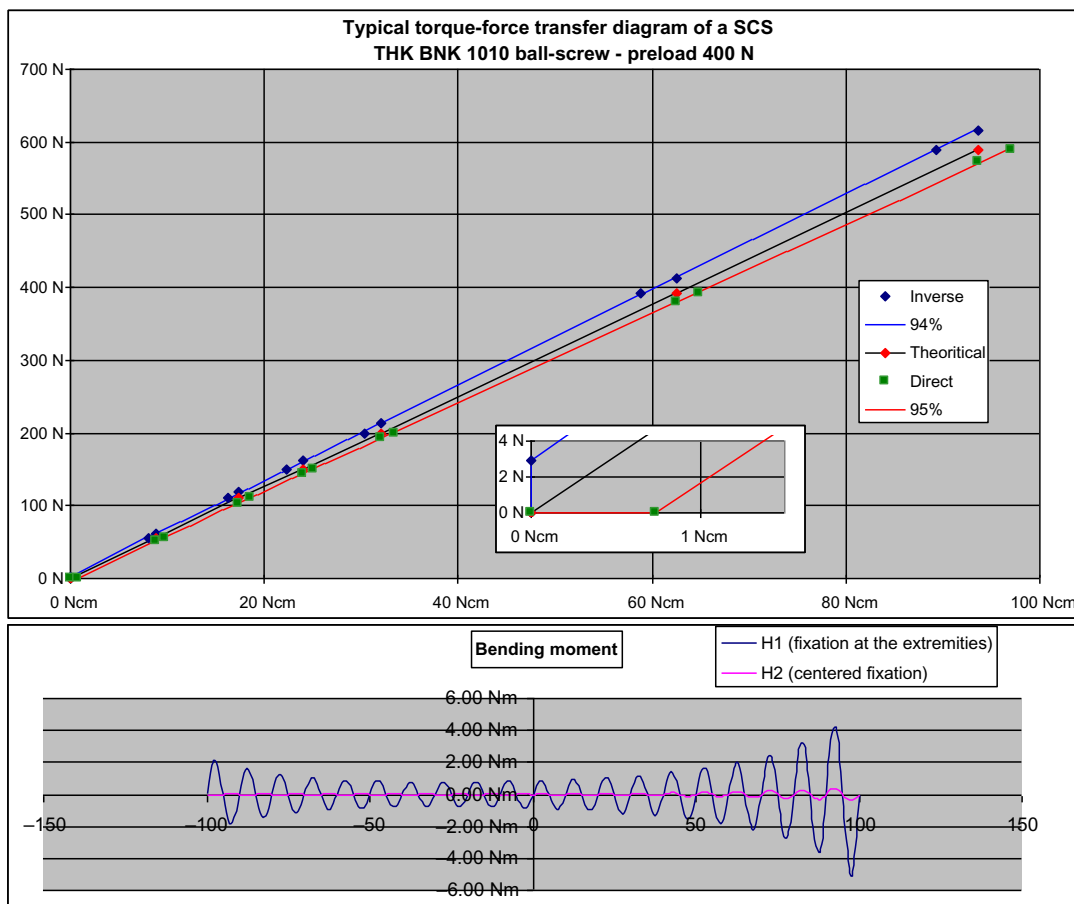
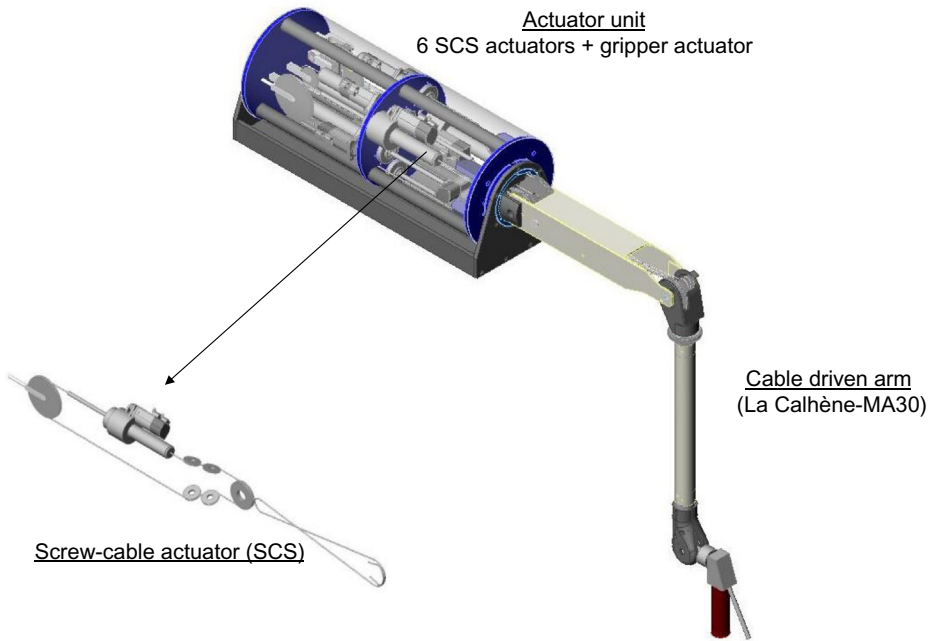


FIGURE 3.7

Torque transfer of a typical SCS and filtering effect of the flexible attachment on torque ripple.

approximately 1/1000 of the capacity of the screw which is a very high performance (according to [13], compared to a mechanical master slave rotative transmission presenting a threshold close to 2% of the torque capacity). The maximum efficiencies are close to 0.94–0.95 both for direct and indirect sense of work conversion.

Fig. 3.8 shows the Virtuose 6D prototype for which the SCS was designed. It combines a cable driven master arm, coming as a part of the mechanical master slave manipulator MA30 constructed by La Calhène, with an actuator unit comprising six SCSs located at its base. The cable actuating the handle is pulled by a seventh motor directly acting on a pulley, providing a feedback on the force exerted by the slave gripper. Virtuose 6D was completed and demonstrated in March 2001 at the exhibition of the 9th American Nuclear Society congress held in Seattle. An upgraded version was designed by CEA and industrialized by Haption under the name MAT6D. It has been mainly

**FIGURE 3.8**

CAD view of the force feedback Virtuose 6D master arm. (Left) A detailed view of its elbow actuator.

used in teleoperation systems such as the Maestro telerobot from CEA-CYBERNETIX and the prototype of the MT200TAO from CEA-AREVA.

3.3 THE FIRST ABLE 4D

At the time of the beginning of the project (end of 2002), upper limb exoskeletons—wearable or not, semi- or complete exoskeletons—had been already pioneered [12,18] and the field was pretty active during this period [19–22]. A few models were simplified enough to be wearable. Some authors were looking for haptic capabilities (i.e., an accurate joint torque control) but the proposed solutions were not well suited to provide altogether substantial and accurate torque. Also structures were generally bulky. The project of ABLE was born as a technological attempt to explore the potential of an exoskeleton arm powered by distributed SCSs rather than by SCSs grouped at its base as with Virtuose 6D. On the Virtuose 6D, the longitudinal alignment of the motors in the base housing gave it a better compactness than the transverse motors previously used in the MA23. However, we realized that it was possible to better exploit the essential advantages of the SCS by integrating it into the moving parts of the arm in order to reduce the length of common transmission cables while maintaining a streamlined shape of the arm. This would result in a reduction in

friction and flexibility of the actuators. Also, thanks to the tolerance of the SCS to misalignment and geometrical uncertainties, we could accept a more deformable structure than with gears, a factor that would allow the reduction of its mass.

To reduce the gravity torque and inertia generated by the moving masses of the motors, we have chosen to move the motor from the driven joint near the previous joint using a light shaft, separating the torque amplifier from the motor [23]. This principle has since been adopted for the design of the EMY Balance and Hercule Slim exoskeletons, using a flexible shaft rotating on ball bearings [24].

In addition, an important requirement was to design a complete exoskeleton including the shoulder joint arrangement which would allow it to be installed on the backrest of a chair and we were also looking for a fully opened mechanical architecture that would avoid the user's apprehension of being caught in a rigid mechanism. These choices resulted in the first version of ABLE 4D integrating two SCS modules in the humerus limb, each of them actuating a transverse axis. In this arrangement, the absence of a bevel gear has obvious advantages in terms of volume and mass (Fig. 3.9).

The shoulder joint takes advantage of the SCS to offer a very simple solution to a known difficulty. Its conventional kinematics is represented with three coincident orthogonal joints forming the equivalent of a rotule (Fig. 3.10).

The main difference with previous designs is that the second joint is made with a circular guide [25–28]. Such an arrangement is at the same time free of singularity and a priori not very invasive. The first two joints are driven by two SCSs attached to the rear module, while the third joint (flexion) is driven transversely by one of the arm modules (Fig. 3.11). The linear coupling between the first two joints is classically decoupled by the control program using the inverse of the transmission matrix. The fourth joint drives the elbow. The result is a simple, integrated and morphologically compatible design with a mass and volume of actuator distributed along the structure.

The SCS rear module occupies only half of the rear module, to allow the integration of a second exoskeleton in the same volume. The main specifications of ABLE 4D are presented in Table 3.2.

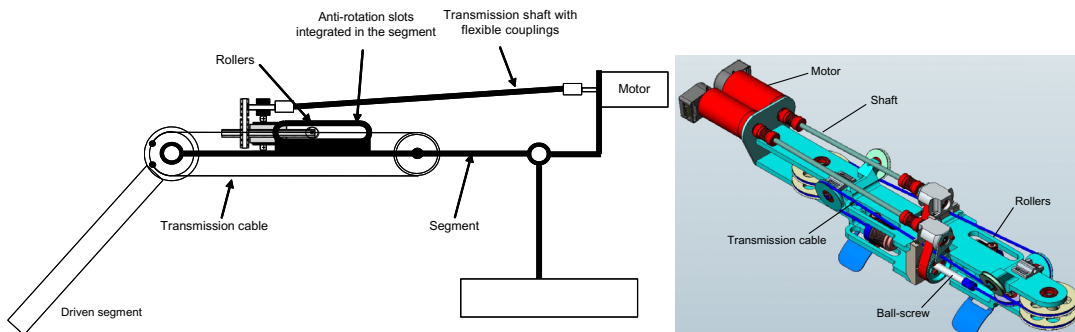


FIGURE 3.9

Shoulder and elbow flexion SCS integrated in the ABLE 4D arm segment with grouped upstream motors.

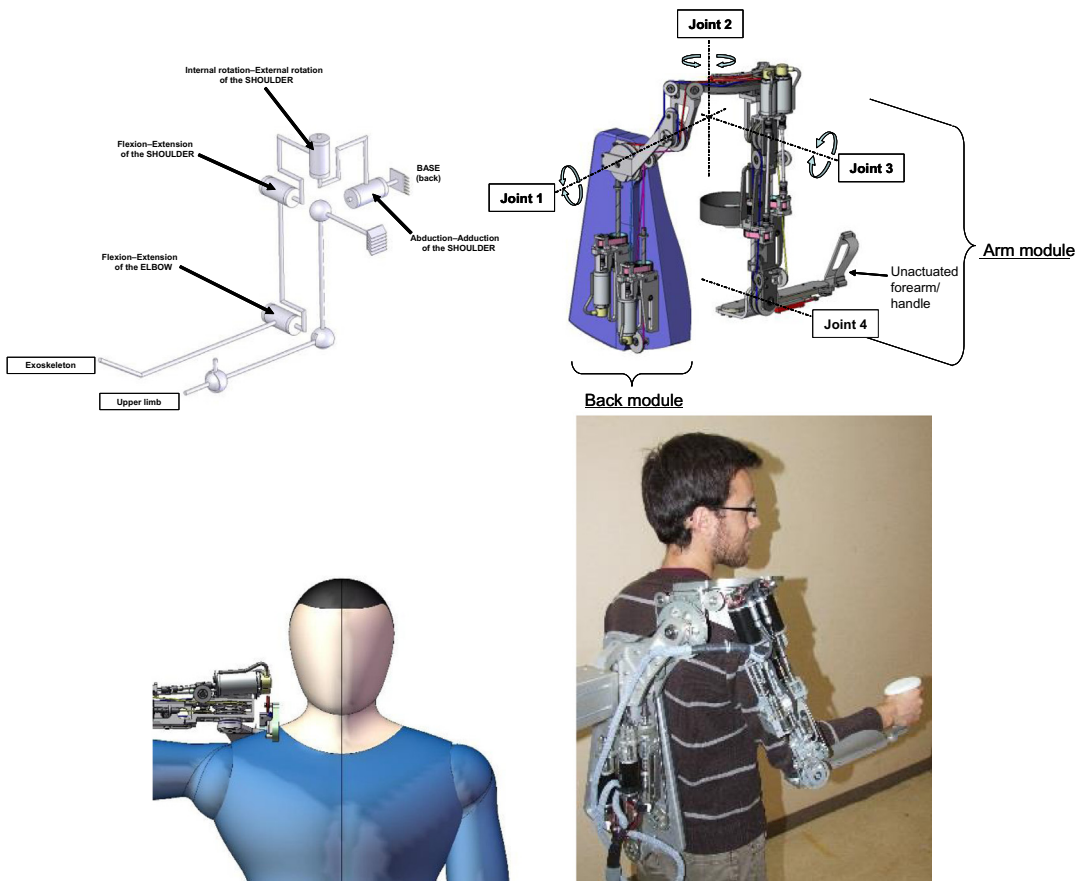


FIGURE 3.10

ABLE—four axis kinematics.

3.4 THE COMPLETION OF ABLE 7D

The main challenge to complete a 7-DOF version of ABLE version (Fig. 3.12) was to design an open forearm structure with a streamlined shape and the best possible transparency (minimum friction and inertia) even under load. We also wanted to replace the existing shoulder articulation with a solution that would avoid the use of a circular guide rail, a component with many disadvantages.

3.4.1 FOREARM–WRIST DESIGN

We found that none of the forearm exoskeletons described in the literature met these requirements [18–21]. It had become clear to our team that the central problem was obtaining a pronosupination movement with an open mechanism surrounding the forearm and whose friction under load and

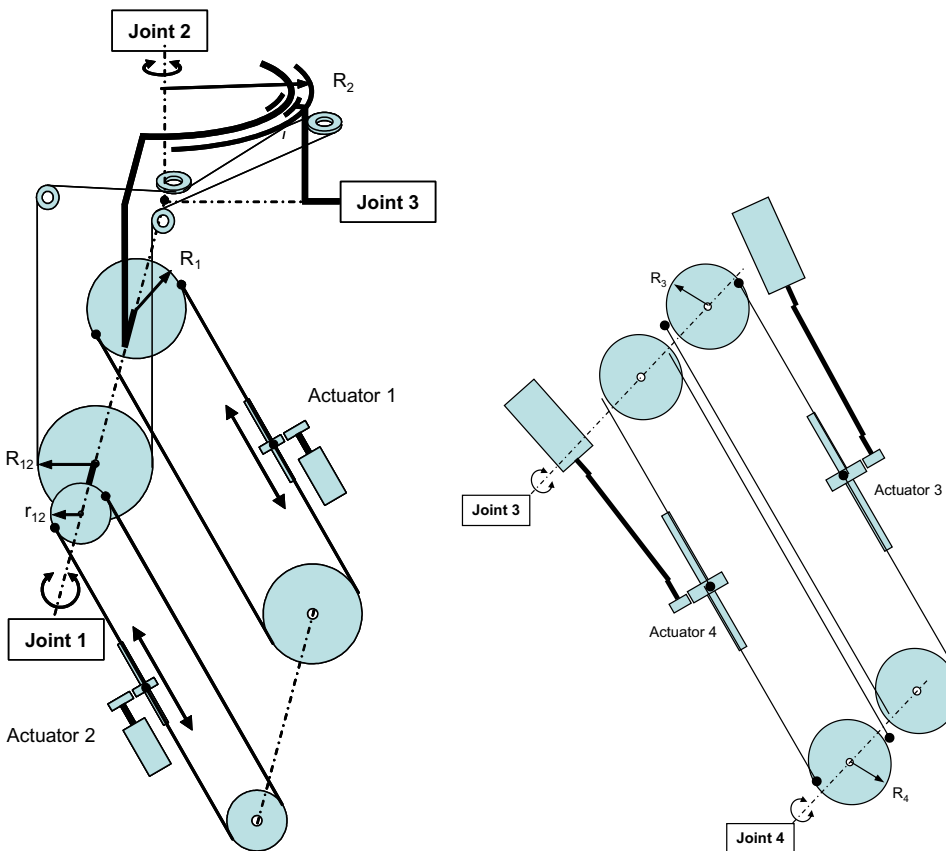


FIGURE 3.11

ABLE—four axis actuator kinematics: (left) back module (Joints 1 & 2); (right) arm module (Joints 3 & 4).

inertia is minimal. We then devised a new mechanism composed of an articulated cage and a fixed mast arranged in parallel [29]. The wrist cradle is connected to the base cradle by three articulated bars on rotules. The mast supports three ball bearings which keep the articulated cage rotating on its longitudinal axis. This association is a particular form of parallel mechanism. One can notice a kind of biomechanical similarity with the movement of the ulna bones and the radius of the human forearm, even if it was not at the origin of the invention. From a mechanical point of view, the desired effect is the conversion of the bending moment into tension—compression in the bars according to the parallelogram principle while the shearing force is transmitted to the mast by a radial support on miniature bearings. Whereas in the previous circular bearing, the bending moment generated high stresses and friction in the carriage, our mechanism is less dependent on the applied transverse load (pivoting and bending friction in the spherical plain bearings under limited loads) (Fig. 3.13).

As an example, the miniature bearings used are dimensioned to support about 50 N of radial load, whereas the rods and ball joint easily transmit the tensile/compressive forces of about 150 N.

Table 3.2 ABLE 4D Main Specifications

Module	Back		Arm	
	Axis 1	Axis 2	Axis 3	Axis 4
Joint	Abduction/ Adduction	Rotation Internal/ External	Flexion/ Extension	Flexion/ Extension
Articulation	Shoulder			Elbow
Amplitude (degree)	110			130
Motors	DC ironless Faulhaber type			
Transmission	Belt + Ball screw and cable (SCS)			
Ratio	106	107	71	71
Max. velocity in hand (approx.) (m/s)	1			
Joint torque (continuous) (Nm)	18	18	13	13
Continuous effort in hand (approx.) (N)	50	50	40	40
No-load friction in hand (approx.) (N)	3		2	

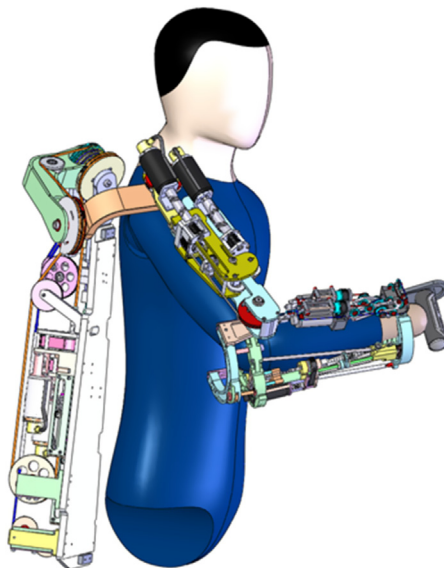
The amplitude of rotation is limited by interference between the rods and the fixed parts. Our model allows about 120 degrees of amplitude which is inferior to the maximum possible for a human but sufficient in practice for rehabilitation and industrial applications. Another aspect is that the wrist cradle exhibits a translation on the longitudinal axis ([Fig. 3.14](#)).

The displacement law as a function of the pronosupination angle is given by the above equation. For the amplitude allowed in our design made for an adult, this represents about 7 mm ([Table 3.3](#)).

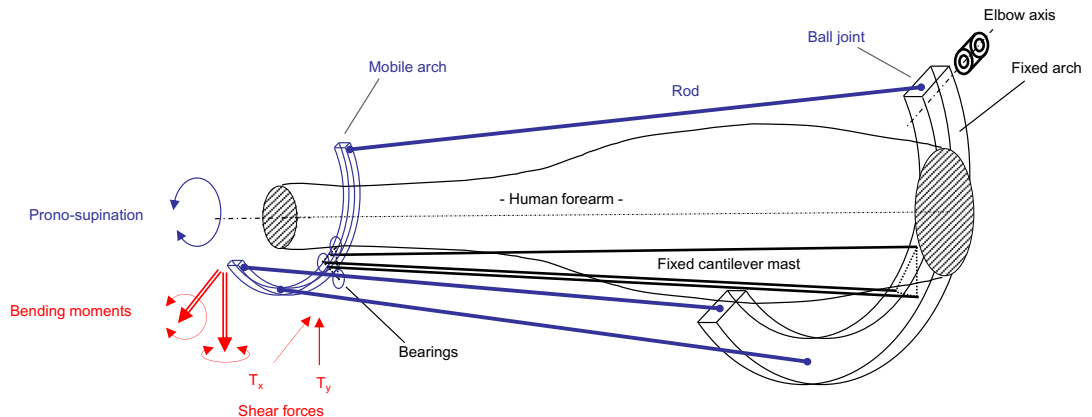
Compared to the flexibility of the skin and muscles, this disturbance is relatively small and is unlikely to be felt by the user. The cumulating effect of play in the ball joints and in the bearing creates some slight perturbations of the motion which are not detectable by the operator. The SCS with its cable transmission provides the necessary tolerance and the desired torque (around 2 Nm) is easily achieved with a miniature ball screw. However, the design of the cable transmission is not obvious, due to the nonlinear longitudinal movement of the wrist cradle [30]. Therefore the grooves machined on the wrist cradle are not portions of circles. The scheme shows the arrangement of the routing of the closed-loop preloaded cable transmission ([Fig. 3.15](#)).

We will detail now the model used to synthesize the grooves. A presentation of the complete design would be too long here because the nontrivial shapes of the grooves, the speed, and the angle of both sections of the cable are not equal. Therefore the cable loop needs to be compensated by a special return idling pulley. In order to synthesize the shape of the grooves, the spatial kinematic problem is studied by unfolding it on a plane ([Fig. 3.16](#)).

The cable is deviated by the pulley $P(p, q)$ and contacts the driving pulley in points T, T', T'' (tangential line at the intersection of the deviating pulley plane and the driving pulley cylinder).

**FIGURE 3.12**

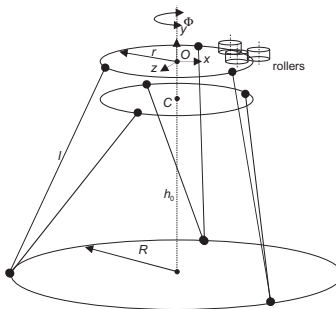
A CAD view of ABLE 7D.

**FIGURE 3.13**

Forearm articulated structure allowing pronosupination.

There is a fixed frame (O, x, y) , with x representing the arc $R\Phi$ and y , the translation of the mobile arch associated with the frame (I, u, v) . The origin of the groove I is such that for $\Phi = 0$, I is confused with T where we also impose $\theta = 0$, leading to the following initial conditions: $v'(0) = v(0) = 0$

The radius of the driving pulley is noted R_0 and the distance between the deviating pulley center and the tangential line is noted L_0 . For $\Phi > 0$, the cable is wrapped on the *blue portion* of the

**FIGURE 3.14**

Axial displacement law of the parallel structure.

Table 3.3 Example of Translation Magnitude for Typical Biomechanical Dimensions

Angular travel		120 degrees
Pronation/supination	Φ_{\max}	60 degrees
Fixed arch radius	R	60 mm
Mobile arch radius	r	60 mm
Nominal distance between arches	h_0	250 mm
Rod length	1	250 mm
Maximum translation	$y_{C_{\max}}$	-7 mm

groove and on the *red portion* for $\Phi < 0$. Since the cable must ideally remain constantly tangent to the groove at contact points T, T', T'' , the groove presents different curvatures for both portions. On the opposite branch, the cable is wrapped on complementary portions of the second groove, due to the symmetry of the problem. By writing that the segment TS is the common tangent to the driving pulley and the deviating pulley, we obtain the following relations:

$$\frac{\rho(\cos\theta - 1) - y - v}{L_0 - \rho\sin\theta} = -R_0^{-1}v' = \tan\theta \quad (3.1)$$

By using the following trigonometric transformations:

$$\begin{cases} \cos\theta = (1 + R_0^{-2}v'^2)^{-\frac{1}{2}} \\ \sin\theta = (1 + R_0^2v'^{-2})^{-\frac{1}{2}} \end{cases} \quad (3.2)$$

We can eliminate θ and finally obtain the nonlinear differential Eq. (3.3) where $v(\Phi)$ is the unknown function.

$$R_0^{-1}v'\left[L_0 - \rho(1 + R_0^2v'^{-2})^{-\frac{1}{2}}\right] + \rho\left[(1 + R_0^{-2}v'^2)^{-\frac{1}{2}} - 1\right] - \sqrt{h_0^2 + 2Rr(\cos\Phi - 1)} - v = 0 \quad (3.3)$$

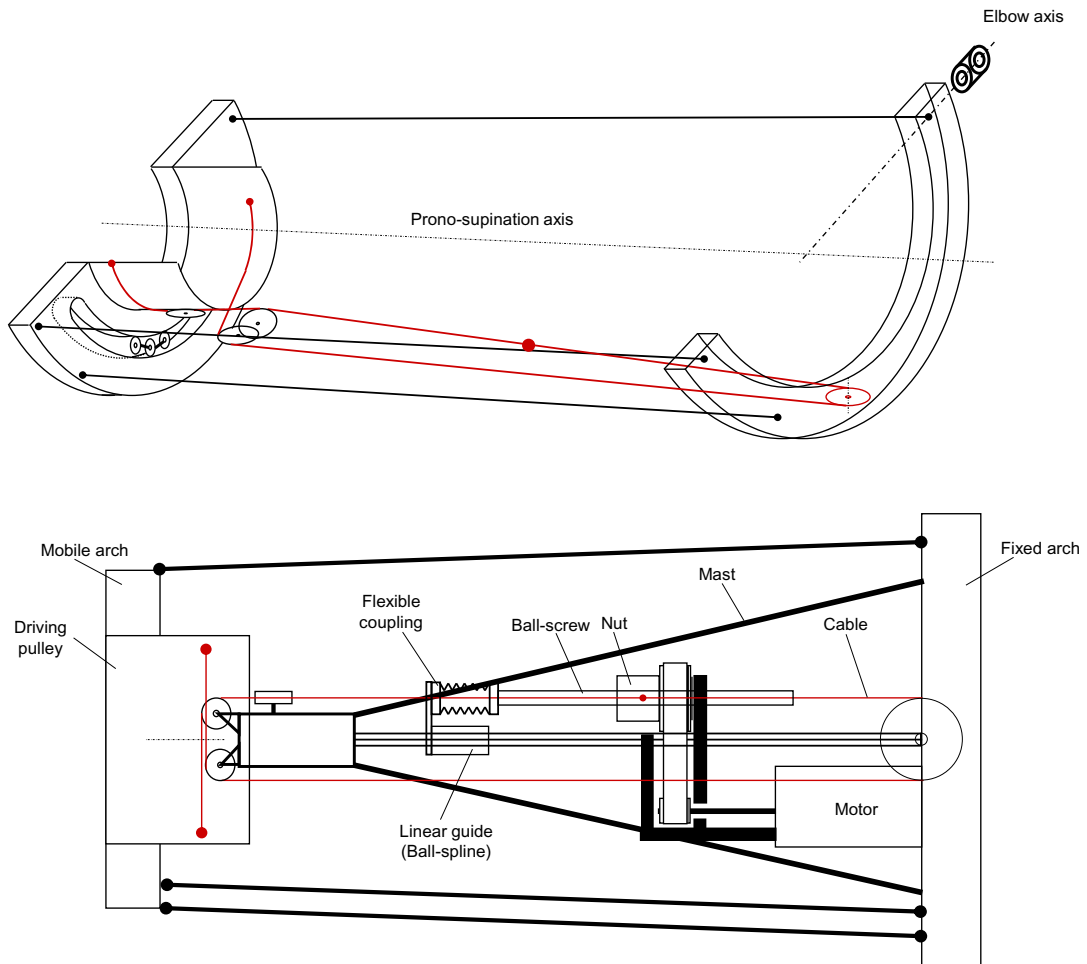


FIGURE 3.15

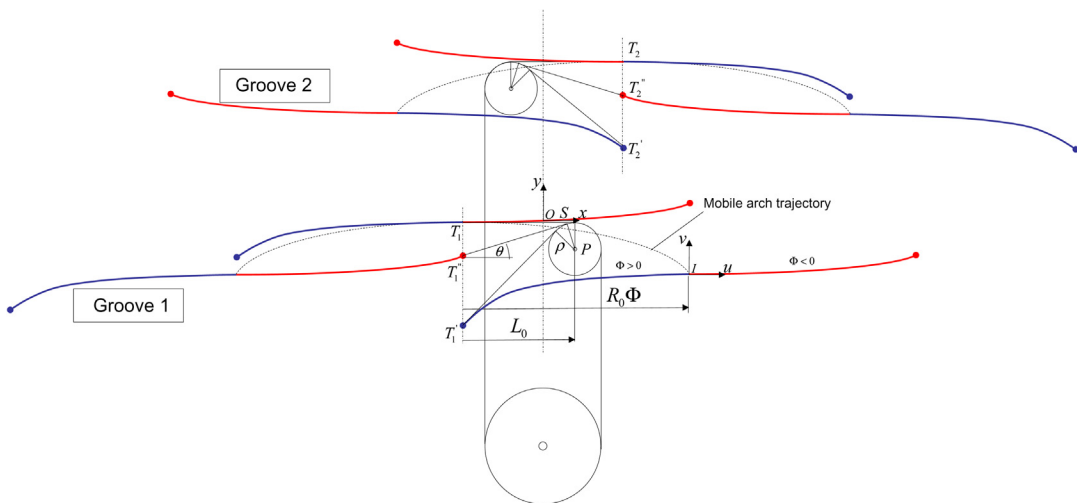
Schematic of the forearm pronosupination actuator.

The groove was discretized into 100 points in order to solve this equation numerically. The computed results are presented below in Fig. 3.17 (coordinates in mm).

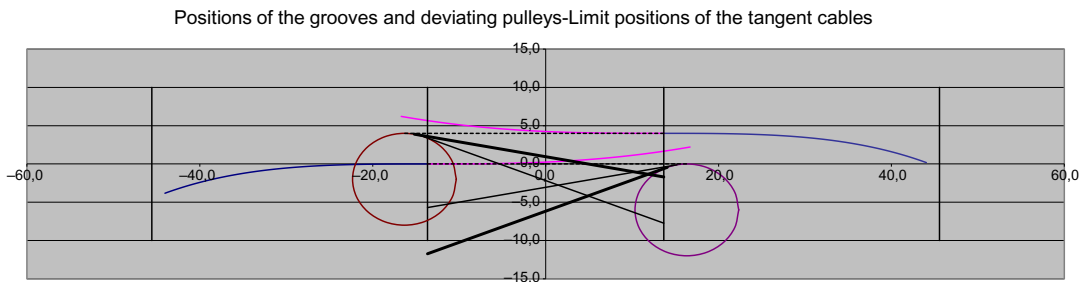
The grooves are milled with a five-axis machine tool programmed with the computed grooves. Fig. 3.18 shows a CAD view of the forearm module with its cable transmission and the special grooves.

The previous structure can be completed by a wrist joint formed by two coincident orthogonal transverse axes (equivalent to a conventional U joint) fixed on the movable arch. Each joint is driven by a SCS mounted on a structure that replaces one of the rods (Fig. 3.19). Linear and nonlinear decoupling are required to control this structure.

The synergy of the SCS actuators with the articulated cage is obvious: the motors are aligned with the rods and their reflected inertia is reduced because they are located near the base. On the

**FIGURE 3.16**

Schematic of the closed-loop cable transmission for the generation of the grooves.

**FIGURE 3.17**

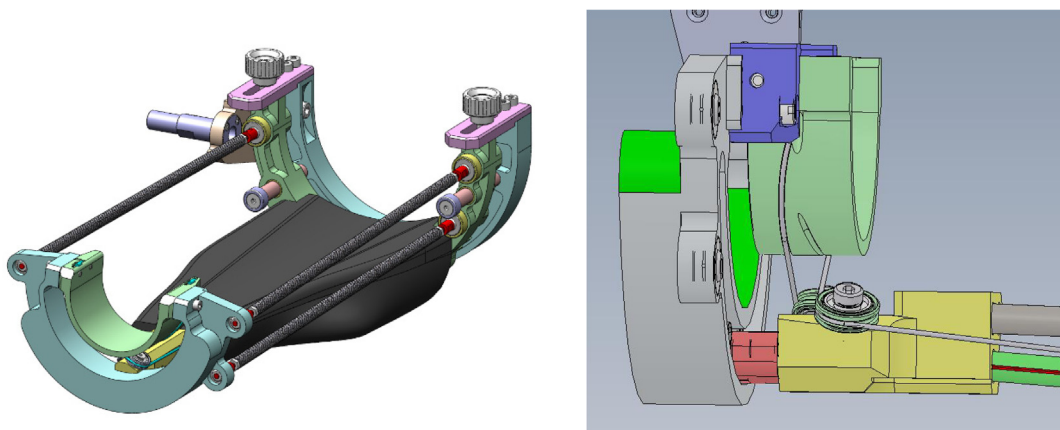
Developed computed grooves showing various positions of the cable on the deviation pulleys.

other hand, the heterogeneous connecting devices on the moving arc (two spherical plain bearings and a pair of orthogonal axes) generate other angular disturbances but fortunately of a small amplitude (less than 1 degree for our design). The main features of the forearm–wrist module are grouped in [Table 3.4](#).

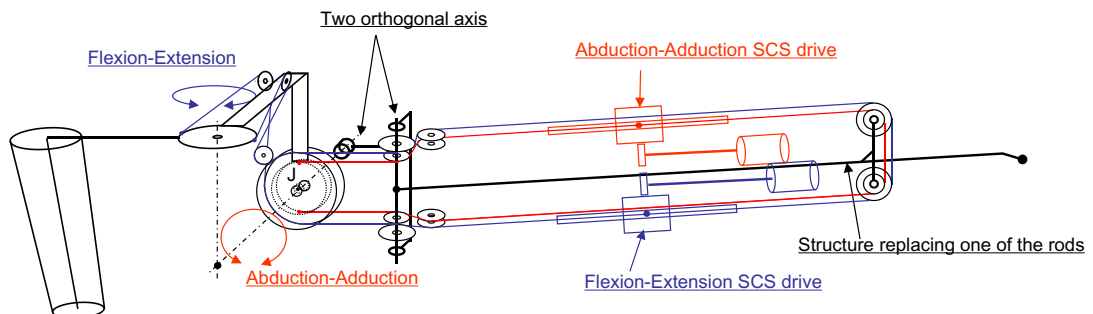
3.4.2 A NEW SHOULDER WITH NONORTHOGONAL JOINTS AND SIMPLE BEARING

The ABLE 4D shoulder effectively avoids any singularity: the joints cannot align 2–2 in the whole humanly acceptable range. However, the circular sliding guide used on axis 2 has many important disadvantages, both kinematically and mechanically:

- low flexural bending capacity due to the small size of the carriage.

**FIGURE 3.18**

Views of the forearm (left) and its pronosupination cable drive showing the computed grooves (right).

**FIGURE 3.19**

Wrist U-joint articulation and their SCS drives with cable routing.

- friction critically increasing with the flexural bending moment; its friction is much higher and much less consistent than for a standard joint rotating on ball bearings like to axis 1 and 3. This generates an inhomogeneous transparency of the arm.
- intrusive shape near the face.
- the 100 mm radius used is the minimum value. This prohibits the scaling of the shoulder, for example, for a child.
- limited displacement (approximately 90 degrees here for the abduction) restraining the expansion of the working volume.
- high cost.

Table 3.4 Forearm–Wrist Main Specifications

Module	Forearm–Wrist		
	Axis 5	Axis 6	Axis 7
Joint/Articulation	Pronosupination	Abduction/Adduction	Flexion/Extension
Articulation	Forearm		
Amplitude (degree)	110		
Motors	DC ironless Faulhaber type		
Transmission	Belt + Ball screw and cable (SCS)		
Ratio	117	49	47
Max. velocity in hand (notional) (m/s)	1		
Joint torque (continuous) (Nm)	2	2	2
Continuous effort in hand (approx.) (N)	19	22	20
No-load friction in hand (approx.) (N)	0		

- only one supplier at the time (2008), long delivery delay for a monobloc rail and instead two rails jointed (shocks and irregular friction).

We also came up with two observations:

- The orientation of the first axis is not required to be normal with respect to the reference planes.
- Since the working space of the human shoulder patella is limited by interference with the torso, it is not mandatory that the three intersecting axis be perpendicular two to two.

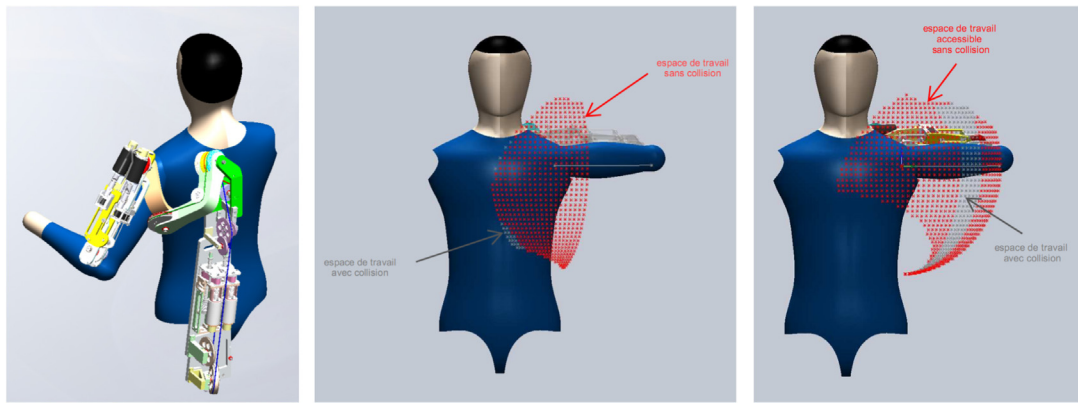
We have therefore sought a geometry of the joints that can equal or increase the previous volume of work by avoiding collisions between parts and ensuring a sufficient safety distance with the body of an operator. A first set of intuitive angle distribution for the three nonorthogonal joints was proposed and confirmed using an optimization method based on computations with Matlab or Adams software (Fig. 3.20).

In addition to this innovative shoulder arrangement [31], the humerus limb was modified to become adjustable in length [32]. The final resulting transmission scheme for the first four joints is shown on Fig. 3.21.

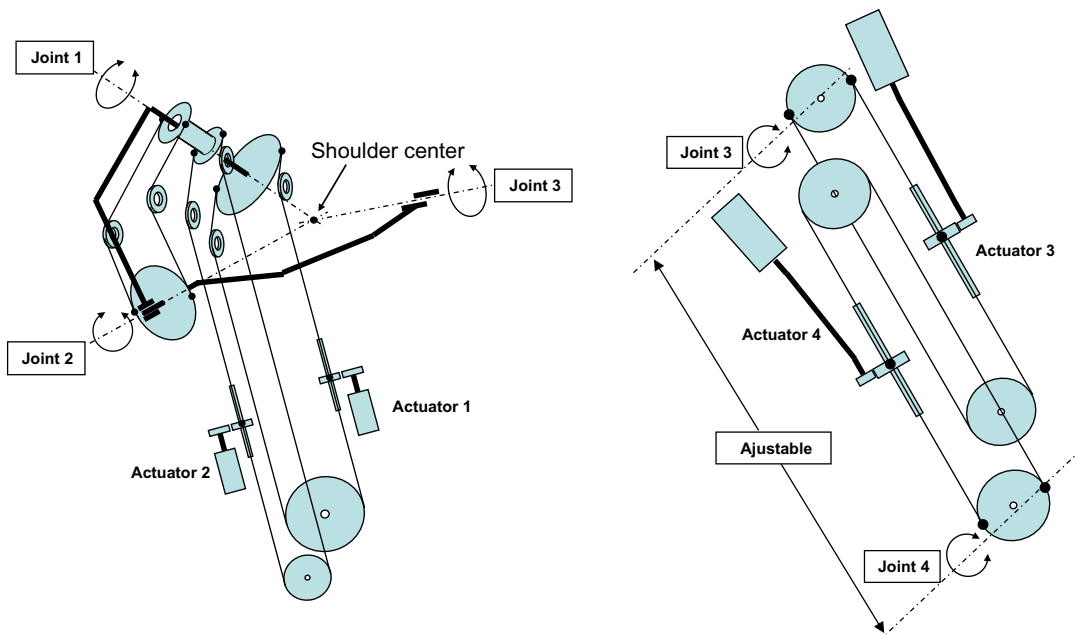
A final integration phase led to the completion of the ABLE 7D prototype in 2011. Later versions have been commercialized by Haption.

3.5 CONCLUSION

The successful integration of the SCS into the ABLE exoskeleton architecture illustrates how a flexible element acts in synergy with the rigid mechanical component to ensure a low and above all reproducible level of friction within a light and relatively deformable host structure. During the collaborative French ANR-BRAHMA project, the ABLE 4D version has been used for rehabilitation

**FIGURE 3.20**

Confirmation of the initial proposed distribution of the three nonorthogonal axes using optimization computations.

**FIGURE 3.21**

Four first joints kinematics of ABLE 7D: (left) back module (Joints 1 & 2); (right) arm module (Joints 3 & 4).

**FIGURE 3.22**

ABLE 7D first prototype (left, ©CEA/C. Dupont) and its bilateral version built by Haption (right, ©CEA/Echord++ / H. Seyfarth).

tests [33,34] and its technology and performances were positively reviewed [35,36]. The first ABLE 7D prototype was completed in 2011 (Fig. 3.22), within the SCALE 1 project (ANR), mainly for haptic applications in which it demonstrates an unexpected texture rendering capacity. The homogeneity of response to forces is enhanced by the homogeneity of its seven torque-controlled actuators. ABLE 7D has also been tested by PSA Peugeot Citroen as a cobotic device to evaluate the ergonomic advantage of force assistance for working posture at height under an automotive assembly line [37]. Overall the successful design of ABLE 7D with its innovative actuation system, has enabled the development of new applications for lower limb exoskeletons in the domain of assistance, with the HERCULE family, for tetraplegics with the four-limb exoskeletons EMY and EMY Balance, as well as for industrial cobotic arms such as COBOMANIP (Sarrazin Technologies) and more recently SYB3 (Isybot).

ACKNOWLEDGMENTS

This work, in part funded by the French ANR (Agence Nationale de la Recherche), has been carried out by the CEA robotic team over several years under the leadership of J. P Friconneau and Y. Perrot who consecutively led the Interactive Robotics Service of CEA. I had the privilege to conduct the design of ABLE with extremely dedicated and professional technicians, engineers and researchers whose experience and knowledge is invaluable and permitted the construction of ABLE 7D. I would like to thank in particular A. Verney, B. Perochon, D. Ponsort, F. Kfouri, J. Langevin, Philippe Pottier, and J. P. Martins. I am also pleased to mention the constant, passionate and inspiring support of former technicians and engineers, in particular. A. Dupuis, M. Férid, M. P. Meyer, M. Itchah, P. Marchal (CEA), and D. François (La Calhène), some of whom were part of the team of designers of the famous MA23 led by the pioneer J. Vertut. Finally, I would like to thank also all the researchers and colleagues outside CEA who tested our prototypes, gave their feedback and suggestions to refine and enrich our initial ideas.

REFERENCES

- [1] D. François, J.C. Germond, P. Marchal, J. Vertut, Cable-operated power manipulator, US Patent 4078670, 1975 (priority 1974).
- [2] J. Vertut, P. Coiffet, Bilateral servo manipulator MA23 in direct mode and via optimized computer control, in: Proceedings of the 2nd Retotely Manned System Technology Conference, 1975.
- [3] A.K. Bejczy, *Teleoperation, telerobotics, Jet Propulsion Laboratory, California Institute of Technology*, 1999, p. 6.
- [4] T.H. Massie, J.K. Salisbury, The PHANTOM haptic interface: a device for probing virtual objects, in: Proceedings of the ASME Winter Annual Meeting, Symposium on Haptic Interfaces for Virtual Environment and Teleoperator Systems, Chicago, IL, November 1994.
- [5] W.T. Townsend, The effect of transmission design on force-controlled manipulator performance, Thesis, MIT AI Laboratory, 1988.
- [6] P. Garrec, Screw transmission, nut and cable attached to the screw, Patent FR2809464/US7073406/WO200192761, 2000.
- [7] P. Garrec, Screw, nut and cable transmission, Patent FR2852373/EP1620664/WO200483683, 2003.
- [8] P. Garrec, J.P. Friconeau, F. Louveau, Virtuose 6D: a new force-control master arm using innovative ball-screw actuators, in: Proceedings of ISIR 35th International Symposium in Robotics, Paris, March 2004.
- [9] R.C. Goertz, et al., Master-slave servo-manipulator model 2, *Proc. 4th Ann. Conf. Hot Lab. and Equip.* 1 (1955).
- [10] L. Galbiati, et al., A compact flexible servo system for master slave electric manipulator, in: Proceedings of 12th Conference Remote System Technology, ANS, 73, 1964.
- [11] C.R. Flatau, Development of servo manipulators for high energy accelerator requirements', in: Proceedings of 12th Conference Remote System Technology, 29, 1965.
- [12] G.-W. Köhler, *Manipulator Type Book*, Verlag Karl Thiemig, München, 1981.
- [13] J. Vertut, P. Coiffet, *Téléopération Evolution des techniques*, Vol. 3A, Hermes, Paris, France, 1984.
- [14] W. Townsend, J.K. Salisbury, The effect of Coulomb friction and stiction on force control, *IEEE Int. Conf. Robot. Autom.* 2 (1987) 883–889.
- [15] P. Garrec, Systèmes mécaniques, in: P. Coiffet and A. Kheddar (Ed.), *Téléopération et télérobotique*, Ch 2., Hermes, Paris, France, 2002.
- [16] P. Garrec, F. Geffard, O. David, F.-X. Russotto, Y. Measson, Y. Perrot, Telerobotics research and development at CEA LIST, in: ANS EPRRSD – 13th Robotics & Remote Systems for Hazardous Environments, 11th Emergency Preparedness & Response Knoxville, TN, August 7–10, 2011.
- [17] J.M. Goubot, P. Garrec, STEP: an innovative teleoperation system for decommissioning operations, in: Workshop “Decommissioning Challenges: An Industrial Reality ?”, French Nuclear Energy Society, Avignon, France, 2003.
- [18] M. Bergamasco, B. Allotta, L. Bosio, L. Ferretti, G. Parrini, G.M. Prisco, et al., An arm exoskeleton system for teleoperation and virtual environments applications, in: *Proc. IEEE Int. Conf. Robot. Autom.*, vol. 2, 1994, pp. 1449–1454.
- [19] A. Gupta, M.K. O’Malley, Design of a haptic arm exoskeleton for training and rehabilitation, *Mech. IEEE/ASME Trans.* 11 (3) (2006) 280–289.
- [20] L. Frisoli, A. Borelli, A. Montagner, et al., Arm rehabilitation with a robotic exoskeleton in Virtual Reality, in: Proceedings of IEEE ICORR 2007, International Conference on Rehabilitation Robotics, 2007.
- [21] J.C. Perry, J. Rosen, S. Burns, Upper-limb powered exoskeleton design, *IEEE/ASME Trans. Mech.* 12 (4) (2007) 408–417.

- [22] P. Letier, M. Avraam, S. Veillerette, M. Horodinca, M. De Bartolomei, A. Schiele, et al., SAM: A 7-DOF portable arm exoskeleton with local joint control, in: Proceedings of IROS 2008, Nice, France, September 2008.
- [23] P. Garrec, Intermediate segment of an articulated arm comprising a screw and nut transmission, Patent FR2852265/US20060169086/WO200482901, 2003.
- [24] P. Garrec, Actuator having an offset motor using a flexible transmission, and robotic arm using such an actuator, Patent FR2990485/US20150096392/WO2013167396, 2012.
- [25] P. Garrec, J.P. Martins, J.P. Friconeau, A new technology for portable exoskeletons, *AMSE* 65 (7/8) (2004) 13–22.
- [26] P. Garrec, J.P. Martins, Shoulder mechanism for an orthosis, Patent FR2932081/US20110098619/WO201000973, 2008.
- [27] P. Garrec, J.P. Martins, F. Gravez, Y. Perrot, Y. Measson, A new force-feedback, morphologically inspired portable exoskeleton, in: Proceedings of 15th IEEE International Symposium on Robot and Human Interactive Communication (RO-MAN - 2006), Hatfield, UK, 2006.
- [28] P. Garrec, J.P. Friconeau, Y. Méasson, Y. Perrot, ABLE, an innovative transparent exoskeleton for the upper-limb, in: Proceedings of IROS 2008, Nice, France, September 2008.
- [29] P. Garrec, Forearm rotation mechanism and orthosis including such mechanism, Patent FR2917323/EP2164432/US20100204804/WO2008155286, 2007.
- [30] P. Garrec, A. Verney, Design of an innovative exoskeletal forearm-wrist mechanism, in: 1st International Conference on Applied Bionics and Biomechanics ICABB-2010, Venice, Italy, 2010.
- [31] P. Garrec, J. Bonnemason, J.P. Martins, A. Verney, Segment de bras mécanique à longueur variable et bras mécanique comprenant ce segment, Patent FR2961424, 2010.
- [32] P. Garrec, Shoulder mechanism for orthosis, Patent FR2949669A1/US20120172769/PCT/EP2010/005452, 2009.
- [33] N. Jarrassé, J. Robertson, P. Garrec, J. Paik, V. Pasqui, Y. Perrot, et al., Design and acceptability assessment of a new reversible orthosis, in: Proceedings of IROS 2008, Nice, France, September 2008.
- [34] N. Jarrasse, M. Tagliabue, J.V.G. Robertson, A. Maiza, V. Crocher, A. Roby-Brami, et al., A methodology to quantify alterations in human upper limb movement during co-manipulation with an exoskeleton, *IEEE Trans. Neural Syst. Rehabil. Eng.* 18 (2010) 389–397.
- [35] D.J. Reinkensmeyer, et al., World Technology Evaluation Center (WTEC), in: Panel Report on “European Research and Development in Mobility Technology for People with Disabilities”, Final Report, 2011, p. 25.
- [36] D.J. Reinkensmeyer, M.L. Boninger, Technologies and combination therapies for enhancing movement training for people with a disability, *J. Neuroeng. Rehabilit.* (2012).
- [37] N. Sylla, V. Bonnet, F. Colledani, P. Fraisse, Ergonomic contribution of ABLE exoskeleton in automotive industry, *Int. J. Ind. Ergon.* 44 (4) (2014) 475–481.

RIGID VERSUS SOFT EXOSKELETONS: INTERACTION STRATEGIES FOR UPPER LIMB ASSISTIVE TECHNOLOGY

4

Domenico Chiaradia¹, Michele Xiloyannis², Massimiliano Solazzi¹, Lorenzo Masia³ and Antonio Frisoli¹

¹PERCRO Laboratory, TeCIP Institute, Scuola Superiore Sant'Anna, Pisa, Italy ²Sensory-Motor Systems (SMS) Lab,

ETH Zurich, Zurich, Switzerland ³Department of Physics and Astronomy, Institute of Technical Informatics ZITI,
Heidelberg University, Heidelberg, Germany

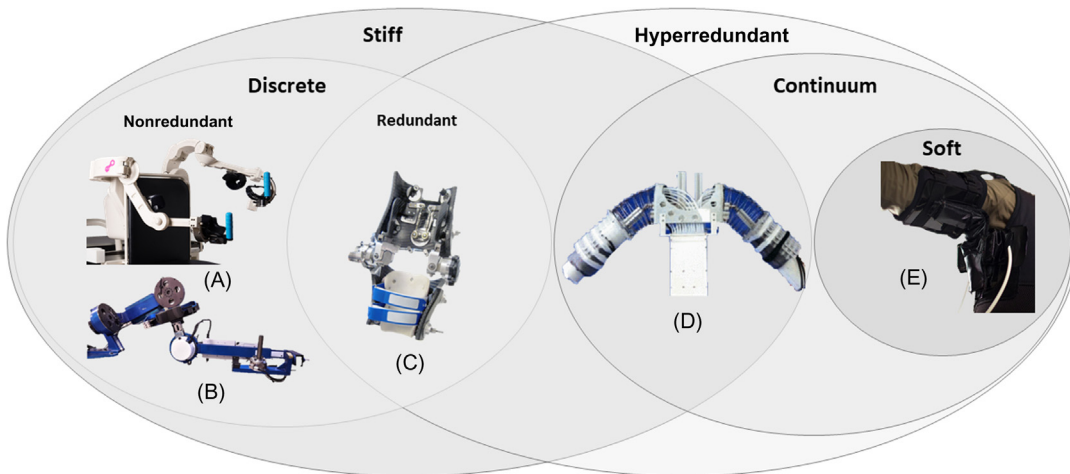
4.1 INTRODUCTION

The need to augment human motor abilities or restore lost motor functions has been one of the key reason to develop wearable robotic devices. Among them, exoskeletons are robotic interfaces for human–robot interaction where the highest physical symbiosis with the operator is achieved. The earliest one, dating back to 1967 [1], was conceived as a *rigid* external frame that would bear heavy loads in parallel with its operator; one of its main limitations was the lack of an intuitive interaction control, which limited the mutual physical communication between the man and the machine. The possibility to interact closely with the robot requires safety and compliance features that were introduced later, either through control strategies or passively with compliant or soft mechanical elements in the design.

In literature, the term “soft robotics” usually refers to two distinct design approaches [2]: (1) robots with compliant joints (active or passive) connecting rigid links [3] and (2) continuum robotic devices [4]. These systems are the result of a design evolution from discrete mechanisms assembled in a series of rigid links, to mechanisms without rigid components but rather composed of elastic structures capable of continuous bending along their length [2]. Fig. 4.1 shows the taxonomy introduced in Ref. [2] adapted to upper-limb exoskeletons.

On one side of the taxonomy, one finds rigid nonredundant exoskeletons, that is, systems where the degrees of freedom (DOFs) are less or equal the ones required to accomplish the specific task. The Rehab-Exos [6] is an example of this category, where the interaction is made possible by torque sensors allowing a direct torque control. In the same category of rigid robots, the ALEX Exoskeleton [5] provides interaction without the use of torque sensors due to its high backdrivability combined with an implicit impedance control and a highly accurate feed-forward compensation.

A higher user motion compliance can be achieved by a kinematically redundant device, where the robot's DOFs are more than the ones required for the task accomplishment, as in the case of

**FIGURE 4.1**

Systems for physical human–robot interaction. From left to right, in (A) the ALEX Exoskeleton (Frisoli [5]) and in (B) the Rehab-Exos (Vertechy [6]) are stiff and nonredundant examples. In (C), the NEUROExos (Vitiello [7]) elbow exoskeleton is a stiff redundant example that provides 13 DOFs. (D) An example of continuum shoulder exoskeleton [8], whereas (E) the shoulder soft exosuit [9] is made of soft materials and actuated pneumatically.

the NEUROExos [7] (13 DOFs for the elbow joint) and the (CADEN)-7 [10] (7 DOFs for the arm movements). Furthermore, the NEUROExos is equipped by a series elastic actuator (SEA) [11] that introduces compliance at the joints’ level. Recently, exoskeletons design is drifting toward an approach where mechanical compliance is distributed across a “continuum,” as in the case of the shoulder exoskeleton presented in [8,12], where the adaptability to human biomechanics is achieved by an ideally infinite number of DOFs [13].

The abovementioned approach can be found on the far side of the spectrum shown in Fig. 4.1: the introduction of soft materials, such as fabric and elastomers, provides the possibility to design wearable assistive devices resembling typical garments with embedded sensing and actuation to work in parallel with our muscles and provide additional power [14]. Representative examples are a soft exosuit for the shoulder [9] made of fabric and pneumatically actuated, or the tendon-driven wearable gloves [15,16]. A characteristic of exosuits is that they rely on the structural integrity of the human biomechanics to transfer reaction forces between body segments, rather than having their own frame, acting more like external muscles than external supporting skeletal structures [14]. For this reason, soft exosuits require a more accurate ergonomic design/study to obtain a comfortable device [17].

To summarize, the multiple classes of this taxonomy provide multiple solutions, all showing advantages and drawbacks. Their choice is related to specific different applications. Rigid links robotic solutions, for example, are commonly used in poststroke neurorehabilitation [18], assistance for limb movements, human power augmentation for lifting heavy loads [19], and teleoperation [20,21]. The use of these exoskeletons provides support to patients with no residual motion

capability and altered biomechanics (i.e., muscular atrophy) or in the case of augmenting technology, they enhance the master immersivity and dexterity.

In general, as stated in Ref. [22], soft and rigid wearable robots are complementary rather than substitutive approaches. The compliance of soft devices strongly limits the amount of forces/torques that the device can provide to the human body as well as the speed of the transmitted motion. This makes soft exosuits suitable only for applications requiring both a limited magnitude of assistance, and wearers with intact and unimpaired biomechanics. On the other hand rigid exoskeletons can deliver higher forces but rigidity of their linkages is paid in terms of power requirements and low force/weight ratio which make them metabolically unoptimal in the case of portable devices.

Another important aspect is that the mechanical characteristics of a wearable device strongly influence the choice of the most appropriate control strategy. Interaction forces can be controlled by means of a direct force control [23], that is, the desired forces are tracked by a feedback loop, or by indirect force control, that is, the controlled forces are linked to kinematics with a predefined relation (admittance or impedance).

This chapter aims to explain in detail the complementarity between the devices on the opposite sides of the taxonomy presented in Fig. 4.1, by highlighting the strengths and weaknesses of rigid and soft wearable robots and objectively quantifying their capability in terms of interaction with a human operator. By comparing the design and performance of a rigid nonredundant exoskeleton and a soft exosuit, the authors aim to provide the guidelines to implement the interaction control strategies for the scenarios where both soft and rigid devices operate. Finally, we compare the performance of a soft exosuit and a rigid exoskeleton while performing a human in the loop assistive task. To quantify the performance we introduce metrics to assess the biomechanical and physiological effects of the devices on movements performed by a population of healthy subjects. Both the devices were controlled to provide assistance by compensating for the gravitational force acting on the arm, and maximize their transparency to the wearer's motion.

An initial section dedicated to the mechanical description of the exoskeleton and exosuit provides the reader with the main distinctions of rigid versus soft devices. The second section is dedicated to physical modeling and control paradigms. Each of the two sections is divided into two parts (rigid and soft) to highlight the differences between the two exoskeleton typologies.

The experimental setup and results sections report the design of the experiments and the performance of the two devices, respectively. Finally, the chapter offers a comparative study and a concluding section with our thoughts on the implications of our findings for the choice of control strategies for soft and stiff exoskeletons.

4.2 EXOSKELETONS DESCRIPTIONS

The two typologies of exoskeleton employed in the present study follow two complementary mechanical design strategies. The Rehab-Exos is an upper-limb exoskeleton [6] conceived for rehabilitation and assistive tasks requiring a high level of force. The device is not portable, but it is a workstation for clinical application, made of rigid aluminum links: according to the categorization provided in Fig. 4.1 the device belongs to the class of rigid exoskeletons.

The Soft Exosuit [24] is an elbow supporting device designed to assist poststroke patients: with relatively low torque, it is a portable system made with a soft harness and an embedded tendon-driven actuation system which transmits torque at the elbow joint.

4.2.1 A RIGID EXOSKELETON: THE REHAB-EXOS

The Rehab-Exos is an active robotic exoskeleton (Fig. 4.2) which is designed with the idea to be compact, easily reconfigurable, and to have a good trade-off between transparency and force replication. The physical interaction between user and exoskeleton is achieved by means of the joint-torque sensors.

The Rehab-Exos is designed in such a way to generate controlled contact forces/torques not only at its end-effector, but due to the colocated sensing at the joint level it is able to deliver the desired interaction at the intermediate links. When the user is wearing the device the interaction is mutual and the robotic assistance is regulated by sensing both the force at the handle and the interaction torques at the joints (wrist, shoulder, elbow).

4.2.1.1 Mechanical design of the Rehab-Exos

Fig. 4.2A shows the exoskeleton which has a serial architecture, isomorphic with the human kinematics. It comprises a shoulder joint which is connected to the fixed frame, and three active joints J_1 , J_2 , and J_3 ; an active elbow joint J_4 ; and a passive revolute joint J_5 allowing for wrist pronosupination.

All the active joints have been designed to satisfy speed, torque, and safety requirements of typical rehabilitative applications. In more detail, as design specifications the exoskeleton joints should have 10 rpm maximum output velocity; 120 Nm (and 80 Nm for J_3) nominal maximum output torque for actively sustaining exoskeleton links and patient limbs, and for generating the desired

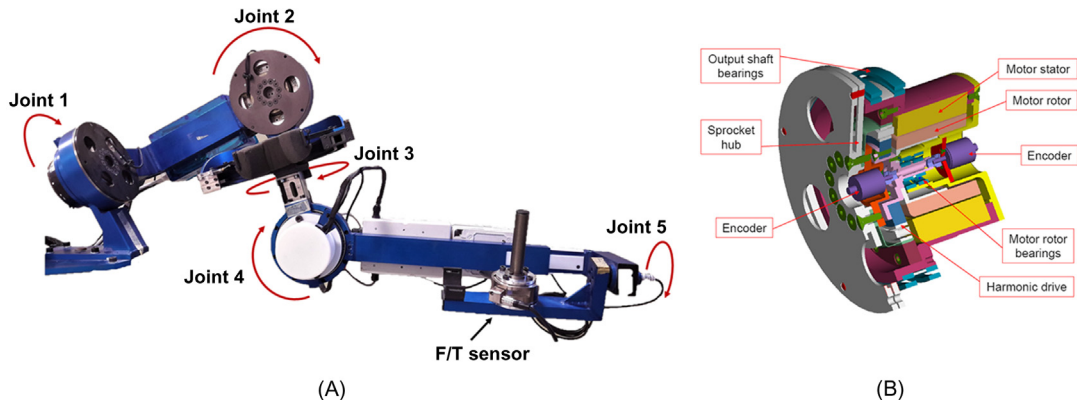


FIGURE 4.2

(A) A schematic representation of the Rehab-Exos exoskeleton. (B) A CAD section of the J_1 , J_2 , and J_4 joint actuator of the Rehab-Exos. The torque sensor (sprocket hub) is a series elastic element between the motor and the link.

contact forces. Joints should exhibit limited joint backdrivability at motor power-off, for guaranteeing patient safety; joint-torque sensing to derive forces at the exoskeleton–patient contact points, as well as torque in the patient joints, and possibly a limited mechanical complexity to ease maintenance and to reduce costs.

The three joints J_1 , J_2 , and J_4 of the exoskeleton are motorized through identical actuation groups (Fig. 4.2B). Each joint features a custom-made frameless brushless torque motor integrating a compact Harmonic Drive (HD) component set. The actuator provides a joint output torque equal to 150 Nm with an overall weight equal to 3.7 kg and a motor shaft inertia reduced to the joint output shaft $J_m = 3.7 \text{ kgm}^2$. The Harmonic Drive performs a reduction equal to 100:1. Due to the adopted mechanical components, the joints feature limited backdrivability at motor power-off and limited mechanical complexity to ease maintenance as well as reduce costs.

Joint J_3 is characterized by a tendon transmission: the motor stator is fixed to the roller slider and it provides the actuation torque through an open semicircular guide rail via the cable drive. The motor has a maximum velocity of 8000 rpm and a nominal stall torque of 0.105 Nm; the gear-head reduction ratio is 33, the cable drive reduction ratio is 23, and the overall weight of the actuation stage of J_3 is 2.2 kg.

The three joints J_1 , J_2 , and J_4 have a torque sensor that consists of two fully balanced strain gauge bridges placed on different beams of the spoke, which is located at the joint output shaft. The overall joint torsional stiffness reduced to the joint output shaft is $k = 11.38 \text{ kNm/rad}$.

Despite further augmenting the actuation group compliance, the availability of joint-torque sensors enables multicontact force control at multiple points distributed over the links and, additionally, makes it possible (1) to close a stable high-bandwidth torque inner loop around each joint which is weakly affected by robot link variable inertia; (2) to suppress robot vibrations produced by the inherent transmission compliance (Harmonic Drive); (3) to reduce internal disturbance torques caused by actuator and reducer (for instance friction losses, actuator's torque ripples and gear teeth wedging actions); and (4) to measure externally applied forces/momenta and complex nonlinear dynamic interactions between joints and links.

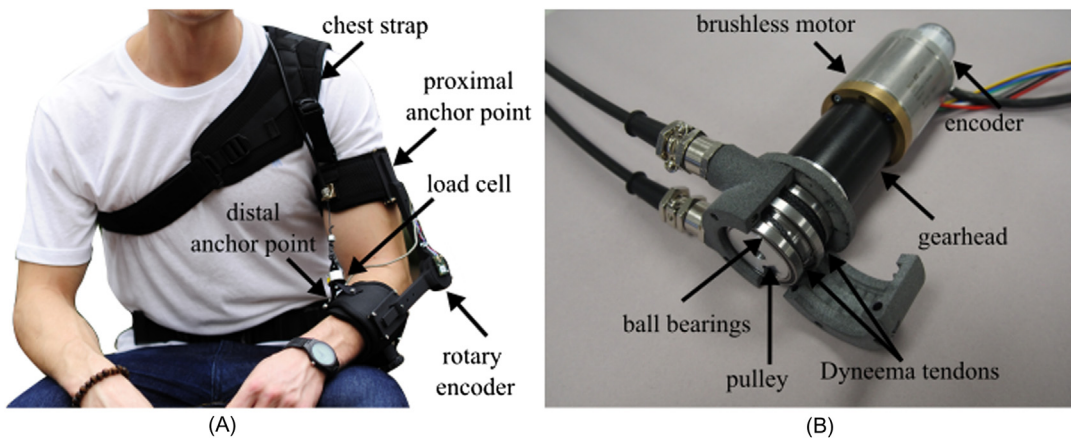
Finally, the Rehab-Exos is provided by a six-axis force/torque sensor (ATI Gamma) that is mounted at the end-effector to evaluate the performance of the joint-torque control and to estimate the torque of the joint J_3 .

4.2.2 ELBOW EXOSUIT (SOFT EXOSUIT)

4.2.2.1 Design of the soft exosuit

The exosuit for assistance of the elbow joint, shown in Fig. 4.3A, comprises three harness: one around the forearm (distal anchor point), one around the arm (proximal anchor point), and a shoulder harness, connected to the arm strap via adjustable webbing bands. Buckles, velcro straps, and a Boa lacing system allow tightening of the suit.

A pair of Bowden cables transmits power from an actuation unit to the anchor points where the cable is secured. The Bowden cables sheaths (Shimano SLR, 5 mm) are attached to the arm strap, while their inner tendons (Dupont, Black Kevlar Fiber, 136 kg max load) attach to the forearm strap. When either of the two tendons is shortened, it pulls together the two anchor points, applying a flexing or extending torque on the elbow.

**FIGURE 4.3**

The soft exosuit for assistance of the elbow joint. (A) A soft frame transmits a torque on the elbow joint by means of Bowden cables. The frame consists of a chest strap and two anchor points. A load cell and a rotary encoder monitor the force on the tendon and the position of the joint, respectively. (B) The actuation unit consists of a brushless electric motor, driving a pulley around which two Dyneema tendons are wrapped in opposite directions.

The shoulder harness is connected via inextensible webbing bands to the arm strap, covers the shoulder and encircles the chest; its purpose is to prevent the arm strap from migrating toward the center of the joint by relying on reaction forces from the shoulder and ribcage. The same is achieved for the forearm strap by tightening it with a boa lacing system, the conic shape of the forearm contributes to prevent slippage.

The proximal and chest straps were made by modifying a commercially available passive orthosis (Master-03, Reh4mat). Their substrate is made of a three-layered fabric: an external layer used to attach hard components (buckles and webbing strips), an intermediate ethylene-vinyl acetate (EVA) foam to avoid peaks of pressure and an internal 3D polyamide structure to provide air permeability. The distal anchor point consists of a flexible plastic sheet, lined with ballistic nylon and covered by a 3-mm-thick layer of polyethylene (PE) sponge at the interface with the skin. A load cell (Futek, LCM300), secured on the distal anchor point, measures the tension in the flexing tendon and an absolute encoder (AMS, AS5047P, 1000 pulses/rev), mounted on a 3D-printed joint (Shapeways, versatile plastic) between the arm and forearm straps, senses the angular position of the elbow.

The unit actuating the Bowden cables is shown in Fig. 4.3B. It consists of a brushless electric motor (Maxon, EC-i 40, 70 W) in series with a planetary gearhead (Maxon, GP 32, 55:1), capable of delivering up to 8.5 Nm of continuous torque at the elbow joint and whose angular position is monitored by an incremental encoder (Scancon, 2RMHF, 5000 pulses/rev).

The gearhead's output shaft drives a pulley around which the two tendons are wrapped in opposite directions, in an antagonistic fashion. The pulley is enclosed in a plastic casing; three ball bearings between the pulley and the plastic prevent the tendons from derailing when they are slack.

4.3 EXOSKELETON MODELS

4.3.1 REHAB-EXOS (RIGID EXOSKELETON)

The Rehab-Exos can be classified as a rigid exoskeleton basically for two reasons: both the robot's links and its actuation are much stiffer than the human arm's mechanical properties. Nevertheless, the exoskeleton joints feature an elasticity that can be modeled to estimate the interaction torques. The elasticity is due to the harmonic drive speed reducer and torque sensor (for joints 1, 2, and 4) and due to tendon transmission for joint 3.

4.3.1.1 Single joint model

The joints of the exoskeleton can be modeled with a lumped parameter model, that is, 2-mass with spring and damper as depicted in Fig. 4.4. The compliance of the joint introduces a deflection between the output joint angle $\theta_{j,i}$ and the motor angle $\theta_{m,i}$ that follows the dynamics formulated by the equations

$$J_{m,i} \ddot{\theta}_{m,i} + c_{m,i} \dot{\theta}_{m,i} + c_{t,i} (\dot{\theta}_{m,i} - \dot{\theta}_{j,i}) + k_{t,i} (\theta_{m,i} - \theta_{j,i}) = \tau_{m,i} + \tau_{d,i} \quad (4.1a)$$

$$J_{l,i} \ddot{\theta}_{j,i} + c_{t,i} (\dot{\theta}_{j,i} - \dot{\theta}_{m,i}) + k_{t,i} (\theta_{j,i} - \theta_{m,i}) = \tau_{l,i} \quad (4.1b)$$

where referring to the i -th joint, $k_{t,i}$ and $c_{t,i}$ are the stiffness and viscous coefficient of the transmission, that were experimentally characterized. $C_{m,i}$ is the viscous coefficient of the motor, $J_{m,i}$ is motor inertia, and $J_{l,i}$ is average link inertia considered as constant. $\tau_{m,i}$ is the motor torque, $\tau_{d,i}$ is a disturbance torque acting on the motor rotor which accounts for internal friction and ripple effects of both motor and harmonic drive, while $\tau_{l,i}$ is the external torque acting directly on the output link. The $\tau_{l,i}$ torque accounts for the exogenous input due to the interaction with the human, and endogenous input accounting for unmodeled nonlinear effects, such as dynamic or gravity forces.

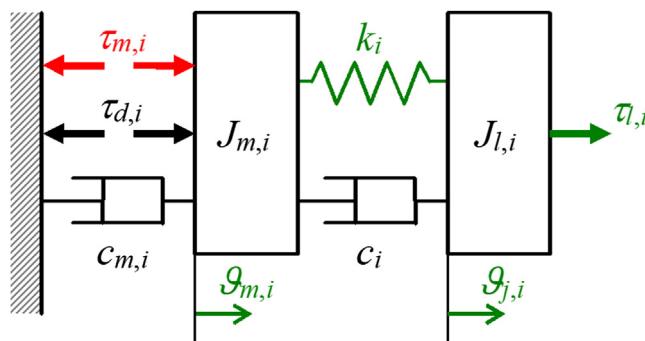


FIGURE 4.4

The 2-mass, spring, and damper model for each joint.

4.3.1.2 Multiple joints model

The multi degree of freedom dynamic model of the exoskeleton can be derived starting from Eqs. (4.1a) and (4.1b) and can be formulated in matrix form as follows:

$$\begin{cases} J_m D \ddot{\theta}_m + B_m D \dot{\theta}_m + C_t (D \dot{\theta}_m - \dot{\theta}_j) + K_t (D \theta_m - \theta_j) = \tau_m + \tau_d \\ M(\theta_j) \ddot{\theta}_j + C(\dot{\theta}_j, \theta_j) \dot{\theta}_j + C_t (\dot{\theta}_j - D \dot{\theta}_m) + K_t (\theta_j - D \theta_m) + G(\theta_j) = J^T F_h \end{cases} \quad (4.2)$$

where J_m , B_m , D , K_t , and C_t are diagonal matrices. J_m and B_m model inertia and viscous friction at motor, respectively. K_t and C_t are the stiffness and the damping of the elastic transmission and D models the gearheads transmission reduction factor. G models the effects of gravity force on links. $M(\theta_j)$ and $C(\dot{\theta}_j, \theta_j)$ models inertial and Coriolis effects, respectively. F_h are the external forces acting on the system due to human interaction and the respective joint-torques are computed by multiplying them by the transposed Jacobian matrix J^T .

Eq. (4.2) can be rewritten in a more convenient form to derive the control law and some consideration can be made by studying the system under static conditions. The application of a motor torque compensating for the nonlinearity due to gravity, estimated as $\hat{G}(D \dot{\theta}_m)$, with:

$$\tau_m = \hat{G}(D \dot{\theta}_m) + u \quad (4.3)$$

where u represents the actual control command, leads to

$$u = -J^T F_h + G(\theta_j) - \hat{G}(D \dot{\theta}_m) = -J^T F_h \quad (4.4)$$

since $\hat{G}(D \dot{\theta}_m) \approx G(\theta_j)$. Under dynamic conditions, the incomplete cancellation of the gravity component due to the elasticity of the joint transmission can be modeled by introducing a disturbance term $\delta g = G(\theta_j) - \hat{G}(D \dot{\theta}_m)$, that can be summed up to F_h as a disturbance noise supported by the operator.

By taking into account that the real dynamics has terms $M(\theta_j)$ and $C(\dot{\theta}_j, \theta_j)$ depending on the actual joint configuration, the first term can be decoupled into a diagonal constant component and a variable component as follows:

$$M \ddot{\theta}_j = \bar{M} \ddot{\theta}_j + \Delta M(\theta_j) \ddot{\theta}_j \quad (4.5)$$

So a variable apparent dynamic force F_{dyn} can be defined such that $J^T \Delta F_{dyn}(\dot{\theta}_j, \theta_j) = -\Delta M(\theta_j) \ddot{\theta}_j - C(\dot{\theta}_j, \theta_j) \dot{\theta}_j$. The new variable ΔF_{dyn} , representing uncompensated and/or unmodeled dynamics, can be considered as a disturbance force and considered as a contribution term to the overall external load force F_l expressed by:

$$F_l = F_h + \delta g + \Delta F_{dyn} \quad (4.6)$$

Introducing the following variable substitution for joint torque τ_s

$$\begin{cases} \tau_s = -K_t (D \theta_m - \theta_j) \\ \dot{\tau}_s = -K_t (D \dot{\theta}_m - \dot{\theta}_j) \\ \ddot{\tau}_s = -K_t (D \ddot{\theta}_m - \ddot{\theta}_j) \end{cases} \quad (4.7)$$

the dynamics Eq. (4.2) can be reformulated as follows:

$$\begin{cases} J_m D \ddot{\theta}_m + B_m D \dot{\theta}_m = K_t^{-1} C_t \dot{\tau}_s + \tau_s + u + \tau_d \\ \ddot{\tau}_s + C_t J_i^{-1} \dot{\tau}_s + K_t J_i^{-1} \tau_s = K_t J_m^{-1} B_m D \dot{\theta}_m + \bar{M}^{-1} K_t J^T F_l - K_t J_m^{-1} \tau_d - K_t J_m^{-1} u \end{cases} \quad (4.8)$$

where we defined $J_i^{-1} = \bar{M}^{-1}[\mathbf{I} + \bar{M}\bar{J}_m^{-1}]$, and \mathbf{I} is an identity matrix. This form of the dynamics equation is useful for defining a full-state feedback control law and an optimal observer for the estimation of joint torque.

4.3.2 EXOSUIT (SOFT EXOSUIT)

The torque applied by the exosuit on the wearer's joint is estimated from the tension measured by load cell on the suit's tendons, using Eqs. (4.11) and (4.12). Fig. 4.5 shows the schematics of the suit's tendon routing across the elbow joint, configured in an agonistic/antagonistic fashion. Using trigonometric relations, one can derive the mapping from a displacement of either tendon to a joint angle; we call these extension functions, $h_f(\theta)$ for the flexor and $h_e(\theta)$ for the extensor:

$$h_f(\theta) = 2\sqrt{a^2 + b^2} \cos\left(\tan^{-1}\left(\frac{a}{b}\right) + \frac{\theta}{2}\right) - 2b \quad (4.9)$$

$$h_e(\theta) = R\theta \quad (4.10)$$

where a is half of the width of the arm, b is the distance from the joint center of rotation to the anchor points, R is the radius of the elbow joint, and θ is the joint angle. From the two extension functions $h_f(\theta)$ and $h_e(\theta)$, we can compute the position-dependent moment arm of the cables' tension on the elbow's axis of rotation:

$$P(\theta) = \frac{dh(\theta)^T}{d\theta} \quad (4.11)$$

$$\tau_{exo} = P(\theta)f \quad (4.12)$$

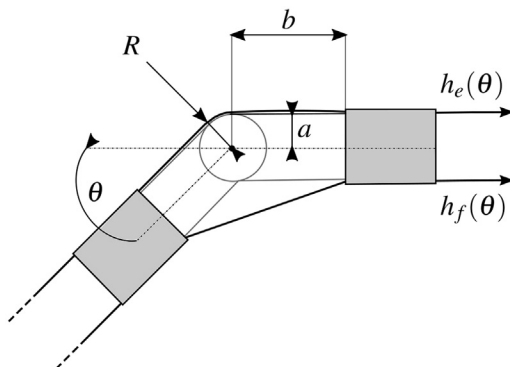


FIGURE 4.5

Planar model of the tendon routing across the elbow joint. In the top view the gray areas indicate the anchor points.

where f is the tension on the exosuit's tendons. This model assumes that the position of the anchor points is fixed: it neglects deformation of the fabric and soft tissues upon the application of a force from the tendons.

4.4 CONTROLS DESIGN

This section introduces the two control strategies that have been adopted to interact with the rigid and soft exoskeletons previously presented. The rigid exoskeleton implements a Direct Torque Control due to the presence of joint-torque sensors, whereas the soft exosuit uses an Admittance Control to interact with the human. The main difference between the two controls is the inner loop: the Direct Torque Control is based on a torque feedback loop, whereas the Admittance Control is based on a reference speed feedback loop compared with the speed computed from the measured force/torque at the joint. The following subsections address in more detail the two designed controls based on the models explained in the previous section.

4.4.1 DIRECT TORQUE CONTROL (RIGID EXOSKELETON)

Starting from the multiple joint dynamic model of the Rehab-Exos, a full-state feedback control law was designed. To implement the control, the state of the system and, more particularly, the joint torque was estimated through a Kalman Filter described in the following subsection. For the human–robot interaction, the proposed control law can be directly used to track a desired torque profile, such as for example, gravity compensation to aid the user with the arm weight during an assistive task.

4.4.1.1 An optimal observer for estimation of joint torque

The full-state feedback joint torque–based interaction control relies on the correct state estimation. From Eq. (4.8), the full system state is defined as $[\tau_{s,i}, \dot{\tau}_{s,i}, \theta_{m,i}, \dot{\theta}_{m,i}, \tau_{d,i}, \tau_{l,i}]$, where $\tau_l = J^T F_l$. The full-state can be estimated by means of the torque sensor raw measurement $\tau_{s,i}$ together with the measured joint position $\theta_{m,i}$. Thus a full-state Kalman filter has been designed to clean out both $\theta_{m,i}$ from quantization noise $w_{\theta,i}$ and $\tau_{s,i}$ from measurement noise $w_{\tau,i}$, as well as to estimate the remaining variables.

Following the work of Vertechy [25], the dynamics of the two state components $\tau_{d,i}$ and $\tau_{l,i}$ can be modeled as two distinct Wiener processes (i.e., as two distinct nonstationary random processes) $\dot{\tau}_{d,i} = v_{d,i}$ and $\dot{\tau}_{l,i} = v_{l,i}$. Starting from Eq. (4.8) the following metasystem can be derived:

$$\begin{cases} \dot{\tau}_i &= A_i \tau_i + B_i \tau_{m,i} + \Gamma v_i \\ y_i &= C \tau_i + w_i \end{cases} \quad (4.13)$$

where $\tau_i^T = [\dot{\tau}_{s,i} \tau_{s,i} \dot{\theta}_{m,i} \theta_{m,i} \tau_{l,i} \tau_{d,i}]$ is the metastate vector, $v_i^T = [v_{l,i} v_{d,i}]$ is the vector of process noises with variances $V_{l,i}$ and $V_{d,i}$, $w_i^T = [w_{\tau,i} w_{\theta,i}]$ is the vector of measurement noises with variances $W_{l,i}$ and $W_{d,i}$, whereas the state matrixes are defined as:

$$A_i = \begin{pmatrix} -c_{t,i} & -k_{t,i} & k_{t,i}b_{m,i} & 0 & k_{t,i} & -k_{t,i} \\ \frac{1}{J_i} & \frac{1}{J_i} & \frac{J_{m,i}}{J_{m,i}} & 0 & \frac{1}{J_{m,i}} & 0 \\ 1 & 0 & 0 & 0 & 0 & 0 \\ \frac{c_{t,i}}{k_{t,i}J_{m,i}} & \frac{1}{J_{m,i}} & \frac{-b_{m,i}}{J_{m,i}} & 0 & 0 & \frac{1}{J_{m,i}} \\ 0 & 0 & 1 & 0 & 0 & 0 \\ 0 & 0 & 0 & 0 & 0 & 0 \\ 0 & 0 & 0 & 0 & 0 & 0 \end{pmatrix} \quad (4.14)$$

$$B_i = \begin{bmatrix} -k_{t,i} \\ \frac{1}{J_{m,i}} \\ 0 \\ \frac{1}{J_{m,i}} \\ 0 \\ 0 \\ 0 \end{bmatrix} \Gamma = \begin{pmatrix} 0 & 0 \\ 0 & 0 \\ 0 & 0 \\ 0 & 0 \\ 1 & 0 \\ 0 & 0 \\ 0 & 1 \end{pmatrix} C = \begin{pmatrix} 0 & 0 \\ 1 & 0 \\ 0 & 0 \\ 0 & 1 \\ 0 & 0 \\ 0 & 0 \end{pmatrix}$$

4.4.1.2 A full-state feedback controller

The joint-torque control law rely on the full state obtained from Eqs. (4.13) and (4.14). The input control u is the sum of two terms: u_f , which implements control force behavior, and another term u_g , which acts as a gravity compensation. The two terms are defined as:

$$u_g = G(D\hat{\theta}_m) \quad (4.15)$$

$$u_f = -J_m K_t^{-1} \ddot{\tau}_s^D + B_m D\dot{\theta}_m + J_m \bar{M}^{-1} J^T \hat{F}_l - \hat{\tau}_d - J_i^{-1} J_m \tau_s^D + K_p e + K_d \dot{e} \quad (4.16)$$

where $e = \tau_s - \tau_s^D$ is the error on sensor torque, given the desired sensor torque τ_s^D . Under the assumption that $\dot{\tau}^D = 0$ and $\ddot{\tau}^D = 0$, so that $\dot{e} = \dot{\tau}_s$ and $\ddot{e} = \ddot{\tau}_s$, the expression (4.16) of u_f can be rewritten as

$$u_f = B_m D\dot{\theta}_m + J_m \bar{M}^{-1} J^T \hat{F}_l - J_i^{-1} J_m \tau_s^D - \hat{\tau}_d + K_p e + K_d \dot{e} \quad (4.17)$$

The use of the control laws (4.15) and (4.17) leads to stable error dynamics equations:

$$\ddot{\theta}_m = \ddot{\theta}_j - K_t^{-1} \ddot{e} \quad (4.18)$$

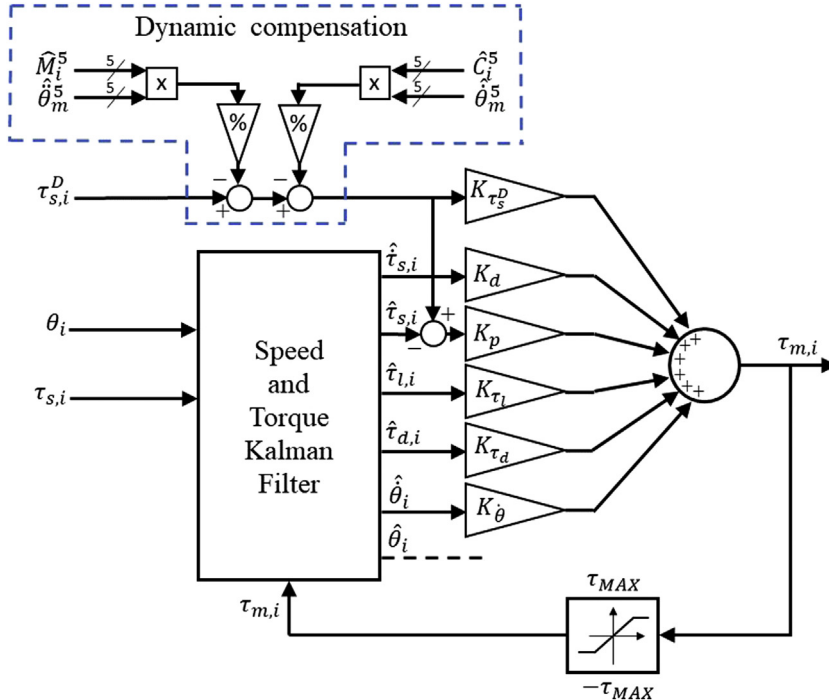
$$0 = \ddot{e} + (C_t J_i^{-1} + K_d K_t J_m^{-1}) \dot{e} + (K_t J_i^{-1} + K_p K_t J_m^{-1}) e \quad (4.19)$$

where the convergence of error e to zero can be tuned by choosing the proportional and derivative gains K_p and K_d , so obtaining the desired dynamic response.

In the schema of the direct force control (depicted in Fig. 4.6) the compensation of inertial effects has been added since the chosen inertial parameters are fixed values (see Eq. 4.5). The computation of dynamic compensation starts from an estimation of the joint acceleration (using a dedicated Kalman filter) and provides a higher accuracy in torque tracking. Note that the torque sensor reads $\tau_{s,i}$ and the commanded motor torques $\tau_{m,i}$ are net of the gravity compensation term u_g .

4.4.2 ADMITTANCE CONTROL (SOFT EXOSUIT)

The interaction controller for the soft exosuit that we propose here is an admittance scheme, in the sense that it has an outer torque loop and an inner velocity loop. The presence of nonlinearities in the

**FIGURE 4.6**

The schema of the full-state control feedback with the dynamic compensation of the i -th joint.

transmission, such as backlash and friction, combined with the complex viscoelasticity of soft human tissue, make a direct force control unpractical. Explicit admittance and impedance controllers are both good candidates, with the former benefiting from the robustness of the inner velocity/position loop [26].

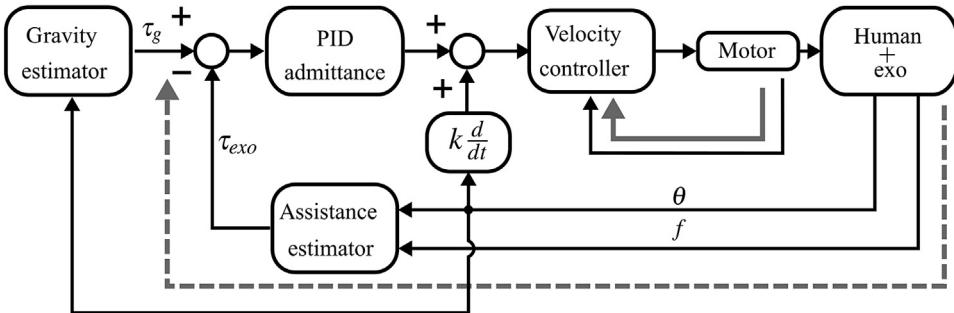
The controller for the soft exosuit for the elbow is shown in Fig. 4.7. Unlike traditional admittance controllers, the inner loop is closed on the motor rather than the joint: this configuration, baptized by Calanca and colleagues [26] *collocated admittance control*, allows the use of a high-gain position/velocity feedback loop to compensate for friction and backlash-related phenomena [27].

The outer loop (dotted arrow in Fig. 4.7) is responsible for tracking a position-dependent torque profile at the elbow, equal and opposite to gravity:

$$\tau_g = mgl_c \sin(\theta) \quad (4.20)$$

So that the torque exerted by the exosuit on the joint τ_{exo} (Eq. 4.12), is equal and opposite to gravity: the main idea is to make transparent the effect of gravity at the elbow joint. The error $\tau_g - \tau_{exo}$, is converted into a velocity for the motor, ω_d , by an admittance block of the form (in the Laplace domain):

$$Y(s) = \frac{\omega_d}{\tau_g - \tau_{exo}} = K_P + \frac{K_I}{s} + K_{DS} \quad (4.21)$$

**FIGURE 4.7**

Collocated admittance controller for indirect force control and gravity compensation. An outer torque loop tracks a position-dependent profile, equal and opposite to gravity, sending a velocity reference to an inner velocity controller. An additional positive feedback increases transparency of the suit.

with the K_P , K_I , and K_D constants governing the characteristics of the relation between the interaction force and the motor's velocity [28].

A low-level, PI velocity loop (continuous arrow in Fig. 4.7) tracks the desired velocity on the motor's axis.

Finally, a positive feedback term is added to the desired velocity, to increase the controller's sensitivity to the user's movement and compensate for the dynamic friction of the cable transmission. This strategy is commonly used to compensate for stick-slip friction phenomena, but it here facilitates initiation of movement, making the exosuit more transparent [29]. The final desired velocity, tracked by the low-level motor driver, has the form:

$$\omega_d = K_P(\tau_g - \tau_{exo}) + \frac{K_I}{s}(\tau_g - \tau_{exo}) + K_D s(\tau_g - \tau_{exo}) + ks\theta \quad (4.22)$$

4.5 EXPERIMENTAL SETUP

The performance of the two proposed controllers have been evaluated by measuring the accuracy in a torque tracking task. The experimental design was conceived to test the devices in their final applications. The last part of this section is devoted to the evaluation of both exoskeletons in performing an assistive task that involves the user's elbow.

4.5.1 EVALUATION OF THE DIRECT TORQUE CONTROL (RIGID EXOSKELETON)

The direct torque control, implemented for the rigid Exos, was used to track both constant and varying desired torques. To evaluate the exoskeleton performance and to quantify how it affects the user motion, we performed the *transparency test*. In this experiment the robot tries to keep the joint torque at zero Nm while the user is moving the exoskeleton.

The control gains (Fig. 4.6) K_{τ_s} , K_{τ_I} , K_{τ_d} , and $K_{\dot{\theta}}$ were set using the model parameters, whereas the proportional and derivative PD gains (K_p and K_d) have been chosen to obtain a desired error dynamics, that is, the form that guarantees the minimum ITAE index (Integral of Time multiplied by the Absolute magnitude of the Error) [30].

4.5.1.1 Transparency

The *transparency test* is designed to involve all the 4 joints of the Rehab-Exos and to test their torque tracking behavior. The user was asked to wear the exoskeleton and to perform a circumference at constant speed. The center of the desired circumference was chosen in the middle of the workspace and with a diameter of 300 mm. An example of the recorded end-effector position during the transparency test is depicted in Fig. 4.8. During the transparency tests the user has been linked with the exoskeleton at two points: at the upper extremity of the arm to transmit the shoulder movement, and at the hand in order to exchange the elbow movement. With the hand, the user grasps the 6-DOF force/torque sensor located at the end-effector of the exoskeleton.

For the transparency index, the measured end-effector norm force $|F_h^*|$ applied by the user and the joint torques estimated by the observer have been used.

4.5.2 EVALUATION OF THE ADMITTANCE CONTROL (SOFT EXOSUIT)

The admittance controller for gravity compensation in the soft exosuit was tested on human subjects to determine its accuracy (*test 1*) and bandwidth (*test 2*). In both tests, we kept the human user in the loop, to replicate the conditions of the application the device was designed for. Two participants, wearing the exosuit, were asked to match the movement of a character on a screen as accurately as possible. The screen showed the reference and actual position of the elbow angle, allowing the subject to intuitively follow the desired profile.

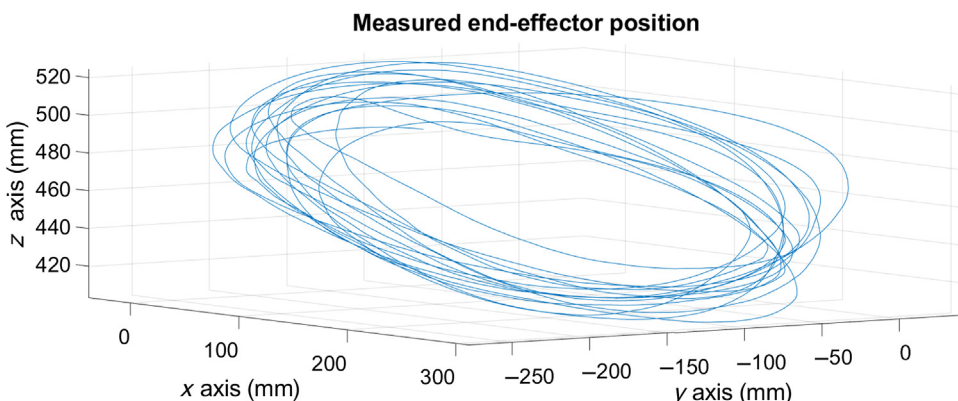


FIGURE 4.8

End-effector positions that were recorded during the transparency tests. The user was able to perform circles due to high transparency of the exoskeleton.

In the *accuracy* test, the reference motion consisted of a series of Minimum Jerk Trajectories (MJT), known to accurately replicate to the movements of healthy subjects [31]. Trajectories to track were presented to subjects at varying peak velocities, chosen to be fractions of the average elbow speed in activities of daily living (ADLs), that is, 126 degrees/s [32]. The performances of the outer and inner loop were evaluated in terms of the Root Mean Square (RMSE) between the desired and measured profiles.

In the *bandwidth* test, the reference trajectory consisted of a sinusoidal signal of the form

$$\theta_d(t) = A_0 + A \sin(2\pi f(t)t) \quad (4.23)$$

with $A_0 = A = 40^\circ$, chosen to cover a reasonable range of motion of the joint, and $f(t)$ being a step-wise varying frequency in increasing steps of 0.05 Hz, between 0.05 and 0.9 Hz. These values were chosen as they correspond to movements with a peak velocity between 12.5 and 226 degrees/s, equivalent to 10%–180% of the speed of the elbow in daily tasks. Each velocity value was held for 20 seconds; the first 5 seconds were discarded to allow evaluation of the response at steady state. For each frequency/velocity, we evaluated the ratio between the Fourier coefficients of the first harmonic of the measured and desired elbow angles, to derive a magnitude and phase plot:

$$H(f_0) = \frac{C_1(\theta_m)}{C_1(\theta_d)}. \quad (4.24)$$

We collected kinematic data (AMS, AS5047P, 1000 pulses/rev) and tension on the exosuits' flexing tendon (Futek, LCM300). The control algorithm and the data acquisition were handled by a National Instrument PCI6025e acquisition board, at a 1 kHz refresh rate.

4.6 RESULTS

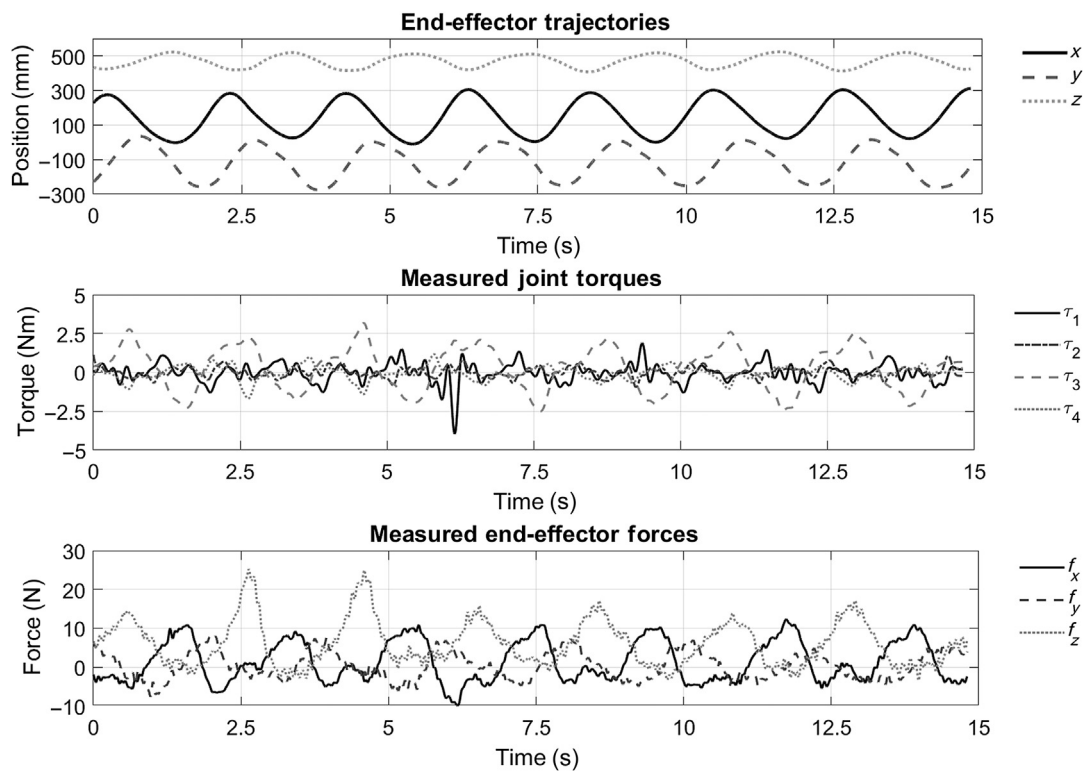
4.6.1 EVALUATION OF THE DIRECT TORQUE CONTROL (RIGID EXOSKELETON)

4.6.1.1 Transparency

The results of the transparency tests are reported in Fig. 4.9 and summarized in Table 4.1. The trajectories performed by the user are reported on the top plot of Fig. 4.9 and show that the user was able to perform smooth ellipses with an average eccentricity of 0.402 ± 0.11 . The user was not hindered in performing the desired path, however a perturbation was introduced by the exoskeleton. Regarding the z axis, the user did not have any cues on the third dimension, so the small oscillation can be neglected.

The forces experienced by the user at the end-effector are reported on the bottom plot of Fig. 4.9. Their shapes clearly follow the position trends that were imposed by the user. From these results we can infer the control error is due to an imperfect or incomplete dynamic compensation, in fact the circular task causes acceleration and deceleration phases during its execution. The same trend is not clearly visible in the measured joint torques reported in the central plot of Fig. 4.9. This is because the task was defined in a 2D plane whereas the exoskeleton contributes to the motion with four DOFs.

As a numerical index, the RMS of the interaction torques as well as the RMS of the force norm highlight a high level of transparency (see Table 4.1). The joints J_1, J_2 , and J_4 exhibit an RMS less

**FIGURE 4.9**

The results of the transparency test of the Rehab-Exos. The user is not hindered by performing a circular trajectory in the XY plane (the z coordinate has a small variation compared to the x and y axis) at constant speed (top plot). The joint torques (central plot) are small compared to the maximum torque that can be exerted by the joints and only the J_3 torque (the dashed gray line) exhibits a sinusoidal evolution. The bottom plot reports the forces measured at the end-effector that are always smaller than 25 N.

Table 4.1 The RMS of the Joint Torques and of the End-Effector Force as an Index of the Exoskeleton Transparency

Joint/end-effector	RMS
J_1	0.9707 (Nm)
J_2	0.9514 (Nm)
J_3	1.4270 (Nm)
J_4	0.6034 (Nm)
End-effector	11.1870 (N)

than 1 Nm, whereas the joint J_3 has an RMS of 1.427 Nm. Despite these values seeming high to some readers, it is worth being reminded that the maximum torque of the Rehab-Exos joints is about 150 Nm and, secondly, the RMS of the end-effector force norm is 11.18 N. This means moving the exoskeleton in transparency mode can be seen by the user as if it is executing the task in free space while handling a 1.1 kg mass.

4.6.2 EVALUATION OF THE ADMITTANCE CONTROL (SOFT EXOSUIT)

4.6.2.1 Transparency

[Fig. 4.10](#) shows the desired and measured profiles of both layers of the admittance controller. The bottom plot displays the tracking accuracy of the outer torque loop, for one subject and movements with a peak velocity of 84 degrees/s. The reference trajectory is a position-dependent estimate of the torque acting on the elbow because of the weight of the forearm. The controller shows overshoots in the rising transient region and before the downward motion. The Root Mean Square Error (RMSE), over subjects and velocities, was found to be 8.7% of the range of desired torques.

The top plot of [Fig. 4.10](#) shows the accuracy of the inner velocity loop, tracking the speed of the pulley on the motor's shaft, for the same repetitions. This PID was tuned to be as stiff as possible, to stably reject nonlinearities in the transmission. The RMSE, over subjects and velocities, was found to be 2.8% of the range of desired motor speeds.

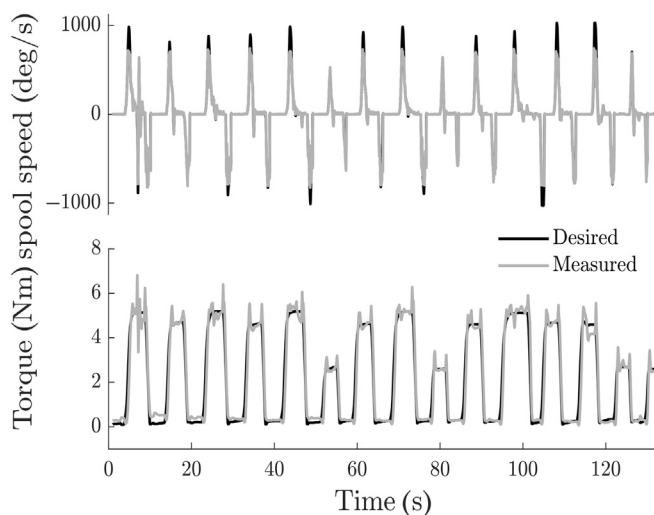
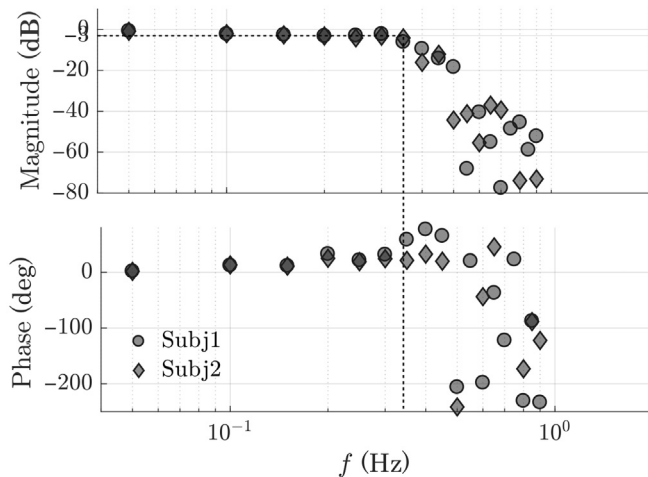


FIGURE 4.10

Tracking accuracy of the admittance controller. The top plot shows the tracking of the inner velocity loop. The bottom plot shows the desired and measured torque delivered at the elbow joint.

**FIGURE 4.11**

Bandwidth of the exosuit with the user in the loop. While wearing the exosuit, subjects could follow a sinusoidal signal of up to 0.35 Hz, corresponding to a peak velocity of 88 deg/s.

4.6.2.2 Control bandwidth

The magnitude and phase of $H(f_0)$ (Eq. 4.24) were calculated to derive a Bode plot of the exosuit's position tracking accuracy, shown in Fig. 4.11.

The system has a bandwidth of 0.35 Hz, corresponding to a peak velocity of movement of 88 degrees/s. This is highlighted with a dotted line in Fig. 4.11, where it corresponds to an average phase of 40 degrees or 0.3 seconds of delay.

4.6.3 ASSISTIVE PERFORMANCE: REHAB-EXOS VERSUS EXOSUIT

The previous experiments were focused on the characterization of the controller performance in order to find their limitations in terms of transparency and control accuracy. In the present section the two devices were used for a further task: to evaluate the biomechanical and physiological effects on the user arm movements and compare them.

Two healthy male subjects (age 27.5 ± 0.7 years, no reported injuries or impairments in the upper limbs) were asked to perform repetitive elbow flexion/extension movements, while holding a 1.25 kg load in their hand.

The tests were performed on a single joint (the elbow), testing separately the same task with the rigid exoskeleton and the soft exosuit. The goal was to investigate the change in muscular activation of the biceps brachii when lifting a light load and comparing the performance of the two exoskeletal systems [33].

The reference movement was shown to the subjects on a screen, by means of a virtual avatar representing a human arm, while the actual position of the subjects' elbow was depicted as a shadowed arm (see Fig. 4.12). The speeds were chosen to be 20%, 30%, and 60% of the average

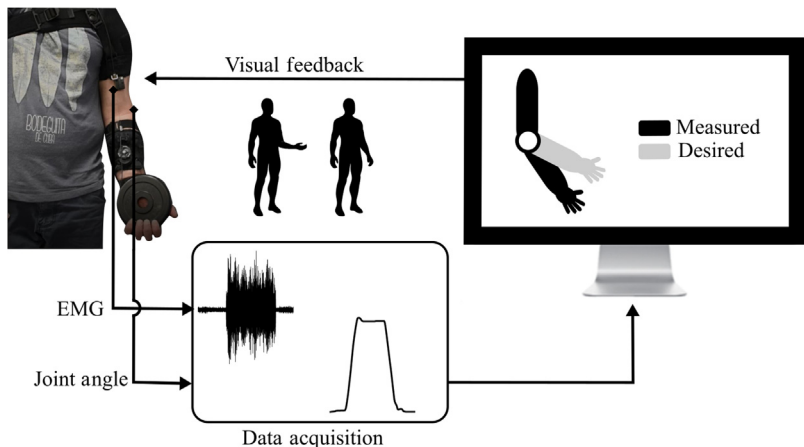


FIGURE 4.12

Schema of the experimental setup. Subjects were asked to follow a visual reference trajectory at three different speeds. During the experiment, the elbow angle, the interaction force (only powered) and EMG activity of the biceps brachii were collected.

elbow velocity in ADLs: 20, 25, and 50 degrees/s, respectively [34]. The experiments were conducted in three distinct randomized phases to avoid predictability and adaptation by the subjects:

- wearing the rigid exoskeleton
- wearing the soft exosuit
- without any assistance

We monitored the assistive torque and estimated the muscular effort from the RMS of the electromyography (EMG) of the biceps brachii. We positioned the electrodes according to the SENIAM standards [35].

Between phases, subjects rested for at least 5 minutes to avoid muscular fatigue. Subjects performed 10 repetitions with and 10 without the exoskeleton/exosuit for each velocity, following a reference trajectory of the joint shown on a screen.

The EMG signal was acquired using an external system, that is, g.USBamp (g.tec Inc.). It was acquired at 1 kHz rate, then preprocessed using a full-wave rectification and low-pass filtered by a second-order Butterworth filter with an 8 Hz cutoff frequency. The real-time postprocessed signal was sent to the main control system to collect synchronized data. A schematic of the assistance task setup is shown in Fig. 4.12.

The goal of the assistive tasks experiment (when wearing the exoskeletons) was to quantify the reduction of the user muscular activation and to provide relief during task execution. The effect on the torque required to flex the elbow resulting from wearing either the Rehab-Exos or the soft exosuit can be seen in Fig. 4.13A. Values are reported as a percentage of the total amount of torque required to perform the lifting movement. The Rehab-Exos provides a slightly higher assistive torque, relieving its wearer from a greater part of the effort required to flex the joint.

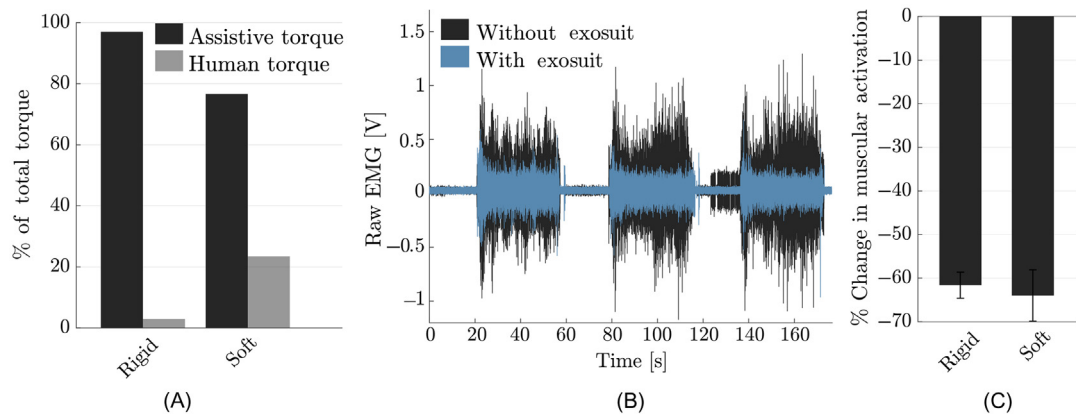


FIGURE 4.13

Comparison of the assistive torque and percentage reduction in muscular activity when wearing the rigid exoskeleton and soft exosuit. (A) The rigid exoskeleton provided nearly the entire torque required to support the elbow position; the torque that the wearer needed to exert was higher when wearing the exosuit. (B) Amplified electromyography from the biceps brachii, comparison between the case of no assistance and assistance with the exosuit. (C) The bar plot presents the reduction in muscular activity resulting from wearing the exoskeleton or exosuit.

As expected the EMG activity from the biceps brachii shows significant reduction between the conditions with versus without assistance, meaning that wearing the devices leads to a decrease of muscular activation during the lifting task.

Fig. 4.13B shows the muscular activity when flexing the elbow in the three conditions with and without the soft exosuit; the difference between them is used to compute the percentage reduction of effort from wearing the device. A similar analysis for both systems, averaged across repetitions and subjects, is shown in Fig. 4.13C: both produce an average reduction in the activation of the biceps brachii, of -61.63% and -63.97% for the rigid and soft device, respectively.

The Rehab-Exos provides a higher part of the torque required to move the arm (97.05%) with respect to the one provided by the soft exosuit (76.63%), this, however, did not result in a greater reduction of muscular activity.

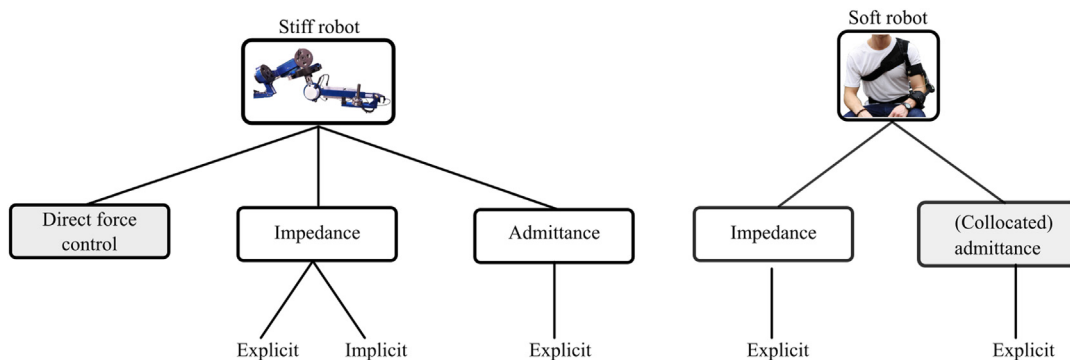
4.7 DISCUSSION

Table 4.2 summarizes the key aspects of the rigid and soft wearable robots tested in the actual study. While the exosuit stands out for its low weight and power consumption, making it ideal for mobile applications, the rigid device has higher torque rating, bandwidth, and power efficiency.

As expected, the Rehab-Exos provides a higher part of the torque required to move the arm but this did not result in a greater reduction of muscular activity. This might be caused by misalignments

Table 4.2 Performance of the Exoskeleton Versus the Exosuit

	Rigid	Soft
Characteristics		
Frame material	Aluminum	Fabric
Motor location	Joints	Waist
Weight (kg)	17	1.2
DOF	5	1
Maximum torque (Nm)	150	10
Bandwidth (Hz)	39.7	1.1
Power Consumption (W)	25.65	13.71
Efficiency	0.26	0.14
Physiological effects (% of the no-exo case)		
Muscular activity	- 61.63	- 63.97
Human torque	- 97.05	- 76.63

**FIGURE 4.14**

Force control paradigms for stiff and soft robots.

between the robot's kinematic chain and the human skeleton, known to be a source of unwanted parasitic torques in the human joints [36]. Further studies are needed to verify this point.

It is worth noting that the comparison was made with two different control architectures driving the devices, both falling under the broad category of force control.

The alternative for the implementation of force control in soft and stiff robots are summarized in Fig. 4.14. Following the notation adopted by Calanca and colleagues [26], “explicit” and “implicit” respectively refer to the presence and lack of a force sensor at the interface between the user and the device.

While the deterministic nature of the Rehab-Exos allowed us to implement a direct force controller, this is an unlikely choice for a soft device, where one would benefit from the combination of a force loop with a position/velocity loop. The presence of elasticity in the soft exosuit

introduces a higher order dynamics and the need for a force sensor at the interface between the robot and the environment. This is similar to how SEAs are controlled, where the deformation of a compliant element of known elasticity is used, in combination with a robust position/velocity controller, to achieve safe and accurate force tracking. Indirect force control, including impedance and admittance controllers, are the most appropriate candidates.

As is often the case in soft devices, moreover, the transmission might be characterized by complex and configuration-dependent effects such as stiction, stick-slip, backlash, and nonlinear stiffness. One could either choose to identify and compensate for these phenomena [37] or, as we did in this work, choose a “lazy” and less principled approach. By choosing an admittance controller and closing a high-gain inner velocity loop on the motor’s axis rather than on the joints’ axis, one can filter out most nonlinearities with very little effort. This approach has been shown to reduce stick-slip phenomena in a legged robot powered by series elastic actuators [27].

4.8 CONCLUSION

The variety of hardware architectures for wearable robots that assist human joints requires an equally rich assortment of control schemes. As compliant and hyperredundant robots attract interest in the context of HRI, it is important to define the advantages and limitations of hardware and control choices.

In this chapter we proposed a simple taxonomy for wearable robots, based on the compliance and redundancy of the hardware, and detailed the control choice for two devices on the opposite side of the spectrum (Fig. 4.1). Our findings highlight the strengths and weaknesses of each approach and can serve as a tutorial for a growing number of engineers and research groups that are designing stiff and soft robots for human motion assistance and augmentation.

REFERENCES

- [1] R. Mosher, Handyman to hardiman, *SAE Trans.* 76 (1) (1967) 588–597.
- [2] T. George Thuruthel, Y. Ansari, E. Falotico, C. Laschi, Control strategies for soft robotic manipulators: a survey, *Soft Robot.* 5 (2) (2018). p. soro.2017.0007.
- [3] A. Albu-Schaeffer, et al., Soft robotics, *IEEE Robot. Autom. Mag.* 15 (3) (2008) 20–30.
- [4] C. Laschi, B. Mazzolai, M. Cianchetti, Soft robotics: technologies and systems pushing the boundaries of robot abilities, *Sci. Robot.* 1 (1) (2016) 1–12.
- [5] E. Pirondini, et al., Evaluation of the effects of the Arm Light Exoskeleton on movement execution and muscle activities: a pilot study on healthy subjects, *J. Neuroeng. Rehabil.* 13 (1) (2016) 1–21.
- [6] R. Vertechy, A. Frisoli, A. Dettori, M. Solazzi, M. Bergamasco, Development of a new exoskeleton for upper limb rehabilitation, *IEEE Int. Conf. Rehabil. Robot.* (2009) 188–193.
- [7] N. Vitiello, et al., NEUROExos: a powered elbow exoskeleton for physical rehabilitation, *IEEE Trans. Robot.* 29 (1) (2013) 220–235.
- [8] K. Xu, D. Qiu, Experimental design verification of a compliant shoulder exoskeleton, *Proc. - IEEE Int. Conf. Robot. Autom.* (2013) 3894–3901.

- [9] C.T. O'Neill, N.S. Phipps, L. Cappello, S. Paganoni, C.J. Walsh, A soft wearable robot for the shoulder: design, characterization, and preliminary testing, *IEEE Int. Conf. Rehabil. Robot.* 02129 (2017) 1672–1678.
- [10] J.C. Perry, J. Rosen, S. Burns, Upper-limb powered exoskeleton design, *IEEE/ASME Trans. Mech.* 12 (4) (2007) 408–417.
- [11] G.A. Pratt, M.M. Williamson, Series elastic actuators, *IEEE/RSJ International Conference on Intelligent Robots and Systems. “Human Robot Interaction and Cooperative Robots 1* (1524) (1995) 399–406.
- [12] K. Xu, Y. Wang, Z. Yang, Design and preliminary experimentation of a continuum exoskeleton for self-provided bilateral rehabilitation, *IEEE International Conference on Information and Automation (ICIA)* (2014) 327–332.
- [13] Y. Jiang, D. Chen, P. Liu, X. Jiao, Z. Ping, Z. Xu, Y. Xu, Fishbone-inspired soft robotic glove for hand rehabilitation with multi-degrees-of-freedom, *IEEE International Conference on Soft Robotics (RoboSoft)* (2018) 394–399.
- [14] A.T. Asbeck, S.M.M. De Rossi, I. Galiana, Y. Ding, C.J. Walsh, Stronger, smarter, softer: next-generation wearable robots, *IEEE Robot. Autom. Mag.* 21 (4) (2014) 22–33.
- [15] H. In, B.B. Kang, M.K. Sin, K.J. Cho, Exo-glove: a wearable robot for the hand with a soft tendon routing system, *IEEE Robot. Autom. Mag.* 22 (1) (2015) 97–105.
- [16] M. Xiloyannis, L. Galli, D. Chiaradia, A. Frisoli, F. Braghin, L. Masia, A soft tendon-driven robotic glove: preliminary evaluation, *Biosyst. Biorobot.* 21 (October) (2019) 329–333.
- [17] M. Xiloyannis, D. Chiaradia, A. Frisoli, L. Masia, Characterisation of pressure distribution at the interface of a soft exosuit: towards a more comfortable wear, *Wearable Robot. Challenges Trends* (2019) 35–38.
- [18] H.S. Lo, S.Q. Xie, Exoskeleton robots for upper-limb rehabilitation: state of the art and future prospects, *Med. Eng. Phys.* 34 (3) (2012) 261–268.
- [19] M.J. Kim, W. Lee, J.Y. Choi, Y.S. Park, S.H. Park, G. Chung, W. K. Chung, Powered upper-limb control using passivity-based nonlinear disturbance observer for unknown payload carrying applications, *IEEE International Conference on Robotics and Automation (ICRA)* (2016) 2340–2346.
- [20] D. Buongiorno, E. Sotgiu, D. Leonardis, S. Marcheschi, M. Solazzi, A. Frisoli, WRES: a novel 3 DoF wrist exoskeleton with tendon-driven differential transmission for neuro-rehabilitation and teleoperation, *IEEE Robot. Autom. Lett.* 3 (3) (2018) 2152–2159.
- [21] D. Buongiorno, D. Chiaradia, S. Marcheschi, M. Solazzi, A. Frisoli, Multi-DoFs exoskeleton-based bilateral teleoperation with the time-domain passivity approach, *Robotica* 37 (9) (2019) 1641–1662.
- [22] C. Walsh, Human-in-the-loop development of soft wearable robots, *Nat. Rev. Mater.* 3 (6) (2018) 78–80.
- [23] S. Oh, K. Kong, High-precision robust force control of a series elastic actuator, *IEEE/ASME Trans. Mech.* 22 (1) (2017) 71–80.
- [24] D. Chiaradia, M. Xiloyannis, C.W. Antuvan, A. Frisoli, L. Masia, Design and embedded control of a soft elbow exosuit, *2018 IEEE Int. Conf. Soft Robot. Robo Soft 2018* (2018) 565–571.
- [25] R. Vertechy, A. Frisoli, M. Solazzi, D. Pellegrinetti, M. Bergamasco, An interaction-torque controller for robotic exoskeletons with flexible joints: preliminary experimental results, *IEEE Int. Conf. Intell. Robot. Syst.* (2012) 335–340.
- [26] A. Calanca, R. Muradore, P. Fiorini, A review of algorithms for compliant control of stiff and fixed-compliance robots,”, *IEEE/ASME Trans. Mech.* 21 (2) (2016) 613–624.
- [27] G.A. Pratt, P. Willisson, C. Bolton, A. Hofman, Late motor processing in low-impedance robots: impedance control of series-elastic actuators, *Proc. Am Control Conf.* 4 (2004) 3245–3251.
- [28] J. Rosen, W. Yu, X. Li, PID admittance control for an upper limb exoskeleton, *Proc. 2011 Am. Control Conf.* (2011) 1124–1129.

- [29] H. Kazerooni, J.L. Racine, L. Huang, R. Steger, On the control of the Berkeley Lower Extremity Exoskeleton (BLEEX), Proc. IEEE Int. Conf. Robot. Autom. (2005) 4353–4360.
- [30] W. Levine, The Control Handbook, Control System Fundamentals, second ed., CRC Press, Boca Raton, 2010.
- [31] T. Flash, N. Hogan, The coordination of arm movements: an experimentally confirmed mathematical model, *J. Neurosci.* 5 (7) (1985) 1688–1703.
- [32] M.A. Buckley, A. Yardley, G.R. Johnson, D.A. Cams, Dynamics of the upper limb during performance of the tasks of everyday living: a review of the current knowledge base, *J. Eng. Med.* 210 (4) (1996) 241–247.
- [33] D. Chiaradia, M. Xiloyannis, M. Solazzi, L. Masia, A. Frisoli, Comparison of a soft exosuit and a rigid exoskeleton in an assistive task, *Biosyst. Biorobot.* 22 (2019) 415–419.
- [34] H.J. Hermens, B. Freriks, C. Disselhorst-Klug, G. Rau, Development of recommendations for SEMG sensors and sensor placement, *J. Electromyogr. Kinesiol* 10 (5) (2000) 361–374.
- [35] M.B. Weinger, M.E. Wiklund, D.J. Gardner-Bonneau, Handbook of Human Factors in Medical Device Design, CRC Press, 2010.
- [36] A. Schiele, F.C.T. Van Der Helm, Kinematic design to improve ergonomics in human machine interaction, *IEEE Trans. Neural Syst. Rehabil. Eng.* 14 (4) (2006) 456–469.
- [37] B.K. Dinh, M. Xiloyannnis, C.W. Antuvan, L. Cappello, L. Masia, Hierarchical cascade controller for assistance modulation in a soft wearable arm exoskeleton, *IEEE Robot. Autom. Lett.* 2 (3) (2017) 1.

EXO-UL UPPER LIMB ROBOTIC EXOSKELETON SYSTEM SERIES: FROM 1 DOF SINGLE-ARM TO (7 + 1) DOFS DUAL-ARM

Yang Shen and Jacob Rosen

Bionics Lab, Department of Mechanical and Aerospace Engineering, University of California, Los Angeles, CA,
United States

5.1 INTRODUCTION

Stroke is a global health care problem that is common, serious, and disabling [1]. According to the American Heart Association report [2], every year there are around 795,000 people who experience a new or recurrent stroke and every 4 minutes someone dies from the disease. After a stroke, over 50% of persons have mild to severe weakness of the affected upper extremity that is managed by physical therapies to try to improve skillful arm and hand movements, strength, speed, and coordination [3]. Due to the lack of experienced physical therapists, engineers and scientists looked into automating the poststroke rehabilitation using machines.

Integrating human and robot into a single system offers remarkable opportunities for creating a new generation of assistive/rehabilitation technology for both healthy and disabled people. Humans possess naturally developed algorithms for control of movement, but they are limited by their muscle strength. In addition, muscle weakness is the primary cause of disability for most people with neuromuscular diseases and injuries to the central nervous system. In contrast, robotic manipulators can perform tasks requiring large forces; however, their artificial control algorithms do not provide the flexibility to perform in a wide range of fuzzy conditions while preserving the same quality of performance as humans. It seems therefore that combining these two entities, the human and the robot, into one integrated system under the control of the human, may lead to a solution that will benefit from the advantages offered by each subsystem. The first wave of attempts generated some manipulandum-like handheld devices, but since multijoint coordination is more of an interest, exoskeleton-like arm-covering robots attracted attention and became the main focus of rehabilitative robotics research.

The exoskeleton robot, serving as an assistive device, is worn by the human (orthotic) and functions as a human-amplifier. Its joints and links correspond to those of the human body, and its actuators share a portion of the external load with the operator.

The goal of this research is to design, build, and study the integration of a powered exoskeleton controlled by the intention of the human arm. The research will pursue this goal through several

objectives: (1) developing an 8 degrees of freedom (DOFs) powered anthropomorphic exoskeleton for the arm, including grasping/releasing; (2) developing control algorithms that will fuse information from multiple sensors and will guarantee stable exoskeleton operation; and (3) evaluating the overall performance of the integrated system using standardized arm/hand function tests. These goals and objectives will be pursued using several experimental protocols aimed at developing the controllers and evaluating the exoskeleton performance. The proposed experimental protocol includes only healthy subjects as the first step in a long-term goal aimed at evaluating the exoskeleton performance with disabled subjects suffering from various neurological disabilities, such as stroke, spinal cord injury, muscular dystrophies, and other neurodegenerative disorders.

The development of this series of upper limb rehabilitation robotic exoskeleton systems in the Bionics Lab (University of Washington, University of California Santa Cruz, and University of California Los Angeles) integrates hardware, firmware, and software that includes human in the loop. This chapter illustrates the process of developing these four generations of upper limb exoskeletons: EXO-UL1 (myosignal-based, single-arm), EXO-UL3 (myosignal-based, single-arm), EXO-UL7 (force/torque-based, dual-arm), and EXO-UL8 (force/torque-based, dual-arm), as well as some ongoing research work.

5.2 EXOSKELETON SYSTEMS

5.2.1 PROTOTYPE 1 (EXO-UL1)

As the beginning of this serial research on rehabilitative robotic exoskeletons, the first exoskeleton mechanism consisted of a two-link, two-joint device corresponding to the upper and the lower arm and to the shoulder and elbow joints of the human body [4–6].

Shown in Fig. 5.1, the system included a weight plate (external load) that can be attached to the tip of the exoskeleton forearm link. The mechanism was fixed to the wall and positioned parallel to the sagittal plane of the operator. The human/exoskeleton mechanical interface included the upper arm bracelet, located at the upper arm link, and a handle grasped by the operator. This two-joint mechanism was used as a 1-DOF system by fixing the system shoulder joint at specific angles in the range of 0–180 degrees. The elbow joint was free to move in an angle range of 0–145 degrees, and included built-in mechanical constraints which kept the exoskeleton joint angle within the average human anthropometric boundaries. Since the human arm and the exoskeleton were mechanically linked the movements of the forearms of both the human and the exoskeleton were identical.

The basic purpose of the exoskeleton system as an assistance device is to amplify the moment generated by the human muscles relative to the elbow joint, while manipulating loads. The exoskeleton's elbow joint was powered by a DC servo motor (ESCAP-35NT2R82) with a stall torque of 360 mNm equipped with a planetary gearbox (ESCAP-R40) with a gear ratio of 1:193 and a maximal output torque of 40 Nm. An optical incremental shaft encoder (HP HEDS 5500) with 500 lines was attached to the motor shaft. Due to the encoder location and the high gear ratio, the practical encoder's resolution for measuring the joint angle was 0.0036 degrees. This setup incorporated a DC motor with the highest torque-to-weight ratio that was available on the commercial market at that time with power consumption that could be provided by a battery. A high energy density of the power supply and an actuator with a high torque-to-weight ratio are two key features of the

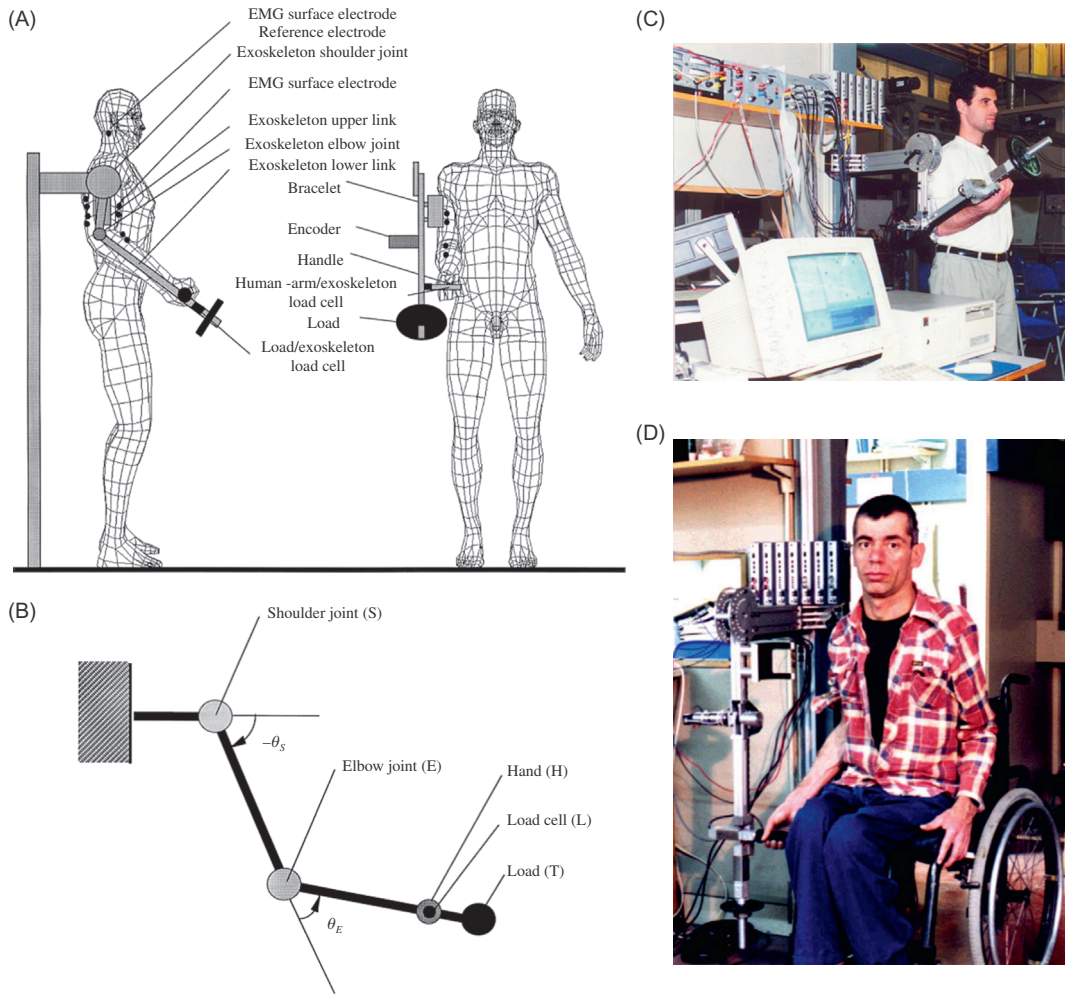


FIGURE 5.1

(A) Frontal and lateral view of the experimental setup: the exoskeleton and human operator. (B) Schema of the two-link, two-joint exoskeleton. (C) A human operator is using the exoskeleton device. (D) The EXO-UL1 system tested with a disabled person suffering from Tay-Sachs [7].

exoskeleton system as a self-contained mobile medical assistance device for the disabled community. Limits imposed by the technologies at that time on these two key components along with design requirements for developing a compact system with a potential of serving as a medical assistance device for disabled person restricted the payload to 5 kg. However, this biomedical-oriented design does not restrict the generality of the exoskeleton concept or its operational algorithms. Using other actuation systems, like a hydraulic system, increases the load capacity substantially.

The exoskeleton forearm was extended by a rod with a special connector for attaching disk-type weights (external load). Two force sensors (TEDEA 1040) were mounted at the interfaces between the exoskeleton and the tip carrying the external load and between the exoskeleton and the human hand. The first load cell, inserted between the rod holding the external load and the exoskeleton forearm link, measured the actual shear force, normal to the forearm axis, applied by the external load. The second load cell was installed between the handle grasped by the human hand and the forearm link of the exoskeleton. This load cell measured the shear force applied by the operator to the handle. Multiplying the sensors' measurements by the corresponding moment arms indicated the moments applied by the weights and by the human hand relative to the elbow joint.

One of the primary innovative ideas of the research was to set the Human Machine Interface (HMI) at the neuromuscular level of the human physiological hierarchy using the body's own neural command signals as one of the primary command signals of the exoskeleton. These signals will be in the form of processed surface electromyography (sEMG) signals, detected by surface electrodes placed on the operator's skin. The originally proposed HMI takes advantage of the electrochemical-mechanical delay, which inherently exists in the musculoskeletal system, between the time when the neural system activates the muscular system and the time when the muscles generate moments around the joints. The myoprocessor is a model of the human muscle running in real-time and in parallel to the physiological muscle. During the electrochemical-mechanical time delay, the system will gather information regarding the physiological muscle's neural activation level based on processed sEMG signals, the joint position, and angular velocity, and will predict, using the myoprocessor, the force that will be generated by the muscle before physiological contraction occurs. By the time the human muscles contract, the exoskeleton will move with the human in a synergistic fashion, allowing natural control of the exoskeleton as an extension of the operator's body.

Surface EMG electrodes (8 mm Ag-AgCl BIOPAC—EL208S) were attached to the subject's skin by adhesive disks for measuring the EMG signal of the biceps brachii and triceps brachii medial-head muscles. The signals were gained by EMG amplifiers (BIOPAC—EMG100A) using a gain factor in the range of 2000–5000 (depending on the subject). The EMG signals and the load cell signal were acquired by an A/D convector (Scientific Solution Lab Master 12-bit internal PC card) with a 1 kHz sampling rate, whereas the encoder signals were counted by custom-made hardware. The entire data set was recorded simultaneously and stored, for later off-line analysis and simulation.

A special real-time software, for operating the system, was written in C and run on a PC-based platform. The software was composed of three main modules. The first module dealt with the hardware/software interface. It controlled the interaction between the PC and the external motor driver and the sensors, through a D/A and an A/D card. The second module included the automatic code generated by the MATLAB—Simulink Real-Time toolbox. The third module was the user interface module which allowed setting of various run time operational parameters. All the modules were compiled and linked for generating an efficient real-time software.

5.2.2 PROTOTYPE 2 (EXO-UL3)

The second exoskeleton mechanism, shown in Fig. 5.2 [7], consisted of a three-link, two-joint device corresponding to the upper and the lower arm and the shoulder and elbow joints of the



FIGURE 5.2

EXO-UL3 Robotic Exoskeleton System.

human body. The hardware is similar to the first mechanism except that it was used as a 2-DOF system: the elbow and the shoulder joints were free to move in their anatomical range of motion.

Four force sensors (TEDEA 1040) were mounted at the interfaces between the exoskeleton and the operator: one at the tip carrying the external load, two between the exoskeleton and the human hand, and one at the interface between the upper arm and the exoskeleton. Like the first generation, the first load cell, inserted between the rod holding the external load and the exoskeleton forearm link, measured the actual shear force, normal to the forearm axis, applied by the external load. The other load cells were installed between the handle grasped by the human hand and the forearm link of the exoskeleton and between the upper arm bracelet and the exoskeleton upper link. These load cells measured the shear forces applied by the operator to the mechanism. Multiplying the sensors' measurements by the corresponding moment arms indicated the moments applied by the weights and by the human arm relative to the elbow and the shoulder joints.

Expanding the DOFs the mechanism could facilitate from three to seven, and eventually eight, took the research team several years—a leap to EXO-UL7.

5.2.3 PROTOTYPE 3 (EXO-UL7)

Note: this generation of anthropometric 7-DOF powered exoskeleton system was once termed as “Cable-Actuated Dexterous Exoskeleton for Neuro-rehabilitation” (CADEN-7) [8], but soon afterward the authors decided to uniform its name under the “EXO-UL” series [9].

Based on the human arm kinematics and dynamics during activities of daily living [10], for the first time in this exoskeleton system series, the EXO-UL7 shown in Fig. 5.3 covers all seven major

**FIGURE 5.3**

EXO-UL7 Robotic Exoskeleton System.

DOFs of the human upper limb including shoulder extension/flexion, shoulder adduction/abduction, shoulder internal/external rotation, elbow extension/flexion, forearm pronation/supination, wrist extension/flexion, and wrist radial/ulnar deviation [7,11–13]. It also contains two arms and enables more training protocols that will be further discussed in the EXO-UL8 section.

At first the controller was based on the sEMG [14,15], but due to the cumbersomeness of setting up an sEMG measuring system in practical rehabilitation applications, the research shifted to using force/torque sensors only. For details of gravity compensation implementation please refer to Ref. [16], of PID control [17,18], and of neural PID control [19].

For more details on the design of this generation of exoskeleton system, readers are encouraged to read the PhD dissertation from Joel C. Perry [12]; for the general control part, readers are encouraged to read the PhD dissertations from Miller [20] and Kim [21].

5.2.4 PROTOTYPE 4 (EXO-UL8)

The strength and maximum power output of EXO-UL7 were limited by the cable-driven mechanism. Therefore the authors modified the design to a motor-gear actuated one. Some of the recent progress in the EXO-UL8 (Fig. 5.4) was covered in Refs. [22–25]. Here the authors try to provide an overview in a more systematic way.

5.2.4.1 System architecture

The dual exoskeleton system includes two major components: (1) hardware—robotic mechanism, actuation, sensing and electronics; and (2) software—control architecture, and virtual reality (VR) environment. The human is physically attached to the exoskeleton system. Contact forces are

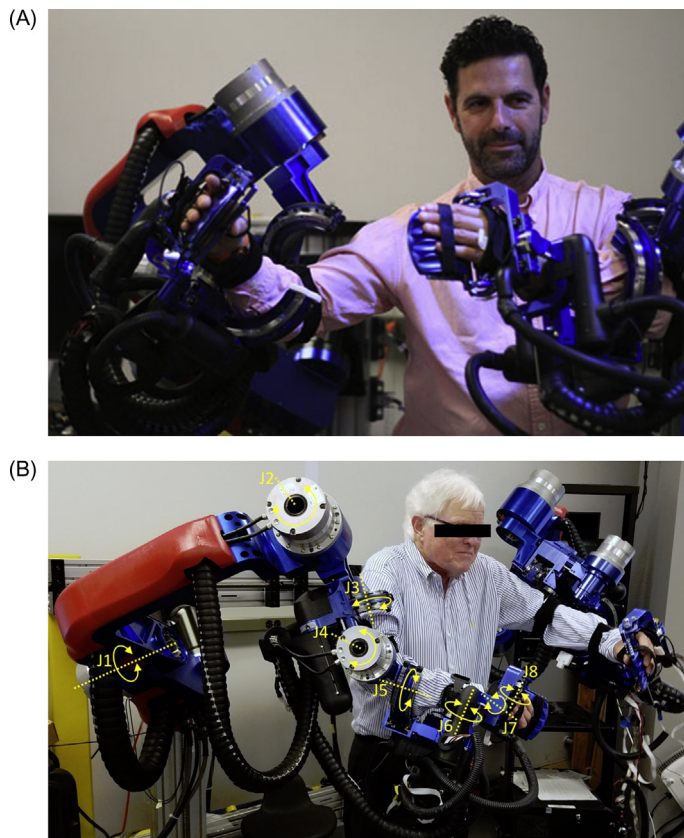


FIGURE 5.4

(A) One of the authors is operating the EXO-UL8 Robotic Exoskeleton System; (B) A poststroke patient is operating the EXO-UL8 Robotic Exoskeleton System.

measured by force sensors placed between the braces (upper arm, forearm, palm, and fingers) and the exoskeleton structure. Joint angles are measured by encoders located on the shafts of the joints. These two types of signals are converted via the A/D and a counter, respectively, by the real-time PC. Using an array of algorithms, encoded into the real-time PC, joint torque commands are generated and converted via the D/C by the real-time PC as inputs to the servo amplifiers. The servo amplifiers operated in a current mode control the actuation system which in turn results in its movement along with the application of the force fields. Feedback control signals are generated based on modes of operation: unilateral or bilateral. Joint angles are also sent via UDP protocol to the VR PC. The VR scene including a representation of the operator's arm along with all the virtual objects is rendered and displayed to the operator on a screen. The physics engine renders the haptic force fields information that is applied to the operator's arms by the exoskeleton system.

5.2.4.2 Mechanism, actuation, and sensing

The fourth generation (EXO-UL8) of a dual anthropometric arm exoskeleton system was designed and fabricated based on lessons learned for the extensive use of the system in the past in both a lab and clinical settings with stroke patients.

- *Mechanism (Adjustable Links Length)*—The mechanism includes a total of 8 DOF (3 DOFs for the shoulder joint, 2 DOFs for the elbow joint, 2 DOFs for the wrist joint, and 1 DOF of the hand). The entire two exoskeleton arms are attached to a portable frame and a chair that allows changing the height and distance (shoulder span) of the two arms. The length of the upper arm and the forearm are adjustable allowing the therapist to fit these two dimensions to various arm lengths in the range of the 5–95 percentile of the populations' anthropometric data. The rotation axes of the exoskeleton system intersect at the centers of the anatomical joints in a way that eliminates any potential joint dislocation. The mechanical joint includes hard joint limits that match the range of motion of the anatomical joint. The first three shoulder joints are oriented with respect to the patient in such a way that they position the singular configuration of the shoulder joint out of the human arm workspace. Furthermore, a single passive DOF was added to the wrist in addition to the existing two actuated DOFs in order to avoid any internal joint torque. The anthropometric design of the exoskeleton allows the user to reach 95% of the workspace accessible to the healthy operator. The human operator is physically attached to the exoskeleton arm and interacts with the system through five physical interfaces. Three braces are attached to the upper arm, the forearm, and the palm. An additional two contact surfaces form the claw-type hand interface.
- *Actuation*—This generation of the system uses actuators that are directly connected to each of the 8 DOFs of the system. Pancake coil brushless DC actuators with harmonic drive are used for the large joints (shoulder and elbow), and small form factor Maxon DC brushed motors with multistage gearboxes are used for the smaller joints (wrist and hand). The selected actuators have the largest torque-to-weight ratio available in an off-the-shelf actuation system at the time it was developed.
- *Hands*—The new generation of the system includes two types of hands: (1) claw-type single DOF hand; and (2) three-finger multi-DOF hand (under development [26]). The exoskeleton arm includes a universal interface at the proximal end of the arm allowing the mounting and interchanging of the two hands. The claw-type single DOF hand separates the fingers into two groups including the thumb and the rest of the fingers. The hand with its two supporting surfaces is rotated with a single actuated axis allowing a claw-type grasp. The three fingers multi-DOF exoskeleton type hand lumps the fingers into three groups: (1) the thumb; (2) the index; and (3) the middle finger, the ring, and the pinky fingers. Lumping the five fingers of the hand into three groups and a special alignment of the joints of the hand interface allow for comfortable manipulations of the fingers throughout the entire common workspace of each group of fingers.
- *Sensing*—There are two types of sensors embedded into the exoskeleton: (1) position sensors; and (2) force torque sensors. Absolute encoders are mounted to the back shaft of all the actuators for measuring the absolute joint angle of every DOF. The human operator is physically attached to the exoskeleton arm and interacts with the system through three physical interfaces of the arm and two to three interfaces at the hand depending on the hand

configuration. Three braces are attached to the upper arm, the forearm, and the palm. An additional two contact surfaces of the claw-type hand interface and three contact interfaces for the three fingers hand transmit forces between the exoskeleton hand and the operator's fingers. Force sensors embedded into the braces and the supporting surfaces of the fingers enable the operator to control the arm and the hand using an admittance controller.

5.3 RELATED RESEARCH

5.3.1 CONTROL ALGORITHMS

Control algorithms on the series of exoskeleton systems have been improved over the years, from sEMG-based to force/torque-based. Adding strength to the mechanism from cable-driven to motor-gear also brings complexity to the control system, making it unruly and easily unstable.

Originally the admittance controller was used for high-level HMI intention detection: forces and torques were fed in and position/velocity commands were generated, and the strategy was compared in joint space and task space on EXO-UL7 [27]. Later on, the performances of hyperparameter-based and Kalman Filter–based admittance controllers were compared on EXO-UL8 [25].

For more details on the most recent progress, readers are encouraged to refer to Ref. [25].

5.3.2 REDUNDANCY RESOLUTION

Both the mechanisms of human upper limb [28] and the EXO-UL7 or EXO-UL8 exoskeleton [29] are redundant in 3D Cartesian space [30]. A variety of studies thus have been done on this topic: a viscoelastic model for redundancy resolution of the human arm was built in [31], the redundancy resolution was incorporated into the task space admittance control algorithm [32] to reduce energy exchange, and it was further studied based on kinematic and dynamic constraints [33].

Depending on the task type, the redundancy resolution of the human upper limb has been investigated for point/reach tasks [34–37], reach-to-grasp tasks [38,39], and reach tasks with gravitational loads [40]. The understanding of redundancy resolution was applied to predict human arm posture [41], as well as the EXO-UL7 exoskeleton configuration [42].

A better understanding of redundancy resolution is beneficial for the design and development of compliant control, force fields (for compensation correction), as well as a resistance training controller. For more details, please refer to the book [43] and the PhD dissertation from Zhi Jane Li [44].

5.3.3 SYNERGY ANALYSIS

While it is common for poststroke patients to have abnormal synergies, the symptom is not well quantified—a common way to access the multijoint coordination/independence is Fugl-Meyer Assessment (FMA) [45]. However, to the authors' understanding, the quantification of FMA is not fine enough for differentiating patients with similar scores. The synergistic effects between joints have been investigated on, in different scenarios, modeling [46,47]; rhythmic effects [48];

stroke-induced synergistic phase shifting [49], etc. For details on the human movement synergies, the readers are encouraged to read the MS thesis from Aimen Hamid Al-Refai [50], and the PhD dissertation from Matt Simkins [51].

5.3.4 DUAL-ARM TRAINING

Compared with unilateral training, dual-arm training may have potential benefits [52]. The dual-arm exoskeleton, which uses interarm teleoperation, has the capability of enabling different dual-arm training modes, including mirror-image symmetric bilateral training mode, and asymmetric (asynchronous) bilateral training mode. For bilateral symmetric training and related analysis, please refer to Refs. [53–57]; for asymmetric dual-arm training, please refer to Ref. [24] for more details. Research on arm motion similarity has also been reported [58,59].

5.3.5 VIRTUAL REALITY

As an accompanying module, VR has been developed along with the R&D of the exoskeleton [60,61]. The newest version of the VR module could be used with an exoskeleton or head-mounted devices (e.g., Oculus Rift). The research has been filed for a patent (No. 62/732,736).

5.4 SUMMARY

This chapter reviews all four generations of the upper limb robotic exoskeleton systems developed in the authors' lab (University of Washington, University of California Santa Cruz, University of California Los Angeles). Related research has also been covered.

REFERENCES

- [1] P. Langhorne, J. Bernhardt, G. Kwakkel, *Stroke rehabilitation*, Lancet 377 (2011) 1693–1702.
- [2] E.J. Benjamin, et al., *Heart disease and stroke statistics-2017 update: a report from the American Heart Association*, Circulation 135 (10) (2017) e146–e603.
- [3] B.H. Dobkin, *Rehabilitation after stroke*, N. Engl. J. Med. 352 (16) (2005) 1677–1684.
- [4] J. Rosen, *Natural Integration of a Human Arm/Exoskeleton System*, Tel-Aviv University, 1997.
- [5] J. Rosen, M.B. Fuchs, M. Arcan, Performances of hill-type and neural network muscle models-toward a myosignal-based exoskeleton, Comput. Biomed. Res. 32 (5) (1999) 415–439.
- [6] J. Rosen, M. Brand, M.B. Fuchs, M. Arcan, A myosignal-based powered exoskeleton system, IEEE Trans. Syst. Man, Cybern. Part A Syst. Humans 31 (3) (2001) 210–222.
- [7] J.C. Perry, J. Rosen, Case study: an upper limb powered exoskeleton, in: J.L. Pons (Ed.), *Wearable Robots: Biomechatronic Exoskeletons*, John Wiley & Sons, 2008.
- [8] J.C. Perry, J. Rosen, S. Burns, Upper-limb powered exoskeleton design, IEEE/ASME Trans. Mechatronics 12 (4) (2007) 408–417.
- [9] J.C. Perry, J.M. Powell, J. Rosen, Isotropy of an upper limb exoskeleton and the kinematics and dynamics of the human arm, Appl. Bionics Biomech. 6 (2) (2009) 175–191.

- [10] J. Rosen, J.C. Perry, N. Manning, S. Burns, B. Hannaford, The human arm kinematics and dynamics during daily activities - toward a 7 DOF upper limb powered exoskeleton, in: 2005 International Conference on Advanced Robotics, ICAR '05, Proceedings, 2005, no. July, pp. 532–539.
- [11] J.C. Perry, J. Rosen, Design of a 7 degree-of-freedom upper-limb powered exoskeleton, in: Biomedical Robotics and Biomechatronics, 2006. BioRob 2006. The First IEEE/RAS-EMBS International Conference on, 2006, pp. 805–810.
- [12] J.C. Perry, Design and development of a 7 degree-of-freedom powered exoskeleton for the upper limb, University of Washington, 2006.
- [13] J. Rosen, J.C. Perry, Upper limb powered exoskeleton, *Int. J. Humanoid Robot.* 04 (03) (2007) 529–548.
- [14] E. Cavallaro, J. Rosen, J.C. Perry, S. Burns, B. Hannaford, Hill-based model as a myoprocessor for a neural controlled powered exoskeleton arm - parameters optimization, in: Proceedings of the 2005 IEEE International Conference on Robotics and Automation, 2005, no. April, pp. 4525–4530.
- [15] E.E. Cavallaro, J. Rosen, J.C. Perry, S. Burns, Real-time myprocessors for a neural controlled powered exoskeleton arm, *IEEE Trans. Biomed. Eng.* 53 (11) (2006) 2387–2396.
- [16] L.M. Miller, Gravity Compensation for a 7 Degree of Freedom Powered Upper Limb Exoskeleton, University of Washington, 2006.
- [17] W. Yu, J. Rosen, A novel linear PID controller for an upper limb exoskeleton, in: Proceedings of the IEEE Conference on Decision and Control, 2010, pp. 3548–3553.
- [18] W. Yu, J. Rosen, X. Li, PID admittance control for an upper limb exoskeleton, in: 2011 American Control Conference, 2011, pp. 1124–1129.
- [19] W. Yu, J. Rosen, Neural PID control of robot manipulators with application to an upper limb exoskeleton, *IEEE Trans. Cybern.* 43 (2) (2013) 673–684.
- [20] L.M. Miller, Comprehensive Control Strategies for a Seven Degree of Freedom Upper Limb Exoskeleton Targeting Stroke Rehabilitation, University of Washington, 2012.
- [21] H. Kim, Systematic Control and Application for 7 DOF Upper-Limb Exoskeleton, University of California, Santa Cruz, 2012.
- [22] Y. Shen, Control and Dynamic Manipulability of a Dual-Arm/Hand Robotic Exoskeleton System (EXO-UL8) for Rehabilitation Training in Virtual Reality, University of California, Los Angeles, 2019.
- [23] Y. Shen, P.W. Ferguson, J. Ma, J. Rosen, Upper limb wearable exoskeleton systems for rehabilitation: state of the art review and a case study of the EXO-UL8 - dual-arm exoskeleton system, in: Wearable Technology in Medicine and Health Care, Elsevier, 2018, pp. 71–90. <http://dx.doi.org/10.1016/B978-0-12-811810-8.00004-X>.
- [24] Y. Shen, J. Ma, B. Dobkin, J. Rosen, Asymmetric dual arm approach for post stroke recovery of motor functions utilizing the EXO-UL8 exoskeleton system: a pilot study, 2018 40th Annual International Conference of the IEEE Engineering in Medicine and Biology Society (EMBC), 2018, pp. 1701–1707. <http://dx.doi.org/10.1109/EMBC.2018.8512665>.
- [25] Y. Shen, J. Sun, J. Ma, J. Rosen, Admittance control scheme comparison of EXO-UL8: a dual-arm exoskeleton robotic system, 2019 IEEE 16th International Conference on Rehabilitation Robotics (ICORR), 2019, pp. 611–617. <http://dx.doi.org/10.1109/ICORR.2019.8779545>.
- [26] P.W. Ferguson, B. Dimapasoc, Y. Shen, J. Rosen, Design of a hand exoskeleton for use with upper limb exoskeletons, in: M.C. Carrozza, S. Micera, J.L. Pons (Eds.), *Wearable Robotics: Challenges and Trends*, Springer International Publishing, Cham, 2019, pp. 276–280.
- [27] L.M. Miller, J. Rosen, Comparison of multi-sensor admittance control in joint space and task space for a seven degree of freedom upper limb exoskeleton, in: Proceedings of the 2010 3rd IEEE RAS & EMBS International Conference on Biomedical Robotics and Biomechatronics, 2010, pp. 70–75.
- [28] H. Kim, L.M. Miller, A. Al-Refai, M. Brand, J. Rosen, Redundancy resolution of a human arm for controlling a seven DOF wearable robotic system, in: Proceedings of the Annual International Conference of the IEEE Engineering in Medicine and Biology Society, EMBS, 2011, pp. 3471–3474.

- [29] L.M. Miller, H. Kim, J. Rosen, Redundancy and joint limits of a seven degree of freedom upper limb exoskeleton, in: Proceedings of the Annual International Conference of the IEEE Engineering in Medicine and Biology Society, EMBS, 2011, pp. 8154–8157.
- [30] H. Kim, L.M. Miller, N. Byl, G.M. Abrams, J. Rosen, *Redundancy resolution of the human arm and an upper limb exoskeleton*, *IEEE Trans. Biomed. Eng.* **59** (6) (2012) 1770–1779.
- [31] H. Kim, J.R. Roldan, Z. Li, J. Rosen, Viscoelastic model for redundancy resolution of the human arm via the swivel angle: applications for upper limb exoskeleton control, in: Conference Proceedings: ... Annual International Conference of the IEEE Engineering in Medicine and Biology Society. IEEE Engineering in Medicine and Biology Society. Annual Conference, 2012, pp. 6471–6474.
- [32] H. Kim, L.M. Miller, Z. Li, J.R. Roldan, J. Rosen, Admittance control of an upper limb exoskeleton - reduction of energy exchange, in: Proceedings of the Annual International Conference of the IEEE Engineering in Medicine and Biology Society, EMBS, 2012, pp. 6467–6470.
- [33] H. Kim, Z. Li, D. Milutinović, J. Rosen, Resolving the redundancy of a seven DOF wearable robotic system based on kinematic and dynamic constraint, in: Proceedings of International Conference on Robotics and Automation, 2012, pp. 305–310.
- [34] B. Kashi, M. Brand, J. Rosen, I. Avrahami, Synthesizing two criteria for redundancy resolution of human arm in point tasks, in: 2011 Third World Congress on Nature and Biologically Inspired Computing (NaBIC), 2011, 63–68.
- [35] Z. Li, J.R. Roldan, D. Milutinovic, J. Rosen, The rotational axis approach for resolving the kinematic redundancy of the human arm in reaching movements, in: Proceedings of the Annual International Conference of the IEEE Engineering in Medicine and Biology Society, EMBS, 2013, no. 2, pp. 2507–2510.
- [36] Z. Li, H. Kim, D. Milutinović, J. Rosen, Synthesizing redundancy resolution criteria of the human arm posture in reaching movements, in: Redundancy in Robot Manipulators and Multi-Robot Systems, 2013, 201–240.
- [37] Z. Li, D. Milutinovic, J. Rosen, *Spatial map of synthesized criteria for the redundancy resolution of human arm movements*, *IEEE Trans. Neural Syst. Rehabil. Eng.* **23** (6) (2015) 1020–1030.
- [38] Z. Li, J.R. Roldan, D. Milutinović, Task-relevance of grasping-related degrees of freedom in reach-to-grasp movements, in: 36th Annual International Conference of the IEEE Engineering in Medicince and Biology Society, EMBS, 2014, pp. 6903–6906.
- [39] Z. Li, K. Gray, J.R. Roldan, D. Milutinović, J. Rosen, The joint coordination in reach-to-grasp movements, in: IEEE International Conference on Intelligent Robots and Systems, 2014, pp. 906–911.
- [40] Y. Shen, B.P. Hsiao, J. Ma, J. Rosen, Upper limb redundancy resolution under gravitational loading conditions: arm postural stability index based on dynamic manipulability analysis, 2017 IEEE-RAS 17th International Conference on Humanoid Robotics (Humanoids), 2017, pp. 332–338. <http://dx.doi.org/10.1109/HUMANOIDS.2017.8246894>.
- [41] B. Kashi, I. Avrahami, J. Rosen, M. Brand, A bi-criterion model for human arm posture prediction, in: 2012 World Congress on Medical Physics and Biomedical Engineering, 2012, 1–4.
- [42] H. Kim, J. Rosen, *Predicting redundancy of a 7 DOF upper limb exoskeleton toward improved transparency between human and robot*, *J. Intell. Robot. Syst.* **80** (2015).
- [43] D. Milutinović, J. Rosen (Eds.), *Redundancy in Robot Manipulators and Multi-Robot Systems*, Springer, 2013.
- [44] Z. Li, *The Synergy of Human Arm and Robotic System*, University of California, Santa Cruz, 2014.
- [45] K.J. Sullivan, et al., Fugl-Meyer assessment of sensorimotor function after stroke: standardized training procedure for clinical practice and clinical trials, *Stroke* **42** (2) (2011) 427–432.
- [46] A. Feldman, Y. Shen, J. Rosen, Modeling of joint synergy and spasticity in stroke patients to solve arm reach tasks, 2017 IEEE Signal Processing in Medicine and Biology Symposium (SPMB), 2017 IEEE, 2017, pp. 1–3. <http://dx.doi.org/10.1109/SPMB.2017.8257046>.

- [47] M. Simkins, A.H. Al-Refai, J. Rosen, Upper limb joint space modeling of stroke induced synergies using isolated and voluntary arm perturbations, *IEEE Trans. Neural Syst. Rehabil. Eng.* 22 (3) (2014) 491–500.
- [48] M. Simkins, A. Burleigh Jacobs, J. Rosen, Rhythmic affects on stroke-induced joint synergies across a range of speeds, *Exp. Brain Res.* 229 (4) (2013) 517–524.
- [49] M. Simkins, A.B. Jacobs, N. Byl, J. Rosen, Stroke-induced synergistic phase shifting and its possible implications for recovery mechanisms, *Exp. Brain Res.* 232 (11) (2014) 3489–3499.
- [50] A.H. Al-Refai, Objectively Characterized Linear Model of Stroke Induced Joint Synergies in Relation to Clinical Measures, University of California, Santa Cruz, 2012.
- [51] M. Simkins, Human Movement Synergies of the Upper Extremities, University of California, Santa Cruz, 2013.
- [52] J.H. Cauraugh, J.J. Summers, Neural plasticity and bilateral movements: a rehabilitation approach for chronic stroke, *Prog. Neurobiol.* 75 (5) (2005) 309–320.
- [53] M. Simkins, H. Kim, G. Abrams, N. Byl, J. Rosen, Robotic unilateral and bilateral upper-limb movement training for stroke survivors afflicted by chronic hemiparesis, in: IEEE International Conference on Rehabilitation Robotics, 2013, pp. 1–6.
- [54] M. Simkins, N. Byl, H. Kim, G. Abrams, J. Rosen, Upper limb bilateral symmetric training with robotic assistance and clinical outcomes for stroke: a pilot study, *Int. J. Intell. Comput. Cybern.* 9 (1) (2016) 83–104.
- [55] N.N. Byl, et al., Chronic stroke survivors achieve comparable outcomes following virtual task specific repetitive training guided by a wearable robotic orthosis (UL-EXO7) and actual task specific repetitive training guided by a physical therapist, *J. Hand Ther.* 26 (4) (2013) 343–352.
- [56] J. Rosen, D. Milutinović, L.M. Miller, M. Simkins, H. Kim, Z. Li, Unilateral and bilateral rehabilitation of the upper limb following stroke via an exoskeleton, in: P. Ardemiadis (Ed.), *Neuro-Robotics: From Brain Machine Interfaces to Rehabilitation Robotics*, Dordrecht, Springer Netherlands, 2014, pp. 405–446.
- [57] H. Kim, et al., Kinematic data analysis for post-stroke patients following bilateral versus unilateral rehabilitation with an upper limbwearable robotic system, *IEEE Trans. NEURAL Syst. Rehabil. Eng.* 21 (2) (2013) 153–164.
- [58] J.R.U. Roldan, D. Milutinovic, Z. Li, J. Rosen, A low-dimensional dissimilarity analysis of unilateral and bilateral stroke-impacted hand trajectories, *J. Dyn. Syst. Meas. Control* 138 (11) (2016) 111007.
- [59] Z. Li, K. Hauser, J.R. Roldan, D. Milutinovic, J. Rosen, A novel method for quantifying arm motion similarity, in: Proceedings of the Annual International Conference of the IEEE Engineering in Medicine and Biology Society, EMBS, 2015, pp. 5716–5719.
- [60] M. Simkins, I. Fedulow, H. Kim, G. Abrams, N. Byl, J. Rosen, Robotic rehabilitation game design for chronic stroke, *Games Health J.* 1 (6) (2012) 422–430.
- [61] M. Simkins, J.R. Roldan, H. Kim, G. Abrams, N. Byl, J. Rosen, Kinematic analysis of virtual reality task intensity induced by a rehabilitation robotic system in stroke patients, in: Proceedings of ASME 2013 Dynamic Systems and Control Conference 2013, 2013, pp. 1–7.

PRISM: DEVELOPMENT OF A 2-DOF DUAL-FOUR-BAR EXOSKELETON SHOULDER MECHANISM TO SUPPORT ELEVATION, DEPRESSION, PROTRACTION, AND RETRACTION

6

Joel C. Perry, Chris K. Bitikofer, Parker W. Hill, Shawn T. Trimble and Eric T. Wolbrecht

Mechanical Engineering Department, University of Idaho, Moscow, ID, United States

6.1 INTRODUCTION

As one of the leading causes of long-term functional deficits in the arm and hand, the annual incidence of stroke is about 800,000 in the United States and about 42 million globally [1]. Losses in arm function and mobility occur in some 85% of strokes and persist at least 3–6 months after stroke in 55%–75% of cases [2]. This number is projected to rise over the next several decades due to the effect of increases in the following four factors: (1) life expectancies, (2) prevalence of stroke with age, (3) number of baby-boomers reaching the age of higher prevalence, and (4) post-stroke survival rates. These growing trends place a large burden on our healthcare system and increase the need for more therapists to perform hands-on and physically demanding rehabilitation treatments. The introduction of robotics onto the therapeutic stage [3–6] brings welcomed characteristics including high strength, precision, and repeatability. Research has demonstrated the efficacy of robotic therapy to match or exceed conventional therapy when provided in equivalent doses [7], and that robotic devices can facilitate far greater numbers of therapeutic repetitions in a single therapy session than can be achieved by therapists alone [8]. Robotics also offer improved elements of quantitative measurement which give meaningful feedback to patients and care providers. This feedback has major implications for care, offering the ability to guide and individualize therapy, gauge compliance, motivate progress, and justify continuation of care to insurers. Furthermore, robotic measures give researchers new ways to study therapy hypotheses and evolve robotic device design. Ensuring accuracy of measurement is therefore of the utmost importance, and is significantly linked to the appropriateness of the robot's design in terms of fit and function to the needs of the human users.

6.1.1 REHABILITATION ROBOTICS: EXOSKELETON VERSUS END-EFFECTOR

Assessing and rehabilitating the deficits caused by stroke and other cerebrovascular accidents has been a major motivating factor behind the proliferation of rehabilitation robotics over the past two decades. In the design and development of robotics for the upper extremity, both exoskeleton [9–13] and end-effector [14–17] approaches are common. Exoskeletons provide structural links in close proximity to, and along the length of, the arm. Their kinematics mimic anatomical movements by aligning robot joint axes with approximations of human joint axes and maintaining alignment throughout the user’s motion. End-effector robots, on the other hand, attach to the user at the hand and/or forearm, and may use any number of joint configurations to enable an end-effector workspace that coincides with a subset of the user’s hand and/or forearm workspace.

In both end-effector and exoskeleton design approaches, safe and comfortable operation requires that robot-induced movements remain within normal ranges of motion at all times and across all joints of the driven human limb. Different approaches can be taken to ensure anatomically appropriate joint motions, which can involve direct control of the joints or, in other cases, an intentional lack of control over specific joints. The latter approach of adding passive joints into the design is referred to as underactuation and is most often applied in robotic hands [18,19] and legs [20]. End-effector-based systems commonly control an end-point position while the inclusion of passive degrees-of-freedom (DOFs) leave some aspect of arm orientation underconstrained. Exoskeleton-based systems, however, rely on proper alignment between joints of the exoskeleton and user [11]. The user must be fully constrained to the device such that the locations and orientations of the user’s anatomical joints are reasonably known.

Consequently, maintaining proper alignment between the joints of the robotic device and the joints of the human user is one of the principal challenges in exoskeleton design. Problems resulting from inadequate joint alignment can include excessive or unwanted forces exerted on the patient and/or exoskeleton, inaccurate measurements, and increased risk of joint injuries such as shoulder subluxation (i.e., partial dislocation). In an attempt to address this concern, current exoskeleton designs are beginning to incorporate features that better accommodate slight misalignments, or that attempt to eliminate them entirely. This has been attempted in the wrist [21], the elbow [22,23], and the shoulder [9,24–26].

While allowing proper alignment, or accommodating for misalignment, is important for all users of exoskeletons, it is especially important when used with individuals having acute-stage neurological impairments (e.g., 1–2 weeks poststroke). A common early sequela poststroke is muscular flaccidity (i.e., no tone) followed by hypotonia (i.e., low tone) [27], both of which lead to instability in the joints and increased risk of injury if not properly supported [9]. This is of particular importance in the shoulder complex where the highest risk for subluxation occurs [28].

6.1.2 EXOSKELETON SHOULDER BACKGROUND

6.1.2.1 State of the art

Over the past decade, a handful of systems have provided varying solutions to address some of the additional DOFs provided by the shoulder complex, but few account for full shoulder mobility [29–33]. In the healthy shoulder, articulation is a combination of four joints: the glenohumeral (GH), acromioclavicular (AC), and sternoclavicular (SC) synovial joints, and a scapulothoracic

(ST) “false” joint formed by musculature between the scapula and thoracic cage (see Fig. 6.1). Together the four joints of the shoulder girdle provide the humerus with the freedom to move within a nearly hemispherical workspace with a rather nonlinear center of rotation [35]. Although the overall shoulder structure has been previously represented by numerous models [36], its replication with an anthropomorphic exoskeleton remains a significant design challenge.

In total, the shoulder complex consists of 5 DOFs [36], but many designs account for only three. In an attempt to simplify the shoulder, the most popular approach with robotic systems has been to represent the shoulder as a 3-DOF spherical joint, mimicking the behavior of the GH joint, and neglecting the articulations of the ST, SC, and AC joints. However, these articulations are vital to achieving full range of motion (ROM) in the shoulder; without them, exoskeletal shoulder alignment is reasonably maintained over a limited range of humeral elevation (<90 degrees), and leads to increased misalignment with higher levels of humeral elevation above horizontal.

Recognizing that increased humeral elevation has a nonlinear relationship to SC, AC, and ST articulation, referred to as scapulohumeral rhythm, shoulder designs have been developed with variations to the standard 3-DOF spherical arrangement in order to further reduce misalignments and increase the allowable workspace. A few of the more notable systems include the MGA, ARMin, MEDARM, and HARMONY exoskeletons (Fig. 6.2), described below.

The *MGA exoskeleton*, built in 2005, is a 6-DOF upper-limb exoskeleton with a 4-DOF shoulder. The MGA models the GH joint as a ball and socket, with three actuated DOFs. A fourth DOF is placed behind the patient in line with the SC joint (Fig. 6.2), which allows for elevation/depression of the shoulder girdle [37,41]. The addition of a 1-DOF SC joint allows for increased GH mobility that supports shoulder elevation (upward) and depression (downward).

The *ARMin I, II, and III*, prototypes developed between 2005 and 2008, each used 3-DOF shoulders with variations of additional shoulder DOFs. The ARMin I used a passive gravity-balanced linear DOF to support vertical translation of the entire exoskeleton, similar to elevation/depression; however, being a passive DOF, the system’s position was not actively determined and became problematic for patients with risk of shoulder subluxation [9]. The ARMin II coupled the passive shoulder elevation/depression DOF with humeral elevation. This achieves a substantially similar result to the single SC-aligned DOF used in the MGA exoskeleton. The ARMin III took this coupling approach a step further by replacing the vertical translation of the GH joint by a circular path that was numerically optimized to minimize anatomical error with typical humeral head movement. Protraction/retraction support was not added as the authors noted that misalignment in this direction could be overcome by torso movements from the patient. It is worth noting that the ARMin III is the only exoskeleton of those discussed here that is commercially available (as the ArmeoPower); so far, the other systems exist in research settings only.

The *MEDARM* is a 6-DOF exoskeleton with a 5-DOF shoulder that claims to be the first rehabilitation robot to fully account for shoulder movement [36]. Two independent DOFs are aligned with the SC joint, one positioned behind the user for elevation/depression and the other positioned above the user for protraction/retraction. As a result, the entirety of shoulder girdle motion is accommodated.

The *HARMONY* is a dual upper-limb exoskeleton developed for rehabilitation. Like the MEDARM, the HARMONY proposes a novel solution to the shoulder mobility problem [34,42]. Scapulohumeral rhythm is accounted for by way of a parallelogram mechanism positioned behind the patient. The parallelogram serves to provide protraction/retraction of the joint while a single

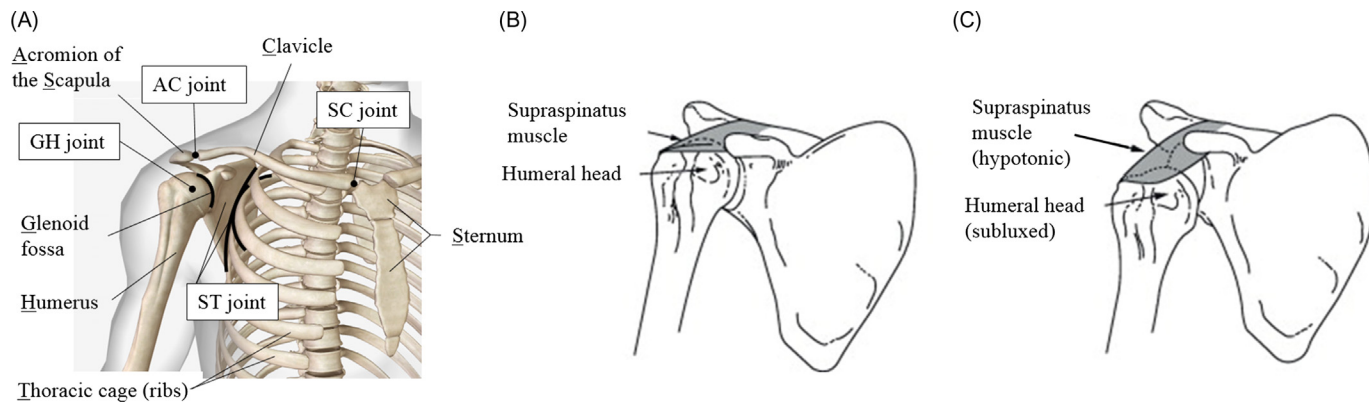


FIGURE 6.1

The shoulder complex (A) is comprised of three bones: the clavicle, humerus, and scapula. Four joints form the entire shoulder girdle: sternoclavicular, acromioclavicular, glenohumeral, and the scapulothoracic joints. In the healthy shoulder, the supraspinatus muscle is a major contributor to proper shoulder stability (B). Under hypotonic conditions, flaccidity of the musculature results in humeral head subluxation (C).

(A) Adapted from D.A. Neumann, *Kinesiology of the Musculoskeletal System-E-Book: Foundations for Rehabilitation*, Elsevier Health Sciences, 2013 [34]. (B and C)

Adapted from M. Murie-Fernandez, M.C. Iragui, V. Gnanakumar, M. Meyer, N. Foley, R. Teasell, *Painful hemiplegic shoulder in stroke patients: causes and management*, *Neurología (English Ed.)* 27 (4) (2012) 234–244.

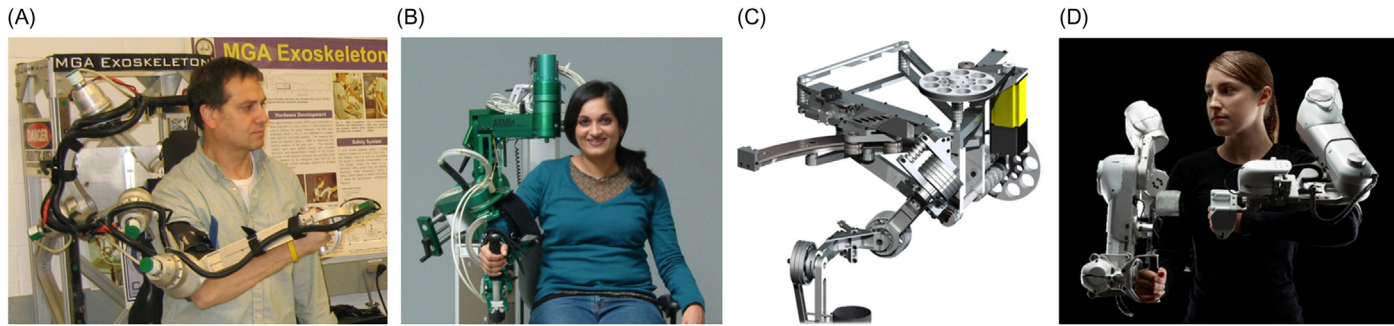


FIGURE 6.2

Notable exoskeleton arms that incorporate aspects of SC, AC, and/or ST articulation: (A) the MGA exoskeleton [37], (B) the ARMin III [38], (C) the MEDARM [39], and (D) the HARMONY [40].

revolute joint permits elevation/depression. Motion of the GH joint is accomplished through three DOFs, but one will note that the angles between the axes are not orthogonal as in most other exoskeleton designs.

Each of the above exoskeletons provide 3 DOFs to support GH ROM, but variations between axes orientation can clearly be seen. In the ARMin, shoulder internal/external rotation is the third GH axis (GH3), while in the others, internal/external rotation is achieved through a combination of all three GH axes (GH1, GH2, and GH3). It is also worth noting that the selection and placement of the first axis has major implications not only on the allowable ROM of the resulting exoskeleton shoulder, but also on the location (or existence) of workspace singularities. A singularity can occur when two axes are aligned, effectively eliminating one of the DOFs of the device. The effect of a singularity is apparent both near and at the alignment of two joint axes as the manipulability of the device degrades. In mechanical systems, a singularity can manifest either as “gimbal lock”, in which case axial alignment prevents the mechanism from being able to move in a given direction, or as an underconstrained system, in which case axial alignment allows multiple movements to achieve the same result. Both are problematic for proper control of the end-effector. Placing the first GH joint (GH1) directly above the shoulder, as was done in the ARMin III, has the potential to create three singularities when the arm is straight down along the side of the body; one between GH1 and GH3 (internal/external rotation), a second between GH3 and forearm pronosupination (PS), and a third between GH1 and PS. In the axial configurations used in the MEDARM and MGA exoskeleton designs, the point of singularity between GH1 and GH3 have been placed in hard-to-reach locations on the edge of, or entirely outside the workspace of the human arm. This minimizes the risk that the singularity is reached and therefore reduces the negative effects of the singularity on the mechanism, such as poor manipulability. In the HARMONY design, it may be noted that the angle between GH1 and GH2, and between GH2 and GH3 are not 90 degrees as in most other exoskeletons. While this does prevent direct alignment between axes GH1 and GH3, it does not prevent the singularity from occurring. Some discussion on the placement of the axes GH1, GH2, and GH3 can be found in Ref. [42].

Although the advantages and disadvantages behind placing the GH axes at various locations is not the focus of this paper, it is important to note that their selection does impact the device's ROM, manipulability, and relative ease (or ability) to incorporate additional proximal DOFs, such as the SC joint, in order to allow a more anthropomorphic shoulder actuation. As can be seen in the designs of Fig. 6.2, the incorporation of SC joint axes into an exoskeleton arm can take up substantial real estate behind or above the user, even to the point where it compromises GH joint ROM. The HARMONY implementation is a great example of an elegant low-profile design that incorporates all 5 shoulder DOFs; however, the elegance comes at the cost of limited bilateral shoulder ROM due to the close placement of motors, and as a result, shoulder abduction is unable to reach the ROM in which the additional SC DOFs contribute most (> 90 degrees). MEDARM's design clearly precludes the ability to extend this device to a bilateral version due to the placement of hardware that drives the exoskeleton's SC axes (SC1 and SC2) whose joints must align with the anatomical SC joint.

6.1.2.2 3-DOF versus 5-DOF shoulder

As previously mentioned, being able to measure the arm orientation accurately is highly important for assessment purposes. Knowing that misalignments alter the accuracy of measurements, adding a

4th or 5th joint to the shoulder is advantageous. Why not just add a coupled DOF to elevate the shoulder along with humeral elevation instead of adding another motor? While this approach does closely match healthy kinematics of the shoulder girdle, impaired individuals do not exhibit healthy kinematics. The shoulder is one of the joints where much of the impairment is evident. Muscular weakness, cocontraction, spasticity, and abnormal joint torque couplings at the shoulder make it difficult for many patients to control abduction without elevating the humeral head via SC, AC, and ST articulation. In this case, the elevation of the humeral head is not coupled with elevation of the humerus and would result in undesirable and potentially harmful forces and torques on the individual if exhibited in an exoskeleton with a fixed or floating 3-DOF GH joint. For assessment purposes, the inclusion of a 2-DOF anthropomorphic clavicle to a 3-DOF GH joint has strong merit.

6.1.2.3 Bilateral versus unilateral shoulder designs

In recent years, there has been a growing interest in bilateral task training [43–47], showing benefits over unilateral and other types of training. Similarly, bilateral assessment offers many advantages over unilateral assessment. It is nothing new to the clinical community who routinely compare impaired and intact sides of the body, but is often neglected in robotic systems for economic reasons. The ARMin provides a design which can be reconfigured for either arm, whereas the HARMONY provides mirrored parts that achieve a left and right version. The HARMONY is one of the few exoskeletons since the EXO-UL7 [11] that was developed from the start for bilateral use with impaired users. The majority of other systems would require substantial redesign to incorporate SC and AC shoulder joints that allow a design with simultaneous bilateral capability.

6.1.3 OVERVIEW

In this work, we propose a novel mechanism that mimics the biomechanics of the clavicle about the AC and SC joints in order to add protraction/retraction and elevation/depression movements to spherical shoulder designs in existing robotic exoskeletons. The resulting mechanism uses a unique dual four-bar spatial design to provide 2 DOFs of shoulder mobility. The design has been termed “PRISM” (Parallel Remote Inclusion of Shoulder Mobility) and will be part of a new exoskeleton arm instrument called BLUE SABINO that takes advantage of key aspects from previous exoskeleton designs including EXO-UL7 [11], EXO-UL8 [48], LIMPACT [23], and HARMONY [42]. The BLUE SABINO concept, the mobility requirements for unimpaired shoulders, and the kinematics of the PRISM mechanism are presented below in [Section 6.2](#), followed by the final design and discussion in [Sections 6.3 and 6.4](#).

6.2 METHODS: PRISM DEVELOPMENT

In the following methods, the approach has been aimed at addressing the needs of a 5-year NSF project called BLUE SABINO. The overarching goal of the project is to develop a new instrument for comprehensive assessment of neurological impairment affecting functional mobility in the arm or hand. The project involves development of two full-arm exoskeletons (shoulder, elbow, wrist, and hand) with a fully integrated EMG/EEG acquisition system. The exoskeleton is modeled after

a previous exoskeleton design, the EXO-UL8, which utilizes a 3-DOF shoulder joint, adjustable link lengths, and direct Harmonic Drive actuation. To improve upon the anthropomorphic fit between user and device throughout the workspace, the PRISM mechanism is developed in the sections that follow.

6.2.1 BLUE SABINO CONCEPT

BLUE SABINO is a rather lengthy but technically appropriate acronym for BiLateral Upper-limb Exoskeleton for Simultaneous Assessment of Biomechanical and Neuromuscular Output. The project aims to create an instrument to help researchers and scientists improve upon our understanding of the fundamental contributors to neurological impairment. A schematic of the overall instrument and interior architecture is shown in Fig. 6.3. As depicted in the figure, the instrument architecture is composed of a task environment, a biosignal acquisition system, a data processing unit, and a storage database. The biosignal acquisition system interfaces with the human at three noninvasive levels: cerebral cortex (visual and motor), neuromuscular (arm musculature), and musculoskeletal (arm and hand exterior). The musculoskeletal interface represents the physical human–machine interface to the exoskeleton.

The BLUE SABINO exoskeleton will have a set of bilateral (left and right) exoskeleton arms supporting anatomical articulations of the shoulder, elbow, wrist, thumb, index finger, and

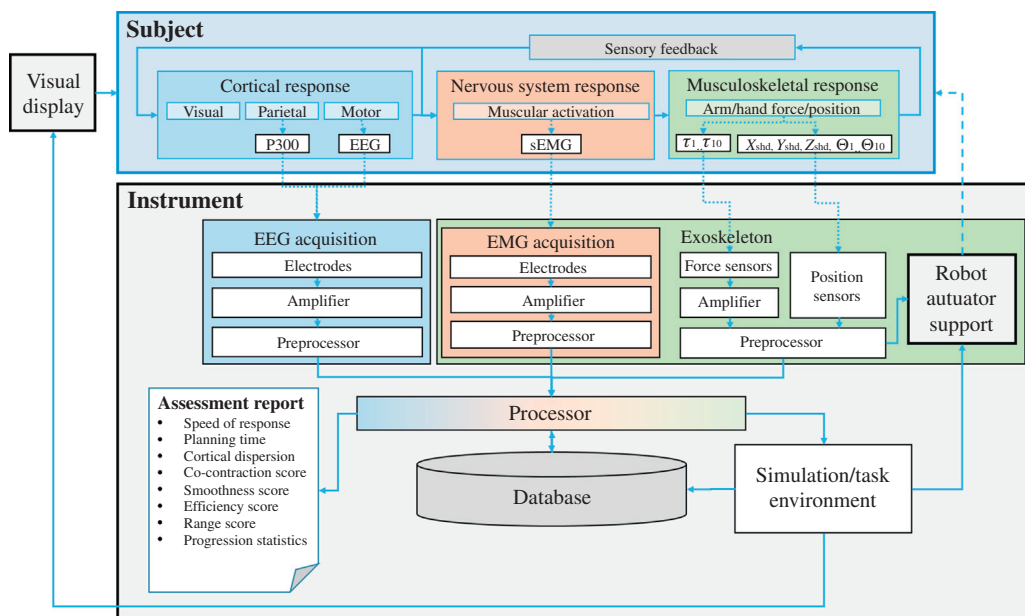


FIGURE 6.3

Instrument architecture with relation to the human subject and the acquisition of brain signals (blue), muscle signals (red), and arm movements and forces (green).

middle/ring/pinky finger combination. In total, each arm includes 15 active (i.e., motorized) and 8 passive (i.e., nonmotorized) joints, or DOFs. For development, exoskeleton subassemblies are divided into a 2-DOF passive base, a 2-DOF active shoulder, a 7-DOF active arm, and a 12-DOF hand (six active, six passive). The arm exoskeleton connects to the user at key points along the arm and hand and must be designed around desired electrode placement in order to minimize the introduction of movement artifacts in the SEMG signals. The bilateral aspect is intended to provide intrasubject measures between impaired and unimpaired limb (in the case of hemiparetic stroke) as well as assessment in performing bilateral tasks. Previous 7-DOF and 8-DOF exoskeleton arms [11,43,49], developed in part by the authors, provide a starting point to the arm and hand design in order to allow a greater focus on extending functionality to SC/AC and finger/thumb articulations.

6.2.2 EXO-UL8 DESIGN APPROACH

The *EXO-UL8* is the second generation of an earlier EXO-UL7 arm, but with an added DOF at the hand for grasp-release training. The EXO-UL7, (aka, CADEN-7) was one of the earliest examples of a 7-DOF exoskeleton with a lightweight and low-profile design (Fig. 6.4A). Features include a cable-driven power transmission from stationary base-mounted actuators, shoulder singularity avoidance through peripheral placement, and open bearing designs at both the upper arm and the forearm. Drawbacks to the system include (1) complexity of cable routing repair in the event of cable rupture, (2) lack of adjustability in arm lengths, (3) a stationary GH joint, (4) no hand grasp functionality, and (5) high-cost precision enclosures around the arm to allow axial rotation. As a second-generation system, the EXO-UL8 (Fig. 6.4B) addressed several of the potential disadvantages of the EXO-UL7 by (1) replacing cable transmissions with direct-drive integrated harmonic drive actuation, (2) adding length adjustment mechanisms for the upper and lower arm, and (3) adding a 1-DOF hand grasp module. It also addressed important strength and robustness concerns

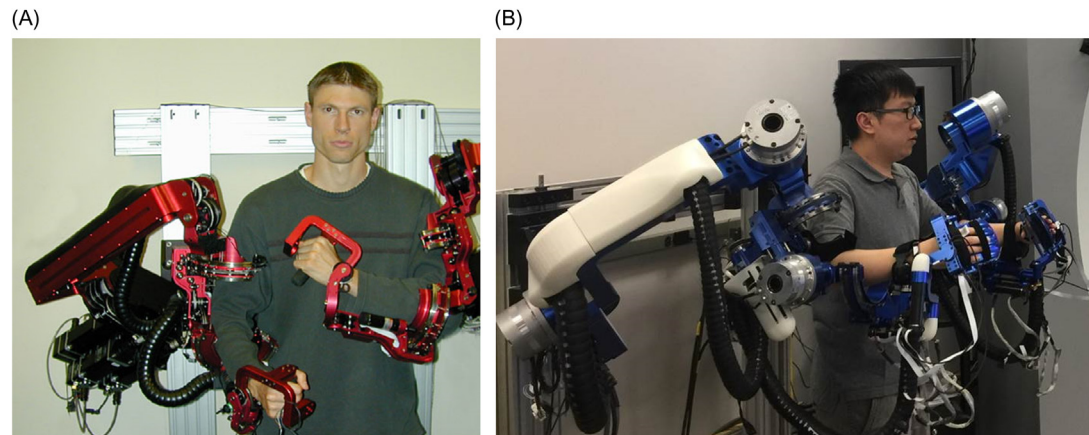


FIGURE 6.4

The EXO-UL7 (A) and EXO-UL8 (B) exoskeletons serve as previous iterations to the BLUE SABINO exoskeleton design.

following user testing with both healthy and impaired populations. The shoulder in both designs was represented by a spherical joint composed of three orthogonal axes intersecting at the estimated center of the shoulder GH joint. The first shoulder axis, GH1, intersects the inferior posterolateral aspect of the shoulder, achieving a combination of abduction and flexion. The second shoulder axis, GH2, is orthogonal to GH1 and sits on the anterolateral aspect of the shoulder when the arm is straight down. GH3 is aligned with the long axis of the humerus. As a result of having already been vetted with stroke patients, the EXO-UL7, with modifications from the EXO-UL8 redesign, was taken as the starting configuration for the BLUE SABINO design.

6.2.3 SHOULDER RANGE OF MOTION REQUIREMENTS ESTIMATION

The requirements at the shoulder depend to some degree on the population of interest and their impairment characteristics. The target population in this case suffers from neurological impairment as a result of conditions such as stroke or cerebral palsy; furthermore, it is necessary to be able to assess both impaired and unimpaired limbs for baseline comparisons. For these reasons, the desired ROM of the system is the full ROM of the unimpaired shoulder including GH, SC, and AC joint contributions. While not all aspects of full ROM will be necessary for impaired limbs, the SC and AC joint inclusion will allow accurate measurement in a greater array of exhibited neuropathies and compensatory strategies, as well as accurate assessment of subjects' unimpaired ipsilesional sides, in the case of stroke.

To assess just how much mobility is needed to accommodate a healthy shoulder girdle, an activities-of-daily-living (ADLs) database [49] was used to estimate the translation of the GH joint during a variety of daily tasks. Most tasks were performed while seated at a desk with target locations for pick and place reaching tasks labeled on the desk and shelf as shown in Fig. 6.5. The dataset was collected using a 12-camera VICON motion capture system that tracked the Cartesian locations of seven markers on a subject at a rate of 120 Hz. The system maps the locations of the markers to an internal kinematic model and exports both Euler angle rotations for rigid bodies representing the arm, and Cartesian locations of the centers of rotation of the shoulder, elbow, and wrist.

The kinematic motions for 24 ADLs were captured for six subjects whose ages ranged from 20 to 41 years. Three of the subjects were male and three were female. Mean and standard deviations of height, weight, and age were 1.72 ± 0.08 m, 76.2 ± 23.1 kg, and 26.2 ± 7.7 years, respectively. Tasks were broken into subgroups of Reaching, Functional ADLs, Eating and Drinking, and Hygiene as follows:

1. Reaching (actions 1–7): Placing hand on desk (RP to Dh), moving an object between desktop positions (D1R to D1L, D0 to D2), *moving an object between shelf positions (S2L to S2R), combination shelf/desktop object motions (D1R to S2L, D1L to S2R, D1 to S2)*.
2. Functional ADLs (actions 8–15): *Opening and closing a door/cabinet/drawer*, answering a table-mounted phone (Dp), overhand/underhand stirring with a utensil (D1), pouring from a pitcher to a cup (Dp to Dc), and pouring from a cup to a pitcher (D1R to D1).
3. Eating and drinking (actions 16–19): Normal eating with a fork (D0), *powered grasp eating with a fork (D0)*, eating with right hand (D0), and drinking from a cup (Dc).

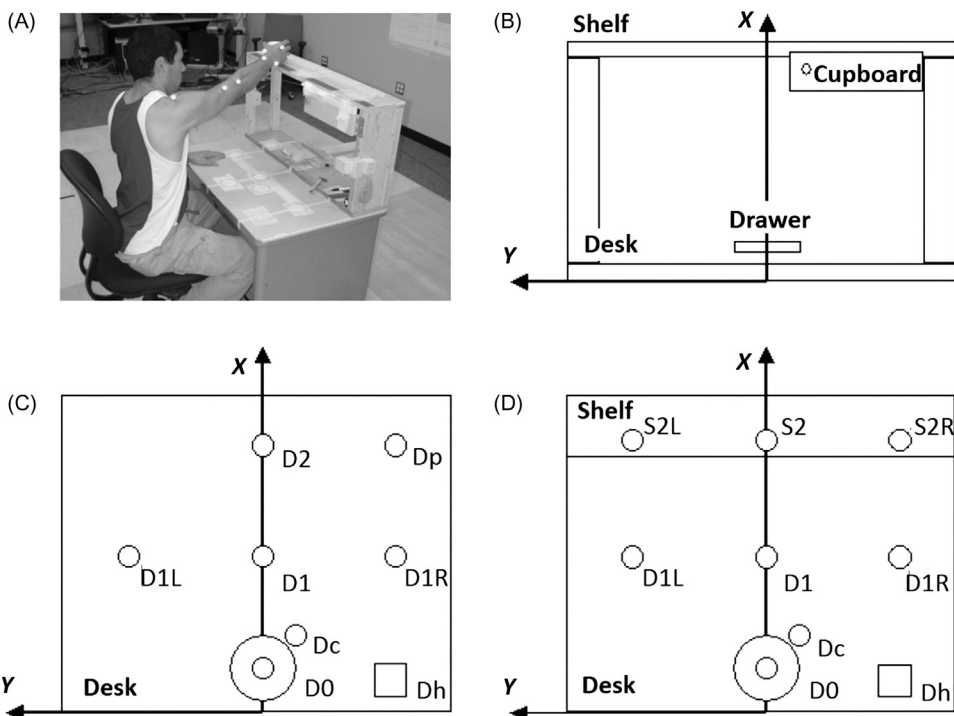


FIGURE 6.5

Desk location from the ADL study. Desk (D) and shelf (S) locations as defined in the ADL study were divided into three medial–lateral, three anterior–posterior, and two superior–inferior positions. Subjects sat in a chair of fixed height for all tasks except opening a door (standing). Reaching actions required moving an object (e.g., a cup) from one location to another and then back (A). A top view of the desktop (C) shows eight target desk locations, more heavily concentrated in the right-hand plane. The three shelf locations were located at the same x -coordinate as desk locations D2 and D_p, only 0.44 m above the desktop in the positive z -direction (D). Also attachable to the desk and shelf were a wood drawer, a cupboard, and a door (B). RP, not shown, refers to the rest pose of the arm lying comfortably along the subject's side.

*Reprinted with permission from J.C. Perry, J.M. Powell, J. Rosen, Isotropy of an upper limb exoskeleton and the kinematics and dynamics of the human arm, *Appl. Bionics Biomech.* 6 (2) (2009) 175–191.*

4. Hygiene (actions 20–24): Combing the hair, washing the face, shaving the face, brushing the teeth, and washing the neck.

For more details on the experimental setup and data collection process, readers are encouraged to review the original publication [49].

In the present analysis, only Cartesian position data is used. The ADL dataset provided shoulder positions in terms of Cartesian coordinates with respect to a global origin. For each ADL action, a shoulder origin was established as the mean position of the shoulder in the first 10 motion capture frames. The shoulder displacement for each frame is then taken as the absolute difference of the

shoulder's recorded position and the shoulder origin. A Euclidean norm is used to calculate the magnitude of shoulder displacement for each frame, and displacement histograms are then generated by placing displacement values in bins, where bin widths are automatically generated in order to represent the data with the same number of bins. Thus bin widths range from about 0.2 to 0.5 mm.

Some of the tasks in the original 24-action database involved a higher potential for torso involvement due to the nature of the task, and were therefore removed from the analysis. These included four pick-and-place tasks involving moving objects to or from a shelf, and a door-opening task (from standing). An additional action was removed that involved a simulated myopathic grasp of a utensil during an eating task. This task was removed in order to represent only natural movements of healthy individuals. Six actions were thus removed from the dataset in an effort to limit actions to those that would most accurately capture healthy shoulder girdle movement with minimal movement from the trunk. These six actions have been italicized in the complete list of actions and subgroups provided above. The data of individual subjects was also compared to see if subject stature might have had an impact on the amount of shoulder translation needed to pick and place objects. No significant differences were seen as a result of subject stature, and therefore all six subjects were included in the shoulder displacement analysis.

In most recordings, the start and end position was a specified location with about 1 second of recording before and after the task. Including the stationary period before movement onset would introduce a bias in the histograms toward positions near the task start and end position. To limit this bias, a velocity trigger is applied. The trigger segments each ADL action according to the velocity of the hand and only processes frames for which hand velocity is above the specified threshold of 50 mm/s.

6.2.4 CONCEPTUAL DESIGN OF A REMOTE BIOMIMETIC SHOULDER MODULE

A central goal of BLUE SABINO is to enable full-arm assessment during reach and grasp tasks, which requires a close fit with human arm kinematics at the shoulder, elbow, wrist, and fingers. Full GH joint ROM cannot be achieved by a shoulder modeled as a spherical joint. Natural movement of the shoulder girdle and subsequent quality of rehabilitation and assessment capabilities are intrinsically linked to the functional performance of the device itself. Some devices have simplified the movement of the shoulder girdle based on typical scapulohumeral rhythm patterns. However, scapulohumeral movements are quite complex, without definitive agreement upon the relationship between scapular and humeral motion. Unimpaired individuals have the ability to volitionally change the ratio between GH and scapular motion to perform desired movements (e.g., a shoulder shrug). Similarly, neurological damage can also alter the patterns observed in scapulohumeral rhythm. For these reasons, a less constrained model of the shoulder girdle has been developed.

In this work, a clavicular design approach has been selected in which the articulation of the SC and AC joints are incorporated. In its simplest form, the clavicle operates as a link with a universal joint at each end. Musculotendinous attachments allow protraction/retraction movement in the anterior-posterior direction and allow elevation/depression movements in the superior-inferior direction. Due to the shape of the ST false joint, the elevation/depression movements are mostly imparting a translation to the GH joint while the smaller radius of ST curvature in protraction/retraction imparts both a

translation and a rotation. For simplicity, this rotation is ignored in the design of the clavicle and instead will be accounted for with the 3-DOF GH joint.

6.2.4.1 Adjustment-free biomimetic clavicle

The first consideration in the design of a biomimetic exoskeleton clavicle is length as this will define the shape of the movement and the ratio between clavicular rotation and the resulting translation of the GH joint center. The range of clavicle lengths vary substantially from about 119 mm in the 5th percentile female to 152 mm in the 95th percentile male [33]. While this appears to be a significant difference in length, the resulting difference in curvature between the two is quite minor over the ROM in question. The largest ROM experienced by the shoulder in regards to elevation/depression or protraction/retraction is approximately 30 degrees. It should be noted that this ROM is due to the contribution of all the shoulder joints combined, and that full ROM of the shoulder is generally not required to perform most ADLs. In most ADL movements, total GH motion does not exceed 120 degrees in flexion and abduction directions [11], and in this range, the clavicle elevates only about 6 degrees and protracts/retracts 15 degrees [50,51]. Thus it is assumed that most of the operation of this device will see a maximum angular displacement of 15 degrees or less in any given direction. Given this condition, Fig. 6.6A, illustrates how closely the 5th percentile female and 95th percentile male clavicular lengths overlap when the distal ends of the clavicle are aligned. In the figure, the 30-degree arclength on the left has been superimposed on the 30-degree arclength on the right to showcase the small amount of GH misalignment that would result from using a single-length clavicle design. As shown in the figure, the curves for both clavicular lengths are

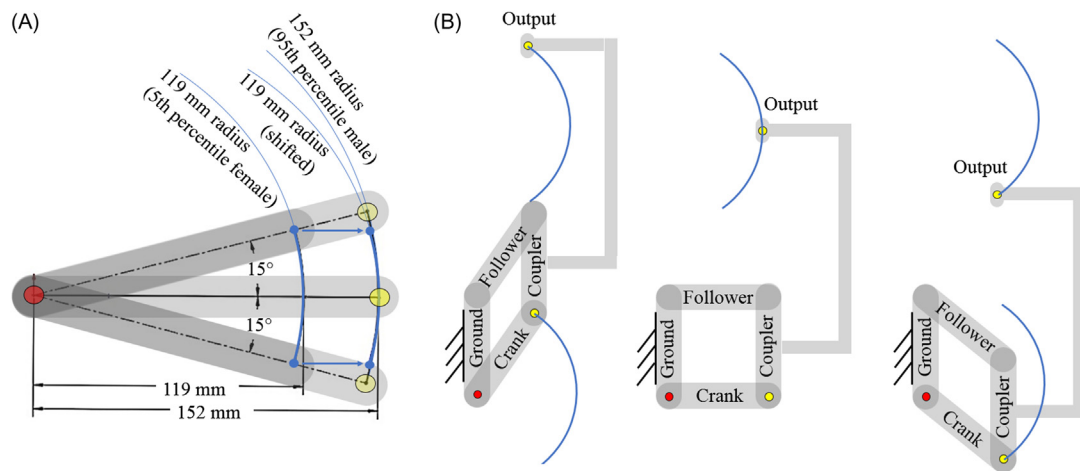


FIGURE 6.6

A comparison between estimated distal endpoint motion of clavicles from a 5th percentile female and a 95th percentile male (A) rotating through a 30-degree arc. The path of the 5th percentile female has been shifted and superimposed on the 95th percentile male path to show the similarity. A planar four-bar mechanism composed of ground, crank, follower, and coupler links (B) illustrates with semicircular paths how points on the remote output mimic the movements of the coupler.

similar over the expected ROM. Not only can full ROM be achieved for the entire span of clavicle lengths with a single 152 mm length, but the curve traveled is nearly identical for all cases. Even at the extremes of the motion the curves are in close agreement, suggesting that a fixed-length link is appropriate.

6.2.4.2 Four-bar mechanism for remote positioning

A limitation of exoskeleton design lies in joint placement. Typically, robot joints are intended to align with the corresponding joints of the user. But what if the desired motion could be achieved remotely, allowing greater freedom in joint placement? This would be advantageous in preexisting designs that want to minimize the revision needed to the existing setup. This concept is the motivation behind the integration of a dual four-bar mechanism in PRISM.

Another motivation for the use of a dual four-bar mechanism in the design of PRISM is the potential for gravity compensation. The elevation and depression DOF continuously bears the weight of the attached exoskeleton system. Without gravity compensation, the system would require the corresponding elevation/depression actuator to provide a continuous load to maintain a stationary vertical position. Other common solutions to increasing available torque involve the use of larger gears (increasing friction and backlash, and reducing backdrivability), or using larger motors (adding size, weight, and cost). Both alternatives come with drawbacks that can be avoided through the use of gravity compensation made possible by the four-bar mechanism.

To understand the kinematics of PRISM's four-bar design, we first consider a parallelogram. A parallelogram is a type of four-bar mechanism, but it has a unique feature in that the coupler link remains parallel to the ground link throughout its prescribed rotation as shown in Fig. 6.6B. In this way, any arbitrary rigid structure affixed to the coupler link will translate in unison with the coupler, thereby transcribing the translation of the distal four-bar joints to any arbitrary point along the rigid structure. This allows such a device to support one-dimensional rotation of the clavicle remotely, which could be used to support elevation/depression or protraction/retraction.

Extending this concept orthogonally out of the plane of the four-bar, a dual parallelogram four-bar mechanism with universal joints in place of pin joints could produce both vertical and horizontal rotation while maintaining a parallel output at any location. This principle has been leveraged in the development of a remote 2-DOF scapulohumeral positioning device.

6.2.4.3 Dual four-bar mechanism preliminary modeling

A dual four-bar model was designed in SolidWorks to verify the combination of the components previously outlined. This included four moving links and one stationary “ground” link (Fig. 6.7). The model is simple in design, with features like bearings modeled by through holes that use bolts to serve as revolute joints.

The main objective of the prototype is to validate the potential for the desired 2-DOF mobility. Gruebler's equation [Eq. (6.1)] is often used to identify the DOFs of multisegment parallel planar mechanisms:

$$F = 3(n - 1) - 2(f_1) - 1(f_2) \quad (6.1)$$

where F is the mobility or DOFs of the system, n is the number of links, and f_n is the number of joints with n DOFs. For a standard planar four-bar, such as that depicted in Fig. 6.7D, n is 4, f_1 is 4, and f_2 is 0, resulting in 1 degree of planar mobility. However, the PRISM mechanism is not

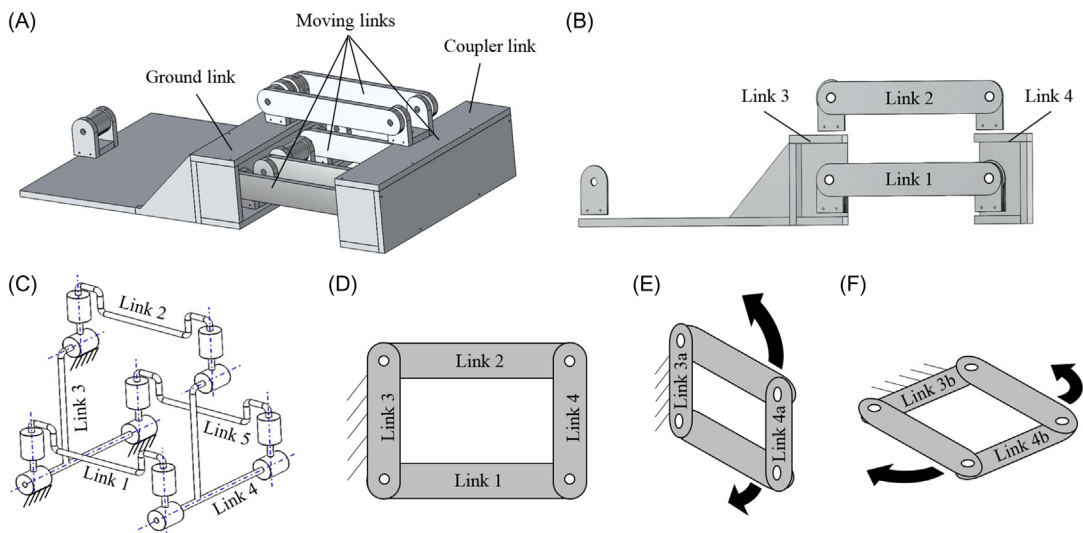
**FIGURE 6.7**

Illustration of the prototype linkage design and kinematics: (A) solid model showing stationary (Ground) link and moving links; (B) side view showing four-bar configuration; and (C) the kinematic diagram of the mechanism. Functionally, the structure has the combined mobility of two standard four-bar mechanisms (D), one oriented in the vertical plane (E), and one oriented in the horizontal plane (F).

restricted to planar movement despite having only 2 DOFs. Rather, the motion of each point on the output side is constrained to the surface of a sphere. In this case, the spatial Gruebler equation [Eq. (6.2), also known as the “mobility equation” or Kutzbach criterion] would be implemented as follows:

$$F = 6(N - 1) - 5(P_5) - 4(P_4) - 3(P_3) - 2(P_2) - P_1 \quad (6.2)$$

where F is the mobility or DOFs of the system, N is the number of links, and P_n is the number of joints with n DOFs removed per joint. Each joint in 3D space has the capability of 6 DOFs. If a revolute joint is considered, its constraints allow for one DOF. Thus it removes 5 DOFs. For example, if three revolute joints were the objects of interest, then P_5 in Eq. (6.1) would be replaced with the number 3. This is synonymous with saying that there are three joints with only 1 DOF each, or in other words, three joints that remove 5 DOFs. Every subsequent joint in the device is analyzed in the same manner. Any terms that do not apply to the system being evaluated are simply omitted from the equation. Unfortunately, as shown in Eq. (6.3), Eq. (6.2) incorrectly predicts PRISM’s mobility as having 0 DOF:

$$F = 6(5 - 1) - 4(6) \Rightarrow 0 \text{ DOFs} \quad (6.3)$$

As occurs with a number of other closed-chain parallel mechanisms, the parallel structure of the PRISM design results in what is known as an overconstrained mechanism. An overconstrained

mechanism is a mechanism that has more DOFs than the mobility equation predicts. This is because the mobility equation does not take into account the relative locations or orientations of joints, nor the length of linkages, both of which can result in configurations where particular geometries allow specific movements. In other words, what Eq. (6.3) actually tells us, is that in most cases a mechanism with five linkages and six 2-DOF joints will result in a fully constrained structure. There are however some configurations, such as that used in the PRISM design and other specific parallel mechanisms, where the particular characteristics of link lengths, joint configurations, and/or joint locations align in ways that allow mobility. As a side note, these designs can result in mechanisms with higher strength and rigidity due to the presence of parallel structures, which in the case of an exoskeleton device can be highly advantageous.

A closer look at the building blocks of the mechanism reveals the design is based on two orthogonal parallel four-bar mechanisms, one oriented in the vertical plane (Fig. 6.7E), and the other oriented in the horizontal plane (Fig. 6.7F). Eq. (6.1) correctly predicts a 1-DOF mobility of a planar four-bar mechanism composed of four links and four 1-DOF joints. When a second 1-DOF parallel four-bar mechanism (with the same link lengths) is attached orthogonal to the first one, and all revolute joints are replaced by properly orientated universal joints, the result is a mechanism that retains mobility in the same 2 DOFs originally contributed by each 1-DOF mechanism. At the same time, the coupler link of the 2-DOF planar configuration (that remains parallel to its ground link) continues to remain parallel to the ground links of both horizontally and vertically oriented four-bar mechanisms in the spatial configuration. In other words, the coupler link is allowed to move in 2 DOFs while remaining parallel to the plane defined by the intersection of the axes on the ground link. The prototype design is shown again in Fig. 6.8 with labeled movement directions and a cross-section view through links 1, 2, and 5 for greater clarity.

6.2.5 GRAVITY COMPENSATION METHODS

The output side of the dual four-bar mechanism will support the entirety of the remaining exoskeleton arm and hand. While the mechanism will experience some internal loading due to the moment arms developed in the coronal plane, a significant amount of external loading will occur simply from maintaining vertical position against gravitational forces. This makes the mechanism an ideal candidate for applying a gravitational compensation method.

Numerous solutions for gravity compensation have been previously developed in the form of zero-length spring gravity equilibrators [52]. The most convenient configuration for this setup is the three-pulley, fixed spring model, shown in Fig. 6.9.

6.3 RESULTS

Results of shoulder displacement estimations from a 2009 ADL dataset [49] are reported below, followed by the preliminary and final designs of the remote four-bar shoulder mechanism.

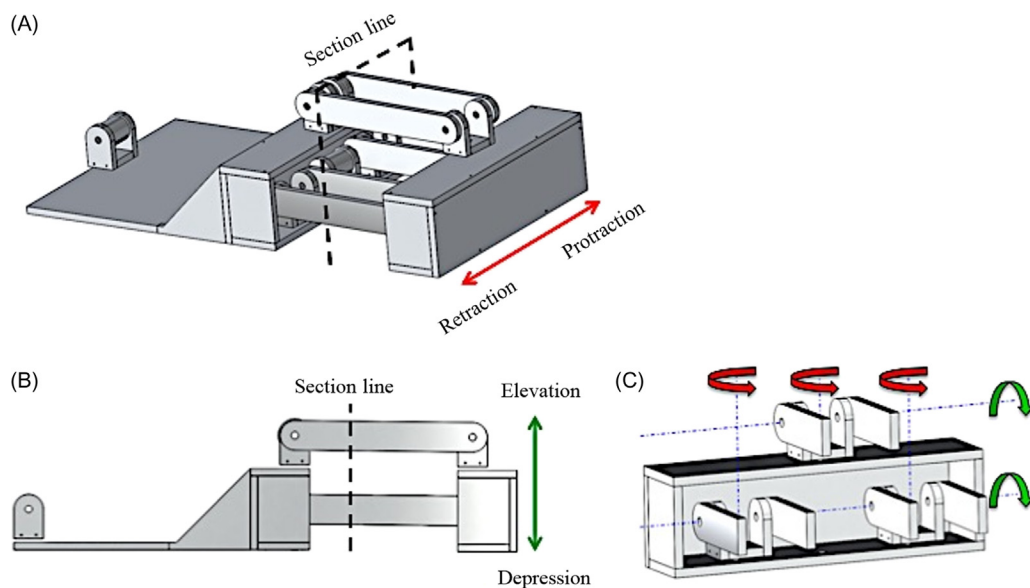


FIGURE 6.8

Isometric view (A) and side view (B) of the solid model. Section lines indicates plane of intersection. Direction of protraction, retraction, elevation, and depression are identified for the given orientation. (C) Section view of the prototype showing the interior of the dual four-bar mechanism with arrows indicating protraction and depression movements.

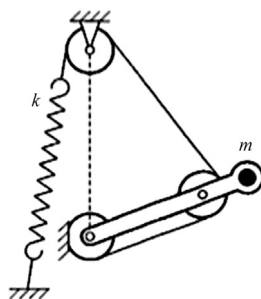


FIGURE 6.9

A three-pulley zero-length spring gravity equilibrator can provide perfect gravity balancing of mass, m , and allow a large degree of freedom in the placement of the spring fixed to ground.

*Reprinted with permission from J.L. Herder, Energy-Free Systems; Theory, Conception and Design of Statically Balanced Spring Mechanisms (Ph.D. thesis), Delft University of Technology, ISBN 90-370-0192-0 (<http://repository.tudelft.nl>), 2001, p. 139.
doi:10.13140/RG.2.1.3942.8966.*

6.3.1 SHOULDER RANGE OF MOTION REQUIREMENTS ESTIMATION

A previous database of 24 ADL tasks was reduced to a set of 18 tasks and used to plot positional variation of the shoulder during all tasks, as well as during specific task subgroups. Computed histograms from the 18-task ADL dataset show that the modeled GH joint position translates between 5 and 15 cm for most tasks with very minimal activity above 15 cm, with the average being around 4 cm. Exclusion of the furthest reaching tasks (i.e., those believed to contain the most artifacts of torso motion) removed most of the displacements above 15 cm (as seen in the comparison between Fig. 6.10A and B). While some level of torso involvement may remain in the reported measures of Fig. 6.10B–F, the amount is believed to be low. A comparison between displacements from select hygiene tasks (i.e., combing hair, washing the face, shaving, brushing teeth, and washing the neck) show similar displacement magnitudes as those seen in the rest of the dataset. Shoulder displacement from torso movement is expected to be negligible in these tasks as a result of the target location being on the body (i.e., the head). This is also the reason that a rather pronounced peak is seen in the hygiene tasks (Fig. 6.10F) between 4 and 5 cm of displacement where a substantial portion of the task time takes place in the vicinity of the head. The displacement similarities between the hygiene tasks and all other tasks indicate that if torso movement is present in the data, it does not result in displacements of the shoulder beyond the levels that the shoulder displaces as a result of its own internal joints. Based on these results, it is anticipated that the reported GH displacements from the 18-task dataset are due primarily to displacements of the GH joint as a result of SC and AC contributions, as opposed to contributions from the torso.

Displacement histograms were also generated for each subject to assess the effect of subject height on shoulder displacement for the given task setup. No significant differences were seen between intersubject displacements, indicating that stature was not a factor in the resulting shoulder displacement values.

From the histograms of Fig. 6.10, it can be seen that variations in GH displacement emerge within different task subgroups. The reaching tasks have most activity from 0 to 5 cm and about $\frac{1}{4}$ of their activity spread out over the range of 5–15 cm. Functional tasks show more than 90% of displacements range from 0 to 9 cm and the remaining activity is spread thinly from 9 to 17 cm. Eating and drinking tasks saw the least amount of GH movement, with about 90% of the data falling below 5 cm. Hygiene tasks saw a distinct peak in the displacement data at around 5 cm, consistent with the magnitudes seen in the eating and drinking tasks and a marked exponential decay with about 90% of the data falling between 0 and 10 cm.

As a result, we estimate that the amount of GH joint translation support needed to accommodate the majority ($\sim 90\%$) of healthy ADL movements is between 10 and 12 cm with an estimated maximum value of 15 cm and an average value between 3 and 5 cm.

6.3.2 DUAL FOUR-BAR MECHANISM PROOF-OF-CONCEPT MOCKUP

A computer-aided drafting model (Fig. 6.11A) and proof-of-concept wood mockup (Fig. 6.11B) were produced to validate the adequacy of the 2-DOF mobility enabled. Constructed of $\frac{1}{4}$ " Baltic birch plywood using a laser cutter, the entire device was assembled and evaluated for ROM, mobility, and potential weak points in the design.

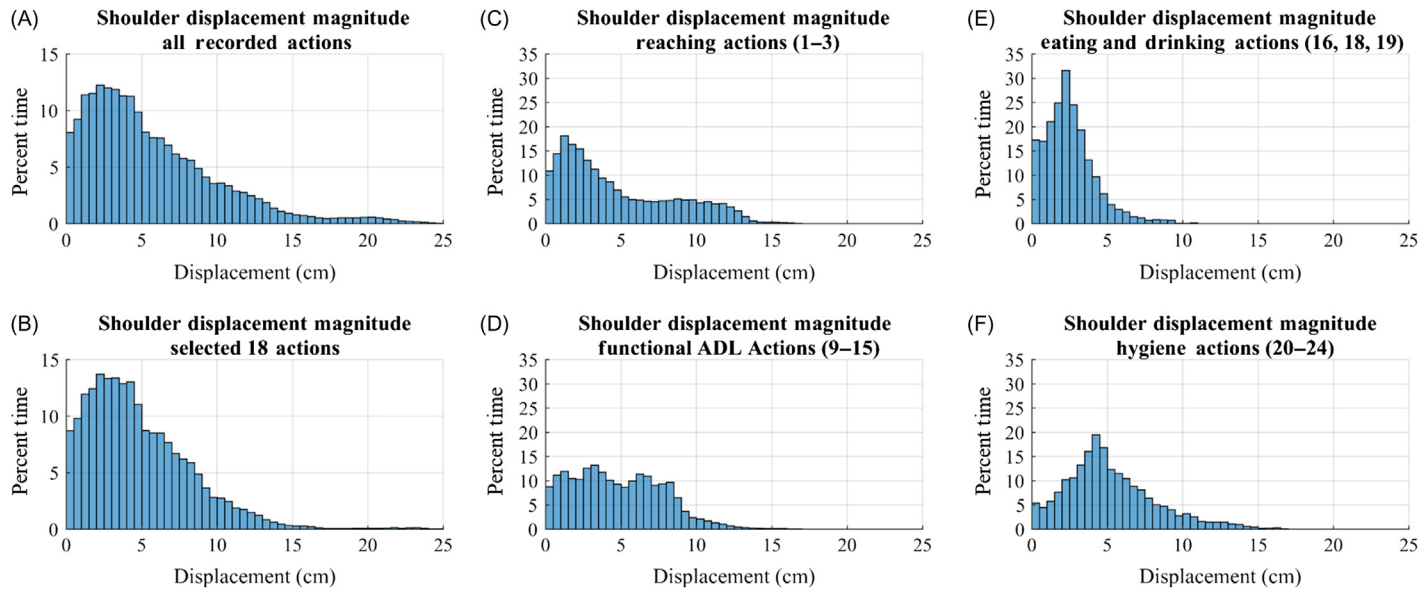
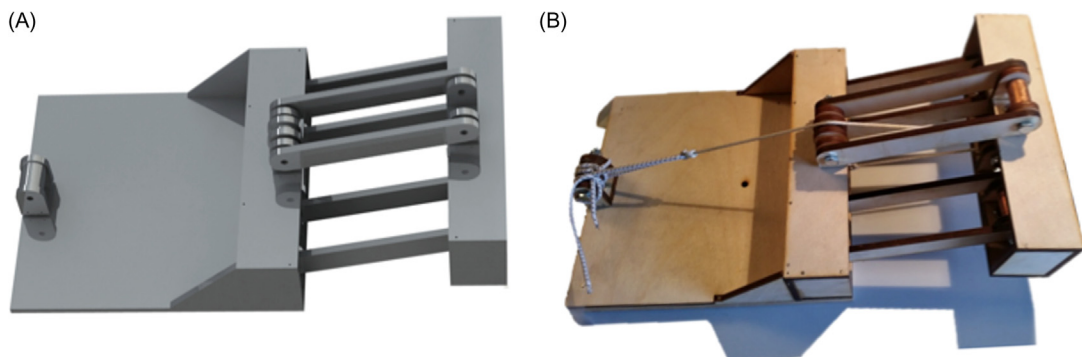


FIGURE 6.10

Histograms of estimated shoulder GH joint displacement from rest as computed from a set of 24 actions (A) and a subset of 18 actions (B) from a 2009 ADL database [49]. Additional histograms show action subgroups from the 18-action subset including: Reaching actions (C), Functional ADL actions (D), Eating and Drinking actions (E), and Hygiene actions (F).

**FIGURE 6.11**

SolidWorks model (A) and laser-cut wood mockup (B) of a proof-of-concept dual four-bar prototype. Revolute joints are created with bolts serving as bearings. Note the three-pulley gravity compensation method was included in the prototype to demonstrate a possible method for its integration.

The physical prototype proved to be an effective evaluation tool. A rudimentary form of gravity compensation was included in the design and although not optimized, its inclusion demonstrated the feasibility of the approach and its potential to compensate weight over a wide range of orientations. To increase torsional stability of the design, a fourth redundant link was added that effectively reduces the loading conditions on the remaining joints, thereby increasing stability. The dual-link setup at each pivot allows for dual bearings, which simultaneously accommodate moment and axial loading, and provide an opportunity to implement solid bearing preload. Despite the added joints, the kinematic behavior is unchanged, and therefore remains a 2-DOF mechanism. Lastly, the desired ROM was easily attained and the parallel function performed as expected, allowing both elevation/depression and protraction/retraction in a single mechanism. Thus the proof of concept verified the use of a dual four-bar mechanism for achieving clavicular motion.

6.3.3 EXOSKELETON CLAVICLE DESIGN AND ASSEMBLY

The clavicular link design ([Fig. 6.12A](#)) is a critical component that enables the desired ROM and overall stability of the mechanism. Each of four links are identically shaped with counterbored through holes for dual bearings that enable elevation/depression ([Fig. 6.12B](#)), and relief cuts on each end for clearance with perpendicularly-oriented shafts that simultaneously accommodate for protraction/retraction ([Fig. 6.12C](#)). In this design, recessed pockets of material have been removed from both sides for weight reduction purposes.

6.3.4 SPRING-BASED GRAVITY COMPENSATION

Although the spring stiffness and cable routing have not been finalized, the preliminary routing of the cable and pulley placement are included in the model. The resemblance to the cable/pulley arrangement of [Fig. 6.9](#) is clearly apparent. The cable resides in a plane midway between the

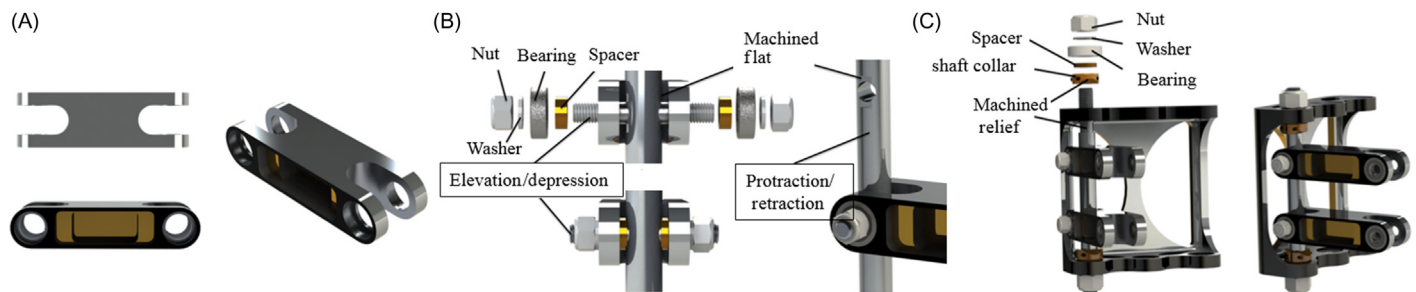
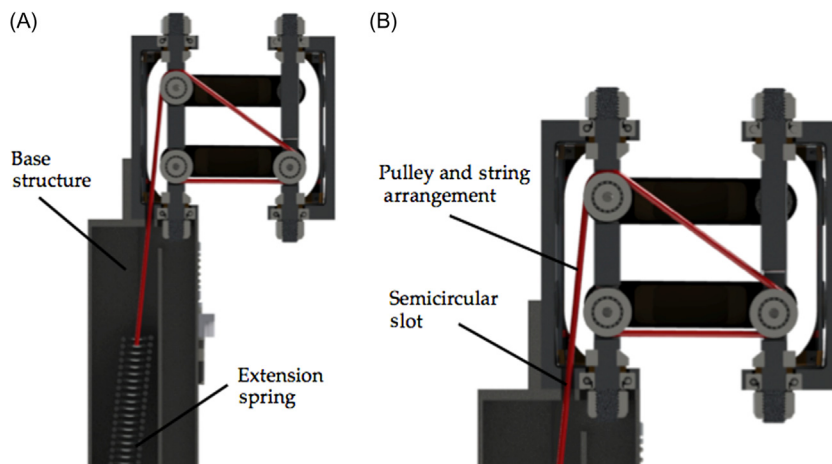


FIGURE 6.12

Renders of the clavicular link design (A); the elevation/depression axis exploded assembly (B); the protraction/retraction axis exploded assembly and the constructed assembly for a single protraction/retraction four-bar mechanism (coupler link is missing from the view) (C).

**FIGURE 6.13**

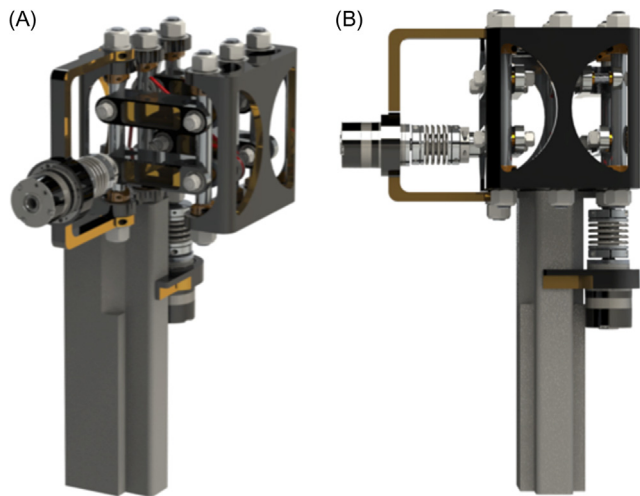
Section view of the entire balancing mechanism (A). The base structure serves as both a mounting surface for the scapulohumeral device and a way to conceal the extension spring. Close-up view (B) to illustrate the three-pulley gravity balancing system and the semicircular slot for cable clearance.

anterior and posterior four-bar mechanisms for elevation/depression, extending from a fixed termination at the bottom of a first pulley, and wrapping around two other pulleys before attaching to a spring fixed to the base. Section views of the mechanism exposing the cable routing are shown in Fig. 6.13.

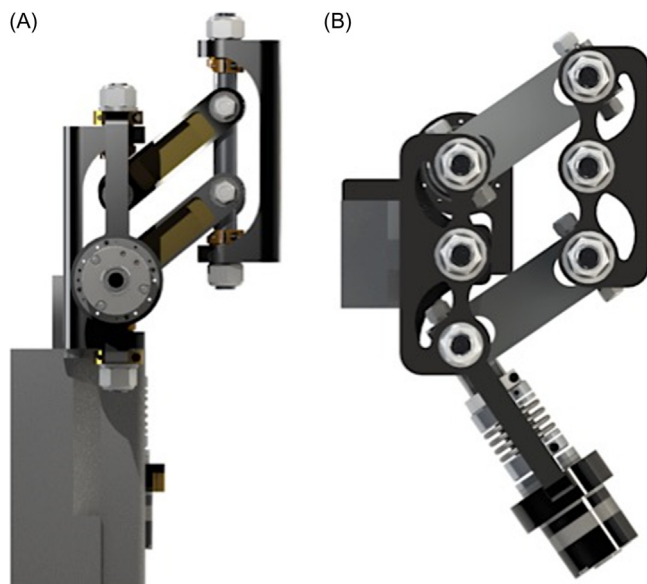
6.3.5 PRISM FINAL DESIGN

In the final assembly, the parallel dual four-bar mechanism is composed of two parallel endplates separated by the four clavicular links attached to each plate via revolute joints on vertical posts. The joints between each part are seated in bearings forming a universal joint between each clavicular link and each endplate. In Fig. 6.14A, the leftmost (or proximal) endplate is fixed, while each point on the rightmost (or distal) endplate is able to translate along the surface of a sphere defined by the distance between the axes of each clavicular link. Torque is transmitted from two actuators (Harmonic Drive, Peabody, MA) through bellows couplings to minimize radial loading due to misalignment. As shown in Fig. 6.14B, the bellows coupling of the lower motor is attached to the proximal anterior post driving the protraction/retraction DOF, and the bellows coupling of the leftmost motor is attached to the proximal end of the lower posterior clavicular link, driving elevation/depression.

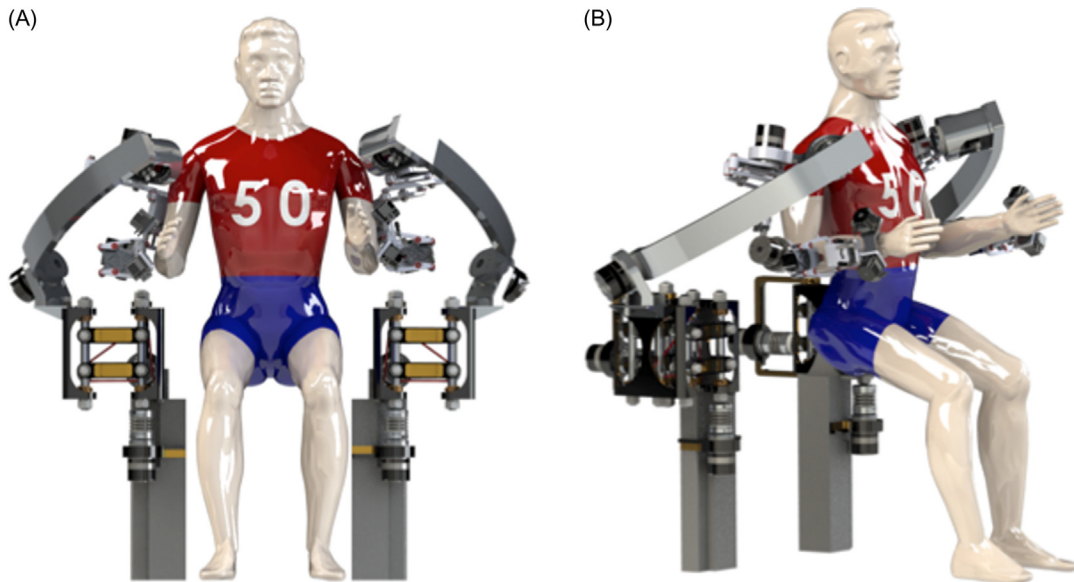
When elevated, the distal endplate translates upward and medially (Fig. 6.15A) and when protracted, the distal endplate translates anteriorly and medially (Fig. 6.15B). In both cases, it can be seen that the distal endplate remains parallel to the fixed base, allowing the actuation to induce a translation on all distally mounted structures. The parallel structure and heavy duty part design are capable of providing the desired level of stability and rigidity to withstand moments from remote exoskeleton loading. From a mechanical perspective, the design is capable of moving the clavicular

**FIGURE 6.14**

Isometric view (A) and front view (B) of the PRISM full assembly.

**FIGURE 6.15**

Side view of PRISM (A) illustrating parallel movement for elevation and depression. Top view (B) showing parallel movement of shoulder protraction and retraction.

**FIGURE 6.16**

BLUE SABINO front view (A) and front isometric view (B). Note the distance from PRISM to the subject. To allow full ROM with the BLUE SABINO, PRISM must be positioned far enough behind the patient to not interfere with posterior arm movements. Note, the design of PRISM allows it to be placed where it best benefits the particular exoskeleton design.

links ± 40 degrees in elevation/depression, 35 degrees in protraction, and 25 degrees in retraction. For the 95th percentile male clavicular length, this equates to ± 9.8 cm in elevation/depression, 8.7 cm in protraction, and 6.4 cm in retraction, for a combined vertical and horizontal displacement of 19.5 and 15.1 cm, respectively.

The parallel nature of the design allows the freedom of placing the mechanism where it is most convenient for the design. In the BLUE SABINO, the PRISM “boxes” will be positioned such that a patient (and wheelchair) can pass between them for easier front or rear loading into the instrument. This places PRISM shoulder mechanisms behind and to the sides of the patient at about the level of the hip joint, as illustrated in Fig. 6.16, while the vertical support structure can be used to house the gravity-compensating spring system.

6.4 CONCLUSION AND DISCUSSION

The design of PRISM extends the classical 1-DOF planar four-bar mechanism to a 2-DOF spatial dual four-bar mechanism. The results show promise as a means of expanding the anthropomorphic shoulder functionality of existing exoskeleton arm systems. The proposed parallel dual four-bar mechanism provides an additional 2 DOFs to the shoulder to enable elevation, depression,

protraction, and retraction movements extending functionality from a 3-DOF design to a 5-DOF shoulder system. The four-bar arrangement keeps the design output parallel to the base, allowing freedom to place the mechanism where desired for specific exoskeleton designs. The parallel design also allows for easy gravity compensation via established gravity equilibrator designs. The biomimetic link size was developed to fit a wide range of individuals from the 5th percentile female to the 95th percentile male providing an adjustment-free solution.

Results of shoulder displacement during seated ADL tasks provide insight on the ROM requirements of the shoulder to support natural movement. Even in relatively small workspaces, it is known that the GH joint of the shoulder does not remain stationary. In common ADL tasks, the unrestrained shoulder leads to GH translations of about 4 cm on average and peak displacements of up to 15 cm or more approaching the edges of the shoulder workspace. A mechanism with a GH displacement capability of 10–12 cm would accommodate approximately 90% of the shoulder displacement seen in this study. The PRISM design accommodates up to 19.5 cm of translation vertically and 15.1 cm horizontally. Combined, these accommodate a peak displacement of up to 24.6 cm when both protraction and elevation are fully engaged. The resulting ROM of PRISM therefore allows full coverage of the ROM experienced during common ADLs. Although in this ADL dataset restraints were not added to isolate shoulder girdle contributions from torso contributions, the authors believe that the vast majority of the shoulder displacement recorded in this study came directly from the joints of the shoulder complex rather than the torso. This indicates that natural arm kinematics at the shoulder may be stifled in exoskeletons that simplify the shoulder to a 3-DOF joint with a static center of rotation.

The PRISM design is being developed as part of a comprehensive exoskeleton instrument for full-arm assessment. As of the publication of this manuscript, the design remains largely virtual and the final hardware has not yet been fabricated beyond proof-of-concept prototypes. Preliminary evaluations look promising as a biomimetic add-on to enable anthropomorphic shoulder movements, but final validations with healthy and impaired individuals are needed in order to verify the appropriateness of enabled movements, physical human–machine interfaces, and control modalities with hypotonic patients.

ACKNOWLEDGMENTS

This work was funded by the National Science Foundation (Award#1532239) and the Eunice Kennedy Shriver National Institute of Child Health & Human Development of the National Institutes of Health (Award#K12HD073945). The content is solely the responsibility of the authors and does not necessarily represent the official views of the National Science Foundation nor the National Institutes of Health.

REFERENCES

- [1] E.J. Benjamin, S.S. Virani, C.W. Callaway, A.M. Chamberlain, A.R. Chang, S. Cheng, et al., Heart disease and stroke statistics—2018 update: a report from the American Heart Association, *Circulation* 137 (12) (2018) e67–e492.

- [2] M.C. Cirstea, A. Ptito, M.F. Levin, Arm reaching improvements with short-term practice depend on the severity of the motor deficit in stroke, *Exp. Brain Res.* 152 (4) (2003) 476–488.
- [3] N. Hogan, H.I. Krebs, J. Charnnarong, P. Srikrishna, A. Sharon, MIT-MANUS: a workstation for manual therapy and training. I, in: *Robot and Human Communication*, 1992. Proceedings, IEEE International Workshop on Sep 1, 1992, 161–165.
- [4] M.L. Aisen, H.I. Krebs, N. Hogan, F. McDowell, B.T. Volpe, The effect of robot-assisted therapy and rehabilitative training on motor recovery following stroke, *Arch. Neurol.* 54 (4) (1997) 443–446.
- [5] C.G. Burgar, P.S. Lum, P.C. Shor, H.M. Van der Loos, Development of robots for rehabilitation therapy: the Palo Alto VA/Stanford experience, *J. Rehabil. Res. Dev.* 37 (6) (2000) 663–674.
- [6] D.J. Reinkensmeyer, L.E. Kahn, M. Averbuch, A. McKenna-Cole, B.D. Schmit, W.Z. Rymer, Understanding and treating arm movement impairment after chronic brain injury: progress with the ARM guide, *J. Rehabil. Res. Dev.* 37 (2000) 653–662.
- [7] A.C. Lo, P.D. Guarino, L.G. Richards, J.K. Haselkorn, G.F. Wittenberg, D.G. Federman, et al., Robot-assisted therapy for long-term upper-limb impairment after stroke, *N. Engl. J. Med.* 362 (19) (2010) 1772–1783.
- [8] N. Shute. How Robots Are Aiding Stroke Rehabilitation, Heart Health, US News. Available: <<http://health.usnews.com/health-news/managing-your-healthcare/heart/articles/2008/09/19/how-robots-are-aiding-stroke-rehabilitation>> (accessed 10.11.16).
- [9] T. Nef, M. Guidali, R. Riener, ARMin III—arm therapy exoskeleton with an ergonomic shoulder actuation, *Appl. Bionics Biomech.* 6 (2) (2009) 127–142.
- [10] A. Gupta, M.K. O’Malley, Design of a haptic arm exoskeleton for training and rehabilitation, *IEEE/ASME Trans. Mechatronics* 11 (3) (2006) 280–289.
- [11] J.C. Perry, J. Rosen, S. Burns, Upper-limb powered exoskeleton design, *IEEE/ASME Trans. Mechatronics* 12 (4) (2007) 408–417.
- [12] A. Frisoli, F. Salsedo, M. Bergamasco, B. Rossi, M.C. Carboncini, A force-feedback exoskeleton for upper-limb rehabilitation in virtual reality, *Appl. Bionics Biomech.* 6 (2) (2009) 115–126.
- [13] A.H. Stienen, E.E. Hekman, F.C. Van Der Helm, H. Van Der Kooij, Self-aligning exoskeleton axes through decoupling of joint rotations and translations, *IEEE Trans. Robot.* 25 (3) (2009) 628–633.
- [14] H.I. Krebs, N. Hogan, M.L. Aisen, B.T. Volpe, Robot-aided neurorehabilitation, *IEEE. Trans. Rehabil. Eng.* 6 (1) (1998) 75–87.
- [15] P.S. Lum, C.G. Burgar, M. Van der Loos, P.C. Shor, M. Majmundar, R. Yap, MIME robotic device for upper-limb neurorehabilitation in subacute stroke subjects: a follow-up study, *J. Rehabil. Res. Dev.* 43 (5) (2006) 631–643.
- [16] J.C. Perry, J. Oblak, J.H. Jung, I. Cikajlo, J.F. Veneman, N. Goljar, et al., A variable structure pantograph mechanism with spring suspension system for comprehensive upper extremity haptic movement training, *J. Rehabil. Res. Dev.* (2010).
- [17] M. Casadio, V. Sanguineti, P.G. Morasso, V. Arrichiello, Braccio di Ferro: a new haptic workstation for neuromotor rehabilitation, *Technol. Health Care* 14 (3) (2006) 123–142.
- [18] T. Laliberté, L. Birglen, C. Gosselin, Underactuation in robotic grasping hands, *Mach. Intell. Robot. Control* 4 (3) (2002) 1–11.
- [19] A. Chiri, N. Vitiello, F. Giovacchini, S. Roccella, F. Vecchi, M.C. Carrozza, Mechatronic design and characterization of the index finger module of a hand exoskeleton for post-stroke rehabilitation, *IEEE/ASME Trans. Mechatronics* 17 (5) (2012) 884–894.
- [20] O.Y. Kanner, A.M. Dollar, Kinematic design of an underactuated robot leg for passive terrain adaptability and stability, *J. Mech. Robot.* 5 (3) (2013) 031006.
- [21] N. Rijnveld, H.I. Krebs, Passive wrist joint impedance in flexion-extension and abduction-adduction, in: *Rehabilitation Robotics*, 2007. ICORR 2007. IEEE 10th International Conference on Jun 13, 2007, IEEE, pp. 43–47.

- [22] N. Vitiello, T. Lenzi, S. Roccella, S.M.M.E. De Rossi, E. Cattin, F. Giovacchini, et al., NEUROExos: a powered elbow exoskeleton for physical rehabilitation, *IEEE Trans. Robot.* 29 (1) (2013) 220–235.
- [23] A. Otten, C. Voort, A. Stienen, R. Aarts, E. van Asseldonk, H. van der Kooij, LIMPACT: a hydraulically powered self-aligning upper limb exoskeleton, *IEEE/ASME Trans. Mechatronics* 20 (5) (2015) 2285–2298.
- [24] M. Ergin, V. Patoglu, Assiston-se: a self-aligning shoulder-elbow exoskeleton, in: Proc. IEEE Int. Conf. Robot. Autom. 2012, pp. 2479–2485.
- [25] D. Galinski, J. Sapin, B. Dehez, Optimal design of an alignment-free two-dof rehabilitation robot for the shoulder complex, in: Proc. IEEE Int. Conf. Rehabil. Robot. 2013, pp. 1–7.
- [26] Y. Jung, J. Bae, Kinematic analysis of a 5-dof upper-limb exoskeleton with a tilted and vertically translating shoulder joint, in: Proc. IEEE/ASME Int. Conf. Adv. Intell. Mechatronics, 2013, pp. 1643–1648.
- [27] M. Murie-Fernandez, M.C. Iragui, V. Gnanakumar, M. Meyer, N. Foley, R. Teasell, Painful hemiplegic shoulder in stroke patients: causes and management, *Neurología (English Ed.)* 27 (4) (2012) 234–244.
- [28] R.D. Zorowitz, D. Idank, T. Ikai, M.B. Hughes, M.V. Johnston, Shoulder subluxation after stroke: a comparison of four supports, *Arch. Phys. Med. Rehabil.* 76 (8) (1995) 763–771.
- [29] R.A.R.C. Gopura, D.S.V. Bandara, K. Kiguchi, G.K.I. Mann, Developments in hardware systems of active upper-limb exoskeleton robots: a review, *Robot. Auton. Syst.* 75 (2016) 203–220.
- [30] W.S. Harwin, T. Rahman, R.A. Foulds, A review of design issues in rehabilitation robotics with reference to North American research, *IEEE. Trans. Rehabil. Eng.* 3 (1) (1995) 3–13.
- [31] H.S. Lo, S.Q. Xie, Exoskeleton robots for upper-limb rehabilitation: state of the art and future prospects, *Med. Eng. Phys.* 34 (3) (2012) 261–268.
- [32] B. Sheng, Y. Zhang, W. Meng, C. Deng, S. Xie, Bilateral robots for upper-limb stroke rehabilitation: state of the art and future prospects, *Med. Eng. Phys.* 38 (7) (2016) 587–606.
- [33] Y. Ren, S.H. Kang, H.S. Park, Y.N. Wu, L.Q. Zhang, Developing a multi-joint upper limb exoskeleton robot for diagnosis, therapy, and outcome evaluation in neurorehabilitation, *IEEE. Trans. Neural. Syst. Rehabil. Eng.* 21 (3) (2013) 490–499.
- [34] D.A. Neumann, *Kinesiology of the Musculoskeletal System-E-Book: Foundations for Rehabilitation*, Elsevier Health Sciences, 2013.
- [35] B.F. Morrey, K.N. An, (Chapter 6) *Biomechanics of the shoulder*, *The Shoulder*, vol. 1, Elsevier Health Sciences, C.A. Rockwood, 2009.
- [36] B. Tondu, Estimating shoulder-complex mobility, *Appl. Bionics Biomech.* 4 (1) (2007) 19–29.
- [37] C. Carignan, J. Tang, S. Roderick, Development of an exoskeleton haptic interface for virtual task training, in: 2009 IEEE/RSJ International Conference on Intelligent Robots and Systems, 2009, pp. 3697–3702.
- [38] T. Nef, M. Guidali, V. Klamroth-Marganska, R. Riener, ARMin - exoskeleton robot for stroke rehabilitation, in: O. Dössel, W.C. Schlegel (Eds.), *World Congress on Medical Physics and Biomedical Engineering, September 7 - 12, 2009, Munich, Germany: Vol. 25/9 Neuroengineering, Neural Systems, Rehabilitation and Prosthetics*, Berlin, Heidelberg, Springer Berlin Heidelberg, 2009, pp. 127–130.
- [39] S.J. Ball, I.E. Brown, S.H. Scott, MEDARM: a rehabilitation robot with 5DOF at the shoulder complex, in: 2007 IEEE/ASME International Conference on Advanced intelligent mechatronics, 2007, pp. 1–6.
- [40] B. Kim, A.D. Deshpande, Controls for the shoulder mechanism of an upper-body exoskeleton for promoting scapulohumeral rhythm, in: 2015 IEEE International Conference on Rehabilitation Robotics (ICORR), 2015, pp. 538–542.
- [41] D. Koo, P.H. Chang, M.K. Sohn, J. Shin, Shoulder mechanism design of an exoskeleton robot for stroke patient rehabilitation, in: 2011 IEEE International Conference on Rehabilitation Robotics, 2011, pp. 1–6.
- [42] B. Kim, A.D. Deshpande, An upper-body rehabilitation exoskeleton Harmony with an anatomical shoulder mechanism: design, modeling, control, and performance evaluation, *Int. J. Robot. Res.* 36 (4) (2017) 414–435.

- [43] J.H. Morris, F. Van Wijck, Responses of the less affected arm to bilateral upper limb task training in early rehabilitation after stroke: a randomized controlled trial, *Arch. Phys. Med. Rehabil.* 93 (7) (2012) 1129–1137.
- [44] A.L. van Delden, C.L. Peper, K.N. Nienhuys, N.I. Zijp, P.J. Beek, G. Kwakkel, Unilateral versus bilateral upper limb training after stroke: the Upper Limb Training After Stroke clinical trial, *Stroke* 44 (9) (2013) 2613–2616.
- [45] M. Simkins, N. Byl, H. Kim, G. Abrams, J. Rosen, Upper limb bilateral symmetric training with robotic assistance and clinical outcomes for stroke: a pilot study, *Int. J. Intell. Comput. Cybern.* 9 (1) (2016) 83–104.
- [46] D. Sethy, P. Bajpai, E.S. Kujur, K. Mohakud, S. Sahoo, Effectiveness of modified constraint induced movement therapy and bilateral arm training on upper extremity function after chronic stroke: a comparative study, *Open J. Ther. Rehabil.* 4 (01) (2016) 1.
- [47] M. Gandolfi, E. Formaggio, C. Geroin, S.F. Storti, I. Boscolo Galazzo, M. Bortolami, et al., Quantification of upper limb motor recovery and EEG power changes after robot-assisted bilateral arm training in chronic stroke patients: a prospective pilot study, *Neural. Plast.* 2018 (2018).
- [48] Y. Shen, B.P. Hsiao, J. Ma, J. Rosen, Upper Limb Redundancy Resolution Under Gravitational Loading Conditions: Arm Postural Stability Index Based on Dynamic Manipulability Analysis. UCLA (2017). Retrieved from: <<https://escholarship.org/uc/item/2p71214x>> (accessed 30.11.18).
- [49] J.C. Perry, J.M. Powell, J. Rosen, Isotropy of an upper limb exoskeleton and the kinematics and dynamics of the human arm, *Appl. Bionics Biomech.* 6 (2) (2009) 175–191.
- [50] P.M. Ludewig, S.A. Behrens, S.M. Meyer, S.M. Spoden, L.A. Wilson, Three-dimensional clavicular motion during arm elevation: reliability and descriptive data, *J. Orthop. Sports Phys. Ther.* 34 (3) (2004) 140–149.
- [51] P.M. Ludewig, V. Phadke, J.P. Braman, D.R. Hassett, C.J. Cieminski, R.F. LaPrade, Motion of the shoulder complex during multiplanar humeral elevation, *J. Bone Jt. Surg.-Am. Vol.* 91 (2) (2009) 378–389.
- [52] J.L. Herder, Energy-Free Systems; Theory, Conception and Design of Statically Balanced Spring Mechanisms (Ph.D. thesis), Delft University of Technology, ISBN 90-370-0192-0 (<http://repository.tudelft.nl>), 2001, p. 139. doi:10.13140/RG.2.1.3942.8966.

DESIGN AND MODELING OF SHOULDER EXOSKELETON USING TWO REVOLUTE JOINTS

7

Carlos Parga and Wen Yu*Center for Research and Advanced Studies of the National Polytechnic Institute, Mexico City, Mexico*

7.1 INTRODUCTION

An exoskeleton is a mechanical structure like the skeleton of humans [1]. It has joints and a mechanical structure that supports and shapes the human body's movement. Interest in exoskeletons has increased due to the benefits offered by these devices. The research and development show more proposals with different applications. There are not many very powerful or versatile exoskeletons. A broad field of study has expanded into the creation of new applications in biomedical, space, industrial, military, and other research technologies. Exoskeletons can be used in four modes of operation:

- Physiotherapy: the exoskeleton can operate in passive or active mode to perform tasks of rehabilitation therapy in patients who have damage to their motor ability [2].
- Force amplifier: a user with an exoskeleton of this type can manipulate heavier objects, also it prevents fatigue and injuries. This type of exoskeleton is of great military interest [3,4].
- Haptic device: it is used to capture body movements to interact with virtual environments [5,6].
- Master device: in a similar way to the haptic device, the exoskeleton is able to operate a real robot through teleoperation [7,8].

The upper limb exoskeleton is one of the most complex robotic systems, due to the mechanical and sensory complexity, especially in two parts of the body: the hand and the shoulder [9,10].

In this chapter we will describe the prototype of an exoskeleton that works on the shoulders. The objective is to allow as much freedom as possible [11,12]. By the limits of the structural design of the exoskeleton, we first perform the structural analysis.

7.2 SHOULDER EXOSKELETON WITH 2 DEGREES OF FREEDOM

The upper limb exoskeleton is one of the most difficult robotic systems of exoskeletons, because both mechanical and sensor systems are complex. The hand robot needs a huge amount of sensations and five articulated fingers. The shoulder joint is spherical. The spherical joints in robotics are particularly complicated, because they have three rotational degrees of freedom (DOF)

coinciding at one point. In addition to the three rotational degrees, it has two additional prismatic DOFs that give the shoulder forward or upward movements [13].

In this section, we will analyze two spherical joints, and show that this 2-DOF configuration allows the complex movements of the human shoulder. The spherical joint used in the robot exoskeleton is a type of universal joint, see Fig. 7.1.

The human shoulder performs three basic movements, flexion–extension shown in Fig. 7.2, abduction–adduction shown in Fig. 7.3, and the circulation that can be considered as the combination of abduction, adduction, flexion, and extension. One of the goals of this design, once placed on the human shoulder, was that it was to allow the performing of the movements of flexion–extension and abduction freely, avoiding the singularity caused by the configuration of the links. In addition, it had to have the possibility of operating in passive or active mode; in passive mode the user must be able to move the exoskeleton with their own strength and in active mode the exoskeleton must be able to move the user's shoulder [14,15].

These movements can be made by the spherical joint that is formed from the union of the head of the human with the shoulder blade, see Fig. 7.4. A spherical joint has 3 DOFs, also known as Euler angles or simply roll, pitch, and yaw. Because the rotation is an orientation movement of the elbow, we do not consider the third movement of the shoulder, the circulation, only the two remaining angles will be studied.

So we have the basic mechanism with two angles of a revolute rotation. The mechanisms are coupled to a structure that is supported centrally to a crosshead joint, which allows for two axes of rotation intersecting perpendicularly at the origin XYZ. The roll movement rotates the angle θ_x around the X axis and the pitch movement rotates the angle θ_y around the Y axis.

The robot that applies the universal joints is driven by two motors and can perform the basic movements of the human shoulder. These movements are performed by the simplified mechanism

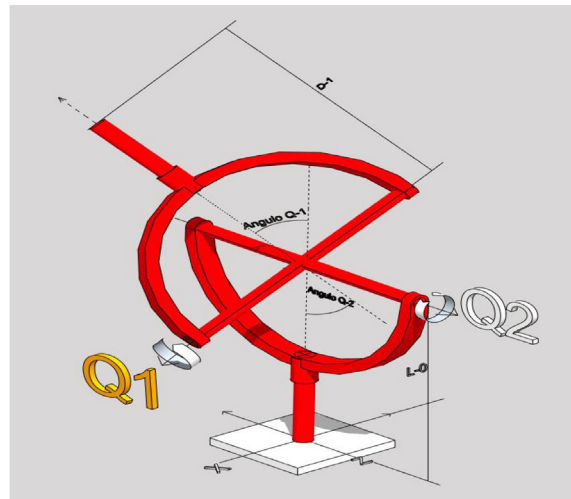


FIGURE 7.1

Two revolute joints.

**FIGURE 7.2**

Flexion–extension movement.

**FIGURE 7.3**

The abduction–adduction movement.

with 2-DOF joints. This exoskeleton allows the natural movement of the shoulder and can be used in passive mode for tasks of movement recording.

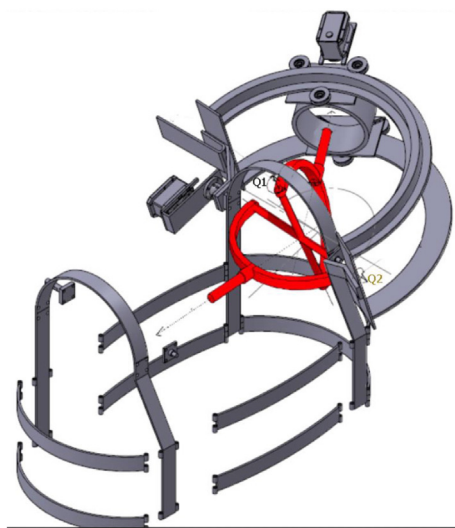
7.3 SHOULDER EXOSKELETON DESIGN

The prototype of the shoulder exoskeleton is shown in [Fig. 7.5](#), and works on the human shoulders as shown in [Fig. 7.6](#). The objective is to allow as much freedom as possible.

In order to know the limits of the structural design of the exoskeleton, it is necessary to perform the structural analysis and find the internal stresses, deformations, and stresses that act on the structure. The exoskeleton is in contact with the human body and exerts force on it, so it is imperative

**FIGURE 7.4**

The universal joints for the shoulder movements.

**FIGURE 7.5**

The shoulder exoskeleton.

**FIGURE 7.6**

The shoulder exoskeleton on a human.

that its operation does not injure the user. The motor forces should not cause damage to the human body and be able to act upon the robot.

The elements subjected to bending are not always straight bars. Sometimes, as in the case of crane hooks, the middle line of the bar is a curve (in the plane of the application of the loads or bending moments). If the curvature is large, the stress distribution differs markedly from that given by the formula of bending $\sigma = M_c/I$ that is deduced for the initially straight bars. If the curved beam subjected to pure bending is considered (Hooke's law)

$$\frac{\sigma_e L_e}{E} = \frac{\sigma_f L_f}{E} \quad (7.1)$$

where $\delta = \sigma L/E$. The length L_e of the fiber e is greater than the length L_f of the fiber f . According to the length ratio of the initial curvature of the fiber, $\sigma_e < \sigma_f$. Therefore the stress distribution is nonlinear.

The resistant forces of tension and compression acting on the rectangular section cannot be balanced. If the neutral line passes through the center of gravity, the neutral axis moves toward the center of the curvature. The linear distribution superimposed on the nonlinear distribution shows not only the displacement of the neutral axis, but also the greater value of the stresses in the inner fibers and their lower value.

To determine the displacement of the neutral axis with respect to the center of gravity and calculate the stresses, the elongation of a fiber at distance and the neutral line is defined as $y d\phi$, the initial length is $(R - e + y)d\theta$, and the unit deformation is

$$\epsilon = \frac{\delta}{L} = \frac{y d\phi}{(R - e + y)d\theta} \quad (7.2)$$

According to Hooke's law,

$$\sigma = E\epsilon = \frac{Ed\phi}{d\theta} \cdot \frac{y}{R - e + y} \quad (7.3)$$

These equations allow determining the bending stresses in curved beams. Their analytical development is complicated in general, so their application is limited to simple cases, such as the rectangular section or the exoskeleton rails. The stress on the end fibers in the curved beams can be calculated by

$$\sigma = K \frac{Mc}{I} \quad (7.4)$$

where K depends on R/c , R is the radius of curvature of the line of centers of the curved beam, and c is the order of the center of gravity of the inner fiber. When $R/c > 20$, the K is almost unity.

Using the above calculations of the curved beams and the rails, the bending stress of the beam is σ , and the moment of inertia of the hyperstatic beam area is defined as

$$\begin{aligned} I_{yy} &= \frac{hb^3}{12}, \quad c = \frac{h}{2}, \quad M_f = \frac{\sigma b^3}{6K} \\ \sigma &= K \frac{M_f c}{I_{yy}} \left(\frac{R}{c} < 20 \right), \quad \sigma = \frac{6KM_f}{b^3} \left(\frac{R}{c} \geq 20 \right) \end{aligned} \quad (7.5)$$

The total bending stress of the entire structure is obtained by

$$\begin{aligned} M_{fy} &= \frac{I_{yy}\sigma_{adm}}{c}, \quad S = \frac{I_{yy}}{c} \\ \overline{I_{yy}} &= 2\overline{I_1} + \overline{I_2}, \quad \overline{I_y} = \frac{hb^3}{12} \end{aligned} \quad (7.6)$$

The designed structure is shown in Fig. 7.7.

The entire design of the exoskeleton is made with the Solid Works software. The physical properties are:

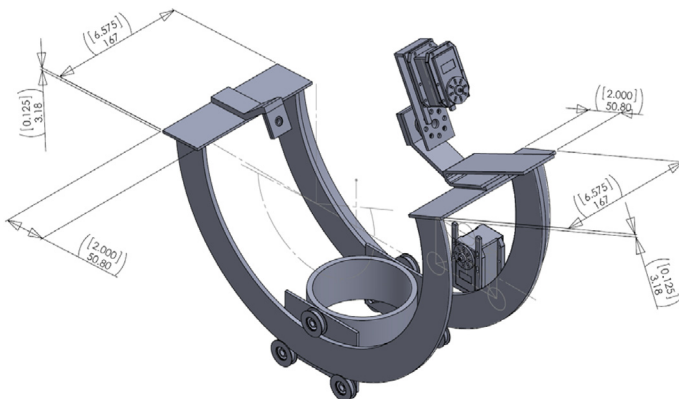


FIGURE 7.7

Curved rail and rack car.

- Link 1 is curved rail, the mass is 1346.46 g, the volume is 498,687.44 mm³, surface area is 196,318.48 mm².
- Link 2 is a carriage, the mass is 471.25 g, the volume is 174,538.12 mm³, surface area is 95,382.72 mm².

7.4 MODELING THE SHOULDER EXOSKELETON

The aim of the kinematic model is to know analytically the acceleration, velocity, and position of the shoulder exoskeleton, and to relate the dynamic model with the forces involved. The mathematical relations between the articulated coordinates (or the coordinates of the end of the robot), their derivatives (speed and acceleration), and the forces. The 2-DOF robot has a type of spherical joint. It is different to the other normal robots.

The rotational articulation of the shoulder of the exoskeleton is designed based on the kinematic model of the universal joint, where two rotation axes of rotational type joints are perpendicular to each other and intersect at the origin. This intersection must also be coincident with the intersection of the same axes of rotation of the spherical joint of the shoulder, see Fig. 7.8.

The DH parameters corresponding to the universal joints are

$$DH = \begin{bmatrix} a & \alpha & d & \theta \\ 1 & 0 & \frac{\pi}{2} & 0 & q_1 \\ 2 & d_1 & \frac{\pi}{2} & 0 & q_2 \end{bmatrix} \quad (7.7)$$

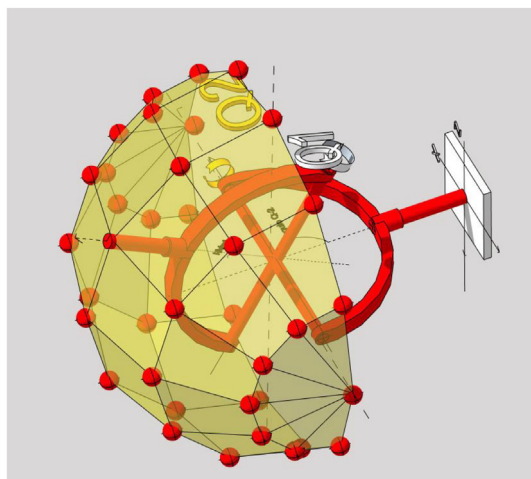


FIGURE 7.8

The work area of the universal joint.

where q_1, q_2 are the two joints and d_1 is the distance from the intersection of the two axes of rotation to the end effector. These parameters can be obtained by the transformation matrix A_i , $i = 1, 2$, as

$${}^0A_1 = \begin{bmatrix} \cos q_1 & 0 & \sin q_1 & 0 \\ \sin q_1 & 0 & -\cos q_1 & 0 \\ 0 & 1 & 0 & 0 \\ 0 & 0 & 0 & 1 \end{bmatrix}, {}^1A_2 = \begin{bmatrix} \cos q_2 & 0 & \sin q_2 & d_1 \cos q_2 \\ \sin q_2 & 0 & -\cos q_2 & d_1 \sin q_2 \\ 0 & 1 & 0 & 0 \\ 0 & 0 & 0 & 1 \end{bmatrix} \quad (7.8)$$

The final transformation matrix is obtained by multiplying the matrix A_i , $i = 1, 2$,

$$T = \begin{bmatrix} R_{3 \times 3} & p_{3 \times 1} \\ f_{1 \times 3} & w_{1 \times 1} \end{bmatrix} = \begin{bmatrix} \cos q_1 \cos q_2 & \sin q_1 & \cos q_1 \sin q_2 & d_1 \cos q_1 \cos q_2 \\ \cos q_2 \sin q_1 & -\cos q_1 & \sin q_1 \sin q_2 & d_1 \cos q_2 \sin q_1 \\ \sin q_2 & 0 & -\cos q_2 & d_1 \sin q_2 \\ 0 & 0 & 0 & 1 \end{bmatrix} \quad (7.9)$$

The Jacobian of the robot is

$$J = \begin{bmatrix} \frac{\partial x}{\partial d_1} & \frac{\partial x}{\partial q_2} & \frac{\partial x}{\partial q_1} \\ \frac{\partial y}{\partial d_1} & \frac{\partial y}{\partial q_2} & \frac{\partial y}{\partial q_1} \\ \frac{\partial z}{\partial d_1} & \frac{\partial z}{\partial q_2} & \frac{\partial z}{\partial q_1} \end{bmatrix} = \begin{bmatrix} \cos q_1 \sin q_2 & d_1 \cos q_1 \cos q_2 & -d_1 \sin q_1 \sin q_2 \\ \sin q_1 \sin q_2 & d_1 \sin q_1 \cos q_2 & d_1 \cos q_1 \sin q_2 \\ \cos q_2 & -d_1 \sin q_2 & 0 \end{bmatrix} \quad (7.10)$$

From the vector $p_{3 \times 1}$ of the final transformation matrix, the solution is obtained at the positions P_x , P_y , and P_z which are given by

$$\begin{aligned} x &= d_1 \cos q_1 \cos q_2 \\ y &= d_1 \cos q_2 \sin q_1 \\ z &= d_1 \sin q_2 \end{aligned} \quad (7.11)$$

The solution for the inverse kinematics is obtained by geometry, where the angles for q_1 and q_2 are known from a position P_x and P_y given by

$$\begin{aligned} q_1 &= \arctan\left(\frac{\sqrt{d_1^2 - x^2 - z^2}}{x}\right) \\ q_2 &= \arcsin\left(\frac{z}{d_1}\right) \end{aligned} \quad (7.12)$$

Given the equations it is possible to find a solution for the angular position at any position P_x , P_z whenever $d_1 > \sqrt{P_x^2 + P_z^2}$. The kinetic energy of the system is

$$E_c = \frac{1}{2} \sum_{i=1}^n \left(m_i \dot{c}_i^T \dot{c}_i + \frac{1}{2} \omega_i^T I_i \omega_i \right) = \frac{1}{2} \sum_{i=1}^n \dot{\theta}^T \bar{I}_i \dot{\theta} \quad (7.13)$$

where \dot{c} is the tridimensional lineal velocity vector, ω is the tridimensional angular velocity vector, m is the mass, the matrix \bar{I}_i and $n \times n$ is determined by $\bar{I}_i \equiv m_i J_{ci}^T J_{ci} + J_{\omega, i}^T I_i J_{\omega, i}$. If the matrix I $n \times n$ is defined by $I = \sum_{i=1}^n \bar{I}_i$ then the kinetic energy from (7.13) is

$$E_c = \frac{1}{2} \dot{\theta}^T I \dot{\theta}$$

The potential energy of the robot due to the gravity g is given by

$$E_p = - \sum_{i=1}^n m_i c_i^T g$$

From (J) and (E), the Lagrangian equation is

$$L = E_c - E_p = \sum_{i=1}^n \left[\frac{1}{2} \dot{\theta}^T \bar{I}_i \dot{\theta} + m_i c_i^T g \right]$$

In q_1 the Lagrangian equations of motion are $\partial/\partial t[\partial L/\partial \dot{q}_1] - \partial L/\partial q_1 = 0$, $\partial/\partial t[\partial L/\partial \dot{\theta}_1] - \partial L/\partial \theta_1 = \tau_1$, where τ_1 and τ_2 are the torque applied to the system. The system state is considered as $q = [\theta_1 \quad \theta_2]^T$. The regulation errors are $\bar{q}_1 = q_1^* - q_1$, $\bar{q}_2 = q_2^* - q_2$, where q_1^* and q_2^* are the desired values. Then $q^* = [\theta_1^* \quad \theta_2^*]^T$, where θ_1^* , and θ_2^* are the desired system positions. The model is transformed into the following standard form:

$$M(q) \ddot{q} + C(q, \dot{q}) \dot{q} + G(q) = \tau \quad (7.14)$$

where $\tau = [\tau_1, \tau_2]^T$, and τ_1 and τ_2 are the torques of the two control motors. To model the torque of the servomotor, we need electrical and mechanical models of the motor.

7.5 CONTROL FOR THE EXOSKELETON

7.5.1 LYAPUNOV STABILITY

Define $q = [x_1 \quad x_2 \quad x_3 \quad x_4]$. The Lyapunov's design allowed us to calculate a global feedback in an analytic way, due to the system stabilizing asymptotically. The final control τ will be calculated in n steps, where n is the number of state variables for the proposed case. The first step calculates a tracking error for x_1 . Defining the tracking error as

$$\varepsilon_1 = x_1 - x_1^*$$

where x_1^* is the desired trajectory of x_1 . The Lyapunov function is selected as

$$V_1(x) = \frac{1}{2} \varepsilon_1^2$$

In the second step, the Lyapunov function is selected as

$$V_2(x_1, x_2) = \frac{1}{2} \varepsilon_1^2 + \frac{1}{2} \varepsilon_2^2$$

In the third step, the Lyapunov function is selected as

$$V_4(x_1, x_2, x_3, x_4) = \frac{1}{2} \varepsilon_1^2 + \frac{1}{2} \varepsilon_2^2 + \frac{1}{2} \varepsilon_3^2 + \frac{1}{2} \varepsilon_4^2$$

Then

$$\dot{V}_4(x_1, x_2, x_3) = -k_1 \varepsilon_1^2 - k_2 \varepsilon_2^2 - k_3 |\varepsilon_3| - k_4 |\varepsilon_4| < 0$$

7.5.2 LINEAR CONTROL

The most popular controller in industrial applications is PID control. It has the form of

$$\tau(t) = K_p e(t) + K_i \int_0^t e(t) dt + K_D \frac{de(t)}{dt} \quad (7.15)$$

where

$$e(t) = q - q*$$

$q*$ is the desired position of the shoulder, q is the real position. K_p , K_i , and K_d are proportional, integral, and derivative gains of the PID controller, respectively. Because $q = [x \ \theta_x \ y \ \theta_y]^T$, besides the desired position of exoskeleton (x , y), we need also the desired angles of the links (θ_x , θ_y). At each equilibrium point $[x_0 \ \theta_{x0} \ y_0 \ \theta_{y0}]^T$, the nonlinear model (7.14) can be approximated in

$$\delta\dot{x} = A\delta x + B\delta u, \quad y = C\delta x$$

Since for each motor, $mx_1 = C(x_3^2/0/x_1^2)$, $u_0 = Ri_0$, $\delta x_1 = x - x_0$, $\delta x_2 = v$, $\delta x_3 = x_3 - i_0$, $\delta u = v - Ri_0$. The PID controller (7.15) is

$$\begin{aligned} \tau_{pid} = K_0 \int_0^t (x_{1ref} - x_1) dt + K_1(x_{1ref} - x_1) + \\ K_2(x_{2ref} - x_2) + K_3(x_{3ref} - x_3) \end{aligned}$$

7.5.3 SLIDING MODE CONTROLLER

The tracking error is defined as

$$e = q - q*$$

Let us define the sliding surface as $S = (d/dt + \lambda)^n e$, when $n = 2$

$$S = \left(\frac{d}{dt} + \lambda \right)^2 e_1 = \ddot{e} + \lambda_1 \dot{e} + \lambda_2 e \quad (7.16)$$

We select the Lyapunov function as

$$V = \frac{1}{2} S^2 \quad (7.17)$$

We use (7.14) and (7.16)

$$S = g_c - \frac{C}{m} \left(\frac{x_3}{x_1} \right)^2 + \lambda_1 x_2 + \lambda_2 (x_1 - x_{1d})$$

We hope the derivative of (7.17) satisfying

$$\dot{V} = S \dot{S} < 0$$

We should use the control as

$$\tau_{smc} = \frac{1}{g_1(x)} \begin{pmatrix} -f_1(x) - \lambda_1 \left(g_c - \frac{C}{m} \left(\frac{x_3}{x_1} \right)^2 \right)^2 \\ -\lambda_2 x_2 - SM \end{pmatrix} \quad (7.18)$$

where $SM = Wsign(S)$, $f_1(x) = (R/L(x))x_3 + (2C/L(x))(x_2x_3/x_1^2)$, $g_1(x) = L^{-1}(x)$. In order to reduce chattering, the saturation function $sat(S)$ is used to replace $sign(S)$, so $SM = Wsat(s)$. When the sliding mode controller (7.18) is applied, the asymptotic stability is guaranteed.

$$\lim_{t \rightarrow \infty} e = 0$$

7.5.4 NEURAL CONTROL

A neural network can approximate the controller (7.18). Here we use the radial base function neural network

$$\tau_{nn} = \sum_{i=1}^n w_i \exp \left(-\frac{\|S - c_i\|^2}{z\rho_i} \right) = W^T \varphi \quad (7.19)$$

where n is the number of hidden layers. An adaptive law is used to adjust the weights for the search of optimal values and to obtain a stable convergence property

$$W_{new} = W_{old} - \eta \frac{\partial S \dot{S}}{\partial W} \mid W = W_{old}$$

That is, $W_{new} = W_{old} - \eta S (\partial S / \partial W) | W = W_{old}$. Because $(\partial \dot{S} / \partial W) = (\partial \dot{S} / \partial u) \times (\partial u / \partial W)$, and $\dot{S} = \ddot{e} + \lambda_1 \ddot{e} + \lambda_2 \dot{e}$, we find the updated law as follows:

$$W_{new} = W_{old} - \eta S \frac{-2C}{Lmx_1^2} \times \frac{\partial u}{\partial W}$$

This gradient updated law can assure that τ_{nn} goes to τ_{smc} in (7.18).

7.6 ELECTRONIC AND CONTROL SYSTEM

The electronic components of the exoskeleton is shown in Fig. 7.9. The electronic issue is reduced because the servomotors are digital and internally the microcontrollers control the serial communication protocol synchronic half duplex, which comprises only the two servos, the UART–USB interface, and a PC.

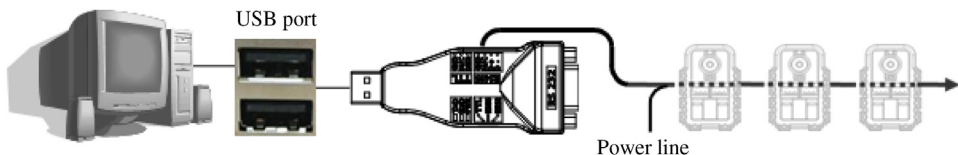


FIGURE 7.9

The electronic components.

Servomotors return information on temperature, voltage, and angular position. Particularly interesting is the angular position as this allows the development of a system of closed loop control, also the exoskeleton works in passive mode. The PC where the control software runs is a Pentium Core2Duo with 2 GB of RAM and a 120 GB hard drive.

The electrical system is based on Kirchhoff's voltage law:

$$U = L_m \dot{I}_m + R_m I_m + K_b \dot{q}$$

where U is input voltage, I_m is armature current, R_m and L_m are the resistance and inductance of the armature, K_b is back emf constant, and \dot{q} is angular velocity. Because the term $L_m \dot{I}_m$ is very small compared with $R_m I_m$ and it can be neglected. The mechanical subsystem is

$$\frac{1}{K_g} (J_m \ddot{q} + B_m \dot{q}) = \tau_m$$

where K_g is the gear ratio, J_m is the effective moment of inertia, B_m is the viscous friction coefficient, and τ_m is the torque. The electrical and mechanical subsystems are coupled to each other through an algebraic torque equation:

$$\tau_m = K_m I_m$$

where K_m is the torque constant of the motor. Assuming that there is no backlash or electric deformation in the gears, the work done by the load shaft is equal to the work done by the motor shaft,

$$\tau = \frac{1}{K_g} \tau_m$$

For each motor, the model is

$$\frac{R_m J_m}{K_m K_g} \ddot{q} + \left(K_b + \frac{R_m B_m}{K_m K_g} \right) \dot{q} = U$$

where q can be the actuators angles q_1 or q_2 . In the model (7.14) the state q represents the position and the angles of the system, while the control input is the torques of the motors.

The position of the exoskeleton $q = [\theta_1 \quad \theta_2]^T$ is the same as the human shoulder because it is mechanically connected. This is reflected like a disturbance h that is added to the torque τ that is applied to the exoskeleton. This modifies the position and the controller must compensate it.

The operating system on which the control software runs is Linux Mint 15 "Olivia." This operating system was chosen because of the development software and the operating system have a GNU General Public License.

The development environment is *Qt4* with language *C++* which allows better performance at runtime without needing a work environment, unlike MATLAB Simulink in which it is necessary to execute the control algorithms that must be compiled every time it is run. Another advantage is that it generates executable programs that can run on any *PC* even if you have installed the development environment.

The application communicates with the servos through the Dinamixel SDK library in which commands are written to send torque to the servos and where the position data is also read. In the GUI interface the reference position q_1 , q_2 and PID are introduced as

$$\tau(t) = K_p e(t) + K_i \int e(t) + K_d \frac{de}{dt} \quad (7.20)$$

where $e(t) = r(t) - y(t)$, $\tau(t)$ is the torque in (7.14), $r(t)$ is the reference position, and $y(t)$ is the current position of the servos, read from the Dinamixel SDK library.

7.7 EXPERIMENTAL RESULTS

To verify the design and modeling of the exoskeleton, we use the following experiments. The PID gains in (7.20) are $K_p = 30$, $K_i = 1$, and $K_d = 5$.

The first experiment is the response to the step. The responses are shown in Fig. 7.10. This test shows the stability and response of the system are satisfied when the exoskeleton takes the trajectory. The figure shows the evolution of q_1 , q_2 angles in response to the reference and its transition. This test demonstrates the stability and correct response of the system in transition of the reference.

The second experiment is the trajectory tracking. Here the shoulder makes cyclical movements, tracking the reference. This test is important due to the basic movements of the shoulder being like the real work. In this test the shoulder makes cyclic movements following the reference, see Figs. 7.11 and 7.12.

Finally, we show the results of simulations of the exoskeleton dynamics with the step response using the sliding mode controllers (7.18) (see Fig. 7.13), and the neural network (7.19) (see Fig. 7.14).

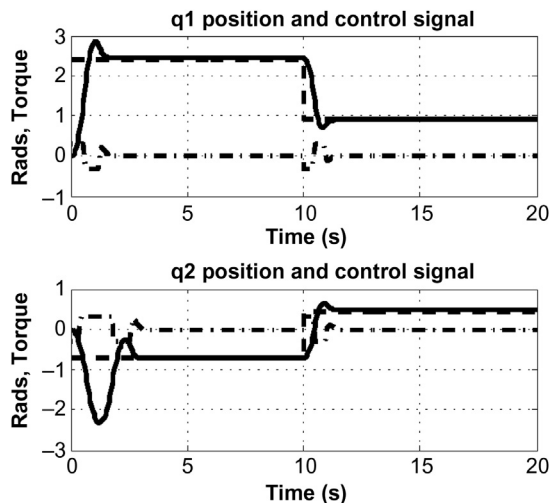
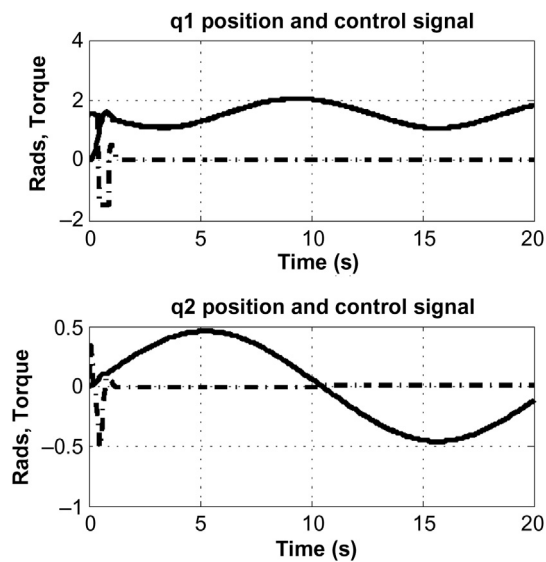
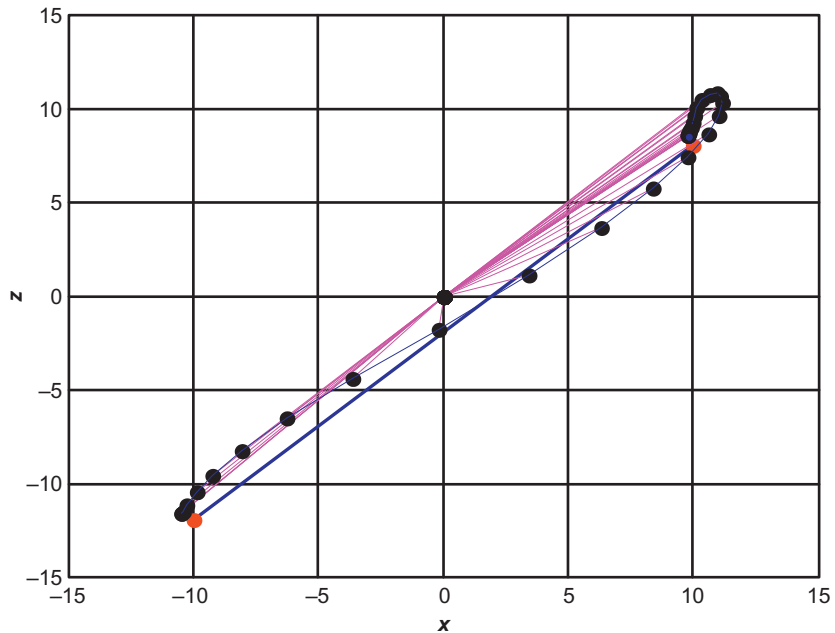


FIGURE 7.10

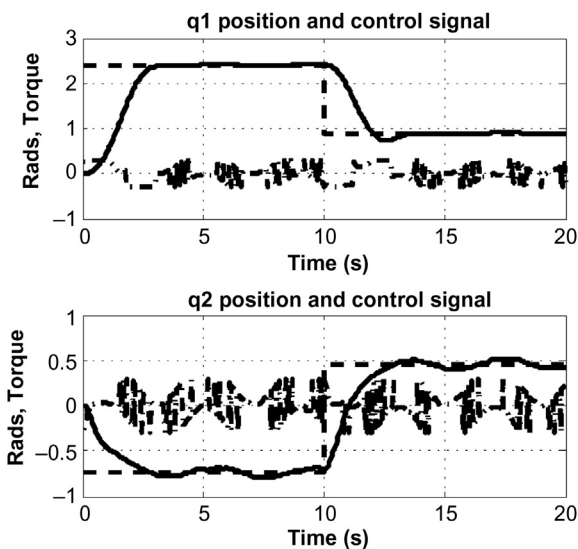
Position regulation with PID controller, (- -) is the reference, (---) is the robot position, (-.-) is the control signal.

**FIGURE 7.11**

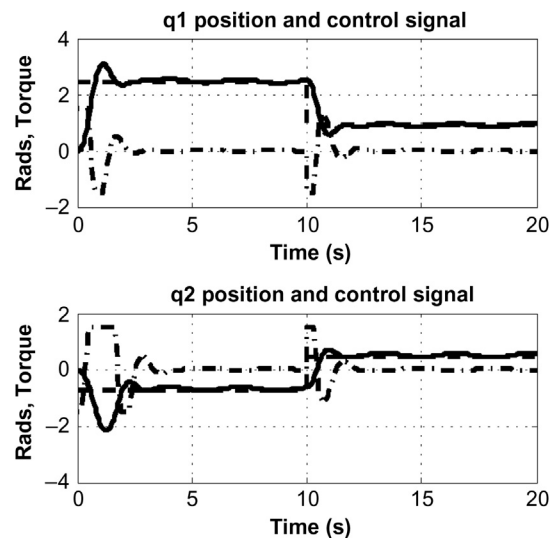
Position tracking with PID controller, (- -) is the reference, (---) is the robot position, (---) is the control signal.

**FIGURE 7.12**

X-Y tracking.

**FIGURE 7.13**

Position regulation with sliding mode controller, (- -) is the reference, (---) is the robot position, (-.-) is the control signal.

**FIGURE 7.14**

Position regulation with neural network controller, (- -) is the reference, (---) is the robot position, (-.-) is the control signal.

7.8 CONCLUSION

The human shoulder has at least three DOFs. In this chapter, we use a 2-DOF robot to complete most movements of the shoulder. We analyze the behaviors of the human shoulder and the shoulder exoskeleton. A prototype of the 2-DOF shoulder exoskeleton is constructed. We also model this robot exoskeleton and apply it in real applications.

REFERENCES

- [1] N. Hogan, H.I. Krebs, J. Charnnarong, P. Srikrishna, A. Sharon, MITMANUS: a workstation for manual therapy and training. I, in: IEEE Int. Workshop Robot Hum. Commun., 1992, pp. 161–165.
- [2] T.W. Williams, Control of powered upper extremity prostheses, in: R.H. Meier, D.J. Atkins (Eds.), *Functional Restoration of Adults and Children with Upper Extremity Amputation*, DemosMedical Publishing, New York, 2004, pp. 207–224.
- [3] J.L.G. Nielsen, Simultaneous and proportional force estimation for multifunction myoelectric prostheses using mirrored bilateral training, *IEEE Trans. Biomed. Eng* 58 (3) (2011) 681–688.
- [4] H. Kazerouni, The human amplifier technology at the University of California, Berkeley, *Robot. Auton. Syst.* 19 (1996) 179–187.
- [5] P. McCool, N. Chatlani, L. Petropoulakis, J.J. Soraghan, R. Menon, H. Lakany, Lower arm electromyography (EMG) activity detection using local binary patterns, *IEEE Trans. Neural Syst. Rehabil. Eng.* 22 (5) (2014).
- [6] J.J. Baker, et al., Continuous detection and decoding of dexterous finger flexions with implantable myoelectric sensors, *IEEE Trans. Neural Syst. Rehabil. Eng* 18 (4) (2010) 424–432.
- [7] M. Zribi, M. Karkoub, L. Huang, Modelling and control of two robotic manipulators handling a constrained object, *Appl. Math. Model.* 24 (12) (2000) 881–898.
- [8] B.M. Jau, Anthropomorphic exoskeleton dual arm/hand telerobot controller, in: IEEE Int. Workshop Intell. Robots, 1988, pp. 715–718.
- [9] D.G. Caldwell, O. Kocak, U. Andersen, Multi-armed dexterous manipulator operation using glove/exo-skeleton control and sensory feedback, in: IEEE/RSJ Int. Conf. Intell. Robots Syst. 1995, Hum. Robot Interaction Cooperative Robots, vol. 2, pp. 567–572.
- [10] J.C. Perry, J. Rosen, S. Burns, Upper-limb powered exoskeleton design, *IEEE/ASME Trans. Mechatronics* 12 (4) (2007).
- [11] K. Kiguchi, T. Fukuda, A 3DOF exoskeleton for upper-limb motion assist - consideration of the effect of bi-articular muscles, in: IEEE International Conference on Robotics and Automation, New Orleans, LA, April 2004.
- [12] N. Chatlani, J. Soraghan, Local binary patterns for 1-D signal processing, in: Proc. 18th Eur. Signal Process. Conf., Aug. 23–27, 2010, pp. 95–99.
- [13] R.W. Wirta, D.R. Taylor, F.R. Finley, Pattern recognition arm prostheses: a historical perspective - a final report, *Bull. Prosthes. Res.* (1978), 10-30: S-35.
- [14] M. Quigley, A. Asbeck, A. Ng, A low-cost compliant 7-DOF robotic manipulator, in: IEEE International Conference on Robotics and Automation, Shanghai, China, 2011, pp. 6051–6058.
- [15] D.W. Repperger, B.O. Hill, C. Hasser, M. Roark, C.A. Phillips, Human tracking studies involving an actively powered augmented exoskeleton, in: 15th Southern Biomed. Eng. Conf., 1996, pp. 28–31.

HAND EXOSKELETON SYSTEMS—OVERVIEW

8

Peter Walker Ferguson, Yang Shen and Jacob Rosen

Bionics Lab, Department of Mechanical and Aerospace Engineering, University of California, Los Angeles, CA,
United States

8.1 INTRODUCTION

This study is a review of development and state-of-the-art techniques of active hand exoskeletons. There exists a considerable difference between exoskeleton techniques in upper-limb, lower-limb, and hand exoskeletons, based on the motivation as well as the technical difficulties. The authors aim to provide an overview of the applications of hand exoskeletons as assistive, rehabilitative, augmentative, and other devices. Both “rigid” exoskeletons and “soft” gloves are reviewed. For the purpose of this paper, only robotic devices that actively control one or more degrees of freedom (DOF) of at least one digit of the hand, and that are grounded in such a way that attaches to the body of the user are considered. By this definition of an active hand exoskeleton, passive devices such as HandSOME [1] or SCRIPT [2] are not considered even though they may accomplish many of the same tasks. Additionally, end-effector robotic systems that are not grounded at the hand or forearm, such as HandCARE [3] or Reha-Digit (<https://reha-stim.com>) are not included. Finally, to prevent redundancy with the first chapter of this book (see Chapter 1), combined arm and hand exoskeletons with more independent active DOFs at the shoulder, elbow, and wrist joints than at the digits of the hand are excluded.

Hand exoskeletons are uniquely qualified to perform a variety of useful functions. Unlike end-effector systems that manipulate the hand with respect to a point remote to the body, exoskeletons attach to the human hand and move synchronously with the joints of the digits. This enables more potential applications such as natural teleoperation, strength augmentation, and provision of additional structure and correction of movement similar to an orthosis. Additionally, the potential for hand exoskeleton portability permits their development for assisting and augmentation outside of a stationary setting. However, hand exoskeletons also bring major challenges in mechanism design and control algorithm development. To solve these challenges typically requires interdisciplinary knowledge of hardware design, software development, and human anatomy and physiology among other fields.

The first powered hand exoskeletons were in development since at least the late 1980s [4,5]. These early devices were not meant for standalone use, but rather as force feedback gloves for teleoperation. They developed naturally out of purely sensory data gloves such as [6] and findings that teleoperation was improved with force feedback. However, within a few years, hand exoskeleton

systems began appearing in the literature for assisting paralyzed individuals [7] and augmenting performance while wearing a space suit [8]. Later, applications extended to rehabilitation, which requires better human-in-the-loop understanding in terms of intention detection and motion control. Lastly, numerous hand exoskeletons have been developed for other purposes such as teleoperation and as haptic devices in VR environments. For all these systems, the historical trend has been for the need for active systems due to the inadequacy of purely passive ones.

This chapter begins with a graphical overview of a sample of existing hand exoskeletons along with a discussion of hand exoskeletons in terms of mechanism design, actuation methods, transmission systems, control algorithms, and intent estimation methods. Afterwards, an overview of a selection of hand exoskeletons for each application is provided.

Hand exoskeleton research is a rapidly growing and evolving field, with many new systems developed and studies published each year. Several publications have previously reviewed hand exoskeletons, and the authors refer interested readers to [9–14] among others for further information on the field.

8.2 OVERVIEW OF HAND EXOSKELETON SYSTEMS

[Fig. 8.1](#) provides a chronological overview of the characteristics of 40 hand exoskeletons found in the literature. The Y-axis categorizes systems by the number of independent active DOFs. Mechanically coupled DOFs are commonly found in hand exoskeleton systems and are indicated by thin lines between coupled DOFs.

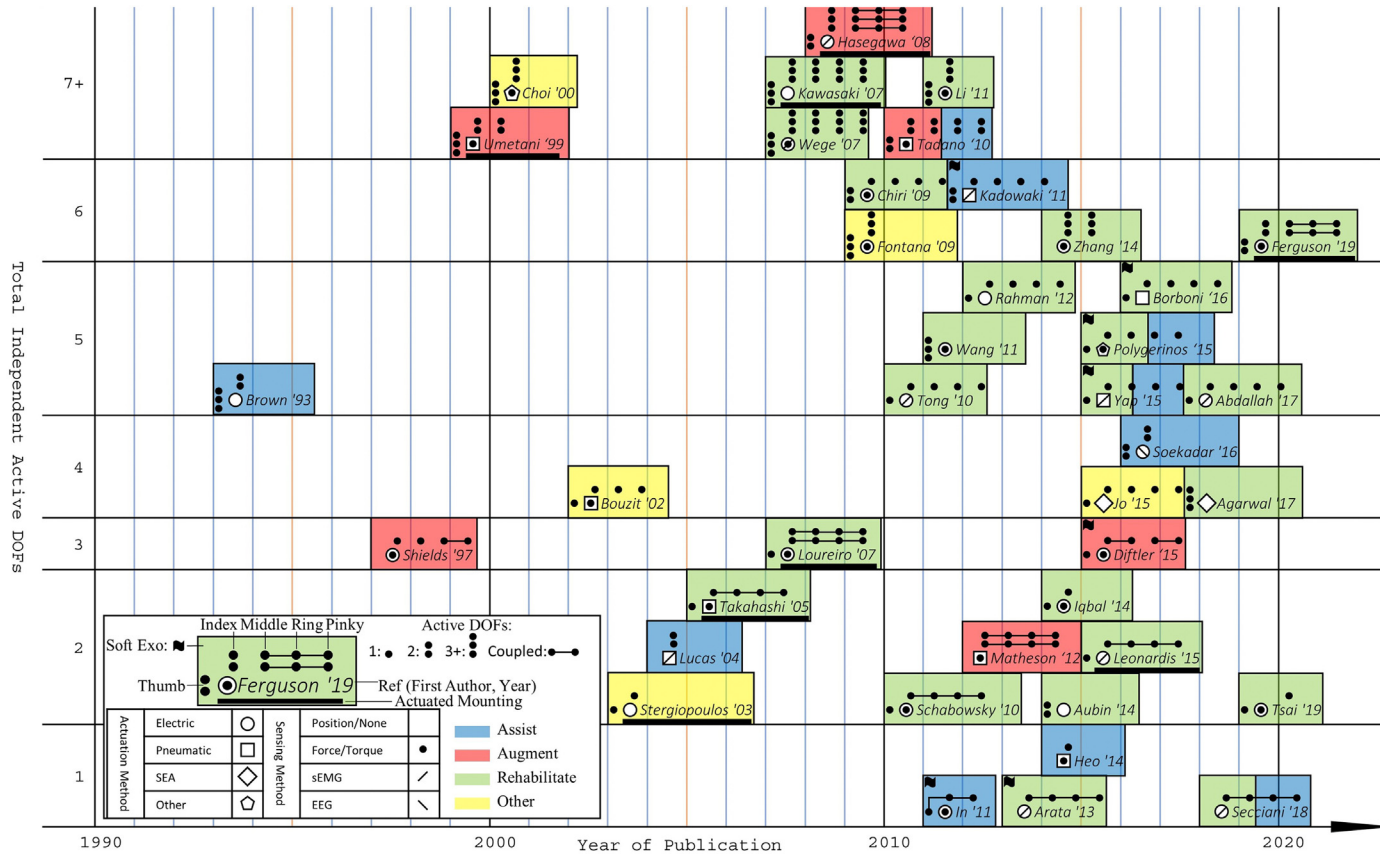
8.2.1 MECHANISM

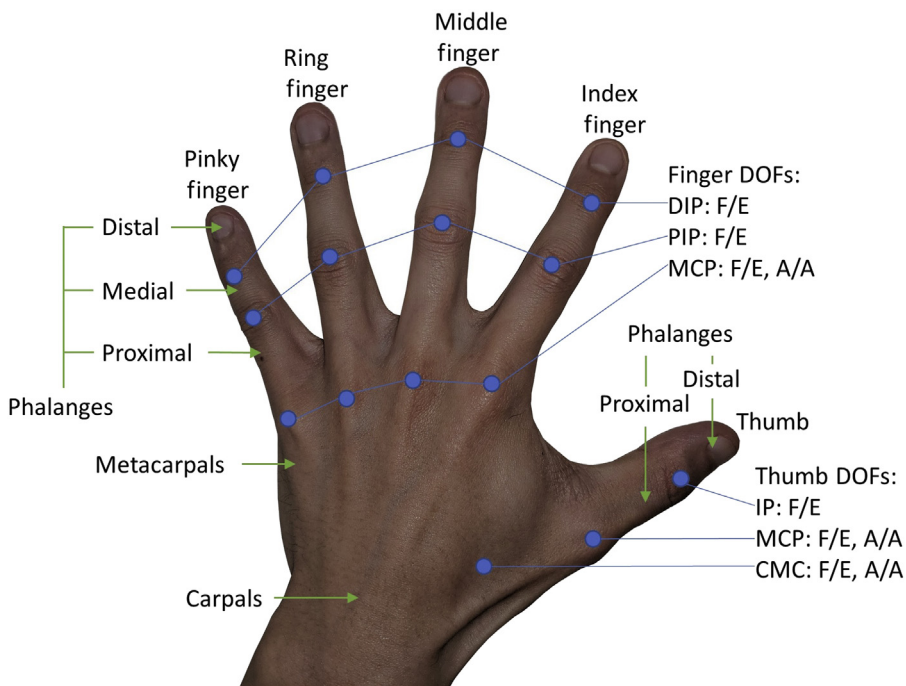
8.2.1.1 Degrees of freedom

A simplified model of the hand that is commonly used for discussion of hand exoskeletons is shown in [Fig. 8.2](#). Each of the four fingers, namely the index, middle, ring, and pinky fingers, are widely agreed upon to contain four DOFs. At the knuckle, or metacarpophalangeal (MCP) joint, each of the four fingers is capable of flexion and extension (F/E) as well as abduction and adduction (A/A). The four fingers are capable of two additional F/E motions each, at their respective proximal interphalangeal (PIP) and distal interphalangeal (DIP) joints.

The thumb is generally regarded as a more complex mechanism than the other digits, and kinematic models for its motion are still being refined [15]. Nonetheless, the prevailing model consists of five rotation axes [16,17]. The carpometacarpal (CMC) and MCP joints of the thumb are each considered to be capable of F/E and A/A, whereas the interphalangeal (IP) joint is capable only of F/E. However, it should be noted that one of the most important movements of the thumb is that of opposition and reposition (O/R). O/R consists of rotation of the plane of F/E of the thumb about an axis through the CMC such that the finger pad of the thumb can touch that of the fingers. This motion occurs as a combination of F/E and A/A of the joints of the thumb.

In total, there are 21 DOFs in this simplified model of the hand that ignores motion of the four finger metacarpals. Given the compact size of the hand, the required ability of the exoskeleton to rotate about hand joints without physically overlapping said joints, actuator size and mass, and

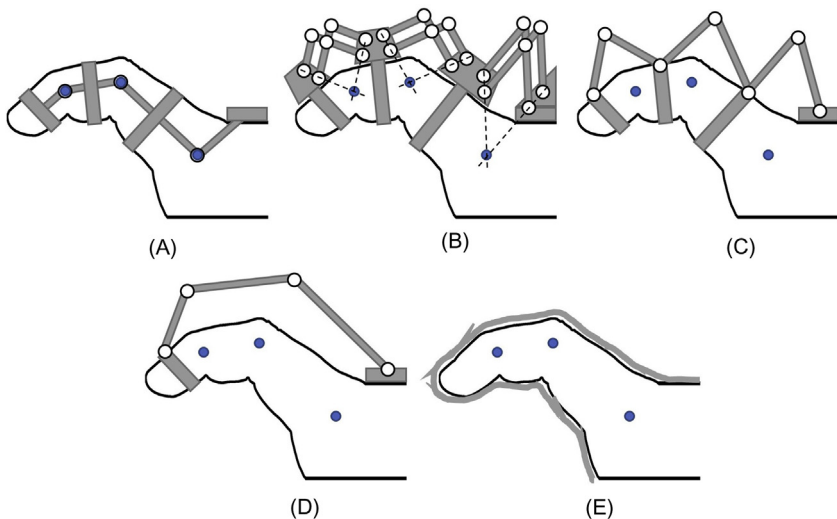


**FIGURE 8.2**

Simplified model of the hand. Bones are indicated by green, and joints in blue.

increasing complexity of intent estimation and control algorithms with more DOFs, it is frequently impractical to actively control every joint. Instead, it is common practice to include passive DOFs. As such, it is necessary when designing a hand exoskeleton to identify which motions must be actuated and which can be left passive. This choice depends largely on application, however even within applications there is not a unanimous consensus as can be seen in the varying designs shown in Fig. 8.1.

In addition to passive joints, most hand exoskeletons also feature either underactuated or coupled joints. This occurs when multiple DOF's are actuated by a single actuator. In hand exoskeletons, this commonly occurs in three ways. The first consists of placing rigid connections between fingers at specific attachment locations such that separate fingers move together. The second method requires a differential or some other mechanism such that multiple DOFs are driven by a single actuator but without a set ratio between joint angles velocities. This method enables some devices to conform grasp shape to a variety of different objects even with a single actuator. These first two methods are indicated on Fig. 8.1 by thin lines between DOFs. The final method involves the use of gears, pulleys, or links such that separate DOFs actuate together with a fixed ratio of joint angle velocities. This last method is frequently used to control multiple F/E DOFs with a single actuator, and is not indicated in Fig. 8.1.

**FIGURE 8.3**

Example schematics of hand exoskeletons in each category. (A) Matched axes, (B) remote center of motion, (C) redundant linkage, (D) base-to-distal, and (E) compliant.

8.2.1.2 Topology

Various studies have classified the topology of hand exoskeleton mechanisms in different ways [10,14]. This chapter classifies topology by categorizing as matched axes, remote center of motion, redundant linkage, base-to-distal, or compliant. Similar categories have been proposed in the literature, although terminology differs. Fig. 8.3 contains example diagrams of each category.

In order for a hand exoskeleton to properly control the desired DOFs of the digits of the hand, it is necessary for actuation of the exoskeleton joints to cause predictable rotations of the joints of the human hand.

The most direct way to cause hand exoskeleton motion to predictably control DOFs of the hand is to place the axis of rotation of the exoskeleton joint coincident with that of the human joint as shown in Fig. 8.3A. Exoskeletons that do so are referred to here as matched axes exoskeletons. Although such a topology may initially present as simple, they are in practice difficult to achieve as placing the exoskeleton F/E joints coincident to those of the fingers requires the structure of the exoskeleton to be laterally adjacent to said fingers. Given that many grasps place the fingers in contact with each other, this topology is usually not feasible for multiple finger systems. It should be noted that, in all systems studied, A/A motions of the four fingers were achieved with a matched axes topology.

An alternative method is for the mechanism of the exoskeleton to cause each link to rotate about remote centers of motion aligned with those of the finger joints as shown in Fig. 8.3B. There are several possible mechanisms to do this, and the problem has been analyzed in Ref. [18]. For hand exoskeletons, common mechanisms in this category include parallelogram mechanisms and circular-prismatic joints. These mechanisms can be low-profile depending on design. Exoskeletons

that feature this topology generally connect to the segments of the hand immediately proximal and distal to each joint such that each exoskeleton joint is coupled to a biological joint.

A redundant linkage topology is another option to couple motion of a specific exoskeleton joint to a single hand joint. These systems also attach to the digit before and after each actuated hand joint, but feature additional linkages and joints between each attachment point as shown in Fig. 8.3C. These extra joints and linkages serve to turn the combined digit-exoskeleton system between adjacent attachment points into four-bar or other mechanisms with well-defined relations between exoskeleton and hand joint motions. The resulting mechanism is typically slightly larger than those that use a remote center of motion topology.

Base-to-distal topology exoskeletons relax the recommendation of coupling specific exoskeleton joints to specific hand joints. Instead, these systems connect a serial linkage from the exoskeleton base, typically the dorsum, to distal to the last actuated joint as shown in Fig. 8.3D. The connecting serial linkage effectively actuates the entire digit together, as opposed to at each joint. Although there is some variability between individuals, it has been shown that F/E of the PIP and DIP joints are in general coupled [19], and multiple studies have reported accurate estimation of finger joint angles based on this coupling. Foremost among the advantages of this topology are simplified design and the removal of required adjustment mechanisms for varying user digit segment lengths with proper selection of link lengths. However, this comes at the costs of larger mechanism size and, despite joint coupling, reduced controllability of the hand.

Compliant topology exoskeletons can appear similar to gloves, and do away with rigid joints altogether, as shown in Fig. 8.3E. The actuation method or transmission is built into the exoskeleton such that there is minimal rigid structure. The structure of the exoskeleton bends with the actuated digits. These exoskeletons bring all the advantages and challenges of soft robots. Extra care must be taken such that forces are not applied inappropriately, as there are not rigid joints to guide torques and forces and thus the user's skeleton becomes the guiding structure.

A common requirement for the topologies of nearly all hand exoskeletons is an open palm. This requirement has a threefold purpose. First, occupying the palm with the mechanism prevents grasp of, and interaction with, most objects. Second, placing the mechanism on the palm prevents full closure of the hand. Lastly, the ability to obtain tactile feedback is an instrumental part of the human hand. Any obstruction of the palmar side of the hand will reduce this ability, and thus have a negative impact on the user.

8.2.2 ACTUATION

All active exoskeleton systems, by definition, require at least one actuator. Requirements for these actuators differ by system and application, but common desirable characteristics are high force/torque, high actuation bandwidth, low mass, backdrivability, and easy and precise control. Fig. 8.1 includes information on actuation method for each exoskeleton.

8.2.2.1 Electric motors

Electric motors are the most common actuator used, and come in several varieties. While standard rotary motors make up the bulk of these systems, a significant number also use linear actuators. Electric motors provide the notable advantages of easy, precise, and high bandwidth actuation, but

they in general have a lower power-to-mass ratio than their main competitor. Via use of gears, the torque provided by electric motors can be easily increased, but at the expense of speed.

8.2.2.2 Pneumatic actuators

Pneumatic actuators account for nearly all other hand exoskeleton systems. Different systems have incorporated pneumatics in different methods, including pneumatic cylinders, pneumatic muscle actuators, and soft elastomeric actuators. Pneumatics are characterized by high power-to-mass ratio, yet also create challenges in control. Additionally, pumps and/or compressed gas containers are required for their use.

8.2.2.3 Series elastic actuators

A relatively small minority of hand exoskeletons feature series elastic actuators (SEAs). This method of actuation typically features an electric motor driving a transmission ending in springs. Despite using electric motors, the addition of springs changes the characteristics of SEAs enough that they can be considered in a different category. By nature, SEAs provide advantages in safety and impact resistance. Additionally, the springs allow the implementation of highly accurate force-control. However, SEAs also suffer from high power requirements, increased mechanical complexity, low actuation bandwidth, and low stiffness. A discussion of the use of SEAs in rehabilitation robotics is provided in Ref. [20].

8.2.2.4 Other actuators

Other actuation methods have been implemented in the remaining few hand exoskeletons. These include hydraulic actuators, ultrasonic motors, and shape memory alloys among others.

8.2.3 TRANSMISSION

8.2.3.1 Direct drive, gear, or linkage

The simplest and most direct way to transfer force/torque from the actuator to the joints of the hand is through direct drive, gears, or rigid links. With this type of transmission, the motor is typically placed on the dorsum or on the finger linkages themselves. While this reduces complexity, it also increases mass at the hand which is undesirable for many systems. Due to limitations in permissible motor size or mass, these systems usually have fewer actuators unless the structure of the exoskeleton is supported externally.

8.2.3.2 Bowden cable

Bowden cable transmission systems offer an attractive alternative to direct drive, gear, or linkage transmission systems due to the ability to place the motor remotely. This option is particularly attractive for nonportable hand exoskeletons, as the motors can be moved to a stationary location to reduce inertia while still permitting the arm to be moved. However, Bowden cable transmissions suffer from friction, backlash, comparatively lower maximum force before breaking, and the sheathes exerting forces on the exoskeleton when moved. Nevertheless, they are a popular choice to reduce inertia of hand exoskeletons.

8.2.3.3 Tendon driven

Another option is to use cables to mimic the functionality of the tendons of the hand. By attaching them at a distal point beyond a joint, and applying tension, they can cause joints to move in a way that closely matches biology. However, tendon transmissions are, in general, unidirectional. In order to achieve bidirectional actuation, a second cable, often from another actuator, must be attached to apply force in the opposite direction. Additionally, tendon transmissions can suffer from cable breakage and sometimes require complex routing. Nonetheless, as they apply force/torque across a digit and not just a joint, they are frequently used in soft exoskeleton gloves. They are often coupled with restorative springs.

8.2.3.4 Compliant

Several other compliant transmissions have been proposed for hand exoskeletons, and theoretically any of the methods used in soft robotics [21] could be applied. Various methods using electric motors, pneumatics, and hydraulics have been tried. These transmissions simultaneously increase safety by absorbing impacts, and can reduce safety if unsafe forces are routed through the hand due to the lack of exoskeleton structure.

8.2.3.5 Restorative springs

Although a passive element, springs are used in most hand exoskeletons with otherwise unidirectional actuation. Frequently, they are coupled with either tendons or pneumatic cylinders that control only flexion or only extension in order to passively provide the other.

8.2.4 SENSING METHOD

In order for a hand exoskeleton to properly accomplish a task, it is necessary to prescribe an overarching strategy for how it is to be controlled. The inputs to this control strategy are the desired actions to perform. The desired action, in turn, is dictated by the state of the system and estimated intention of the user. There are a variety of sensors used to acquire this information, and some of the more common strategies are discussed.

8.2.4.1 Position sensors

The vast majority of hand exoskeletons have some method of detecting the joint angles and/or the position of the various links with respect to the exoskeleton base. There are a variety of different choices to establish this information including encoders on the motors, encoders or potentiometers placed at joints, flex sensors, and linear variable differential transducers among others. Position sensors are required to obtain the physical configuration of the exoskeleton, and are therefore critical to many control strategies.

8.2.4.2 Force/torque sensors

Numerous applications require knowledge of the forces/torques experienced by the hand exoskeleton. This information can be used to enable admittance or force control, provide information on rehabilitation progress to a physical therapist, and for interactive use as a teleoperation or virtual reality haptic device. Inclusion of force/torque sensors are varied, with some systems omitting

them, others building them into the fundamental structure of the device, and others placing them at human–robot interface locations.

8.2.4.3 Electromyogram

Surface electromyogram (sEMG) is a method for detecting the electrical activity in muscle [22]. In healthy individuals, these electrical signals accompany all movements. With sEMG used to detect these signals, a hand exoskeleton can generate trajectories with complementary movements. This ideally enables real-time control of an exoskeleton without requiring the user to exert forces or torques on the system, creating greater transparency. However, sEMG faces a variety of challenges as a method for intent estimation. Every time the system is donned/doffed, electrodes must be reattached, and changes in position will result in changes in detected electrical activity requiring recalibration. Additionally, there are challenges with using electrodes with hairy, dirty, or wet skin. Finally, the resolution of sEMG is relatively low and the number of electrodes used may be less than the number of active DOFs, and thus it is challenging to use to control a high DOF system.

8.2.4.4 Electroencephalogram

Similar to sEMG, electroencephalogram (EEG) is used to detect electrical biosignals. However, EEG is used to noninvasively detect brain signals, in the form of electrical activity, through the scalp. As with sEMG, EEG could be used to control a hand exoskeleton without applying forces/torques. Additionally, it can be used with users that do not have proper muscle functioning, such as victims of stroke or spinal cord injury. It has also been shown to be capable of controlling a variety of complex robotic systems, such as mobile or humanoid robots [23,24]. EEG suffers from many of the same challenges as sEMG, as well as low signal-to-noise ratios, significant required processing, and long reaction times.

8.2.5 CONTROL

There exist several control strategies used by hand exoskeletons to correctly actuate the hand to accomplish tasks. A brief summary of some of the more common strategies are detailed below.

8.2.5.1 Passive motion

Passive motion ignores the intention of the user entirely, and attempts to control the hand exoskeleton along a trajectory as if the user was not there. This strategy typically uses a position or velocity low-level controller. The passive motion can be used to test functionality of a device, or to bring the exoskeleton to a specific state, such as a neutral position for donning/doffing. However, the most significant application is as continuous passive motion (CPM) [25]. Applied in the initial stages after an injury or surgery, CPM can be effective in preventing the development of stiffness. However, it has been shown that interactive treatment with a rehabilitation robot can provide benefits that CPM cannot [26]. For this reason, as well as for applications outside of rehabilitation, active intent estimation is necessary.

8.2.5.2 Master/slave system

The first active hand exoskeletons were developed as haptic devices and data gloves to control other robotic systems. It is therefore logical that one strategy for controlling a hand exoskeleton is

to use it as the slave of a master/slave system. Of particular interest is the use of two hand gloves, one a master system and one a slave hand exoskeleton system, where the movements of the hand in the master system are mirrored to the other by the hand exoskeleton. This is a commonly proposed technique for bimanual rehabilitation of stroke, and has been shown to be effective [27–29].

8.2.5.3 Biosignal control

This category consists of strategies for controlling the exoskeleton based upon biological signals measured from the body through EMG, EEG, electrooculogram (EOG), or other methods. Depending on the sensing method, the biological signals can be obtained even from users who have impaired motor functioning. As such, biological control strategies are primary candidates for real-time control of assistive exoskeletal devices, although they are also not uncommon for rehabilitation exoskeletons. The challenge of biosignal control strategies is how to convert the biological signals to control inputs, as there is rarely unambiguous or independent mapping between the measured signals and the DOFs to be controlled. There are also options of whether the signals are used as binary switches [30] or for proportional control [31].

8.2.5.4 Force-based strategies

Force-based control strategies are those that control the hand exoskeleton based upon the interaction forces and torques applied between the human hand and exoskeleton. These include low-level control of impedance, admittance, and force. Further, these strategies can be divided into assistive strategies that help the user move, and resistive strategies that hinder movement. Assistive force-based control strategies are common across all hand exoskeleton applications. Resistive strategies are found primarily in systems made as haptic devices (to simulate virtual objects it is necessary to resist movements of the hand that would penetrate said objects), as well as rehabilitation devices for the latter stages of physical therapy.

8.3 ASSISTIVE HAND EXOSKELETONS

Assistive hand exoskeletons are a popular area of research in academia and have even begun to be commercialized. One of the primary design requirements of these systems is portability. A consequence of this is that systems are heavily limited in the number and size of actuators. It is not at present a viable strategy to attempt to independently control all, or even most of, the DOFs of the hand, as the required motor mass would be prohibitive for use by the intended functionally impaired audience.

Hand exoskeletons in this category include:

8.3.1 BROWN ET AL

The assistive hand exoskeleton by Brown et al. [7] dates back to 1993 and consists of rigid joints placed between aluminum blocks with bands that wrap around the fingers between joints. The overall mechanism falls under the redundant linkage topology category. It uses a motor and tendon actuation system to control unidirectional actuation of three DOFs of the thumb and two DOFs of

the index finger, and restoring actuation occurring due to passive springs connecting between the aluminum blocks.

8.3.2 LUCAS ET AL

Lucas et al. [30] developed a two active DOF exoskeleton for actuation of the index finger. It features pneumatic linear actuators controlled using sEMG using either binary or variable control algorithms. One of the actuators controlled MCP joint F/E, while passive MCP A/A movements were allowed. The other pneumatic actuator controlled coupled F/E of the DIP and PIP joints. The actuators are directly connected to the redundant linkage topology to actuate the system.

8.3.3 IN ET AL

In et al. [32] developed a soft exoskeleton glove to actuate the thumb, index, and middle fingers with a single motor. Flexion is achieved with a unidirectional motor and tendon actuation system combined with a differential mechanism to compliantly enable different grasps of the index and middle fingers. Extension is passively achieved with springs.

8.3.4 KADOWAKI ET AL

Kadowaki et al. [33] published on a power-assist soft exoskeleton glove for hand grasping in daily life by the elderly or disabled. The system compliantly actuates F/E of all five full digits using five pneumatic sheet-like curved rubber muscles and O/R of the thumb with a pneumatic spiral rubber muscle. The hand module consists entirely of cloth and rubber, and consequently weighs just 135 g, not including remotely located valves and air pressure source. Control is demonstrated both as a master/slave system with a data glove, and with EMG.

8.3.5 OFX

Heo and Kim [34] created the Open Fingerpad eXoskeleton, OFX, with a single active DOF of the index finger. The OFX, as the name describes, is distinct in that the finger pad is unobscured due to use of cantilever load cells on either side of the index finger, allowing the user to naturally interact with and feel surfaces. A pneumatic cylinder directly actuates rotation of the entire index finger about the MCP F/E joint with a rigid finger module designed with a matched axes topology. A thumb module with a locking mechanism enables pinching.

8.3.6 EXOGLOVE

The fabric-based ExoGlove [35,36] features interchangeable pneumatically actuated soft elastomeric actuators. These actuators, which attach with Velcro dorsally to each finger and thumb, each produce specific motions depending on the distributed stiffness within the actuator. The actuators are customizable for different grasps and can be manufactured in an hour. The ExoGlove uses a combination of EMG and radio frequency identification (RFID) for intent detection. The ExoGlove is also intended for use as a rehabilitation hand exoskeleton.

8.3.7 POLYGERINOS ET AL

Polygerinos et al. [37,38] developed a hydraulically actuated, compliant, portable hand exoskeleton glove for assistance and at-home rehabilitation. The system is low-profile (<2 cm), lightweight (<500 g), and capable of 2 hours of continuous use powered by a waist pack weighing less than 3 kg. Each of the five digits is driven by a separate hydraulic soft actuator made of molded elastomeric chambers with fiber reinforcements. These actuators are designed to actuate F/E motions of the four fingers and combined F/E and O/R motions of the thumb along natural trajectories. Different actuators can be made for different sized hands and different motion profiles. Fluidic pressure sensors are placed in line with the actuators to regulate pressure with a sliding-mode controller.

8.3.8 HX

The HX hand exoskeleton published in Ref. [39] is a rigid, underactuated, cable-driven exoskeleton for the index finger and thumb. Each digit has one actuated DOF controlling all F/E motion, the index finger possesses an actuated MCP A/A joint, and the thumb has an active joint for CMC O/R. The exoskeleton features a combination of matched axes and remote center of motion mechanism topologies for different joint axes. The HX was shown in Ref. [40] to be controllable with intent estimation based upon a combination of EEG and EOG.

8.3.9 SECCIANI ET AL

Secciani et al. [41] present their work on several generations of light, low-cost, 3D-printed, portable assistive and rehabilitation hand exoskeletons. The most recent design is compact, entirely portable, and customizable for different users. A single servomotor, combined with a transmission system with varying pulley diameters, enables actuation of all four fingers with natural grasping patterns using a base-to-distal topology that attaches to the medial phalanges. Intention detection is enabled via EMG.

8.4 REHABILITATION HAND EXOSKELETONS

Hand exoskeletons have also been developed for rehabilitation, and a wide variety of them have been presented in the literature. As opposed to assistive hand exoskeletons, rehabilitation hand exoskeletons do not, by nature, need to be portable. Instead, the most important requirement is the ability to enable the exercises required for physical therapy. This has enabled the development of extremely complex hand exoskeletons to enable independent control of many movements, although this complexity is not ubiquitous. Indeed, the two hand exoskeletons with greater than 15 active DOFs, as seen in Fig. 8.1, were developed more than a decade ago. Although these systems can reproduce almost any hand motion, the complexity also equates to bulkiness and introduces greater challenges for control and intent estimation. Many recent designs have instead limited the number of independent active DOFs, and therefore enable smaller, sleeker, and potentially less expensive designs that still permit the majority of motions required for rehabilitation. Rehabilitation

exoskeletons are also generally designed not to be used by a single patient, but by a variety of users. As such, ability to accommodate hands of different sizes and impairments is a common requirement.

The goal of hand rehabilitation exoskeletons is to restore, or at least improve, the ability of the patient to use the hand without the exoskeleton. This is done to enable the patient to resume normal activities of daily living (ADL) without the need to constantly wear an assistive device. Many ADL involving the hand are reach-and-grasp tasks that also require movement of the arms. As it is not uncommon for patients with hand impairments to also have impairments in the arm, it is a logical step to design a single exoskeleton combining both a multi-DOF hand exoskeleton and a full arm exoskeleton. However, there are relatively few examples of this in the literature. Instead, many upper-limb exoskeletons with hand modules actuate just one DOF to permit a single simple grasp.

There are several challenges limiting the development of arm exoskeletons with multi-DOF hand modules. Typically, the more DOFs a hand exoskeleton can actuate, the more complex and heavier the system becomes. This creates problems if the hand exoskeleton is attached to the distal end of an upper-limb system, as it increases mass and inertia. Additionally, power and control signals for the hand must be routed in such a way that does not interfere with motion of the arm. Though feasible, this becomes more difficult with more hand DOFs. Furthermore, the combined human arm and hand system possesses dozens of DOFs. As the number of DOFs of the combined exoskeleton system increases, questions of intent estimation and redundancy resolution become more difficult to answer.

A common addition to rehabilitation robotic systems is a virtual reality or computer game environment [1,3,42–45]. These games are intended to engage the patient and keep them motivated to perform greater repetitions of tasks, increase possible training session durations, and potentially reduce the need for supervision by a physical therapist. The tasks are designed to require motions similar to those normally performed during physical therapy sessions. They have been proven as effective strategies for rehabilitation in multiple studies.

Numerous rehabilitative hand exoskeletons exist in the literature, and a sample are shown in Fig. 8.1.

8.4.1 HWARD

HWARD [46,47], the Hand-Wrist Assisting Robotic Device, is a three active DOF pneumatically actuated and backdriveable exoskeleton designed for repetitive grasp and release movements. One of the actuators controls a mechanically coupled grouping of all F/E motions of the four fingers, another the F/E motions of the thumb, and the final controls F/E of the wrist. The coupling of the four fingers permits the mechanism to use a matched axes topology without placement of exoskeleton structure between the fingers.

8.4.2 GENTLE/G

Gentle/G [48] consists of a three active DOF hand exoskeleton combined with the active three DOF HapticMaster [49] system and a passive three DOF Connection Mechanism. The HapticMaster and Connection Mechanism together serve to enable active positioning and passive orienting of the hand exoskeleton module. Similar to the HWARD, the Gentle/G has a single

actuator for controlling thumb F/E, and groups the F/E of the four fingers with a matched axes topology. However, the Gentle/G uses two actuators to flex/extend the MCP and PIP joints independently.

8.4.3 WEGE ET AL

Wege et al. [50,51] developed a rehabilitation hand exoskeleton with 20 independent active DOFs. To the authors' knowledge, no other existing hand exoskeleton has as many active DOFs of the hand. The exoskeleton estimates user intention with force sensors and 10 EMG electrodes placed along the forearm. Each digit is controlled in A/A at the most proximal joint and all three F/E motions with a motor and Bowden cable transmission combined with a redundant linkage topology.

8.4.4 KAWASAKI ET AL

Kawasaki et al. [52,53] created an 18 active DOF hand and wrist exoskeleton. Two of these DOFs are located at the wrist. The thumb is controlled in CMC A/A and all F/E, whereas each of the four fingers are controlled in MPC A/A, MPC F/E, and PIP F/E. The mechanism uses matched axes for the A/A motions and redundant linkages with motors placed on the links for F/E motions. The device is controlled as a master/slave system using “mirror therapy” with a Cyber Glove (Virtual Technologies Co.).

8.4.5 HANDEXOS

HANDEXOS [54,55] is a multiphalanges device intended for poststroke rehabilitation. The device is designed to minimize human/exoskeleton rotational axes misalignment. For each digit, flexion is passively accomplished with three springs and cables, while extension is controlled for all MCP, PIP, and DIP joints by a single motor and cable. The thumb features one additional active DOF for CMC O/R driven by an on dorsum motor directly actuating a slider-crank mechanism. The system features a remote center of motion topology for each of the four finger MCP joints, and a matched axes topology for each DIP, PIP, and IP joint. The O/R joint is approximated and slightly offset dorsally. It should be noted that despite being comparatively compact, the matched axes topology inherently prevents fully adducting the fingers together.

8.4.6 TONG ET AL

Tong et al. [56,57] developed the hand exoskeleton that was later commercialized as the Hand of Hope (<http://www.rehab-robotics.com/>). It is intended for use with stroke rehabilitation. F/E of each of the digits is controlled independently by five linear actuators that directly drive linkages to move about remote centers of rotation aligned with the finger joints. User intent is estimated from EMG signals.

8.4.7 HEXORR

HEXORR [58] consists of two modules, one for the thumb and one for the fingers. Each module possesses one independent active DOF. The thumb mechanism can be passively adjusted to enable active control of different motions. The finger mechanism mechanically couples all fingers at attachment points, and causes F/E using a four-bar linkage system with link lengths chosen to maximize backdrivability. The mechanism uses a matched axes topology.

8.4.8 ATX

The ATX [59] is a thumb exoskeleton with five independent active DOF. The five DOFs were chosen to match a model of the thumb consisting of DOFs for CMC F/E and A/A, MCP F/E and A/A, and IP joint F/E. The ATX uses a matched axes for CMC F/E, but redundant linkages for MCP and IP F/E.

8.4.9 IHANDREHAB

iHandRehab [60] is a cable-driven rehabilitation hand exoskeleton with eight independent active DOF. The index finger modules have the same overall design, enabling each of the three F/E and the A/A motion of the respective digit. The mechanism is based on a parallelogram structure that adds a redundant link topology but places joints at matched axes locations. Range of motion (ROM) of each joint can be mechanically adjusted to prevent injuring patients.

8.4.10 RAHMAN ET AL

Rahman et al. [61] presented a five digit hand exoskeleton for stroke rehabilitation by mirroring motions from a custom control glove worn on the unaffected hand. This device features an independent linear actuator controlling a novel L-shaped sliding bar mechanism for F/E of each digit. This sliding mechanism effectively creates a remote center of motion topology through the combination of active rotation and passive translations.

8.4.11 ARATA ET AL

Arata et al. [62] created a compliant hand exoskeleton based on a sliding spring mechanism. Coupled F/E of the three DOFs of all fingers are controlled by sliding a spring blade with respect to two others and rigid connection points on each finger, causing the blades to bend.

8.4.12 IOTA

The IOTA [63], or Isolated Orthosis for Thumb Actuation, is a thumb exoskeleton designed for rehabilitation of pediatric patients with thumb-in-palm deformity. It is capable of independently actuating CMC A/A and MCP F/E with a matched axes topology. Five control modes were proposed, including manual control, teach & learn, cyclic control, wrist control, and functional assistance modes.

8.4.13 HEXOSYS-I

Iqbal et al. [64,65] developed HEXOSYS-I, a portable index finger and thumb exoskeleton device designed to facilitate therapy exercises. It features underactuated base-to-distal topology that is directly driven by a single motor for each joint and is able to apply up to $45N$ of bidirectional force in F/E. The link lengths were selected via a multiparametric optimization procedure that considered isotropy, dexterity, and the ability to exert force perpendicular to the finger phalanges.

8.4.14 ZHANG ET AL

Zhang et al. [66] made a portable rehabilitation hand exoskeleton featuring a novel “circuitous joint” that functions as a remote center of motion mechanism. The six active DOF device independently controls each of the three F/E joints of the index and middle fingers using a Bowden cable transmission system with a motor pack that mounts to the forearm.

8.4.15 BRAVO

The BRAVO hand exoskeleton [67] was developed for rehabilitation exercises involving cylindrical grasps. The four fingers are rigidly mechanically coupled at a shared driving shaft, are driven by a single motor that causes coupled F/E of all finger joints. The thumb features a spatial four-bar linkage mechanism, the plane of actuation is passively adjustable in six DOFs, and actuates coupled F/E of the distal two joints. The entire mechanism uses the redundant linkage topology. The BRAVO is specifically designed to be integrated with the L-Exos upper-limb exoskeleton [68,69].

8.4.16 SINFONIA

The Gloreha Sinfonia (<https://www.gloreha.com>) soft exoskeleton glove developed from [70] is a commercialized device for stroke rehabilitation. The glove independently controls F/E of the five digits via linear actuation by five pneumatic cylinders of flexible rods routed dorsally along the digits and attached to the fingertips. The Sinfonia can be purchased with an optional arm module for passive gravity compensation called the Gloreha Aria. The glove is controlled for either CPM or with mirror therapy with a sensorized glove on the other hand.

8.4.17 AGARWAL ET AL

Agarwal et al. [71,72] published prototypes of thumb and index finger exoskeletons that feature similar designs with redundant linkage topologies. Each of these devices independently actuate each F/E and an A/A motion of their respective digit using SEAs with Bowden cable transmission systems. The devices are highly transparent to the user, and accurate torque control is demonstrated.

8.4.18 ABDALLAH ET AL

An EMG controlled, portable, low-cost, hand exoskeleton is presented by Abdallah et al. in Ref. [73]. The design is 3D-printed, and all actuators and electronics are contained within a forearm splint module that attaches to the dorsal side of the palm, wrist, and forearm. The mechanism topology is that of the redundant linkage type, but with additional links added to couple F/E motions. The joints of each of the five digits of the hand are controlled in coupled F/E motions by a servo-motor each, while A/A is passively permitted.

8.4.19 FERGUSON ET AL

In Ref. [74], Ferguson et al. created a three finger hand exoskeleton with reconfigurable mechanical coupling to actuate all five digits. Each exoskeleton finger consists of a base-to-distal mechanism that independently controls two DOF F/E motions using an electric motor and Bowden cable transmission system. The device was designed to be integrated with the EXO-UL8 [75,76] and BLUE SABINO [77] upper-limb exoskeletons. A second-generation hand exoskeleton with an active thumb O/R is under development.

8.4.20 DEXOHAND

The DexoHand [78] was developed and tested for use with stroke patients with spasticity. It was used to actuate F/E of the MCP, PIP, and DIP of the middle finger, as well as of the MCP and IP joints of the thumb with a remote center of motion mechanism driven by one actuator for each digit. The device was tested by a group of healthy and impaired individuals who reported high usability and satisfaction.

8.5 AUGMENTATION HAND EXOSKELETONS

Compared to other categories, few hand exoskeletons for augmentation were found in the literature. There are a number of significant obstacles to the development of an ideal augmentation hand exoskeleton for general use by healthy individuals. Foremost among these obstacles is low mass. In order for a hand exoskeleton to truly augment a healthy individual in tasks without unusual burdens, it is necessary for the mechanism to be of low enough mass to be mostly ignored. To the authors' knowledge, no existing combination of mechanical structure, materials, actuator, and power supply can fulfill this requirement while providing meaningful augmenting force. Power supply and actuators may be placed remotely to reduce mass at the hand, but this necessarily introduces at least some restriction of arm motion due to the resulting connector routing. The requirement can be relaxed if the mass of the hand exoskeleton can be offset to the environment through a supporting device.

Another significant challenge is for the augmentation hand exoskeleton to permit all the motions of a healthy hand. Even the most simplified kinematic models of the hand assume more than 20 DOFs. Although not all DOFs must be actively controlled to achieve augmentation, relatively few designs even passively permit all motions.

Additional challenges for augmentation hand exoskeletons come in the forms of intent estimation and control. Given the high number of DOFs and compact size it is difficult to accurately estimate the desired motion of all joints. Additionally, the exoskeleton must be capable of being extremely transparent.

In addition to general power augmentation hand exoskeletons, augmentation exoskeletons for specific challenging tasks can be found in the literature. A commonly stated application for these exoskeletons is for use in extravehicular activity (EVA) gloves in space. EVA gloves can be bulky and stiff, particularly at the MCP joint, and are fatiguing when used for extended periods of time. The augmentation hand exoskeletons for EVA gloves are intended to reduce the strain of hand activities on astronauts while wearing the gloves. It is important to note that the EVA gloves are already somewhat restrictive, and thus the hand exoskeletons that reduce the required effort to use the glove would not necessarily purely augment a user that is not wearing such a glove.

8.5.1 SHIELDS ET AL

Shields et al. [8] presented a three finger hand exoskeleton for use with EVA gloves. The exoskeleton features a rigid body that extends over the dorsal side of the hand, and encloses the four fingers in protective brackets with the ring and pinky fingers grouped together. The mechanism is based on a remote center of motion topology, and uses motors with cable transmissions.

8.5.2 SKIL MATE

Skil Mate [79] is a combination elbow–wrist–hand augmentation exoskeleton for use in hostile environments with seven independent active DOFs at the hand. Index and middle finger MCP and PIP joints, as well as F/E of thumb CMC, MCP, and IP joints are actuated in flexion by pneumatic cylinder actuators and restored in extension by coil springs. The wrist module passively allows two DOFs while the elbow is controlled in F/E by McKibben artificial muscles.

8.5.3 HASEGAWA ET AL

Hasegawa et al. [80] published their work on a portable wrist-hand augmentation exoskeleton with 11 DOFs and a matched axes topology. Three DOFs were dedicated to actuate a wrist five-parallel-link mechanism in all rotations. The hand module is capable of simulating variable compliance at the fingertips for grasping stability using a polyarticular tendon-driven transmission. The thumb is actuated in O/R as well as in biarticular MCP and IP F/E. The little, ring, and middle fingers are mechanically coupled at the attachment points. The index finger and the grouped three fingers are driven by three motors and tendon pairs each. For each finger grouping, one motor and tendon drives MCP flexion, one motor and tendon drives biarticular MCP and PIP flexion, and the last motor and tendon pair drives polyarticular flexion of all three finger joints. The system is force controlled based on detected sEMG signals.

8.5.4 TADANO ET AL

Tadano et al. [81] created a 10 DOF hand exoskeleton for power amplification driven by pneumatic artificial rubber muscles (PARM). On each of the four fingers, one PARM is used to control MCP F/E, another causes biarticular F/E of the PIP and DIP joints. The thumb features a cable and pulley system for CMC A/A, as well as a PARM for biarticular F/E of MCP and IP joints. Despite use of (mostly) compliant actuators, the system features rigid joints and thus is not a soft glove. The device does not easily fall into one of the discussed topologies, as the joint rotations are misaligned with those of the finger but the attachment points have passive tolerances to accommodate. The PARMs, cable and pulley, as well as “balloon type” force sensors contain no electronics at the hand, enabling the system (excluding remotely located pressure sensors and servo valves) to be waterproof. The system can also be used as an assistive exoskeleton.

8.5.5 MATHESON ET AL

Matheson and Brooker [82] developed two augmentation hand exoskeletons for use with EVA gloves based on the same design principle. Each exoskeleton powered extension of the four fingers by pneumatic muscle actuators. For the first prototype, flexion was obtained due to the initial state of the elastic composite material that composed the structure of the compliant exoskeleton. However, material fatigue and poor ROM were observed in testing. The second prototype used torsion springs, coupled F/E of the PIP and DIP, decreased coupling of extension via use of a second pneumatic muscle actuator, and had slightly offset joint axes with the hand. For both prototypes, all four fingers were coupled together.

8.5.6 ROBOGLOVE

The RoboGlove [83] is a spinoff of the Robonaut 2 system developed by General Motors and NASA. It is a soft exoskeleton glove capable of providing steady-state grasp force of 15–20 Lbs. Three electric motors drive ball screws to linearly actuate tendons that together drive F/E of all five digits, with index and middle fingers and pinky and little fingers coupled. Actuators, drive electronics, and microprocessor are contained within a forearm module. At the time of publication, the system had not yet been integrated into an EVA glove.

8.6 OTHERS

In addition to hand exoskeletons for assistance, rehabilitation, and augmentation, there exist a number of systems in the literature that are classified in this chapter as “other” hand exoskeletons. Whereas assistive, rehabilitative, and augmentative hand exoskeletons are primarily intended to move the user for the user’s sake, hand exoskeletons that fall in the “other” category are primarily intended to simulate interaction. Applications for these exoskeletons vary, but a significant subset of them are used as virtual reality haptic devices or for teleoperation of other systems. Although these devices were typically developed for industry and academia, the recent boom in consumer virtual reality systems has sparked the creation of a number of commercial systems intended for

consumers. It should be noted that these commercial systems are not usually accompanied by publications providing information on specifications, and thus some of them are excluded from Fig. 8.1.

8.6.1 SKK HAND MASTER

The SKK Hand Master [84] is a seven DOF exoskeletal haptic device with a redundant linkage topology driven by ultrasonic motors. These actuators were selected for their light weight, quiet operation, high power-to-weight ratio, high transparency, and no electromagnetic noise. However, they also have disadvantages of hysteresis and temperature rise with operation that were addressed with a PWM/PS driving method. The presented design features two modules, a four DOF index finger and a three DOF thumb, though it is noted that it could be expanded to include the other digits.

8.6.2 RUTGERS MASTER II-ND

The Rutgers Master II-New Design [85] force-feedback glove is a haptic interface designed for virtual environments. Although it may be considered a base-to-distal system, it is unique in the reviewed hand exoskeletons in that the mechanism is placed on the palm. Pneumatic cylinder actuators attach between universal joints at the palm and the fingertips of the thumb, index, middle, and ring fingers. Although this design does prevent interaction with most physical objects, it creates a very compact and lightweight design; the glove exoskeleton structure is just 80 g while the electric wires and pneumatic tubing connecting to the glove is 105 g.

8.6.3 STERGIOPoulos ET AL

Stergiopoulos et al. [86] developed a base-to-distal hand exoskeleton for VR grasping simulation. The system underactuates the three F/E DOFs of each digit with a single actuator each, and the thumb passively permits A/A. The device is used with the Virtuose 6D commercial six DOF haptic arm to allow simulation of external forces and compensate for mechanism weight.

8.6.4 FONTANA ET AL

Fontana et al. [87,88] presented a portable haptic hand exoskeleton for accurate force displaying and precision grasp simulation. The system has “quasianthropomorphic” kinematics in that it uses a remote center of motion topology such that the exoskeleton moves about axes aligned with those of the hand, but it is also a base-to-distal topology as the linkages only attach at the base and distal phalanges. The thumb and index finger are each actuated in A/A and two F/E motions by three motors mounted on their respective first links to simplify cable routing.

8.6.5 JO ET AL

Jo et al. [89] created a five DOF redundant linkage hand exoskeleton for interaction with virtual reality. Each digit is controlled in F/E by a separate compact SEA featuring a linear electric motor. Linear potentiometers were used with the SEAs to estimate force and implement accurate force-control.

8.7 CONCLUSION

Despite the many advancements made and systems developed over recent decades, active hand exoskeletons still primarily exist in the realm of academia. Functionality for various applications has been demonstrated in lab settings, yet only a few hand exoskeletons have been commercialized. This is speculated to be due to limitations not only in the state-of-the-art of hand exoskeleton design, but also in related fields. It is likely that significant breakthroughs will require or accompany innovations in actuator technology, material science, transmission methods, sensor technology, and control algorithms.

Perhaps the greatest challenges for development and commercialization of hand exoskeletons stem from the many DOF in a relatively compact area. In lower-limb and arm exoskeletons, mechanical designs have tended to converge toward actuation capabilities for similar DOFs, with further improvements still being made in control, actuation method, materials, and power supply. However, for hand exoskeletons, no such trend is immediately apparent and very few systems even approach independent actuation of every motion of the hand.

A popular and growing area is that of using soft robotics for hand exoskeletons, as the systems are often lighter, lower profile, and feature inherent safety. However, existing systems typically have five or fewer independent DOFs and therefore couple motions. Although compliance permits the generated motions to adapt to grab a variety of objects, not all desirable motions can be actuated. Additionally, actuator design and precise control of soft robotic hand exoskeletons have not been refined to the same extent as their rigid counterparts.

Despite the potential for hand exoskeletons to be built onto full arm exoskeletons to improve functionality, few systems have been developed that enable active control of multiple DOF of both the hand and arm. This can be attributed to multiple factors including physical constraints, high required complexity, challenges with intent estimation, and potentially opposing design requirements. However, it should be noted that synthesis of combined arm and hand exoskeleton systems is an active area of research with significant future potential [42,68,74,90].

Another area with room for improvement is that of portability. Numerous portable systems have been developed, yet various systems face issues with operation time, system weight, low number of independently controlled motions, and low torque capabilities. A significant limiting factor is actuator mass, and therefore alternative actuation methods may provide improvements to the state of the art.

There is reason for the increasing call for the application of hand exoskeleton systems. As the global society ages, the need arises for assistive technologies to keep the elderly mobile and functional. Similarly, as medicine improves, the number of patients that survive stroke, spinal cord injuries, and other conditions that require rehabilitation, potentially from robotic systems, increases. Further, augmenting exoskeletons have the potential to improve strength of laborers, resulting in higher worker output, as well as endurance of astronauts, potentially improving mission capabilities even as space flight is entering a new phase with the private sector. Lastly, future and emerging markets such as virtual reality entertainment may create demand for hand exoskeletons that cannot currently be predicted.

This chapter was intended to review the literature on hand exoskeleton systems by providing a summary of the state-of-the-art, and by discussing techniques and challenges related to these devices.

REFERENCES

- [1] E.B. Brokaw, S. Member, I. Black, R.J. Holley, P.S. Lum, Hand spring operated movement enhancer (HandSOME): a portable, passive hand exoskeleton for stroke rehabilitation, *IEEE Trans. Neural Syst. Rehabil. Eng.* 19 (2011) 391–399.
- [2] S. Ates, J. Lobo-Prat, P. Lammertse, H. Van Der Kooij, A.H.A. Stienen, SCRIPT passive orthosis: design and technical evaluation of the wrist and hand orthosis for rehabilitation training at home, *IEEE Int. Conf. Rehabil. Robot.* (2013) 1–6. Available from: <https://doi.org/10.1109/ICORR.2013.6650401>.
- [3] L. Dovat, O. Lambery, R. Gassert, T. Maeder, T. Milner, T.C. Leong, et al., HandCARE : a cable - actuated rehabilitation system to train hand function after stroke, *IEEE Trans. Neural Syst. Rehabil. Eng.* 16 (2008) 582–591. Available from: <https://doi.org/10.1109/TNSRE.2008.2010347>.
- [4] S.C. Jacobsen, E.K. Iversen, C.C. Davis, D.M. Potter, T.W. McLain, Design of a multiple degree of freedom, force reflective hand master/slave with a high mobility wrist, in: *Third Top. Meet. Robot. Remote Syst.*, 1989.
- [5] G. Burdea, T.H. Speeter, Portable dexterous force feedback master for robot telemanipulation, in: *NASA Conf. Sp. Telerobotics*, 1989, pp. 153–161.
- [6] S.S. Fisher, Telepresence Master Glove Controller for Dexterous Robotic End-Effectors, in: D.P. Casasent (Ed.), *Intell. Robot. Comput. Vis. V*, 1987, p. 396. <https://doi.org/10.1117/12.937753>.
- [7] P. Brown, D. Jones, S.K. Singh, J.M. Rosen, The exoskeleton glove for control of paralyzed hands, *Proc. IEEE Int. Conf. Robot. Autom.*, IEEE Comput. Soc. Press, 1993, pp. 642–647. Available from: <https://doi.org/10.1109/ROBOT.1993.292051>.
- [8] B.L. Shields, J.A. Main, S.W. Peterson, A.M. Strauss, An anthropomorphic hand exoskeleton to prevent astronaut hand fatigue during extravehicular activities, *IEEE Trans. Syst. Man, Cybern. A Syst. Humans.* 27 (1997) 668–673.
- [9] S. Balasubramanian, J. Klein, E. Burdet, Robot-assisted rehabilitation of hand function, *Curr. Opin. Neurol.* 23 (2010) 661–670. Available from: <https://doi.org/10.1097/WCO.0b013e32833e99a4>.
- [10] P. Heo, G.M. Gu, S. Lee, K. Rhee, J. Kim, Current hand exoskeleton technologies rehabilitation and assistive engineering, *Int. J. Precis. Eng. Manuf.* 13 (2012) 807–824. Available from: <https://doi.org/10.1007/s12541-012-0107-2>.
- [11] Z. Yue, X. Zhang, J. Wang, Hand rehabilitation robotics on poststroke motor recovery, *Behav. Neurol.* 2017 (2017) 1–20. Available from: <https://doi.org/10.1155/2017/3908135>.
- [12] C.Y. Chu, R.M. Patterson, Soft robotic devices for hand rehabilitation and assistance: a narrative review, *J. Neuroeng. Rehabil.* 15 (2018) 1–14. Available from: <https://doi.org/10.1186/s12984-018-0350-6>.
- [13] T. Shahid, D. Gouwanda, S.G. Nurzaman, A.A. Gopalai, Moving toward soft robotics: a decade review of the design of hand exoskeletons, *Biomimetics.* 3 (2018) 17. Available from: <https://doi.org/10.3390/biomimetics3030017>.
- [14] M. Sarac, M. Solazzi, A. Frisoli, Design requirements of generic hand exoskeletons and survey of hand exoskeletons for rehabilitation, assistive or haptic use, *IEEE Trans. Haptics*, 2019, pp. 1–1. <https://doi.org/10.1109/TOH.2019.2924881>.
- [15] Y. Kawanishi, K. Oka, H. Tanaka, K. Okada, K. Sugamoto, T. Murase, In vivo 3-dimensional kinematics of thumb carpometacarpal joint during thumb opposition, *J. Hand Surg. Am.* 43 (2018) 182.e1–182.e7. Available from: <https://doi.org/10.1016/j.jhsa.2017.07.028>.
- [16] D.J. Giurintano, A.M. Hollister, W.L. Buford, D.E. Thompson, L.M. Myers, A virtual five-link model of the thumb, *Med. Eng. Phys.* 17 (1995) 297–303. Available from: [https://doi.org/10.1016/1350-4533\(95\)90855-6](https://doi.org/10.1016/1350-4533(95)90855-6).
- [17] F.J. Valero-Cuevas, M.E. Johanson, J.D. Towles, Towards a realistic biomechanical model of the thumb: the choice of kinematic description may be more critical than the solution method or the variability/

- uncertainty of musculoskeletal parameters, *J. Biomech.* 36 (2003) 1019–1030. Available from: [https://doi.org/10.1016/S0021-9290\(03\)00061-7](https://doi.org/10.1016/S0021-9290(03)00061-7).
- [18] G. Zong, X. Pei, J. Yu, S. Bi, Classification and type synthesis of 1-DOF remote center of motion mechanisms, *Mech. Mach. Theory.* 43 (2008) 1585–1595. Available from: <https://doi.org/10.1016/j.mechmachtheory.2007.12.008>.
- [19] J.N.A.L. Leijnse, P.M. Quesada, C.W. Spoor, Kinematic evaluation of the finger's interphalangeal joints coupling mechanism-variability, flexion-extension differences, triggers, locking swanneck deformities, anthropometric correlations, *J. Biomech.* 43 (2010) 2381–2393. Available from: <https://doi.org/10.1016/j.jbiomech.2010.04.021>.
- [20] H. Vallery, J. Veneman, E. van Asseldonk, R. Ekkelenkamp, M. Buss, H. van Der Kooij, Compliant actuation of rehabilitation robots, *IEEE Robot. Autom. Mag.* 15 (2008) 60–69. Available from: <https://doi.org/10.1109/MRA.2008.927689>.
- [21] D. Rus, M.T. Tolley, Design, fabrication and control of soft robots, *Nature* 521 (2015) 467–475. Available from: <https://doi.org/10.1038/nature14543>.
- [22] K.R. Mills, The basics of electromyography, *Neurol. Pract.* 76 (2005) 32–35. Available from: <https://doi.org/10.1136/jnnp.2005.069211>.
- [23] J. del, R. Millan, F. Renkens, J. Mourino, W. Gerstner, Noninvasive brain-actuated control of a mobile robot by human EEG, *IEEE Trans. Biomed. Eng.* 51 (2004) 1026–1033. Available from: <https://doi.org/10.1109/TBME.2004.827086>.
- [24] C.J. Bell, P. Shenoy, R. Chalodhorn, R.P.N. Rao, Control of a humanoid robot by a noninvasive brain–computer interface in humans, *J. Neural Eng.* 5 (2008) 214–220. Available from: <https://doi.org/10.1088/1741-2560/5/2/012>.
- [25] S.W. O'Driscoll, N.J. Giori, Department of Veterans Affairs Continuous passive motion (CPM): theory and principles of clinical application, *J. Rehabil. Res. Dev.* 37 (2000) 179–188.
- [26] B.T. Volpe, M. Ferraro, D. Lynch, P. Christos, J. Krol, C. Trudell, et al., Robotics and other devices in the treatment of patients recovering from stroke, *Curr. Atheroscler. Rep.* 6 (2004) 314–319. Available from: <https://doi.org/10.1007/s11883-004-0064-z>.
- [27] P.S. Lum, C.G. Burgar, M. Van Der Loos, P.C. Shor, M. Majmundar, R. Yap, The MIME robotic system for upper-limb neuro-rehabilitation: results from a clinical trial in subacute stroke, *Proc. 2005 IEEE 9th Int. Conf. Rehabil. Robot.* 2005 (2005) 511–514. Available from: <https://doi.org/10.1109/ICORR.2005.1501153>.
- [28] C.G. Burgar, P.S. Lum, A.M.E. Scrimin, S.L. Garber, H.F.M. Van der Loos, D. Kenney, et al., Robot-assisted upper-limb therapy in acute rehabilitation setting following stroke: Department of Veterans Affairs multisite clinical trial, *J. Rehabil. Res. Dev.* 48 (2011) 445. Available from: <https://doi.org/10.1682/JRRD.2010.04.0062>.
- [29] H. Kim, L.M. Miller, I. Fedulow, M. Simkins, G.M. Abrams, N. Byl, et al., Kinematic data analysis for post-stroke patients following bilateral versus unilateral rehabilitation with an upper limb wearable robotic system, *IEEE Trans. Neural Syst. Rehabil. Eng.* 21 (2013) 153–164. Available from: <https://doi.org/10.1109/TNSRE.2012.2207462>.
- [30] L. Lucas, M. Dicicco, Y. Matsuoka, An EMG-controlled hand exoskeleton for natural pinching, *J. Robot. Mechatronics.* 16 (2004) 1–7.
- [31] M. Mulas, M. Folgheraiter, G. Gini, An EMG-controlled exoskeleton for hand rehabilitation, *Proc. 2005 IEEE 9th Int. Conf. Rehabil. Robot.* 2005 (2005) 371–374. Available from: <https://doi.org/10.1109/ICORR.2005.1501122>.
- [32] H. In, K. Cho, K. Kim, B. Lee, Jointless Structure and Under-Actuation Mechanism for Compact Hand Exoskeleton, in: 2011 IEEE Int. Conf. Rehabil. Robot., 2011.
- [33] Y. Kadokawa, T. Noritsugu, M. Takaiwa, D. Sasaki, M. Kato, Development of soft power-assist glove and control based on human intent, *J. Robot. Mech.* 23 (2011) 281–291. Available from: <https://doi.org/10.20965/jrm.2011.p0281>.

- [34] P. Heo, J. Kim, Power-assistive finger exoskeleton with a palmar opening at the fingerpad, *IEEE Trans. Biomed. Eng.* 61 (2014) 2688–2697. Available from: <https://doi.org/10.1109/TBME.2014.2325948>.
- [35] H.K. Yap, J.H. Lim, F. Nasrallah, J.C.H. Goh, R.C.H. Yeow, A soft exoskeleton for hand assistive and rehabilitation application using pneumatic actuators with variable stiffness, in: 2015 IEEE Int. Conf. Robot. Autom., 2015, pp. 4967–4972.
- [36] H.K. Yap, B.W.K. Ang, J.H. Lim, J.C.H. Goh, C.H. Yeow, A fabric-regulated soft robotic glove with user intent detection using EMG and RFID for hand assistive application, in: Proc. - IEEE Int. Conf. Robot. Autom., June 2016, pp. 3537–3542. <https://doi.org/10.1109/ICRA.2016.7487535>.
- [37] P. Polygerinos, Z. Wang, K.C. Galloway, R.J. Wood, C.J. Walsh, Soft robotic glove for combined assistance and at-home rehabilitation, *Rob. Auton. Syst.* 73 (2015) 135–143. Available from: <https://doi.org/10.1016/j.robot.2014.08.014>.
- [38] P. Polygerinos, K.C. Galloway, E. Savage, M. Herman, K. O'Donnell, C.J. Walsh, Soft robotic glove for hand rehabilitation and task specific training, in: Proc. - IEEE Int. Conf. Robot. Autom., June 2015, pp. 2913–2919. <https://doi.org/10.1109/ICRA.2015.7139597>.
- [39] M. Cempini, M. Cortese, N. Vitiello, A powered finger-thumb wearable hand exoskeleton with self-aligning joint axes, *IEEE/ASME Trans. Mech.* 20 (2015) 705–716. Available from: <https://doi.org/10.1109/TMECH.2014.2315528>.
- [40] S.R. Soekadar, M. Witkowski, C. Gómez, E. Opisso, J. Medina, M. Cortese, et al., Hybrid EEG/EOG-based brain/neural hand exoskeleton restores fully independent daily living activities after quadriplegia, *Sci. Robot.* 1 (2016). Available from: <https://doi.org/10.1126/scirobotics.aag3296>.
- [41] N. Secciani, M. Bianchi, A. Ridolfi, F. Vannetti Yary Volpe, L. Governi, M. Bianchini, et al., Tailor-made hand exoskeletons at the university of florence: from kinematics to mechatronic design, *Machines* 7 (2019) 22. Available from: <https://doi.org/10.3390/machines7020022>.
- [42] Y. Ren, H.S. Park, L.Q. Zhang, Developing a whole-arm exoskeleton robot with hand opening and closing mechanism for upper limb stroke rehabilitation, in: 2009 IEEE Int. Conf. Rehabil. Robot. ICORR 2009, 2009, pp. 761–765. <https://doi.org/10.1109/ICORR.2009.5209482>.
- [43] T. Nef, M. Mihelj, G. Kiefer, C. Perndl, R. Müller, R. Riener, ARMin - Exoskeleton for arm therapy in stroke patients, in: 2007 IEEE 10th Int. Conf. Rehabil. Robot. ICORR'07, 2007, pp. pp. 68–74. <https://doi.org/10.1109/ICORR.2007.4428408>.
- [44] M. Simkins, I. Fedulow, H. Kim, G. Abrams, N. Byl, J. Rosen, Robotic rehabilitation game design for chronic stroke, *Games Health J.* 1 (2012) 422–430. Available from: <https://doi.org/10.1089/g4h.2012.0044>.
- [45] M. Simkins, J.R. Roldan, H. Kim, G. Abrams, N. Byl, J. Rosen, Kinematic analysis of virtual reality task intensity induced by a rehabilitation robotic system in stroke patients, in: Proc. ASME 2013 Dyn. Syst. Control Conf. 2013, 2013, pp. 1–7.
- [46] C.D. Takahashi, V.H. Le, S.C. Cramer, A robotic device for hand motor therapy after stroke, in: 2005 IEEE 9th Int. Conf. Rehabilitation Robot., 2005, pp. 17–20.
- [47] C.D. Takahashi, L. Der-Yeghaian, V. Le, R.R. Motiwala, S.C. Cramer, Robot-based hand motor therapy after stroke, *Brain.* 131 (2008) 425–437. Available from: <https://doi.org/10.1093/brain/awm311>.
- [48] R.C.V. Loureiro, W.S. Harwin, Reach & grasp therapy: design and control of a 9-DOF robotic neuro-rehabilitation system, 2007 IEEE 10th Int. Conf. Rehabil. Robot., IEEE, 2007, pp. 757–763. Available from: <https://doi.org/10.1109/ICORR.2007.4428510>.
- [49] R.Q. Van Der Linde, P. Lammertse, HapticMaster – a generic force controlled robot for human interaction, *Ind. Robot An Int. J.* 30 (2003) 515–524. Available from: <https://doi.org/10.1108/01439910310506783>.
- [50] A. Wege, G. Hommel, Development and control of a hand exoskeleton for rehabilitation of hand injuries, in: 2005 IEEE/RSJ Int. Conf. Intell. Robot. Syst. IROS, 2005, pp. 3046–3051. <https://doi.org/10.1109/IROS.2005.1545506>.

- [51] A. Wege, A. Zimmermann, Electromyography sensor based control for a hand exoskeleton, in: 2007 IEEE Int. Conf. Robot. Biomimetics, ROBIO, 2007, pp. 1470–1475. <https://doi.org/10.1109/ROBIO.2007.4522381>.
- [52] H. Kawasaki, S. Ito, Y. Ishigure, Development of a hand motion assist robot for rehabilitation therapy by patient self-motion control, in: 2007 IEEE 10th Int. Conf. Rehabil. Robot. ICORR'07, 2007, pp. 234–240.
- [53] S. Ueki, H. Kawasaki, S. Ito, Y. Nishimoto, M. Abe, T. Aoki, et al., Development of a hand-assist robot with multi-degrees-of-freedom for rehabilitation therapy, IEEE/ASME Trans. Mech. 17 (2012) 136–146. Available from: <https://doi.org/10.1109/TMECH.2010.2090353>.
- [54] M.C. Carrozza, HANDEXOS: towards an exoskeleton device for the rehabilitation of the hand, in: 2009 IEEE/RSJ Int. Conf. Intell. Robot. Syst., 2009, pp. 1106–1111.
- [55] A. Chiri, N. Vitiello, F. Giovacchini, S. Roccella, F. Vecchi, M.C. Carrozza, Mechatronic design and characterization of the index finger module of a hand exoskeleton for post-stroke rehabilitation, IEEE/ASME Trans. Mech. 17 (2012) 884–894. Available from: <https://doi.org/10.1109/TMECH.2011.2144614>.
- [56] K.Y. Tong, S.K. Ho, P.M.K. Pang, X.L. Hu, W.K. Tam, K.L. Fung, et al., An intention driven hand functions task training robotic system, in: 2010 Annu. Int. Conf. IEEE Eng. Med. Biol., IEEE, 2010, pp. 3406–3409. <https://doi.org/10.1109/IEMBS.2010.5627930>.
- [57] N.S.K. Ho, K.Y. Tong, X.L. Hu, K.L. Fung, X.J. Wei, W. Rong, et al., An EMG-driven exoskeleton hand robotic training device on chronic stroke subjects: task training system for stroke rehabilitation, in: IEEE Int. Conf. Rehabil. Robot., 2011. <https://doi.org/10.1109/ICORR.2011.5975340>.
- [58] C.N. Schabowsky, S.B. Godfrey, R.J. Holley, P.S. Lum, Development and pilot testing of HEXORR: hand EXOskeleton Rehabilitation Robot, J. Neuroeng. Rehabil. 7 (2010) 1–16.
- [59] F. Wang, M. Shastri, C.L. Jones, V. Gupta, C. Osswald, X. Kang, et al., Design and control of an actuated thumb exoskeleton for hand rehabilitation following stroke, in: Proc. - IEEE Int. Conf. Robot. Autom., 2011, pp. 3688–3693. <https://doi.org/10.1109/ICRA.2011.5980099>.
- [60] J. Li, R. Zheng, Y. Zhang, iHandRehab : an Interactive Hand Exoskeleton for Active and Passive Rehabilitation, in: 2011 IEEE Int. Conf. Rehabil. Robot., 2011.
- [61] M.A. Rahman, A. Al-Jumaily, Design and development of a hand exoskeleton for rehabilitation following stroke, Proc. Eng. 41 (2012) 1028–1034. Available from: <https://doi.org/10.1016/j.proeng.2012.07.279>.
- [62] J. Arata, K. Ohmoto, R. Gassert, O. Lambercy, H. Fujimoto, I. Wada, A new hand exoskeleton device for rehabilitation using a three-layered sliding spring mechanism, in: 2013 IEEE Int. Conf. Robot. Autom., 2013, pp. 3902–3907.
- [63] P. Aubin, K. Petersen, H. Sallum, C. Walsh, A. Correia, L. Stirling, A pediatric robotic thumb exoskeleton for at-home rehabilitation: the isolated orthosis for thumb actuation (IOTA), Int. J. Intell. Comput. Cybern. 7 (2014) 233–252. Available from: <https://doi.org/10.1108/IJICC-10-2013-0043>.
- [64] J. Iqbal, N.G. Tsagarakis, D.G. Caldwell, Human hand compatible underactuated exoskeleton robotic system, Electron. Lett. 50 (2014) 7–8. Available from: <https://doi.org/10.1115/1.4024981>.
- [65] J. Iqbal, H. Khan, N.G. Tsagarakis, D.G. Caldwell, A novel exoskeleton robotic system for hand rehabilitation – conceptualization to prototyping, Biocybern. Biomed. Eng. 34 (2014) 79–89. Available from: <https://doi.org/10.1016/j.bbe.2014.01.003>.
- [66] F. Zhang, L. Hua, Y. Fu, H. Chen, S. Wang, Design and development of a hand exoskeleton for rehabilitation of hand injuries, Mech. Mach. Theory. 73 (2014) 103–116. Available from: <https://doi.org/10.1016/j.mechmachtheory.2013.10.015>.
- [67] D. Leonardis, M. Barsotti, C. Loconsole, M. Solazzi, M. Troncossy, C. Mazzotti, et al., An EMG-controlled robotic hand exoskeleton for bilateral rehabilitation, IEEE Trans. Haptics. 8 (2015) 140–151. Available from: <https://doi.org/10.1109/TOH.2015.2417570>.

- [68] A. Frisoli, F. Salsedo, M. Bergamasco, B. Rossi, M.C. Carboncini, A force-feedback exoskeleton for upper-limb rehabilitation in virtual reality, *Appl. Bionics Biomech.* 6 (2009) 115–126. Available from: <https://doi.org/10.1080/11762320902959250>.
- [69] A. Frisoli, F. Rocchi, S. Marcheschi, A. Dettori, F. Salsedo, M. Bergamasco, et al., Arm exoskeleton for haptic interaction in virtual environments, in: Proc. First Jt. Eurohaptics Conf. Symp. Haptic Interfaces Virtual Environ. Teleoperator Syst., 2005, pp. 195–201. <https://doi.org/10.1109/WHC.2005.15>.
- [70] A. Borboni, M. Mor, R. Faglia, Gloreha—hand robotic rehabilitation: design, mechanical model, and experiments, *J. Dyn. Syst. Meas. Control.* 138 (2016) 111003. Available from: <https://doi.org/10.1115/1.4033831>.
- [71] P. Agarwal, J. Fox, Y. Yun, M.K.O. Malley, A.D. Deshpande, An index finger exoskeleton with series elastic actuation for rehabilitation: design, control and performance characterization, *Int. J. Rob. Res.* 34 (2015) 11772–17470. Available from: <https://doi.org/10.1177/0278364915598388>.
- [72] P. Agarwal, Y. Yun, J. Fox, K. Madden, A.D. Deshpande, Design, control, and testing of a thumb exoskeleton with series elastic actuation, *Int. J. Rob. Res.* 36 (2017) 355–375. Available from: <https://doi.org/10.1177/0278364917694428>.
- [73] I. Ben Abdallah, Y. Bouteraa, C. Rekik, *Design and development of 3d printed myoelectric robotic exoskeleton for hand rehabilitation*, *Int. J. Smart Sens. Intell. Syst.* 10 (2017) 341–366.
- [74] P.W. Ferguson, B. Dimapascoc, Y. Shen, J. Rosen, Design of a hand exoskeleton for use with upper limb exoskeletons, in: M.C. Carrozza, S. Micera, J.L. Pons (Eds.), *Wearable robotics: Challenges and trends. WeRob 2018. Biosystems & Biorobotics*, Springer International Publishing, Cham, 2019, pp. 276–280. Available from: https://doi.org/10.1007/978-3-030-01887-0_53.
- [75] Y. Shen, P.W. Ferguson, J. Ma, J. Rosen, *Upper limb wearable exoskeleton systems for rehabilitation: state of the art review and a case study of the EXO-UL8—dual-arm exoskeleton system*, *Wearable Technol. Med. Heal. Care*, Academic Press, 2018, p. 71.
- [76] Y. Shen, J. Sun, J. Ma, J. Rosen, Admittance control scheme comparison of EXO-UL8 : a dual-arm exoskeleton robotic system, 2019 Int. Conf. Rehabil. Robot., IEEE, 2019, pp. 1–7.
- [77] J.C. Perry, R. Maura, C.K. Bitikofer, E.T. Wolbrecht, BLUE SABINO: development of a bilateral exoskeleton instrument for comprehensive upper-extremity neuromuscular assessment, in: L. Masia, S. Micera, M. Akay, J.L. Pons (Eds.), *Converging Clin. Eng. Res. Neurorehabilitation III*, Springer International Publishing, Cham, 2019, pp. 493–497.
- [78] Y.-L. Tsai, J.-J. Huang, S.-W. Pu, H.-P. Chen, S.-C. Hsu, J.-Y. Chang, et al., Usability assessment of a cable-driven exoskeletal robot for hand rehabilitation, *Front. Neurorobot.* 13 (2019) 1–11. Available from: <https://doi.org/10.3389/fnbot.2019.00003>.
- [79] Y. Umetani, Y. Yamada, T. Morizono, T. Yoshida, S. Aoki, “Skil Mate” wearable exoskeleton robot, 1999 IEEE Int. Conf. Syst. Man, Cybern., IEEE, 1999, pp. 984–988. Available from: <https://doi.org/10.1109/ICSMC.1999.812544>.
- [80] Y. Hasegawa, Y. Mikami, K. Watanabe, Y. Sankai, Five-fingered assistive hand with mechanical compliance of human finger, 2008 IEEE Int. Conf. Robot. Autom., IEEE, 2008, pp. 718–724. Available from: <https://doi.org/10.1109/ROBOT.2008.4543290>.
- [81] K. Tadano, M. Akai, K. Kadota, K. Kawashima, Development of grip amplified glove using bi-articular mechanism with pneumatic artificial rubber muscle, in: Proc. - IEEE Int. Conf. Robot. Autom., 2010, pp. 2363–2368. Available from: <https://doi.org/10.1109/ROBOT.2010.5509393>
- [82] E. Matheson, G. Brooker, Augmented robotic device for EVA hand manoeuvres, *Acta Astronaut.* 81 (2012) 51–61. Available from: <https://doi.org/10.1016/j.actaastro.2012.06.006>.
- [83] M.A. Diftler, L.B. Bridgewater, J.M. Rogers, RoboGlove – a grasp assist device for earth and space, in: 45th Int. Conf. Environ. Syst., 2015, pp. 1–8.
- [84] B.H. Choi, H.R. Choi, SKK hand master-hand exoskeleton driven by ultrasonic motors, in: 2000 IEEE/RSJ Int. Conf. Intell. Robot., 2000, pp. 1131–1136.

- [85] M. Bouzit, G. Burdea, G. Popescu, R. Boian, The rutgers master II - new design force-feedback glove, *IEEE/ASME Trans. Mech.* 7 (2002) 256–263. Available from: <https://doi.org/10.1109/TMECH.2002.1011262>.
- [86] P. Stergiopoulos, P. Fuchs, C. Laugeau, Design of a 2-finger hand exoskeleton for VR grasping simulation, in: Eurohaptics, 2003, 80–93.
- [87] M. Fontana, A. Dettori, F. Salsedo, et al., Mechanical design of a novel hand exoskeleton for accurate force displaying, in: Proc. - IEEE Int. Conf. Robot. Autom., 2009, pp. 1704–1709. <https://doi.org/10.1109/ROBOT.2009.5152591>.
- [88] M. Fontana, S. Fabio, S. Marcheschi, M. Bergamasco, Haptic hand exoskeleton for precision grasp simulation, *J. Mech. Robot.* 5 (2013) 041014. Available from: <https://doi.org/10.1115/1.4024981>.
- [89] I. Jo, J. Bae, Design and control of a wearable hand exoskeleton with force-controllable and compact actuator modules, in: Proc. - IEEE Int. Conf. Robot. Autom., June 2015, pp. 5596–5601. <https://doi.org/10.1109/ICRA.2015.7139982>.
- [90] E.A. Kirchner, N. Will, M. Simnofske, L.M.V. Benitez, B. Bongardt, M.M. Krell, et al., Exoskeleton Technology with Integrated Biosignal Analysis for Sensorimotor Rehabilitation, in: Tech. Unterstützungssysteme, Die Die Menschen Wirklich Wollen (2016) 504–517.

A PORTABLE TAILOR-MADE EXOSKELETON FOR HAND DISABILITIES

9

Benedetto Allotta, Matteo Bianchi, Enrico Meli, Alessandro Ridolfi and Nicola Secciani

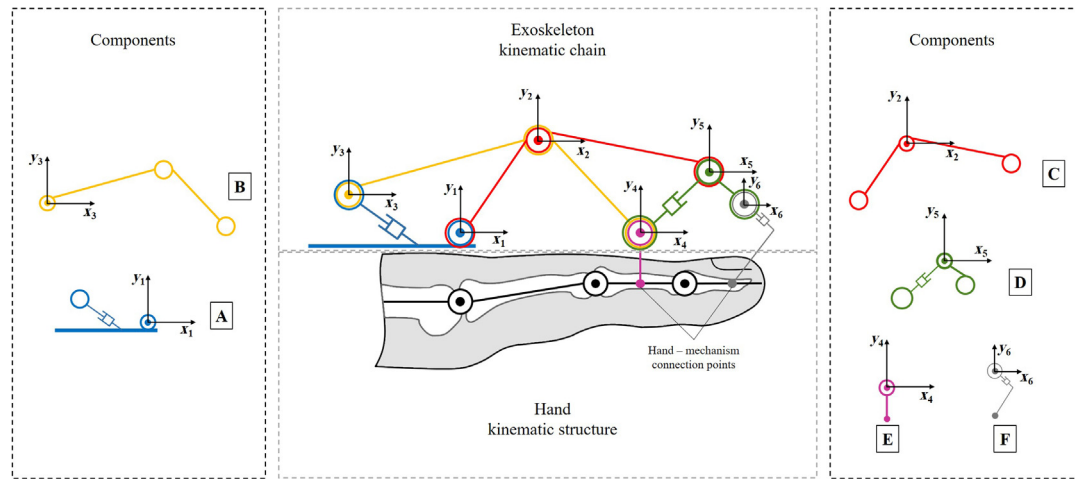
Department of Industrial Engineering (DIEF), University of Florence, Florence, Italy

9.1 INTRODUCTION

In a society where robots are increasingly more pervasive and the number of wearable robotic devices is remarkably growing, investigating the robot interactions with the human hand plays a key role. In fact since the hand has a crucial part in everyday life, much effort has been undertaken in providing robotic assistance to those people who have lost their manual dexterity [1,2]. One of the most ambitious aspects in this field is represented by the users' acceptance of the device, which depends on several features: comfort, lightness, small dimensions, user-friendly design, and straightforward active use of these hand exoskeletons. The development of a compact and tailor-made device capable of accurately following the fingers' natural trajectories represents a challenging aspect in this scenario. In this chapter the development process of a low-cost and fully wearable hand exoskeleton will be discussed. Starting from a one-degree-of-freedom (DOF) kinematic architecture, three different versions of the prototype have been sequentially developed to match step-by-step the user's needs both in terms of comfort and usability. Three dedicated sections will describe the main accomplishments each version has reached, from the manufacturability assessment of the developed finger mechanism kinematic chain to an assistive device directly actuated by the user.

9.2 KINEMATIC ANALYSIS AND SYNTHESIS

This section will describe the analytical study of the kinematics of a case study finger mechanism. The discussed model will represent the mathematical ground which will allow the exoskeleton to be made to properly adapt to different fingers' trajectories. However, before going into the details of the kinematics it is appropriate to give a brief overview of the concept of the hand exoskeleton under examination. The device that will be investigated throughout this chapter is thought to be composed of two base modules: the first module—referred to as the “finger mechanism”—is a planar mechanism which is placed over a finger, characterized by a single DOF and in charge of actuating the extension movement of the finger itself; the second one—referred to as the “back case”—is instead a case, placed over the back of the hand, designed to house a cable-driven transmission

**FIGURE 9.1**

Finger mechanism kinematic model.

system and the electronics, but also to serve as an anchor point for each finger mechanism. In the following, an overview of the kinematic analysis is reported to introduce the way the mechanism geometry has been chosen and optimized. Fig. 9.1 shows the 1-DOF kinematic chain exploited in the finger mechanism module.

Reference systems x_1y_1 , x_2y_2 up to x_6y_6 are respectively integral with components A, C, B, E, D, and F. To simplify the notation each reference frame will also be related to a specific joint following the numerical progression (e.g., joint 1 is related to frame x_1y_1 , joint 2 to frame x_2y_2 , and so on). Component A represents a part of the back case, which means that the corresponding reference frame (x_1y_1)—thought to be positioned right above the metacarpophalangeal (MCP) joint—is hence integral with the hand and can be used as a global reference system for the mechanism. Components C, B, and D are the ones responsible for reproducing the correct trajectory of the end-effector of the mechanism, represented by component E, while component F is just an idle thimble.

The study of the mechanism's forward kinematics starts from the equations describing the revolute joints 1, 2, and 4:

$$\mathbf{0} = {}^1p_2 + R_2^1 {}^2p_1 \quad (9.1)$$

$${}^1p_2 = {}^1p_3 + R_3^1 {}^3p_2 \quad (9.2)$$

$${}^1p_4 = {}^1p_3 + R_3^1 {}^3p_4 \quad (9.3)$$

where, according to the same mathematical notation also exploited in Ref. [3], the vector ${}^i p_i = ({}^i p_i^{xx} {}^i p_i^{yy})^T \in \mathbb{R}^2$ and the rotation matrix R_i^j , respectively, denoted the position of the origin and the orientation—resulting in a rotation about the z_i axis through an angle α_i —of x_iy_i with respect to x_jy_j .

The equations of joint 3 and 5—which are cylindrical joints—can now be added to the system:

$$a_1 {}^1 p_3^{xx} + b_1 {}^1 p_3^{yy} + c_1 = 0 \quad (9.4)$$

$$a_2 {}^4 p_5^{xx} + b_2 {}^4 p_5^{yy} + c_2 = 0 \quad (9.5)$$

where a_1, b_1, c_1 and a_2, b_2, c_2 are constants indicating the translational constraints of the joints, and, finally, considering joint 5 (rotational):

$${}^1 p_5 = {}^1 p_2 + R_2^1 {}^2 p_5 \quad (9.6)$$

$${}^1 p_5 = {}^1 p_4 + R_4^1 {}^4 p_5 \quad (9.7)$$

At this point, the trajectory of the end-effector—namely the origin of x_4y_4 —can be calculated by varying the only DOF of the kinematic chain, α_2 , and solving the equation system thus composed. However, for the sake of completeness, the equation of joint 6 is also added:

$${}^1 p_6 = {}^1 p_4 + R_4^1 {}^4 p_6 \quad (9.8)$$

Referring to Eqs. (9.1)–(9.8), the state of the system is thus represented by the vector:

$$q = [{}^1 p_2^{TT} {}^1 p_3^{TT} {}^1 p_4^{TT} {}^1 p_5^{TT} {}^1 p_6^{TT} \alpha_2 \alpha_3 \alpha_4]^T \in \mathbb{R}^{13} \quad (9.9)$$

where α_2 represents the only control variable. A priori known geometrical parameters of the mechanism are gathered in vector $S \in \mathbb{R}^{16}$:

$$S = [{}^2 p_1^{TT} {}^2 p_2^{TT} {}^2 p_5^{TT} {}^2 p_4^{TT} {}^5 p_6^{TT} a_1 b_1 c_1 a_2 b_2 c_2]^T. \quad (9.10)$$

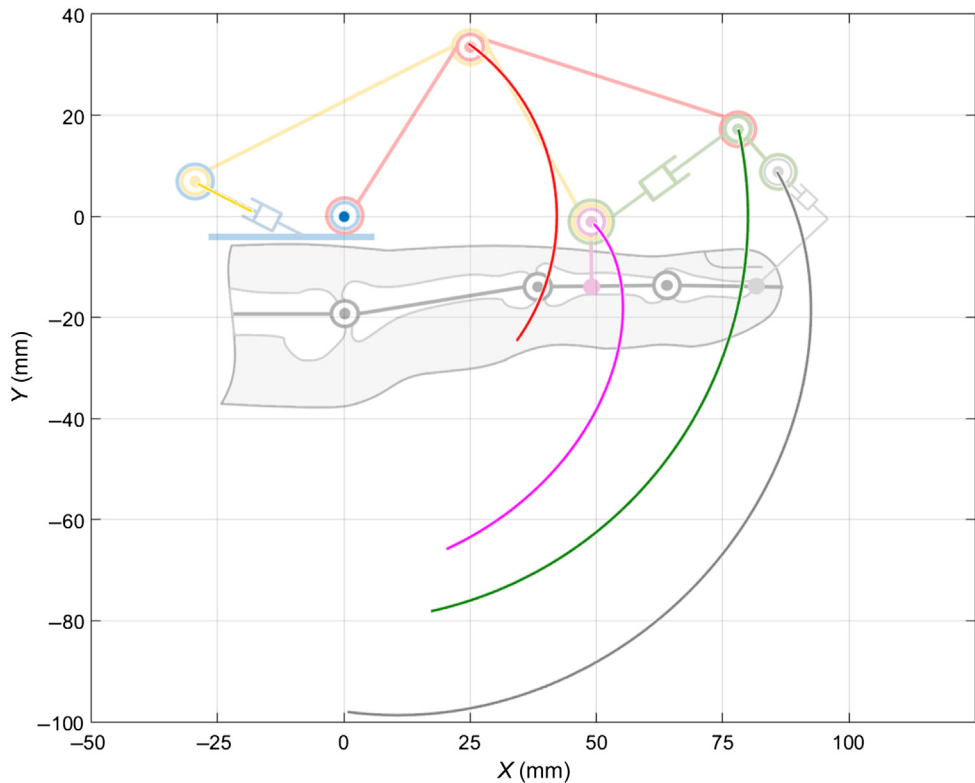
By introducing $\tilde{q} = [{}^1 p_2^{TT} {}^1 p_3^{TT} {}^1 p_4^{TT} {}^1 p_5^{TT} {}^1 p_6^{TT} \alpha_3 \alpha_4]^T = f(\alpha_2, S)$ as the unknown part of the state vector q (see Eq. 9.9), the direct kinematics of the mechanism is solved—and so the trajectory of the end-effector with respect to the fixed reference system x_1y_1 is identified—by calculating the function $f(\alpha_2, S)$ for different values of α_2 .

Fig. 9.2 shows the trajectories of the 1-DOF finger mechanism joints, providing a qualitative overview of the resulting kinematics of the mechanism when fingers are actuated. The reported three mechanical solutions embody such a kinematic model leading, in the final version, to an adaptable and ergonomic solution for different patients' hands.

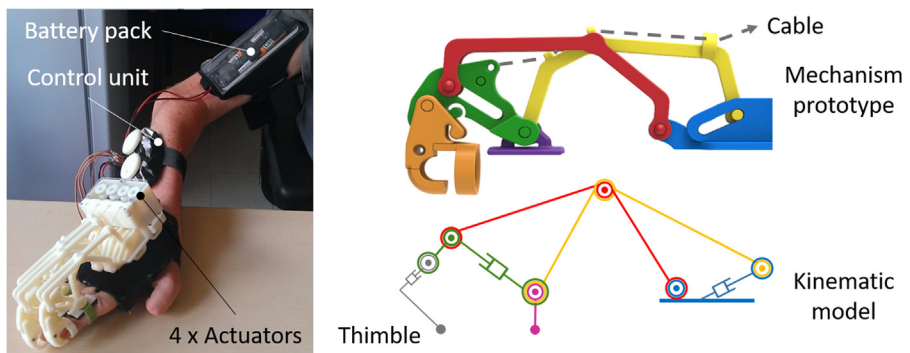
9.3 KINEMATIC CHAIN ASSESSMENT: FIRST DEVICE

The first version of the hand exoskeleton prototype (Fig. 9.3, [4]) has been produced by the Department of Industrial Engineering of the University of Florence (DIEF) to assess the real output of the kinematic synthesis presented in the previous section. A patient, affected from birth by Spinal Muscular Atrophy (SMA), has been enrolled in this test phase and this prototype has been specifically designed around his needs. In particular, the SMA had produced on him a selective damage of the extensor muscles of the forearm leading to the clenched fist deformity of both hands. Therefore, the exoskeleton has been designed to assist him in opening the fingers and allowing him to grasp and handle objects of daily use.

The remainder of this section will detail this process, separately analyzing the mechanical design, and the electronics and the strategy exploited in the control of the device.

**FIGURE 9.2**

Joint trajectories of the 1-DOF finger mechanism.

**FIGURE 9.3**

First prototype of the exoskeleton designed by the DIEF.

9.3.1 MECHANICAL DESIGN

Lightness was one of the main goals to achieve during the design phase. This led to the choice of 3D-printing all of the structural parts in a thermoplastic polymer, acrylonitrile butadiene styrene (ABS), which well matches the imposed requirement of very low weight while ensuring good mechanical characteristics. The embodiment of the 1-DOF mechanism required several manufacturing choices (Fig. 9.4) leading to a practical manufacturable and mountable device. Referring to Fig. 9.1, components C, D, and F have been designed in two parts to be assembled together while component E has been designed to wrap only the back side of the second phalanx and to be tightened to the finger by means of a Velcro strap. Moreover, shafts and pins have been directly integrated into the ABS components as lateral rods to save as much lateral room as possible. Finally, the shapes of all the components have been modified to avoid contact with the finger during hand closure. Fig. 9.4 shows these steps.

Once the kinematic chain and the overall geometry of the finger mechanism was defined, an optimization procedure was run to make the end-effector precisely reproduce the patient's finger trajectory. The procedure started by acquiring the 2D trajectory of a marker placed over the second phalanx of the index finger of the patient—the open source software “Kinovea” has been exploited

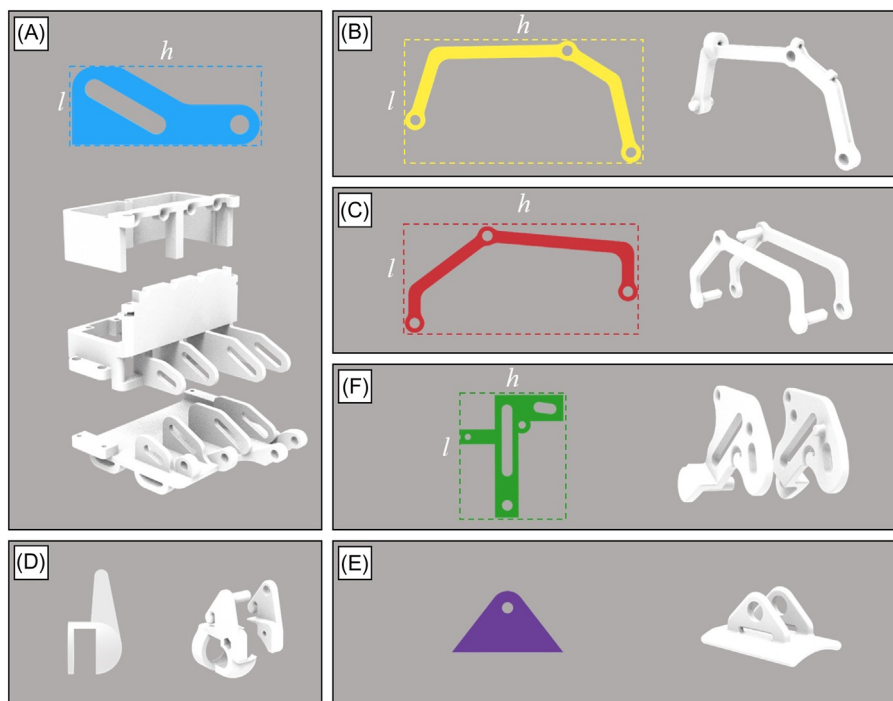


FIGURE 9.4

Design process of the exoskeleton parts. Parts A-F represents the embodiment of the kinematic components reported in Fig. 9.1, which are indicated by the same letter.

to extract the $x-y$ coordinates from a video. The acquired trajectory has then been fed to an optimization algorithm in charge of minimizing a constrained nonlinear multivariable function representing the error between the natural finger motion and the one imposed by the mechanism; not only the maximum was evaluated but also the average error [5]. Although this algorithm proved to output remarkable solutions, the goodness of the results was strongly dependable on the initial state from which the optimization started.

9.3.2 ELECTRONICS AND CONTROL ARCHITECTURE

As shown in Fig. 9.3, the system—except for the control unit and the battery pack—is directly mounted on the back of the hand. It can be easily understood that the reduction of the total mass was one of the main requirements of the device not only from the mechanical design point of view and this led to the choice of high-power density actuators and small electronic parts. Moreover, the direct interaction between the user and the device forced the choice of low-power components to avoid possible hazardous conditions. Four Savox SH-0254 servomotors, one per long finger, have been chosen as they well matched the design requirements thanks to their small dimensions and low weight. All the motors have been modified to allow for the continuous rotation of their shaft and a specific cable-driven transmission has been designed. Finally the actuators have undergone some experimental tests, which confirmed their characteristics and their capacity to easily actuate the exoskeleton—and so opening the user’s fingers—by pulling the cable connected to the corresponding finger mechanism. The closing gesture is passively allowed by releasing the same cables. The behavior of the actuators was managed by a six-channel MicroMaestro control board also connected to two triggering buttons. The two buttons were mapped over two commands: open and close; the control code had hence only to check whether one of the two were pressed and held down and to react by sending the corresponding command to the actuators, which were all activated at once. A compact four-cell Lithium battery pack—6 V output, fixed to the upper part of the arm—powered the whole system.

9.3.3 TESTING AND DISCUSSION

The last step of the development of the first prototype involved some clinical tests on the patient introduced at the beginning of this section. Although the results regarding the compliant kinematic synthesis of the finger mechanism were encouraging, being still a very preliminary embodiment of the device, these tests pointed out also several defects which had a negative impact on its usability, such as an uncomfortable feeling of duress caused by the thimble that wrapped the third phalanx and by the finger mechanisms themselves which did not allow for the fingers’ ab/adduction movements; a very unintuitive actuation method since, as it was, the patient had to use the other hand to trigger the exoskeleton; the lack of an automatic control over the range of motion (ROM) did not make the movement management safe; the algorithm exploited for the kinematic optimization of the device, for intrinsic reasons, proved to be very low-adaptable to different hands. After assessing the effectiveness of the design process—theorized over the kinematic analysis of Section 9.2—by means of real-usage tests, the aforementioned weaknesses represented the starting point for the future developments towards the further version of the prototype.

9.4 ERGONOMICS IMPROVEMENTS: SECOND DEVICE

Comfort and high adaptability to different users are two crucial requirements that have to be kept in mind when developing devices, whatever the type, that interact with people; even more attention has to be paid when dealing with patients suffering from some sort of disability. With this in mind and aiming to go beyond the limits of the first device, a second prototype has been developed. The clinical tests conducted on the previous version provided guidelines on how to make changes to the prototype, guiding the design process toward a more lightweight, wearable and adaptable device (Fig. 9.5). The development of this second version particularly focused on resolving the ergonomics issues highlighted by the previous one, but, at the same time, also the portability and the optimization procedure were improved.

9.4.1 MECHANICAL DESIGN

The first important change in the mechanical design has been made to answer the request of comfort. According to the collected feedback, the thimble has been removed and a passive DOF has been added upstream of joint 1 to act on the ab/adduction plane (see Fig. 9.6). This additional joint has the only aim of letting the finger mechanisms freely follow the natural ab/adduction movement of the fingers, always keeping the mechanism plane of action aligned with the flexo/extension one of the fingers. After that, a new optimization procedure has been developed and exploited, achieving a higher—quicker and more precise—adaptability to several users [6]. The software “Kinovea” has been replaced by the motion capture system “BTS SMART-suite” allowing for the acquisition of the fingers’ trajectories by considering the three-dimensionality of the motion. The modifications to the mechanical design ended with the introduction of two encoder houses aligned with joint 1 of the index and the little finger mechanisms—the only fingers where the lateral space was enough to insert a sensor—and a new transmission system that, exploiting just two motors instead of four, would have actuated the index finger and, separately, the other three long fingers. Since dimensions differ from finger to finger, a custom pulley—composed of three pulleys with different diameters bound together—has been developed and mounted on one of the actuators in order to assure the

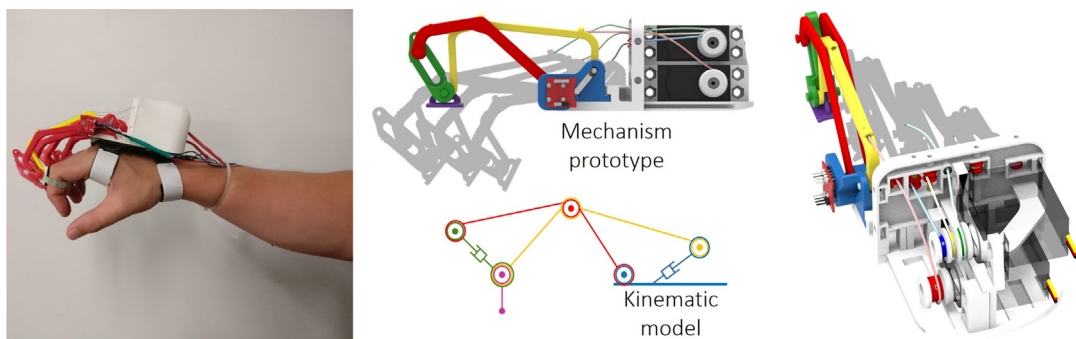
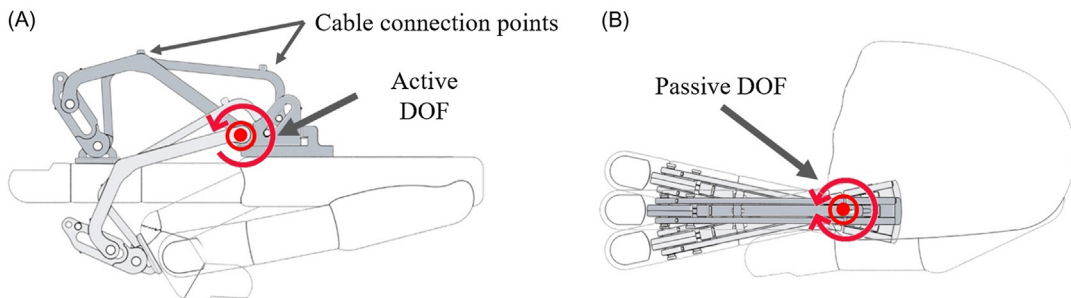


FIGURE 9.5

Second version of the exoskeleton prototype by the DIEF.

**FIGURE 9.6**

Lateral (A) and top (B) view of the finger mechanism mounted on the hand. The active and the passive DOF of the mechanism are highlighted in red.

same angular velocity for the middle, ring, and little finger (Fig. 9.5). This solution reduced weight by 41% with respect to the previous version (405 vs 242 g).

9.4.2 ELECTRONICS AND CONTROL ARCHITECTURE

Hand in hand with the exoskeleton mechanics, also the electronics and the control strategy have undergone significant changes; some of those have been already introduced in [Section 9.4.1](#). Firstly, the previous four servomotors have been replaced by two HS-5495BH High-Torque Servo from Hitec, one of which is specifically dedicated just for the index finger. These new motors have been once again modified to allow for the continuous rotation of their shafts, and a motor controller—the Supermodified V3.0 for RC-servos from 01 Mechatronics—has been interposed between them and the control board. Through this motor driver, which also comprehends a 15-bit magnetic encoder, a more efficient and accurate control over the motors' motion has been achieved; exploiting custom I2C libraries for AVR microcontrollers it was, in fact, possible to monitor the motors' status at any time and control them over the same two-wire bus—the wiring itself has been much reduced. Then, two MagEnc V3.0 Low Rev from 01 Mechatronics—based on the same magnetic encoder as above—have been mounted on joint 1 of the index and little finger mechanism, achieving a continuous feedback on the state of the fingers (angular position and velocity), which was not available with the previous prototype. Since in this version the index was the only finger independently moved and hypothesizing that the mechanics of the system assured a synchronous motion of the other three long fingers, two encoders were enough to have a complete view of the state of all the mechanisms. This overall resulted in a safer control on the limits of the ROM—identified during a preliminary tuning phase—and in the possibility to automatically detect when an object was grasped by comparing motors and fingers angular velocity. In light of the new actions required for the control system, the MicroMaestro board has been replaced by an Arduino Nano which offers the same ease in controlling servomotors and interfacing with sensors, and, at the same time, keeps dimensions and price low while offering improved performance. Customized libraries have been exploited to communicate through I2C protocol with the peripherals.

9.4.3 TESTING AND DISCUSSION

This testing phase began with the enrollment of 13 healthy subject on the kinematics evaluation of the results of the new adopted optimization strategy. Exploiting the “BTS Smart Suite” motion capture system, the trajectory of the index finger during three consecutive flexion/extension movements has been acquired for each subject. Then, the optimization algorithm has been run separately for each of the different patients’ hand sizes and the error between the tracked trajectory and the one generated by the finger mechanism kinematic model has been calculated. This study highlighted an average maximum error of 3.16 mm (standard deviation 1.47 mm) which, considering the necessarily slack couplings between the exoskeleton and the hand/fingers and the relative sliding between skin and bones, has been considered as acceptable. Finally, a 3D printed ABS prototype—optimized on the patient’s hand size—has been manufactured and tested. The new tests have proved the efficacy of the changes made to the mechanical architecture towards the improvement of the device portability. The removal of the distal thimble, the addition of the passive DOF and the integration of an active control over the ROM have liberated the user from uncomfortable feelings of duress and insecurity. Although progress has been made regarding the ergonomics and wearability of the prototype, the intuitiveness of the actuation strategy still remains a point to be opened up for further investigations.

9.5 USER-BASED ACTUATION STRATEGY: FINAL DEVICE

[Fig. 9.7](#) shows the last developed version of the hand exoskeleton prototype. It represents a solution really close to the requirements of portability, wearability, and customizability that would make it a suitable tool to be clinically used both for rehabilitative and assistive purposes. Its design process is centered on the specific users’ needs to satisfy their daily requirements and increase their overall social interaction capabilities. However, this is not a point of arrival but another starting point: within the Department of Industrial Engineering of the University of Florence the research on this topic continues.

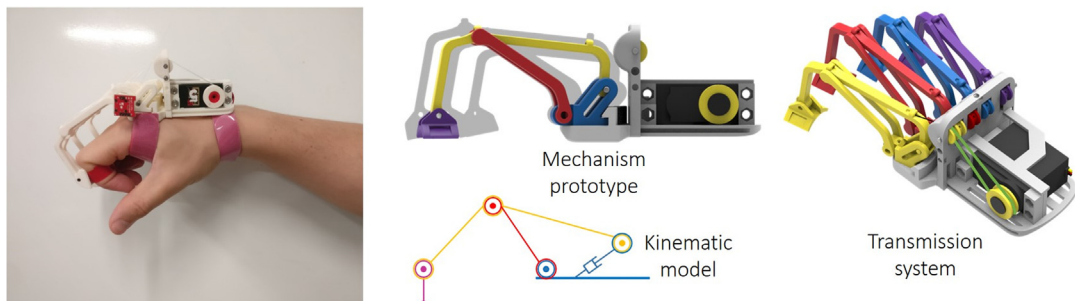


FIGURE 9.7

Final prototype by the DIEF.

9.5.1 MECHANICAL DESIGN

The mechanics has been slightly modified to achieve a more lightweight solution without influencing the obtained results in terms of kinematic accuracy. Aiming to further reduce the complexity and the weight of the device, the transmission system has been redesigned to actuate all the long fingers using just one motor: a shaft is set in rotation through a belt transmission and, integral with the shaft, four different pulleys house the cables connected to each finger mechanism. Finally, component D has been removed and, consequently, component C and B have been thickened to bear the new load program.

9.5.2 ELECTRONIC COMPONENTS AND CONTROL ARCHITECTURE

Both the electronics and the control system have been deeply modified to make it a one-hand device. Beyond the exploitation of a single motor and of a single encoder, and since the mechanism is already optimized for the tracking of the trajectories of the fingers [6], the real changes concerned the triggering system. Tests conducted on the first two versions of the prototype have stressed the importance for the user of being able to use both hands independently. An electromyography (EMG)-based control system has been then implemented following the most recent research trends in literature [7,8]. According to the guideline of simplicity on which this prototype was born, but also to the stringent constraints that the specific application imposes in terms of encumbrance and lightness, the electronics of the system has been reduced to the minimum necessary. For these reasons, only two MyoWare Muscle Sensors (AT-04-001) by Advancer Technologies have been employed for collecting EMG signals. Small and low-powered sensors, they measure the electrical activity of a muscle, outputting either raw or enveloped signals. The pseudo code of the proposed control strategy, detailed in Ref. [9], is reported in Fig. 9.8.

The first part of the code takes care of classifying the user's intentions relying on the measurements of the forearm muscular activity captured by the EMG sensors. Once the current user's intention has been classified, the corresponding signal is passed to the second part of the code, which translates it into appropriate control commands for the actuation system. As done in the previous version, a nested control loop is in charge of continuously checking that the system does not overcome a fixed ROM while another one is meant to check if an object is grasped, in which case the control system intervenes to stop the motor and make it hold position. Real-time information about the position and the velocity of the index finger is collected by means of the magnetic encoder mounted on the exoskeleton corresponding to the MCP joint of the finger. For the considered scenario, an accurate classification of a user's intentions starting from sEMG signals represents a highly challenging task. The human hand can indeed perform lots of different movements which require high dexterity, moreover, the muscles that converge on the tendons for the handling of the hand are many and are very close to each other and, finally, signals coming from surface electromyography are usually very low and noisy; these are the main reasons that make the use of high computational power machines with long training phases necessary to teach complex algorithms to precisely discriminate every possible hand movement from the others and to teach the user how to emit appropriate muscle signals. However, linking the exoskeleton to something which is usually heavy and fixed in place (e.g., a workstation) is definitely far away from representing a wearable solution. The proposed strategy for EMG classification is, instead, thought to be implemented on

Algorithm 1: Pseudo code of the control strategy

Every sample time interval

Input:

F_p = current finger position

F_v = current finger velocity

M_a = current muscular activity

Classification:

```
if  $M_a$  compatible with opening gesture then
    | open
else if  $M_a$  compatible with closing gesture then
    | close
else
    | rest
```

Actuation:

```
if open then
    if  $F_p$  compatible with range of motion then
        | run motor to pull the cables to assist the
        | hand opening
    else
        | maximum opening reached: stop motor and
        | wait for a new close command
if close then
    if  $F_p$  compatible with range of motion then
        | run motor to release the cables to follow the
        | hand closing
        if  $F_v <$  velocity threshold then
            | object grasped: stop motor and wait for
            | a new open command
    else
        | maximum closure reached: stop motor and
        | wait for a new open command
if rest then
    | do nothing: wait for a new different command
```

FIGURE 9.8

Pseudo code of the control strategy.

an embedded microcontroller board, which can be directly mounted on the system, and not require long training phases. To reach these goals, a trade-off between the number of different movements that can be classified and the computational power provided by the defined hardware had to be reached. As a result of the aforementioned reasons, only hand opening, hand closing, and hand resting have been considered as possible user's intentions to be classified, where hand resting, which represents the safe mode of the system because it does not imply any motion, has been thought to enclose every EMG pattern different from hand opening and hand closing, including unwanted

movements (UMs), similar to the base idea of what is presented in Ref. [10]. Among all the other EMG signals features that literature recommends to extract [11], a preliminary principal components analysis has identified the EMG envelope, which is directly output by the EMG sensors and which is known to work well with microcontrollers' analog-to-digital converters, as a representative feature to discriminate between the three gestures. The choice of limiting the possible user's intentions to three, together with the possibility of exploiting the EMG envelope, turned out to be very advantageous in reducing the computational power required by the classifier: these gestures can be indeed discriminated with the use of just two EMG sensors placed on the antagonist muscle bands responsible for fingers/wrist extension and flexion and so, since the input signals are just two (one per sensor), the classification problem results in being bidimensional. Fig. 9.9 shows an example of the positioning of the EMG sensors attached to a healthy subject's forearm.

For the classification phase a point-in-polygon algorithm has been chosen for its good performance and its light code (Fig. 9.10). This algorithm is a ray-casting to the right: it takes as inputs the number of the polygon vertices, their coordinates, and the coordinates of a test point; for each iteration of the loop, the line drawn rightwards from the test point is checked against one of the polygon edges and the number of times this line crosses the edge is counted; once the loop has ended if the number of crosses is an odd number of times, then the point is outside, if an even number, the point is inside.

Although it is a fairly simple classifier, it still requires tuning by means of a preliminary training phase that will likely take place at the hospital/rehabilitation center before the patient gets discharged. Hence, a custom Qt graphical user interface (GUI), visible in Fig. 9.11, has been designed

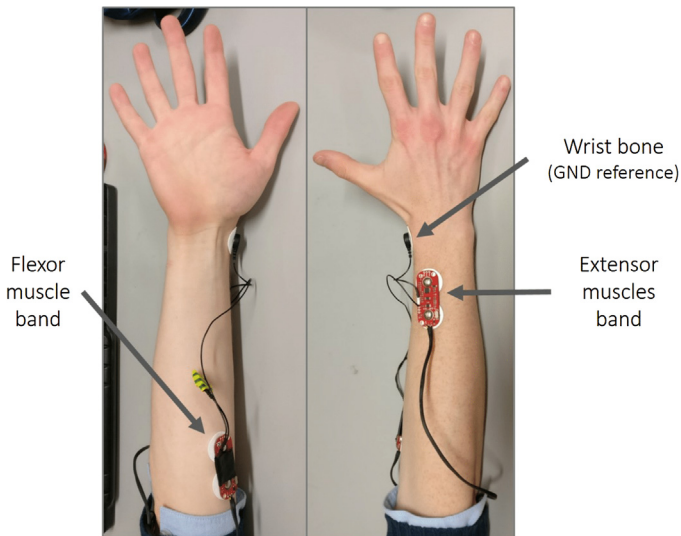


FIGURE 9.9

The picture shows a healthy subject wearing the EMG sensors. One sensor is placed on the fingers/wrist extension muscles band, the other one on the flexor muscles band. An electrode is placed on the wrist bone and serves as ground reference.

Algorithm 2: Point-in-Polygon algorithm**Input:**

```

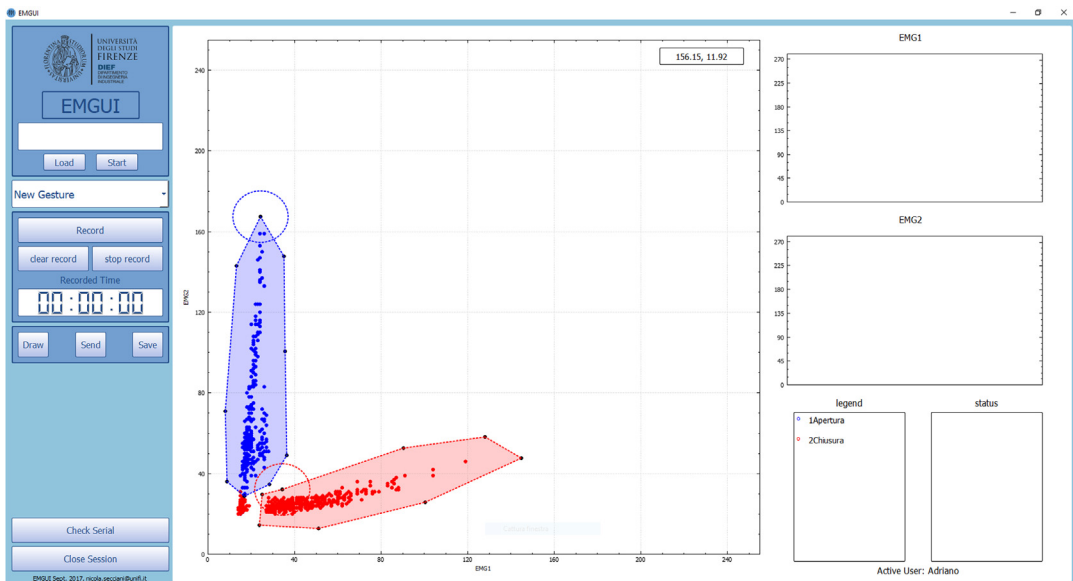
int Nv = number of the polygon vertices
float Vx = array of x-coordinate of all vertices
float Vy = array of y-coordinate of all vertices
float Tx = x-coordinate of the test point
float Ty = y-coordinate of the test point

int j = Nv - 1;
bool inside = false;
for ( int i = 0; i < Nv; i ++ ) do
    if ( ( Vy [ i ] < Ty and Vy [ j ] ≥ Ty ) or ( Vy [ j ] < Ty && Vy [ i ] ≥ Ty ) ) and ( Vx [ i ] ≤ Tx or Vx [ j ] ≤ Tx ) then
        inside ^= ( Vx [ i ] + ( Ty - Vy [ i ] ) / ( Vy [ j ] - Vy [ i ] ) * ( Vx [ j ] - Vx [ i ] ) < Tx );
    j = i;
return inside

```

FIGURE 9.10

Point-in-polygon algorithm.

**FIGURE 9.11**

Example of the classification training phase exploiting the developed custom GUI.

to represent a user-friendly tool which can be used to easily and quickly upload onto the microcontroller from a standard PC all the data needed by the classifier. In particular, it allows the collection of EMG data concerning different gestures, to display them within a scatter plot on a 2D Cartesian plane on whose axes are reported the signals from the EMG sensors and straightforwardly draw the polygons which delimit the clouds of points belonging to the same gesture. Choosing the number of vertices, the shape, and the size of the polygons represents a key point of the classification phase which is meant to be done manually by a professional who has followed the patient during previous supervised physiotherapy sessions. Properly tuning these parameters on a patient's needs can hence improve classification accuracy and disturb rejection.

9.5.3 TESTING AND DISCUSSION

No proper clinical tests have been performed at the time of writing. An application for an experimental campaign protocol is currently being written. Only a few preliminary tests have been conducted and their results can be found in Ref. [9].

9.6 CONCLUSIONS

The chapter reports the process which has led the researchers of the Department of Industrial Engineering of the University of Florence to develop a low-cost and fully wearable prototype of a hand exoskeleton for assistive and rehabilitative purposes. The designed robotic device has been revised twice to get, each time, closer to the user's needs. That is has brought a resulting system deeply adapted to the patient from both the ergonomics and from the usability point of view.

Starting from a detailed mathematical study of the kinematics of a 1-DOF finger mechanism, which has been used as a reference, three versions of the exoskeleton have been presented in sequential order of development. The first version allowed assessment of the actual manufacturability of the novel finger kinematic chain. Then, versions two and three differ from their respective previous ones both in their mechanical design and in their control strategy. Changes and improvements have been made based on the results of several intermediate tests, and users' feedback, allowing the embodied kinematic model on each step to better fit the patients' needs. The final prototype presents two personalization levels for the end-user.

The first one is characterized by the 1-DOF finger mechanism. Thanks to an optimization strategy based on the patient's motion analysis, this specific mechanism is able to follow the fingers' natural motion, although the device is actuated by only one servomotor. This choice led to a very compact and lightweight system without compromising a comfortable feeling even during prolonged use.

A second personalization for the user is given by the particular implemented control strategy. An EMG-based actuation system makes the patient completely in charge of actuating the device on their own and ensures the complete control of the exoskeleton approaching as much as possible the natural use of the hand.

The possibility of wearing the whole robotic system on the arm of the user, freeing them from space constraints, and the remarkable reduction of system complexity, allowing for a more

straightforward learning and managing, are encouraging signs for further developments and pave the way to the design of several tailor-made robotic applications capable of helping people with disabilities.

REFERENCES

- [1] P. Heo, G. Gu, S.-J. Lee, K. Rhee, K. Jung, Current hand exoskeleton technologies for rehabilitation and assistive engineering, *Int. J. Precision Eng. Manuf.* 13 (5) (2012) 807–824.
- [2] M. Troncossi, M. Mozaffari-Foumashi, V. Parenti-Castelli, An original classification of rehabilitation hand exoskeletons, *J. Robot. Mech. Eng. Res.* 1 (4) (2016) 17–29.
- [3] B. Siciliano, O. Khatib, *Springer Handbook of Robotics*, Berlin Heidelberg, Springer, 2016.
- [4] B. Allotta, R. Conti, L. Governi, E. Meli, A. Ridolfi, Y. Volpe, Development and experimental testing of a portable hand exoskeleton, in: Proceedings of the 2015 IEEE/RSJ International Conference on Intelligent Robots and Systems (IROS), Hamburg, Germany, September 2015, pp. 5339–5344.
- [5] R.H. Byrd, J.C. Gilbert, J. Nocedal, A trust region method based on interior point techniques for nonlinear programming, *Math. Prog.* 89 (1) (2000) 149–185.
- [6] M. Bianchi, F. Fanelli, E. Meli, A. Ridolfi, F. Vannetti, M. Bianchini, et al., Optimization-based scaling procedure for the design of fully portable hand exoskeletons, *Meccanica* 53 (11–12) (2018) 3157–3175.
- [7] J. Lobo-Prat, P.N. Kooren, A.H. Stienen, J.L. Herder, B.F. Koopman, P.H. Veltink, Non-invasive control interfaces for intention detection in active movement-assistive devices, *J. NeuroEng. Rehabilit.* 11 (1) (2014) 168–190.
- [8] A.A. Adewuyi, L.J. Hargrove, T.A. Kuiken, Evaluating EMG feature and classifier selection for application to partial-hand prosthesis control, *Front. Neurorobot.* 10 (15) (2016).
- [9] N. Secciani, M. Bianchi, E. Meli, Y. Volpe, A. Ridolfi, A novel application of a surface ElectroMyoGraphy-based control strategy for a hand exoskeleton system: a single-case study, *Int. J. Adv. Robot. Syst.* 16 (1) (2019).
- [10] X. Li, S. Chen, H. Zhang, O.W. Samuel, H. Wang, P. Fang, et al., Towards reducing the impacts of unwanted movements on identification of motion intentions, *J. Electromyogr. Kinesiol.* 28 (2016) 90–98.
- [11] B. Hudgins, P. Parker, R.N. Scott, A. New, Strategy for multifunction myoelectric control, *IEEE Trans. Biomed. Eng.* 40 (1) (1993) 82–94.

FURTHER READING

R. Conti, E. Meli, A. Ridolfi, M. Bianchi, L. Governi, Y. Volpe, et al., Kinematic synthesis and testing of a new portable hand exoskeleton, *Meccanica* 52 (11–12) (2017) 2873–2897.

OPTIMAL KINEMATIC DESIGN OF THE LINK LENGTHS OF A HAND EXOSKELETON 10

Peter Walker Ferguson, Brando Dimapasoc and Jacob Rosen

*Bionics Lab, Department of Mechanical and Aerospace Engineering, University of California, Los Angeles, CA,
United States*

10.1 INTRODUCTION

A hand exoskeleton is an assistive device that is worn by a stroke patient to assist in therapeutic exercises during rehabilitation. The device can aid in, guide, and/or react in specific ways to the patient's motions in order to facilitate therapy exercises, the goal of which is to allow the patient's brain to relearn the motor function it has lost for the hemiparetic limb. Hand exoskeletons have taken on many forms and have used different mechanisms to help the patient perform different types of movements and grasps. In terms of movement, exoskeletons can be designed to aid in binary opening and closing of the hand [1–3], aid in the motions of each digit individually [4–8], and facilitate pinching [9]. Other devices implement a tendon-like actuation system to aid in flexion and extension of the entire hand [10–12].

One important consideration to take into account when designing a hand exoskeleton is the variability in human hand and digit sizes. Common ways of dealing with this are implementing adjustable or movable links, shims, and component configurations of various sizes [5,11,13,14].

The alternative to these solutions is designing manipulators with fixed lengths and sizes that are capable of accommodating a wide range of digit sizes. Some previous works in optimization for hand exoskeletons have focused on maximizing torque transmission on the fingertip being manipulated [15,16]. Others have also included perpendicular forces and contact forces at the digit-manipulator interface [17,18] or followed a certain trajectory or digit position throughout operation [19].

As discussed in Chapter 8, “base-to-distal” topology is a common method for allowing hand exoskeletons with fixed link lengths to accommodate different digit sizes [20–23]. In this topology, each digit mechanism consists of a serial linkage connecting from the base of the exoskeleton, typically at the dorsum, to distal to the last actuated joint of the human digit. In this way, the joints of the exoskeleton linkages do not correspond one-to-one with those of the human digits. Instead, the connecting serial linkage effectively moves the entire human digit together. The advantages of this topology are low mechanism complexity and built-in capability to accommodate different digit sizes. An infinite variety of link lengths could be used to actuate any particular digit size through the full relevant workspace. However, depending on the selected link lengths, mechanism

performance and size are directly affected. As it is desirable to minimize mechanism size while maximizing performance, proper selection of link lengths is crucial.

In this chapter, we present a kinematic optimization strategy for the manipulators of a second-generation three-linkage robotic hand exoskeleton with a base-to-distal topology and demonstrate the process for a single linkage. The optimization method presented here focuses on combining kinematic performance measured by the mechanism isotropy with mechanism size measured by the planar area occupied between the mechanism and digit. This method contributes a study into aspects of hand exoskeleton manipulator optimization that are often not discussed in detail. As optimizations, such as the one presented here, are intended to be used as design tools, the scope of this paper encompasses the manipulator design process in the early stages of the hand exoskeleton development.

First, we describe models for both the mechanism and the digits of interest. Second, we present a brute force algorithm that grades each potential mechanism based on a predefined *Design Score* equation, with the goal of accommodating a variety of hand sizes with fixed link lengths and achieving the best kinematic performance within the workspace. Finally, the theoretically optimal solution from the algorithm is compared to the actual mechanism, which was physically realized as a prototype under various constraints.

10.2 METHOD

The following sections discuss how the digits and manipulator linkages were modeled, the form of the exoskeleton manipulator optimized, and the strategy of the optimization itself.

10.2.1 MODELING THE HUMAN DIGITS

The prevailing simplified kinematic model of the human hand considers the five digits to possess 21 degrees of freedom (DOFs) between them [24,25]. In this model, each of the four fingers consists of four DOFs: abduction/adduction (A/A) and flexion/extension (F/E) of the metacarpophalangeal (MCP) joint, F/E of the proximal interphalangeal (PIP) joint, and F/E of the distal interphalangeal (DIP) joint. Anatomically, the simplified model of the thumb possesses five DOFs: A/A and F/E of the carpometacarpal (CMC), A/A and F/E of the MCP joint, and F/E of the interphalangeal (IP) joint [26,27]. The A/A and F/E axes of rotation for both the CMC and the thumb MCP have been shown to neither be perpendicular nor intersect [25,28]. As a result of the nonperpendicular axes, flexion and abduction of the CMC can result in pronation of the thumb [27,29]. This combined motion results in an important physical motion of the thumb, namely opposition/reposition (O/R). O/R effectively rotates the plane of F/E of the thumb about an axis through the CMC in order for the thumb pad to face the palm. Therefore, exoskeletons have been developed for opposition that treat the kinematics of the thumb as an O/R rotation of the CMC followed by a 3R planar mechanism for F/E [30]. As such, if A/A of the thumb MCP is ignored, the kinematic chain of all five digits of the hand can be treated as 3R planar mechanisms attached to a nonplanar rotation at the digit base.

A design goal of the exoskeleton presented in this chapter is to be capable of covering the full workspace of digits whose hand segments fall in the middle 95th percentile for length. In order to

accomplish this, it was necessary to characterize the size of each relevant hand segment and range of motion of each joint. [Table 10.1](#) shows the minimum, mean, and maximum lengths considered of each relevant hand segment, which correspond to small, medium, and large hands. The maximum and minimum lengths were obtained by adding to and subtracting from the mean segment length, respectively, twice the standard deviation as listed in [\[31\]](#). The range of motion of each F/E joint is listed in [Table 10.2](#). Joint ranges were obtained from [\[32\]](#) and authors' observations of desirable ranges. Hyperextension was not considered for any joint for safety purposes.

10.2.2 EXOSKELETON TOPOLOGY

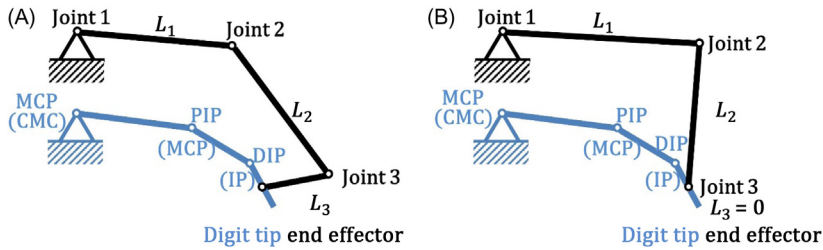
The designed exoskeleton hand is comprised of a three-linkage mechanism. Two of these linkages control the fingers while the last controls the thumb. This configuration was chosen because 95% of human grasps can be achieved with three digits—a thumb and two fingers—and the human hand is largely redundant in having five digits [\[33\]](#). All mechanisms are placed on the dorsal side of the hand so as to enable users to grasp real objects while performing exercises.

Table 10.1 Minimum, Mean, and Maximum Considered Segment Lengths

Digit	Segment	Minimum (cm)	Mean (cm)	Maximum (cm)
Thumb	Metacarpal	3.834	4.622	5.410
	Proximal Phalanx	2.531	3.157	3.783
	Distal Phalanx	1.847	2.167	2.487
Index	Proximal Phalanx	2.990	3.978	4.966
	Medial Phalanx	1.736	2.238	2.740
	Distal Phalanx	1.130	1.582	2.034
Ring	Proximal Phalanx	3.363	4.137	4.911
	Medial Phalanx	1.907	2.565	3.223
	Distal Phalanx	1.286	1.730	2.174

Table 10.2 Considered Range of Motion of Joints in F/E

Digit	Joint	Range of Motion (°)
Thumb	Carpometacarpal	56
	Metacarpophalangeal	73
	Interphalangeal	85
Fingers	Metacarpophalangeal	100
	Proximal Interphalangeal	105
	Distal Interphalangeal	85

**FIGURE 10.1**

Schematics of the two considered options for 3R planar linkages and digit. (A) Manipulator used in the first-generation hand exoskeleton with nonzero L_3 length. (B) Manipulator used in the second-generation hand exoskeleton with zero L_3 length. A/A and O/R joints are not shown. Digit joints are labeled for the fingers (thumb).

The finger linkages consist of A/A joints placed above the MCP of the fingers, followed serially by 3R planar mechanisms for F/E. The location of the base of each finger linkage can be adjusted by sliding in the radial/ulnar directions to accommodate different hand widths and align the linkages with different fingers. One finger linkage is intended to always control the index finger, while the other always controls the ring and pinky fingers. Different attachment structures can be interchanged to associate the middle finger with either linkage. This choice was made to increase the variety of common hand shapes/grasps that can be actuated [34]. The thumb linkage consists of an O/R joint running through the CMC followed serially by a 3R planar mechanism for F/E. As A/A and O/R motions can be matched one-to-one by the first joint, and they do not affect motion in the F/E plane, their ranges of motions were not considered in the optimization and thus were not listed in [Table 10.2](#).

3R planar mechanisms were chosen to match the capabilities of the human digits. In the F/E plane, each digit has a dexterous workspace over two positions and one orientation. The first-generation hand exoskeleton of the UCLA Bionics Lab matched the human digits in having three nonzero link lengths corresponding to the three phalanges [22], as shown in [Fig. 10.1A](#). However, as only the first two F/E joints were actuated, it was found that the passive distal-most joint enabled undesirably large uncontrolled motions of the user's digits. This was because the position of the fingertip could passively move in a circle with radius equal to the link length of the distal-most link.

To address this issue without adding additional motors, which would have resulted in greater mass and complexity, the second-generation hand exoskeleton was designed with zero length for the third link as shown in [Fig. 10.1B](#). This was accomplished by aligning the axis of rotation such that it intersects the distal phalanx. By doing so, the two actuated F/E joints can fully define the position of the connection point, while orientation is left passive. As there is well established coupling between the F/E motions of the PIP and DIP joints [35], and from the authors' observations wearing prototypes, it was anticipated that this would have a significant benefit on the ability of the exoskeleton to precisely control each digit. However, in order to place the final joint axis such that it intersects the distal phalanx, it was necessary to place at least the end of the mechanism lateral to the actuated digit.

As shown in Fig. 10.1, the exoskeleton linkages do not connect all the way to the tip of the digits they actuate. They were designed to connect to the distal phalanx 1 cm past the distal-most digit joint. This choice was made to leave the finger pads as unobstructed as possible to permit users to feel the objects with which they interact.

10.2.3 MODELING THE 3R PLANAR MECHANISMS

Each linkage of the considered exoskeleton device ends in 3R planar mechanisms for F/E motions. For the following analysis, L_1 , L_2 , and L_3 refer to the lengths of the first, second, and third links of the 3R mechanism, respectively. As previously mentioned, L_3 was set to zero for the second-generation hand exoskeleton. θ_1 , θ_2 , and θ_3 refer to the joint angles of the first, second, and third joints, respectively.

For a general 3R planar mechanism, the position of the end-effector can be described by coordinates (x,y) and orientation ϕ . The forward kinematics equations are given in Eq. (10.1).

$$\begin{bmatrix} x \\ y \\ \phi \end{bmatrix} = \begin{bmatrix} L_1 c_1 + L_2 c_{12} + L_3 c_{123} \\ L_1 s_1 + L_2 s_{12} + L_3 s_{123} \\ \theta_1 + \theta_2 + \theta_3 \end{bmatrix} \quad (10.1)$$

where

$$\begin{aligned} s_1 &= \sin\theta_1, \quad s_{12} = \sin(\theta_1 + \theta_2), \quad s_{123} = \sin(\theta_1 + \theta_2 + \theta_3), \\ c_1 &= \cos\theta_1, \quad c_{12} = \cos(\theta_1 + \theta_2), \quad c_{123} = \cos(\theta_1 + \theta_2 + \theta_3) \end{aligned} \quad (10.2)$$

By taking the derivative of Eq. (10.1), the Jacobian matrix with respect to the ground frame was obtained:

$${}^0J = \begin{bmatrix} -L_1 s_1 - L_2 s_{12} - L_3 s_{123} & -L_2 s_{12} - L_3 s_{123} & -L_3 s_{123} \\ L_1 c_1 + L_2 c_{12} + L_3 c_{123} & L_2 c_{12} + L_3 c_{123} & L_3 c_{123} \\ 1 & 1 & 1 \end{bmatrix} \quad (10.3)$$

The singular values of the Jacobian matrix were then found and were used to calculate mechanism isotropy.

Similar to the exoskeleton mechanisms, each hand digit was considered to end in a 3R planar mechanism for the purposes of the presented optimization algorithm. The forward kinematics equations given in Eq. (10.1) hold true, with substitution of variables. For the fingers, L_1 and L_2 correspond to the hand segment lengths for the proximal and medial phalanges while θ_1 , θ_2 , and θ_3 are the F/E angles of the MCP, PIP, and DIP. For the thumb, L_1 and L_2 correspond to the hand segment lengths for the metacarpal and proximal phalanx while θ_1 , θ_2 , and θ_3 are the F/E angles of the CMC, MCP, and IP. For the fingers and thumb, L_3 was set to 1 cm to account for the desired attachment point.

10.2.4 THE OPTIMIZATION ALGORITHM

The leading factors of this optimization are the size and kinematic performance of the exoskeleton. The overall goal of the algorithm is to determine the set of manipulator link lengths that gives the best kinematic performance within the workspace of the digit compared to alternative designs with the same topology. The optimized manipulator ensures comfortable movement in the exoskeleton while allowing the device to be as small as possible.

There were a few criteria that automatically invalidated a design if they were not met. The first criterion was overlapping workspace area. The workspace of the manipulator must completely overlap the workspace of the digit, that is, the end-effector of the manipulator must be able to attach to the distal phalanx in the desired location anywhere the digit moves within its planar workspace. To address this, the algorithm checked for a valid solution to the inverse kinematics for all points in the workspace. An optional second criterion was interference between the manipulator links and the digit. If the inverse kinematics solution for the set of potential link lengths showed that in order to reach the fingertip, a joint of the manipulator must have lain within the flesh of the digit, the design was marked as unacceptable, as this indicated there would be interference.

In the first-generation hand exoskeleton developed by the UCLA Bionics Lab, it was determined that each linkage should be placed entirely on the dorsal side of the hand. Additionally, A/A motion of the two finger linkages were accounted for by a passive joint distal to the 3R mechanism, as opposed to proximal. As such, L_3 had a minimum length due to mechanical constraints. This, combined with the requirement for zero interference between manipulator links and digit, resulted in a significantly larger mechanism. In the second-generation hand exoskeleton, it was determined that zero length of L_3 was more desirable as it reduced mechanism size and increased ability to control fingertip position. As stated, this required the end of each linkage to be located laterally to the digits actuated. In order to reduce mechanism size further by removing the no interference requirement, the entirety of the planar 3R portion of each linkage was placed laterally to the digits they control.

The first step of the optimization algorithm is the generation of a range of potential link length sets. It was determined that permutations generated with a resolution of 1 mm were sufficient. In addition to the $L_3 = 0$ cm constraint, minimum length constraints were placed on different links to enable use of various sensors and mechanical components. Maximum lengths were determined by running the algorithm at low resolution to find a reasonable range.

Second, the algorithm calculated the workspace of three versions of the primary digit that were to be manipulated by the linkage. For the three linkages, these are the thumb, index, and ring fingers, respectively. For a given digit, three sizes were checked, corresponding to small, medium, and large digits with lengths listed in [Table 10.1](#). For each of these digit sizes, the workspace was calculated using forward kinematics of the biological digit as it was varied in three-degree increments for each joint across the considered joint ranges in [Table 10.2](#).

Next, each potential set of link lengths was checked for validity. The workspace and, optionally, the interference criteria were checked against all three digit sizes. If any of the criteria failed for any configuration of any of the three digit sizes, the evaluated set of link lengths was considered invalid and a *Design Score* of zero was assigned. To compare valid sets of link lengths, a *Design Score* based on kinematic performance and size was calculated for each.

The measure used in the optimization to determine kinematic performance is based on mechanism isotropy (*ISO*). Mechanism isotropy is a measure of the ability of a mechanism to move its end-effector in any direction. It is a function of the joint angles ($\theta_1, \theta_2, \theta_3$) and ranges from 0 to 1. Mechanism isotropy can be defined as in [\[36,37\]](#) as the inverse of the condition number of the Jacobian matrix or:

$$ISO(\theta_1, \theta_2, \theta_3) = \frac{\sigma_{min}}{\sigma_{max}} \in [0, 1] \quad (10.4)$$

where σ_{min} and σ_{max} are the minimum and maximum singular values of the Jacobian matrix. An isotropy value of zero indicates a singularity and the loss of a degree of freedom, while an isotropy

of 1 indicates that the end-effector can move equally well in all directions. Note that this built-in normalization to a range of 0 to 1 is an advantage of using the isotropy to evaluate kinematic performance as it bounds the *Design Score*.

For each potential set of manipulator link lengths, the mechanism isotropy was calculated for the joint angles obtained from inverse kinematics for each end-effector configuration generated in the workspace of the digit for each of the three digit sizes.

Potential mechanisms should have an increase in *Design Score* in accordance with higher mechanism isotropy values within the digit workspace. The isotropy was incorporated into the score by summing isotropy values over the digit workspace. Because the size of the in-plane digit workspace was the same for all sets of link lengths, it was possible to compare the sum of isotropy quantities between potential manipulator designs. Potential mechanisms were rewarded for having a higher sum of isotropy.

However, a *Design Score* based only on the sum of *ISO* would output a design that has excellent kinematic performance in much of the workspace, but extremely poor in places. More specifically, it would not sufficiently punish a near-zero isotropy value. If there is a position where the isotropy is zero within the digit workspace, the *Design Score* should be zero as well because this indicates a singularity. To account for this, the optimization factored in a minimax approach to *ISO*. In addition to optimizing the design for overall performance (sum of *ISO*) in the workspace, it was also preferred to have a design that had the best (or “good”) worst-case performance within the workspace, that is, one with higher minimum *ISO* values across potential designs. Therefore the minimum *ISO* value within the digit workspace was included in the numerator of the *Design Score* equation. Specifically, the numerator consists of the sum of *ISO* across all configurations of all digit sizes times the minimum *ISO* score of each digit size.

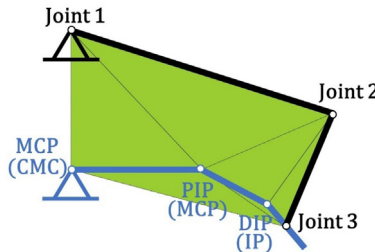
Another factor to consider in the design of an exoskeleton hand is the bulkiness of the system. As link lengths increase, the envelope of the device around the hand of the user becomes larger. This is not favorable because the mechanism will be more likely to interfere with surrounding objects during therapeutic tasks and may prevent proper interaction with certain physical objects. Additionally, greater mass due to larger links increases the strain on the user if he/she must manually lift the device during use, or requires larger actuators of an external active support system if one is used. For these reasons, designs were penalized for excessive size.

The most straightforward way to include size in the *Design Score* is to penalize link lengths directly as in Eq. (10.5).

$$\text{Design Score} = \frac{\sum_K ISO \times \text{MIN}_S ISO \times \text{MIN}_M ISO \times \text{MIN}_L ISO}{L_1 + L_2 + L_3} \quad (10.5)$$

where *S*, *M*, *L*, and *K* were the sets of all checked points in the workspace of the small digit, medium digit, large digit, and all digit sizes, respectively. However, it was found that the derivative of the numerator term with respect to link length was greater than unity unless links were unreasonably long. Consequently, such a *Design Score* would result in excessively large designs. As such, a tunable weighting factor, *A*, would need to be added to result in a compact design as in Eq. (10.6).

$$\text{Design Score} = \frac{\sum_K ISO \times \text{MIN}_S ISO \times \text{MIN}_M ISO \times \text{MIN}_L ISO}{(L_1 + L_2 + L_3)^A} \quad (10.6)$$

**FIGURE 10.2**

Example configuration for calculation of *AREA*. The green polygon is the largest possible with all vertices coincident with joints of either the digit or linkage.

Although A could be tuned to result in reasonable designs based on requirements, as was done in the first-generation hand exoskeleton, physical meaning behind the link length factor in the *Design Score* would be lost. As such, the link length term was replaced in the second-generation hand exoskeleton optimization algorithm by a term intended to directly measure the envelope of the digit-exoskeleton system of a given set of link lengths.

In order to evaluate the size of the envelope of the digit-exoskeleton system, an area-based measurement was used. Specifically, for each point in the workspace of each digit size, the area (*AREA*) of the largest polygon with all vertices placed at the joints of the digit or exoskeleton 3R mechanism was found. As every potential set of link lengths was evaluated for the same points in the workspace of the three digit sizes, it was possible to directly compare different link length sets by summing *AREA* for all points in the workspace of the three digit sizes. The sum of *AREA* was set as the denominator in the *Design Score* in order to reward smaller designs. It should be noted that the designed exoskeleton placed each 3R mechanism lateral to the digits, and thus *AREA* is a representation of the digit-exoskeleton envelope instead of a physical planar area. An example configuration with an overlaid shaded polygon area is shown in Fig. 10.2.

Thus the final *Design Score* equation can be expressed as:

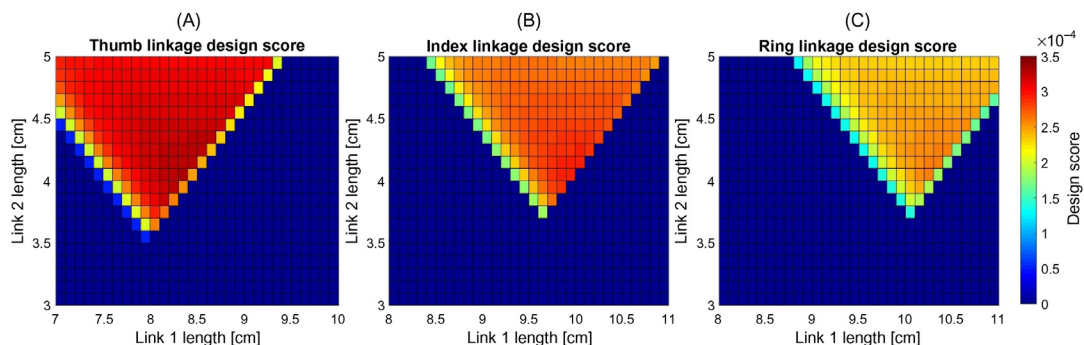
$$\text{Design Score} = \frac{\sum_K ISO \times MIN_S ISO \times MIN_M ISO \times MIN_L ISO}{\sum_K AREA} \quad (10.7)$$

Each valid potential set of link lengths was assigned a *Design Score* according to Eq. (10.7). The sets of link lengths with the highest *Design Score* for each digit were considered the optimal solutions and were used to construct a physical prototype.

10.3 RESULTS

10.3.1 SIMULATION RESULTS

Fig. 10.3 shows the results of the optimization algorithm for the thumb, index finger, and ring finger. For the input constraints, including specified locations of the base of the 3R mechanisms, Table 10.3 shows the optimal link lengths and corresponding *Design Score*.

**FIGURE 10.3**

Optimization results for the (A) thumb, (B) index finger, and (C) ring finger.

Table 10.3 Optimal Link Lengths

Linkage	L_1 (cm)	L_2 (cm)	L_3 (cm)	Design Score
Thumb	8.3	4.0	0	3.283×10^{-4}
Index	9.9	4.0	0	2.943×10^{-4}
Ring	10.3	4.1	0	2.597×10^{-4}

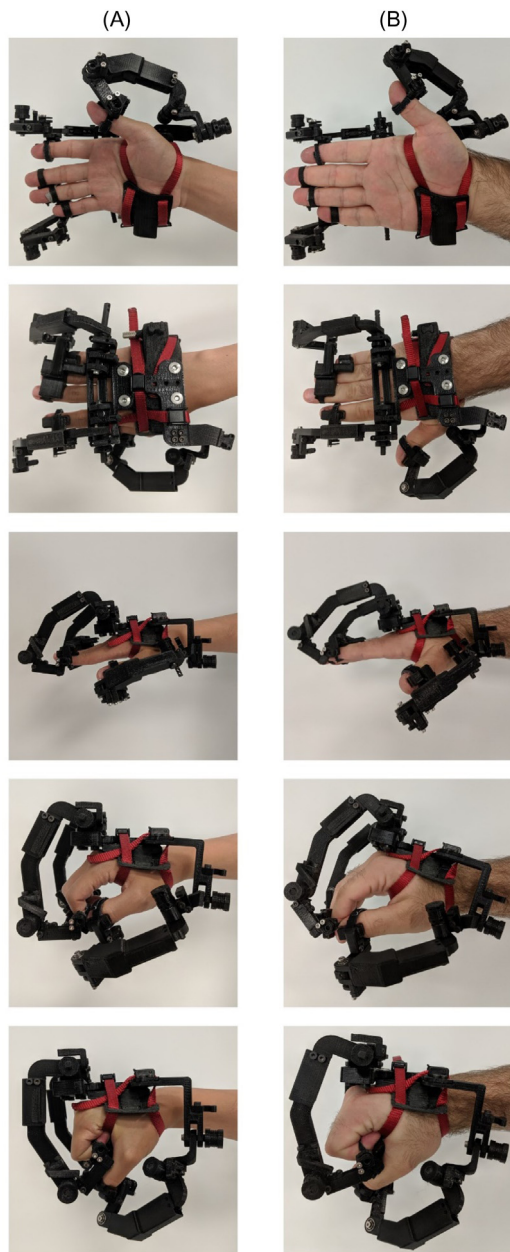
10.3.2 PHYSICAL PROTOTYPE EVALUATION

An unactuated physical prototype was constructed based upon the link lengths obtained from the optimization algorithm. The prototype was evaluated for comfort and workspace coverage of the human hand without approaching singularity. Ten volunteers with varying hand sizes tested the prototype. All volunteers reported the device attached securely and comfortably. Nine of the users reported that the device did not constrain their motions in unintended ways, and were able to form a variety of hand shapes. The tenth volunteer possessed a hand in the 99th percentile for size, and reported the inability to reach specific hand poses and singular configurations of the device. Fig. 10.4 provides images of the prototype across different angles and grasp shapes for two volunteers with digits in the 20th and 80th percentiles for length.

10.4 DISCUSSION

10.4.1 LINK LENGTH EVALUATION

The *Design Scores* for possible link length sets for each linkage are shown in Fig. 10.3. The designs on the edge of the valid link length sets possessed near-singular configurations in at least

**FIGURE 10.4**

Physical prototype based on optimized link lengths. Experimentally validated for comfort, workspace coverage, and interference with different hand sizes for various hand shapes. (A) 20th percentile hand size. (B) 80th percentile hand size.

part of the workspace for at least one of the digit sizes. As such, the minimum *ISO* term significantly reduced their *Design Score*. *Design Score* generally decreased as link lengths increased, indicating that smaller designs were preferred as intended by the *AREA* term. However, the smallest valid designs (those in the bottom left) were not the most optimal. The sum of the *ISO* term tended to reward longer link lengths, particularly longer L_1 . Collectively, the optimal link length sets had near minimal total length, with longer L_1 preferred to longer L_2 , and without near-singular configurations within the tested workspaces.

The optimization results show that L_1 should be significantly longer than L_2 for all three linkages. This result is reasonable. First, the proximal phalanx (or metacarpal in the case of the thumb), is significantly longer than the medial phalanx (or proximal phalanx for the thumb). Second, the origins of the linkages were placed dorsally to the first joint of each digit, and thus there is a minimum distance required between the first joint of each 3R linkage and the first joint of the digit. This offset is nonnegligible as A/A joints were placed prior to the first F/E joint of the 3R finger linkages, and an O/R joint was placed proximally to the first F/E joint of the 3R thumb linkage. As the *AREA* is roughly related to the cross product of the vectors corresponding to the lengths and orientations of L_1 and L_2 , *AREA* increases for a given total mechanism length the closer L_1 and L_2 are to equal. As such, it is anticipated that an ideal L_1 should account for the required offset and proximal phalanx (metacarpal) length while L_2 should account for medial phalanx (proximal phalanx) length and the 1 cm length along the distal phalanx where the digit-exoskeleton attachment point is located. It is therefore reasoned that, for the given topology, the second joint of each linkage should roughly align with the second joint of each digit when the digit is fully flexed. This near-alignment can be observed in Fig. 10.4.

10.4.2 PROTOTYPE WORKSPACE EVALUATION

Although the mechanism produced is not as low profile as some devices in the literature with other topologies, the overall size is reasonable given the required ability to fit 95% of the population. The mechanism was tested by ten volunteers, with digit lengths ranging from the 15th to 99th percentiles. All volunteers from the 15th to 95th percentile reported that the design comfortably permitted all intended desired motions without approaching singular configuration. Although the volunteer with the hand in the 99th percentile was restricted from creating certain hand poses, this was anticipated as their hand segment lengths exceeded the maximum designed for. It also suggests that the optimized link lengths are not excessively large for the design requirements.

The ability of the volunteers from the 15th to 95th percentile hand lengths to reach all intended desired hand postures indicates that the designed hand is robust to the assumption of a rigid connection between user and exoskeleton. The human palm is not a rigid structure, as the carpal and metacarpals can each move slightly with respect to each other. Encasing the hand in a rigid structure such that these palm motions are eliminated is uncomfortable for the user, and thus a less constraining attachment was used. The attachment in turn permits some motions of the palm, which means that the base of the digits can move slightly with respect to the base of the exoskeleton linkages. Despite this undesired but required motion, near-singular configurations are still avoided throughout the workspace.

10.5 CONCLUSION

The optimization method presented in this study was used to determine the optimal set of link lengths of a dexterous hand exoskeleton manipulator. The *Design Score* defined in this work focuses on the kinematic performance measure of mechanism isotropy, as well as the physical envelope of the hand exoskeleton system. The optimal link lengths were used to construct a physical prototype that was demonstrated to achieve design goals.

Although this study presents a specific case in which a 3R planar manipulator is the mechanism of interest, the methodology behind the optimization could be applied with modification to other types of mechanisms in which an end-effector must control a body part that interfaces with it at a fixed point, provided that the kinematics and inverse kinematics are solvable.

ACKNOWLEDGEMENT

This work was funded in part by the National Science Foundation through Award #1532239 MRI: Development of an exoskeleton for simultaneous assessment of brain, muscular, and nervous system output during functional arm and hand tasks. Subcontracted from the University of Idaho.

REFERENCES

- [1] C.D. Takahashi, V.H. Le, S.C. Cramer, A robotic device for hand motor therapy after stroke, in: 2005 IEEE 9th Int. Conf. Rehabilitation Robot., 2005, pp. 17–20.
- [2] E.B. Brokaw, S. Member, I. Black, R.J. Holley, P.S. Lum, Hand spring operated movement enhancer (HandSOME): a portable, passive hand exoskeleton for stroke rehabilitation, IEEE Trans. Neural. Syst. Rehabil. Eng. 19 (2011) 391–399.
- [3] C.N. Schabowsky, S.B. Godfrey, R.J. Holley, P.S. Lum, Development and pilot testing of HEXORR: hand EXOskelton rehabilitation robot, J. Neuroeng. Rehabil. 7 (2010) 1–16.
- [4] Y. Fu, S. Wang, Development of a multi-DOF exoskeleton based machine for injured fingers, in: IEEE/RSJ Int. Conf. Intell. Robot. Syst., 2008, pp. 22–26.
- [5] T.T. Worsnopp, M.A. Peshkin, J.E. Colgate, D.G. Kamper, An actuated finger exoskeleton for hand rehabilitation following stroke, in: 2007 IEEE 10th Int. Conf. Rehabil. Robot. ICORR’07, 2007, pp. 896–901. doi:10.1109/ICORR.2007.4428530.
- [6] A. Wege, A. Zimmermann, Electromyography sensor based control for a hand exoskeleton, in: 2007 IEEE Int. Conf. Robot. Biomimetics, ROBIO, 2007, pp. 1470–1475. Available from: <https://doi.org/10.1109/ROBIO.2007.4522381>.
- [7] I. Ben Abdallah, Y. Bouteraa, C. Rekik, Design and development of 3D printed myoelectric robotic exoskeleton for hand rehabilitation, Int. J. Smart Sens. Intell. Syst. 10 (2017) 341–366.
- [8] M.A. Rahman, A. Al-Jumaily, Design and development of a hand exoskeleton for rehabilitation following stroke, Proc. Eng. 41 (2012) 1028–1034. Available from: <https://doi.org/10.1016/j.proeng.2012.07.279>.
- [9] C.L. Jones, S. Member, F. Wang, R. Morrison, S. Member, N. Sarkar, et al., Design and development of the cable actuated finger exoskeleton for hand rehabilitation following stroke, IEEE/ASME Trans. Mech. 19 (2014) 131–140.

- [10] S.W. Lee, K.A. Landers, H. Park, Biomimetic hand exotendon device (BiomHED) for functional hand rehabilitation in stroke, in: IEEE Int. Conf. Rehabil. Robot., 2013, pp. 13–16.
- [11] A. Chiri, N. Vitiello, F. Giovacchini, S. Roccella, F. Vecchi, M.C. Carrozza, Mechatronic design and characterization of the index finger module of a hand exoskeleton for post-stroke rehabilitation, *IEEE/ASME Trans. Mech.* 17 (2012) 884–894. Available from: <https://doi.org/10.1109/TMECH.2011.2144614>.
- [12] H. In, K. Cho, K. Kim, B. Lee, Jointless structure and under-actuation mechanism for compact hand exoskeleton, in: 2011 IEEE Int. Conf. Rehabil. Robot., 2011.
- [13] P. Agarwal, J. Fox, Y. Yun, M.K.O. Malley, A.D. Deshpande, An index finger exoskeleton with series elastic actuation for rehabilitation: design, control and performance characterization, *Int. J. Rob. Res.* 34 (2015) 11772–17470. Available from: <https://doi.org/10.1177/0278364915598388>.
- [14] S. Ueki, H. Kawasaki, S. Ito, Y. Nishimoto, M. Abe, T. Aoki, et al., Development of a hand-assist robot with multi-degrees-of-freedom for rehabilitation therapy, *IEEE/ASME Trans. Mech.* 17 (2012) 136–146. Available from: <https://doi.org/10.1109/TMECH.2010.2090353>.
- [15] M. Sarac, M. Solazzi, E. Sotgiu, M. Bergamasco, A. Frisoli, Design and kinematic optimization of a novel underactuated robotic hand exoskeleton, *Meccanica* 52 (2017) 749–761. Available from: <https://doi.org/10.1007/s11012-016-0530-z>.
- [16] J. Iqbal, N.G. Tsagarakis, D.G. Caldwell, Design optimization of a hand exoskeleton rehabilitation devicein: *Proc. RSS Work. Underst. Hum. Hand Adv. Robot. Manip.*, 2009, pp. 44–45.
- [17] R. Unal, V. Patoglu, Optimal dimensional synthesis of force feedback lower arm exoskeletons, in: IEEE Int. Conf. Biomed. Robot. Biomechatr., 2008, pp. 329–334.
- [18] Z. Ma, P. Ben-Tzvi, Design and optimization of a five-finger haptic glove mechanism, *J. Mech. Robot.* 7 (2016) 1–8. Available from: <https://doi.org/10.1115/1.4029437>.
- [19] H. Taheri, J.B. Rowe, D. Gardner, V. Chan, D.J. Reinkensmeyer, E.T. Wolbrecht, Robot-assisted Guitar Hero for finger rehabilitation after stroke, in: Proc. Annu. Int. Conf. IEEE Eng. Med. Biol. Soc. EMBS, 2012, pp. 3911–3917. doi:10.1109/EMBC.2012.6346822.
- [20] N. Secciani, M. Bianchi, A. Ridolfi, F. Vannetti Yary Volpe, L. Governi, M. Bianchini, et al., Tailor-made hand exoskeletons at the university of florence: from kinematics to mechatronic design, *Machines*. 7 (2019) 22. Available from: <https://doi.org/10.3390/machines7020022>.
- [21] M. Fontana, S. Fabio, S. Marcheschi, M. Bergamasco, Haptic hand exoskeleton for precision grasp simulation, *J. Mech. Robot.* 5 (2013) 041014. Available from: <https://doi.org/10.1115/1.4024981>.
- [22] P.W. Ferguson, B. Dimapason, Y. Shen, J. Rosen, Design of a Hand Exoskeleton for Use with Upper Limb Exoskeletons, in: M.C. Carrozza, S. Micera, J.L. Pons (Eds.), *Wearable Robotics: Challenges and Trends. WeRob 2018. Biosystems & Biorobotics*, Springer International Publishing, Cham, 2019, pp. 276–280. Available from: https://doi.org/10.1007/978-3-030-01887-0_53.
- [23] P. Stergiopoulos, P. Fuchs, C. Laуреau, Design of a 2-finger hand exoskeleton for VR grasping simulation, in: *Eurohaptics*, 2003.
- [24] A. Erol, G. Bebis, M. Nicolescu, R.D. Boyle, X. Twombly, A review on vision-based full dof hand motion estimation, in: 2005 IEEE Comput. Soc. Conf. Comput. Vis. Pattern Recognit. - Work, 2006, pp. 75–75. doi:10.1109/cvpr.2005.395.
- [25] I.M. Bullock, J. Borras, A.M. Dollar, Assessing assumptions in kinematic hand models: a review, in: Proc. IEEE RAS EMBS Int. Conf. Biomed. Robot. Biomechatronics, 2012, pp. 139–146. doi:10.1109/BioRob.2012.6290879.
- [26] D.J. Giurintano, A.M. Hollister, W.L. Buford, D.E. Thompson, L.M. Myers, A virtual five-link model of the thumb, *Med. Eng. Phys.* 17 (1995) 297–303. Available from: [https://doi.org/10.1016/1350-4533\(95\)90855-6](https://doi.org/10.1016/1350-4533(95)90855-6).
- [27] F.J. Valero-Cuevas, M.E. Johanson, J.D. Towles, Towards a realistic biomechanical model of the thumb: the choice of kinematic description may be more critical than the solution method or the variability/

- uncertainty of musculoskeletal parameters, *J. Biomech.* 36 (2003) 1019–1030. Available from: [https://doi.org/10.1016/S0021-9290\(03\)00061-7](https://doi.org/10.1016/S0021-9290(03)00061-7).
- [28] A. Hollister, W.L. Buford, L.M. Myers, D.J. Giurintano, A. Novick, The axes of rotation of the thumb carpometacarpal joint, *J. Orthop. Res.* 10 (1992) 454–460.
 - [29] P. Aubin, K. Petersen, H. Sallum, C. Walsh, A. Correia, L. Stirling, A pediatric robotic thumb exoskeleton for at-home rehabilitation: the isolated orthosis for thumb actuation (IOTA), *Int. J. Intell. Comput. Cybern.* 7 (2014) 233–252. Available from: <https://doi.org/10.1108/IJICC-10-2013-0043>.
 - [30] M. Cempini, M. Cortese, N. Vitiello, A powered finger-thumb wearable hand exoskeleton with self-aligning joint axes, *IEEE/ASME Trans. Mech.* 20 (2015) 705–716. Available from: <https://doi.org/10.1109/TMECH.2014.2315528>.
 - [31] B. Alexander, K. Viktor, Proportions of hand segments, *Int. J. Morphol. Int. J. Morphol.* 28 (2010) 755–758.
 - [32] M.C. Hume, H. Gellman, H. McKellop, R.H. Brumfield, Functional range of motion of the joints of the hand, *J. Hand Surg. Am.* 15A (1990) 240–243.
 - [33] I.A. Kapandji, fifth ed, *The Physiology of the Joints Upper Limb*, vol. 1, Edinburgh, Churchill Livingstone, 1983.
 - [34] M.R. Cutkosky, On grasp choice, grasp models, and the design of hands for manufacturing tasks, *IEEE Trans. Robot. Autom.* 5 (1989) 269–279.
 - [35] J.N.A.L. Leijnse, P.M. Quesada, C.W. Spoor, Kinematic evaluation of the finger's interphalangeal joints coupling mechanism-variability, flexion-extension differences, triggers, locking swan-neck deformities, anthropometric correlations, *J. Biomech.* 43 (2010) 2381–2393. Available from: <https://doi.org/10.1016/j.jbiomech.2010.04.021>.
 - [36] J. Rosen, B. Hannaford, R. Satava (Eds.), *Surgical Robotics: Systems Applications and Visions*, Boston, MA, Springer, 2010. <https://doi.org/10.1007/978-1-4419-1126-1>.
 - [37] J.P. Merlet, Jacobian, manipulability, condition number, and accuracy of parallel robots, *J. Mech. Des.* 128 (2006) 199. Available from: <https://doi.org/10.1115/1.2121740>.

LOWER LIMB EXOSKELETON SYSTEMS—OVERVIEW

11

Hao Lee, Peter Walker Ferguson and Jacob Rosen

Bionics Lab, Department of Mechanical and Aerospace Engineering, University of California, Los Angeles, CA,
United States

11.1 INTRODUCTION

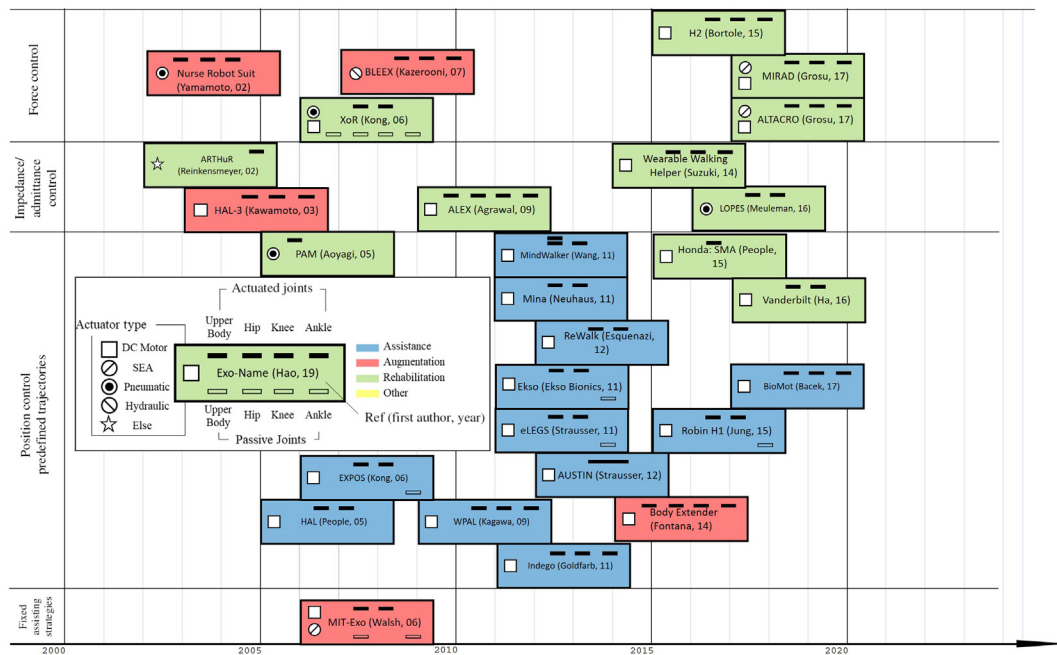
Wearable robots have long been dreamed of in science fiction. They are often described as a mixture of robot and clothing: tools and users are no longer separated. This idea has been realized both in industry and academia in the past decade. Compared to normal clothing, which serves no more purpose than providing coverage, exoskeletons can act on their own. If the exoskeleton assists the user, they can accomplish tasks they originally find difficult or impossible. In this review, we will discuss the design and current state of lower limb exoskeletons. A number of reviews have been carried out by various researchers [1–5].

There are three major categories of lower limb exoskeletons: assistive exoskeletons, rehabilitation exoskeletons, and augmentation exoskeletons [6]. Fig. 11.1 lists many of the lower limb exoskeletons that have been developed. The horizontal axis shows the development date and the vertical axis the control methods. Each marker shows the active/passive degrees of freedom and actuator types.

Assistive lower limb exoskeletons are those that help users to complete daily activities that they are no longer able to do. For instance, they may assist the user to walk when they are normally unable to due to spinal cord injury, stroke, or age deterioration. As shown in Table 11.1, exoskeletons within this group are often controlled with predefined trajectories triggered by the user's moving intention. High precision control is required; most assistive exoskeletons are driven with DC motors.

Rehabilitation exoskeletons, on the other hand, are designed to restore abilities such that patients can live without the device. These exoskeletons focus on "how the tasks are done." In most designs, such systems require online adjustments that only "help when necessary" and reduce assistance as the user gradually improves. It is expected that the user will regain their lost ability via training with decreasing assistance. As listed in Table 11.2, control for this kind of exoskeleton is usually partially predefined since patients need guidance for correct motion profile, but it also adjusts itself based on patient feedback. Portability is usually not considered; the whole system may be fixed to a treadmill under the supervision of a physician.

The last category is the human performance augmentation lower limb exoskeleton (augmentation exoskeletons). The design concept of augmentation exoskeletons can be summarized in one

**FIGURE 11.1**

The development of lower limb exoskeletons. The linked bar represent joints are coupled.

statement: “making the user superhuman.” Augmentation exoskeleton users are generally healthy individuals. For healthy users, predefined trajectories are not necessary. Instead, control algorithms that follow the user’s limb motion, such as admittance/impedance control or even positive feedback sensitivity amplification control, are used. Inaccurate but high power/weight ratio actuators, such as series elastic actuators (SEA) and pneumatic actuators, are more commonly used in this category, as shown in [Table 11.3](#).

Despite separation into categories, there are still some common characteristics. For instance, actuation methods are not specific to only one category and will be reviewed in the last part of the chapter.

11.2 ASSISTIVE EXOSKELETONS

Assistive exoskeletons are mostly used by thoracic-level motor-complete spinal cord injury (SCI) patients. Many of these patients permanently lose the ability to walk and consequently use wheelchairs. However, the accessibility of the wheelchair is limited; common environments such as stairs are not navigable or require extra assistance. Additionally, research has found that remaining seated for long periods induces health issues. It is suggested that passive mechanical loading is necessary for maintaining bone mineral density (BMD). BMD of long-time wheelchair users is statistically

Table 11.1 Some Assistive Exoskeletons

Assistive Exoskeleton			
Name	Degrees of Freedom (DoF)	Intention Estimation Method/ Trajectories Generating Method	Actuator Type
eLEGS [7]	6, 4 actuated (hips and knees), passive ankle joint	1. Force sensors on foot pads and crutches, IMU on arms for estimate the arm angle. Measurements are fed into finite state machine to estimate the walking stage 2. Predefined joint trajectories related to the finite state machine to assist bipedal walking and sit-to-stand	DC motors
Ekso [8]	6, 4 actuated, 2 hips and 2 knees, 2 passive ankles	Predefined joint trajectories based on clinical gait analysis	DC motors
AUSTIN [9]	4, 2 actuators, hip and knee joints are coupled	Function selector on forearm and tilt sensor on torso to trigger predefined motion profile	DC motors
ReWalk [10,11]	6, 4 actuated, 2 hips and 2 knees, passive ankles	Predefined joint trajectories based on healthy subject wearing Mina. Can switch between rigid position control mode and compliant assist mode	DC motors
Mina [12]	4, 2 hips and 2 knees	N/A	DC motors
REX [13]	5 actuated each leg	1. Myoelectric sensors	DC motors
HAL [14–16]	4 actuated, 2 hip and 2 knees	2. Gyroscope and accelerometer on torso/ground reaction force (GRF) sensors 3. Assist sit-to-stand motion, bipedal walking 4. Estimate walking speed and generate desired trajectories with inverse kinematics	DC motors
ROBIN H1 [17]	6, 4 actuated, 2 hips and 2 knees, 2 passive ankles	IMU, encoders and foot sensors (can be replace with neuron network-based classifier with IMU and encoders' measurements)	DC motors
WPAL [18,19] (Wearable Power Assist Locomotor)	6 actuated with a walker	1. Trigger with angle-acceleration sensor on the walker and foot pressure sensor 2. Calculate minimum jerk trajectories with desired toe position	DC motors
MindWalker [20–23]	6 actuated, 4 hips and 2 knees	1. Estimate CoM position with IMU located near hip 2. Swing stage: Modified joint trajectories recorded from healthy subjects and online correction 3. Weight shifting: Interpolation between start and end points	DC motors with series elastic actuators

(Continued)

Table 11.1 Some Assistive Exoskeletons *Continued*

Assistive Exoskeleton			
Name	Degrees of Freedom (DoF)	Intention Estimation Method/ Trajectories Generating Method	Actuator Type
By G. Belforte [24]	4 Actuated, 2 hips and 2 knees	Apply maximum assistance when need assistance, stop by mechanical hard stop	Pneumatic
Indego/Vanderbilt Exoskeleton [25–27]	4 Actuated, 2 hips and 2 knees. Standard ankle orthosis	Using joint angles to estimate the distance between CoP and forward foot to trigger finite state machine	DC motors
BioMot [28]	6 actuated on sagittal plane (hips, knees, and ankles)	<ol style="list-style-type: none"> During ankle push-off and heel-off, actuators provide fixed ramp torque assistance The rest of the time the interacting force between the exo and the user is minimized 	Variable stiffness actuators
EXPOS [29]	4 actuated (hips and knees), 2 passive (ankles) DoF, flexible frame for transverse, frontal plane motion	<ol style="list-style-type: none"> Pressure sensors are installed at human–exoskeleton interacting points, the measurement will increase due to muscle contraction Generate assistive torque proportional to the contact pressure difference between the front and rear sides of the leg 	Motor-cable driven

lower than that of individuals who stand with assisting tools [57]. Wheelchair users also suffer from pressure sores and ischial tuberosities since a high amount of pressure is applied on the seating surface for long durations [58]. As a result, assisting devices that keep users standing upright with better maneuverability are required. ABLE [59], a device that keeps the user standing upright while moving with wheels attached under the feet, was introduced to address this issue, nonetheless, such simplification in human motion limits navigability. To overcome this, the adaptability and robustness of bipedal walking must be retained. This requires the development of assistive exoskeletons, wearable biped robotic suits that enable paralyzed patients to move with human-like gait patterns.

Few lower limb exoskeletons have been made to resolve this issue and manage to have users walk independently [10–14,60–62]. Table 11.1 is a brief list of some assistive exoskeletons. However, these exoskeletons still lack the full mobility of healthy people, and the motion between the human and the exoskeleton is not yet perfectly synchronized.

The development of assistive exoskeletons can be traced back to reciprocating gait orthosis (RGO) [1]. RGO is a passive device that has only one degree of freedom (DoF) in each leg and mechanical constraints that alternately enable the DoFs. While it has aided users with extra mobility, drawbacks such as long and difficult donning/doffing time, overuse of patients' upper limbs, and required supervision to avoid falling have limited its usage. To address these issues, active walking assisting devices later known as assistive exoskeletons were developed. Similar to

Table 11.2 Some Rehabilitation Exoskeletons

Rehabilitation Exoskeleton				
Name	Configuration	Degrees of Freedom (DoF)	Trajectory Generating/Actuator Control Method	Actuator
Stationary				
Lokomat	Treadmill + overhead harness body weight support + orthosis	4 DoFs, 2 (hip, knee) DoFs each leg in sagittal plane	1. Prerecorded, adjusted by the physicians 2. Impedance control, adaptive control by Riener et al. [30]	Electric motors located at each joint
ARTHuR [31]	Treadmill + back-drive able external linkage connecting the user	2 Sagittal plane DoFs on the linkage connected to the shoe	Simple force control generated by constant impedance force field	Moving coil forcer
LOPES [32]	Treadmill + overhead harness body weight support + orthosis (robot legs connect to shanks)	4 DoFs, 2 (hip, knee) DoFs each leg in sagittal plane	1. Predefined joint trajectories/stiffness profile can be adjusted based on how much assistance is needed 2. Admittance controller measures human–robot interaction force, combines it with desired support, outputs desired joint trajectories	Pneumatic actuators
ALEX [33–36]	Treadmill + orthosis (motors located away from the user to reduce inertia of each link)	12 DoFs, 4 at the pelvis and 4 for each leg	1. Desired joint torque calculated by impedance controller 2. Applied torque is calculated by canceling human interaction force, friction, and gravity	DC motors
PAM [37]	Pneumatic cylinder constraint pelvis + treadmill	6 DoFs at the pelvis	Predefined and adjusted with real-time feedback of foot switches	Pneumatic
ALTACRO [38]	Stiffness adjustable compression springs + treadmill	6 DoFs (hips, knee, ankles in sagittal plane)	Predefined joint torque profile with actively controlled degree of assistance	Mechanical spring with motor adjusting equilibrium point

(Continued)

Table 11.2 Some Rehabilitation Exoskeletons *Continued*

Rehabilitation Exoskeleton				
Name	Configuration	Degrees of Freedom (DoF)	Trajectory Generating/Actuator Control Method	Actuator
Mobile				
MIRAD [38]	Manual adjustable stiffness springs + motor-actuated exoskeleton	6 actuated on sagittal plane (hips, knees, and ankles)	Predefined joint torque but manual adjusted degree of assistance for assisting human sit-to-stand motion	Motor-driven joints with manual preloaded tension springs
XoR [39,40]	Hybrid pneumatic muscle + motor actuators full lower body exoskeleton	13 DoFs with 4 actuated (2 hips and 2 knees)	Predefined torque profile for torque control	Pneumatic muscle + electric motors
H2 [41]	Electric motor-driven full lower body exoskeleton	6 actuated DoFs	Predefined joint trajectory and real-time modified with exoskeleton–human interaction force	Electric motors
HAL (Rehabilitation) [16,42]	Electric motor-driven full lower body exoskeleton	6 actuated DoFs	Estimate user's moving intention via GRF or pelvis tilt angles, and gait period with double support time to generate gait trajectories by defining initial and end-points	Electrical motors
Wearable Walking Helper [43]	Electric motor-driven full lower body exoskeleton	6 actuated DoFs	Generate desired trajectories based on spring-mass model and used in impedance control	DC motors with linear actuators
Honda: SMA [44]	Hip joints actuated exoskeleton	2 actuated DoFs	Generate symmetric hip joint trajectory with angle measurements feed into CPG.	DC motors.
Vanderbilt lower limb exo [45]	Exoskeleton with FES electrodes placed at quadriceps and hamstrings	4, 2 hips and 2 knees in sagittal plane	Predefined joint trajectories triggered with finite state machine combines with FES stimulates users. Stimulation will stop if muscle fatigue is detected	DC motors with FES

RGOs, assistive exoskeletons provide stand-upright ability to users, but also extra DoFs and embedded actuators that allow active control. This results in smoother motion and less energy consumption of the upper limbs.

Table 11.3 Some Augmentation Exoskeletons

Augmentation Exoskeleton			
Name	Degree of Freedom (DoF)	Intention Estimation Method/Trajectories Generating Method	Actuator
Nurse Robot Suit [46–48]	5 actuated DoFs (arms, waist, knees)	Generate assisting torque proportional to muscle hardness	Pneumatic actuators
HAL-3 [49]	6 actuated DoFs (hips, knees, ankles in sagittal plane)	1. Defined the ratio of assistance/effort without the assistance based on finite state machine 2. Measure effort with myoelectric sensors	DC motors
MIT Exoskeleton [50–52]	4 actuated DoFs, while hips (sagittal) are actuators and knees are dampers. 4 passive DoFs at the ankles and hip (frontal)	1. Trigger assistance with finite state machine 2. Assist the hip with fixed force profile 3. Adjust knee damping according to angular velocity	Hip: SEA + DC motors Knee: magnetorheological damper Ankle: passive spring
BLEEX/ HULC [53]	8 actuated DoFs (hips, knees, and ankles in sagittal plane, hips' frontal plane)	Follow user's intention with sensitivity amplification	Hydraulic actuators
XOS [54]	N/A		
Body Extender [55]	22 actuated DoFs. 3 hips, 1 knee, and 2 ankles (excluded arm DoF here)	1. For swing phase, minimize the interaction force between the human and the exoskeleton 2. At least one foot is considered fixed to the ground at all times	DC motors with worm gears to transform rotation to linear motion
Panasonic Power Loader [56]	N/A		

The control of assistive exoskeletons is mainly a combination of a high-level central controller and low-level joints controllers. In general cases, the goal of the controller is to plan the joint trajectories. Counter to the intuition that wearable robots should follow users' motion, assistive exoskeletons usually generate the motion profile disregarding the user. To be more specific, the details of the motion (e.g., gait length, gait period) are generated solely by the exoskeleton. The user only gives high-level commands such as "walk forward," "stand up," and "sit down" because, for patients that have fully lost their motor skills, the exoskeletons no longer have "motion" to follow.

To capture high-level commands, exoskeletons need to estimate the user's intention. The easiest method is having the users manually input the command. A common design is placing a console besides the user's wrist. However, this will limit users' upper limbs and cause delay since commanding legs by hands is not intuitive. Direct estimation from biological signals has been developed, yet biological signals are often noisy and difficult to measure. More accessible signals such as EMG are not usable because paralyzed patients have often lost the connection between the brain and the limbs. Thus, indirect measurement has been introduced [14]. Additional sensors are added, such as inertial measurement unit (IMU) or ground reaction force (GRF) sensors. It is known that the center of mass (COM) velocity is highly related to the intention of motion. For example, COM forward movement is associated with walking forward. With IMU located near the torso or force sensor under users' feet, the motion of COM can be estimated. In addition, posture can also insinuate the moving intention. By measuring the torso angle, the exoskeleton can tell whether the user wants to initiate forward motion. These sensors do not need high sample frequency or filtering since they only provide a rough estimation of human intention.

After the task is determined, the exoskeleton will generate the required joint force/position profile to accomplish the task. These trajectories are preprogrammed and linked to specific motions. In most cases, trajectories are generated with a finite state machine. A finite state machine is a controller that divides the single full motion cycle into different phases. For each phase, the controller may have a different control scheme. This is due to the natural discontinuity in lower limb motions such as bipedal walking [63] because different phases of walking present different dynamics. For example, the model of single support (with only one foot contacting the ground) can be viewed as an inverted pendulum, while the double support phase (both feet are on the ground) cannot.

It is important to know that the generated trajectory may not be identical to a healthy subject's motion profile, but it can still complete the task. For example, one feature that is commonly seen in many assistive exoskeletons is unactuated or fixed ankle joints. While humans rely on ankle-push-off torque as the main thrust during walking, researchers have shown that actuating only the hip joints can create stable gaits for passive walkers [64,65]. Thus, for individuals with complete loss of motor skills, human-like gait patterns can be replaced with simpler gait patterns and fewer actuated joints to reduce exoskeleton weight and complexity. Despite the fact that the human lower limbs are 12-DoF mechanisms (for each leg, three at the hip, one at the knee, and two at the ankle), most assistive exoskeletons exclude the DoF in the transverse plane and active DoF at the ankle.

Lower limb exoskeletons with simple sit-to-stand function have been developed [66,67]. Note that while sit-to-stand seems simpler than the task that most lower limb exoskeletons do—walking—it is less developed in exoskeletons due to its high torque requirement and large range of motion.

Some lower limb exoskeletons, such as ReWalk [10,11], use a control panel and tilt sensor. Others, such as Robin H1 [17], estimate the user's intention by measuring the center of pressure (COP). To increase comfort and stability, instead of developing the exoskeleton with a rigid human robot interface and position control, Mina [12] and Indego [25–27] add a compliant assisting mode to partially preserve users' walking ability. BioMot [28] developed a novel variable stiffness actuator to further control the torque and stiffness at each joint.

Instead of purely relying on predefined joint trajectories, some assistive lower limb exoskeletons generate motion profiles with online calculation. Wearable Power-Assist Locomotor (WPAL) [18,19] generates the trajectories based on “not falling back” and “provide ground clearance.”

Desired hip and toe positions are given, and trajectories are generated with minimum jerk. MindWalker [20,21] also applied a similar idea but only during the weight-shifting phase (double support phase), the predefined trajectories are corrected online if the exoskeleton senses imbalance.

While many lower limb exoskeletons control each joint individually, the relationship between different joints has been studied. Researchers have found that the motion of the knee and hip are coupled due to biarticular muscle connections. AUSTIN [68] takes advantages of this coupling and reduces the requirement of actuation by one.

One of the biggest challenges is keeping users balanced during motion. Most assistive exoskeletons require extra support (support besides legs) to maintain balance. MindWalker addresses this issue by estimating the XCoM (the position of the center of mass combined with momentum, during walking) to prevent falling, yet full self-balancing is not accomplished. One of the exceptions is REX, a lower limb exoskeleton developed by REX Bionics in New Zealand, which moves slowly to statically balance itself with only two legs [13]. Nevertheless, for bipedal systems to maintain dynamic balance, the properties of human limbs, such as center of mass, inertia, and link length need to be precisely measured, which is still not possible with current technology.

The results of assistive exoskeletons have been reviewed [69]. It is claimed that around 30% of assistive exoskeletons have high potential to be effective. However, further studies and effectiveness criteria need to be established for better comparing assistive exoskeletons with traditional methods.

11.3 REHABILITATION EXOSKELETONS

In addition to helping paralyzed patients to conduct normal human gait-like motion, researchers have also focused on rehabilitating patients to regain mobility with lower limb exoskeletons. Typically, the loss of walking ability is due to cognitive and sensory deficits. The neuron connections between the brain and muscles are damaged, thus impairing motor ability. While these connections may not be restorable, the plasticity of the human neuron system [70,71] makes it possible to find an alternative neuron path. In order to trigger such neuronal reorganization, repetitive and labor-intensive training is needed [72]. Currently, most rehabilitation processes are done with physical therapists. These therapists assist the patients while they are asked to use the paretic limb. Unfortunately, most of these tasks keep therapists in ergonomically undesirable postures and require high labor intensity, which result in occupational injuries and fatigue. This limits rehabilitation as the efficacy is proportional to the duration of the strenuous work. In other words, the effectiveness of rehabilitation not only depends on the patient's, but also the therapist's strength.

11.3.1 REHABILITATION WITH WEIGHT SUPPORT

To address this issue, tireless robots have been introduced. The first product that came to the market is the Body Weight-Supported Treadmill Training (BWSTT) system [73–78]. The main muscle effort of walking, supporting body weight, is transferred to overhead or around-the-waist cables/harnesses while keeping the feet in contact with a treadmill. Therapists gradually increase the treadmill speed to normal walking speed and decrease the supported weight to zero during training.

Although the labor is reduced compared to traditional methods, it still requires around three therapists for each session. In addition, leaving the patient's lower limbs without constraints cannot assure correct gait patterns. Some research groups have attempted to add extra constraints on the patients. The Pelvic Assist Manipulator (PAM) [37] uses six pneumatic cylinders to control the motion of the pelvis while walking on a treadmill. The desired position of the pelvis is predefined and adjusted with the patient's footsteps. Other research groups dealt with this problem with constraints at the ankles. HapticWalker [79] and GaitMaster [80] replaced the treadmill with manipulators. The patient's feet are restricted by these manipulators while they are replaying the desired gait pattern. LokoHelp [81], on the other hand, keeps the treadmill but guides the patient's feet during the swing phase. These extra constraints help patients maintain and repeat the correct gait cycle during rehabilitation training.

Still, only adding constraints at one contact point may not be enough since human lower limbs are redundant in the sagittal plane. Possible injuries may take place if the leg configuration is incorrect during ankle push-off. To address this issue, driven gait orthosis (DGO) has been introduced. These orthosis-BWSTT combined machines have orthoses that attach to the patient's lower limbs. In each episode, the orthosis is driven with a symmetric walking gait cycle that has equal walking speed with the treadmill. One of the most commonly seen DGO is the Lokomat, a Swiss-made DGO that attaches to the user's thigh and calf that is already commercialized and has had significant results in patients [82].

A common issue with these examples of wearable rehabilitation robots is low compliance. Compared to other types of lower limb exoskeletons, compliance plays an important role in rehabilitation. Unlike assistive exoskeletons that do not take the user's motion into consideration, rehabilitation exoskeletons focus on human–exoskeleton contact and interaction with the user. Rehabilitation exoskeletons need to correct the user's motion when it deviates from the desired trajectory and assist the user when they do not have the strength to achieve required tasks. In other words, human–exoskeleton interaction force is the key for rehabilitation, only when the user has recovered will he/she synchronize with the exoskeleton.

There are two primary ways to make exoskeletons compliant: simulate with control or add an elastic component in the actuators. The first method is also known as impedance or admittance control, depending on whether the input/output relationship is position/force or force/position. In impedance control, a common scheme is to create a virtual environment and determine torque output by simulating the robot as interacting with a compliant material. This method is mainly used to guide the patient during rehabilitation training. Based on such a concept, Riener et al. proposed a “patient-cooperative” strategy on Lokomat [30,83,84]. In their experiments, the exoskeleton generates a virtual impedance to guide the patients, while patients can determine the timing of the trajectories. The results showed that patients' participation increased.

However, only assisting the patients with predefined trajectories may lead to passively following the machine as opposed to actively controlling it, thus reducing the activity of the neural circuit. As shown in experiments on mice by Cai et al. [85], with the introduction of an adaptive assisting method called “assist as needed” (AAN), the rehabilitation results significantly improved compared to fixed trajectories training. This concept has also been applied in human rehabilitation training. Meuleman et al. implemented admittance control that only assisted patients when they needed it [32]. The result was that these patients produced greater torques than in training with pre-defined trajectories, which can be interpreted as a better rehabilitative result.

11.3.2 REHABILITATION WITHOUT WEIGHT SUPPORT

Nonetheless, even with BWSTT and DGO systems, some crucial functions of walking cannot be restored, such as balance [77]. On top of that, BWSTT systems are typically large, and therefore can only be used in hospitals or rehabilitation centers. To address this issue, portable lower limb exoskeletons were introduced.

A major difference between BWSTT and lower limb rehabilitation exoskeletons is that BWSTT supports body weight with overhead cables/harness, while the exoskeleton does not. This enables the exoskeleton system to be portable. For example, H2 [41] exoskeleton supports the body by attaching the user to the exoskeleton through waist, thigh, and calf straps. However, safety concerns appeared due to possible falling. The solution to this problem is having the user use a walker, similar to assistive exoskeletons. In addition, the required torque of the actuators increases since extra power is needed for user weight supporting. Some high-power density actuators have been introduced, XoR uses a combination of pneumatic artificial muscles and DC motors to have higher torque output [39,40]. Control of the exoskeletons in this category is mostly through impedance control since the machine needs to “correct” the user’s motion during training. A virtual impedance is generated when the user deviates from the trajectory that the physician has assigned.

Forcing the user to put in as much effort as possible has always been a challenge in rehabilitation exoskeletons. Estimating whether the user is already applying maximum effort is usually based on the therapist’s experience. To cause the user to increase their effort, functional electrical stimulation (FES) has been implanted in some lower limb exoskeletons, with this combination known as “hybrid exoskeletons.” By artificially triggering muscle contraction, leg locomotion is generated [86,87]. Different control methods are developed for this type of exoskeleton. The Vanderbilt Lower Limb Exoskeleton has combined FES with a traditional position control method [45]. The control system consists of two loops, a PD position control loop and a muscle control loop. The exoskeleton first functions like an assistive exoskeleton with joint actuators following the desired trajectories, and during these steps a nominal torque of the motors is calculated. It is expected when later FES is applied to the user, the required actuator torque will be reduced. The difference between current actuator output and the nominal torque reflects the effort that the user has put in. Note that while human torque is positively related to FES, the relationship is unclear and varies with fatigue. To address this problem, the controller estimates the FES-induced motor torque reduction and combines it with real-time measurement to create an adaptive muscle stimulation model. FES will keep stimulating the muscles until the measured torque output is less than one third under the same stimulation due to muscle fatigue. The result has shown consistent gaits with a reduction in motor output.

Table 11.2 summarizes some of the existing lower limb exoskeletons that have been applied to rehabilitation. Many of the devices have converged to feature similar design and control methods, which suggests further improvements may require an improved understanding of rehabilitation. The future of rehabilitation lower limb exoskeletons may also be correlated to novel strategies used by physicians and physical therapists.

11.4 AUGMENTATION EXOSKELETONS

Lower limb exoskeletons/orthoses are often viewed as medical devices, yet there are also applications for healthy users. For these users, exoskeletons do not replace or help the user regain any abilities, but instead provide augmentations.

There are two main branches for augmenting humans with exoskeletons. One is making tasks transparent to the user. For example, if a user wants to hold a heavy object, the exoskeleton will directly engage with that object, requiring little effort from the user. For the other branch, the exoskeleton may only affect the user and require the user to perform the task. However, the exoskeleton will assist the user to reduce the required effort. For the first method, the exoskeletons can accomplish tasks that a normal human cannot, but it often significantly increases the overall weight and reduces the range of motion of the human–exoskeleton system. The latter method can be achieved with simple, light, and more comfortable exoskeletons, yet the tasks will be limited by users' physical capability since it will first interact with the user.

11.4.1 ASSISTANCE DIRECTLY APPLIED TO TASKS

Humans have focused on the first task since the Industrial Revolution. Robots built for labor-intensive and repetitive jobs are widely used in industry. However, most of them can only operate in controlled environments such as the production line. Unfortunately, not all environments can be controlled. For example, loading/unloading the missiles of fighter jets on an aircraft carrier, or carrying extra load while hiking. Fortunately, this limitation can be resolved by combining the adaptivity of humans and the strength of robots.

Currently, researchers have developed various exoskeletons for weight-lifting tasks. Yamamoto et al. [46–48] built a Nurse Robotic Suit to help nurses lift patients up to 60 kg from wheelchairs to beds. Assisting torque was generated proportional to the hardness of the related muscles. However, their design did not consider mobility and only the arm, waist, and knees are actuated, resulting in extra loading acting on users' ankle joints. Kazerooni et al. presented a moveable load-carrying full lower limb exoskeleton BLEEX, which was later commercialized as Ekso [88–90]. BLEEX can achieve “transparency,” which means the user cannot feel the carrying load, by transferring the loading weight to the ground through mechanical structures. Linear hydraulic actuators are selected for their high force density. The common control method: Sensitivity amplification was first introduced. A standard sensitivity amplification controller considers the human and exoskeleton as one system. The controller embeds a positive-feedback loop that mathematically induces short rise time and high overshoot. The major advantage of this architecture is that the exoskeleton can be driven purely by sensing its own joints' angles, which eliminates the problem of donning and misplacement of the sensors. On the other hand, human interaction with respect to the exoskeleton would be equivalent to a negative-feedback loop. By viewing the human also as a part of its controller, BLEEX could carry the load during stable walking.

Yet, there is a dilemma with the sensitivity amplification controller, if one wants to increase the sensitivity of the exoskeleton, the user needs to exert more effort to stabilize the system. To compensate for this defect, researchers have applied a hybrid control method on the BLEEX [89]. Instead of sensitivity amplification control, position control was used on the stance leg during the single support phase. With additional sensors to measure the human joints' angles, the hybrid controller minimizes the angular difference between the user and the exoskeleton. Nonetheless, the result is inferior to pure sensitivity amplification, not only the load carrying but also the walking speed were reduced, and the user had issues with balance.

Traditional sensing methods induce delay since the exoskeleton can only take actions after the user starts to move [91]. While every system in the real world is causal, delay is inevitable, but

estimation is possible. Some attempts have already been published. Although not estimating the motion in real-time, Lim et al. believes that with sufficient recorded data, one can generate the whole joint trajectory based on the initial and final conditions of each gait period [92,93].

While most of the control methods are based on kinetic sensors, researchers have wondered if exoskeletons can be controlled directly with neuron systems. The Hybrid Assistive Limb (HAL) uses electromyogram (EMG) signals [49]. These, and other biological signals, are hypothetically the only category of sensing that can estimate the user's intention without a time delay [94], but they are much noisier than other measurements (force, position, etc.). As such, bioelectrical signals are difficult to use for precise control. Moreover, the effort systems based on EMG can provide is also limited because, the more assistance the user receives, the less bioelectrical signals he/she will generate, and vice versa. In other words, the exoskeleton can never provide full assistance, otherwise the exoskeleton will receive no input [62].

Although a goal of augmentation exoskeletons can be to reduce the effort when carrying loads, the total metabolic cost may be higher due to balancing and the extra weight of the exoskeleton. Luckily, both increasing stability and reducing weight can be addressed simultaneously with a simple method: adding compliance. Compared to traditional actuators, mechanical springs have high power density. On top of that, simple passive elastic systems also increase stability during bipedal walking [95]. On the other hand, passive elastic systems lack adaptivity, and one design may not fit the needs of different users. The remedy to this problem is combining active and passive systems. Walsh et al. developed a load-carrying quasi-passive lower limb exoskeleton which transfers 80% of the payload weight to the ground during walking, but only requires 2-watt motors [50–52]. In their design, both the hips and the ankles were actuated with passive springs with a mechanical clutch. These springs would store negative work during walking and return it as assistance when useful. On the other hand, the knee joint was only controlled with a variable damper. Despite the assistance transferring payload weight to the ground, the energy consumption of the users was increased by 10% compared to having the user directly bear the weight. This may be due to limited degrees of freedom and conflict during the operating between human and exoskeleton.

Some lower limb exoskeletons have reached the market. Raytheon XOS has been developed for military usage. It is a full body exoskeleton that helps soldiers to do strenuous work and shows moving ability on both flat ground and slopes. Nevertheless, while the details are classified, it is clear in the release videos that XOS is tethered to a power supply that limits portability and operating range.

11.4.2 ASSISTANCE APPLIED ON USERS

However, these rigid lower limb exoskeletons have the same bottleneck: weight, as much as 150 kg [55]. While the lower limb exoskeleton can balance the weight with gravity compensation, the increment in inertia will make it difficult to move agilely. To decrease the weight of the lower limb exoskeleton, researchers began to wonder: is it necessary to have a full lower body exoskeleton? While helping humans dealing with intensive labor was the original objective, the actual goal is often to “reduce metabolic cost.” Thus, instead of removing the task’s load on the user, we can view human and exoskeleton as one system with the goal of reducing the overall metabolic cost to the user.

Assistance can be applied on any part of the human body. It is known that if provided external assistance, an individual will reduce his/her own effort to maintain the same force profile [96,97]. Researchers have assumed that if the user is assisted properly, they can perform the same task with a lower metabolic cost. To properly assist humans, the mechanism of bipedal walking has been analyzed. The energy efficiency of bipedal walking has been troubling researchers for decades. Other than for overcoming friction, passive walkers do not need additional effort to walk [65,98]. This is not the case for humans, as there is significant energy loss in the step-to-step transition [99]. The common explanation is smoothly switching the center of mass between steps is difficult for humans because the vertical projection of the COM (known as COP) has to move out of the supporting plane (feet), resulting in intentional falling [63] and creating impact when the other leg touches the ground. This induces energy lost during the transition state and is often referred to as “heel strike,” which is the primary source of energy lost during ground level walking.

To reduce the energy consumption, researchers first attempted to replace muscle activity with the lower limb exoskeleton’s assistance. Norris et al. suggested that metabolic cost would be reduced with assistance at the ankle plantar flexor [100]. However, providing the correct assistance is challenging. Sawicki and Ferris tested the metabolic rate change while being assisted with a powered ankle exoskeleton [101,102], and showed that the decrease in ankle joint mechanical power is not proportional to net metabolic power change. In other words, assistance from the exoskeleton may cause unknown energy consumption if it is unnatural.

Researchers have also attempted to assist different joints. Besides walking, Gams designed a novel oscillator-based controlled lower limb exoskeleton to assist the knee joint during squatting [103]. It showed that muscle activity statistically decreased. However, oscillator-based controllers require periodic motion, which is uncommon for squatting. Seo, on the other hand, applied an oscillator-based controller on the hip joint, and successfully reduced the metabolic cost of walking by 13% [104]. Full lower body exoskeletons have also been developed, although they tend to be very different from those developed for other applications. The previously mentioned lower limb exoskeletons are mostly made from hard materials. Full-body exoskeletons in this category are often soft, for example, the soft exosuits [105–107] use elastic material as tendons to link different joints to provide assistance.

However, lower limb exoskeletons are limited in their operation time. Around 72% of exoskeletons are driven by electric motors [6], most are servo motors due to their mature position-based control method. Nevertheless, the efficiency of such systems is limited by the fundamental difference between motors and human joints. For example, the human knee joint angular position may range from +20 to +110 degrees, and the angular velocity generally is less than 30 rpm but with high torque output [108]. Alternatively, most motors operate in 360 degrees and have maximized efficiency and torque output at a specific rpm. Practically, gear reduction is applied to compensate for these differences. However, the dilemma of gear ratio appears, which is that a high gear ratio creates larger torque but reduces angular velocity in human joints.

Some attempts have been made to improve motor efficiency. Alò et al. [109] designed a transmission system between the motors and the knee joint. It contains a fly wheel with an infinitely variable transmission. Since the motor could operate at optimal speed, energy efficiency was improved. Although the effective motor efficiency was improved, the effect of the extra weight on the system is unknown.

On the other hand, many researchers believe there is potential to harvest energy from human motion [110,111]. Malcolm et al. [112] showed theoretically that it is possible to reduce the metabolic cost of walking by applying assistive torque at a specific time (i.e., at the supporting leg, just before the heel strike of the swinging leg) without using any external energy source. Instead, energy is recycled from the negative work inherent in bipedal walking. A similar idea can be seen in orthosis design [113]. Collins et al. [114] designed a passive device using a clutch and spring system based on Malcolm's idea, which assists the ankle joint with a more energy-efficient structure. The overall metabolic cost of walking was reduced by $7.2\% \pm 2.6\%$.

However, it is known that the ankle joints are the most energy-efficient joint, as they have the Achilles tendon to store negative work. Thus, the potential for improvements is not as high as for other joints. Rogers et al. [115] reduced the negative work of the knee while descending stairs by using a quasi-passive air spring to absorb the impulse. The knee joints are connected to an air cylinder that creates deceleration by compressing air, resulting in a 15% decrease in EMG activity in the rectus femoris. Nevertheless, the compressed air is just dissipated. Yamada et al. [116] designed a pneumatic walking assistive device that successfully used the energy recycled from the knee joint during the beginning of the double support phase and reused it on the same joint later.

Thus, the optimal design to address this will likely be to recycle energy from the joints that produce the most negative work and apply it on those that require the most positive work. Similar ideas have been seen in prosthesis design. CYBERLEGs Alpha-Prototype [117] uses a passive mechanism to transfer the energy harvested from the knee's negative work to assist the ankle at push-off. The result was positive and shows energy transfer from knee to ankle. As for exoskeletons, van den Bogert [118] and Van Dijk [119] connected multiple joints of their exoskeletons with artificial tendons. However, the metabolic costs were not reduced due to extra restrictions that affected human motion.

Exoskeletons within this category have largely been designed as proofs of concept. Commercial products have not yet been made. The biggest bottleneck is the limitation of actuation and precision of compliant actuators. Although compliant actuators can have weight similar to normal clothing, without precision control, such products cannot be used in industry or our everyday life.

11.5 ACTUATION OF LOWER LIMB EXOSKELETONS

One of the most important factors that affects an exoskeleton's design is the actuation system, since it generally determines the performance, efficiency, and portability [3]. There are mainly four types of actuators used in modern exoskeletons: electrical motors, pneumatic actuators, hydraulic actuators, and series elastic actuators. Most exoskeletons use electric motors due to their ability to be precisely controlled and easily access the energy source. Still, some choose the other options for higher power/weight ratio or better compliance.

As mentioned previously, around 72% of modern exoskeletons are electrical motor driven. For assistive exoskeletons this number is even higher. This is because, for the users of assistive exoskeletons, the most important criterion is the precision of the joint trajectories since the users cannot correct it themselves. In addition, the efficiency of electric motors is usually superior to other

choices. For example, BLEEX has been built in both electric motor and hydraulic versions. It turned out that the electric motor version is 92% more power efficient than the hydraulic version [3]. Nevertheless, the weight of the electric version is twice that of the hydraulic version due to the fact that the power/weight ratio of electric motors is usually the worst among all the four actuation methods.

For higher power output, electric motor users will face a dilemma, which is larger power output requires larger and heavier motors. This makes pneumatic/hydraulic actuators a better solution. Augmentation exoskeletons, such as BLEEX, XOS, and Nurse Robot Suit are all pneumatic/hydraulic driven.

While hydraulic actuators suffer from leakage issues, pneumatic actuators can just leak to the air and inhale back with an air compressor later. The control of pneumatic actuators suffers from imprecision and low control frequency due to the compressibility of air. In addition, to achieve linear control, proportional air valves are needed, which are often expensive, inefficient, and heavy. Some researchers have used solenoid valves with high operating frequencies to reach similar control [120]. Belforte et al. [24] have applied a similar idea to their lower limb exoskeleton, but this method is still uncommon in the community.

11.6 FUTURE FOR LOWER LIMB EXOSKELETONS

Lower limb exoskeletons have shown potential in medical, industrial, and military usages. However, their practicality is still far from perfect due to operation times and difficulty in controlling the interacting force between the user and the exoskeleton.

Human–exoskeleton interaction has troubled researchers for decades. To have exoskeletons cooperate with the user, the motion profiles need to match. Nonetheless, in most cases, interaction is necessary for the exoskeleton to “feel” the user’s intention. This dilemma causes either delay or instability of the exoskeleton. Data analysis techniques have also been used to study human motion. It is believed that human joint trajectories are just combinations of a few basic patterns [93]. Yet, these basic patterns are independent from gait period, which must be estimated when implementing the controller.

In addition, undesired interaction also reduces the comfort of the user. Having additional mass or less range of motion are not only uncomfortable but also increase the metabolic cost of the user. Current improvements are mainly focusing on introducing compliance in the actuators (soft exoskeleton) and reducing weight. However, as mentioned previously, the controllability and support that these soft exoskeletons can provide are limited.

Currently, portable lower limb exoskeletons are limited by operating time. Larger energy sources (e.g., batteries) typically are accompanied by higher mass, and thus are not ideal. Energy harvesting and recycling systems may provide a solution.

Current lower limb exoskeletons still do not completely meet the desire for a machine that can cooperate with the users seamlessly. Fortunately, with the rapid developments in actuators, energy storage systems, materials, and artificial intelligence, it is only a matter of time before the dream for exoskeletons comes true.

REFERENCES

- [1] A. Esquenazi, M. Talaty, A. Jayaraman, Powered exoskeletons for walking assistance in persons with central nervous system injuries: a narrative review, *PM R* 9 (2017). Available from: <https://doi.org/10.1016/j.pmrj.2016.07.534>.
- [2] V. Lajeunesse, C. Vincent, F. Routhier, E. Careau, F. Michaud, Exoskeletons' design and usefulness evidence according to a systematic review of lower limb exoskeletons used for functional mobility by people with spinal cord injury, *Disabil. Rehabil. Assist. Technol.* 11 (2016). Available from: <https://doi.org/10.3109/17483107.2015.1080766>.
- [3] W. Huo, S. Mohammed, J.C. Moreno, Y. Amirat, Lower limb wearable robots for assistance and rehabilitation: a state of the art, *IEEE Syst. J.* 10 (2016). Available from: <https://doi.org/10.1109/JSYST.2014.2351491>.
- [4] D.R. Louie, J.J. Eng, Powered robotic exoskeletons in post-stroke rehabilitation of gait: a scoping review, *J. Neuroeng. Rehabil.* 13 (2016). Available from: <https://doi.org/10.1186/s12984-016-0162-5>.
- [5] T. Yan, M. Cempini, C.M. Oddo, N. Vitiello, Review of assistive strategies in powered lower-limb orthoses and exoskeletons, *Rob. Auton. Syst.* 64 (2015). Available from: <https://doi.org/10.1016/j.robot.2014.09.032>.
- [6] A.J. Young, D.P. Ferris, State of the art and future directions for lower limb robotic exoskeletons, *IEEE Trans. Neural. Syst. Rehabil. Eng.* 25 (2017) 171–182. Available from: <https://doi.org/10.1109/TNSRE.2016.2521160>.
- [7] K.A. Strausser, T.A. Swift, A.B. Zoss, H. Kazerooni, B.C. Bennett, Asme, mobile exoskeleton for spinal cord injury: development and testing, Amer Soc Mechanical Engineers, New York, 2012.
- [8] Ekso, n.d. <https://eksobionics.com/>.
- [9] W.Y.-W. Tung, M. McKinley, M.V. Pillai, J. Reid, H. Kazerooni, Design of a minimally actuated medical exoskeleton with mechanical swing-phase gait generation and sit-stand assistance, in: Vol. 2 Control. Monit. Energy Harvest. Vibratory Syst. Coop. Networked Control. Delay Syst. Dyn. Model. Diagnostics Biomed. Syst. Estim. Id Energy Syst. Fault Detect. Flow Therm. S, ASME, 2013, p. V002T28A004. Available from: <https://doi.org/10.1115/DSCC2013-4038>.
- [10] A. Esquenazi, M. Talaty, A. Packel, M. Saulino, The ReWalk powered exoskeleton to restore ambulatory function to individuals with thoracic-level motor-complete spinal cord injury, *Am. J. Phys. Med. Rehabil.* 91 (2012) 911–921. Available from: <https://doi.org/10.1097/PHM.0b013e318269d9a3>.
- [11] M. Talaty, A. Esquenazi, J.E. Briceño, Differentiating ability in users of the ReWalkTM powered exoskeleton: an analysis of walking kinematics, in: 2013 IEEE 13th Int. Conf. Rehabil. Robot., 2013, pp. 1–5. Available from: <https://doi.org/10.1109/ICORR.2013.6650469>.
- [12] P.D. Neuhaus, J.H. Noorden, T.J. Craig, T. Torres, J. Kirschbaum, J.E. Pratt, Design and evaluation of Mina: a robotic orthosis for paraplegics, in: 2011 IEEE Int. Conf. Rehabil. Robot., 2011, pp. 1–8. Available from: <https://doi.org/10.1109/ICORR.2011.5975468>.
- [13] Rex Bionics, REX, n.d. <https://www.rexbionics.com/>.
- [14] K. Suzuki, Y. Kawamura, T. Hayashi, T. Sakurai, Y. Hasegawa, Y. Sankai, Intention-based walking support for paraplegia patient, in: 2005 IEEE Int. Conf. Syst. Man Cybern., 2005, vol. 3, pp. 2707–2713. Available from: <https://doi.org/10.1109/ICSMC.2005.1571559>.
- [15] Y. Sankai, HAL: hybrid assistive limb based on cybernetics, in: M. Kaneko, Y. Nakamura (Eds.), *Robot. Res.*, Springer, Berlin, Heidelberg, 2011, pp. 25–34.
- [16] A. Tsukahara, Y. Hasegawa, K. Eguchi, Y. Sankai, Restoration of gait for spinal cord injury patients using HAL with intention estimator for preferable swing speed, *IEEE Trans. Neural. Syst. Rehabil. Eng.* 23 (2015). Available from: <https://doi.org/10.1109/TNSRE.2014.2364618>.
- [17] J.-Y. Jung, W. Heo, H. Yang, H. Park, A neural network-based gait phase classification method using sensors equipped on lower limb exoskeleton robots, *Sensors* 15 (2015) 27738–27759. Available from: <https://doi.org/10.3390/s151127738>.

- [18] T. Kagawa, Y. Uno, Gait pattern generation for a power-assist device of paraplegic gait, in: RO-MAN 2009 18TH IEEE Int. Symp. Robot Hum. Interact. Commun. VOLS 1 2, IEEE, 345 E 47th st, New York, NY, 2009, pp. 34–39.
- [19] T. Kagawa, Y. Uno, A human interface for stride control on a wearable robot, in: 2009 IEEE-RSJ Int. Conf. Intell. Robot. Syst., IEEE, 345 E 47th st, New York, NY, 2009, pp. 4067–4072. Available from: <https://doi.org/10.1109/IROS.2009.5353899>.
- [20] S. Wang, L. Wang, C. Meijneke, E. vanAsseldonk, T. Hoellinger, G. Cheron, et al., Design and control of the MINDWALKER exoskeleton, IEEE Trans. Neural. Syst. Rehabil. Eng. 23 (2015) 277–286. Available from: <https://doi.org/10.1109/TNSRE.2014.2365697>.
- [21] L. Wang, S. Wang, E.H.F. vanAsseldonk, H. van derKooij, Actively controlled lateral gait assistance in a lower limb exoskeleton, in: 2013 IEEE/RSJ Int. Conf. Intell. Robot. Syst., 2013, pp. 965–970. Available from: <https://doi.org/10.1109/IROS.2013.6696467>.
- [22] S. Wang, W. vanDijk, H. van derKooij, Spring uses in exoskeleton actuation design, in: 2011 IEEE Int. Conf. Rehabil. Robot., 2011, pp. 1–6. Available from: <https://doi.org/10.1109/ICORR.2011.5975471>.
- [23] F. Sylos-Labini, V. LaScaleia, A.D.’ Avella, I. Pisotta, F. Tamburella, G. Scivoletto, et al., EMG patterns during assisted walking in the exoskeleton, Front. Hum. Neurosci. 8 (2014). Available from: <https://doi.org/10.3389/fnhum.2014.00423>.
- [24] G. Belforte, L. Gastaldi, M. Sorli, Pneumatic active gait orthosis, Mechatronics. 11 (2001) 301–323. Available from: [https://doi.org/10.1016/S0957-4158\(00\)00017-9](https://doi.org/10.1016/S0957-4158(00)00017-9).
- [25] S.D., FDA approves Vanderbilt-designed Indego exoskeleton for clinical and personal use, 2016. <https://news.vanderbilt.edu/2016/03/10/fda-approves-vanderbilt-designed-indego-exoskeleton-for-clinical-and-personal-use/>.
- [26] H.A. Quintero, R.J. Farris, M. Goldfarb, Control and implementation of a powered lower limb orthosis to aid walking in paraplegic individuals, IEEE 2011 (2011) 5975481. Available from: <https://doi.org/10.1109/ICORR.2011.5975481>.
- [27] R.J. Farris, H.A. Quintero, M. Goldfarb, Performance evaluation of a lower limb exoskeleton for stair ascent and descent with Paraplegia, in: 2012 Annu. Int. Conf. IEEE Eng. Med. Biol. Soc., 2012, pp. 1908–1911. Available from: <https://doi.org/10.1109/EMBC.2012.6346326>.
- [28] T. Bacek, M. Moltedo, K. Langlois, G.A. Prieto, M.C. Sanchez-Villamañan, J. Gonzalez-Vargas, et al., BioMot exoskeleton - towards a smart wearable robot for symbiotic human-robot interaction, in: IEEE Int. Conf. Rehabil. Robot., 2017. Available from: <https://doi.org/10.1109/ICORR.2017.8009487>.
- [29] K. Kong, D. Jeon, Design and control of an exoskeleton for the elderly and patients, IEEE-ASME Trans. Mechatron. 11 (2006) 428–432. Available from: <https://doi.org/10.1109/TMECH.2006.878550>.
- [30] R. Riener, L. Lunenburger, S. Jezernik, M. Anderschitz, G. Colombo, V. Dietz, Patient-cooperative strategies for robot-aided treadmill training: first experimental results, IEEE Trans. Neural. Syst. Rehabil. Eng. 13 (2005) 380–394. Available from: <https://doi.org/10.1109/TNSRE.2005.848628>.
- [31] D. Reinkensmeyer, J.H. Wynne, S.J. Harkema, A robotic tool for studying locomotor adaptation and rehabilitation, in: Proc. Second Jt. 24th Annu. Conf. Annu. Fall Meet. Biomed. Eng. Soc. [Engineering Med. Biol., IEEE, 2002, pp. 2353–2354. Available from: <https://doi.org/10.1109/IEMBS.2002.1053318>.
- [32] J. Meuleman, E. VanAsseldonk, G. VanOort, H. Rietman, H. Van DerKooij, LOPES II - design and evaluation of an admittance controlled gait training robot with shadow-leg approach, IEEE Trans. Neural. Syst. Rehabil. Eng. 24 (2016). Available from: <https://doi.org/10.1109/TNSRE.2015.2511448>.
- [33] P. Stegall, K.N. Winfree, S.K. Agrawal, Degrees-of-freedom of a robotic exoskeleton and human adaptation to new gait templates, in: 2012 IEEE Int. Conf. Robot. Autom., 2012, pp. 4986–4991. Available from: <https://doi.org/10.1109/ICRA.2012.6225092>.
- [34] D. Zanotto, P. Stegall, S.K. Agrawal, ALEX III: a novel robotic platform with 12 DOFs for human gait training, in: 2013 IEEE Int. Conf. Robot. Autom., 2013, pp. 3914–3919. Available from: <https://doi.org/10.1109/ICRA.2013.6631128>.

- [35] K.N. Winfree, P. Stegall, S.K. Agrawal, Design of a minimally constraining, passively supported gait training exoskeleton: ALEX II, IEEE Int. Conf. Rehabil. Robot (2011) 1–6. Available from: <https://doi.org/10.1109/ICORR.2011.5975499>.
- [36] T. Lenzi, M.C. Carrozza, S.K. Agrawal, Powered hip exoskeletons can reduce the user's hip and ankle muscle activations during walking, IEEE Trans. Neural. Syst. Rehabil. Eng. 21 (2013) 938–948. Available from: <https://doi.org/10.1109/TNSRE.2013.2248749>.
- [37] D. Aoyagi, W.E. Ichinose, S.J. Harkema, D.J. Reinkensmeyer, J.E. Bobrow, An assistive robotic device that can synchronize to the pelvic motion during human gait training, in: Proc. 2005 IEEE 9th Int. Conf. Rehabil. Robot., 2005, pp. 565–568. Available from: <https://doi.org/10.1109/ICORR.2005.1502026>.
- [38] V. Grosu, C. Rodriguez-Guerrero, S. Grosu, B. Vanderborght, D. Lefeber, Design of smart modular variable stiffness actuators for robotic-assistive devices, IEEE/ASME Trans. Mechatron. 22 (2017) 1777–1785. Available from: <https://doi.org/10.1109/TMECH.2017.2704665>.
- [39] S.H. Hyon, T. Hayashi, A. Yagi, T. Noda, J. Morimoto, Design of hybrid drive exoskeleton robot XoR2, IEEE Int. Conf. Intell. Robot. Syst. (2013) 4642–4648. Available from: <https://doi.org/10.1109/IROS.2013.6697024>.
- [40] S.-H. Hyon, J. Morimoto, T. Matsubara, T. Noda, M. Kawato, XoR: hybrid drive exoskeleton robot that can balance, in: 2011 IEEE/RSJ Int. Conf. Intell. Robot. Syst., IEEE, 2011, pp. 3975–3981. Available from: <https://doi.org/10.1109/IROS.2011.6095079>.
- [41] M. Bortole, A. Venkatakrishnan, F. Zhu, J.C. Moreno, G.E. Francisco, J.L. Pons, et al., The H2 robotic exoskeleton for gait rehabilitation after stroke: early findings from a clinical study, J. Neuroeng. Rehabil. 12 (2015) 54. Available from: <https://doi.org/10.1186/s12984-015-0048-y>.
- [42] O. Jansen, D. Grasmuecke, R.C. Meindl, M. Tegenthoff, P. Schwenkreis, M. Sczesny-Kaiser, et al., Hybrid assistive limb exoskeleton HAL in the rehabilitation of chronic spinal cord injury: proof of concept; the results in 21 patients, WORLD Neurosurg. 110 (2018) E73–E78. Available from: <https://doi.org/10.1016/j.wneu.2017.10.080>.
- [43] S. Suzuki, Y. Hirata, K. Kosuge, Walking support by wearable system based on the spring-mass model, IEEE/ASME Int. Conf. Adv. Intell. Mechatronics, AIM (2014) 285–290. Available from: <https://doi.org/10.1109/AIM.2014.6878093>.
- [44] C. Buesing, G. Fisch, M.O.' Donnell, I. Shahidi, L. Thomas, C.K. Mummidisetti, et al., Effects of a wearable exoskeleton stride management assist system (SMA®) on spatiotemporal gait characteristics in individuals after stroke: a randomized controlled trial, J. Neuroeng. Rehabil. 12 (2015) 69. Available from: <https://doi.org/10.1186/s12984-015-0062-0>.
- [45] K.H. Ha, S.A. Murray, M. Goldfarb, An approach for the cooperative control of FES with a powered exoskeleton during level walking for persons with paraplegia, IEEE Trans. Neural. Syst. Rehabil. Eng. 24 (2016). Available from: <https://doi.org/10.1109/TNSRE.2015.2421052>.
- [46] K. Yamamoto, K. Hyodo, M. Ishii, T. Matsuo, Development of power assisting suit for assisting nurse labor, JSME Int. J. Ser. C Mech. Syst. Mach. Elec. Manuf. 45 (2002) 703–711. Available from: <https://doi.org/10.1299/jsmec.45.703>.
- [47] K. Yamamoto, M. Ishii, K. Hyodo, T. Yoshimitsu, T. Matsuo, Development of power assisting suit (miniaturization of supply system to realize wearable suit), JSME Int. J. Ser. C. 46 (2003) 923–930. Available from: <https://doi.org/10.1299/jsmec.46.923>.
- [48] K. Yamamoto, M. Ishii, H. Noborisaka, K. Hyodo, Stand alone wearable power assisting suit - sensing and control systems, in: RO-MAN 2004. 13th IEEE Int. Work. Robot Hum. Interact. Commun. (IEEE Cat. No.04TH8759), 2004, pp. 661–666. Available from: <https://doi.org/10.1109/ROMAN.2004.1374841>.
- [49] H. Kawamoto, Suwoong Lee, S. Kanbe, Y. Sankai, Power assist method for HAL-3 using EMG-based feedback controller (2004) 1648–1653. Available from: <https://doi.org/10.1109/icsmc.2003.1244649>.

- [50] C.J. Walsh, K.E.N. Endo, H. Herr, A. Quasi-Passive, LEG exoskeleton for load-carrying augmentation, *Int. J. Humanoid Robot.* 04 (2007) 487–506. Available from: <https://doi.org/10.1142/S0219843607001126>.
- [51] C.J. Walsh, K. Pasch, H. Herr, An autonomous, underactuated exoskeleton for load- carrying augmentation, *IEEE Int. Conf. Intell. Robot. Syst.* (2006) 1410–1415. IEEE Press.
- [52] C.J. Walsh, D. Paluska, K. Pasch, W. Grand, A. Valiente, H. Herr, Development of a lightweight, underactuated exoskeleton for load-carrying augmentation, *Proc. IEEE Int. Conf. Robot. Autom.* 2006 (2006) 3485–3491. Available from: <https://doi.org/10.1109/ROBOT.2006.1642234>.
- [53] H. Kazerooni, A. Chu, R. Steger, That which does not stabilize, will only make us stronger, *Int. J. Rob. Res.* 26 (2007) 75–89. Available from: <https://doi.org/10.1177/0278364907074472>.
- [54] S. Jacobsen, On the development of XOS, a powerful exoskeletal robot, in: *Proc. IEEE/RSJ Int. Conf. Intell. Robot. Syst.* San Diego, CA, 2007. <http://ci.nii.ac.jp/naid/20000716738/en/> (accessed 20.03.19.).
- [55] M. Fontana, R. Vertechy, S. Marcheschi, F. Salsedo, M. Bergamasco, The body extender: a full-body exoskeleton for the transport and handling of heavy loads, *IEEE Robot. Autom. Mag.* 21 (2014) 34–44. Available from: <https://doi.org/10.1109/MRA.2014.2360287>.
- [56] Creating a future together with our customers — the development of activelink’s power assist suit, 2016. <https://news.panasonic.com/global/stories/2016/45161.html>.
- [57] S. Goemaere, M. VanLaere, P. DeNeve, J.M. Kaufman, Bone mineral status in paraplegic patients who do or do not perform standing, *Osteoporos. Int.* 4 (1994) 138–143.
- [58] T. Sumiya, K. Kawamura, A. Tokuhiro, H. Takechi, H. Ogata, A survey of wheelchair use by paraplegic individuals in Japan. Part 2: prevalence of pressure sores, *Spinal Cord* 35 (1997) 595.
- [59] Y. Mori, J. Okada, K. Takayama, Development of a standing style transfer system “ABLE” for disabled lower limbs, *IEEE/ASME Trans. Mechatron.* 11 (2006) 372–380. Available from: <https://doi.org/10.1109/TMECH.2006.878558>.
- [60] C.L. Dembia, A. Silder, T.K. Uchida, J.L. Hicks, S.L. Delp, Simulating ideal assistive devices to reduce the metabolic cost of walking with heavy loads, *PLoS. One* 12 (2017). Available from: <https://doi.org/10.1371/journal.pone.0180320>.
- [61] K.A. Witte, J. Zhang, R.W. Jackson, S.H. Collins, Design of Two Lightweight, High-Bandwidth Torque-Controlled Ankle Exoskeletons, in: 2015 IEEE Int. Conf. Robot. Autom., 2015, pp. 1223–1228.
- [62] J.R. Koller, C. David Remy, D.P. Ferris, Comparing neural control and mechanically intrinsic control of powered ankle exoskeletons, in: *IEEE Int. Conf. Rehabil. Robot.*, 2017. Available from: <https://doi.org/10.1109/ICORR.2017.8009262>.
- [63] D.A. Winter, Human balance and posture control during standing and walking, *Gait. Posture* 3 (1995) 193–214. Available from: [https://doi.org/10.1016/0966-6362\(96\)82849-9](https://doi.org/10.1016/0966-6362(96)82849-9).
- [64] S.Collins, A.Ruina, R.Tedrake, M.Wisse, Efficient bipedal robots based on passive-dynamic walkers, *Science* (80-.). 307 (2005) 1082–1085. Available from: <https://doi.org/10.1126/science.1107799>.
- [65] T. McGeer, Passive dynamic walking, *Int. J. Rob. Res.* 9 (1990) 62–82. Available from: <https://doi.org/10.1177/027836499000900206>.
- [66] K. Junius, B. Brackx, V. Grosu, H. Cuypers, J. Geeroms, M. Molledo, et al., Mechatronic design of a sit-to-stance exoskeleton, in: 5th IEEE RAS/EMBS Int. Conf. Biomed. Robot. Biomechatronics, 2014, pp. 945–950. Available from: <https://doi.org/10.1109/BIOROB.2014.6913902>.
- [67] M.K. Shepherd, E.J. Rouse, Design and validation of a torque-controllable knee exoskeleton for sit-to-stand assistance, *IEEE/ASME Trans. Mechatron.* 22 (2017). Available from: <https://doi.org/10.1109/TMECH.2017.2704521>.
- [68] W.Y.W. Tung, M. McKinley, M. VPillai, J. Reid, H. Kazerooni, Design of a minimally actuated medical exoskeleton with mechanical swing-phase gait generation and sit-stand assistance, *Mech. Eng.* 136 (2014) 68–71.

- [69] S. Federici, F. Meloni, M. Bracalenti, M.L. DeFilippis, The effectiveness of powered, active lower limb exoskeletons in neurorehabilitation: a systematic review, *NeuroRehabilitation*. 37 (2015). Available from: <https://doi.org/10.3233/NRE-151265>.
- [70] C. Calautti, J.-C. Baron, Functional neuroimaging studies of motor recovery after stroke in adults, *Stroke* 34 (2003) 1553–1566. Available from: <https://doi.org/10.1161/01.STR.0000071761.36075.A6>.
- [71] R.J. Nudo, E.J. Plautz, S.B. Frost, Role of adaptive plasticity in recovery of function after damage to motor cortex, *Muscle Nerve* 24 (2001) 1000–1019. Available from: <https://doi.org/10.1002/mus.1104>.
- [72] A. Pennycott, D. Wyss, H. Vallery, V. Klamroth-Marganska, R. Riener, Towards more effective robotic gait training for stroke rehabilitation: a review, *J. Neuroeng. Rehabil.* 9 (2012) 65. Available from: <https://doi.org/10.1186/1743-0003-9-65>.
- [73] L. Finch, H. Barbeau, B. Arsenault, Influence of body weight support on normal human gait: development of a gait retraining strategy, *Phys. Ther.* 71 (1991) 842–855. Available from: <https://doi.org/10.1093/ptj/71.11.842>.
- [74] A. Wernig, S. Müller, Laufband locomotion with body weight support improved walking in persons with severe spinal cord injuries, *Spinal Cord* 30 (1992) 229–238. Available from: <https://doi.org/10.1038/sc.1992.61>.
- [75] S. Hesse, C. Bertelt, M.T. Jahnke, A. Schaffrin, P. Baake, M. Malezic, et al., Treadmill training with partial body weight support compared with physiotherapy in nonambulatory hemiparetic patients, *Stroke* 26 (1995) 976–981. Available from: <https://doi.org/10.1161/01.STR.26.6.976>.
- [76] R.S. Goncalves, H.I. Krebs, MIT-Skywalker: considerations on the design of a body weight support system, *J. Neuroeng. Rehabil.* 14 (2017). Available from: <https://doi.org/10.1186/s12984-017-0302-6>.
- [77] T. Susko, K. Swaminathan, H.I. Krebs, MIT-Skywalker: a novel gait neurorehabilitation robot for stroke and cerebral palsy, *IEEE Trans. Neural. Syst. Rehabil. Eng.* 24 (2016) 1089–1099. Available from: <https://doi.org/10.1109/TNSRE.2016.2533492>.
- [78] AlterG®Anti-Gravity Treadmill™ for Rehab & Training, n.d. <https://www.alterg.com/>.
- [79] H. Schmidt, S. Hesse, R. Bernhardt, J. Krüger, HapticWalker - a novel haptic foot device, *ACM. Trans. Appl. Percept.* 2 (2005) 166–180. Available from: <https://doi.org/10.1145/1060581.1060589>.
- [80] H. Yano, S. Tamefusa, N. Tanaka, H. Saitou, H. Iwata, Gait rehabilitation system for stair climbing and descending, in: 2010 IEEE Haptics Symp. HAPTICS 2010, 2010, pp. 393–400. Available from: <https://doi.org/10.1109/HAPTIC.2010.5444627>.
- [81] S. Freivogel, J. Mehrholz, T. Husak-Sotomayor, D. Schmalohr, Gait training with the newly developed 'LokoHelp'-system is feasible for non-ambulatory patients after stroke, spinal cord and brain injury. A feasibility study, *Brain. Inj.* 22 (2008) 625–632. Available from: <https://doi.org/10.1080/02699050801941771>.
- [82] M. Wirz, D.H. Zemon, R. Rupp, A. Scheel, G. Colombo, V. Dietz, et al., Effectiveness of automated locomotor training in patients with chronic incomplete spinal cord injury: a multicenter trial, *Arch. Phys. Med. Rehabil.* 86 (2005) 672–680. Available from: <https://doi.org/10.1016/J.APMR.2004.08.004>.
- [83] A. Duschau-Wicke, Jv onZitzewitz, A. Caprez, L. Lunenburger, R. Riener, Path control: a method for patient-cooperative robot-aided gait rehabilitation, *IEEE Trans. Neural. Syst. Rehabil. Eng.* 18 (2010) 38–48. Available from: <https://doi.org/10.1109/TNSRE.2009.2033061>.
- [84] A. Duschau-Wicke, A. Caprez, R. Riener, Patient-cooperative control increases active participation of individuals with SCI during robot-aided gait training, *J. Neuroeng. Rehabil.* 7 (2010). Available from: <https://doi.org/10.1186/1743-0003-7-43>.
- [85] J. Mehrholz, S. Thomas, B. Elsner, Treadmill training and body weight support for walking after stroke, *Cochrane Database Syst. Rev.* (2017). Available from: <https://doi.org/10.1002/14651858.CD002840.pub4>.
- [86] S.R. Chang, M.J. Nandor, L. Li, R. Kobetic, K.M. Foglyano, J.R. Schnellenberger, et al., A muscle-driven approach to restore stepping with an exoskeleton for individuals with paraplegia, *J. Neuroeng. Rehabil.* 14 (2017) 48. Available from: <https://doi.org/10.1186/s12984-017-0258-6>.

- [87] A.J. del-Ama, A.D. Koutsou, J.C. Moreno, A. de-los-Reyes, A. Gil-Agudo, J.L. Pons, Review of hybrid exoskeletons to restore gait following spinal cord injury, *J. Rehabil. Res. Dev.* 49 (2012) 497–514. Available from: <http://www.ncbi.nlm.nih.gov/pubmed/22773254>.
- [88] R. Steger, S.H. Kim, H. Kazerooni, IEEE, Control scheme and networked control architecture for the Berkeley Lower Extremity Exoskeleton (BLEEX), in: 2006 IEEE Int. Conf. Robot. Autom., 2006, pp. 3469–3476.
- [89] H. Kazerooni, R. Steger, L.H. Huang, Hybrid control of the Berkeley Lower Extremity Exoskeleton (BLEEX), *Int. J. Rob. Res.* 25 (2006) 561–573. Available from: <https://doi.org/10.1177/0278364906065505>.
- [90] A.B. Zoss, H. Kazerooni, A. Chu, Biomechanical design of the Berkeley lower extremity exoskeleton (BLEEX), *IEEE/ASME Trans. Mechatron.* 11 (2006) 128–138. Available from: <https://doi.org/10.1109/TMECH.2006.871087>.
- [91] D.P. Ferris, G.S. Sawicki, M.A. Daley, A physiologist’s perspective on robotic exoskeletons for human locomotion, *Int. J. Humanoid Robot.* 04 (2007) 507–528. Available from: <https://doi.org/10.1142/S0219843607001138>.
- [92] L.Bokman, R.Syungkwon, F.C.Park, Movement primitives, principal component analysis, and the efficient generation of natural motions, in: Proc. 2005 IEEE Int. Conf. Robot. Autom., 2005, pp. 4630–4635. Available from: <https://doi.org/10.1109/ROBOT.2005.1570834>.
- [93] B. Lim, K. Kim, J. Lee, J. Jang, Y. Shim, IEEE, An event-driven control to achieve adaptive walking assist with gait primitives, in: 2015 IEEE/RSJ Int. Conf. Intell. Robot. Syst., 2015, pp. 5870–5875.
- [94] P.R. Cavanagh, P.V. Komi, Electromechanical delay in human skeletal muscle under concentric and eccentric contractions, *Eur. J. Appl. Physiol. Occup. Physiol.* 42 (1979) 159–163. Available from: <https://doi.org/10.1007/BF00431022>.
- [95] H. Geyer, A. Seyfarth, R. Blickhan, Compliant leg behaviour explains basic dynamics of walking and running, *Proc. R. Soc. B Biol. Sci.* 273 (2006) 2861–2867. Available from: <https://doi.org/10.1098/rspb.2006.3637>.
- [96] C.L. Lewis, D.P. Ferris, Invariant hip moment pattern while walking with a robotic hip exoskeleton, *J. Biomech.* 44 (2011) 789–793. Available from: <https://doi.org/10.1016/J.JBIOMECH.2011.01.030>.
- [97] P.C. Kao, C.L. Lewis, D.P. Ferris, Invariant ankle moment patterns when walking with and without a robotic ankle exoskeleton, *J. Biomech.* 43 (2010) 203–209. Available from: <https://doi.org/10.1016/j.jbiomech.2009.09.030>.
- [98] S.H. Collins, A. Ruina, A bipedal walking robot with efficient and human-like gait, in: Proc. 2005 IEEE Int. Conf. Robot. Autom., 2005, pp. 1983–1988. Available from: <https://doi.org/10.1109/ROBOT.2005.1570404>.
- [99] J.M. Donelan, R. Kram, A.D. Kuo, Mechanical work for step-to-step transitions is a major determinant of the metabolic cost of human walking, *J. Exp. Biol.* 205 (2002) 3717 LP –3727. <http://jeb.biologists.org/content/205/23/3717.abstract>.
- [100] J.A. Norris, K.P. Granata, M.R. Mitros, E.M. Byrne, A.P. Marsh, Effect of augmented plantarflexion power on preferred walking speed and economy in young and older adults, *Gait. Posture* 25 (2007) 620–627. Available from: <https://doi.org/10.1016/J.GAITPOST.2006.07.002>.
- [101] G.S. Sawicki, D.P. Ferris, Mechanics and energetics of level walking with powered ankle exoskeletons, *J. Exp. Biol.* 211 (2008) 1402–1413. Available from: <https://doi.org/10.1242/jeb.009241>.
- [102] G.S. Sawicki, D.P. Ferris, Powered ankle exoskeletons reveal the metabolic cost of plantar flexor mechanical work during walking with longer steps at constant step frequency, *J. Exp. Biol.* 212 (2009) 21–31. Available from: <https://doi.org/10.1242/jeb.017269>.
- [103] A. Gams, T. Petric, T. Debevec, J. Babic, Effects of robotic knee-exoskeleton on human energy expenditure, *IEEE. Trans. Biomed. Eng.* 60 (2013) 1–9. Available from: <https://doi.org/10.1109/TBME.2013.2240682>.

- [104] K. Seo, J. Lee, Y. Lee, T. Ha, Y. Shim, Fully autonomous hip exoskeleton saves metabolic cost of walking, in: A. Okamura, A. Menciassi, A. Ude, D. Burschka, D. Lee, F. Arrichiello, H. Liu, H. Moon, J. Neira, K. Sycara, K. Yokoi, P. Martinet, P. Oh, P. Valdastri, V. Krovi (Eds.), 2016 IEEE Int. Conf. Robot. Autom., 2016, pp. 4628–4635.
- [105] A.T. Asbeck, K. Schmidt, I. Galiana, D. Wagner, C.J. Walsh, Multi-joint soft exosuit for gait assistance, in: Proc. - IEEE Int. Conf. Robot. Autom., 2015. Available from: <https://doi.org/10.1109/ICRA.2015.7140069>.
- [106] A.T. Asbeck, S.M.M. DeRossi, I. Galiana, Y. Ding, C.J. Walsh, Stronger, smarter, softer: next-generation wearable robots, IEEE Robot. Autom. Mag. 21 (2014). Available from: <https://doi.org/10.1109/MRA.2014.2360283>.
- [107] Y. Ding, F.A. Panizzolo, C. Siviy, P. Malcolm, I. Galiana, K.G. Holt, et al., Effect of timing of hip extension assistance during loaded walking with a soft exosuit, J. Neuroeng. Rehabil. 13 (2016). Available from: <https://doi.org/10.1186/s12984-016-0196-8>.
- [108] T.F. Novacheck, The biomechanics of running, Gait. Posture 7 (1998) 77–95. Available from: [https://doi.org/10.1016/S0966-6362\(97\)00038-6](https://doi.org/10.1016/S0966-6362(97)00038-6).
- [109] R. Alo, F. Bottiglione, G. Mantriota, Artificial knee joints actuators with energy recovery capabilities: a comparison of performance, J. Robot (2016). Available from: <https://doi.org/10.1155/2016/4802474>.
- [110] R. Chin, E.T. Hsiao-Wecksler, E. Loth, Fluid-power harvesting by under-foot bellows during human gait, J. Fluids Eng. Asme. 134 (2012) 7. Available from: <https://doi.org/10.1115/1.4005725>.
- [111] R. Riemer, A. Shapiro, Biomechanical energy harvesting from human motion: theory, state of the art, design guidelines, and future directions, J. Neuroeng. Rehabil. 8 (2011) 22. Available from: <https://doi.org/10.1186/1743-0003-8-22>.
- [112] P. Malcolm, W. Derave, S. Galle, D. DeClercq, A simple exoskeleton that assists plantarflexion can reduce the metabolic cost of human walking, PLoS. One 8 (2013) e56137. Available from: <https://doi.org/10.1371/journal.pone.0056137>.
- [113] A.M. Oymagil, J.K. Hitt, T. Sugar, J. Fleeger, Control of a regenerative braking powered ankle foot orthosis, in: 2007 IEEE 10th Int. Conf. Rehabil. Robot., 2007, pp. 28–34. Available from: <https://doi.org/10.1109/ICORR.2007.4428402>.
- [114] S.H. Collins, M.B. Wiggin, G.S. Sawicki, Reducing the energy cost of human walking using an unpowered exoskeleton, Nature 522 (2015) 212. Available from: <https://doi.org/10.1038/nature14288>.
- [115] E. Rogers, P. Polygerinos, S. Allen, F.A. Panizzolo, C.J. Walsh, D.P. Holland, A quasi-passive knee exoskeleton to assist during descent, in: J. GonzalezVargas, J. Ibanez, J.L. Contreras Vidal, H. Van Der Kooij, J.L. Pons (Eds.), Wearable Robot. Challenges Trends, 2017, pp. 63–67. Available from: https://doi.org/10.1007/978-3-319-46532-6_11.
- [116] Y. Yamada, G. Endo, E.F. Fukushima, Pneumatic walking assistive device for use over long period, Adv. Robot. 28 (2014) 1253–1264. Available from: <https://doi.org/10.1080/01691864.2014.920722>.
- [117] L. Flynn, J. Geeroms, R. Jimenez-Fabian, B. Vanderborght, N. Vitiello, D. Lefeber, Ankle–knee prosthesis with active ankle and energy transfer: development of the CYBERLEGs Alpha-Prosthesis, Rob. Auton. Syst. 73 (2015) 4–15. Available from: <https://doi.org/10.1016/j.robot.2014.12.013>.
- [118] A.J. van denBogert, Exotendons for assistance of human locomotion, Biomed. Eng. Online. 2 (2003) 17. Available from: <https://doi.org/10.1186/1475-925X-2-17>.
- [119] W. vanDijk, H. VanderKooij, XPED2: a passive exoskeleton with artificial tendons, IEEE Robot. Autom. Mag. 21 (2014) 56–61. Available from: <https://doi.org/10.1109/MRA.2014.2360309>.
- [120] A. Messina, N.I. Giannoccaro, A. Gentile, Experimenting and modelling the dynamics of pneumatic actuators controlled by the pulse width modulation (PWM) technique, Mechatronics 15 (2005) 859–881. Available from: <https://doi.org/10.1016/J.MECHATRONICS.2005.01.003>.

WALKON SUIT: A MEDALIST IN THE POWERED EXOSKELETON RACE OF CYBATHLON 2016

12

Jungsu Choi¹ and Kyoungchul Kong²

¹*The Department of Robotics Engineering, Yeungnam University, Gyeongbuk, Korea* ²*The Department of Mechanical Engineering, Korea Advanced Institute of Science and Technology, Daejeon, Korea*

12.1 INTRODUCTION

Spinal cord injury (SCI) can be caused by various accidents and diseases such as traffic accidents, fall-down injury, tumor, myelitis, etc. [1]. Advances in the medical care of patients with SCI have significantly reduced the mortality rate and improved the life expectancy [2,3]. Nevertheless, the SCI patients still suffer from the side effects of sitting for a long-term period, which frequently causes serious damage to the skin, the digestive system, etc. In many aspects, walking is not only a necessary movement for daily living activities, but also an essential exercise for paraplegics to maintain their health condition.

Powered exoskeletons for paraplegics have been studied in academia and even commercialized by several companies, such as ReWalk Robotics [4–6], Ekso Bionics [7], Rex Bionics [8], Parker Hannifin [9]. It still, however, may not be an easy decision for customers to purchase a powered exoskeleton, not only because of its high price, but also due to its limited functionality for assisting activities in daily lives. The powered exoskeleton race in the Cybathlon 2016 [10] directly tackled this question; it asked researchers and engineers to develop the necessary functions for powered exoskeletons to assist the activities in daily lives, such as sitting down and standing up from a sofa, walking through a slalom, passing on a ramp and opening a door, walking on randomly-positioned stones, walking on a tilted path, and ascending and descending six stairs.

In this article, a powered exoskeleton that won the Bronze medal in the Cybathlon 2016, called WalkON Suit, shown in Fig. 12.1, is introduced. The WalkON Suit was developed based on several special technologies, such as a hybrid actuation mechanism, a biarticular transmission system, distributed batteries, and distributed actuators, which made the WalkON Suit powerful and unique. In addition to the technical aspects of the WalkON Suit, this article also introduces the training procedure throughout the preparation for participating in the Cybathlon 2016.

**FIGURE 12.1**

A pilot wearing the WalkON Suit. Since 1998 when he became completely paraplegic, he has sat on a wheelchair. After almost 20 years, he stood up with his legs with the help of a powered exoskeleton and won a bronze medal in the Cybathlon 2016.

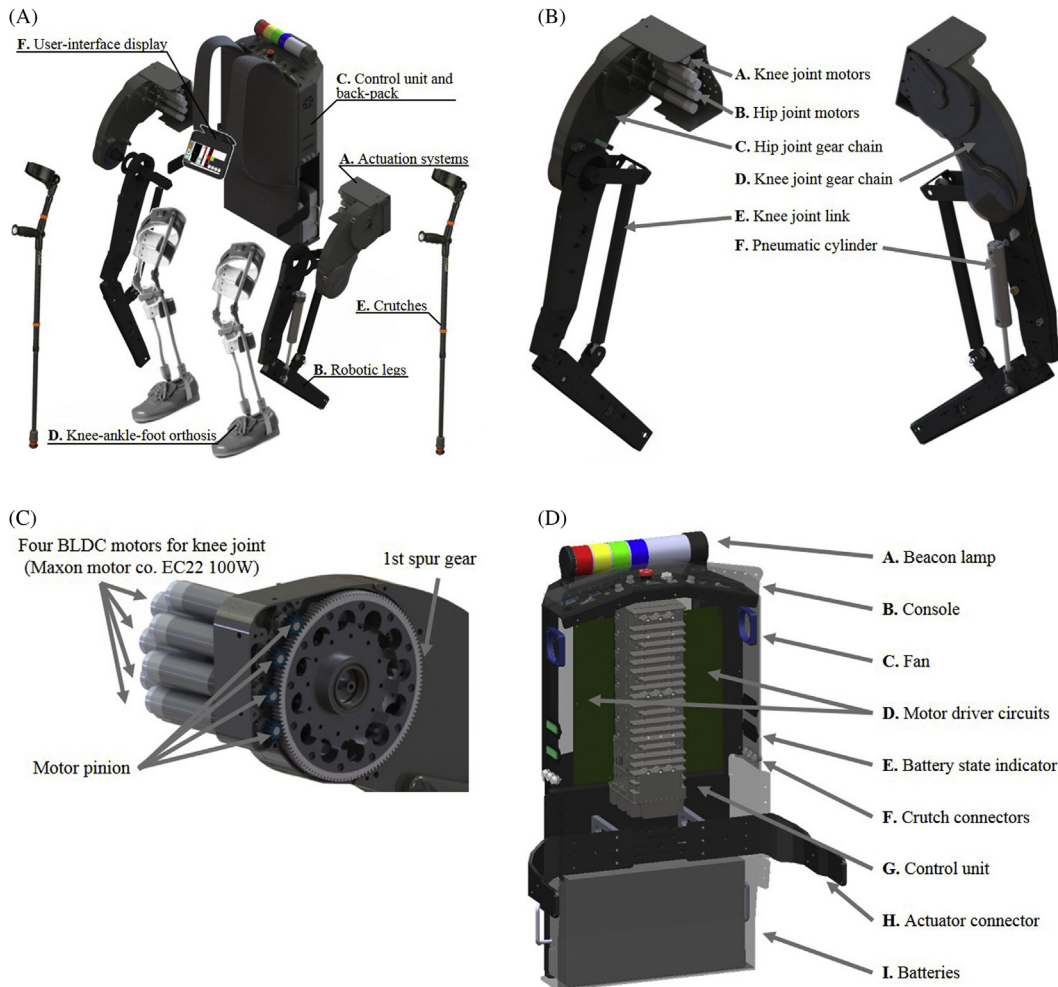
12.2 DESIGN OF WALKON SUIT

12.2.1 OVERALL CONFIGURATION

The WalkON Suit system consists of a pair of actuation systems, a pair of robotic legs, a backpack that includes a control unit, circuits, and batteries, a pair of crutches, and a user display, as shown in Fig. 12.2. Table 12.1 shows the specification of the WalkON Suit.

12.2.2 ACTUATION SYSTEMS

The requirements of the actuation systems were determined based on the power requirement of a sit-to-stand motion. Several clinical studies reported that the required knee extensor and hip extensor torques are at most 1.170 and 0.914 Nm/kg, respectively [11,12]. These normalized values in the previous study were converted into the absolute values by multiplying the weight of the pilot and the WalkON Suit. Since the weights of the pilot and the WalkON Suit are 75 and 27 kg, respectively, the required knee assist torque is at least 120 Nm and hip assist torque is 94 Nm. In addition, the efficiency of the gear transmission is assumed as 60%. From these data the

**FIGURE 12.2**

Design of WalkON Suit; (A) the overall configuration, (B) the robotic legs and actuation systems, (C) synchronization of the four motors, and (D) the backpack.

specification of the WalkON Suit was set as shown in Table 12.1. Note that the peak torque value was calculated from the stall torque of each motor, specified in the specification of the motor.

The biggest challenge was that the Cybathlon requested appropriate solutions to safety issues based on ISO13482-2014, “Robot and robotic devices – Safety requirements for personal care robot” [13], and ISO22523-2011 “External limb prostheses and external orthoses – Requirements and test methods” [14]. It took more than a month to seek solutions for reducing the risk factors in the WalkON Suit.

Table 12.1 Mechanical Specification of WalkON Suit

Specification	WalkON Suit	
Dimension (mm)	Height	1400
	Width	550
	Depth	350
Weight (kg)	27	
Degree of freedom	Active	4
	Passive	2
Torque (Nm) (continuous)	Hip	172
	Knee	168
Torque (Nm) (Peak)	Hip	740
	Knee	720
Speed (RPM)	Hip	33
	Knee	34
Range of motion (deg.)	Hip	−30 to 120
	Knee	0–115
	Ankle	−20 to 20

Among many risk management strategies in the WalkON Suit, one of the most successful methods was the synchronous actuation module, shown in Fig. 12.2C. Four electric motors were used for actuation of each joint, which were not only for obtaining a large actuation force, but also for reducing the risk of motor failure. For the synchronization of multiple motors, one motor was controlled in a position mode with high controller gains, and the other motors were controlled in a current (torque) mode, as in [15]. A brushless direct current (BLDC) motor manufactured by Maxon Motor Company, EC22, with a maximum speed of 29,900 revolutions per minute (RPM); 100 W rated power, and a continuous torque of 0.05 Nm, and a stall torque of 0.857 Nm, was used as a subactuator. The motors were used in combination with gears to generate the large assistive joint torques, as in Table 12.1.

12.2.3 ROBOTIC LEGS

While the hip joints were directly actuated by the BLDC motors except the gears for torque amplification, the knee joints were actuated through a linkage mechanism as shown in Fig. 12.2B. Since the linkage was connected between the trunk (i.e., the backpack) and the shank upright, the knee joint was biarticularly actuated by the motors. The biarticular mechanism showed a great advantage in the torque to force transformation efficiency [16]. Namely, compared with monoarticular mechanisms, which are typical robotic joint mechanisms, the biarticular mechanisms could generate larger end-effector forces with less motor torque in particular motions. Therefore the biarticular mechanism greatly contributed to the improvement of overall power efficiency [17].

12.2.4 CONTROL UNIT AND BACKPACK

The backpack was a main control unit, which included a CompactRIO, cRIO-9038, manufactured by National Instruments. The cRIO-9038 is an extremely powerful computing device that has a 1.33 GHz dual-core Intel Atom processor, 8 GB nonvolatile storage, 2 GB DDR3 memory, and Xilinx Kintex-7 160 T FPGA. The large computation capability of the CompactRIO and the great performance of the FPGA system enabled accurate control of the motions of the WalkON Suit.

The WalkON Suit is powered by four separated batteries; two batteries with the nominal voltage of 11.1 V are for the CompactRIO, while the other two batteries with the nominal voltage of 44.4 V are for actuation powers of the left and right legs, respectively. When the batteries are fully charged, their maximum voltages are 12.6 V and 49.8 V, respectively. The batteries are strictly isolated from each other, such that even if one of the batteries is deeply discharged due to any accidental situation, the remaining parts remain functional. All the batteries are made of Lithium-Polymer cells, and battery management circuits are embedded in the battery packs.

12.2.5 CRUTCHES

Crutches were utilized for the pilot to maintain the overall body balance. In addition, the pilot controlled the WalkON Suit using switches on the crutches. While the left crutch has no switch, the right crutch has two button switches at the handles. This is because the pilot has to hold the guard-rail with his left hand in the stairs and ramp tasks. The functions of the two buttons on the right crutch include:

- a STOP button: Locomotion-phase Stop
- a START button: Locomotion-phase Start, Locomotion-phase Change, Task Change, and Shutdown

The crutch handles and the forearm holders are covered by soft materials to minimize pressure sores on the palm and related injuries.

12.2.6 USER DISPLAY

The Mini DisplayPort of cRIO-9038 made it possible to provide the pilot with a graphical user interface without any other peripherals; through a small monitor installed on stomach straps, the pilot could monitor the control status of the WalkON Suit.

12.3 SENSOR SYSTEM

The sensor system of the WalkON Suit was developed to measure the trunk inclination, the joint angle, and the ground contact.

The inertial measurement unit (IMU) was used to measure the trunk inclination for the safety of the pilot. A three-axis accelerometer, a three-axis gyroscope and a three-axis magnetometer were embedded in IMU. An abnormal trunk inclination of the pilot is defined according to the trunk inclination angle. In the case of the WalkON Suit, the continuous unintended trunk inclination of

Table 12.2 Encoders of the WalkON Suit

Name	Type	Resolution	Max. Speed (RPM)	Output Data
MR 22	Incremental	128 cpr	37,500	A, B, A-, B-
RMB30SC	Absolute	13 bit	2500	RS422A

10 degrees or more is defined as the abnormal trunk inclination of the pilot. When the abnormal trunk inclination of the pilot is measured by the IMU, an automatic fault detection algorithm in the main control program detects the risk and provides a management plan. The detailed explanations of the automatic fault detection algorithm and the management plan are described in Section 12.5.2.

The joint angles of the WalkON Suit were measured by the absolute encoder and the incremental encoder, as shown in [Table 12.2](#). The absolute encoder could measure the absolute joint angle of the WalkON Suit with 13 bit resolution. The resolution of the absolute encoder, however, was not sufficient for precise control of the joints of the WalkON Suit. Therefore additional incremental encoders with high resolution were applied to the motors. Since the incremental encoders could not measure the absolute angle, the incremental encoders were initialized by the absolute angle measured by the absolute encoder at the initial state.

The Smart Shoes system was utilized to determine the ground contact. The Smart Shoes system consisted of a silicon tube and differential air pressure sensors. The information of the ground contact was used to distinguish the gait phase, that is, the stance and swing.

12.4 HUMAN FACTORS

12.4.1 PILOT

At initial evaluation for admission to Cybathlon, bone mineral density was within normal limits (*t*-score of femoral neck is 2.6, L1 2.7, L2 2.6, and L3 3.1) and T10-L1 spine was stably fixated on radiographic examination. However, the range of motion (RoM) of his knee joints was limited because he has used a wheelchair for about 20 years. The X-ray picture in [Fig. 12.3A](#) clearly shows the contracture of his knee joints. This can be mathematically modeled as

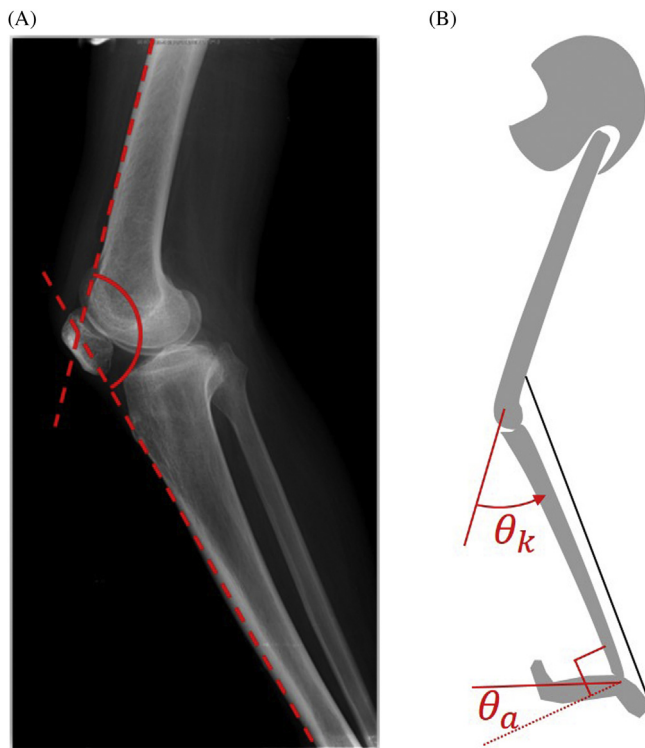
$$0 < \underline{\theta}_k < \theta_k(t) < \overline{\theta}_k \quad (12.1)$$

where $\theta_k(t)$ is the knee joint angle, and $\underline{\theta}_k$ and $\overline{\theta}_k$ are the lower and upper bounds of the knee joint angle, respectively.

In addition to the knee joint contracture, the RoM of his ankle joint was also limited. Unlike the knee joint, the characteristics of the RoM of the ankle joints were complicated, because the contracture resulted from the stiffened gastrocnemius muscle, which is biarticularly connected between the thigh and the foot. Therefore the RoM of the ankle joint is expressed as

$$\underline{\theta}_a < \theta_a(t) < \min(\theta_k(t), \overline{\theta}_a) \quad (12.2)$$

where $\theta_a(t)$ is the ankle joint angle measured between the shank and the foot, and $\underline{\theta}_a$ and $\overline{\theta}_a$ are the upper and lower bounds of the ankle joint angle, respectively. Note that the RoM of the ankle joint

**FIGURE 12.3**

Contracture of legs: (A) the knee joint with full extension and (B) a schematic model.

angle is a function of the knee joint angle. These mathematical models of the joint contracture, Eqs. (12.1) and (12.2), were considered in the generation of joint angle trajectories to prevent any damage to the pilot's body.

12.4.2 KNEE–ANKLE–FOOT ORTHOSIS

A knee–ankle–foot orthosis (KAFO) is a device that connects the pilot's body parts and the robotic legs as shown in Fig. 12.2A, and thus it is one of the most important components that determine the safety and usability of a powered exoskeleton. Since the actuation force of the WalkON Suit is transferred to the human body through the KAFO, the KAFO must be perfectly fitted to the human body shape. In particular, as the WalkON Suit is for the use of people with complete paraplegia, the pilot does not generate any voluntary muscular force at all. Therefore unless the human body part is tightly fastened to the robotic legs through the KAFO, the actuation force may not be transferred to the human body part properly, which causes an abnormal gait or even the failure in gait. More seriously, the use of an inappropriate KAFO may cause serious chronic pressure sores,

as well as scratches or bruises on the skin. Since a pressure sore is fatal to people with complete paraplegia, the KAFO must be customized for each user by an orthotist.

For the design of the KAFO of the WalkON Suit, the pilot's body shape was accurately measured by a 3D-scanning method. Through the 3D-scanned object, the musculoskeletal structure and the anthropometric data of the pilot were accurately identified. Based on the anthropometric data of the pilot, a KAFO, which consists of metal uprights, bands, and cuffs, was designed and manufactured. As the KAFO was fabricated based on the accurate measurement, it allowed a perfect fit between the human body and the robotic legs, as well as easy don and doff. The inner and outer surfaces of the bands were all covered with shock-absorbent materials such that an impact applied to the pilot's body was minimal.

As in the case of the pilot of the WalkON Suit, many complete paraplegics experience joint contracture. Due to the contracture, the RoM is limited, as shown in Fig. 12.3, and thus the KAFO should be designed taking into account the limited RoM. Even if the KAFO is carefully designed considering the contracture, nevertheless, the misalignment of the joint positions can be unavoidable during the operation of powered exoskeletons. Once the misalignment occurs, the gait stability may be lost, and the operation must be stopped. In order to avoid the misalignment of the knee joints during walking, ergonomically designed knee caps were additionally utilized in the WalkON Suit system. In particular, patients with complete paraplegia due to cauda equina injury who have frail legs without spasticity are liable to wear and tear injuries of weight-bearing joints during assisted gait using a powered exoskeleton.

12.5 CONTROL SYSTEM

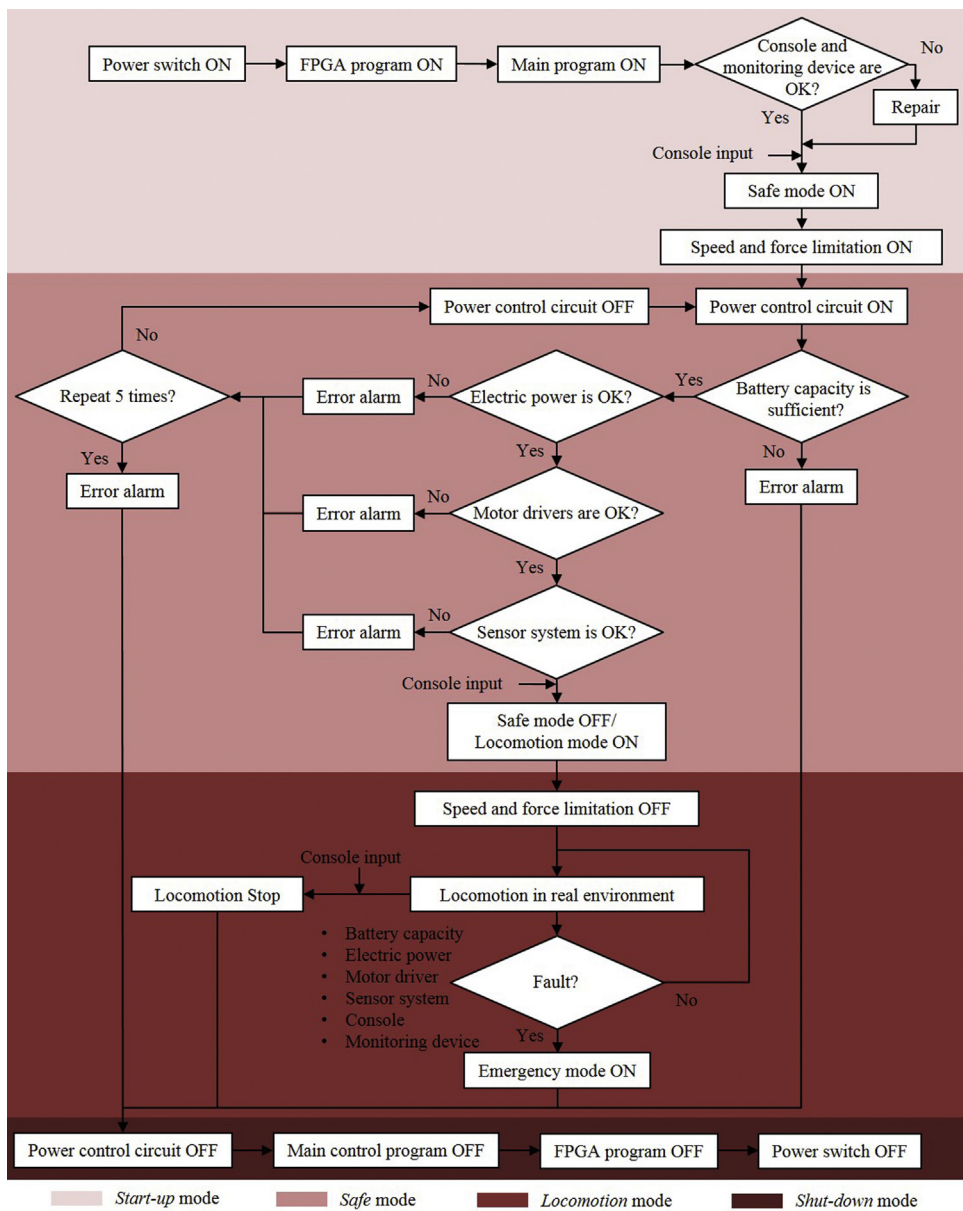
12.5.1 PROCESSES OF OVERALL CONTROL SYSTEM

The processes of the overall control system of the WalkON Suit consist of:

- Start-up mode;
- Safe mode;
- Locomotion mode; and
- Shut-down mode.

The processes of the overall control system are shown in Fig. 12.4. The detailed explanations on each process follow.

- *Start-up mode* is the first process to initiate the robot operation after mechanical power switches are all turned on. The mechanical power switch should be manually turned on by the pilot. Once it is turned on, the battery power is supplied to the CompactRIO and the power control circuits. If the CompactRIO is successfully started up and the real-time operating system is booted up, a program embedded in the FPGA level is first loaded. Once the FPGA program is successfully deployed without any error, the main control program is loaded onto the real-time target of the CompactRIO.
- *Safe mode* is a process where the hardware status and the software status are carefully checked while the outputs of the actuation systems (i.e., the speed and actuation torque) are limited.

**FIGURE 12.4**

The overall program processes consist of Start-up mode, Safe mode, Locomotion mode, and Shut-down mode.

If the hardware and software inspection processes are all passed, the pilot is able to don the WalkON Suit.

- *Locomotion mode* is a process of trajectory generation and motion control of actuation systems according to the pilot's commands. The pilot is able to change a locomotion phase according to the environmental situation. The locomotion phase is divided into walking, standing up/sitting down, uphill/downhill, stones, tilted path, and upstairs/downstairs. In order to guarantee the safety of the pilot, an automatic fault detection algorithm is run in the main control program. The automatic fault detection algorithm continuously observes the overall status of the WalkON Suit. Once any risk of failure is detected (i.e., the abnormal trunk inclination, the battery power, the motor driver fault signal, the absolute encoder fault or the incremental encoder fault, the IMU failure, etc.), an appropriate message is generated automatically, such that the pilot can react to the potential failure actively.
- *Shut-down mode* is a process of termination of the overall operation after doff. Shut-down mode follows the reciprocal process of Start-up mode.

12.5.2 MAIN FUNCTIONS OF THE CONTROL SYSTEM

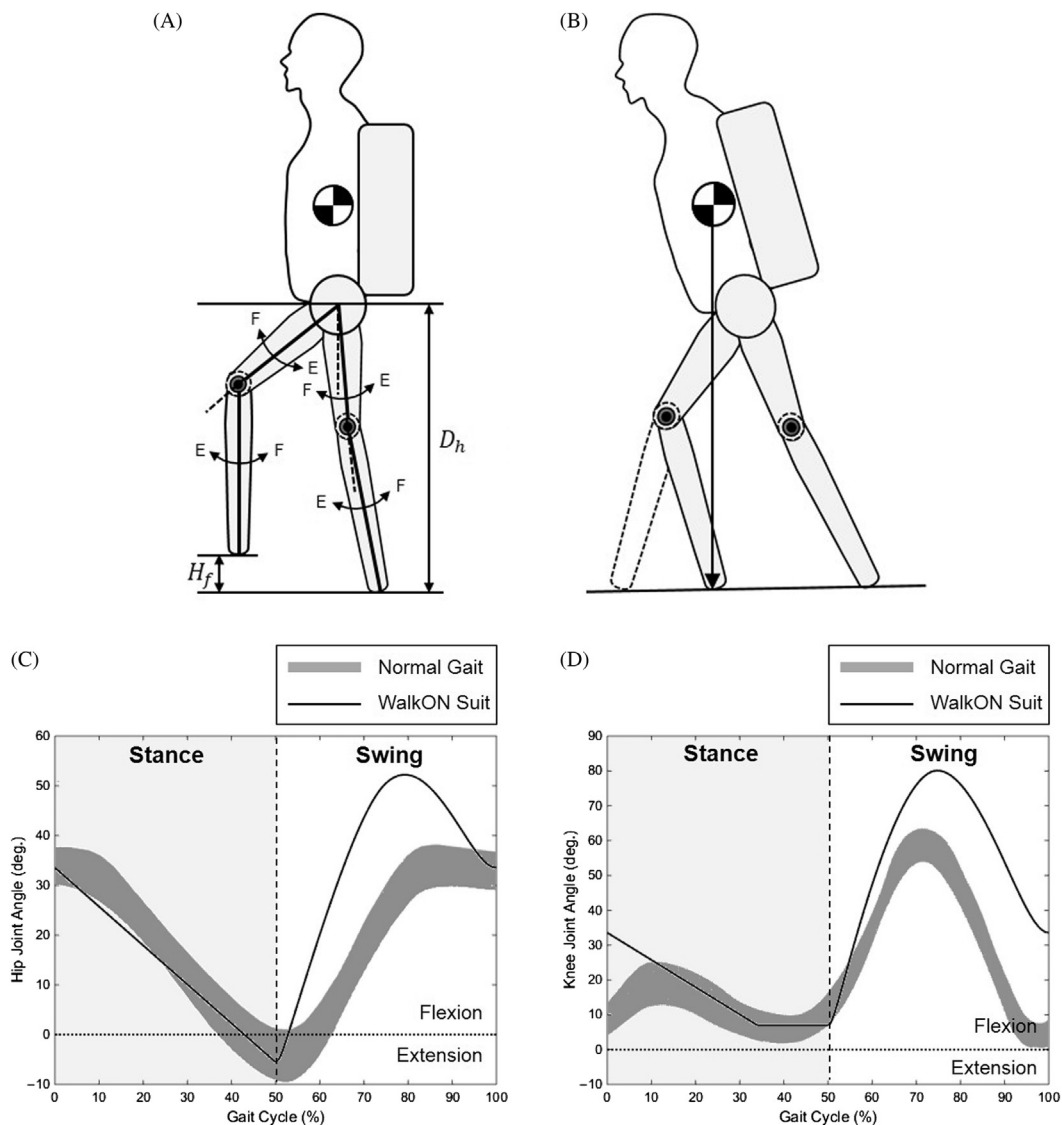
The main functions of the control system included

- Joint trajectory generation function;
- Motion control function; and
- Real-time risk assessment and management function.

The detailed explanations on each function follow.

- *Joint trajectory generation:* For robust stability, controlling the center of gravity (CoG) may be the most important issue in a powered exoskeleton during walking. If the CoG is located around the foot in a swing phase, the powered exoskeleton loses balance and will fall sideways even with crutches. Therefore the CoG should be always located in the foot area of a stance phase, that is, the leading leg. Since complete paraplegics have not used their legs for a long time, most complete paraplegics experience the muscle loss of the legs. The lower body weight of complete paraplegics are extremely lighter than the upper body weight due to the muscle loss, and thus all the weight of complete paraplegics is concentrated in the upper body. In addition, the weight of the WalkON Suit is concentrated in the waist position, because the biarticular mechanism is applied to the WalkON Suit here. Therefore it can be simply assumed that the CoG of complete paraplegics with the powered exoskeleton is close to the center of the upper body. The upper body should be tilted to the front in order that the CoG of complete paraplegics is located at the leading leg. A new gait pattern, forward inflection walking (FIW), enables the upper body to be tilted to the front by the height difference between the leading and the trailing leg under the knee joint constraint as shown in [Fig. 12.5A](#). D_h represents the height of the trailing leg and H_f is the height difference between the leading and trailing leg (i.e., H_f in [Fig. 12.5A](#)). The joint constraint of the FIW is

$$\theta_k(t) = -\theta_h(t) \quad (12.3)$$

**FIGURE 12.5**

The schematic of the forward inflection walking and the joint angle trajectories for a gait speed of 18 m/min: (A) the height difference between the leading and trailing leg, (B) comparison with the normal walking, (C) hip joint angle trajectory ($\theta_{r,hip}$), and (D) knee joint angle trajectory ($\theta_{r,knee}$).

where $\theta_k(t)$ is the knee joint angle, and $\theta_h(t)$ is the hip joint angle. Following this constraint, the shank is always parallel to the body even when H_f changes, and the knee joint is not fully extended at the beginning of the stance phase as opposed to normal walking. If the knee joint is fully extended at the beginning of the stance phase, the CoG is not located at the leading leg even if the upper body is tilted to the front as shown in Fig. 12.5B (see the dashed line in the figure). The CoG, however, is located at the leading leg in the proposed FIW method, because the knee joint flexion occurs through the knee joint constraint.

Also, the proposed FIW walking method is applied to the uphill, the stairs, and the stones, as well as the level walking. Since the control system of the WalkON Suit was developed for accomplishing all the tasks of the Cybathlon 2016, the information about the tasks (i.e., the degree of the uphill, the distance of each stone, and the height of the stairs) was set to a fixed value specified by the Cybathlon organizers. Based on the information provided by the Cybathlon organizers, the joint angle trajectories for each task were tuned by adjusting H_f .

The calculated joint angle trajectories of the level walking are shown in Fig. 12.5. Notice that $\theta_{r,knee}$ in Fig. 12.5D is always greater than about 10 degrees, which is due to the knee joint contracture of the pilot. The resultant joint angle trajectories are slightly different from those in a normal gait. The gray bands represent joint angle trajectories in a normal gait, while the black solid lines are the joint angle trajectories of the WalkON Suit. Since the normal walking utilizes the natural dynamics of the human body, the gray bands have a continuous sinusoidal waveform. In contrast, the motions of the WalkON Suit are quasistatic, and thus the joint angle trajectories were designed to continuously propel the body forward in a stance phase and to guarantee a large clearance in a swing phase.

- *Motion control algorithms:* A motion control algorithm is depicted in Fig. 12.6. Once a command is exerted from the pilot through the switches on the crutches, the desired positions of the feet, x_d and z_d , are determined in real time. Then the desired joint angle trajectories, $\theta_{r,hip}$ and $\theta_{r,knee}$ are calculated by the inverse kinematics of the robotic leg, that is, $I.K$ in the figure. The control input for each joint actuator, $u_{hip}(k)$ and $u_{knee}(k)$, is calculated as

$$u(k) = f_1 \theta_r(k) + f_2 \theta_r(k-1) + c_1 e(k) + c_2 e(k-1) + c_3 e_c(k) \quad (12.4)$$

where k is a current discretized time, and $e(k) = \theta_r(k) - \theta(k)$ is a tracking error for each joint, respectively. The subscripts, *hip* and *knee*, are omitted for simplicity. f_1 and f_2 are feedforward

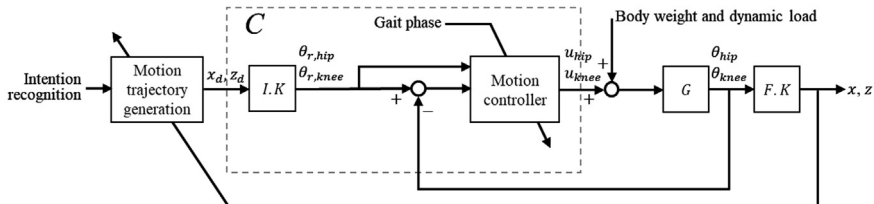


FIGURE 12.6

A motion control system for each leg. *I.K*, Inverse kinematics; *G*, the system model of the WalkON Suit; *F.K*, forward kinematics.

Table 12.3 Setting of Controller Gains

Phase	f_1 and f_2	c_1 and c_2	c_3	s
Stance	0	170,000, 4000	0	0
Swing	45,000, 950	6500, 150	500,000	1

controller gains, and c_1 , c_2 , and c_3 are feedback controller gains. $e_c(k)$ is an accumulated error, that is,

$$e_c(k) = s[e_c(k - 1) + e(k)T] \quad (12.5)$$

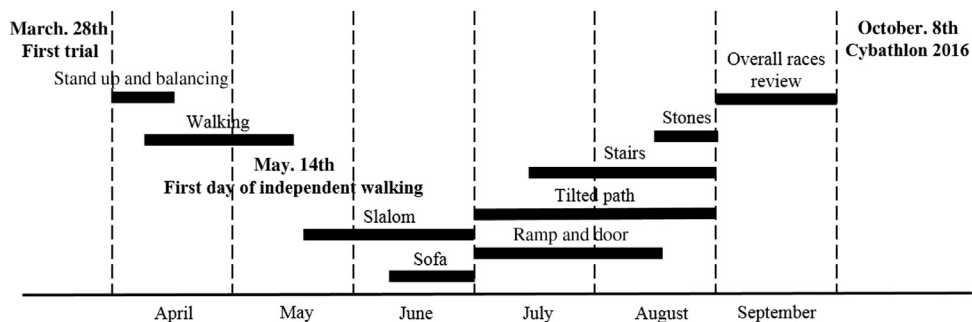
where T is the sampling period, and s is a switching variable. Note that $e_c(k)$ is reset to zero if $s = 0$.

During the operation of the WalkON Suit, the controller gains were changed according to the gait phase. In the stance phase, the robotic legs are exposed to large disturbances due to the body weight and dynamic load. Also the disturbances are continuously changed according to walking conditions, such as walking speed, ground condition, and crutch position. Therefore high gain control is not preferred, because the control input is drastically changed according to the change of the disturbance, which causes instability of the overall control system and makes the pilot uncomfortable and nervous. Therefore the robotic leg was controlled by the feedback control gains related to the proportional and derivative control, that is, c_1 and c_2 , while the other control actions depend on the phases as described in [Table 12.3](#).

In contrast, since the joint movements in the swing phase are larger than the joint movements in the stance phase as shown in [Fig. 12.5](#), a faster movement of the robotic leg is required in the swing phase. In addition, the disturbances are not significant in this phase. Therefore the feedforward control gains, f_1 and f_2 , and the integral control action, c_3 and s , were activated.

The gain scheduling method was effective, but it caused sudden impacts when the gait phase changed. The low gain control during the stance phase might increase the tracking error. This large tracking error, however, may cause an impulsive control input, as the controller gains suddenly become large as the swing phase starts. In such a case, the pilot may feel discomfort and lose balance. Therefore the joint angle trajectory was adaptively changed, such that $\theta_{r,hip}$ and $\theta_{r,knee}$ should start from θ_{hip} and θ_{knee} in the swing phase.

- *Real-time risk assessment and management:* Failures of components may occur during the operation of the WalkON Suit, and the failures may or may not cause a serious problem related to the safety of the pilot. Therefore an automatic fault detection algorithm during operation continuously monitors almost all possible risk factors in the entire robot system, and provides a management plan if any failure is detected. The risk of fault is distinguished into multiple degrees according to its severity, and the degrees of risk are defined as follow.
- *Caution:* The risk of a fault is minor, but operation for a prolonged period of time without the risk management can significantly increase the risk. It is recommended to stop operating the robot within 30 minutes.
- *Warning:* The risk of a fault is meaningful, and continuous operation without the risk management can significantly increase the risk. It is recommended to stop operating the robot within 10 minutes.

**FIGURE 12.7**

The training schedule for Cybathlon 2016.

- *Danger:* The risk of a fault is critical, and continuous operation without the risk management can cause an emergency situation immediately.
- *Emergency:* The risk of a fault is fatal, and an injury of the pilot may occur. It is mandatory to prepare for an accidental fall-down or an emergency disembarkation immediately.

12.6 EVALUATION

12.6.1 TRAINING

In order to succeed in the powered exoskeleton race, the pilot performed training twice a week for 6 months as shown in Fig. 12.7.

- *First trial:* At the very first day for the pilot to wear the WalkON Suit, the pilot was too nervous of the awkward body posture, as well as the mechanical sound of the robot, that the pilot wanted to immediately stop the first trial.
- *Stand up and balancing:* The pilot received intensive psychological training to overcome the fear of standing up, as well as training to balance the body with crutches and to control the robot, for a half month in Severance hospital as shown in Fig. 12.8.
- *Walking and slalom:* At the first trial of walking, the joint trajectories of a normal gait were applied to the WalkON Suit as a reference input. In normal walking, it is possible to transfer the CoG by the natural dynamics of the human body, ab/adduction movement of the hip joint, and generate the ankle joint torque. The pilot, however, is able to voluntarily move neither his legs nor his waist, and thus the pilot could not generate the ab/adduction motion of the hip joint and the ankle torque. Therefore, the pilot was not able to control the CoG even with the help of the WalkON Suit. In order to solve these problems, we proposed the FIW, and the pilot could start walking successfully by himself in May, 2016. In addition, the pilot was able to make a turn by using the crutches while walking. After tens of training sessions for walking, the pilot started accomplishing Cybathlon tasks. The pilot could walk up to 1.082 km/h with the WalkON Suit through repeated training until the Cybathlon 2016. While training walking with the WalkON

Suit, the gait efficiency and performance were monitored with objectively measured data, such as an oxygen cost. The oxygen cost data are measurements of energy expenditure per unit distance of walking, and thus are a good means to measure how the pilot consumes energy while walking with a powered exoskeleton. As shown in Fig. 12.9, the oxygen cost data were collected during level walking by Cosmed k4b2 manufactured by COSMED Co., USA. At an early training period, oxygen cost was about 30 times higher than that of a normal person without a disability. It decreased from 100% to 25% after training and algorithm optimization, meaning improved gait efficiency.



FIGURE 12.8

The training for stand up and balancing.

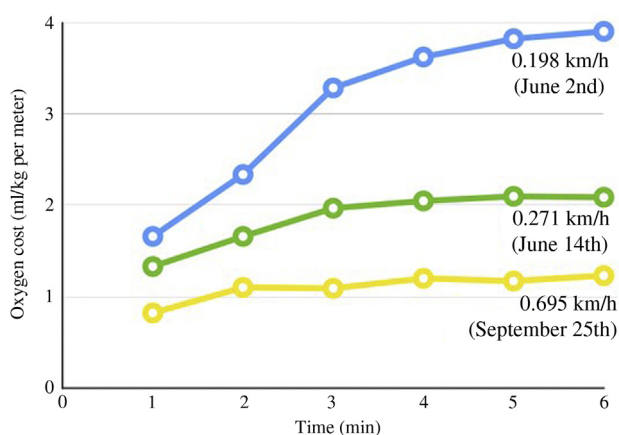


FIGURE 12.9

The performance measurements during level walking.

- *Sofa*: Since standing up and sitting down are repeated in every training, it took only 1 day for him to master the sofa task.
- *Ramp and stairs*: The ramps and stairs tasks required much more time; it took about 2 months for him to master the tasks. In the first version of rules of Cybathlon, it was not clear if the pilot could hold the guardrails, and thus the pilot practiced these two challenging tasks without holding the guardrail. However, the rule was specified to allow holding the guardrail, and then the ramps and stairs tasks had become easier for him.
- *Stones and tilted path*: After practicing the stones task for a month, the pilot could clear the task, but the success rate was not 100%. In particular, the pilot has relatively shorter legs compared to the other pilots, and thus the distance between stones was particularly challenging to him. In the case of the tilted path, the pilot had to spend too much time to clear it (about 2 minutes), because the tilted path had two ramps without a guardrail and maintaining balance was more difficult than the level walking. Therefore we decided to dismiss the tilted path task in the Cybathlon 2016.
- *Race simulation*: Race simulation training was started a month before the Cybathlon 2016. In order to create an environment similar to the actual stadium, we installed all the tasks in the Sogang University gymnasium. In addition, we recruited the crowd to create the same noise as in the actual stadium. In these conditions, the best time record to clear all the six tasks during practicing was 9 minutes 42 seconds, and the best time record for the five tasks excluding the tilted path was 7 minutes 30 seconds.

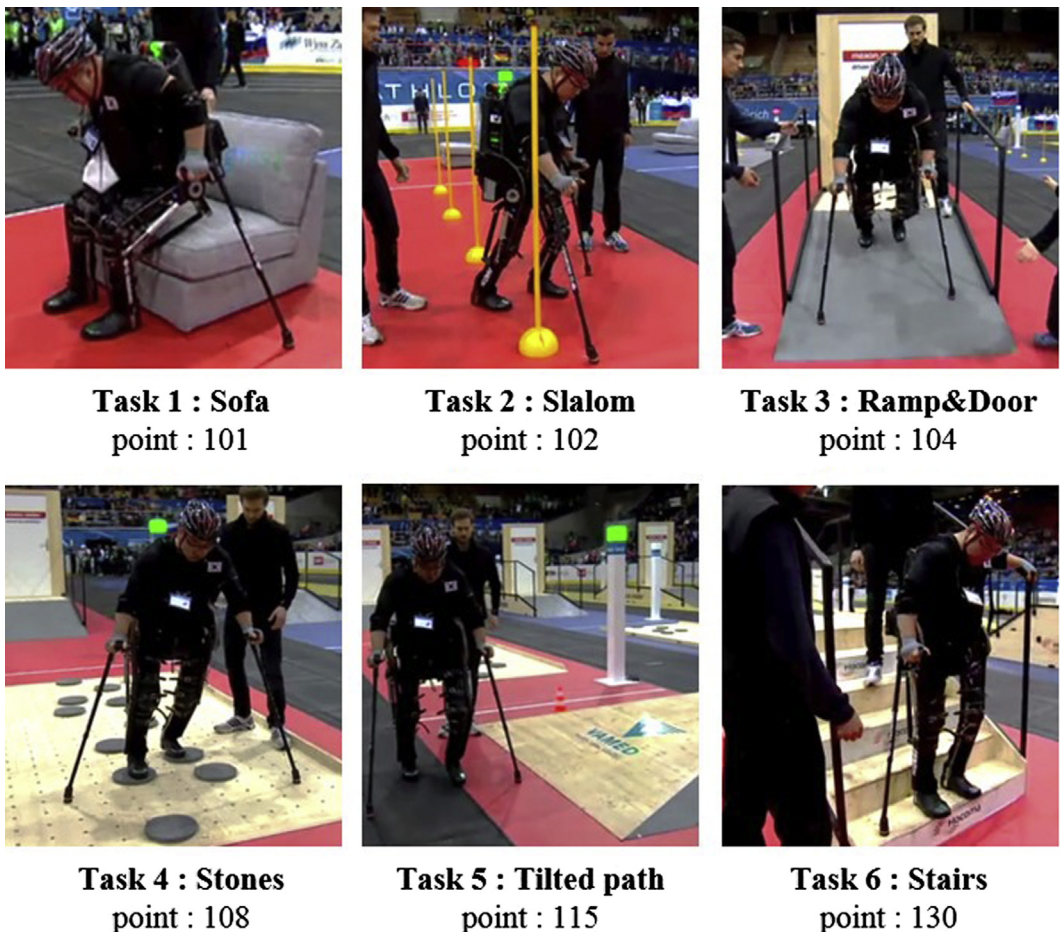
12.6.2 CYBATHLON 2016

On October 8, the Cybathlon was held in the SWISS Arena. In the qualification race, the pilot successfully cleared the five tasks as planned, as shown in Fig. 12.10, but he received scores only for the first four tasks due to the time limit. A video of the qualification race can be found at YouTube: <https://youtu.be/KGHf5AWm3gs>.

In the final race, the pilot made a critical mistake on the stones task; his foot touched the floor and he eventually lost the balance. The pilot had to spend much time to overcome this mistake. Eventually the pilot finished up to the stairs task. Although the stairs task was not counted due to the time limit, everyone was standing up and congratulating his success. The pilot won the bronze medal in the Powered Exoskeleton Race in Cybathlon 2016. Table 12.4 shown the scores of the qualification and final race.

12.6.3 ANALYSIS OF CYBATHLON 2016

Table 12.5 shows the comparison of the top three teams in the Powered Exoskeleton Race in Cybathlon 2016. The walking speed of the WalkON Suit, however, was slower than the ReWalk. It was expected, because the step length of the WalkON Suit was limited by the proposed walking method, that is, the FIW method. In contrast, ReWalk and Mina ver.2 applied the joint trajectory similar to normal walking, which is advantageous to improve the walking speed. However, the normal walking motion is dynamic, and thus it is not a stable gait motion for complete paraplegics who should walk carefully maintaining the balance for each step. For this reason, the WalkON Suit was controlled based on the proposed FIW method. However, we realized that once the pilot is

**FIGURE 12.10**

Clearing tasks in the Powered Exoskeleton Race.

fully trained to walking with a robot, he/she can maintain the body balance even in dynamic motions. If we participate in the next Cybathlon, the WalkON Suit will probably be controlled to have more dynamic motions such that the walking speed is much improved.

12.7 AFTER THE CYBATHLON

The Cybathlon remained numerous presents to the pilot and to the Team SG Mechatronics. First of all, a powered exoskeleton, WalkON Suit, could be intensively developed in a short time. All the

Table 12.4 Result of Tasks in Exoskeleton Race

Race	Qualification	Final
Sofa	Clear	Clear
Slalom	Clear	Clear
Ramp & Door	Clear	Clear
Stones	Clear	Fail
Tilted path	Dismissed	Dismissed
Stairs	Overtime fault	Overtime fault
Points	415	307
Time	404	252
Ranking	3	3

Table 12.5 Result of Tasks in Exoskeleton Race

Specification	ReWalk	Mina ver. 2	WalkON Suit
Weight (kg)	30	34	27
DoF (Active)	4	6	4
Gait speed (km/h)	2.6	1.0	1.1
Task preparation	ReWalk	Mina ver. 2	WalkON Suit
Sofa	Prepared	Prepared	Prepared
Slalom	Prepared	Prepared	Prepared
Ramp and Door	Prepared	Prepared	Prepared
Stones	Dismissed	Prepared	Prepared
Tilted path	Prepared	Dismissed	Dismissed
Stairs	Prepared	Prepared	Prepared

team members of the Team SG Mechatronics including the pilot are strongly tied, and they are very determined to develop powered exoskeletons for more people with complete paraplegia. The Cybathlon left unforgettable memories and strong motivations in our minds.

ACKNOWLEDGMENT

The authors appreciate Mr. Byeongwook Kim for his contribution and desire to overcome his difficulty.

REFERENCES

- [1] National Spinal Cord Injury Statistical Center, Spinal Cord Injury (SCI) facts and figures at a glance, 2016.

- [2] M.J. DeVivo, J.S. Krause, D.P. Lammertse, Recent trends in mortality and causes of death among persons with spinal cord injury, *Arch. Phys. Med. Rehabil.* 80 (11) (1999) 1411–1419.
- [3] M.J. DeVivo, Epidemiology of traumatic spinal cord injury: trends and future implications, *Spinal Cord* 50 (5) (2012) 365–372.
- [4] A. Esquenazi, M. Talaty, A. Packel, M. Saulino, The ReWalk powered exoskeleton to restore ambulatory function to individuals with thoracic-level motor complete spinal cord injury, *Am. J. Phys. Med. Rehabil.* 91 (11) (2012) 911–921.
- [5] G. Zeilig, H. Weingarden, M. Zwecker, I. Dudkiewicz, A. Bloch, A. Esquenazi, Safety and tolerance of the ReWalk exoskeleton suit for ambulation by people with complete spinal cord injury: a pilot study, *J. Spinal Cord Med.* 35 (2) (2012) 96–101.
- [6] ReWalk Robotics, <http://rewalk.com/>.
- [7] Ekso Bionics, <http://eksobionics.com/>.
- [8] Rex Bionics, <http://www.rexbionics.com/>.
- [9] Paker Hannifin-Indego, <http://www.indego.com/indego/en/home>.
- [10] R. Riener, The Cybathlon promotes the development of assistive technology for people with physical disabilities, *J. Neuro-Eng. Rehabil.* 13 (2016) 49–52.
- [11] A.B. Schultz, N.B. Alexander, J.A. Ashton-Miller, Biomechanical analyses of rising from a chair, *J. Biomech.* 25 (12) (1992) 1383–1391.
- [12] M.K. Mak, O. Levin, J. Mizrahi, C.W. Hui-Chan, Joint torques during sit-to-stand in healthy subjects and people with Parkinsons disease, *Clin. Biomech.* 18 (3) (2003) 197–206.
- [13] Standard ISO 13482, Robots and robotic devices - Safety requirements for personal care robots.
- [14] Standard ISO 22523, External limb prostheses and external orthoses - Requirements and test methods.
- [15] Y. Ito, S. Nozawa, J. Urata, T. Nakaoka, K. Kobayashi, Y. Nakanishi, K. Okada, M. Inaba, Development and verification of lifesize humanoid with high-output actuation system, in: IEEE International Conference on Robotics and Automation (ICRA), Hong Kong, pp. 3433–3438, 2014.
- [16] S. Oh, K. Kong, Two-degree-of-freedom control of a two-link manipulator in the rotating coordinate system, *IEEE Trans. Ind. Electr.* 62 (9) (2015) 5598–5607.
- [17] H. Choi, S. Oh, K. Kong, Control of a robotic manipulator in the polar coordinate system using a biarticular actuation mechanism, *Int. J. Control Automation Syst.* 14 (4) (2016) 1095–1105.

DESIGN OF LOWER-LIMB EXOSKELETONS AND EMULATOR SYSTEMS 13

Kirby Ann Witte¹ and Steven H. Collins²

¹*Department of Mechanical Engineering, Carnegie Mellon University, Pittsburgh, PA, United States* ²*Department of Mechanical Engineering, Stanford University, Stanford, CA, United States*

13.1 INTRODUCTION

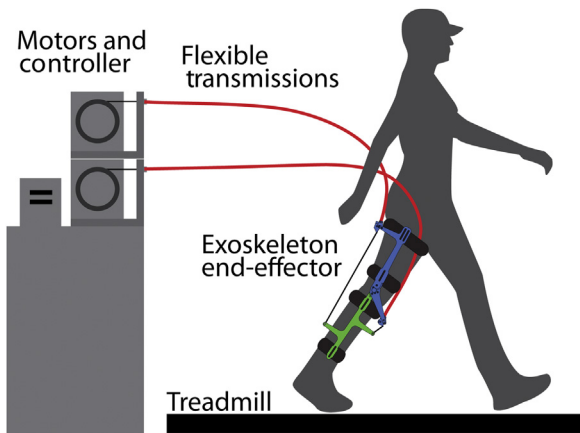
Designing lower-limb exoskeletons is a difficult process with many inherent challenges. All exoskeletons add mass and inertia to their user, which makes locomotion more energetically costly. Exoskeletons also restrict natural movement by increasing the overall volume of the leg and by resisting or completely inhibiting motion in some directions. The assistance provided by exoskeletons must effectively offset these innate costs before the user's performance can be improved. This requires exoskeletons to be lightweight and compact while ensuring safety and conforming to constraints such as desired degree of adjustability.

Designs range from soft to rigid and single jointed to full body, but all exoskeletons have the same key components: frames, actuators, sensors, control hardware, and physical interfaces that connect to the user. These features can be distributed in various ways, from a fully untethered system with all components mounted on the user to an emulator testbed with many components located off-board.

This chapter provides guiding principles for design and case studies of effective approaches to help developers begin the process of designing their own lower-limb exoskeletons. Topics include the pros and cons of exoskeleton testbeds, selection of actuators, development of free body diagrams for evaluating loading and stresses, comfort and safety measures, tips for frame and joint design, sensor selection, materials and manufacturing, series elasticity for improved torque tracking, and a brief description of low-level control strategies.

13.2 EXOSKELETON EMULATOR TESTBEDS

Exoskeleton hardware is often complicated and expensive. Exoskeletons are usually built as an untethered system with onboard power supply, control hardware, and actuation. Fitting all of this into a compact package that fits on a user without impeding movement often requires complex custom parts. Researchers often build exoskeletons and discover unsatisfactory details, resulting in the need for adjustments that require substantial redesign. This is discouraging, time-consuming, and expensive, and can be largely avoided by beginning development with an exoskeleton emulator system.

**FIGURE 13.1**

Example of an emulator system with a knee exoskeleton end-effector. Powerful off-board motors transmit mechanical power to the exoskeleton end-effector via flexible transmissions known as Bowden cables. Power is supplied by a three-phase wall outlet and control is managed by off-board control hardware. Any number of end-effectors can be used on a single emulator system.

Adapted from K.A. Witte, A.M. Fatschel, S.H. Collins, Design of a lightweight, tethered, torque-controlled knee exoskeleton, in: 2017 International Conference on Rehabilitation Robotics (ICORR), July 2017, pp. 1646–1653 [1].

Exoskeleton emulators are laboratory testbeds that are used to emulate existing systems or to test candidate exoskeleton designs before they are developed. The key components of an exoskeleton emulator include an exoskeleton end-effector worn by a user and off-board components, including actuation, control hardware, and power supply (Fig. 13.1). Placing these components off-board makes the exoskeleton simpler, which reduces design time and expense, while simultaneously improving performance.

Several research groups have adopted emulator testbeds with success. The details of their exoskeleton design vary widely while still using the same general approach (Fig. 13.2).

Most testbed systems are used to test general strategies or candidate designs for untethered systems before prototyping them, but sometimes testbeds are used with the intent of remaining testbeds forever. For example, the MIT Anklebot is intended to be used in a clinical setting to characterize the stiffness and impedance of ankles [10], and it has been used to identify the active, passive, and dissipative behavior of the ankle joint during walking [11].

Emulator testbeds can be affordable and efficient tools for both researchers and clinicians. Developing a testbed can deliver benefits for years, but not without some minor drawbacks.

13.2.1 EMULATOR PROS AND CONS

Exoskeleton emulators are fast, inexpensive, and flexible, but restricted to a laboratory setting. Emulators are fast to design, manufacture, and adjust. Placing the motor, power, and control hardware off-board removes the problem of designing mounts and mechanical transmissions on the leg,

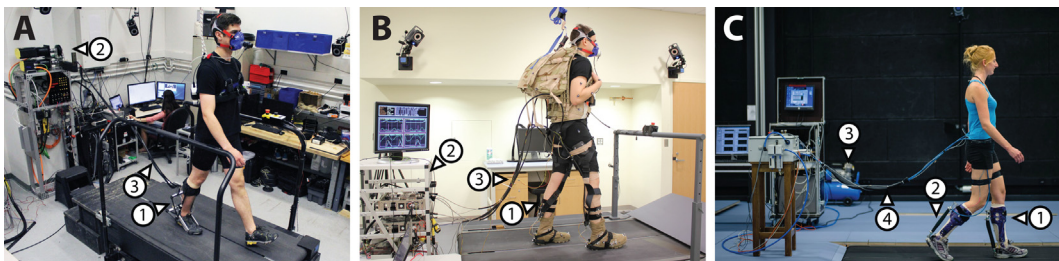


FIGURE 13.2

Testbeds keep devices simple and lightweight by placing heavy high-power components off-board and enable timely walking experiments on a treadmill. (A) Carnegie Mellon University's Emulator testbed [2] includes (1) a rigid ankle exoskeleton actuated by (2) an off-board electric motor with (3) a flexible Bowden cable transmission [2–6]. (B) The Harvard Biodesign Lab [7,8] actuates their (1) soft exoskeleton end-effector with (2) off-board motors and (3) Bowden cable transmission. (C) The Sport Science Laboratory at Ghent University [9] uses a pneumatic exoskeleton testbed which includes (1) two rigid ankle-foot orthoses actuated by (2) pneumatic artificial muscles with (3) an air compressor located off-board and mechanical power transmitted through (4) pneumatic tubes.

(A) Adapted from J. Zhang, P. Fiers, K.A. Witte, R.W. Jackson, K.L. Poggensee, C.G. Atkeson, et al., *Human-in-the-loop optimization of exoskeleton assistance during walking*, *Science* 356 (6344) (2017a) 1280–1284; (B) Adapted from Y. Ding, I. Galiana, A. Asbeck, B. Quinlivan, S.M.M. De Rossi, C. Walsh, *Multi-joint actuation platform for lower extremity soft exosuits*, in: 2014 IEEE International Conference on Robotics and Automation (ICRA), May 2014, pp. 1327–1334; (C) Photo by Cedric Verhelst, adapted from C. Verhelst, Sport Research Laboratory, Ghent University, <https://www.ugent.be/ge-bsw/en/sportlab> (accessed 22.07.19).

which eliminates the most complex elements of the design. Without these components the number of parts on the end-effector is drastically reduced, which reduces both design time and the cost of manufacturing. The greatest time-saving feature is that any device behavior can be programmed in without changing hardware. Let's say we think a passive clutch and spring system, such as that developed by North Carolina State and Carnegie Mellon Universities [12], could be beneficial. The proposed system can be emulated by programming in the expected torque profiles. Changing the virtual spring stiffness or clutch timing is done with a keystroke rather than replacing parts, tuning finicky components, or building an entire exoskeleton. In this way a single end-effector can be used to test any number of candidate mechanical systems.

Emulators are cost-effective largely because the most expensive components are off-board, which allows them to be used and reused for any number of end-effectors over the course of years. Batteries and motors that are small and light enough to mount on a user, but powerful enough to get the job done are expensive, while wall power and reusable motors that sit on a shelf are much cheaper with greater capability. Lastly, precise design requirements can be determined based on experimental results before designing complex untethered systems, so mass, space and money are not wasted building in too much capability, or worse: too little.

The only major con is that the tether to power and actuation restricts exoskeletons to treadmill walking. While this seems like a major limitation, exoskeletons have been under development for more than 120 years, yet the first measurable benefits were recorded using a pneumatic emulator in 2013 [13]. While some research groups may be ready to step out into the world to address

behaviors not easily captured on a treadmill, substantial basic research remains to be done in the laboratory.

13.2.2 OFF-BOARD COMPONENTS—POWER, ACTUATION, AND CONTROL HARDWARE

Selecting off-board components with more capability than required by the current application has the benefit of keeping additional strategies available for future endeavors. The cost of overdesigning off-board components is very low as they can be used for years to come.

Common actuators include pneumatic artificial muscles [13,14], Bowden cable transmissions connected to powerful off-board electric motors [4], and linear actuators [7]. In this chapter, we will focus mainly on Bowden cable systems. Regardless of the actuator you select, there is a trade-off between joint torque and velocity. The actuator must produce the required torques at velocities that can match or exceed the demands of the assisted biological joints.

Bowden cables attached to large electric motors are a common option for actuation because they are simple to implement and require little maintenance. An example of a Bowden cable is a bicycle brake cable. It is a thin cable that travels through a tough, flexible outer housing. Forces acting on the ends of the housing are equal and opposite to the tension on the inner cable. These equal and opposite forces result in no net force, meaning the brakes are not pulled towards the handle bars and exoskeleton end-effectors will not be pulled towards off-board motors. The exoskeleton just needs a small clamp for the housing to attach to and a lever or drum onto which to tie the inner cable. Another benefit of Bowden cable actuation is that it is extremely backdrivable. The motor can simply let the cable go slack for the exoskeleton to switch to a zero-torque mode.

Overdesigning off-board components allows for a highly responsive system. Off-board actuators can often provide higher peak torque than the exoskeleton frame can withstand, but that torque can be used to accelerate the rotor quickly. This allows for higher force bandwidth and greater disturbance rejection. The more bandwidth you have, the more types of assistance you can accurately apply. Disturbance rejection is important as torque can be developed in two ways: the motor can turn, or the user can disturb the system by flexing a joint to tighten the Bowden cable. This means your motor will need to get out of the way quickly to achieve accurate torque tracking.

13.3 UNTETHERED SYSTEMS

While testbeds give researchers a high degree of flexibility, untethered systems are needed for over-ground walking and are often the end goal of research performed on a testbed. Many untethered systems are currently in use and several have been shown to reduce the metabolic cost of walking. An untethered ankle exoskeleton from MIT effectively reduced the metabolic cost of walking during load carriage [15]. This exoskeleton is likely successful because it allows the ankle to maintain mobility in uncontrolled directions and its mass is kept to a minimum by eliminating explicit joints and taking advantage of lightweight materials such as fiberglass leaf springs and cord. Researchers at Samsung developed a sleek product-like hip exoskeleton that reduced the metabolic cost of walking by 20% with maximum torque as small as 10 Nm [16].

Some untethered exoskeletons have particularly unique designs. North Carolina and Carnegie Mellon Universities collaborated on a passive ankle exoskeleton with a mechanical clutch and spring that stored and released energy during walking resulting in a metabolic energy reduction of about 7% [12]. The Harvard Biodesign Lab has untethered versions of their soft exoskeletons with power and actuation located in a backpack. These untethered soft exoskeletons have been used to reduce the metabolic cost of walking during load carriage by 7% compared to walking without the mass of the exoskeleton and 14% compared to an unpowered mode [17]. The physical structure of the soft exoskeleton is unique and impressive as it can be worn under clothing, is lightweight, and the materials of the exoskeleton are exceptionally inexpensive to manufacture. Lastly, Simon Fraser University and Bionic Power have produced an energy harvesting knee exoskeleton that generates electricity while decelerating the knee at the end of the swing phase [18]. This is similar to regenerative braking in a hybrid vehicle. The negative work performed by the exoskeleton, which powers the generator, replaces positive work in human muscle, so the additional metabolic cost of wearing the device is small. This energy harvesting knee exoskeleton may provide power to medical devices or allow charging in remote areas.

Several position-controlled exoskeletons are currently available for assisting individuals with spinal cord injuries. One such device is the ReWalk which senses the tilt of the torso and commands a predetermined hip and knee trajectory that results in a step when the user leans forward [19]. The user can also use a remote to command the exoskeleton to aid with several tasks such as sit-to-stand transitions.

Some exoskeletons have been well designed, but have not produced measurable benefits for the user. The Achilles exoskeleton developed at Delft University of Technology is cleverly designed with an efficient leaf spring and linear actuator drive system [20]. However, it did not reduce the metabolic cost of walking, likely due to the weight of the hardware and details of its current control scheme [21].

13.4 MECHANICAL DESIGN OF ONBOARD COMPONENTS

Regardless of whether an exoskeleton is untethered or part of an emulator system, the same principles of exoskeleton design apply. Exoskeleton design requires balancing competing design goals and constraints. In general, we would like to minimize mass, inertia, and volume while maintaining safety, comfort, mechanical strength, and peak torque and power capabilities. In this section we will discuss general approaches for addressing comfort and safety, frame design, joint design, sensing, series elasticity, and materials and manufacturing.

13.4.1 LOADING ANALYSIS—FREE BODY DIAGRAMS

Free body diagrams enable designers to understand the forces applied to the user and stresses in the exoskeleton. This allows designers to make better decisions to produce lightweight designs while ensuring comfort and safety. Free body diagrams will reveal whether or not a design will operate as intended. They can also reveal the relationships between design parameters and outcomes such as the magnitude of forces applied to users and mechanical stresses in components. This chapter

assumes a basic understanding of free body diagrams. If some background is needed, we recommend referring to a textbook on Engineering Statics or Physics, such as *Introduction to Statics and Dynamics*, available online [22].

Here are some helpful techniques for generating free body diagrams of exoskeletons:

1. Simplify free body diagrams of the exoskeleton and user by including only a portion of the user. It is acceptable to make a “cut” and include only the user’s leg, but you must include internal forces and moments at the “cut.” Make certain that any other forces applied at the boundaries of your free body are also included.
2. The mass of exoskeletons and the accelerations experienced during walking are often small compared to the driving forces and moments, so the gravitational and dynamic loads can usually be safely neglected. Complexity can be added as the design takes shape.
3. Assumptions that are in line with design goals can simplify analysis and verify that the exoskeleton will operate as expected. For example, if you do not want straps to apply shear force to your user, assume straps only apply forces normal to the user. If you cannot achieve static equilibrium with this assumption in place, you know your design will not function as intended.

Once free body diagrams are composed, you can solve the static equilibrium equations for outcomes of interest. This allows you to see the effect of changing design parameters such as component lengths on outcomes like the magnitude of force applied to a user. If static equilibrium cannot be achieved, you will need to make adjustments to your assumptions or change the overall design of your system.

Comparing candidate architectures and identifying issues early in the design process can greatly impact performance and avoid costly alterations later. After load analysis is performed, dimensions can be selected to minimize forces and stresses, which allows for a mass-efficient design.

See the case study in [Section 13.4.2.4](#) for an example of free body diagrams and how they were used to develop an ankle exoskeleton.

13.4.2 SAFETY STOPS AND PHYSICAL INTERFACES

An exoskeleton has limited usefulness if it is unsafe or too uncomfortable to be worn. We can ensure safety by preventing the user’s natural range of motion from being exceeded, and we can improve comfort by placing physical interfaces far apart, keeping forces acting normal to the user, and restricting natural motion as little as possible.

13.4.2.1 Safety stops

Hard stops should prevent an exoskeleton from applying force to the user outside their natural range of motion. Placing hard stops far away from the assisted joint will reduce the magnitude of force applied to the hard stop. A singularity may be an acceptable replacement for a hard stop in some cases. A singularity works by aligning the inner Bowden cable with the joint center. In this configuration, tension in the rope can be very high and still apply zero torque to the user’s leg at the maximum allowable angle. This approach is less desirable than the hard stop. A large portion of the exoskeleton frame still experiences large forces and stresses, and the user is not protected against hyperextension of joints due to other causes such as trips or the momentum of the leg itself.

Other safety measures such as mechanical fuses and in-software safeties should be in place. A breakaway cable can be tied in line with the inner Bowden cable at the motor. If tension in the cable rises higher than expected, the breakaway cable will break and separate the end-effector from the motor. Software safeties can command zero torque when certain limits are exceeded, but software safeties should be used with caution as sensor malfunctions or wiring problems can render them ineffective. Including redundant sensors can improve our confidence in software safeties.

13.4.2.2 Case study—knee exoskeleton end-effector utilizes hard stops

The Carnegie Mellon University (CMU) knee exoskeleton end-effector utilizes safety hard stops to prevent flexing or extending the knee beyond acceptable limits (Fig. 13.3). The Bowden cable housing termination and the inner cable termination press against each other to counteract the tension in the cable. This type of hard stop is preferable compared to a singularity because all the force is reacted through these two components and the rest of the exoskeleton remains unloaded.

13.4.2.3 Straps

Placing interfaces far apart maximizes lever arm lengths and minimizes forces applied to the user. It is also more comfortable for force to be applied directly towards the leg (normal to) than along its surface (in shear). Not only do shear forces cause rubbing and pain, but skin doesn't support them well [23]. This can be demonstrated by gripping your wrist and pressing directly toward the bone. There is little movement between your hand and wrist. Now grip your left forearm tightly

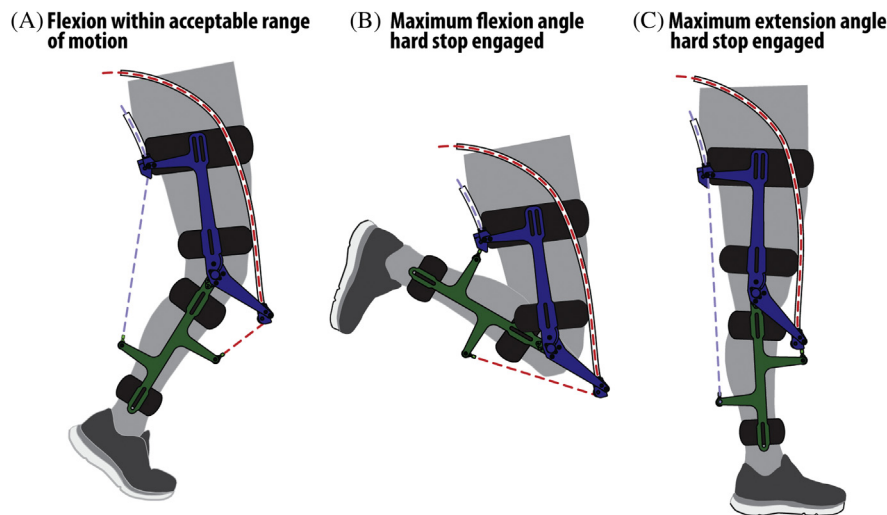


FIGURE 13.3

(A) The exoskeleton experiences a flexion angle within the acceptable range. (B) The exoskeleton has reached its maximum allowable flexion angle. The Bowden cable housing termination collides with the inner cable termination thus preventing the exoskeleton from flexing any further. (C) The exoskeleton is in its straight leg configuration and will not allow further extension of the knee.

and force your right hand alternatingly towards the left elbow and hand. Your hands slide with respect to each other with little resistance as your soft tissues deform. This motion is undesirable and will be worse in very fleshy areas like the thigh. For these reasons exoskeletons should apply forces mainly normal to the user whenever possible.

Straps are key to the success of exoskeletons and should be prototyped early in the development process. The best strapping locations have a shape conducive to preventing downward migration, experience little change in muscle volume, and are bony. One of the best strapping locations is at the top of the calf. The large size of the gastrocnemius muscle prevents a calf strap from sliding down the leg. The top of the calf also sees very little change in volume allowing for inextensible straps. The shin is bony and an excellent location for applying force without losing mechanical power to the deformation of soft tissues. The thigh is less convenient and requires more thoughtful design as it is shaped like an inverted cone and thigh straps tend to slide down.

Some mechanical power loss is experienced at all human-exoskeleton interfaces due to movement of the device relative to the user, deformation of soft tissues and compliance in the straps themselves. Some measures of power loss at interfaces are as high as 55% [24]. While some of this power is returned viscoelastically, the timing of its return is difficult to anticipate.

Applying forces to the user at bony locations and making straps out of inextensible material can help avoid relative motion between the exoskeleton, mitigate rubbing, and reduce mechanical power loss, but the changing shape of the user may require some elasticity at locations that experience large volume changes. For example, a strap above the knee may be comfortable for walking, but uncomfortably tight for running or squats.

Straps must be able to resist gravity and dynamic loads. These loads are often neglected during component design as they are small and cause low stress, but will cause exoskeletons to migrate with respect to the user over time. Legs experience high rotational velocity during locomotion which acts along with gravity to force exoskeletons down the leg. This problem can be mitigated by reducing mass. Additional suspension straps may also help. Knee exoskeletons often utilize a strap to the waist to prevent downward migration. The distribution of mass is important as laterally offset mass can cause the exoskeleton to spin around the leg as the user walks. The coefficient of friction between the user and straps can be improved using self-adhering sport wrap such as Coban or prosthesis socket liner. Developing straps is often a matter of trial and error, as mechanical engineers, clinicians, and biomechanists are not typically expert in apparel design. Comfort may be best maintained by adapting straps already well-developed for sports, weight lifting, or safety equipment.

13.4.2.4 Case study—ankle exoskeleton end-effector designed for low forces and safety

In the first stages of designing the ankle exoskeleton, we used free body diagrams to select among architectures, set major geometric parameters, and estimate loads on the device and the body (Fig. 13.4). The exoskeleton interfaces with the user at three locations: a strap above the calf, a rope under the heel of the shoe, and a plate embedded in the toe of the shoe. These diagrams adhere to the recommendations listed in Section 13.1.

It is assumed that the force applied by the calf strap acts normal to the user's shin (Fig. 13.4B). This assumption ensures that it is physically possible for the exoskeleton to work as intended and makes solving the force balance equations easier. If force balance could not be achieved with this assumption in place, it would be understood that the exoskeleton must apply undesirable shear

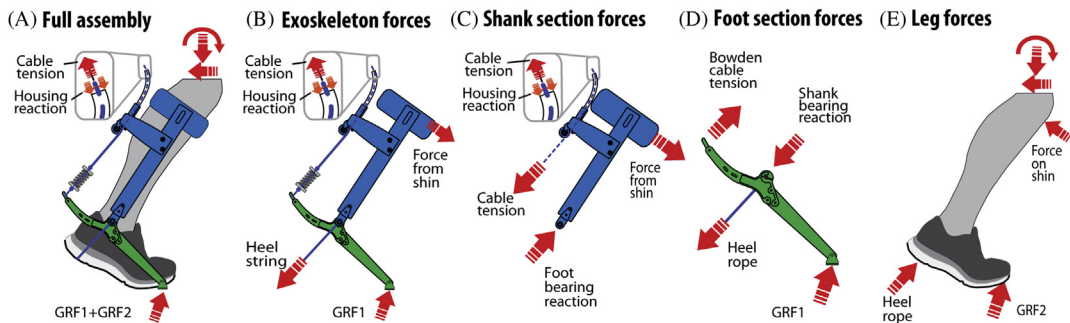


FIGURE 13.4

Free body diagrams of an ankle exoskeleton. (A) The full system including the exoskeleton and user's leg. Forces in the Bowden cable housing act equal and opposite to tension in the cable resulting in zero net force on the exoskeleton. (B) The exoskeleton interfaces with the user in three locations: a strap at the shin, a rope embedded in the heel of the shoe, and a plate in the toe of the shoe. (C) The shank section experiences force from the calf strap, force at the Bowden cable housing termination that is equal and opposite to the tension in the inner Bowden cable, and a reaction force at the bearing. Note that the force from the redirection of the inner Bowden cable around a pulley is not included as it is internal to the free body. If the inner Bowden cable were not included then the redirection force would be needed. (D) Forces acting on the foot section of the exoskeleton. (E) Forces acting on the user.

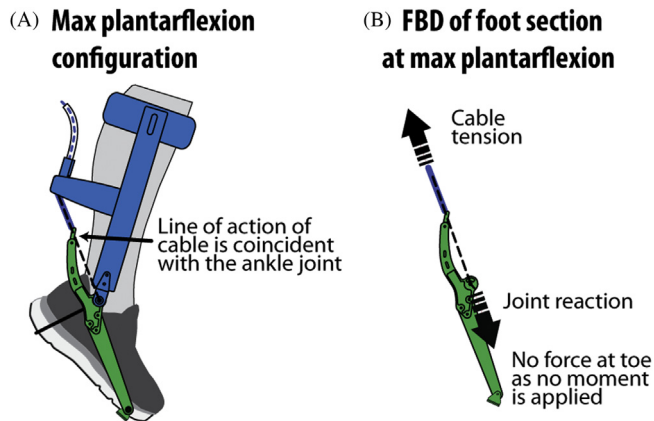
Adapted from K.A. Witte, J. Zhang, R.W. Jackson, S.H. Collins, Design of two lightweight, high-bandwidth torque-controlled ankle exoskeletons, in: IEEE International Conference on Robotics and Automation (ICRA), 2015, pp. 1223–1228 [5].

force to the shin and calf. The no-shear assumption is reasonable as the straps and soft tissues have low stiffness in shear loading and disallow the development of large forces except in the case of large displacements.

The interfaces at the calf, heel, and toe are placed as far apart as possible to reduce forces on the user. For example, if a moment balance is taken about the bearing in Fig. 13.4C, the force in the calf strap is inversely proportional to the distance between the strap and the bearing. Placing the strap half way down the shin would decrease the overall size of the exoskeleton, but would also double the force on the user's leg for the same applied torque.

Free body diagrams can be used to answer many design questions. For example, why is the heel rope included? If we start with known tension in the Bowden cable, the joint reaction force between the shank and foot section can be solved for using Fig. 13.4C and static balance equations. This joint force can then be used in Fig. 13.4D to solve for the three unknowns: tension in the heel rope, the ground reaction force, and the direction of the ground reaction force. Three static balance equations (sum of the forces in the x and y directions along with a moment balance) can be used to solve for our three unknowns. If the heel rope was not included, the problem would be underconstrained with two unknowns and three equations. Static balance would not be possible without additional forces, such as a shear force on the shank.

The ankle exoskeleton features a singularity (Fig. 13.5) to prevent the exoskeleton from applying torque to the user outside their normal range of motion. As the ankle approaches its maximum allowable plantarflexion angle, the inner Bowden cable aligns with the joint center, ensuring that

**FIGURE 13.5**

Singularity on an ankle exoskeleton. (A) As the ankle approaches its maximum allowable plantarflexion angle, the inner Bowden cable aligns with the joint center. (B) A Free body diagram of the foot section demonstrates that zero torque is applied at this maximum angle.

zero torque is applied at this maximum angle. Furthermore, if the plantarflexion angle exceeds this maximum angle, a restoring dorsiflexion torque will be applied. However, a large portion of the frame is loaded when the singularity is reached. This means that the frame must be reinforced to a greater degree when using the singularity as a safety instead of a hard stop.

13.4.3 FRAME AND JOINT DESIGN

We would like to minimize mass, inertia, and volume while allowing the device to fit many different users comfortably without inhibiting gait. The energy cost of carrying mass increases drastically as the location of the added weight becomes more distal [25]. Components should be mass efficient and heavier components should be as close to the torso as possible. Adding an exoskeleton also increases the overall volume of the leg, which requires the user to increase circumduction (swing their legs further to the side) to avoid collisions between legs during walking. This is very tiresome as the net rate of energy expenditure during walking increases with the square of circumduction amplitude [26]. With this in mind, protrusions from the leg on the medial aspect should be kept to a minimum.

13.4.3.1 Frame design

Attaching to people is difficult. Not only are people squishy and oddly shaped, but there is wide variability in the shape of individuals. Variation in leg length, leg diameter, shoe size, levels of valgus or varus alignment in the knee (knock-kneed or bow-legged), and external rotation of the toe, among other things can make fitting multiple individuals with one exoskeleton difficult. Developing an exoskeleton that is one-size-fits-all is likely impossible without including some amount of adjustability, modularity, or compliance.

Adjustability can be a time-saver when running lots of experiments. Sliders can extend or shorten struts to fit legs of different lengths, but add weight and complexity to the design. Users of different sizes can be accommodated through modularity by making multiple sizes of select components. Addressing fit with modularity is simple, but can be time-consuming to adjust as connective hardware needs to be removed and replaced and wires might need to be rerouted.

In some cases, sizing can be addressed through compliance in select directions. Frames with built-in flexibility can flex in or out to accommodate users of different leg sizes. Selective compliance can also be used to provide passive degrees of freedom to a joint. This is desirable as biological joints usually have many degrees of freedom, but an exoskeleton may be designed to assist only one or two. Allowing some motion in the unassisted directions through compliance keeps locomotion relatively uninhibited while maintaining a simple design.

13.4.3.2 Case study—Carnegie Mellon University's ankle exoskeleton

- *Modularity*—The shoe, toe strut, and calf strut of the CMU ankle exoskeleton (Fig. 13.6) can be exchanged to fit different users, but the joints, Bowden cable termination, and heel spur are one-size-fits-all. The exoskeleton can be shifted by adding spacers of unequal size to the top of the calf. Often the calf is not symmetric around the center of the leg—more muscle mass can be located on the lateral side of the leg, which shifts the exoskeleton towards the lateral side. This is a problem if the medial malleolus of the biological ankle joint contacts the frame. This can be fixed by adding a wide spacer to the medial side and a thin (or no) spacer to the lateral side.

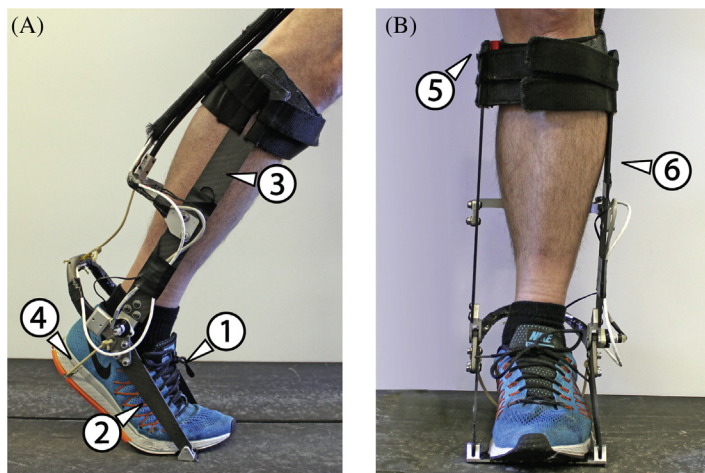
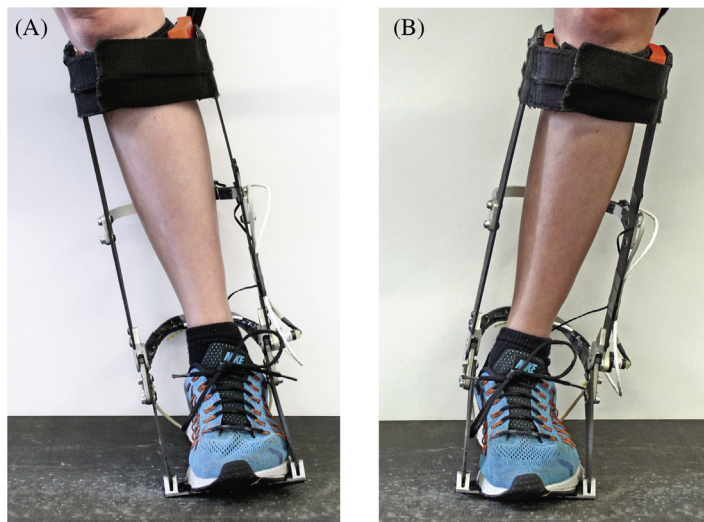


FIGURE 13.6

Modularity ensures a good fit on different users. (A) The shoe (1), toe struts (2), calf struts (3), and heel rope (4) can be exchanged to fit users of different foot and calf lengths, while the rest of the components are one-size-fits-all. (B) This subject's natural ankle configuration requires a wide spacer (5) under the strap on the medial aspect of the calf to ensure that the ankle is centered in the exoskeleton. Other subjects may require spacers on the lateral aspect, or none at all. Note that while the ankle is relatively centered in the exoskeleton, the calf is not. There is no space (6) between the exoskeleton frame and the lateral aspect of the leg.

**FIGURE 13.7**

Selective compliance allows freedom of motion in several degrees of freedom without complex joint design. Flexibility in the shoe, straps, struts, and heel rope allow for comfortable inversion (A) and eversion (B) of the ankle.

- *Selective compliance for fit*—The tops of the calf struts on this ankle exoskeleton can flex towards and away from the leg to accommodate legs of differing diameter. The struts are thin in the frontal plane to allow flexing, but wide in the sagittal plane to ensure that they are rigid in the directions in which large forces are applied.
- *Selective compliance for passive degrees of freedom*—The biological ankle acts mainly in the plantarflexion/dorsiflexion direction, but is also capable of rotation and roll. The CMU ankle exoskeleton only assists plantarflexion and uses a simple pivot joint, but still allows freedom for the ankle to roll through compliance in the shoe, heel rope, strap, and struts (Fig. 13.7). High compliance in the heel rope is particularly useful for allowing inversion and eversion of the ankle, although ankle rotation is still limited.

Note: Complete design files for this ankle exoskeleton are available at [27].

13.4.3.3 Joint design

Simple pivot joints are lightweight and functional as they simplify attachment and sensing. For example, a knee exoskeleton can depend largely on the calf strap to prevent the entire structure from sliding down the leg if the joint has only 1 degree of freedom. However, if translation between the thigh and calf sections of the exoskeleton is allowed by a more complex joint, the calf strap cannot support the thigh portion. More degrees of freedom require better strapping. Additionally, many control strategies require real-time measurement of the joint angle. This is most easily accomplished by attaching an encoder to a pivot joint.

Deliberately designing for structural compliance in unassisted directions allows simple joint designs to be effective. Biological joints are complex and have multiple degrees of freedom, but each of these may not need to be explicitly addressed by the mechanical joint if there is sufficient compliance in soft tissues, straps, and the exoskeleton structure. However, small natural movements in the unassisted degrees of freedom of biological joints will result in undesirable large forces if the exoskeleton and its interface with the user are both very stiff.

Several successful exoskeletons have been developed without explicit joints. A jointless autonomous ankle exoskeleton has reduced the metabolic cost of walking [15]. Soft exoskeletons typically lack explicit joints and are extremely lightweight and allow freedom of motion [28]. However, the magnitude of torque applied can be limited using this strategy as some shear forces must be applied by straps, which can be uncomfortable. The range of available control strategies can also be limited as the measurement of joint angle is more difficult without an explicit joint.

13.4.3.4 Case study—5-degree-of-freedom knee exoskeleton

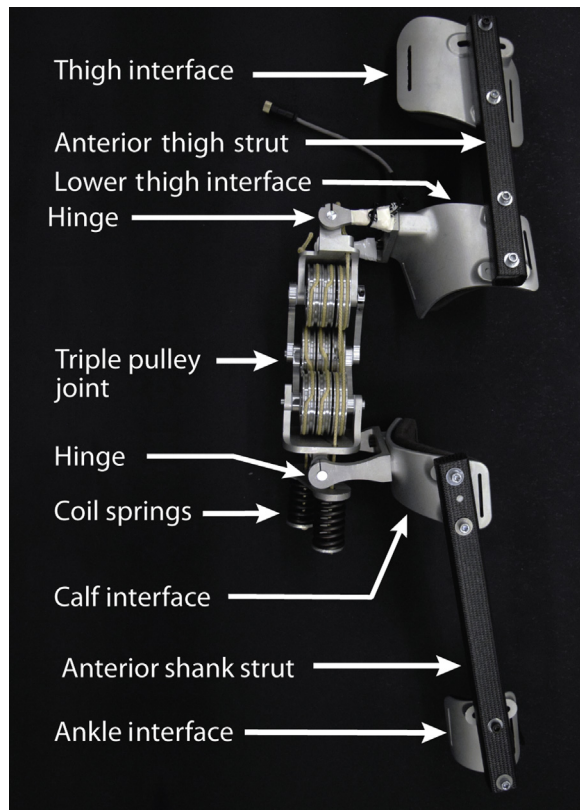
Complex designs to address multiple degrees of freedom and fitting issues can be time-consuming to design, expensive to manufacture, and heavy, while a simpler, lighter design may suffice. Consider the 5-degree-of-freedom knee exoskeleton developed by Carnegie Mellon University in collaboration with Boston Dynamics shown in Fig. 13.8.

Five degrees of freedom were selected so the center of rotation of the exoskeleton could match the center of rotation of the biological joint and accommodate all natural degrees of freedom other than knee rotation. Internal/external knee rotation was omitted to prevent torque application in unintended directions.

The joint of the knee exoskeleton comprised three sets of triple pulleys: one for extension torque, one for flexion, and one for a safety hard stop to prevent hyperextension. Straps at four physical interfaces attached at the top of the thigh, above the knee, calf, and above the ankle.

This exoskeleton had many desirable traits, but failed to be useful in walking experiments. It featured no rigid components on the medial aspect of the leg, which avoided increased circumduction during walking. It could fit a wide range of adults easily regardless of leg-length, degree of varus or valgus alignment of the knee, or leg diameter without the need for modularity. Similar to another exoskeleton developed by Boston Dynamics [29], it also delivered a near pure moment (limited by friction at the bearings) to the biological knee, meaning internal joint forces were not increased due to the use of the exoskeleton. Unfortunately, the weight and bulk of the complex joint limited the utility of the device. The offset mass caused it to gradually rotate around the leg during walking, and the long length of the hard stop cable reduced its stiffness and effectiveness. A simpler knee exoskeleton was developed as a replacement (Fig. 13.9).

Our second knee exoskeleton (Fig. 13.9) was developed using simple pivot joints and planar struts on the medial and lateral aspects of the leg. We found the single degree of freedom to be adequate as compliance allowed for comfortable use. The rigid components on the medial aspect of the leg are not desirable, but the exoskeleton has enabled walking experiments and was relatively simple to design and build. Information gained from this simple exoskeleton can be applied to more complex designs with more desirable form factors later on.

**FIGURE 13.8**

A 5-degree-of-freedom exoskeleton designed to provide a pure moment to the knee joint. The exoskeleton consists of four aluminum strap interfaces at the upper thigh, lower thigh, calf, and ankle. These interfaces are connected by anterior struts formed of rectangular carbon fiber tubes. The joint is composed of two hinges and three sets of triple pulleys, which allow for 5 degrees of freedom.

Adapted from K.A. Witte, A.M. Fatschel, S.H. Collins, Design of a lightweight, tethered, torque-controlled knee exoskeleton, in: 2017 International Conference on Rehabilitation Robotics (ICORR), July 2017, pp. 1646–1653.

13.4.4 SENSING

Emulator systems should include enough sensors to allow flexibility in the design of control strategies. Including sensors for joint angle, torque measurement, and heel contact keep most control strategies available for testing. For example, joint angle may not be needed to implement proportional electromyographic control, but it would be necessary to emulate the behavior of a spring-loaded passive device or to detect different phases of gait.

Joint encoders make measurement of joint angle simple. Magnetic encoders are recommended as they can be found in very small sizes and are relatively robust to misalignment compared to optical encoders.

**FIGURE 13.9**

Knee exoskeleton featuring a simple pivot joint and plate carbon fiber frame.

Torque can be measured directly by lightweight strain gauges. Strain gauges can be configured in a Wheatstone bridge to improve sensitivity. The arrangement of the strain gauges can be designed to measure strain from specific types of loading while rejecting others. Torque can also be calculated by measuring tension in the Bowden cable with a load cell and multiplying by the effective lever arm which is calculated considering geometry and joint angle. Placing the load cell on the motor side of the Bowden cable in order to reuse the load cell across end-effectors is not recommended. Friction between the Bowden cable housing and the inner cable can result in lower (or higher) tension in the cable on the end-effector side compared to the motor side, resulting in inaccurate torque measurements [30].

A switch in the heel and/or toe of the shoe can provide information on the user's place in the gait cycle. A pressure sensor may be more desirable than a simple on/off switch as it would open up more assistance strategies.

Sensors can often be moved off-board. For example, pressure sensors may be replaced by ground reaction forces as measured by an instrumented treadmill. Joint angle can be sensed by motion capture cameras. However, moving sensors off-board may involve delays or additional setup time for experiments.

If electromyographic (EMG) sensors are required for control strategies such as proportional EMG control [31] or for locomotion mode identification [32], then extra space is needed between the user's leg and the exoskeleton frame near the instrumented muscles. Contact between EMG sensors and the exoskeleton can cause spikes in measured EMG data.

Wiring problems can be hard to diagnose and can result in large development delays. Wiring issues can be largely mitigated by making plans early in the design process. Routing wires over or near the axis of joints to avoid sharp repeated bends will reduce fatigue and prevent internal breaks in the cable that are hard to find. Buying cable with high flexibility will reduce the chances of failure due to fatigue. Including snaps or guides for cables will reduce the need for tape or cable ties. Routing all the cables for sensors into a single connector rigidly mounted on the exoskeleton frame will allow for a single cable extending from the exoskeleton to power and the controller. This reduces mass and makes unplugging the exoskeleton easy and reduces dangling cables which get in the way during maintenance and adjustments. Wireless sensors may be an option, but larger latencies are likely.

13.4.5 SERIES ELASTICITY FOR IMPROVED TORQUE TRACKING

Placing an elastic element like a spring in series with an actuator creates a series-elastic actuator [33]. This can improve torque tracking by improving disturbance rejection, but may also reduce bandwidth [34]. It is easiest to think of disturbance rejection in extremes. Consider the following scenario: the motor is being held still, the inner Bowden cable is taut, and the user suddenly flexes the exoskeleton. If the Bowden cable has high stiffness, a large increase in force is generated quickly. If the Bowden cable has extremely low stiffness, like a rubber band, the user can quickly flex their joint without developing a large change in force. However, greater compliance in the transmission also reduces force bandwidth. If the transmission is very stiff, the Bowden cable is taut and there is a step increase in desired torque, the motor turns a tiny amount to create tension in the cable and a large force is quickly generated. If the transmission has very low stiffness, the motor must turn much further to generate the same amount of force, as force is equal to the stiffness of the transmission multiplied by displacement. Because the motor must turn more when the transmission is less stiff, it takes more time to develop torque and lag is experienced between the desired and measured torque, which limits force bandwidth.

There is some intermediate stiffness that supplies some disturbance rejection without reducing bandwidth below acceptable levels. The optimal stiffness depends on the frequency content of the desired torque and the magnitude and frequency of disturbances. The best stiffness for an ankle exoskeleton was shown to be that which most closely approximated desired torque patterns while holding the motor in a fixed position during walking [35]. Additionally, the stiffness of the entire transmission—the cable, the added spring, the straps, the structure of the exoskeleton, and the soft tissues of the user—needs to be considered. In some cases, the user's soft tissues may reduce the stiffness of the exoskeleton/user system below the ideal stiffness for torque tracking. When this occurs, adding a spring cannot improve torque tracking.

13.4.6 MATERIALS AND MANUFACTURING

Components for end-effectors can be machined, 3D-printed, or made by carbon fiber layup. Most other manufacturing techniques are too expensive, as these devices are made in batches of only one or two. Each of these manufacturing techniques has pros and cons that should be considered.

Computer Numerical Control (CNC) machining is widely available and somewhat complex shapes can be achieved affordably, allowing for a more closely fitting exoskeleton than that possible with a few simple planar parts. CNC machining is a highly repeatable method and the material properties of CNC machined metals, such as aluminum, are well understood. It is helpful as a designer to have a good understanding of material properties and expected fatigue life.

3D-printing is attractive for exoskeleton design as very complex geometry can be easily achieved. Flowing 3D shapes can be made to wrap elegantly around the leg and small details for attachment to other components are simple to create. Complex or hollow cross sections can be created to achieve mass efficient designs. However, 3D-printed materials have less predictable bulk material properties as the strength of the material is higher within a printed layer and lower between layers.

An exoskeleton's life likely involves more than a million steps, so fatigue becomes a real concern and predicting the fatigue life of 3D-printed materials is currently extremely difficult. Little information is available on the performance of 3D-printed materials in high cycle applications. Fatigue life of parts depends on surface finish and the size and quantity of internal defects. Printed materials are porous by nature and high residual stresses are created as a result of the additive manufacturing process. This makes printed materials more susceptible to fatigue than similar conventionally machined materials [36].

When small or noncyclic loads are expected and fatigue is not an issue, inexpensive plastic 3D-printed parts can be lightweight and convenient. Spacers, sensor protectors, cable guides, and bump guards can all be produced easily and relatively cheaply using 3D-printing processes such as fused deposition modeling or stereolithography.

Carbon fiber is an attractive material for exoskeletons as it has a high strength to weight ratio. Carbon fiber is expensive both in terms of raw material and manufacturing costs. The complexity of 3D parts made by carbon fiber layup is limited by how fine the weave is. Carbon fiber does not easily conform to sharp bends and cannot achieve small complex geometry. Custom carbon fiber layups can result in very nice form-fitting exoskeletons, but care needs to be taken in their design. The orientation of the fibers needs to be considered and the bulk properties stated for the epoxy or carbon fiber material should be considered rough estimates as they depend on the quality of the layup itself. Additionally, carbon fiber is extremely susceptible to wear through abrasion and care should be taken to avoid any rubbing between carbon fiber components and other parts.

Sheets of carbon fiber, fiberglass, metals, and plastics can all be interesting materials if planar parts are being considered. Planar parts are very quick and cheap to form by a variety of processes including waterjet cutting, plasma cutting, and laser cutting. Waterjet cutting of carbon fiber is particularly attractive because it is very inexpensive and the hazardous dust is captured in the cutting fluid. The cost-effectiveness of parts becomes especially important when addressing sizing and fit through modularity. Making the majority of a frame out of planar parts makes having three or more sizes more affordable than if utilizing complex three-dimensional parts. In addition to being affordable, planar parts also have very predictable beam stiffness, which allows compliance in select directions for fit and freedom of motion.

In general, 3D-printing is advantageous where extremely complex geometry is necessary, CNC machining is appropriate for moderately complex parts, and waterjet cutting of carbon fiber plates is effective for large parts that will be replicated in multiple sizes or where compliance in select directions is needed.

13.4.6.1 Case study—the evolution of the CMU ankle exoskeleton

The frame of the first iteration of the ankle exoskeleton was composed of planar carbon fiber parts to allow for high compliance in the frontal plane and to reduce cost (Fig. 13.10A). The next three iterations use simple rectangular carbon fiber struts (Fig. 13.10B–D). These shapes have lower compliance, but are well suited to the expected loading, make manufacturing multiple sizes inexpensive, and provide compliance at the tops of the struts to fit calves of different diameters. Adjustability was added for the fourth iteration (Fig. 13.10D). The fourth ankle exoskeleton is part of a larger Bilateral Lower Limb Exoskeleton Emulator (BiLLEE) capable of assisting the ankles, knees, and hips.

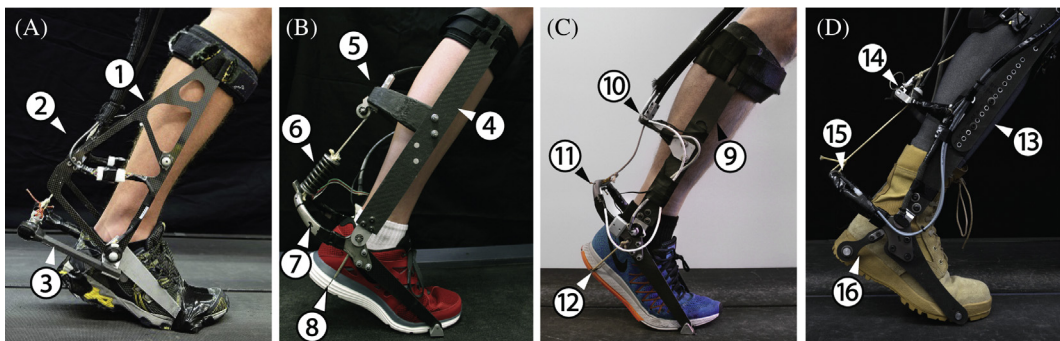


FIGURE 13.10

Evolution of ankle exoskeleton end-effectors (A) The original ankle exoskeleton is comprised almost entirely of (1) planar carbon fiber parts with (2) a rectangular Bowden cable termination connecting the medial and lateral aspects of the frame. (3) Fiberglass leaf springs provide series elasticity and leverage. (B) A more recent iteration of the ankle exoskeleton featuring (4) rectangular carbon fiber frame, (5) a hollow carbon fiber Bowden cable termination, (6) a steel coil spring, (7) a hollow titanium heel spur, and (8) a heel rope. (C) (9) The rectangular carbon fiber frame was reused and the Bowden cable termination was replaced with (10) a CNC aluminum component. (11) The titanium heel spur and (12) heel rope were also reused. The coil spring was removed as elasticity in the inner Bowden cable itself was found to be sufficient. (D) This ankle exoskeleton is a small part of a Bilateral Lower Limb Exoskeleton Emulator (BiLLEE). Discrete adjustability was added to the (13) frame. (14) The Bowden cable termination and (15) titanium heel spur remain mostly unchanged. The heel rope was replaced with (16) a carbon fiber link attached to a rod extending through the heel of the shoe to allow compressive loads to be carried.

(A) Adapted from J. Zhang, P. Fiers, K.A. Witte, R.W. Jackson, K.L. Poggensee, C.G. Atkeson, et al., *Human-in-the-loop optimization of exoskeleton assistance during walking*, *Science* 356 (6344) (2017a) 1280–1284; (B) Adapted from K.A. Witte, J. Zhang, R.W. Jackson, S.H. Collins, *Design of two lightweight, high-bandwidth torque-controlled ankle exoskeletons*, in: *IEEE International Conference on Robotics and Automation (ICRA)*, 2015, pp. 1223–1228.

A heel rope is used in three of the ankle exoskeleton iterations (Fig. 13.10 A–C). It is strong and stiff in tension, but allows for free motion of the ankle in rotation and inversion and eversion, which would be difficult to match with other more conventional materials. The heel rope was replaced with a carbon fiber link in the fourth iteration (Fig. 13.10D) to allow loading in compression, as part of the BiLLEE system.

The Bowden cable housing termination connects the medial and lateral aspects of the shank portion of the frame. The frame of the first iteration had to be large and extend far behind the calf to allow a rectangular shaped termination to work along with the fiberglass leaf springs (Fig. 13.10A). This configuration was easy to produce, but created a large boxy device envelope. The envelope was too large to allow for bilateral testing as frequent collisions occurred between the left and right exoskeletons. For this reason, we changed to a sweeping, U-shaped Bowden cable housing termination that fit the leg more closely (Fig. 13.10B–D). The first U-shaped termination was made out of hollow carbon fiber (Fig. 13.10B). This part was formed by casting a wax mold of the component, performing a carbon fiber layup around the wax form, and melting the wax out by submerging the part in warm water. While this produced a lightweight component, it was very time-consuming to manufacture. For ease of manufacturing, the Bowden cable housing termination was changed to a machined aluminum component (Fig. 13.10C and D).

Series elasticity was originally supplied by fiberglass leaf springs (Fig. 13.10A). It was believed that this design would be lightweight as the leaf springs could act as both springs and as a lever. But bulky connective hardware was needed to allow for robust attachment that prevented cracks from developing in the leaf springs. A coil spring was later used to provide series elasticity. The spring was heavy and torque tracking was acceptable without it. So the spring was removed in subsequent iterations (Fig. 13.10C and D).

The lever supplied by the leaf springs was replaced with a 3D-printed titanium heel spur (Fig. 13.10B–D). The complex loading experienced in the part was well addressed by a complex flowing shape easily produced by additive manufacturing. Torsion experienced in the middle of the horseshoe shape is well addressed by a hollow tube while bending stresses at the tips of the horseshoe can be reduced by using an I-beam cross section. The majority of the heel spur is hollow, which would not be possible with conventional machining. The first iteration of the titanium spur experienced failure due to fatigue after 2 years of use (Fig. 13.11). It is likely the next iteration of the heel spur will be conventionally machined because the fatigue life of conventional materials can be better predicted. This change will be made at the cost of added mass as hollow cross sections will not be possible using conventional machining.

13.5 CONTROL

Control of robotic systems can be split into high-level control of behaviors and low-level control of positions or torques. High level control determines *what* you want your device to do while low level control is *how* your device achieves it. The high-level controller determines the desired torque or position, and the low-level control attempts to track the desired signal as closely as possible. Emulator systems are most often used to give the user the experience of using a candidate device, and so the low-level controller typically aims to match the torques that would have been produced by that device.

**FIGURE 13.11**

Titanium heel spur created by electron beam melting (EBM). Additive manufacturing allows for simple manufacturing of (1) sweeping shapes with hollow cross sections and small complex geometry such as the (2) split hub clamp. However, this manufacturing process has some drawbacks. The printed material cannot be reliably threaded, so (3) a slot was required for capturing a nut for tightening the clamp. Hollow cross sections are filled with partially sintered titanium dust which require (4) vents to be included. The vent holes must be large enough to allow a small pick access to the hollow area to forcibly remove the dust. These vents limit the strength of the part and reduce the usefulness of the hollow cross sections. Other additive manufacturing techniques such as selective laser sintering require smaller holes and the dust can be simply blown out with compressed air. Material made through additive manufacturing is especially susceptible to fatigue failure due to its porosity and poor surface finish. (5) Fatigue cracking began at the bottom of the part, propagated up to the vent hole and continued to the top of the component after 2 years of consistent use.

The simplest form of closed-loop low-level control is proportional control. The measured torque is subtracted from the desired torque to calculate the torque error which is then multiplied by a gain. This value then becomes the motor velocity command. In this way, the motor turns to take up slack when torque is too low and spins the other direction to let out slack when torque is too high. The speed that the motor turns is proportional to the error, so the bigger the error, the faster the motor turns.

Stability can be added to proportional control by adding damping injection. A damping gain is applied to the measured motor velocity and the product is subtracted from the motor velocity command such that there is resistance to further speeding up the motor when the motor is already moving very rapidly.

An iterative learning term can be added to the motor command to correct for error that is consistent across multiple consecutive steps. Iterative learning takes advantage of the repetitive nature of walking to create a feed-forward term based on past torque tracking error. Zhang et al. [34] provide information on how to implement iterative learning.

If a series elastic actuator is being used, other methods of improving disturbance rejection include disturbance observers [37,38], acceleration feedback [39], and model-based environment-adaptive control [40].

13.5.1 CASE STUDY—CONTROL OF ANY CMU EMULATOR

In the case of the CMU ankle and knee exoskeletons, the low level torque controller consists of proportional control plus damping injection and iterative learning as described in Eq. (13.1).

$$\dot{\theta}_{des}(i, n) = K_p * e_{\tau}(i, n) - K_{damp} * \dot{\theta}_m(i, n) + \dot{\theta}_{learn}(i + d, n) \quad (13.1)$$

There are two indices in Eq. (13.1). i indicates the time step, which is set to zero at the moment of heel strike and is updated at a rate of 500 Hz. n refers to the number of the current stride which is updated at every heel strike of the same foot. d is a delay equal to the number of time steps required for a change in motor velocity to be reflected in applied torque. $\dot{\theta}_{des}$ refers to the desired motor velocity. K_p is the proportional gain applied to e_{τ} , the error in torque tracking. K_{damp} is the damping gain applied to $\dot{\theta}_m$, motor velocity. $\dot{\theta}_{learn}$ is a learning term calculated in Eq. (13.2).

$$\dot{\theta}_{learn}(i, n) = \beta * \dot{\theta}_{des}(i, n - 1) - K_l * e_{\tau,filt}(i, n - 1) \quad (13.2)$$

where β is a “forgetting” term that acts as a weight on the learned trajectory and K_l is a gain applied to the filtered torque error, $e_{\tau,filt}$, which is calculated in Eq. (13.3).

$$e_{\tau,filt}(i, n) = (1 - \gamma) * e_{\tau,filt}(i, n - 1) + \gamma * e_{\tau}(i, n) \quad (13.3)$$

where γ is a weighting term on the learned error. For more information on this approach refer to [34].

Many other control strategies have been tried on the CMU emulator system, but proportional control with damping injection and iterative learning have proven to be the most effective. It is important to note that iterative learning, as implemented on the CMU emulator, has limited utility during nonsteady-state behavior as the cyclic nature of walking cannot be exploited. Other low-level control strategies may be required for accurate torque or position tracking during nonsteady-state behaviors.

Time-based control has been used extensively on the ankle exoskeleton. After performing individualized optimization of control parameters, the time-based controller has delivered a 23% reduction in metabolic energy on average with some subjects experiencing reductions as high as 37% [2]. Proportional electromyographic control and electromyographic control with a virtual muscle tendon model are currently under evaluation.

13.6 MAKING STRIDES IN THE FUTURE

Emulator testbeds are accelerating exoskeleton development and will help researchers and industry partners to quickly develop viable commercial products that improve lives. Emulators allow more rapid progress than that possible using complex untethered systems based mainly on intuition without experimental data to guide design.

Whether designing exoskeletons as emulator end-effectors or as standalone untethered devices, many of the same guiding principles apply: keep designs simple, allow for natural motion, and minimize weight while maintaining safety and comfort.

While some researchers may develop untethered product-like devices to address problems like nonsteady-state locomotion and uneven terrain, there are more questions we can answer in the lab

before making the leap to mobile systems. How can exoskeletons best improve stability and prevent falls? Which joints should we assist to improve maximum running speed? How does exoskeleton use affect muscle–tendon dynamics? How can we best facilitate user adaptation to assistive devices? Is there a single control strategy that is effective for multiple gaits? Can we use exoskeletons to teach novel skills such as dancing or football punting? How do the answers to these questions affect the design of our devices? It is our hope that researchers will tackle these questions and more by applying our guidelines for design and taking on the testbed strategy to help their exoskeletons evolve into effective tools efficiently and affordably.

REFERENCES

- [1] K.A. Witte, A.M. Fatschel S.H. Collins, Design of a lightweight, tethered, torque-controlled knee exoskeleton, in: 2017 International Conference on Rehabilitation Robotics (ICORR), July 2017, pp. 1646–1653.
- [2] J. Zhang, P. Fiers, K.A. Witte, R.W. Jackson, K.L. Poggensee, C.G. Atkeson, et al., Human-in-the-loop optimization of exoskeleton assistance during walking, *Science* 356 (6344) (2017) 1280–1284.
- [3] J.M. Caputo, S.H. Collins, An experimental robotic testbed for accelerated development of ankle prostheses, in: 2013 IEEE International Conference on Robotics and Automation (ICRA), 2013, pp. 2645–2650.
- [4] J.M. Caputo, S.H. Collins, A universal ankle–foot prosthesis emulator for human locomotion experiments, *J. Biomech. Eng.* 136 (3) (2014) 035002.
- [5] K.A. Witte, J. Zhang, R.W. Jackson, S.H. Collins, Design of two lightweight, high-bandwidth torque-controlled ankle exoskeletons, in: IEEE International Conference on Robotics and Automation (ICRA), 2015, pp. 1223–1228.
- [6] M. Kim, T. Chen, T. Chen, S.H. Collins, An ankle–foot prosthesis emulator with control of plantarflexion and inversion–eversion torque, *IEEE Trans. Robot.* 99 (2018) 1–12.
- [7] Y. Ding, I. Galiana, A. Asbeck, B. Quinlivan, S.M.M. De Rossi, C. Walsh, Multi-joint actuation platform for lower extremity soft exosuits, in: 2014 IEEE International Conference on Robotics and Automation (ICRA), May 2014, pp. 1327–1334.
- [8] Y. Ding, I. Galiana, A.T. Asbeck, S.M.M. De Rossi, J. Bae, T.R.T. Santos, et al., Biomechanical and physiological evaluation of multi-joint assistance with soft exosuits, *IEEE Trans. Neural Syst. Rehabil. Eng.* 25 (2) (2017) 119–130.
- [9] C. Verhelst, Sport Research Laboratory, Ghent University, <https://www.ugent.be/ge-bsw/en/sportlab> (accessed 22.07.19)
- [10] A. Roy, H.I. Krebs, S.L. Patterson, T.N. Judkins, I. Khanna, L.W. Forrester, et al., Measurement of human ankle stiffness using the anklebot, in: 2007 IEEE 10th International Conference on Rehabilitation Robotics, IEEE, June 2007, pp. 356–363.
- [11] H. Lee, E.J. Rouse, H.I. Krebs, Summary of human ankle mechanical impedance during walking, *IEEE J. Transl. Eng. Health Med.* 4 (2016) 1–7.
- [12] S.H. Collins, M.B. Wiggin, G.S. Sawicki, Reducing the energy cost of human walking using an unpowered exoskeleton, *Nature* 522 (7555) (2015) 212.
- [13] P. Malcolm, W. Derave, S. Galle, D. De Clercq, A simple exoskeleton that assists plantarflexion can reduce the metabolic cost of human walking, *PLoS One* 8 (2) (2013) e56137.
- [14] D. Ferris, G. Sawicki, A. Domingo, Powered lower limb orthoses for gait rehabilitation, *Topics Spinal Cord Injury Rehabil.* 11 (2) (2005) 34–49.

- [15] L.M. Mooney, E.J. Rouse, H.M. Herr, Autonomous exoskeleton reduces metabolic cost of human walking during load carriage, *J. Neuroeng. Rehabil.* 11 (1) (2014) 80.
- [16] J. Lee, K. Seo, B. Lim, J. Jang, K. Kim, H. Choi, Effects of assistance timing on metabolic cost, assistance power, and gait parameters for a hip-type exoskeleton, in: 2017 International Conference on Rehabilitation Robotics (ICORR), IEEE, July 2017, pp. 498–504.
- [17] F.A. Panizzolo, I. Galiana, A.T. Asbeck, C. Siviy, K. Schmidt, K.G. Holt, et al., A biologically-inspired multi-joint soft exosuit that can reduce the energy cost of loaded walking, *J. Neuroeng. Rehabil.* 13 (1) (2016) 43.
- [18] J.M. Donelan, Q. Li, V. Naing, J.A. Hoffer, D.J. Weber, A.D. Kuo, Biomechanical energy harvesting: generating electricity during walking with minimal user effort, *Science* 319 (5864) (2008) 807–810.
- [19] A. Esquenazi, M. Talaty, A. Packel, M. Saulino, The ReWalk powered exoskeleton to restore ambulatory function to individuals with thoracic-level motor-complete spinal cord injury, *Am. J. Phys. Med. Rehabil.* 91 (11) (2012) 911–921.
- [20] C. Meijneke, W. van Dijk, H. van der Kooij, Achilles: an autonomous lightweight ankle exoskeleton to provide push-off power, in: 2014 5th IEEE RAS & EMBS International Conference on Biomedical Robotics and Biomechatronics, IEEE, 2014, pp. 918–923.
- [21] W. van Dijk, C. Meijneke, H. Van Der Kooij, Evaluation of the Achilles ankle exoskeleton, *IEEE Trans. Neural Syst. Rehabil. Eng.* 25 (2) (2017) 151–160.
- [22] A. Ruina, R. Pratap, Introduction to Statics and Dynamics, 2015, accessed 1 May 2018, <http://ruina.tam.cornell.edu/Book/>.
- [23] J.E. Sanders, B.S. Goldstein, D.F. Leotta, Skin response to mechanical stress: adaptation rather than breakdown—a review of the literature, *J. Rehabil. Res. Dev.* 32 (3) (1995) 214.
- [24] M.B. Yandell, B.T. Quinlivan, D. Popov, C. Walsh, K.E. Zelik, Physical interface dynamics alter how robotic exosuits augment human movement: implications for optimizing wearable assistive devices, *J. Neuroeng. Rehabil.* 14 (1) (2017) 40.
- [25] R.C. Browning, J.R. Modica, R. Kram, A. Goswami, The effects of adding mass to the legs on the energetics and biomechanics of walking, *Med. Sci. Sports Exerc.* 39 (3) (2007) 515–525.
- [26] K.A. Shorter, A. Wu, A.D. Kuo, The high cost of swing leg circumduction during human walking, *Gait Posture* 54 (2017) 265–270.
- [27] K.W. Witte, S.H. Collins, Ankle Exoskeleton Designs, 2018. <https://biomechatronics.stanford.edu/exo-design>.
- [28] B.T. Quinlivan, S. Lee, P. Malcolm, D.M. Rossi, M. Grimmer, C. Siviy, et al., Assistance magnitude versus metabolic cost reductions for a tethered multiarticulate soft exosuit, *Sci. Robot.* 2 (2) (2017). p.eaah4416.
- [29] S.D. Potter, C.E. Thorne, M.P. Murphy, Google Inc, 2016. Brace system. U.S. Patent 9,333,107.
- [30] A. Schiele, P. Letier, R. Van Der Linde, F. Van Der Helm, Bowden cable actuator for force-feedback exoskeletons, in: International Conference on Intelligent Robots and Systems, 2006 IEEE/RSJ, October 2006, pp. 3599–3604.
- [31] D.P. Ferris, C.L. Lewis, Robotic lower limb exoskeletons using proportional myoelectric control, in: Engineering in Medicine and Biology Society, 2009. EMBC 2009. Annual International Conference of the IEEE, IEEE, September 2009, pp. 2119–2124.
- [32] H. Huang, F. Zhang, L.J. Hargrove, Z. Dou, D.R. Rogers, K.B. Englehart, Continuous locomotion-mode identification for prosthetic legs based on neuromuscular–mechanical fusion, *IEEE Trans. Biomed. Eng.* 58 (10) (2011) 2867–2875.
- [33] G.A. Pratt, M.M. Williamson, Series elastic actuators, in: Intelligent Robots and Systems 95.' IEEE/RSJ International Conference on Human Robot Interaction and Cooperative Robots', Proceedings, IEEE, August 1995, Vol. 1, pp. 399–406.

- [34] J. Zhang, C.C. Cheah, S.H. Collins, Torque control in legged locomotion, in: M. Sharbafi, A. Seyfarth (Eds.), *Bio-Inspired Legged Locomotion: Models, Concepts, Control and Applications*, with editors, Butterworth-Heinemann, 2017, pp. 347–395.
- [35] J. Zhang, S.H. Collins, The passive series stiffness that optimizes torque tracking for a lower-limb exo-skeleton in human walking, *Front. Neurorobot.*, 11, 2017.
- [36] T.A. Book, M.D. Sangid, Strain localization in Ti-6Al-4V Widmanstätten microstructures produced by additive manufacturing, *Mater. Charact.*, 122, 2016, pp. 104–112.
- [37] S. Oh, K. Kong, High-precision robust force control of a series elastic actuator, *IEEE/ASME Trans. Mech.* 22 (1) (2017) 71–80.
- [38] Z. Li, C.Y. Su, L. Wang, Z. Chen, T. Chai, Nonlinear disturbance observer-based control design for a robotic exoskeleton incorporating fuzzy approximation, *IEEE Trans. Ind. Electr.* 62 (9) (2015) 5763–5775.
- [39] A. Calanca, P. Fiorini, A rationale for acceleration feedback in force control of series elastic actuators, *IEEE Trans. Robot.* (2018).
- [40] A. Calanca, P. Fiorini, Understanding environment-adaptive force control of series elastic actuators, *IEEE/ASME Trans. Mechatr.* 23 (1) (2018) 413–423.

PHYSICAL ASSISTANT ROBOT SAFETY

14

Yoji Yamada and Yasuhiro Akiyama

Nagoya University, Nagoya, Japan

14.1 INTRODUCTION

Securing human safety is indispensable in the use of human coexistent robots and robotic devices. Initiated by a strong demand from society, safety standard ISO 13482 [1], in which a wearable robot is defined as a restrain-type physical assistant robot, was published in February, 2014. The standard compiles safety requirements for personal care robots which are defined as several types of service robots, including wearable robots, which perform actions contributing directly toward improvement in the quality of life of humans. This chapter deals with two hazards, human skin abrasion and falls, which are identified in the first process of conducting a risk assessment and associated with typical risks which are not negligible.

Skin abrasion can occur between human skin and the cuff which is used to clamp a wearable robot on a part of the human body, generating such wounds as blisters, scratches, etc. This risk can be considered as being unacceptable not because of the severity of harm, but the probability of occurrence is high due intrinsically to continuous wearing of the robot.

On the other hand, the risks associated with a fall by a human wearing a robot are estimated to be intrinsically high. However, this is not specifically shown in the safety standard ISO 13482 simply because there have been few studies on this risk analysis. In the following sections of this chapter, the first half deals with a description of human skin abrasion and the second with human falls.

14.2 CONTACT SAFETY OF THE PHYSICAL ASSISTANT ROBOT

14.2.1 INTRODUCTION

This standard is followed by another standard for the safety verification and validation (V&V) of personal care robots to be published as a technical report (ISO/TR). The article describes a typical example of a V&V test method developed by the author's research group for estimating the wound risk in the use of wearable robots.

The target is blister generation. Physical stress hazards are identified from the statement in 5.9.2 of ISO 13482 stating that a personal care robot shall be designed to minimize or reduce physical stress or strain to its user from continuous use. After conducting intensive studies to identify any

hazards originating in the ergonomic mismatch between the wearer's body part and the cuff of a wear, we concluded that the risk of generating skin wounds becomes nonnegligible in the use of wearable robots where the cuff parts are in direct contact with the human skin, with or without clothing. Later it was also reported that friction blisters were observed to be generated relatively easily with the use of a wearable robot by a wearer suffering from liver cirrhosis [2].

It is to be stressed that this type of risk is unique to a wearable robot because the probability of occurrence can be high, while the severity of such wounds as blisters is estimated to be very low when this type of robot is worn by a wearer.

14.2.2 VERIFICATION AND VALIDATION TEST PROCEDURE

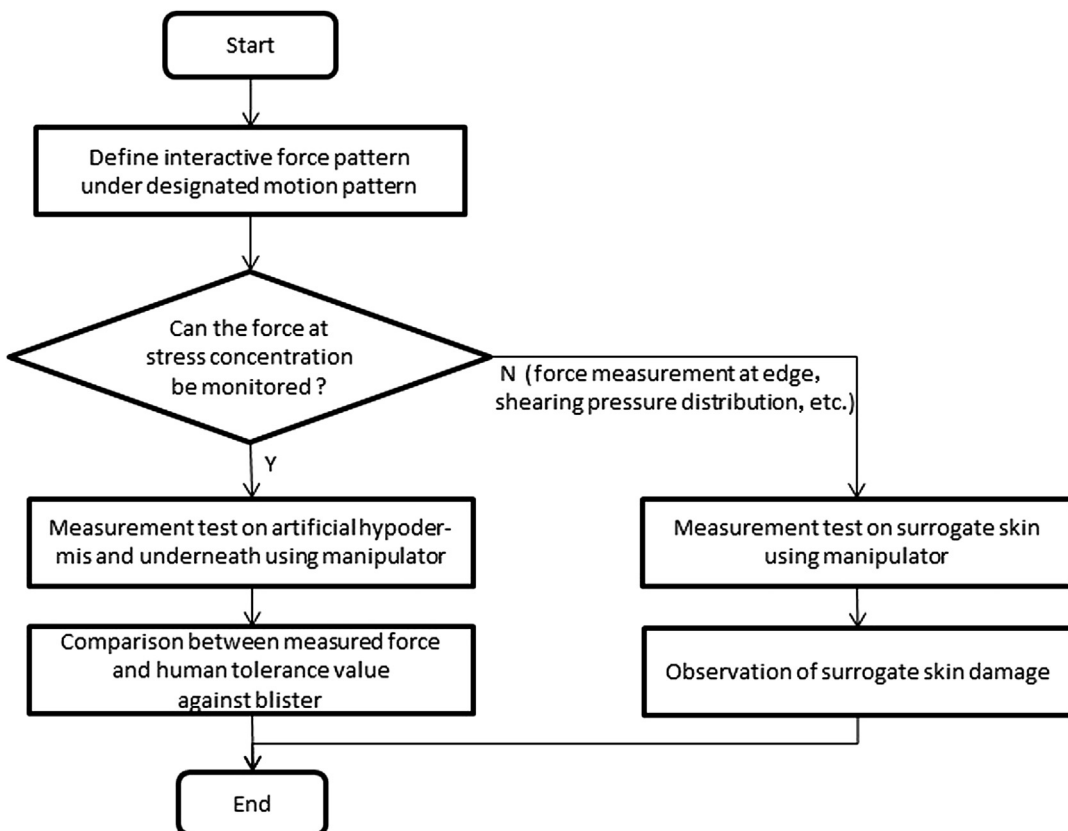
In the test methods, we developed a test of the physical hazard characteristics for wearable robots. The test procedure consists of three steps: (1) defining contact states and the pattern of maximum load on the human body when the robot is worn in his/her predetermined periodical motion of interest; (2) preparing material simulating human hypodermis and underneath under the contact surfaces of such body parts as upper/lower extremities, waist, and so on, where contact parts of wearable robots such as cuffs are attached, and a surrogate for a human skin piece is fixed, if necessary, between the surfaces of the cuff and the simulated material; (3) replicating and recording the pattern of maximum/average load exerted on the surrogate skin piece in the same contact states as those defined in (1). The surrogate tissue can be inspected for injury during the test. An overview of the V&V test procedure from (1) above is illustrated in Fig. 14.1, where the test flow is classified into two cases: (1) measurement of shearing force/pressure if the stress concentration area is identified and monitored at the contact point of risk; and (2) observation of damage to the surrogate skin piece if the stress concentration is not well monitored. The following sections describe the test method in detail.

14.2.3 VERIFICATION EXPERIMENTS FOR OBTAINING AN INHERENTLY SAFE REGION AGAINST BLISTER GENERATION

14.2.3.1 *Verification procedure*

We developed a novel blister generation method for establishing a safety verification test system focusing on skin friction trauma [3,4]. The surrogate skin used as the experimental subject was excised from the anterior part of a pig's shank shortly after its death, and delivered to the laboratory within 16 hours under 4°C. Before the experiments, the skin surface was dehaired using scissors, cleaned by alcohol, and the excessive fat underneath was also removed. In the study, the representative direction (shear direction) of the force component was selected to emulate the skin surface-rubbing phenomenon.

To conduct a horizontal reciprocating rubbing action, a rheometer (DHR: TA Instrument Co.) was used to exert oscillating rotational rubbing on the surrogate skin with high calibration accuracy. The surrogate skin for the test was extended and firmly clamped between a plate with a sheet of sandpaper (40#) attached and a fixation frame as shown in Fig. 14.2. After a set period of rubbing under oscillating shear force, the structure of the surrogate skin was examined by serial sectioning

**FIGURE 14.1**

Overview of the V&V test procedure.

at intervals of 10 μm and the microsection was analyzed by hematoxylin and eosin (H&E) staining, and the stained sections were observed sequentially with a microscope.

The shear stress distribution (traction) of the porcine skin surface under the stainless steel circular plate of DHR $\tau(r)$ should be a function of the detected point r distant from the center of the circle according to the skin's viscosity η , shear rate $\dot{\gamma}$, angular velocity Ω , and thickness H

$$\tau(r) = \eta \dot{\gamma} = \eta \frac{\Omega}{H} r$$

The torque T exerted at the contacting area of the circular plate, whose radius is R , can be measured by DHR and the traction under rubbing can be finally calculated as

$$\tau(r) = \frac{2T}{\pi R^4} \cdot r$$

We can accurately set a traction value to be exerted on the target area of the porcine skin surface which contacts with the rubbing head of the DHR.

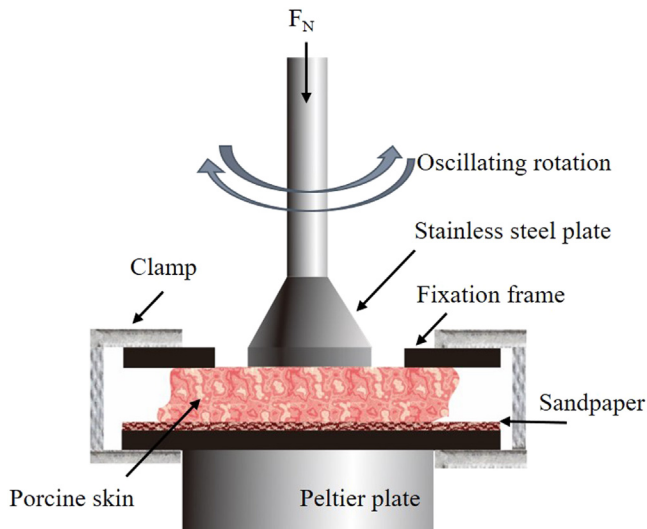
**FIGURE 14.2**

Diagram of surrogate skin fixation and the main parts of the experimental apparatus.

14.2.3.2 Verification experiments

After each rubbing test, the experimental subject was fixed with 10% formalin for 8 hours, and then 20% sucrose and 30% sucrose for 8 hours sequentially, and sectioned with a cryostat (Leica Microsystems Co.) at 10 μm . The skin structure was then analyzed with H&E staining. The section of original porcine skin without rubbing and the microscopic appearance of porcine skin after the first rubbing experiment are shown in Fig. 14.3A and B, respectively.

It can be seen from Fig. 14.3A that the main epidermal structure of porcine skin, including the stratum corneum, stratum granulosum, stratum spinosum, and epidermal basal layer, are intact before rubbing test. As supposed to the previous experimental blister generation studies on normal human skin by Naylor [5], friction force can be transmitted through the “stratum corneum and granulosum” of the epidermis, degenerating the stratum spinosum, and finally producing clefts between the stratum granulosum and basal layer. Once they are filled with fluid from the dermis, these clefts develop friction blisters rapidly. Compared with the section of original porcine skin shown in Fig. 14.3A and the section after 1200 seconds of rubbing under shear stress value 3.2×10^4 Pa shown in Fig. 14.3B, it can be observed clearly that there is severe splitting generated in the stratum spinosum layer of the porcine skin.

According to Sulzberger's study [6], the blister cleft or cavity always appears at the same intraepidermal layer, with the blister roof composed of the stratum corneum, stratum granulosum, and a segment of traumatically degenerated stratum spinosum. Therefore, the cleft in Fig. 14.3B, with intact stratum granulosum and stratum corneum, can be regarded as evidence of the first stage of blister generation.

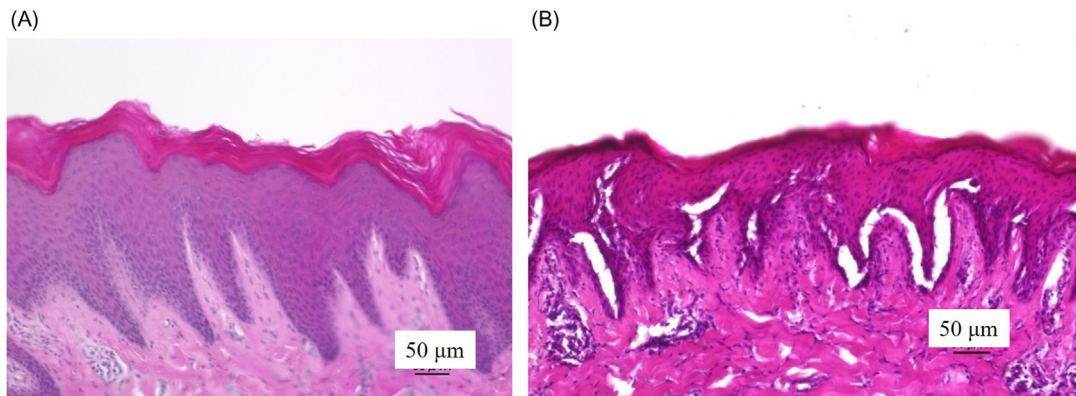


FIGURE 14.3

Cross-sectional photos of porcine tissue. (A) Appearance of the structure of the original porcine skin surface; (B) intraepidermal clefts after 1200 s of rubbing under a shear stress value of 3.2×10^4 Pa.

In order to confirm the availability of porcine skin, the characteristics of blister generation shall match those obtained in the previous blister generation test using human skin as the subject, which was conducted by Naylor. In our experimental model, we set traction as a unit of the interactive force between the porcine skin and the rubbing head. In the case of the human skin test reported in Naylor's study, only the compression and average friction force were described in detail. Therefore a condition-matching calculation is necessary for us to convert the friction force in Naylor's study to the corresponding traction for comparing their blister generation characteristics. Since the rubbing head applied in Naylor's study was a small hemisphere, the tested traction value can be calculated approximately based on Hertz theory

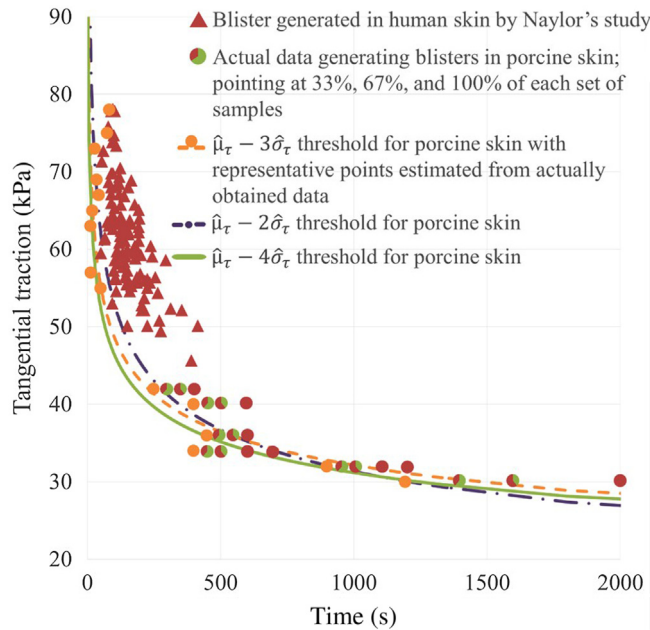
$$\tau(r) = \frac{3\mu P}{2\pi a^2} \frac{\sqrt{a^2 - r^2}}{a}$$

$$a = \left(\frac{3PR}{4E^*}\right)^{\frac{1}{3}}$$

where P is the total load compressing the skin surface, μ is the friction coefficient, R is the relative curvature of the hemispherical indenter, and E^* can be calculated by the elasticity moduli and Poisson's ratios of the two surfaces in contact with each other.

14.2.3.3 Analysis for the safety verification test

We calculated a regression curve from the inherently safe time points, regarding it as an inherently safe threshold, and combines it with the human subject's blister generation conditions to produce a new tangential traction–time characteristic for blister generation, as shown in Fig. 14.4. It can be seen that the threshold is located in the safety region left of and below the points representing human blister generation. We claim from these results that it is feasible to utilize a surrogate skin as a reliable safe verification test model to confirm that a defined action is effective in avoiding the

**FIGURE 14.4**

Combination of a porcine skin's inherently safe conditions and human subjects' blister generation conditions.

generation of friction blisters. However, more appropriate calculation for the inherently safe time points and drawing the threshold line may require a larger number of samples.

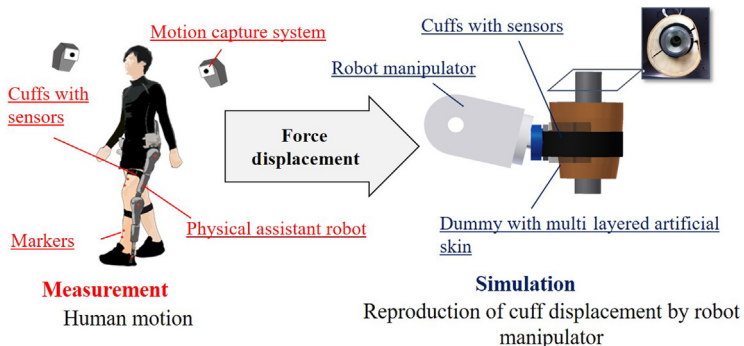
14.2.4 VALIDATION TEST METHOD FOR WOUND RISK

14.2.4.1 Principles and procedure

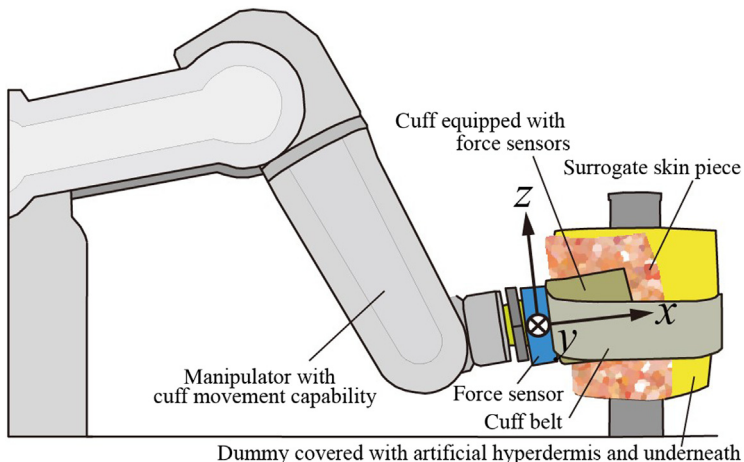
We developed a validation test method [7] which was applied to lower limb wearable robots, each supported by cuffs tied by belts to make firm contact with human skin. The validation test procedure comprises the following three steps. Beginning by defining test conditions, we conducted validation tests mainly using the cuff motion reproduction apparatus of our development, and ended with data logging. Fig. 14.5 shows an overview of the flow of the V&V testing methodology.

First, such motion parameters as shown below are measured in the state where a subject takes actions while wearing a lower limb wearable robot. The first parameter is the relative displacement of the motion of one of the cuffs which support the robot on the subject's lower limbs, with respect to the coordinate frame defined on the lower limb. The second parameter is the interaction force exerted at the contact surface between the lower limb surface and the cuff.

Second, the data sequence of the motion parameters are reflected on the cuff, which is mounted at the end effector of a conventional six-axis manipulator and makes contact with artificial skin (hypodermis and underneath), whose viscoelastic characteristics are similar to those of human skin.

**FIGURE 14.5**

Overview of the flow of the V&V testing methodology.

**FIGURE 14.6**

A manipulator grasps the cuff covering the upper/lower limb.

Fig. 14.6 shows a manipulator and artificial skin system in which the manipulator grasps the cuff covering the upper/lower limb.

We call this data transfer contact motion reproduction. This complies with one of the recommended V&V methods specified in Section 5.9.2 of ISO 13482, and the following specifies the validation test procedure.

1. The first step is to define the test conditions in view of the specifications of the wearable robot to be tested.
 - a. Physical frame of the user

The test will be conducted on the assumption that the user possesses the lower thigh, femur, and lumbar shape based on the average physical frame of target users. If the limitations are to be imposed on the physical frame of the wearable robot user, modifications may be made after consultations with the manufacturer over the conditions.

b. Robot wearing condition

The test shall be conducted under robot wearing conditions anticipated in normal use (standing and sitting, walking, and picking up objects).

c. Load pattern on a robot cuff

In the patterns of the movement in normal use anticipated in robot wearing conditions, the states of the robot cuff in contact with the human body where the robot is worn are selected to define the pattern of maximum load as well as that of maximum relative displacement and velocity vectors, with attention to target robot mass and attachment method.

d. Load time on the robot cuff

The load time is defined with attention to maximum time of use in one robot operation anticipated in normal use.

2. Test

a. Preparations

i. Production of jig tools

Due to attachment of the robot cuff in contact with the human body to a 3-D load device, jig tools adapted to the target robot are produced for the test.

ii. Replicate of the attachment areas

The robot cuff with a 3-D load device is attached to the dummy with artificial skin under specified attachment conditions. Note that the 3-D load device which is embedded in the inner side of a cuff for measuring the contact force/pressure should be small enough to satisfy the condition of observing the maximal traction.

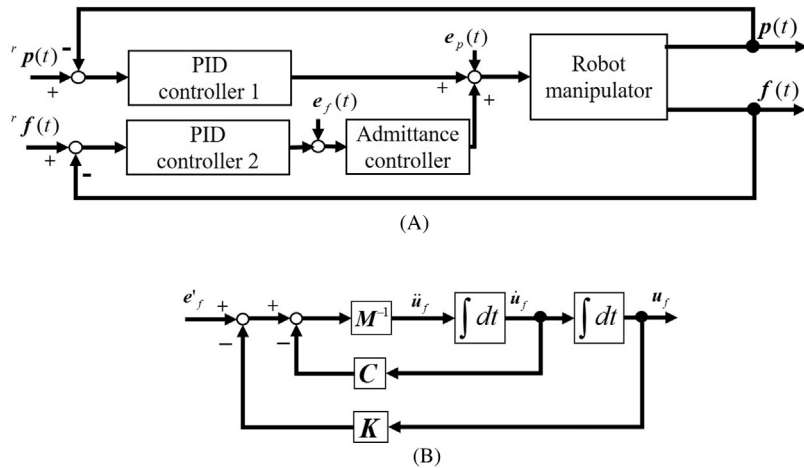
b. Measurement

The wearable robot cuff with the 3-D load device embedded is attached to the dummy with artificial skin, and is operated for the length of load time specified in the previously defined test condition, in order to generate the load pattern specified again in the test condition. The pattern of maximum load on the human body skin simulation is data logged.

The load data are organized in time series, synchronized with the cuff movement pattern, recording the pattern of maximum load and average load in the media.

14.2.4.2 Optimization for Reproduction of the Cuff Motion

A piece of surrogate (porcine) skin is attached around the artificial skin. Technically, the cuff motion reproduction means that both relative displacement generated and interactive force exerted, respectively, at a contact point on the cuff are similar to those at a corresponding contact point between human skin and the cuff of a wearable robot. Fig. 14.7A shows the control system of the manipulator to realize the cuff motion reproduction on the artificial skin surface. It enables the cuff mounted at the end effector of the manipulator to reproduce the motion on the artificial skin. At the stage of designing the control system, optimization of human skin–cuff contact motion was discussed. Fig. 14.7B shows in detail the admittance control system which converts a force vector

**FIGURE 14.7**

(A) Control system of the manipulator; (B) admittance controller part.

signal into a velocity one. Note that the control system architecture is well examined from such a viewpoint that the viscoelastic parameters of the artificial skin [8] are one of the targets to be standardized within certain ranges. Only the gains of PID controller 2, not including the gains of the admittance controller, need to be adaptively tuned for the test objective since the admittance gains are supposed to correspond to the viscoelastic parameters. They were actually measured from the artificial skin.

We adopted an adaptive controller called IFT (Iterative Feedback Tuning) [9], which can optimize the errors based on the sequential quadratic programming under constraint conditions. PID gains are optimized through performing experiments repeatedly, and the errors caused through the adaptive tuning are fed back to the inputs. The index function for the optimization is defined in the following formula, with weighing vectors w_p and w_f appropriately chosen for high performance of motion reproduction.

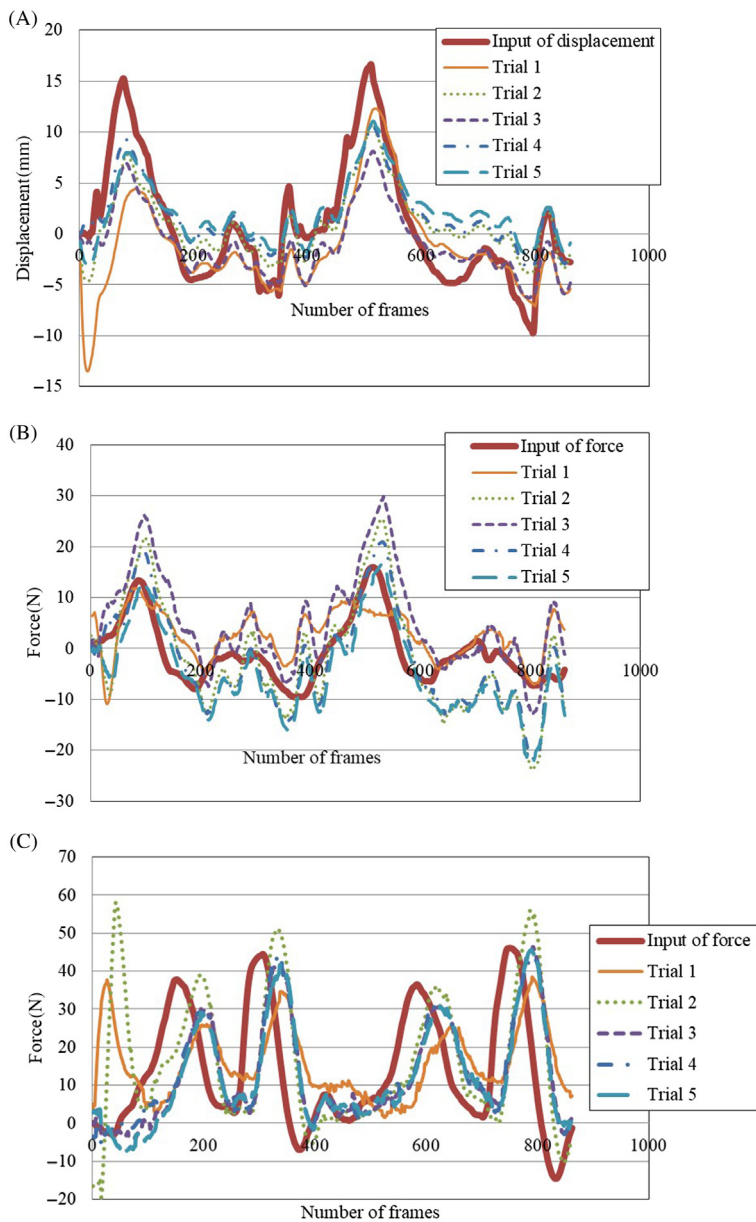
$$J = \frac{1}{N} \sum_{t=1}^N \left\{ \mathbf{e}_p^T(t, \rho) \mathbf{w}_p \mathbf{e}_p(t, \rho) + \mathbf{e}_f^T(t, \rho) \mathbf{w}_f \mathbf{e}_f(t, \rho) \right\}$$

where N is the number of data, and \mathbf{e}_p and \mathbf{e}_f are the error vectors of the relative displacement and force, respectively.

The amount of change of the gain vector ρ_k consisting of the PID gains in the k -th iteration is adjusted by use of the following adjustment parameter vector γ .

$$\rho_{k+1} = \rho_k + \gamma^T \Delta \rho_k$$

We conducted experiments reproducing the motions of the cuff on the artificial skin. The original motion pattern data were obtained when a subject worked on flexion and extension tasks while having a wearable robot attached. The cuff motions were reproduced for the y and z axes illustrated in Fig. 14.6, and therefore, the data in the x direction are omitted. Fig. 14.8A–C show the results

**FIGURE 14.8**

Motion and force exerted at the contact surface: (A) y-direction displacement of the cuff on the artificial skin; (B) y-direction force exerted at the surface of the artificial skin; (C) z-direction force exerted at the contact surface of the artificial skin.

of the displacement and force in the y -direction, and the force in the z -direction, respectively, which represent the cuff motion on the artificial skin reproduced in the experiment.

14.2.5 APPLICATION OF A SURROGATE SKIN FOR SAFETY VALIDATION

We conducted an experiment validating a cuff attachment in the use of a wearable robot after confirming the feasibility of using a surrogate (porcine) skin for a safety verification test. We focused on a human subject's "stand-up and sit-down" motion, which is considered to exhibit the largest level of relative displacement between the cuff and the skin surface of the subject. The interaction force between the robot's cuff and the user's thigh skin can be exerted repeatedly using the validation test apparatus consisting primarily of the manipulator described in Section 14.3. Fig. 14.9 shows an overview of the test experiments. Note that a piece of a surrogate skin is firmly fixed on the top surface of the artificial skin.

During the series of experiments, three pieces of surrogate skin were tested for safety validation of a cuff–human skin surface system, and each test lasted for 1800 seconds. Since the smallest contact area between urethane and surrogate skin was about $12 \times 10^{-4} \text{ m}^2$ and the largest shear force applied on the surrogate skin was 27.7 N, the highest traction applied to the porcine skin was calculated approximately as $2.3 \times 10^4 \text{ Pa}$. According to the inherently safe region shown in Fig. 14.6, no blisters should have been generated on the porcine skin within 3350 seconds, even under the highest traction.

The safety validation test was repeated three times. After each test, three samples were taken from the higher, middle, and lower parts, respectively, where the porcine skin was in contact with the urethane-made cuff.

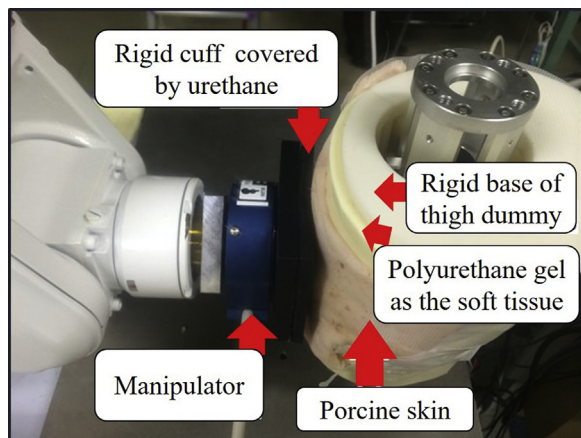


FIGURE 14.9

Overview of the test experiment.

14.2.6 SUMMARY

In this chapter, integrated studies on a validation test method for estimating the risk of blister generation have been introduced for the use of wearable robots, together with a verification experiment to determine the inherently safe region in the traction–rubbing time relationship. The validation test used a manipulator which was controlled adaptively by IFT (iterative feedback tuning) to reproduce contact states between the cuff of a wearable robot mounted at the end effector of the manipulator and artificial skin. The data to reproduce were originally monitored in the contact states of a human skin–cuff system when a human wearing a lower limb wearable robot stood up and sat down. A study to verify the safety in the traction–rubbing time relationship was also described to clarify an inherently safe condition region by use of pieces of surrogate skin.

Such wounds as blisters are estimated to have a high risk because the probability of occurrence is high while the severity is low. These studies comply with the safety requirement against a physical stress hazard stated in ISO 13482 and followed by a V&V test method; the latter method appearing in the document will be published as a technical report (ISO/TR).

The author considers that further studies are desired to be conducted for better performance of the V&V test methodology. The safety validation test method can detect the interaction force more accurately at the cuff–artificial skin contact system in a distributed way. Further, the results of the verification experiments can be analyzed to a full extent using the concept of survival analysis.

14.3 FALL RISK DURING GAIT USING A WEARABLE ROBOT

14.3.1 INTRODUCTION

14.3.1.1 Installation of wearable robots in society

A number of lower limb wearable robots have been developed for gait assist recently. They were previously developed for rehabilitative uses on treadmills. In such cases, it is reasonable to fix a wearable robot on a treadmill because the robot and wearer do not deviate from the treadmill [9,10,11]. Some other wearable robots are designed for rehabilitation on walking lanes instead of treadmills [12]. In such situations, the wearer can grasp handrails or be supported by a therapist to avoid falling while walking.

Some other wearable robots have been developed for use in daily living, and not necessarily in hospitals. The potential users of these robots include people who cannot stand or walk by themselves owing to paralyses or other related symptoms [13]. Other robots have been developed to compensate for the frailty of users due to aging or after injury or other disabilities [14]. The latter robots are used to improve the gait ability of the wearer who can stand and walk by themselves. Thus, the applications of wearable robots in society differ from those used for rehabilitation because they are intended to improve the quality of life directly by supporting the mobility of wearers. Though the risk of fall inevitably exists during biped gait, such a risk has not yet been intensively analyzed.

14.3.1.2 Risk of fall related to wearable robots

When using wearable robots in society, robots cannot be fixed to the ground or supported by the therapist. Thus, such wearable robots are constantly exposed to the risk of falling because of the

static instability of biped walking. Although humans sometimes fall during natural walking, the problem of product liability may occur if a fall occurs during assisted walking. In particular, if a wearable robot interferes with the motion of the wearer, the robot may be responsible for the fall. Unsteady gait, such as tripping, sudden acceleration and deceleration, and curving will increase the probability of motion interference.

Generally, wearable robots apply assisted torque by sensing the gait pattern [15], which is based on the periodicity of gait motion, or a biosignal of motion [16], such as a myoelectric signal. Thus, incorrect detection or a sudden change in the wearer's motion may cause a mismatch of motion between the robot and wearer. Furthermore, because gait motion mostly relies on motion in the sagittal plane, some wearable robots have none or only a limited range of motion (RoM) in rotation of the frontal and horizontal planes, which are controlled by abduction/adduction and rotation of the hip joint. Such a limitation of the degree of freedom (DoF) may disturb the reaction motion against perturbation and curving motion. In addition, an increase in the weight, inertia, and size of the body owing to the wearable robot may also affect the motion of the wearer. Experimental studies, which have observed gait motion when attaching weight or inertia, have suggested an increase in gait instability [17,18].

14.3.1.3 Reaction motion against a trigger for falling

Human gait and fall motion have been researched for a long time. Fall during gait is not only a familiar phenomenon for many people but also a social problem, because fall-related injuries have a medical cost and cause loss of labor [19,20].

When analyzing gait motion, it is general to separate continuous motion from the gait cycle (GC), which was determined as the motion between a heel contact (HC) to the next HC of the same foot, resulting in the periodicity of gait motion [21]. Because the gait motion of humans is similar to a degree when the age, speed, and other conditions are similar, average motion patterns such as joint angle and posture have been reported [22]. Furthermore, the trend of gait timing, such as walking speed, cadence, and step length and width, has been also statistically analyzed for each gait condition and subject attributes [22,23].

Most falls that occur in the daily living environment are caused by a slip or trip [24]. Slips mainly occur when the foot slips on the floor at HC owing to low friction between the sole and ground. On the other hand, trips occur when the leg swing is stopped by an obstacle. Many experimental results suggest that there are two major motion strategies against trip [25]. The “elevating” strategy overcomes the obstacle using the tripped swing leg which steps forward earlier. In contrast, the “lowering” strategy uses a motion which places the tripped leg before the obstacle. Then, the other leg is stepped forward. In both strategies, the length and speed of the recovery step, which is the forward step just after the tripping, have a critical role in avoiding falling because the faster and longer recovery step helps to cancel the forward moment caused by tripping [26]. Because of the complexity and variety of reaction patterns, the mismatch between a wearable robot and the wearer can easily occur when the perturbation occurs during the swing phase, such as in tripping.

A mismatch of assist timing is a perturbation unique to the wearable robot. If the assist torque, which generally assists the leg swing and body support, is applied at the wrong time, the applied torque may disturb the leg swing. Although most wearable robots do not exert torque sufficiently to directly stop leg swing, motion interference may cause a loss of balance, which can cause a fall. Furthermore, contact of the wearable robot to an environmental object may be another perturbation

which occurs during the swing phase. Because most wearable robots expand the body size in a lateral direction, there is an increased possibility that the robot may come into contact with an object, such as a door or furniture, especially in narrow spaces. The mismatch of somatic sensation also amplifies the risk of contact. However, such fall triggers, which are unique to wearable robots, have been rarely studied. Thus, the analysis of reaction motion against new fall triggers is required for the safety use of wearable robots.

14.3.2 MISMATCH BETWEEN THE MOTION OF THE WEARABLE ROBOT AND THE WEARER

14.3.2.1 *Methods which detect the wearer's intention*

The function of detecting signs of motion of the wearer is essential for the algorithm of wearable robots, which can apply assist torque along with the intention of the wearer. Otherwise, the delay in detection or misdetection of motion intention causes a mismatch of motion between the wearable robot and wearer, causing discomfort and interfering with the motion of the wearer.

A representative method to detect the motion intention of the wearer is to observe the motion of the robot caused by the wearer. Motion detection using sensors such as an encoder is widely used to apply assisted torque, which helps in the detection of motion [11]. For wearers whose muscles are too weak to move the robot by themselves, an electromyogram (EMG) or interaction force at the contact part between the robot and wearer is suitable for anticipating the motion intention. Furthermore, EMG sensing can decrease the time delay between the motion of the robot from the intention of the wearer.

In the case of gait assistance, methods using the periodicity of gait motion have been developed to synchronize with the GC. When gait motion can be successfully anticipated, assist torque can be applied proactively [15]. Such methods are based on an algorithm which estimates the GC, such as the central pattern generator (CPG) [27]. These algorithms can synchronize with the gait motion within a few GCs.

14.3.2.2 *Factors which cause a mismatch and their risks*

The balance loss probably occurs when the motion of the wearer is disturbed by the mismatch of motion between the wearable robot and the wearer. Such mismatches are caused by various factors depending on the method used to detect the motion sign of the wearer. Furthermore, the mode of motion interference also differs by the cause of the mismatch.

When detecting the motion sign or the motion of the wearer, the time delay of motion detection causes a mismatch. Furthermore, because such algorithms sometimes limit motion speed to avoid divergence of feedback, a mismatch of motion speed may occur. Except for mechanical and electrical problems, such as reliability of the sensor and stability of the controller, these mismatches are caused by a fundamental limitation of the assist algorithm and sensing method. To reduce such mismatches, the use of motion signs, which appear quicker than the actual motion, such as an EMG, and improvement in the responsibility of the sensor and actuator are essential. It should be also considered that such mismatches probably occur when the wearer starts, changes, and stops the motion.

On the other hand, as long as the gait motion remains stable, the motion delay does not occur if the algorithm anticipates gait motion by estimating the gait period. However, the assumption of periodicity has the risk that the algorithm cannot deal with a rapid change in the gait timing, which is sometimes caused by tripping, stumbling, or other perturbations. In the assist pattern, which is synchronized with the original gait pattern, the assist torque may disturb the motion of the wearer, especially in an emergency. In contrast, if the gait estimation is sensitive to following the change of gait timing flexibly, the risk of sudden change of assist pattern, caused by a misdetection of the gait timing, increases. Motion interference may occur during normal walking in this case.

14.3.2.3 Experimental setup which artificially causes a mismatch of the assist pattern

The reaction motion of the wearer against the motion mismatch should be observed experimentally because the motion strategy to recover from motion interference has not been modeled. Thus, motion mismatch was artificially applied to the wearer during gait to observe and analyze the reaction motion.

In this experiment, a Motor-Actuated Lower-limb Orthosis (MALO), which was a lower limb exoskeleton developed for gait experiments, was used (Fig. 14.10). MALO was made of a corset, lower limb orthosis, and actuated joint mechanisms. When wearing MALO, it was fixed to the wearer at the pelvis, thigh, shank, and foot using a corset, cuffs, and shoes. Thus, the weight of the MALO could be supported by itself when standing still. The hip, knee, and ankle joints were the single DoF rotation joint in the sagittal plane. Both the hip and knee were actuated by DC motors to apply assist torque. These motors were powered and controlled online outside the robot by a wired connection, because MALO was designed for experimentation in the laboratory.

Among the above-mentioned assist strategies, the assist algorithm, which anticipated the gait motion from the periodicity of the GC, was tested here because such an algorithm was generally used and exerted high performance when synchronized with the GC. The situation of motion mismatch is described below. The pattern of assist torque applied by MALO, which is shown in Fig. 14.11, aimed to help body thrusts during the stance phase and leg swings in the swing phase. In the stance phase, the hip extension torque was applied during 15%–45% of the GC and the knee flexion torque was applied during 30%–60% of the GC. The magnitude of assist torque was set at 7 Nm for the hip and 8 Nm for the knee, respectively. These corresponded to approximately 20% of the average moment exerted by a human during the stance phase [21]. In the swing phase, the hip flexion torque was applied during 65%–95% of the GC and the knee extension torque was applied during 75%–95% of the GC. The application of assist torque started and stopped smoothly to avoid a sudden change in the assist torque.

The motion mismatch that occurred in this experiment assumed the situation when the timing of the assist pattern shifted suddenly and disturbed the gait motion because of the misdetection of gait timing. As mentioned above, there are many modes of motion mismatch. However, because the mechanical performance and individual motion of each wearer affected the modes of mismatch differently, it is difficult to estimate the occurrence of such a mismatch accurately. Among such mismatches, the occurrence of a shift in the assist timing, which was caused by misdetection of the gait event, was assumed and applied in this experiment because it could happen without any perturbation from outside, meaning the robot was probably responsible for the mismatch. The shifted assist torque will disturb leg swing at the early swing phase, which may be hazardous for the walker, as shown in Fig. 14.12.

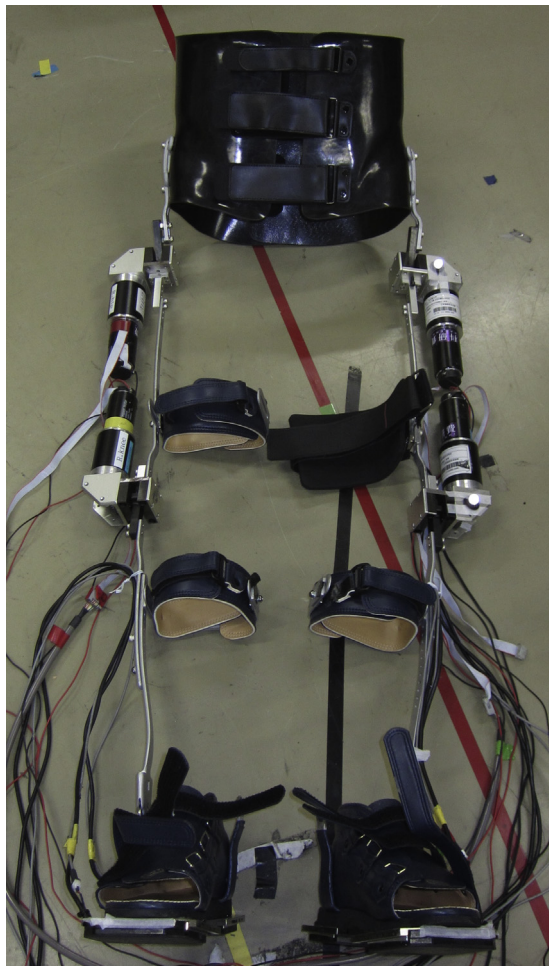
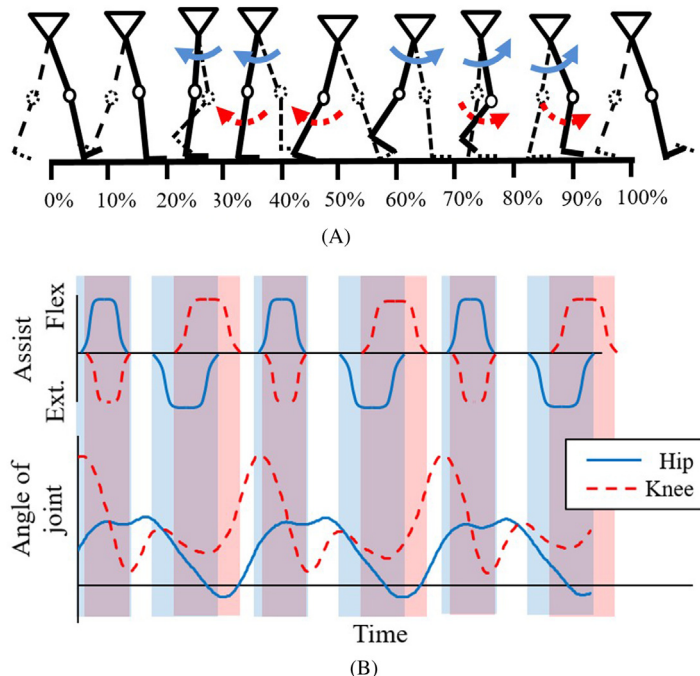


FIGURE 14.10

Motor-actuated lower-limb orthosis (MALO).

14.3.2.4 Observation of reaction motion against mismatch of the assist pattern

In this experiment, the motion of subjects in a walking lane was recorded using a motion capture system. The walking lane had 5 m of recording area and 3 m of acceleration area. To record the ground reaction force exerted on the toe and heel of each foot, four mobile force plates were attached under the sole. Thus, gait timings and parameters such as speed, foot position, joint patterns, center of pressure (CoP), and center of mass (CoM) could be calculated. For the safety of subjects, safety measures such as a harness, protector, and leg supporters were used. The experiment was performed with the permission of the institutional review board of Nagoya University.

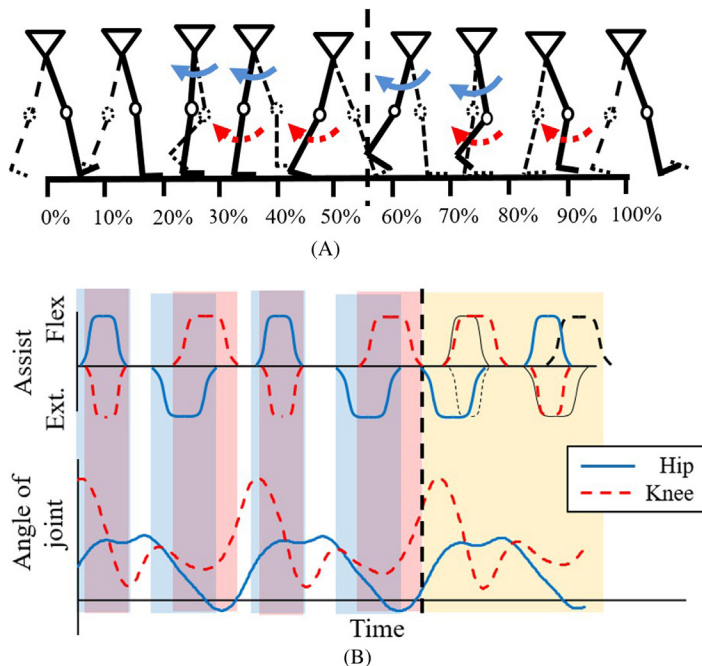
**FIGURE 14.11**

Normal assist: (A) timing and direction of assist torque; (B) pattern of joint angle and assist torque.

The subjects of this experiment were nine young male adults. Subjects wore MALO and walked a sufficient amount of time for adjustment before recording trials. After these training trials, subjects walked on the lane repeatedly with gait assist. The mismatch torque was applied on randomly selected trials.

None of the subjects fell in this experiment because they were sufficiently strong compared to the perturbation torque applied from the MALO. Thus, it was possible for subjects to continue to walk even when the mismatch torque was applied. In this experiment, although some subjects decreased their walking speed after a mismatch, others continued walking. Thus, it was suggested that the individual differences in the intentions of each subject affected the reaction strategies.

The mismatch torque disturbed the leg swing by applying hip extension torque on the early swing phase and knee flexion torque on the middle to late swing phase. The influence of this mismatch appeared during the double-stance phase soon after the perturbed swing. During the double-stance phase, the peak flexion angle of lower limb joints was increased. This change of joint angle meant that the wearer lowered the hip position and became closer to the half-rising posture. Furthermore, the CoP trajectory on the perturbed leg in the double-stance phase differed from that of the normal gait. The time series of CoP position in the longitudinal direction of a foot is drawn in Fig. 14.13. The vertical axis is the distance from the heel. When the mismatch occurred, CoP moved forward quicker than in a normal assist trial, which meant that the wearer maintained the forward movement of the body.

**FIGURE 14.12**

Irregular assist: (A) timing and direction of assist torque; (B) pattern of joint angle and assist torque.

To complete this reaction motion, the joint torque of lower limb joints should become larger than that in normal gait. In particular, the knee joint has to exert sufficient extension torque to control the CoM, which may be moved forward rapidly, even though the knee is flexed. Although the required torque was not large for young adult subjects, it is perhaps difficult for potential users of wearable robots such as the elderly and frail people to complete the reaction motion observed in this experiment. Thus, further analysis to understand the relationship between the reaction motion against the mismatch and the risk of falling during gait is required because such a wearer may use compensation motion which differs from the observed reaction strategy.

14.3.3 CONTACT WITH AN ENVIRONMENTAL OBJECT

14.3.3.1 Motion in the daily living environment and risk of collision

As long as wearable robots are used for gait rehabilitation, the risk of collision can be neglected because the wearer usually walks in a walking lane or on a treadmill. However, if the wearable robot is used in the daily living environment, the probability of contact with an environmental object increases drastically because the wearer may walk through narrow spaces, such as doors or the interspace between furniture. Furthermore, the body width of the wearer is expanded with the

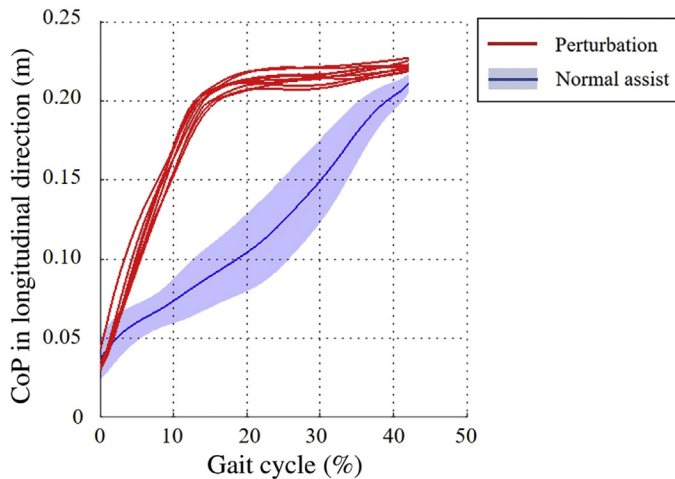


FIGURE 14.13

CoM trajectory in the longitudinal direction of the foot.

wearable robot equipment. Thus, the risk of collision of the wearer with an object should be considered when the wearable robot is used in the daily living environment.

The risk of falls caused by general perturbations, such as trips or slips, has been studied for a long time. Thus, the pattern of reaction motion against such perturbation and the factors which affect the motion have been collected and analyzed [25]. The knowledge obtained from such experiments will be also helpful to estimate the risk of falling during assisted walking. However, the risk of falling caused or increased by a wearable robot has not been studied.

A collision of the side of the wearable robot with an environmental object is a representative mode of the hazards unique to a wearable robot. Such a collision is caused and amplified by the expansion of the physical frame, which increases the risk of collision. Moreover, the body expansion also increases the rotation moment of the body when the collision occurs. Furthermore, the interaction force and torque exerted when the side of the robot collides with an obstacle causes a rotation moment in the horizontal plane. This differs from that caused by previously studied perturbations such as tripping and slipping. Because the body rotation probably increases the risk of falls and causes severe hazards such as falls from the lateral side of the body, the reaction motion against side contact should be observed and analyzed.

14.3.3.2 Observation of reaction motion against side contact of the wearable robot

Side contact during assisted walking was artificially caused to observe reaction motion in the laboratory. The MALO, the above-mentioned wearable robot, was also used with a modification in which aluminum plates were attached to the lateral side of the thigh as the contact part. The obstacle, the height of which was adjustable, was made from an aluminum frame as shown in Fig. 14.14.

Young male adult subjects participated in the experiment by walking in a walking lane repeatedly with the MALO fitted. The obstacle was fixed either to the left or right side of the walking lane, so that the side of the MALO hit the obstacle. The height of the obstacle was adjusted to 55 or 80 cm. Furthermore, to observe the effect of gait phase at contact timing on the reaction motion, the position of the obstacle in the traveling direction was varied because the perturbation timing affected the reaction motion in the case of tripping.

Contact of the side of MALO applied a rotation moment on the subject and caused body rotation in the horizontal plane in this experiment. Representative step positions of the reaction motion are shown in Fig. 14.15. The three steps drawn in these figures are the sequence starting from the step immediately before the contact. In some trials, as shown in Fig. 14.15A, the subject stopped his body rotation quickly and attempted to continue to walk forward. In contrast, as shown in Fig. 14.15B, sometimes the subject stopped walking and stepped sideways to avoid body rotation.

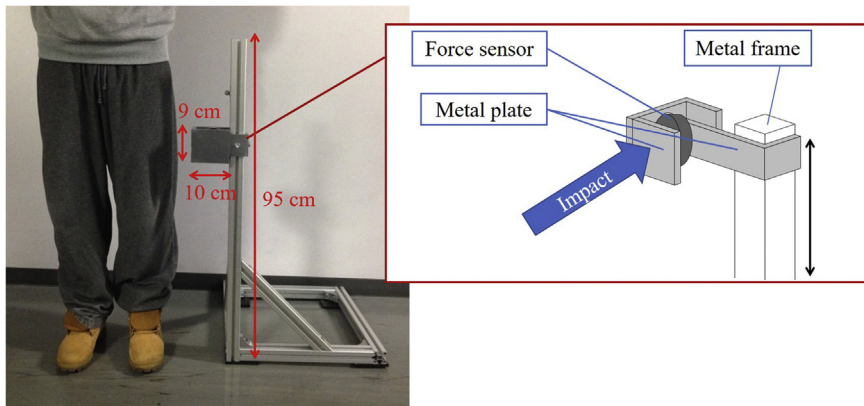


FIGURE 14.14

Side contact obstacle.

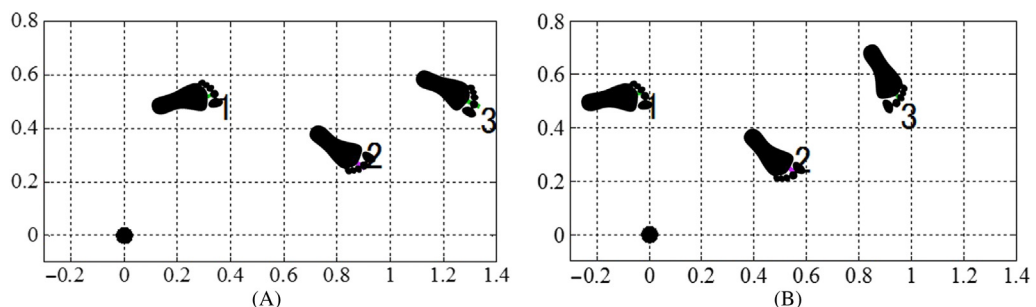


FIGURE 14.15

Position of footsteps after the side contact (meter unit): (A) continue to walk; (B) side step.

The former reaction motion appeared when the rotation motion was small. However, when a large rotation moment was applied by heavier contact, the latter reaction was exerted. In addition, no subjects fell during any of these trials.

Although the MALO does not have DoF of hip rotation and abduction/adduction, step positions in reaction motion suggested the existence of a certain amount of hip rotation and abduction. In this experiment, the lower leg muscles of the wearer were probably stronger than the stiffness of the frame of the MALO. Thus, it should be considered that a wearable robot, whose DoF limitation is strong, may make it difficult to execute the reaction motion observed in this experiment. This will increase the risk of falling by disturbing the reaction motion to stop the body rotation.

14.3.4 CURVING MOTION UNDER LIMITED DEGREE OF FREEDOM

14.3.4.1 *Motions required in a daily living environment*

The DoF of the lower limb joints of many wearable robots were limited on the sagittal plane because they were designed for straight walking rehabilitation. However, as mentioned in the section above, hip rotation and abduction/adduction is necessary in a daily living environment. Furthermore, curving gait, which is also necessary in a daily living environment [28], also requires the additional DoF of the hip joint.

However, motion using hip rotation and abduction/adduction was not considered in many wearable robots. Thus, the structure and assist algorithm of wearable robots was not designed to turn corners smoothly. Although some wearable robots are equipped with a mechanism to adjust the alignment and angle of joints for each wearer, most are passive and usually fixed during walking.

14.3.4.2 *Natural curving motion and required degree of freedom*

When turning a corner in a daily living environment, the angle and width of the corner will affect the curving motion, such as rotation radius and CoM trajectory. Thus, the natural curving motion of humans appears when they can curve freely. Despite an enormous variety of curving motions, previous studies discovered characteristics of the motion in relation to the curving condition. According to such studies, “spin” and “pivot” motions were observed when turning a square corner at a sharp angle [29,30]. In contrast, subjects combined the straight step and the step which loosely altered the gait direction when turning a round corner with a large radius [31]. Thus, the walking path became polygonal. The natural turning motion can be observed continuously when turning corners with 1–2 m radius [32,33].

The walking experiment suggested that the hip rotation and abduction/adduction are used for natural turning motions [34]. Although the gait timing when the subject started turning affects the joint pattern, maximally approximately 30 degrees of rotation and 15 degrees of abduction/adduction were observed. Furthermore, it was also reported that the smaller corner radius decreased the gait speed [35]. Thus, when the wearable robot restricts the hip joint other than flexion/extension, such a natural curving motion cannot be done and some compensation motion will appear.

14.3.4.3 Observation of the compensation motion of degree of freedom restriction when turning in a curve

The effect of the restriction of hip rotation and abduction/adduction on curving gait was analyzed using a wearable robot [36]. In this experiment, subjects wore the MALO, which is the above-mentioned wearable robot, and turned a round corner with a radius of 0.5 m. In this experiment, the MALO was not actuated to concentrate on observing the effect of joint restriction. To control the gait timing when starting turning, the first step was integrated to the inner step as shown in Fig. 14.16. The gait motion in the corner section was recorded by a motion capture system and kinematic parameters such as body angle, step position, and CoM trajectory were calculated. The connection of the hip joint to the MALO was detached to observe the gait motion without joint restriction. However, other parts of the MALO were retained to integrate other conditions such as weight and RoM of other lower limb joints.

Although rotation and abduction/adduction of the hip joint were possible to some degree owing to the flexibility of the robotic frame, RoM decreased drastically when they were restricted. Representative motion trajectories observed in this experiment are displayed in Fig. 14.17. A decrease in step length and increase in step width were observed in the restricted case. The ability to alter the gait direction of each stride became smaller in the restricted case. Thus, a decreased step length was essential to maintain the rotation radius, which was determined by the corner shape in this experiment. On the other hand, the restriction of hip adduction disturbed the step inside of the body and increased the step width. In addition, the trajectory of CoM and step positions separated because the CoM could not be controlled smoothly.

In this experiment, compensated curving motion against the restriction of the DoF of hip rotation and abduction/adduction was observed. However, it should be also considered that the compensation motion may be different in a different walking environment. For example, a decrease in step length in the compensation motion to ease the difficulty of changing the gait direction may be substituted by an increase in the turning radius, whereas it was fixed in this experiment by using a walking lane. An increase in the turning radius may be another compensation motion against the restriction of hip rotation.

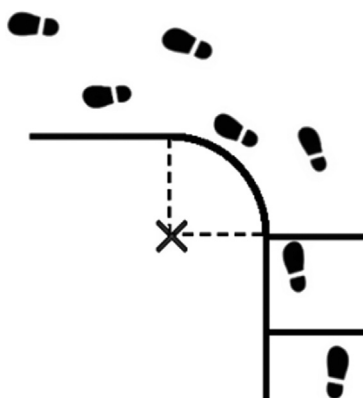
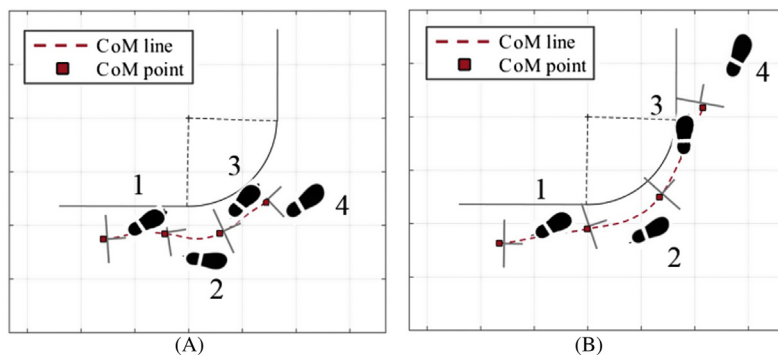


FIGURE 14.16

Overview of the corner turning experiment.

**FIGURE 14.17**

Position of footsteps. (A) restricted; (B) free.

14.3.5 SUMMARY

The use of wearable robots has started to expand from rehabilitation in the hospital to wider society. However, the safety of wearable robots has not matched the expansion of this usage yet because of the variety of daily living environments. In this chapter, mismatch of assist pattern, contact between the side of the robot and an obstacle, and corner curving/turning have been introduced, among the risk factors for falling. Although falling did not occur in the experiment because subjects were young healthy adults, the reaction motion against the perturbation was affected by the wearable robot. Thus, the effect of the wearable robot on the reaction and compensation motion of the elderly wearer should be considered carefully.

14.4 CONCLUSIONS

The risks of blister generation and falls from the point of view of using wearable robots were discussed in this chapter. The first half of the chapter is concerned with the blister generation risk. Verification experiments were demonstrated to clarify traction–rubbing time characteristics with the use of porcine tissue. A safety validation process was also developed in which a manipulator-based test bed was introduced to reproduce the contact motion between dummy skin and the cuff of wearable robots. Following the publication of ISO 13482: 2014, which is an international standard for the safety of personal care robots including wearable robots for nonmedical use, a technical report on the safety V&V test methods is scheduled to be published in which the above safety validation test procedure as well as the experimental results of the safety verification test are described.

The fall risk during assisted walking is a serious problem from the point of view of product liability, especially when the fall is caused by the wearable robot. The effect of the wearable robot on gait stability and fall avoidance motion were discussed based on motion observation in an experimental space in the second half of this chapter. Although research in this field is immature, it has become important for the expansion of the wearable robot to the daily living environment.

Consideration of wearable robots has to proceed without exposing humans to hazards for ethical reasons. Thus, alternative methods have to be devised. Experiments using animals and dummies, which were used for the V&V process of blister generation, are the representative method. On the other hand, an experiment was done within a safe environment to estimate the risk of falling. This is an approach to estimate the safety threshold by extrapolating the experimental result. Estimation of the frequency and severity of risks of new technologies, such as wearable robots, is an essential part of the discussion to enable their social acceptance.

REFERENCES

- [1] ISO 13482: robots and robotic devices—safety requirements for personal care robots, February 2014.
- [2] K. Okamoto, Current status of the introduction of lower extremity functional training with the robot suit HAL in our hospital, *Proc. Pressure Ulcers Jpn.* 16 (3) (2014) 289. in Japanese.
- [3] X. Mao, Y. Yamada, Y. Akiyama, S. Okamoto, K. Yoshida, Development of a novel test method for skin test verification of physical assistant robots, in: IEEE Int. Conf. Rehabil. Robot. 2015, 319–324.
- [4] X. Mao, Y. Yamada, Y. Akiyama, S. Okamoto, K. Yoshida, Safety verification method for preventing friction blisters during utilization of physical assistant robots, *Adv. Robot.* 30 (13) (2017) 680–694.
- [5] P.F.D. Naylor, Experimental friction blisters, *Brit. J. Dermatol.* 67 (10) (1955) 327–342.
- [6] M.B. Sulzberger, T.A. Cortese Jr, L. Fishman, Studies on blisters produced by friction I. Results of linear rubbing and twisting techics, *J. Invest. Dermatol.* 47 (5) (1966) 456–465.
- [7] K. Yoshida, Y. Yamada, Y. Akiyama, S. Hara, S. Okamoto, Development of a safety validation test equipment for severity estimation of wounds caused by physical assistant robots, *The 20th Robotics Symposia, 2015*, , pp. 483–488. in Japanese.
- [8] M. Aso, Y. Yamada, K. Yoshida, Y. Akiyama, Y. Ito, Development of complex artificial skin tissues by evaluating the mechanical characteristics of human thighs, in: IEEE Conf. Robot. Biomimet., 2013, pp. 1450–1455.
- [9] H. Hjalmarsson, “Iterative feedback tuning – an overview”, *Int. J. Adapt. Contr. Signal Process.* 16 (2002) 373–395.
- [10] J. Hidler, D. Nichols, M. Pelliccio, K. Brady, D.D. Campbell, J.H. Kahn, et al., Multicenter randomized clinical trial evaluating the effectiveness of the Lokomat in subacute stroke, *Neurorehabil. Neural. Repair.* 23 (1) (2009) 5–13.
- [11] J.F. Veneman, R. Kruidhof, E.E. Hekman, R. Ekkelenkamp, E.H. Van Asseldonk, H. Van Der Kooij, Design and evaluation of the LOPES exoskeleton robot for interactive gait rehabilitation, *IEEE. Trans. Neural. Syst. Rehabil. Eng.* 15 (3) (September 2007) 379–386.
- [12] K. Suzuki, G. Mito, H. Kawamoto, Y. Hasegawa, Y. Sankai, Intention-based walking support for paraplegia patients with robot suit HAL, *Adv. Robot.* 21 (12) (2007) 1441–1469.
- [13] K. Raab, K. Krakow, F. Tripp, M. Jung, Effects of training with the ReWalk exoskeleton on quality of life in incomplete spinal cord injury: a single case study, *Spinal Cord Ser. Cases* (2)(2016) 15025.
- [14] P.D. Neuhaus, J.H. Noorden, T.J. Craig, T. Torres, J. Kirschbaum, J.E. Pratt, Design and evaluation of mina: a robotic orthosis for paraplegics, in: IEEE Int. Conf. Rehabil. Robot., 2011, pp. 1–8.
- [15] R. Ronsse, N. Vitiello, T. Lenzi, J. van den Kieboom, M.C. Carrozza, A.J. Ijspeert, Human–robot synchrony: flexible assistance using adaptive oscillators, *IEEE. Trans. Biomed. Eng.* 58 (4) (2011) 1001–1012.
- [16] S.C. White, D.A. Winter, Predicting muscle forces in gait from EMG signals and musculotendon kinematics, *J. Electromyogr. Kinesiol* 2 (4) (1992) 217–231.

- [17] R.C. Browning, J.R. Modica, R. Kram, A. Goswami, The effects of adding mass to the legs on the energetics and biomechanics of walking, *Med. Sci. Sports Exerc.* 39 (3) (2007) 515–525.
- [18] J. Meuleman, W. Terpstra, E.H. van Asseldonk, H. van der Kooij, Effect of added inertia on the pelvis on gait, in: *IEEE Int. Conf. Rehabil. Robot.*, 2011, pp. 1–6.
- [19] H.J. Lipscomb, J.E. Glazner, J. Bondy, K. Guarini, D. Lezotte, Injuries from slips and trips in construction, *Appl. Ergon.* 37 (3) (2006) 267–274.
- [20] D.G. Tate, Workers' disability and return to work, *Am. J. Phys. Med. Rehabil.* 71 (2) (1992) 92–96.
- [21] A.N. Donald, N. David, *Kinesiology of the Musculoskeletal System*, Mosby, Inc, Orlando, 2002.
- [22] F.R. Finley, K.A. Cody, Locomotive characteristics of urban pedestrians, *Arch. Phys. Med. Rehabil.* 51 (7) (1970) 423.
- [23] D.J. Blanke, P.A. Hageman, Comparison of gait of young men and elderly men, *Phys. Ther.* 69 (2) (1989) 144–148.
- [24] F. Englander, T.J. Hodson, R.A. Terregrossa, Economic dimensions of slip and fall injuries, *J. Forensic. Sci.* 41 (5) (1996) 733–746.
- [25] J.J. Eng, D.A. Winter, A.E. Patla, Strategies for recovery from a trip in early and late swing during human walking, *Exp. Brain Res.* 102 (2) (1994) 339–349.
- [26] M.J. Pavol, T.M. Owings, K.T. Foley, M.D. Grabiner, Mechanisms leading to a fall from an induced trip in healthy older adults, *J. Gerontol. A Biol. Sci. Med. Sci.* 56 (7) (2001) M428–M437.
- [27] T.G. Brown, On the nature of the fundamental activity of the nervous centres; together with an analysis of the conditioning of rhythmic activity in progression, and a theory of the evolution of function in the nervous system, *J. Physiol.* 48 (1) (1914) 18–46.
- [28] B.C. Glaister, G.C. Bernatz, G.K. Klute, M.S. Orendurff, Video task analysis of turning during activities of daily living, *Gait. Posture* 25 (2) (2007) 289–294.
- [29] M.J. Taylor, P. Dabnichki, S. Strike, A three-dimensional biomechanical comparison between turning strategies during the stance phase of walking, *Human Movement Sci.* 24 (4) (2005) 558–573.
- [30] D. Xu, J.W. Chow, Y.T. Wang, Effects of turn angle and pivot foot on lower extremity kinetics during walk and turn actions, *J. Appl. Biomech.* 22 (1) (2006) 74–79.
- [31] T. Imai, S.T. Moore, T. Raphan, B. Cohen, Interaction of the body, head, and eyes during walking and turning, *Exp. Brain Res.* 136 (1) (2001).
- [32] M.S. Orendurff, A.D. Segal, J.S. Berge, K.C. Flick, D. Spanier, G.K. Klute, The kinematics and kinetics of turning: limb asymmetries associated with walking a circular path, *Gait. Posture* 23 (1) (2006) 106–111.
- [33] A.D. Segal, M.S. Orendurff, J.M. Czerniecki, J.B. Shofer, G.K. Klute, Local dynamic stability in turning and straight-line gait, *J. Biomech.* 41 (2008) 1486–1493.
- [34] Y. Akiyama, H. Toda, T. Ogura, S. Okamoto, Y. Yamada, Classification and analysis of the natural corner curving motion of humans based on gait motion, *Gait. Posture* 60 (2018) 15–21.
- [35] Y. Akiyama, S. Okamoto, H. Toda, T. Ogura, Y. Yamada, Gait motion for naturally curving variously shaped corners, *Adv. Robot.* 32 (2) (2018) 77–88.
- [36] Y. Fukui, Y. Akiyama, Y. Yamada, S. Okamoto, The change of gait motion when curving a corner owing to the motion restriction caused by a wearable device, in: *IEEE Int. Conf. Syst. Man Cybernet.*, 2017, pp. 525–530.

CURRENT EVIDENCE FOR USE OF ROBOTIC EXOSKELETONS IN REHABILITATION

15

Arun Jayaraman^{1,2,3,4}, Borislav Marinov⁵, Yashna Singh⁶, Sheila Burt¹ and William Zev Rymer^{2,6,7}

¹Shirley Ryan AbilityLab, Center for Bionic Medicine & The Max Nader Lab for Rehabilitation Technologies and Outcomes Research, Chicago, IL, United States ²Department of Physical Medicine & Rehabilitation, Northwestern University, Chicago, IL, United States ³Department of Medical Social Sciences, Northwestern University, Chicago, IL, United States ⁴Department of Physical Therapy & Human Movement Sciences, Northwestern University, Chicago, IL, United States ⁵Exoskeleton Report LLC, San Jose, CA, United States ⁶Shirley Ryan AbilityLab, Single Motor Unit Laboratory, Chicago, IL, United States ⁷Department of Physiology, Northwestern University, Chicago, IL, United States

15.1 BRIEF HISTORY OF EXOSKELETONS

15.1.1 EARLY DESIGNS

Although several exoskeleton technologies are just now becoming developed and commercialized, wearable devices that perform physical work have been around for more than a century. The first known drawing of what can be considered an exoskeleton was a satirical piece published in London in the late 1820s entitled “Locomotion—Walking by Steam, Riding by Steam, Flying by Steam” by Robert Seymour [1]. Seymour depicted a comical steam car (driving by steam), a steam helicopter (flying by steam), and a lower-body exoskeleton (walking by steam). A few other exoskeleton-like designs appeared in newspapers. The first patent for an exoskeleton, however, did not come until several decades later when, in 1890, Nicholas Yagn of St. Petersburg, Russia, patented his device called an “Apparatus for Facilitating Walking” [2]. A mechanism worn on the legs, the device was designed for walking, jumping, and running assistance. Two versions were powered either with a giant bow spring or compressed gas bag. This patent represents the first known separation of passive vs. active (powered) exoskeletons. Although these early formulations of exoskeletons never became products, their basic structure and design formed the foundations for establishing powered armor and intuitively controlled force-amplification suits that appeared in science fiction, most notably the book *Starship Troopers* (1959) and the Marvel comic book character *Iron Man* (1963).

15.1.2 FIRST PROTOTYPES 1961–73

In the real world, powered exoskeletons began to take shape during the Man-Amplifier Project, an initiative spearheaded by the Cornell Aeronautical Labs from 1961 to 1962 focused on developing

technologies that augmented human ability [3]. Researchers envisioned both military and aeronautical applications for the technologies. While the Man-Amplifier was never powered, the project was the first proof of concept demonstrating that human and machine could work together to perform complex tasks. The lab envisioned full-body exoskeletons as rigid mechanical frames with sufficient degrees of motion to adhere to the human body without significantly limiting the degrees of freedom. Motors, controllers, and power supply would jut out of the device without compromising mobility, but greatly increasing the volume of space the apparatus and user would take.

In the following years, General Electric, the Japanese company ATOUN, and the American company Sarcos Robotics commenced their own exoskeleton projects, building upon the same ideas as the Man-Amplifier Project. Researchers at the University of Belgrade, Yugoslavia (modern-day Serbia), in the Mihailo Pupin Institute led the development of the first medical powered exoskeleton [4]. The Institute actively researched lower and upper body exoskeletons for paralyzed individuals, and in 1972 had several units in rehabilitation clinics for use and evaluation.

Between 1974 to the late 1990s, industrial robotics revolutionized manufacturing and became a multibillion dollar industry. However, understanding walking kinematics and developing new exoskeletons significantly lagged behind, with the exception of wearable robots for teleoperation. As a result of these limitations, development of exoskeletons struggled, in part because the devices were heavy and usually had to be externally supported.

15.1.3 THE EXOSKELETON AWAKENING: 2001–08

At the turn of the century, several labs and start-up companies led the way in re-invigorating interest in exoskeleton development. In Japan, Cyberdyne led by Yoshiyuki Sankai introduced the Hybrid Assistive Limb (HAL) series. In Korea, Chang-Soo Han built a portfolio of more than two dozen exoskeletons under the brand Hexar Systems. Around the same time in North America, Homayoon Kazerooni of the University of California, Berkeley, cofounded Ekso Bionics, the late Stephen Jacobsen of the University of Utah transformed Sarcos Robotics into an exoskeleton developer, and Hugh Herr of MIT began popularizing the concept that there is no such thing as “disabled people” but only “disabled technology.” Meanwhile, in Europe, Hocoma began selling a robotic treadmill called the Lokomat. Keeping all these companies in mind, a total of 1000 devices have been sold across all these companies.

15.1.4 THE NEW EXOSKELETON RENAISSANCE: 2015–18 AND ONWARDS

In recent years, the number of companies working on exoskeletons has skyrocketed [5]. In East Asia, the increase in interest primarily is fueled by an aging population and workforce. In North America, exoskeletons designed to prevent work injuries or reduce the number of physical therapists needed in rehabilitation sessions are considered potential solutions for rapidly increasing healthcare costs. The European Union, in contrast, has more active kinematics and biomechatronics labs that have recently started to produce commercial products.

15.1.5 EXOSKELETONS IN DEVELOPMENT

As of August 2018, well over 100 commercial and research exoskeleton projects are in development. Exoskeletons broadly can be categorized into four main types: military, industrial, medical,

Table 15.1 Types of Exoskeletons

Medical
<ul style="list-style-type: none"> • Rehabilitation—designed to be an additional tool for physical therapists, these devices usually will not leave a rehabilitation clinic • Assistive—designed to supplement lost physical ability and to motivate the user to use their underperforming body part(s), these devices are meant to be used in-house
Military
<ul style="list-style-type: none"> • Logistics—designed to move supplies quickly • Armor carriers—intended to drive the weight of body armor and/or ballistic shields directly into the ground • Energy salvaging—utilize normal movement while walking to recharge batteries • Augmentation—decrease the energy required to move for dismounted soldiers
Industrial
<ul style="list-style-type: none"> • Chairless-chairs—lock in position while crouching to reduce fatigue • Back support—reduce the stress on the back muscles and spine while lifting • Ergonomic—remind the user of correct posture while lifting and transferring objects • Shoulder support—assist in keeping the arms raised while working at or above waist level • Tool holding—drive the weight of heavy tools directly into the ground • Power gloves—assist the user in holding tools and packages (note that power gloves can also be a subclass of both rehabilitation and assistive medical devices)
Consumer
<ul style="list-style-type: none"> • Educational—introduce students to coding and robotics, building of muscle memory • Sports—reduction of stress and strain on the human body while skiing

and consumer. These categories include powered devices that consist of a rigid outer framework and sensors, and other modular or soft technologies that use textile-based materials to conform to the body. Other categories will likely be added in the future; for example, exoskeletons designed to be worn by first responders. In some cases, the same device can fall into multiple categories, such as the Keeogo (B-Temia Inc., QC, Canada) and the Harvard soft exoskeleton, which have both medical and military applications. In [Tables 15.1–15.4](#), we outline the major categories of exoskeletons, various power sources, materials used, and the control scheme.

15.1.6 CURRENT FOOD AND DRUG ADMINISTRATION—APPROVED DEVICES

Although hundreds of exoskeletons are in development, only four have received approval from the Food and Drug Administration (FDA) as of August 2018. The Ekso (Ekso Bionics, Richmond, CA, US) and Indego (Parker Hannifin Corp., Cleveland, OH, US) are approved for use with persons who have sustained stroke and spinal cord injury (SCI). (The Indego is approved for home use in patients who have a SCI and clinical use for stroke and SCI, while the Ekso is solely a clinical device.) ReWalk (ReWalk Robotics, Inc., Marlborough, MA, US) is approved for persons with SCI (home and clinical use), and the company is collaborating with The Wyss Institute for Biologically Inspired Engineering at Harvard University on a soft exoskeleton for persons with a wide range of lower limb disabilities, including stroke and multiple sclerosis (MS). Finally, the Hybrid Assistive Limb (HAL) (Cyberdyne, Inc., Ibaraki, Japan) received approval in the categories of neurological devices and physical medicine devices. All of these devices are recognized as Class II (moderate to

Table 15.2 Types of Exoskeleton by Their Power Source

Powered exoskeletons use batteries or electric cable connections to run sensors and actuators

- Static exoskeletons: the actuators need to be turned on at all times in order for the device to maintain its shape
- Dynamic exoskeletons: actuators do not need to be turned on at all times and the device can be many times more energy efficient. This type of exoskeleton is further differentiated by what they are designed to do

Passive exoskeletons do not have any electrical power source and can be used for:

- Weight redistribution: springs and locking mechanisms divert the weight of an object around the user and into the ground
- Energy capture: ankle spring-clutch exoskeletons have been shown to improve walking efficiency, while spring-dynamo knee exoskeletons can be used to charge a battery
- Dampening: some spring or spring-damper passive exoskeletons have been designed as shock absorbers (high-speed skiing—Ski Mojo) or vibration reducers (small high-speed boat—Marine Mojo)
- Locking: some passive exoskeletons are designed to be unobtrusive until they are locked into place, allowing the user to sit or crouch in the same position for a prolonged period of time

Pseudo-passive exoskeletons have batteries, sensors, and other electronics, but they are not used to provide actuation

Hybrid-exoskeletons are wearables that have all of the controllers and sensors of a powered exoskeleton but use FES (functional electrical stimulation) of the muscles as actuators

Table 15.3 Type of Exoskeleton by Construction

Materials

Rigid materials such as metals or carbon fiber

Flexible materials in the entire construction commonly referred to as an exosuit

Adherence to the user

The exoskeleton can closely follow the contours of the human body or the device can be distant, connecting only at a few points

The wearable can also match the joints in the human body or it can have fewer or more

Coverage

Full body—the exo extends from the legs to the arms

Lower body—the exoskeleton extends from the legs to the torso

Upper body—the exoskeleton covers the arms and/or torso but does not extend below the waistline

Mobility

Fixed—the device is tethered, attached to a wall, a bracket, or suspended from the air by a fixed hook and harness

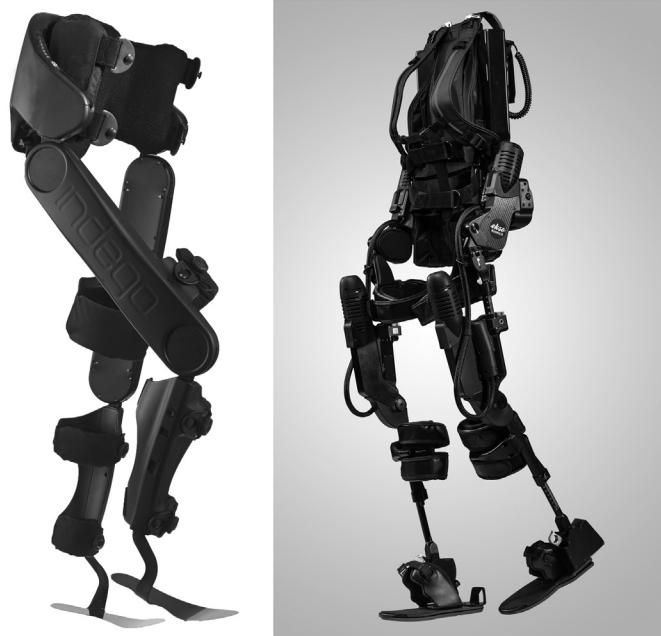
Supported—the exoskeleton is attached to an overhead rail, is supported by a moving frame or, in some cases, supported by an adjacent wheeled robot

Mobile—the user and exoskeleton can move around freely

high risk) primarily due to the risk of falling while in the device. Another device from New Zealand, the RexRehab, has received CE certification and is undergoing evaluation as part of a multicenter clinical trial in the United Kingdom, Australia, and New Zealand for use in SCI [6]. In smaller clinical trials, researchers also are evaluating its potential use for persons with stroke, MS, or other neuromuscular conditions (Fig. 15.1).

Table 15.4 Control Schemes for Exoskeletons

- Joystick: usually reserved for exoskeletons that provide 100% of the energy for motion needed by the wearer
- Buttons or control panels: the exoskeleton is placed in different preprogrammed modes. The control surface does not have to be on the exoskeleton, previous designs have them on a wrist strap, integrated into walking aids such as crutches or held by a supervisor adjacent to the user
- Brain-machine interface: usually utilizing an electrode skull cap
- Predictive control: anticipate the motion of the user using integrated sensors that monitor rotation, torque, tilt, pressure, or EMG sensors that capture nerve signals in the spine, arms, or legs
- No direct control: for example, passive exoskeletons

**FIGURE 15.1**

The Indego (left) and EksoGT (right) exoskeletons, two of four exoskeleton devices that have received FDA approval.

Images courtesy of Parker Hannifin Corporation and Ekso Bionics.

15.2 OVERVIEW OF CLINICAL EVIDENCE

Clinical evidence on the therapeutic efficacy of exoskeletons remains limited and incomplete. To date, studies have not yet proven that exoskeletons are better than either the standard of care provided with treadmill training, or than therapy provided by other high-intensity robotic training devices such as the Lokomat. A recent Cochrane analysis, for example, found that when combined

with conventional physical therapy, electromechanical-assisted training for walking in stroke patients increased the ability to achieve independent walking ability but it did not significantly increase walking velocity or capacity [7]. This (Cochrane) review included use of treadmill-based exoskeletons like the Lokomat and mobile exoskeletons and was not singularly focused on powered exoskeletons. The authors noted that gait training with electromechanical or robotic devices may benefit patients in the first 3 months after stroke rather than in the chronic phase of recovery. These results suggest that what is most important in the effort to improve walking ability may not be the type of device used but rather the application of high-intensity training by the machine at a specific and early time point in recovery. However, extensive research is ongoing in chronic stroke populations. Within the next few years, we anticipate that more high-level evidence will be available on the clinical and mobility efficacy of these devices in the stroke population.

Data on SCI remain ongoing and are similarly inconclusive. A Spinal Cord Outcomes Partnership Endeavor (SCOPE) review found that of 79 trials listed, only 11 involved exoskeletons [8]. A recent review by Mekki et al., in which the authors reviewed recent trials in the SCI population using robotics, recognized the promise of robotic interventions, in particular for providing a high volume of repetitious movement to potentially promote neuroplasticity and to reduce burden on the therapist [9]. However, the authors also argued that more extensive studies of both upper and lower limb exoskeletons are needed to specifically define dose requirements and to establish objective outcome measures.

In order to review the number and type of trials currently ongoing, we searched for studies using the database ClinicalTrials.gov using the search terms: (exoskeletons), (SCI), (stroke), (active/passive exoskeletons), (HAL), (EKS0), (Indego), and (ReWalk). Of the 56 ongoing exoskeleton clinical trials we reviewed as of July 2018, more than half of current trials (about 60%) were either uncontrolled studies, including early efficacy and feasibility studies, or limited controlled trials with a varying range of sample size (from 8 to 160 subjects). These limited controlled trials often have subjects serve as their own controls, usually are not fully randomized or blinded, and do not include a prospective matched group cohort.

More recently, randomized controlled trials evaluating the use of exoskeletons have begun and are often considered the gold standard in research, though some research has pointed to the limitations of conducting these studies in the rehabilitation setting and distinguishing between natural recovery and recovery due to a specific intervention when conducted at the acute stage [10]. These studies include large multisite trials, such as the Walking Improvement for SCI with Exoskeleton (WISE) trial, and controlled trials in single-site settings. The goal of the WISE trial is to compare exoskeleton gait training with standard gait training or no gait training in community-dwelling participants with chronic incomplete SCI. Some outcome measures include walking efficiency and walking endurance.

Training sessions—Most clinical trials with exoskeletons are conducted from 8 to 12 weeks. These trials begin with initial training sessions where a therapist may trigger the device and set the parameters, and slowly progress to having the user (patient) control the device through movements of their steps or trunk in order to complete more complicated tasks, such as walking on uneven terrain or stairs. It remains unclear, however, if this time frame is optimal and what specific doses of therapy are needed for each type of patient. Again timing, dosage, and variability of the trials depend on the aims of the study: whether therapeutic or mobility-based, for example, and the inclusion/exclusion criteria of participants chosen. Participants with incomplete SCI have the capability

to improve from being maximally dependent on the devices at the beginning of the study, to being weaned off the device and becoming independent outside of the device at the end of the study. The timing and distribution of sessions may vary depending on the skill set desired (e.g., using the device to navigate curbs in the community with a certain level of independence), current clinical evidence on nonexoskeleton gait training for improvements in walking function, or the complexity of the hardware/software of the devices.

Primary outcome measures—Standardized outcome measures for exoskeletons have yet to be established. In the studies we reviewed that focused on gait training, the investigators used standardized walking measures such as the 10-Meter Walk Test, 6-Minute Walk Test, and the Timed Up and Go Test. Other measures included changes in bilateral muscle volume, bone mineral density, and change in functional ambulation categories. While these measures may provide a basic framework for understanding patient progress, exoskeleton-specific outcome measures could better define patient-specific progress when training with these devices, and provide a future framework for more objective measures of recovery [11]. Furthermore, these measures are not sensitive enough to give feedback to the engineers and clinicians involved in the design and development of exoskeletons. Below, we summarize some findings from published early-stage feasibility studies and larger randomized controlled trials.

15.2.1 EARLY-STAGE FEASIBILITY AND CASE STUDIES

Early-stage trials of powered exoskeletons—some of which were industry-sponsored—investigated safety and clinical efficacy, primarily in patients with SCI and stroke. An important feature of these studies, which was used for FDA applications, was to look at the risk of falls or bone fractures, and the ability of the machine to allow safe ambulation in either the clinic or within a home setting. Some of these studies also looked at physiological changes such as cardiorespiratory status in the stroke and SCI patient populations.

In summary, studies have found exoskeletons to be safe in limited controlled settings and with trained personnel for persons with stroke and SCI [12–14]. However, as home studies and in-clinic trials require participants to complete more complex tasks (such as climbing stairs), longer-term studies should continue to look at the risk of falling and other adverse events. Some of these studies are ongoing.

Spinal cord injury—A systematic review by Miller et al., which reviewed 14 studies involving 111 patients, found that exoskeletons could allow subjects with SCI to safely ambulate in settings that replicated real-world conditions [15]. Among the studies the authors evaluated, no serious adverse events were reported and incidence of falls and fractures was relatively low (4.4% for falls and 3.4% for bone fractures). The authors noted that falls or minor fractures could be addressed with device modifications, and that these events occurred using an early prototype exoskeleton. Clinical effectiveness was less certain. While the authors found that training with an exoskeleton allowed patients to train at an intensity that may allow for sustained health benefits, they noted inconsistent health benefits, such as improvements in bowel movement or reduced spasticity, among the studies they reviewed.

Another systematic review by Fisahn et al. investigated the effectiveness and safety of exoskeletons for the SCI population but found that while there may be benefits to using a powered exoskeleton, no data exist comparing locomotion assistance with exoskeleton training compared to the use

of a conventional Knee Ankle Foot Orthosis (KAFO) [16]. In our experience, trials such as these are necessary in order to delineate the effects of powered exoskeletons from other forms of gait training. Preliminary research suggests that the devices can be used for overground mobility training, but understanding the long-term therapeutic effects of these devices is ongoing and will require longer clinical trials.

Stroke—Similar to SCI, studies on stroke also looked at the safety and effectiveness of gait training for FDA and CE mark certification. In summary, several studies have found general safety and efficacy, but evidence for therapy is still ongoing. Few early studies have shown positive evidence toward superiority in outcomes compared to traditional care. A review by Louie et al., for example, found that for patients with chronic stroke, gait training with exoskeletons is equivalent to traditional therapy. Persons with stroke in the subacute period (3–6 months poststroke), however, may benefit from exoskeleton therapy due to the effect the training may have on inducing neural plasticity [17].

Some organizations are acknowledging the potential clinical impact of robotics. In 2016, the American Heart Association set forth guidelines on stroke rehabilitation, acknowledging the growing number of studies focused on robotics but also the need for long-term studies that will define training protocols and patient-specific device selection [18]. The review highlighted the ability of exoskeletons to reduce therapist workload as a key benefit. Similar discussions and guidelines on the potential benefits and limitations of robotic devices may be released by additional clinical and professional associations in forthcoming years.

Other conditions—Research is limited but exoskeletons have also been evaluated for other neurological conditions, including cerebral palsy, Parkinson’s disease, and MS [19,20]. In our review of current trials listed on ClinicalTrials.gov, six studies focused on these conditions. We expect to see more clinical trials devoted toward these patient populations, though such trials need to consider the alterations in neural impairment that may require radically different types of robotic interventions.

15.2.2 RANDOMIZED CONTROLLED TRIALS

Larger randomized controlled trials are also underway. Of the 56 trials we evaluated on ClinicalTrials.gov, 22 were randomized controlled trials or controlled trials that we consider to reach Level I or II of evidence [21]. As noted earlier, one of the larger ongoing trials is the WISE trial, which will focus on persons with chronic incomplete SCI and compare exoskeleton gait training with standard gait training or no gait training. [22]. Results are underway at 10 institutions and 164 participants are expected to be recruited.

Another study led by Ann Spungen, EdD of the James J. Peters VA Medical Center in the Bronx, New York—Powered Exoskeletons in Persons with SCI (PEPSCI)—is comparing participants who use an exoskeletal-assisted walking device in the home for 4 months compared to participants who use a wheelchair (standard of care) [23]. Exoskeleton training may also have psychological and physical effects on participants, as measured by the Mental Health Component Summary (MCS) of the Veterans Rand-36 and SCI-QOL Physical Medical Health domain.

15.3 A LOOK TO THE FUTURE

Exoskeletons have evolved from machines primarily built for military applications to potentially powerful therapeutic tools that are being increasingly developed at research institutions and businesses across the world. Although exoskeletons represent a promising technology to provide over-ground walking training and may potentially reduce secondary health effects associated with physical disabilities, longer-term studies are needed in order to evaluate their clinical efficacy. Most literature so far has focused on stroke and SCI. We anticipate this trend will continue as these persons are in great need of different therapeutic devices to promote walking, balance, and strength postinjury. However, as research on these devices advances and their design improves, so likely will their clinical application for other populations with movement disorders, including MS, cerebral palsy, and Parkinson's disease.

Further long-term follow-up data are necessary for understanding the efficacy of exoskeletons and to develop guidelines for their use within clinics and rehabilitation centers. One limitation is that year-long trials are often cost-prohibitive, though long-term data will be critical to understand the efficacy and limitations of the devices. Some gait limitations of exoskeletons, in particular for the rigid devices designed for people with severe impairments, must also be addressed. The gait allowed by these exoskeletons is largely discontinuous and intermittent, yet some animal data suggest that the gait motion should be continuous for optimal recovery. Lastly, we expect that clinical outcome measures will become more specific to exoskeletons. These measures will likely include the use of wearable technologies and other "smart" systems such as the GAITRite mat that can track steps as well as other physiological measures [24]. These data may provide a more detailed analysis of patient diagnosis and progress that can help clinicians better understand issues related to timing and dosage and efficacy of the device.

REFERENCES

- [1] Locomotion: walking by steam, riding by steam, flying by steam, Metropolitan Museum of Art, 2018. [Online]. Available from: <<https://www.metmuseum.org/art/collection/search/383480>>.
- [2] N. Yagn, Apparatus for facilitating walking, US420179A, 1890.
- [3] Man Amplifiers, Popular Science, 1965, pp. 70–78.
- [4] Pioneer work on development of active exoskeletons—the first step to the humanoid robotics robotics laboratory, Mihailo Pupin Institute. [Online]. Available from: <<http://www.pupin.rs/RnDProfile/history.html>>.
- [5] List of exoskeleton companies, businesses and startups, exoskeleton report, Exoskeleton Report, 2018. [Online]. Available from: <<https://exoskeletonreport.com/2015/02/businesses-that-have-or-are-exploring-exoskeleton-products-in-alphabetical-order/>> (accessed 08.08.18.).
- [6] N. Birch, et al., Results of the first interim analysis of the RAPPER II trial in patients with spinal cord injury: ambulation and functional exercise programs in the REX powered walking aid, *J. Neuroeng. Rehabil.* (2017).
- [7] J. Mehrholz, S. Thomas, C. Werner, J. Kugler, M. Pohl, B. Elsner, Electromechanical-assisted training for walking after stroke: a major update of the evidence, *Stroke* (2017).

- [8] Current SCI clinical trials of rehabilitation and technological interventions to improve functional outcomes, Spinal Cord Outcomes Partnership Endeavor (*SCOPE*, www.scope-sci.org), 2018. [Online]. Available from: <<http://scope-sci.org/wp-content/uploads/2018/06/SCOPE-Rehab-AT-SCITrialsTable-2018.06.06.pdf>> (accessed 24.07.18.).
- [9] M. Mekki, A.D. Delgado, A. Fry, D. Putrino, V. Huang, Robotic rehabilitation and spinal cord injury: a narrative review, *Neurotherapeutics*. (2018).
- [10] J.E. Graham, A.M. Karmarkar, K.J. Ottenbacher, Small sample research designs for evidence-based rehabilitation: issues and methods, *Arch. Phys. Med. Rehabil.* (2012).
- [11] R.B. van Dijsseldonk, H. Rijken, I.J.W. van Nes, H. van de Meent, N.L.W. Keijsers, A framework for measuring the progress in exoskeleton skills in people with complete spinal cord injury, *Front. Neurosci.* (2017).
- [12] S.A. Kolakowsky-Hayner, Safety and feasibility of using the EksoTM bionic exoskeleton to aid ambulation after spinal cord injury, *J. Spine* (2013).
- [13] A. Nilsson, K.S. Vreede, V. Häglund, H. Kawamoto, Y. Sankai, J. Borg, Gait training early after stroke with a new exoskeleton—the hybrid assistive limb: a study of safety and feasibility, *J. Neuroeng. Rehabil.* (2014).
- [14] A. Esquenazi, M. Talaty, A. Packel, M. Saulino, The rewalk powered exoskeleton to restore ambulatory function to individuals with thoracic-level motor-complete spinal cord injury, *Am. J. Phys. Med. Rehabil.* (2012).
- [15] L.E. Miller, A.K. Zimmermann, W.G. Herbert, Clinical effectiveness and safety of powered exoskeleton-assisted walking in patients with spinal cord injury: systematic review with meta-analysis, *Med. Devices (Auckl.)*. (2016).
- [16] C. Fisahn, et al., The effectiveness and safety of exoskeletons as assistive and rehabilitation devices in the treatment of neurologic gait disorders in patients with spinal cord injury: a systematic review, *Glob. Spine J.* (2016).
- [17] D.R. Louie, J.J. Eng, T. Lam, Gait speed using powered robotic exoskeletons after spinal cord injury: a systematic review and correlational study, *J. Neuroeng. Rehabil.* (2015).
- [18] C.J. Winstein, et al., Guidelines for adult stroke rehabilitation and recovery: a guideline for healthcare professionals from the American Heart Association/American Stroke Association, *Stroke* 47 (6) (2016) e98–e169.
- [19] M.B. Rietberg, D. Brooks, B.M.J. Uitdehaag, G. Kwakkel, Exercise therapy for multiple sclerosis, *Cochrane Database Syst. Rev.* (2005).
- [20] M. Matsuda, et al., Robot-assisted training using Hybrid Assistive Limb® for cerebral palsy, *Brain. Dev.* (2018).
- [21] B. Lombardi, M. Paci, G. Briganti, Levels of evidence of articles published in physical and rehabilitation medicine journals, *J. Rehabil. Med.* 43 (3) (2011) 264–267.
- [22] The WISE trial—walking improvement for SCI with exoskeleton. [Online]. Available from: <<https://clinicaltrials.gov/ct2/show/NCT02943915?cond=WISE+Trial&rank=1>> (accessed 06.07.18.).
- [23] Powered exoskeletons in persons with SCI (PEPSCI), 2016. [Online]. Available from: <<https://clinicaltrials.gov/ct2/show/NCT02658656>> (accessed 13.08.18.).
- [24] C. Buesing, et al., Effects of a wearable exoskeleton stride management assist system (SMA®) on spatiotemporal gait characteristics in individuals after stroke: a randomized controlled trial, *J. Neuroeng. Rehabil.* (2015).

STRUCTURAL EXOSKELETONS AND SOFT FABRIC EXOSUITS FOR ASSISTIVE WALKING

16

Lawrence J. Jasinski

ReWalk Robotics, Southborough, MA, United States

This chapter will discuss the data, challenges, and progress of exoskeleton designs for those who have no capacity to walk on their own and about the extension of these technologies with the advent of soft exosuits using sensors and software that are designed to provide dynamic situational mechanical assistance in walking.

ReWalk Personal System (ReWalk) is a powered, robotic, lower body exoskeleton that enables individuals who are paralyzed due to spinal cord injury (SCI) to walk. The activity levels achieved through walking have been shown to improve quality of life (QoL) and significantly reduce healthcare utilization, presenting an opportunity to improve health outcomes in this patient segment while containing overall healthcare costs.

Individuals with SCI are often relegated to prolonged sitting due to their inability to walk and the absence of capable products and treatments to restore their walking abilities. Recovery of locomotion is a main priority for SCI patients [1]. The implications for loss of ambulatory function are profound and costly for individuals living with SCI. With current treatment options, estimates of the overall direct lifetime cost of individuals with SCI are known to be as high as \$2.3 Million (MM) per patient [2].

The ReWalk was cleared by the FDA on June 26, 2014, and was the first device of its kind designed for home and community use. It is intended for individuals with SCI to perform ambulatory functions with the supervision of a trained companion. Subsequently, three other systems have been approved for use by the FDA: the Indego for home and community use with SCI patients in March 2016; the EksoGT for institutional use with SCI and stroke patients in April 2016; and Medical HAL for institutional use with SCI patients in December 2017.

The *core value of the ReWalk is to restore walking function and improve QOL* in this otherwise sedentary patient population. The standard of care for the large majority of conditions causing mobility impairments is to return the individual to their highest level of mobility function. Restoring walking function to patients with SCI has significant potential to improve health outcomes and contain the overall costs associated with care. The restoration of walking in paraplegic patients is physiologically, psychologically, and functionally desirable.

There is sufficient clinical data demonstrating the safety and efficacy of powered exoskeletons in a variety of complex and community settings. Multiple studies achieved expected endpoints demonstrating minimal adverse events (AEs) and feasibility of safe use of the ReWalk. Miller et al.

reviewed the experiences of 48 SCI patients among 954 sessions with exoskeletons in various environments in a meta-analysis published in 2016 [3]. The cumulative data demonstrated that *exoskeleton users could successfully and safely ambulate in complex environments in the community setting.*

In summary, exoskeletons have been shown to be a safe and effective treatment for patients with paraplegic SCI. In cases where individuals fit the specific FDA indications for use and demonstrate safe operation of the system, there is a high likelihood that patients will experience improved QoL and reduced healthcare utilization.

16.1 BURDEN OF SPINAL CORD INJURY

Incidence: SCI has a very small incidence rate which is calculated at around 54 cases per 1MM people in the United States, or 17,000 new cases per year [2].

Prevalence: The number of people in the US living with SCI in 2016 has been estimated to be approximately 282,000 [2].

Approximately 42% of SCI cases are paraplegic and 58% are tetraplegic [2]. This equates to approximately 118,000 individuals living with paraplegia in the United States and is on a par with the FDA's definition of a rare disease in the United States (prevalence rate of <200,000). Patients with lesions from T7 to L1 (levels indicated for ReWalk) are a more limited subset of the paraplegic cases. Approximately 26% of all SCI cases are at the levels T7–L1. This equates to approximately 73,320 individuals living with SCI that would qualify for the ReWalk based solely on level of injury (LOI). The group of eligible patients is further reduced by conditions such as weight, lower extremity tone or contracture, compromised bone density, inadequate core control, inadequate companion support, and inappropriate use environment, among others. Based upon study enrollment data and manufacturers' experience qualifying patients, a conservative estimate of between 50% and 75% of the individuals who qualify for ReWalk (by LOI) would be disqualified due to existing comorbidities or the lack of an appropriate companion or use environment. *The net result is a qualified patient group estimated to be between 18,000 and 36,000 in the United States.*

16.1.1 DEMOGRAPHICS

Gender: Males account for 80% of new SCIs [2].

Race/ethnicity: More injuries to non-Hispanic blacks (22%) in proportion to the general population (12%) [2].

Etiology: Motor vehicle accidents (38%), falls (30%), violence (13.5%), sports (9%), and medical/surgical (5%) [2].

16.1.2 ADVERSE HEALTH OUTCOMES

In a 2013 World Health Organization (WHO) paper on SCI by Dr. Margaret Chan, she summarized that:

the consequences of SCI are commonly either premature mortality or at best social exclusion. Trauma care systems are frequently inadequate. For many, access to high quality rehabilitation and assistive devices is unavailable. Ongoing health care is lacking, which means that a person with spinal cord injury is likely to die within a few years from urinary tract infections or pressure sores. Even when individuals are lucky enough to receive the health and rehabilitation care they require, they are likely to be denied access to the education and employment which could enable them to regain their independence and make a contribution to their families and their society [4].

SCI is a serious medical condition that results in functional, psychological, and socioeconomic disorder, causing patients to experience significant impairments in various aspects of their life. These medical issues are widespread as they can be a direct result of the primary deficits created by SCI, but are often amplified by prolonged sitting and the lack of physical activity that is prevalent in this patient segment. It is estimated that more than half of the patients living with SCI are completely sedentary and 65% do not achieve the minimum activity level needed to avoid secondary medical complications [5].

Both acute and long-term secondary medical complications are common. However, chronic complications most negatively impact patients' functional independence and QoL. Complications are a frequent cause of morbidity and mortality and lead to increased rates of rehospitalization, loss of employability, and decreased QoL [6–8]. Prevention, early diagnosis, and treatment of chronic secondary complications in patients with SCI is critical for limiting these complications, improving survival, community participation, and health-related QoL.

As a direct result of SCI, patients typically experience loss of ambulatory function, loss of normal bowel and bladder function, reduced musculoskeletal activity, altered autonomic nervous system function, altered sexual function, and loss of sensory function, among other comorbidities.

The most common secondary long-term complications after SCI include:

- pressure ulcers;
- respiratory complications;
- cardiovascular complications;
- urinary and bowel complications;
- spasticity;
- pain syndrome;
- osteoporosis; and
- bone fractures [6,9].

Patients with SCI commonly utilize a variety of pharmaceuticals to manage their secondary complications. Prescription medications are often dispensed for pain, spasticity, depression, diabetes, bowel management, and a host of other health issues. Many of these drugs are costly and have unwanted side effects, including addiction, changes in mood, and increased risk of suicide. Opioid abuse and addiction has reached epidemic proportions in the United States and is extremely costly, both in terms of direct medical care and the societal impact. The frequent use of opioids in this patient population puts this group at higher risk for addiction. Any interventions that have potential to reduce the utilization of opioids for pain control should be strongly considered.

Increased utilization of healthcare services to treat the above conditions is prevalent among individuals living with SCI. Dryden et al. concluded that compared with a control group, persons with SCI experienced:

- 2.6 times more rehospitalization;
- 3.3 days longer hospital stay;
- 2.7 times more physician contact; and
- 30 times more hours of home care services [7].

Ultimately, this patient segment has a very high rate of adverse health outcomes, which tracks closely with the lack of walking and suppressed general activity levels that are associated with long-term wheelchair use. As a result, mortality rates of individuals who suffer an SCI have remained unchanged since the 1980s [2].

Powered exoskeletons provide a unique solution to reduce the secondary medical complications of SCI and improve patients' QoL. By restoring walking function and supplying a means by which patients can simultaneously unweight from a sitting position and perform aerobic levels of activity, many of these medical complications are diminished.

16.2 CURRENT TREATMENT OPTIONS

Recovery of walking function is a main priority for patients with SCI [1]. However, it is clear that patients have had limited options available to them to regain walking function following severe injury causing paresis or paralysis. No existing treatment or device allows users to perform sustained ambulation in the same manner and efficiency as the modern exoskeleton. Before the availability of exoskeletons, treatment options for standing, walking, or mobility for personal use outside of the rehabilitation setting were limited to:

- wheelchairs;
- leg braces (HKAFOs, RGOs);
- functional electrical stimulation (FES) systems; and
- standing frame and standing mobility devices.

The existing clinical literature supports that powered exoskeletons are a more effective and beneficial treatment for qualified individuals as compared to current existing options. Furthermore, exoskeletons provide a modern solution to mobility that is more in line with the standard of care interventions used to treat other mobility impairments, such as amputation or severe osteoarthritis.

16.2.1 WHEELCHAIRS

Conventional manual wheelchairs are the primary assistive devices used by people with paraplegic SCI. The result of wheelchair use is prolonged sitting and uninterrupted sedentary behavior. In a national cohort study of nearly 8000 adults, Diaz et al. found that uninterrupted bouts of sedentary time are associated with an increase in all-cause mortality [8]. Additionally, 3.3 METs of activity maintained for 1 hour, 3 days per week is associated with preventative health benefits including

all-cause mortality risk reduction of 20% in the general adult population, and is the level of aerobic effort that a powered exoskeleton can provide [3]. Walking in a powered exoskeleton has obvious and significant benefits when compared to the uninterrupted sedentary behavior that is commensurate with wheelchair use.

16.2.2 LEG BRACES

Leg braces require excessive metabolic demand, causing a high rate of discontinued use by patients. In a randomized controlled trial, Arazpour et al. reported that velocity and distance during a 6-minute walk test were superior with a powered exoskeleton compared with RGO and HKAFO and further that the physiological cost index was approximately 50% lower with a powered exoskeleton versus RGO and HKAFO [10]. Miller also found that, “the main limitation of these [orthotic] devices is a high metabolic demand such that most patients eventually discontinue their use” [11]. Leg braces have a high rate of nonuse over time, leading to a poor outcome with regards to restoring walking function and providing increased activity to individuals living with SCI.

Platz et al. published results of an observational study with seven participants during a 4- to 5-week intensive inpatient device training for nonambulatory individuals with SCI using a powered exoskeleton for technically assisted mobility. The key metrics observed were achieved level of control of the system after training, user satisfaction, and impact on QoL. Importantly, the authors in Platz found that:

- Unpowered orthoses such as passive mechanical hip–knee–ankle–foot orthoses can be regarded as training tools for individuals with SCI.
- *Unpowered orthotic devices are not suitable for routine mobility use; and*
- *Robotic exoskeletons provide a major advantage over passive orthoses because they can provide coordinated and controlled joint movements rather than limited hip range of motion coupled with mandatory rigid knee and ankle fixation [12].*

Studies reviewed in Miller identified concrete health benefits from the use of a robotic exoskeleton, such as increased cardiac activity, improved bowel movements, and improved muscle spasticity. *The clinical benefits identified in these patients from the use of a robotic exoskeleton were significant and could not have been achieved by patients using conventional therapy, such as a standing frame or knee–ankle–foot–orthosis (“KAFO”)/ankle–foot–orthosis (“AFO”) braces [3].*

In summary, the use of leg braces for patients living with SCI is largely ineffective due to the high metabolic cost, lack of functional, prolonged gait, and poor long-term patient compliance.

16.2.3 FUNCTIONAL ELECTRIC STIMULATION

FES systems stimulate a user’s muscles by electrical impulses to generate joint movement. However, they have limited application due to a high rate of fatigue and limited walking capabilities. During FES, all motor units in a muscle group are stimulated simultaneously, which induces muscle fatigue and results in high energy consumption and limiting walking distance [13,14]. Furthermore, indications for use stipulate that patients must have complete sensory loss to tolerate the significant electrical stimulation needed to produce muscle contraction [13]. Additional

complicating factors include fatigue and electrode contact stability. At best, FES provides only physiological walking in a very limited segment of patients. The consistent community ambulation that an exoskeleton provides exceeds the walking capabilities of an FES system by a large margin.

16.2.4 STANDING FRAMES AND STANDING MOBILITY DEVICES

Standing frames and standing mobility devices are both interventions for patients living with SCI. Neither intervention has proven to be effective in providing sustained ambulatory function. Standing frames have demonstrated modest improvements in bone integrity, but provide no cardiovascular benefits as they are a passive modality.

16.3 RATIONALE FOR EXOSKELETONS

The referenced clinical literature supports that exoskeletons are a more effective and beneficial treatment for qualified individuals. Patients living with SCI often suffer from a host of secondary complications resulting from their lack of ambulation. Furthermore, the use of a wheelchair to provide mobility can perpetuate issues with digestion and pressure sores, and cause additional chronic injuries to the shoulder, elbow, and wrist, while failing to offer the benefits that can be achieved by using an exoskeleton and walking.

Increased reliance on pharmaceuticals to manage a host of complications only increases the utilization of care or creates tertiary complications such as cardiovascular disease (CVD) or drug dependency. Compared to existing care options, exoskeletons fill an unmet need and provide a unique solution for this patient segment by restoring walking function at sustainable metabolic demand with minimal and manageable AEs.

Exoskeletons fill a crucial mobility need for individuals living with SCI much like a lower limb prosthetic enables individuals with amputations to remain mobile and ambulatory. Amputation and chronic osteoarthritis are two examples of conditions where the standard of care is to provide a high dollar intervention with the overall goal of maintaining mobility function. It is commonly accepted that these interventions preserve the individual's normal function and therefore have a major influence on their overall health profile and healthcare costs.

Exoskeletons can provide a similar standard of mobility for individuals living with SCI. The technology has matured to the stage where it clearly provides a safe and functional mobility alternative to wheelchairs that closely resembles able-bodied walking. With the advancement of such high-tech ambulatory solutions as prosthetics and exoskeletons, the concept of leaving either of these patient groups confined to a wheelchair is antiquated and highly likely to result in a poor outcome. The consequences of not providing an advanced and modern mobility solution to qualified individuals is increased comorbidities, reduced QoL, and a shortened life expectancy.

Exoskeletons are a superior treatment option for patients with SCI and should be a covered item for patients that fit the FDA criteria and demonstrate competent and safe use.

16.4 REWALK PRODUCT SUMMARY

ReWalk is a wearable computerized robotic exoskeleton that provides powered hip and knee motion to enable individuals with SCI to walk. The ReWalk helps treat SCI and related secondary medical conditions due to prolonged sitting in a wheelchair by allowing paraplegic patients to ambulate at home and in the community.

ReWalk consists of a fitted metal brace that supports the legs and part of the upper body; motors that supply movement at the hips, knees, and ankles; a tilt sensor which senses subtle changes in posture; and a waist pack that contains the computer and power supply. Through a series of sensors, ReWalk users can autonomously initiate standing, sitting, and walking, as well as control speed and direction, through a combination of controller commands and shifts in body positions.

16.4.1 REWALK COMPONENTS AND SPECIFICATIONS

The ReWalk consists of three main components:

1. communicator,
2. exoskeleton, and
3. waist pack.

16.4.2 COMMUNICATOR

The remote control communicator (Fig. 16.1) is a small wireless device that provides two-way communication between the user and the ReWalk unit. It provides control of selection between modes and presents a visual indication of the status of the system, which includes the mode in which the device is operating (walking, standing, sitting, etc.). Communication between the

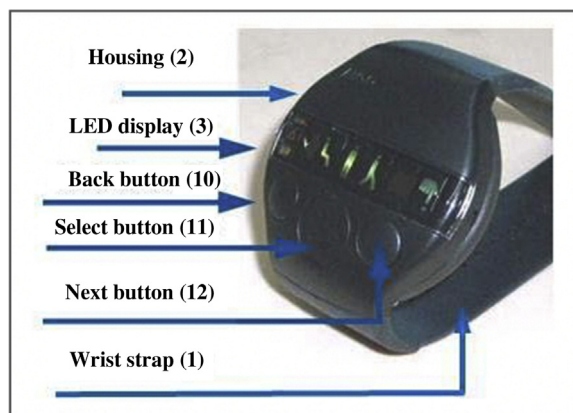


FIGURE 16.1

Remote control communicator.

communicator and the main computer is performed wirelessly at 2.4 GHz with a frequency hopping protocol.

16.4.3 EXOSKELETON

The exoskeleton consists of four components (Fig. 16.2):

- *Articulating legs:* The legs consist of left and right segments that are secured to the thigh and calf and interconnect robotic joints located over the patient's hips and knees. The main structural component of each segment carries the load generated across the ReWalk. Multiple attachment straps are mounted along the length of each leg. DC motors, gearing, and electronics are located at each hip and knee joint to provide motion. Cabling for communication and power is contained within the leg unit.
- *Pelvic band:* The pelvic band support provides a structure to join the two legs together and the pelvic strap helps hold the user firmly in the system. A tilt sensor is mounted on the left side of the pelvic band.
- *Straps, padding, and knee bracket:* Six straps hold the user in the exoskeleton at the following locations: chest, waist, thigh, upper knee, lower knee, and calf. The rigid front of the knee bracket holds the user's knee joint in line with the axis of rotation of the exoskeleton.
- *Ankle–foot plate:* The ankle–foot plate holds the user's foot to the system and fits into the user's shoe.

16.4.4 WAIST PACK

A lightweight waist pack (Fig. 16.2) is attached to the pelvic band of the exoskeleton. The waist pack consists of a rigid outer shell and an inner compartmentalized shell with the power management and computer control system components. The main battery is a lithium ion battery that is capable of allowing a user to walk continuously for more than 2 hours on a charge. Once the battery reaches a predetermined charge the power switches to the lithium polymer battery which provides the user with at least an additional 15 minutes of continuous walking.

16.4.5 SYSTEM CONFIGURATION

After meeting specific criteria for use, the ReWalk is custom fit and programmed to the patient by a ReWalk-trained healthcare professional. The adjustability of the system allows for a precise fit to enable safe and efficient use. Patients undergo a structured training program with objective skill assessments to assure proper competency for home and community use.

16.4.6 VIDEO LINKS

Patient testimonial: <https://youtu.be/aNgf8sPAer8>

How ReWalk works: <https://youtu.be/d5zl7fglMgo>

Community use: <https://youtu.be/DPhYdSxNZnk>



FIGURE 16.2

Exoskeleton and waist pack.

16.4.7 LEVELS OF PATIENT TRAINING

ReWalk patients also complete two levels of training that correspond with the certification levels.

- The Basic Skill Assessment helps guide and monitor patients as they perform initial training in the rehabilitation setting to achieve the core skills of device operation and safe beginner walking.
- The Advanced Skill Assessment is administered following basic skill achievement and focuses on all home and community-based activities needed for personal use.

Both the Basic and Advanced Skill Assessments contain a battery of specific objective tests that patients and their companions must complete in order to achieve full certification and be allowed to take their ReWalk home and use it outside of the supervised setting of a rehabilitation facility.

16.5 SAFETY AND EFFICACY PROFILE

16.5.1 PATIENT SELECTION

Patients with lesions from T7 to L1 (levels indicated for ReWalk) are a subset of the paraplegic cases. In addition, there are a number of other physical criteria that must be met in order to effectively use an exoskeleton at home and in the community.

According to the FDA, candidates for the ReWalk should meet the following criteria:

- SCI injury at T7–L1.
- Meet the height and weight requirements.
- Full use of hands and arms.
- Can tolerate walking activities.
- Demonstrate safe use of the system by passing advanced skills.
- Have an appropriate use environment and companion.

As a result of the limited patient group, exoskeleton research cannot be held to the same standards as pharmaceutical studies or devices which are applicable to a wider population. Conducting large, randomized, or double-blinded studies is simply not feasible. There is no plausible method by which a subject could be double-blinded during an exoskeleton trial. Mimicking the use of an exoskeleton is not a tenable design. Recruiting more than 10 patients for a single-site exoskeleton trial has proven to be challenging even in densely populated cities that have established SCI centers of excellence with a known group of paraplegic patients. The limited patient group will naturally yield a smaller sample size for studies.

For this very limited patient group, it is important that studies with small sample sizes be considered as evidence that exoskeletons can be used safely and provide health benefits. The data from these smaller studies can in fact yield valid and reliable information. The Florida Department of Administrative Hearings ruled in case 17–01723 with the Department of Management Services, Division of State Group Insurance on April 13, 2017, that as a matter of fact and law, the ReWalk is not investigational or experimental; “it is impossible to find large numbers of SCI patients who could be appropriate subjects” and thus “it is necessary to rely on data that can be assembled,” that

“available data demonstrates that ReWalk is not experimental or investigational at this point in time.” Therefore studies involving durable medical equipment (DME) used in rehabilitation medicine cannot follow the same testing paradigms utilized by drug studies or new operative procedures, and the existing research should be given due consideration as credible scientific evidence.

16.5.2 SAFE AMBULATORY FUNCTION AND PATIENT TOLERANCE

There are sufficient clinical data demonstrating safety and efficacy of using exoskeletons in a variety of complex and community settings. Multiple studies have addressed the feasibility of exoskeleton-assisted walking (EAW), examining patient’s ability to learn the skills to walk both in and outside of a rehabilitation center [13,15,16]. AEs have been observed during such trials to understand the inherent risks associated with EAW.

Two early studies on exoskeletons focused primarily on safety, feasibility, and patient tolerance. A 2012 study by Zeilig et al. published in the *Journal of Spinal Cord Medicine* consisted of six subjects, all with complete long-standing SCI. The results demonstrated that all patients successfully completed the training and *no incidents of falls* were reported during more than 80 training sessions [15].

Esquenazi et al. also studied the safety and feasibility of the ReWalk. Their results were published in the *American Journal of Physical Medicine and Rehabilitation* in 2012. Twelve subjects with chronic SCI were trained to use the ReWalk at limited community speeds and participated in sessions up to three times per week for 2 months. During the trial *no falls or serious adverse events (SAEs) were reported*. Dr. Esquenazi went on to conclude that, “ReWalk may improve some of the health problems reported in this population, thereby possibly lessening the inherent risks associated with their management” [13].

Robust clinical data from studies performed at various Veteran Administration (VA) sites also demonstrate the safety and effectiveness of exoskeleton use in the community. Dr. Ann Spungen, Associate Professor, Icahn School of Medicine at Mount Sinai, New York, and Associate Director and Principal Investigator, VA Bronx, NY, Center for Spinal Cord Injury, presented data from the VA sites to the American Academy of Physical Medicine and Rehabilitation (AAPM&R) in November 2014. These clinical data demonstrated that *ReWalk was used in various indoor and outdoor environments without incident* which illustrate exoskeleton users in various community environments.

A specific example of Dr. Spungen’s findings is contained in her 2013 paper, “Exoskeletal-assisted walking for persons with motor-complete paraplegia.” Her team observed and analyzed the use of the ReWalk with patients in the home and community setting and concluded that the subjects were able to *safely and effectively use the ReWalk on a variety of surfaces and conditions in the community and home settings*:

In addition to demonstrating achievement of walking ability, this study showed that persons with motor-complete paraplegia could perform other indoor skills such as reaching for an item in a cabinet above the head, navigating an automatic door and an elevator, and walking on carpet. Additional support for community-based use of this device was demonstrated in some of the participants who were able to perform outdoor mobility skills such as walking on concrete, uneven ground surfaces, slight slopes, and up or down a curb [16].

The FDA conducted an extensive review of ReWalk's clinical data in complex and community settings. Specifically, the following data were provided by ReWalk to the FDA—[K131798, June 26, 2014] Retrospective Analysis of Walking Surfaces—ReWalk Clinical Study Sites (CLN10531):

- Retrospective Analysis of Walking Surfaces—ReWalk Clinical Training Site (CLN0002);
- Retrospective Analysis of Walking Surfaces—ReWalk Personal Use (CLN0001);
- Ann M. Spungen Ed. D—Report on Community-Based Exoskeleton-Assisted Walking; and
- Performance Evaluation of ReWalk Reciprocating Gait Orthosis—Final Report (RW003).

Dr. Miller further analyzed the FDA data that were included in the three retrospective studies. These data were summarized in a white paper titled “Evaluation of the ReWalk Computerized Exoskeleton for Patients with Spinal Cord Injury in Community Settings” [3]. He reviewed the experiences of 48 SCI patients among 954 sessions with the ReWalk in various environments. The cumulative data demonstrated that ReWalk users could successfully ambulate in various environments in the community setting.

- Environments included outdoor sidewalks, homes, stores, restaurants, and offices.
- Terrains included grass, ramps, inclines, curb cutouts, outdoor sidewalks.
- Surfaces included smooth and carpeted surfaces, concrete, asphalt, grass, gravel, tile, wood, granite, brick, and mild irregular surfaces.
- Tasks included crossing streets with traffic lights in a timely fashion, entering and exiting elevators, navigating ADA accessible and nonelectric doors including revolving doors.
- In all these situations, the individuals demonstrated effective use of the computerized exoskeleton.
- Most importantly, no falls or SAEs were reported.

Dr. Miller concluded that *the ReWalk allows for safe ambulation across a wide variety of settings*, including indoor and outdoor surfaces, challenging community environments, uneven surfaces, curb cutouts, and ramps.

A summary of all AEs reported in existing scientific literature on exoskeletons indicates that there have been few SAEs. Seven studies have provided AE data on 106 subjects who received powered exoskeleton gait training. No falls, joint injury, pressure ulcers, or dysreflexia were reported in these studies of exoskeleton use. The most commonly reported AEs were minor to moderate skin abrasions. **Table 16.1** is a representation of the AEs reported through existing scientific literature on powered exoskeletons.

The data provided to the FDA on all exoskeletons as described here and in the previous section, combined with the existing literature on exoskeletons, clearly demonstrate that exoskeletons are safe and effective in a community setting and not investigational. Furthermore, FDA controls, including the training standards and companion requirement, insure that patient safety is maintained and serve to mitigate the risk of falls or other AEs.

16.5.3 EXOSKELETON-ASSISTED WALKING SIMULATES NORMAL PHYSIOLOGICAL EFFECTS

The literature largely supports that *EAW produces a physiological effect similar to that of an able-bodied person walking at normal walking speeds* [3,10]. Similarities have been demonstrated in

Table 16.1 Adverse Events Reported in Studies of Powered Exoskeletons

respiratory function, metabolic demand, rate of perceived exertion [10,21,22], gait speed [23], and ground reaction force (GRF) [24].

16.5.3.1 Energy expenditure

Multiple studies support that the energy demand observed during EAW produces a cardiorespiratory response very close to able-bodied walking, which is sustainable and likely to produce positive effects on health [10,21,22].

In 2012 Arazpour et al. compared the energy consumption between walking with a Powered Gait Orthosis (PGO) versus an HKAFO or RGO. The physiological cost index was measured during a self-selected walking test. The results demonstrated a significantly lower energy expenditure with PGO walking compared with the other two options. The authors concluded that, “patients with SCI walk faster and more efficiently using a PGO and its use should therefore be proposed for the SCI patient” [10].

A 2015 study by Asselin et al. measured oxygen uptake (VO_2) and heart rate (HR) during powered EAW during consecutive 6-minute periods of sitting, standing, and walking. They found, “that participants performed EAW at about half of their estimated max HR reserve, which represents a moderate level of intensity.” They concluded that walking in a powered exoskeleton has the possibility to be used routinely and improve the adverse health-related consequences [21].

The Miller 2016 meta-analysis analyzed the energy expenditure of subjects using three cleared exoskeletons. Based on a review of these studies the author determined that the physiologic demand of powered EAW was 3.3 metabolic equivalents [3]. In addition, the analysis found that the rating of perceived exertion during exoskeleton walking was 10 on the Borg 6–20 scale. The authors stated that this intensity is comparable to the self-reported exertion of an able-bodied person walking at 3 miles per hour. Physical activity from EAW of 3.3 METs for only 1 hour per day, 3 days per week, corresponds to 10 MET hours per week, is associated with preventive health benefits including cardiovascular and all-cause mortality risk reduction of 20% in the general adult population. The authors concluded that the use of a powered exoskeleton in SCI patients allows safe ambulation in real-world settings at a physical activity intensity conducive to prolonged use and known to yield health benefits [3].

16.5.3.2 Gait speed

A multiple subject review examining the capabilities of seven different exoskeletons demonstrated safe ambulation at moderate speeds by thoracic-level nonambulatory patients [23].

In 2015 Louie et al. conducted a systematic review of 15 studies to determine the efficacy of powered exoskeletons and gait speed attained by individuals with SCI when using a powered exoskeleton. “Twelve studies reported individual participant gait speed, which ranged from 0.031 to 0.71 m/s. The mean gait speed attained by the 84 participants in these 12 studies was 0.26 m/s.” The authors concluded that exoskeletons have the potential to allow individuals with thoracic-level motor-complete SCI the ability to walk at moderate speeds. The variables related to speed were also examined and it was found that “Those who were able to train for several weeks to months were generally able to achieve ambulation at faster speeds with a powered exoskeleton” and concluded that “daily use (of exoskeletons) may help exoskeleton users attain higher gait speeds quickly” [23].

This multipublication review clearly demonstrates that functional walking is achievable by non-ambulatory patients through the use of modern exoskeletons. When users are properly selected and trained they can ambulate safely and functionally at limited community speeds.

16.5.3.3 *Ground reaction force*

The forces demonstrated by SCI patients during EAW were similar in magnitude and pattern to those observed during able-bodied walking at self-selected ambulation speeds [24].

In 2013 Fineberg et al. compared the vertical ground reaction forces (vGRFs) of able-bodied subjects to those performing EAW. Using an in-shoe pressure-mapping system they captured the vGRF. All subjects in the EAW group had thoracic motor-complete SCI. Walking speeds were self-selected by the able-bodied participants. All subjects who achieved unassisted walking speeds of 0.29 m/s or greater displayed maximal vGRFs that were at or in excess of 99% of body weight or greater. The able-bodied control group demonstrated similar vGRF measurements. They concluded that EAW “in persons with motor-complete SCI generated vGRF similar in magnitude and pattern to that of able-bodied walking” [24].

The scientific literature to date clearly suggests that EAW consists of many of the same attributes of able-bodied ambulation and that limited community speeds are achievable with the current technology. It is a reasonable expectation that the stimuli produced by intermittent use of an exoskeleton would have similar physiological effects as seen in able-bodied individuals performing normal ambulation, including cardiovascular and bone density benefits. The aerobic effort and weight-bearing demands of EAW are a unique combination that is currently not achievable through existing treatment options. This stimulus has the potential to not only improve these two areas, but to also counteract many of the adverse secondary health complications that are common to individuals living with SCI.

16.5.4 **IMPACT ON QUALITY OF LIFE**

There is evidence to support that EAW reduces immobility, minimizes spasticity, improves cardio-pulmonary, bowel, and bladder function, provides psychological benefits, and results in improved QoL. [Table 16.2](#) represents the published literature on EAW that supports positive health outcomes and QoL.

Improved health outcomes in this patient population provide a key metric which demonstrates the utility and medical benefits that exoskeletons provide. The existing evidence demonstrates that the benefits from EAW exceed any existing treatment options for SCI, and that such positive benefits should be strongly considered regarding the medical appropriateness of providing exoskeletons to qualified individuals.

Bowel and bladder dysfunction is prevalent among individuals living with SCI. According to Glickman, 95% of patients with SCI require at least one therapeutic method to initiate defecation and that bowel function is a source of distress in more than half of these patients [28]. According to French et al., the leading cause of rehospitalization in patients living with SCI is bowel and bladder dysfunction, including urinary tract infections (UTIs), leading to increased healthcare utilization [29].

Patients living with SCI have difficulty achieving normal continence. The daily act of toileting is a time-consuming task, requiring a regular schedule, assistance from a caregiver, and

Table 16.2 Positive Health Outcomes of Exoskeleton-Assisted Walking

Author/Year	Bowel/Bladder	Pain	Spasticity	Sleep	Quality of Life
Esquenazi et al. (2012) [13]	✓	✓	✓		
Hong et al. (2017) [25]	✓				
Raab et. al. (2016) [26]					
Spungen et al. (2014) [16]	✓	✓		✓	✓
Stampacchia et al. (2016) [27]	✓	✓	✓		

pharmaceutical intervention. It is common for these patients to need laxatives, suppositories, digital stimulation, and specialized DME to assist with bowel evacuation. Long-term bowel and bladder dysfunction can negatively affect many organ systems, impacting QoL and increasing morbidity rates [30,31].

Multiple studies have demonstrated marked improvements in bowel and bladder function in SCI patients due to the use of powered exoskeletons [13,16,27]. The systematic review performed by Miller et al. identified several studies which collected data regarding improved bowel movement regularity and concluded that 61% of participants reported improvements with exoskeleton training [3].

In data presented at the AAPM&R Annual Meeting in 2014, Spungen et al. reported significant positive improvements in bowel function. Ten subjects performing EAW consisting of an average of 36 sessions reported increased frequency of bowel evacuations, decreased time to evacuation, reduced accidents, and reduced utilization of associated bowel medications. QoL as measured by the SF-36 also demonstrated significant improvements in bowel and bladder management and complications.

Interim data from 2017 published by Hong et al. in the *Journal of Spinal Cord Medicine* further indicated that EAW can positively affect bladder management and improve QoL. Participants included individuals with SCI ASIA A through D who were injured at least 6 months prior to enrollment. Bladder management was self-reported at baseline and after 12 weeks of usual activity and after 36 sessions of EAW using both the EksoGT and ReWalk devices. Results in 14 participants demonstrated clinical improvements in 50% of the group after EAW versus 14% after usual activity. Following EAW, bladder management was also shown to improve during sleep and reduced distress in the participants [25].

Pain and spasticity are common secondary complications that require ongoing healthcare utilization and medical or pharmaceutical intervention. In a 2015 study on the chronic complications of SCI, Sezar et al. reported the following findings:

- Spasticity affects 70% of patients with SCI and causes considerable disability for many;
- 80% of patients with SCI reported suffering from chronic pain;
- Chronic pain may lead to functional disability, emotional discomfort, and decreased QoL;
- The use of simple analgesics, nonsteroidal antiinflammatory drugs, and opioids is frequently reported for treatment of patients with musculoskeletal pain after SCI [9].

Pain and spasticity can be so acute in these patients that surgical implantation of pumps to deliver local medication intrathecally is a commonly used intervention. Participants in studies performing EAW have reported significantly reduced pain [13,16,27] and spasticity [13,27] and a decrease in medications used to control pain and spasticity [19] following SCI. Miller's 2016 meta-analysis reviewed five publications regarding spasticity and concluded that "clinically relevant improvements were found in self-reports for muscle spasticity following exoskeleton training" [3].

A study by Esquenazi in 2012 demonstrated a strong trend toward the reduction of tonal abnormalities in the initial cohort. Twelve participants with chronic motor-complete cervical and thoracic SCI were trained for up to 24 sessions over 8 weeks. Pain and spasticity were measured pre and post training sessions. The data suggested immediate gains may be made in pain management and spasticity, lessening the inherent risks associated with their management, thus improving QoL [13].

Stampacchia et al. examined the effects of EAW on pain and spasticity. Twenty-one participants with SCI were measured pre and post session using the Numeric Rating Scale (NRS), the Modified Ashworth scale, and the Penn scale to assess spasticity and global impression of change (PGIC) scale to measure pain. The postwalking assessment showed a significant decrease in muscle spasticity and pain intensity. The authors concluded that EAW "has positive effects in terms of spasticity and pain reduction" [27].

Further indicators of positive health outcomes and improved QoL have been demonstrated through examining the emotional, social, and psychological components of well-being. The SF-36 is a patient-reported measure of health status, and is commonly used in health economics as a variable in the quality-adjusted life year calculation to determine the cost-effectiveness of a health treatment.

The eight sections are:

1. vitality,
2. physical functioning,
3. bodily pain,
4. general health perceptions,
5. physical role functioning,
6. emotional role functioning,
7. social role functioning, and
8. mental health.

In a case study published by Raab in 2016, the authors found a positive effect on QoL as six of the eight thematic areas of the SF-36 showed significant improvement over 6 months of walking in the ReWalk. The highest percentage change (50%) was in the area of physical functioning. Data also demonstrated significant improvements in areas such as vitality, general health, and physical pain. The author stated that "ReWalk training has a positive effect on QoL" [26].

In data presented at the AAPM&R Annual Meeting in 2014, Spungen et al. reported significant positive improvements in QoL as measured by the SF-36. Ten subjects completed the SF-36 pre- and post-EAW training. The group recorded a 9-point improvement in overall score. Items demonstrating significant improvements post training included bowel and bladder function, sleep disturbance, daytime fatigue, pain, and mental health status.

Overall, EAW has proven to provide individuals who have no other options for ambulation a viable and safe means of recapturing walking function. The return of ambulation creates a positive

cascade of physical and psychological benefits that help to combat the primary and secondary comorbidities that are so prevalent in this vulnerable patient segment.

16.6 ECONOMIC IMPACT

SCI is a traumatic, life-disrupting event with an annual incidence rate of 17,000 cases in the United States. Despite efforts to develop medical and surgical interventions to minimize chronic neurological deficits, less than 1% of patients experience full neurological recovery by hospital discharge [11]. On completion of inpatient rehabilitation when patients are discharged home, most will begin a chronic period of progressive physical deconditioning due to lack of mobility function and limited options for physical activity [32]. This period is characterized by lifelong physical deterioration of major body systems such that the life span of SCI patients is 18 years shorter than age- and sex-matched healthy individuals. In fact, life expectancy in the SCI population has not changed since the 1980s [2]. Furthermore, these patients will endure severe long-term medical, functional, and psychological complications following the injury, requiring an exponential increase in healthcare utilization and hospitalization rates. They will face significant limitations in their employability, which further decreases QoL, and results in tremendous social cost [9].

Direct medical expenses for SCI are often well in excess of 1 million dollars. According to the National Spinal Cord Injury Statistical Center, the first year of medical care for a paraplegic patient is approximately \$518,000, with each subsequent year averaging nearly \$70,000 [2]. However, direct medical expenses can be just the tip of the iceberg in terms of the overall cost of SCI. Decreased employability of individuals with SCI bears a tremendous cost as well.

Four years postinjury only 25% of individuals with SCI are employed, well below the preinjury employment rate of 85% [11]. Consequently, the loss of earning potential is one of the most significant expenses for SCI survivors. Assuming an average annual salary of \$26,000 and a patient injured at age 25, the survivor would experience a loss of potential earnings at over 1 million dollars. Higher earners can expect to lose even more. According to Miller, over the lifetime of a patient with SCI, indirect costs can total as much as \$2.3MM, with a total economic burden of \$5.3MM [11].

Exoskeletons have the potential to positively affect QoL and reduce overall healthcare utilization by improving health outcomes and reducing secondary complications. For example, pressure sores are one of the most common complications of chronic wheelchair use. This condition often requires rehospitalization and surgical intervention to repair the tissue, which often leads to a high-cost course of treatment resulting in an average hospital stay of 22 days [7].

Similarly, individuals with SCI have significantly greater risk for CVD, largely due to lower energy expenditure. Other risks that increase in this group include a greater prevalence of obesity, lipid disorders, metabolic syndrome, and diabetes [32]. According to Nichols et al., on average the annual cost of treating CVD alone is nearly \$20,000 and it can be upwards of \$62,000 when hospitalization is necessary [33].

Reducing or eliminating these types of issues, as well as the incidence of UTIs and frequency of pharmaceutical use, could create significant overall cost offsets. It is reasonable to expect that the increased activity level afforded by consistent exoskeleton use would bring a host of benefits

that would result in improvements of multiple body system functions, therefore reducing secondary medical complications and enhancing overall QoL.

16.6.1 CHALLENGES OF EXOSKELETONS

A disruptive change in lifestyle, patterns of function, and with technology that is not well understood are all limitations on acceptance of exoskeletons. The dominant technology of wheelchairs dates back nearly 2000 years without dramatic changes in the fundamental operation. The user community has such a dramatic change in their life and in their physical health; and for most, their health deteriorates postinjury. The medical community has limited experience with the technology and awaits more publications and experience to gain comfort with prescribing this technology. The insuring and payer community does not have processes that are well defined for new technologies. This limits the capacity to gain reimbursement for the system. The advocacy groups for SCI in particular are limited in reach and size, which limits their role in advancing technology. All of these combine to limit the rate of growth and acceptance of the technology initially. The groups with the most direct experience have been the first to provide coverage. Specifically, this occurred with the Veteran's Administration (VA) in the United States and with the German MDD in establishing a national code for the German population. In the US individual cases are covered after multiple appeals at a high rate, but no insurer has followed the VA, Germany, or Italy in establishing a policy as of October 2018.

Continuing education through medical publications, public media, ongoing larger scale clinical studies such as the currently active randomized trial of 160 patients at the VA, seminars, and user experiences gained through the systems awarded by the courts and the insurance appeal systems will all combine to expand coverage rapidly over the next 2–3 years.

As exoskeletons achieve the status as a standard of care as an option considered immediately postinjury, the field will have achieved the mission that began in earnest in the late 1990s.

16.6.2 EXOSUITS

The use of exoskeletons for other applications was a common experience as the systems were provided to rehab centers for SCI patients. Initially use in stroke, multiple sclerosis, and Parkinson's have been the most studied uses. Most of the early work was conducted with structural exoskeletons with software modifications for the various patient groups; however, the original design, size, weight, and cost were not made and not ideal for these applications. These users typically need assistive devices rather than designs which dominate the body. The advent of using the software, battery, and sensor components in designs specifically suited to these new populations resulted in the development of a lightweight and lower cost series of designs that are commonly referred to as exosuits.

The first of these designs came out of the Wyss Institute at Harvard University's school of engineering. It was done in parallel with efforts for military and industrial applications using fabric-based structures as the primary housing for the support. These have now progressed over the past 5 years toward commercialization. The first of these efforts is expected to be on the market in the United States and Europe in 2019.



FIGURE 16.3

ReStore soft wearable exosuit system.

16.6.3 DESIGN OF THE RESTORE EXOSUIT

The ReStore is designed to be a versatile, cost-effective gait therapy solution with lightweight components, real-time analytics, and that offers coordinated plantar/dorsiflexion assistance ([Fig. 16.3](#)).

The ReStore transmits power to a key joint of the legs with motor-driven cable technologies, applying software and mechanics similar to the technologies employed in the currently marketed

ReWalk structural exoskeleton systems. The system is designed to allow a user's unimpaired leg to adjust and assist the leg with mobility impairments affected by stroke. The exoskeletal suit consists of a lightweight fabric-based structure that wraps around the waist and supports an actuator with a motor, computer, and cable, along with sensors attached to a stable point on the user's calf and footplate in the user's shoe. This design transfers force in a controlled manner, enabling both powered plantarflexion, or bending to decrease the angle between the sole of the foot and the back of the leg, and powered dorsiflexion, or bending to decrease the angle between the upper surface of the foot and the front of the leg. The ReStore system's soft, lightweight material will facilitate a natural walking pattern for patients using the device. The ReStore system is also designed to provide advantages to stroke rehabilitation clinics and therapists as compared to other traditional therapies and devices by minimizing setup time, supplying real-time analytics to optimize session productivity, and generating ongoing data reports to assist with tracking patient progress.

We expect the device may also provide other secondary benefits for rehabilitation clinics, including reducing staffing requirements, staff fatigue, and the risk for potential staff injuries. The company has conducted a prospective clinical trial on the ReStore system to assess the safety of the ReStore system during gait training in stroke patients in a rehabilitation setting. The study involved 40 patients each partaking in seven training sessions at five designated stroke research centers.

16.7 CONCLUSION

The acceptance of structural exoskeletons as a standard of care for healthcare policy in Germany; through the VA in the United States; and with a significant base of commercial US insurers through case-by-case coverage decisions has occurred due to the functional effectiveness of the current designs and supports expansion of research into additional designs and therapies.

Expansion to larger patient populations with wearable, lightweight, soft exosuits for assistive walking has reached the stage of multiple clinical studies and ongoing regulatory reviews with commercialization anticipated in 2019. Designs for stroke therapy are the initial areas of focus with future designs for multiple sclerosis, Parkinson's, and other applications for the elderly currently being pursued.

REFERENCES

- [1] P.L. Ditunno, M. Patrick, M. Stineman, J.F. Ditunno, Who wants to walk? Preferences for recovery after SCI: a longitudinal and cross-sectional study, *Spinal Cord.* 46 (7) (2008) 500–506.
- [2] National Spinal Cord Injury Statistical Center, Facts and Figures at a Glance. University of Alabama at Birmingham, Birmingham, AL, 2017.
- [3] L.E. Miller, A.K. Zimmerman, W.G. Herbert, Clinical effectiveness and safety of powered exoskeleton assisted walking in patients with SCI: systematic review with meta-analysis, *Med. Devices Evid. Res.* 9 (2016) 1–12.
- [4] M. Chan, International Perspectives on Spinal Cord Injury, World Health Organization, 2013.

- [5] K.A.M. Ginis, A.E. Latimer, K.P. Arbour-Nicitopoulos, A.C. Buccholz, S.F. Bray, B.C. Craven, et al., Leisure time physical activity in a population-based sample of people with spinal cord injury part I: demographic and injury-related correlates, *Arch. Phys. Med. Rehabil.* 91 (5) (2010) 722–728.
- [6] W.O. McKinley, A.B. Jackson, D.D. Cardenas, M.J. DeVivo, Long-term medical complications after traumatic spinal cord injury: a regional model systems analysis, *Arch. Phys. Med. Rehabil.* 80 (1999) 1402–1410. PMID: 10569434.
- [7] D.M. Dryden, L.D. Saunders, B.H. Rowe, L.A. May, N. Yiannakoulias, L.W. Svenson, et al., Utilization of health services following spinal cord injury: a 6-year follow-up study, *Spinal Cord.* 42 (2004) 513–525.
- [8] K.M. Diaz, V.J. Howard, B. Hutto, N. Colabianchi, J.E. Vena, M.M. Safford, et al., Patterns of sedentary behavior and mortality in U.S. middle-aged and older adults, *Ann. Intern. Med.* (2017). Available from: <https://doi.org/10.7326/M17-0212>.
- [9] N. Sezer, S. Akkus, F.G. Ugurlu, Chronic complications of spinal cord injury, *World J. Orthop.* 6 (1) (2015) 24–33.
- [10] M. Arazpour, M.A. Bani, S.W. Hutchins, R.K. Jones, The physiological cost index of walking with mechanical and powered gait orthosis in patients with SCI, *Spinal Cord.* 51 (5) (2013) 356–359.
- [11] L.E. Miller, W.G. Herbert, Health and economic benefits of physical activity for patients with spinal cord injury, *Clin. Econ. Outcomes Res.* 8 (2016) 551–558.
- [12] T. Platz, A. Gillner, N. Borgwaldt, S. Kroll, S. Roschka, Device-training for individuals with thoracic and lumbar SCI using a powered exoskeleton for technically assisted mobility: achievements and user satisfaction, *Biomed. Res. Int.* 2016 (2016) 8459018.
- [13] A. Esquenazi, M. Talaty, A. Packel, M. Saulino, The ReWalk powered exoskeleton to restore ambulatory function to individuals with thoracic-level motor-complete spinal cord injury, *Am. J. Phys. Med. Rehabil.* 91 (11) (2012) 911–921. PMID: 23085703.
- [14] A.J. Del-Ama, A.D. Koutsou, J.C. Moreno, A. de-Los-Reyes, A. Gil-Agudo, J.L. Pons, Review of hybrid exoskeletons to restore gait following spinal cord injury, *J. Rehabil. Res. Dev.* 49 (4) (2012) 497–514. PMID: 22773254.
- [15] G. Zeilig, H. Weingarten, M. Zwecker, I. Dudkiewicz, A. Bloch, A. Esquenazi, Safety and tolerance of the ReWalk exoskeleton suit for ambulation by people with complete spinal cord injury: a pilot study, *J. Spinal Cord Med.* 35 (2) (2012) 96–101. PMID: 22333043.
- [16] A.M. Spungen, P. Asselin, D.B. Fineberg, S.D. Kornfeld, N.Y. Harel, Exoskeletal-assisted walking for persons with motor-complete paraplegia. Research and Technology Organization, Human Factors, and Medicine Panel: North Atlantic Treaty Organization, 2013. Meeting proceedings available from: <<http://www.cso.nato.int>>.
- [17] C.B. Baunsgaard, U.V. Nissen, A.K. Brust, A. Frotzler, C. Ribeill, Y.B. Kalke, et al., Gait training after spinal cord injury: safety, feasibility and gait function following 8 weeks of training with the exoskeletons from Ekso Bionics, *Spinal Cord* (2017). Available from: <https://doi.org/10.1038/s41393-017-0013-7>.
- [18] I. Benson, K. Hart, D. Tussler, J.J. van Middendorp, Lower-limb exoskeletons for individuals with chronic spinal cord injury: findings from a feasibility study, *Clin. Rehabil.* (2015). Available from: <https://doi.org/10.1177/0269215515575166>. Epub ahead of print. Also available: PMID: 25761635.
- [19] A.J. Kozlowski, T.N. Bryce, M.P. Dijkers, Time and effort required by persons with spinal cord injury to learn to use a powered exoskeleton for assisted walking, *Topics Spinal Cord Injury Rehabil.* 21 (2) (2015) 110–121.
- [20] A. Yang, P. Asselin, S. Knezevic, S. Kornfeld, A.M. Spungen, Assessment of in-hospital walking velocity and level of assistance in a powered exoskeleton in persons with spinal cord injury, *Topics Spinal Cord Inj. Rehabil.* 21 (2) (2015) 100–109. Available from: <https://doi.org/10.1310/sci2102-100>.

- [21] P. Asselin, S. Knezevic, S. Kornfeld, C. Cirigliaro, I. Agranova-Breyter, W.A. Bauman, et al., Heart rate and oxygen demand of powered exoskeleton-assisted walking in persons with paraplegia, *J. Rehabil. Res. Dev.* 52 (2) (2015) 147–158.
- [22] J. Kressler, C.K. Thomas, E.C. Field-Fote, J. Sanchez, E. Widerström-Noga, D.C. Cilien, et al., Understanding therapeutic benefits of overground bionic ambulation: exploratory case series in persons with chronic, complete spinal cord injury, *Arch. Phys. Med. Rehabil.* 95 (10) (2014) 1878–1887.
- [23] D.R. Louie, J.J. Eng, T. Lam, Gait speed using powered roboticexoskeletons after spinal cord injury: asystematic review and correlational study, *J. Neuroeng. Rehabil.* 12 (2015) 82.
- [24] D.B. Fineberg, P. Asselin, N.Y. Harel, I. Agranova-Breyter, S.D. Kornfeld, W.A. Bauman, et al., Vertical ground reaction force-based analysis of powered exoskeleton-assisted walking in persons with motor-complete paraplegia, *J. Spinal Cord Med.* 4 (36) (2013) 313–321.
- [25] Hong E of the James J. Peters VA Medical Center in Bronx, NY. *J. Spinal Cord Med.* 40 (5) (2017) - ASCIP 2017 Conference Abstracts Published July 30, 2017.
- [26] K. Raab, et al., Effects of training with the ReWalk exoskeleton on quality of life in incomplete spinal cord injury: a case study, *Spinal Cord Ser. Cases* 2 (2016) 15025.
- [27] G. Stampacchia, et al., Walking with a powered robotic exoskeleton: subjective experience, spasticity and pain in spinal cord injured persons, *NeuroRehabilitation*. 39 (2016) 277–283.
- [28] S. Glickman, M.A. Kamm, Bowel dysfunction in spinal-cord-injury patients, *Lancet* 347 (9016) (1996) 1651–1653.
- [29] D.D. French, R.R. Campbell, S. Sabharwal, A.L. Nelson, P.A. Palacios, D. Gavin-Dreschnack, Health care costs for patients with chronic spinal cord injury in the veterans health administration, *J. Spinal Cord Med.* (30)(2007) 5.
- [30] S.A. Stiens, S. Biener Bergman, L.L. Goetz, Neurogenic bowel dysfunction after spinal cord injury: clinical evaluation and rehabilitative management (focused review), *Arch. Phys. Med. Rehabil.* 78 (1997). S-86–S-102.
- [31] W.C. Lien, T.S. Kuan, Y.C. Lin, F.W. Liang, P.C. Hsieh, C.Y. Li, Patients with neurogenic lower urinary tract dysfunction following spinal cord injury are at increased risk of developing type 2 diabetes mellitus, *Medicine* 95 (2016) 2.
- [32] J. Myers, M. Lee, J. Kiratli, Cardiovascular disease in spinal cord injury: an overview of prevalence, risk, evaluation, and management, *Am. J. Phys. Med. Rehabil.* 86 (2007) 142–152.
- [33] G. Nichols, T.J. Bell, K.L. Pedula, M. O'Keeffe-Rosetti, Medical care costs among patients with established cardiovascular disease, *Am. J. Manag. Care.* 16 (3) (2010) e86–e93.
- [34] P.R. Geigle, M. Kallins, Exoskeleton-assisted walking for people with spinal cord injury, *Arch. Phys. Med. Rehabil.* 98 (2017) 1493–1495.
- [35] R.H. Carmona, J. Cabe, Improving the health and wellness of persons with disabilities: a call to action, *Am. J. Public Health* 95 (11) (2005) 1883.

HYBRID EXOSKELETONS TO RESTORE GAIT IN INDIVIDUALS WITH PARALYSIS FROM SPINAL CORD INJURY

17

Sarah R. Chang¹, Rudi Kobetic² and Ronald J. Triolo^{2,3}

¹*Orthocare Innovations, LLC, Edmonds, WA, United States* ²*Department of Veterans Affairs, Advanced Platform Technology Center, Louis Stokes Cleveland Department of Veterans Affairs Medical Center, Cleveland, OH, United States* ³*Department of Biomedical Engineering, Case Western Reserve University, Cleveland, OH, United States*

17.1 INTRODUCTION

Spinal cord injury (SCI) can result in lower limb paralysis. In the United States, there are approximately 243,000 individuals living with SCI. Approximately 41% of all SCIs result in paraplegia, which is an injury at or below the thoracic level of the spine and primarily compromises the motor and/or sensory function of the trunk and lower limbs [1,2]. Individuals with lower limb paralysis have limited mobility options, with the majority of individuals utilizing wheelchairs as the main mode of transportation. Restoring or improving the ability to walk is one of the top priorities among individuals with paraplegia due to SCI [3]. Walking can enable independence in performing activities of daily living, as well as improve overall health and community interaction.

17.2 TECHNOLOGIES TO RESTORE WALKING

Various technologies have been developed to restore and improve walking in individuals with paraplegia due to SCI. Conventional approaches to assist or restore walking include functional neuromuscular stimulation (FNS), lower limb orthoses, and powered exoskeletons.

17.2.1 FUNCTIONAL NEUROMUSCULAR STIMULATION SYSTEMS

FNS involves applying small current pulses to the intact peripheral nerves innervating the paralyzed muscles via surface, percutaneous, or implanted electrodes [4–7]. The resulting contractions can generate sufficient joint moments to stabilize the lower limbs and trunk, and enable functional standing or stepping motions [8,9]. Neural stimulation uses the individual's own muscle power to achieve standing and stepping, and also provides a form of exercise for the otherwise paralyzed muscles. Restoration of standing and stepping using FNS in individuals with SCI increases

cardiovascular fitness, improves bladder and bowel function, results in higher bone density, reduces spasticity, and slows the onset of pressure sores [10–13].

One of the first FNS systems to restore walking over short distances was the Parastep, which applied stimulation to the peripheral nerves via electrodes on the surface of the skin. Hip and knee flexion for swing phase in stepping were produced by stimulating the peroneal nerve to elicit the flexion withdrawal reflex [10]. Knee and hip extension during the stance phase of gait was achieved by activating the quadriceps and hamstring muscles, respectively. Individuals who used Parastep showed increased muscle mass and blood flow in the lower limbs, reduced muscle spasticity, and psychological benefits [14,15].

Neural stimulation can also be delivered via percutaneous or implanted electrodes, which can facilitate system donning for daily use and improve muscle selectivity with stimulation [5]. Gait has been restored in individuals with paraplegia due to SCI using a percutaneous system with intra-muscular electrodes that activated up to 48 muscles [9]. Eight- and 12-channel stimulation systems based on implanted pulse-generators were later developed [16]. The implantable systems are able to elicit contractions of trunk and lower limb muscles to achieve stability and weight bearing in standing and generate stepping motions [17]. Patterns of stimulation are typically applied in an open-loop or “feed-forward” manner, and stimulation parameters (pulse duration, frequency, and amplitude) on each channel are adjusted to coordinate the actions of several muscles simultaneously to produce the desired limb movements [9]. Although FNS can effectively restore stepping and provides health benefits to the user, FNS-driven gait still requires more physical effort than normal walking. Oxygen consumption per minute and metabolic cost per meter are significantly greater than for nondisabled walking [18]. To provide sufficient body weight support and postural stability against gravity, high stimulation levels and duty cycles are required that can lead to high metabolic energy demands during stepping [18,19]. Muscle fatigue eventually occurs and can make it difficult to generate repeatable limb trajectories, especially during the swing phase of gait when stimulation levels may be at their maxima. Despite these challenges, FNS is a useful technology that can effectively restore mobility and provide health benefits to its users.

17.2.2 LOWER LIMB ORTHOSES

Orthoses can restore standing and walking by passively locking the hip and knee joints to support the body against collapse. The four main types of lower limb orthoses used to assist with gait restoration include the ankle-foot orthosis (AFO) [20], knee-ankle-foot orthosis (KAFO) [21], hip-knee-ankle-foot orthosis (HKAFO) [22], and trunk-hip-knee-ankle-foot orthosis (THKAFO). The reciprocating gait orthosis (RGO) is a THKAFO that supports upright posture and restores gait by reciprocally coupling the hip joints, that is, ipsilateral hip extension is coupled to contralateral hip flexion [23]. These orthoses typically lock the knee and ankle joints during standing and walking to support the body against collapse, resulting in users walking with a stiff-legged type of gait and using compensatory mechanisms such as hip hiking or reliance on excessive upper body effort to advance the legs [24].

17.2.3 POWERED EXOSKELETONS

In general, powered exoskeletons have electric motors at each hip and knee joint to move the lower limbs through preprogrammed joint trajectories. These wearable robotic walking systems usually

have ankle joints that are fixed at neutral, articulated with spring-assisted dorsiflexion, or powered to produce dorsi- or plantarflexion. Exoskeletons can be designed to actuate single or multiple joints. This chapter focuses on bilateral multijoint exoskeletons. Users initiate movements in the exoskeleton using interfaces such as a joystick, control pad, or wrist watch. The exoskeletons have sensors that detect various motions or intent to step by the user. For example, a tilt sensor will detect forward lean and execute a preselected motorized function such as standing up or initiating a step [25]. Powered exoskeletons can be limited in their achievable gait speeds and distances for full community ambulation [26]. Exoskeletons generally do not have the ability to fully engage their users by contracting the paralyzed muscles, as with FNS. Conventional powered exoskeletons are wearable walking robots that rely on actuators at each joint to support the body and move the entire weight of the lower limb through the predefined range of motion for walking.

17.3 CURRENT STATE-OF-THE-ART SYSTEMS FOR RESTORATION OF WALKING

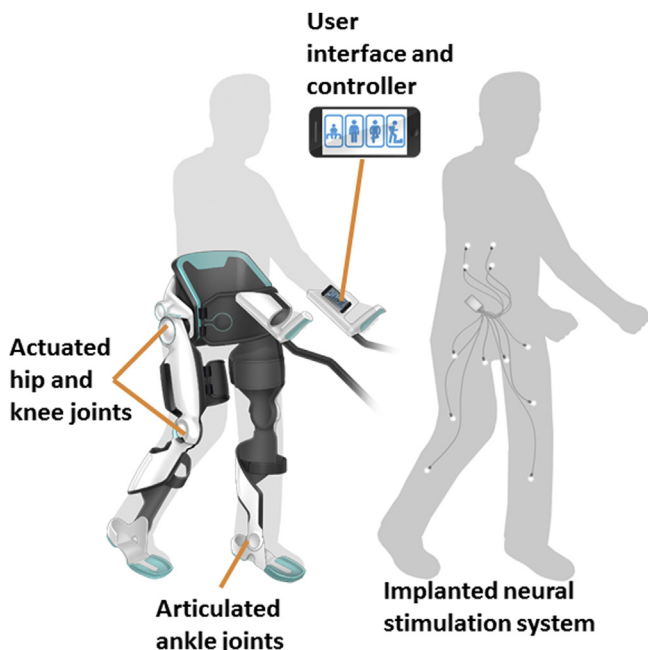
Hybrid neuromechanical systems (Fig. 17.1) are designed to take advantage of the complementary strengths of individual technologies while simultaneously minimizing their drawbacks. In short, the total is greater than the sum of the individual parts in a hybrid system. In this context, different gait restoration technologies (neural stimulation and lower limb orthoses or robotic exoskeletons) can be combined to enable persons with paraplegia to stand up, walk, negotiate stairs, and perform the stand-to-sit maneuver in ways that outperform any one of them applied independently.

17.3.1 HYBRID NEUROPROSTHESIS

The hybrid neuroprosthesis (HNP) is a neuromechanical system that combines the FNS technology to generate muscle contractions with a controllable lower limb orthosis (exoskeleton) to stabilize or assist joint movements during activities such as standing up, walking, stair climbing, and the stand-to-sit maneuver. The lower limb controllable exoskeleton can lock the joints during the stance phase of gait and limit the degrees of freedom to the sagittal plane, or can assist with movements as needed. Neural stimulation can generate joint moments for stepping and also reduce compensatory mechanisms needed for walking with lower limb orthoses.

Walking was restored with an early HNP system that combined surface or intramuscular FNS systems with standard THKAFOs [27–29]. For example, forward progression during gait was enabled by combining neural stimulation of the ipsilateral hip extensor muscles and contralateral hip flexor muscles with an RGO [18,19,30]. Advancement of the HNP led to the current state-of-the-art that combines an implanted neural stimulation system with independently controlled hydraulic hip and knee joints in an RGO [31].

In one configuration, the exoskeleton of the HNP included a variable constraint hip mechanism (VCHM) that could lock, remain free, or reciprocally couple the hip joints [32,33]. When locked, the VCHM provided up to 60 Nm of resistive moment, which was sufficient to support against bilateral hip flexion for postural stability [32,33]. When reciprocally coupled, the VCHM provided hip flexion and contralateral hip extension similar to a conventional RGO. Walking with the

**FIGURE 17.1**

Representation of a user in a hybrid neuromechanical device that combines implanted FNS with a powered exoskeleton.

Illustration courtesy of the APT Center.

VCHM in the HNP significantly reduced forward lean by 36% compared to FNS only; reduced maximum upper limb forces compared to walking with either an isocentric RGO or FNS only (17% and 36%, respectively); and increased walking speed compared to an isocentric RGO [32,33].

The HNP system also included a dual-state knee mechanism (DSKM) that locked the knee joint during the stance phase of gait and freed the knee during the swing phase. When locked, the DSKM supported up to 70 Nm of knee flexion moment and was able to unlock when up to 50 Nm of flexion moment was applied on the joint [34], an important feature during the stand-to-sit maneuver. The DSKM was shown to have low passive resistance, allowing unrestricted knee joint flexion during the swing phase, while providing sufficient locking moment for supporting the body and maintaining knee extension during the stance phase of gait without the need to activate knee extensor muscles with stimulation [34].

While the DSKM provided support during the stance phase by locking the knee joint, normal stance phase knee flexion was not possible. A variable impedance knee mechanism (VIKM) for the HNP was developed to emulate eccentric muscle control during the stance phase of gait. The VIKM uses a magnetorheological fluid damper with a linkage transmission to substitute for eccentric control of the knee extensor muscles during stance knee flexion [35–37]. Sufficient knee stiffness was provided by the VIKM while allowing stance phase knee flexion. Providing knee

damping reduced the impact at loading, maintained forward progression, and decreased the required knee extensor stimulation by up to 40% during gait. The VIKM was also used to assist an individual with SCI in stair descent. Damping with the VIKM regulated stair descent, resulting in reduced descent speed and reliance on upper limb support assistance to approximately 40%–45% body weight as compared to using FNS only (70% body weight) [38].

The HNP has also been designed to assist with the stand-to-sit (STS) maneuver. Individuals with SCI rely on their upper limbs to control the maneuver with stimulation only, thus having high knee angular velocities and a high impact with the seating surface [39]. For a more controlled STS maneuver, kinematic constraint or damping mechanisms can be utilized [40]. The constraint mechanism coordinated the hip and knee joints such that they were kinematically constrained to a 1:1 ratio. The hydraulic damping mechanism provided a resistive torque to emulate the knee extensor muscles that typically control the STS maneuver. Both the kinematic constraint and damping mechanisms improved coordination between hip and knee joints and decreased upper limb support forces by 70% during the STS maneuver. The damping mechanism provided lower and more constant knee angular velocities over the knee joint range of motion during the maneuver. The impact force with the seating surface was reduced by half when using the kinematic constraint and damping mechanisms [40].

Recently, there has been an effort to develop devices capable of restoring walking in the home environment. To achieve this, devices must be untethered from the laboratory environment and able to function independently of stationary computer systems. A self-contained HNP combines implanted FNS with an instrumented exoskeleton, and onboard hardware for controlling the exoskeletal joints and neural stimulation [41]. The untethered HNP prototype has been evaluated in three individuals with SCI and showed potential for use outside of the laboratory. Studies that use commercialized exoskeletons in combination with surface stimulation also show potential to implement the systems in the home environment.

17.3.2 POWERED EXOSKELETONS AND FUNCTIONAL NEUROMUSCULAR STIMULATION

Several motorized exoskeletons have been developed to assist individuals with walking disabilities (e.g., Rex, ReWalk, HAL, Ekso, Indego) [42]. Some of these devices are FDA approved for use in the home with an assistant (ReWalk, Indego, Ekso), while others can only be used in rehabilitation centers or laboratory testing facilities. The addition of neural stimulation technology with a powered exoskeleton has recently gained more attention, in order to restore gait and fully engage the user in the walking motion when using the motorized exoskeleton.

One approach involved a cooperative control structure with a motor control loop and a muscle control loop in order to minimize the motor torque contribution of the powered exoskeleton (Indego, Parker Hannifin, OH) and maximize muscle-generated joint torques via surface stimulation [43]. The motor control loop adjusted the joint outputs based on hip and knee joint angle feedback to follow a set joint trajectory, whereas the muscle control loop adjusted the stimulation parameters based on an estimated joint moment profile. The system was evaluated in three individuals with SCI (levels T6–T10) and showed consistent and repeatable gait motions, while reducing the motor torque and power needed to restore walking in the exoskeleton without stimulation.

Another powered exoskeleton (Ekso, Ekso Bionics, CA) was combined with transcutaneous electrical spinal cord stimulation at selected sites over the spine in an individual with SCI (AIS A, T9–L1). The combination of the two technologies enabled the participant to “voluntarily assist” the exoskeleton during weight-bearing overground stepping. The presence of stimulation reduced the step assistance needed by the exoskeleton [44].

Another approach, called Kinesis, combined a knee-ankle-foot (KAF) powered exoskeleton with surface stimulation. The cooperative control for the joint motor torque controller was designed to provide additional torque at the knee joint when the knee angle deviated from a desired trajectory, the stimulation controller adjusted knee flexor and extensor stimulation parameters, and the muscle fatigue estimator measured the exoskeleton to limb interaction torque [45,46]. Nondisabled volunteers demonstrated the system’s ability to balance the stimulation-generated muscle moment with the motor torque of the KAF exoskeleton.

17.3.3 POWERED EXOSKELETONS AND IMPLANTED FUNCTIONAL NEUROMUSCULAR STIMULATION

Currently, there are two main technologies that exhibit the best potential to restore functional stepping in individuals with paraplegia: FNS and motorized exoskeletons. As these technologies reach their full potentials and approach their natural limitations, their convergence and combination may result in a system with even greater potential for clinical benefit to persons with paralysis. If approached from the FNS side, implanted systems provide stronger, more consistent, and more isolated contractions of more paralyzed muscles than any other stimulation delivery technique. A “muscle-first” approach utilizing implanted technology with an exoskeleton would engage the user’s own muscles to power stepping movements and allow the muscles to act as the main motors in the system. Because stimulation-activated muscles will eventually fatigue, or may be of inadequate strength to complete the required motion, the powered actuators in the exoskeleton can help make walking more robust and consistent across all users, potentially increasing the usage time and walking distances. Using the joint moments generated via neural stimulation would fully engage the user and provide the physiological and health benefits of exercise, while simultaneously reducing the demands on the exoskeleton motors and allowing smaller, lighter external actuators to be incorporated into the exoskeleton, since they only need to be engaged when the appropriate joint trajectories for gait are not achieved. Furthermore, when an implanted FNS system is incorporated into such a hybrid system, the user can still experience the benefits of neural stimulation even when the exoskeleton is not donned.

It is important to note that use of FNS in the hybrid system may not work for all individuals, such as those with denervation and peripheral nerve damage. Powered exoskeletons may be the best and only option to restore gait for these individuals, including but not limited to the large segment of the SCI population with cauda equina injuries at T12 through lumbar and sacral levels.

17.3.4 THE NEED FOR SPEED

The commonly accepted speed for full community ambulation is 0.8 m/s [47] and functional walking distances are considered to be over 500 m [26,48]. However, the technologies available for

Table 17.1 Summary of Hybrid Exoskeleton Systems for SCI

Exoskeleton	Population	Design	Speed	Distance
HNP [18–41]	SCI	Implanted FNS with controllable orthosis	0.25 m/s [18], 0.29 m/s [32], 0.15 m/s [34], 0.38 m/s [35], 0.03–0.06 m/s [41]	350 m [18]
Indego ^a [43]	SCI	Motorized with surface FNS	NR	133 steps
Ekso ^a [44]	SCI	Motorized with surface FNS	NR	NR
Kinesis KAF [45,46]	SCI	Motorized orthosis with surface FNS	NR	NR

NR, Not reported.
^aIndego and Ekso are FDA approved for use in the home without the combination of stimulation.

restoring gait in individuals with SCI are not always sufficient to enable full community ambulation (Table 17.1). Individuals using FNS-only walked between 0.2–0.4 m/s [49], with some reaching peak speeds of 0.9 m/s, and maximal distances of 300–400 m [5,8]. Using bilateral KAFOs, individuals with paraplegia walked an average speed of 0.28 m/s [50]. With powered exoskeletons only, individuals with SCI were able to walk distances between 11 and 170 m [51,52] and at speeds averaging 0.22–0.27 m/s [25,53]. Theoretically, maximal walking distances with powered exoskeletons will depend on the electrical power specifications of the device batteries. However, the actual walking distance depends on the user's upper body strength and endurance, since walking with the powered exoskeletons also requires considerable upper limb and trunk effort to provide stability and assist with propulsion.

On the other hand, an individual with paraplegia was able to walk in a hybrid system (RGO and FNS) at an average speed of 0.42 m/s [28]. Individuals with SCI using the HNP were able to walk between 0.03 and 0.38 m/s [35,41]. The current approaches for restoring gait in individuals with SCI do not consistently achieve functional speeds and distances for walking in the community. To assist individuals with SCI in becoming community ambulators, there is a need to increase the speed and distance that hybrid system users are able to achieve.

17.3.5 EASE OF USE AND COSMESIS

Hybrid systems require a considerable amount of time to don and doff, calibrate, and set up with each user. As the devices continue to advance, the donning time should decrease. With the majority of hybrid systems, users are still required to apply surface electrodes prior to each use and ensure proper placement for optimal muscle selectivity and activation. There is an additional limitation in that surface electrodes cannot efficiently activate deep muscles, such as the hip flexors that are important during the swing phase of gait. Implanted FNS provides an alternative to surface stimulation to improve system donning for daily use and allows for greater muscle selectivity with neural stimulation. Powered exoskeletons also require donning and doffing for each use, since the devices are currently not designed to be worn throughout the day. Similar to lower limb orthoses, powered exoskeletons must improve the donning and doffing time as well as ease of use to avoid

abandonment. Additionally, cosmesis is of concern since the majority of exoskeletons only have the option to be worn over the clothes. Although society is beginning to accept exoskeletons and other visible assistive technologies, users may be self-conscious when wearing the system in public. Full acceptance of the hybrid systems into society may be dependent on providing efficient donning and doffing as well as acceptable cosmesis, in addition to the walking speeds and distances to ambulate in the community.

17.3.6 OTHER APPLICATIONS OF HYBRID SYSTEMS

Other central nervous system disorders that leave the peripheral motor nerve intact, such as stroke and multiple sclerosis (MS), can result in lower limb paralysis or weakness that compromises walking. In the United States, there are about 800,000 people who have a new or recurrent stroke every year [54], and many of these individuals experience hemiparesis which can impact gait. There are more than 400,000 individuals with MS in the United States [55], with 41% reporting difficulty walking [56]. Similar to individuals with SCI, restoring or improving mobility in people with stroke or MS has the potential to improve their overall health, independence, societal participation, and quality of life. The AFO can be used for a variety of needs and is an orthotic option to prevent foot drop, common in stroke survivors and individuals with MS. AFOs, however, tend to be passive devices and provide limited options for active ankle movements such as plantarflexion, which is important to achieve the walking speeds required for community ambulation. Simple surface stimulation systems are commercially available to actively produce ankle dorsiflexion and prevent foot drop after stroke or MS. Such systems, however, only provide at most two channels of stimulation and thus restrict interventions to gait deficits arising from the distal joints. Case studies have shown that an implanted FNS system with eight channels of stimulation can significantly improve the walking of stroke survivors [57] and individuals with MS [58] by intervening at multiple joints including the hips, knees, and active powering of ankle plantarflexion. Preliminary studies report initial applications of powered exoskeletons to stroke survivors [59] and individuals with MS [60]. Because they can be designed to be modular, powered exoskeletons can be customized and scaled down from the bilateral multijoint version used in paraplegia to provide “assist as needed” to any joint depending on the user’s gait deficit [61].

17.4 CONCLUSIONS

Restoration of gait is a high priority for individuals with paraplegia due to SCI, and similarly stroke survivors, individuals with MS, and potentially others with neurological diseases affecting walking. There are hardware and control system challenges that need to be addressed for take-home exoskeleton-based systems capable of restoring full community ambulation, as well as assisting standing balance and reducing reliance on walking aids, before such technologies are user-friendly and functional enough for routine activities of daily living.

The continued development of the hybrid technology has the potential to make a major impact on quality of life and restoring function in individuals with gait deficits from neurological disorders and aging.

Hybrid neuromechanical systems are improving quality of life by providing the opportunity to restore stepping in individuals with paraplegia and fully engage their users by contracting the otherwise paralyzed muscles to maximize the benefits of exercising the large lower limb muscles. While the technology has advanced, lower limb orthoses have a high abandonment rate [62], which could be the major challenge for acceptance into the general public's daily use. The current limitations of the hybrid neuromechanical technology such as speed, distance, and effort in addition to ease of donning, doffing, and cosmesis should be addressed to design a more practical system that is more acceptable to consumers and rehabilitation professionals in the future.

REFERENCES

- [1] Spinal cord injury facts and figures at a glance, National Spinal Cord Injury Statistical Center, Birmingham, Alabama, <<https://www.nscisc.uab.edu/Public/Facts%202016.pdf>>, October 2016.
- [2] One degree of separation: stats about paralysis, Christopher and Dana Reeve Foundation, Short Hills, New Jersey, <<https://www.christopherreeve.org/living-with-paralysis/stats-about-paralysis>>.
- [3] K.D. Anderson, Targeting recovery: priorities of the spinal cord-injured population, *J. Neurotrauma* 21 (10) (2004) 1371–1383.
- [4] A. Kralj, T. Bajd, R. Turk, Electrical stimulation providing functional use of paraplegic patient muscles, *Med. Prog. Technol.* 7 (1) (1980) 3–9.
- [5] E.B. Marsolais, R. Kobetic, Development of a practical electrical stimulation system for restoring gait in the paralyzed patient, *Clin. Orthop.* 223 (1988) 64–74.
- [6] P. Gallien, R. Brissot, M. Eyssette, L. Tell, M. Barat, L. Wiart, et al., Restoration of gait by functional electrical stimulation for spinal cord injured patients, *Paraplegia* 33 (11) (1995) 660–664.
- [7] R. Kobetic, R.J. Triolo, J.P. Uhlir, C. Bieri, M. Wibowo, G. Polando, et al., Implanted functional electrical stimulation system for mobility in paraplegia: a follow-up case report, *IEEE Trans. Rehabil. Eng.* 7 (4) (1999) 390–398.
- [8] R. Kobetic, R.J. Triolo, E.B. Marsolais, Muscle selection and walking performance of multichannel FES systems for ambulation in paraplegia, *IEEE Trans. Rehabil. Eng.* 5 (1) (1997) 23–29.
- [9] R. Kobetic, E.B. Marsolais, Synthesis of paraplegic gait with multichannel functional neuromuscular stimulation, *IEEE Trans. Rehabil. Eng.* 2 (2) (1994) 66–79.
- [10] P.L. Jacobs, M.S. Nash, K.J. Klose, R.S. Guest, B.M. Needham-Shropshire, B.A. Green, Evaluation of a training program for persons with SCI paraplegia using the Parastep 1 ambulation system: part 2. Effects on physiological response to peak arm ergometry, *Arch. Phys. Med. Rehabil.* 78 (8) (1997) 794–798.
- [11] M.H. Granat, A.C.B. Ferguson, B.J. Andrews, M. Delargy, The role of functional electrical stimulation in the rehabilitation of patients with incomplete spinal cord injury – observed benefits during gait studies, *Paraplegia* 31 (4) (1993) 207–215.
- [12] L. Vodovnik, Therapeutic effects of functional electrical stimulation of extremities, *Med. Biol. Eng. Comp.* 19 (4) (1981) 470–478.
- [13] D. Graupe, K.H. Kohn, Functional neuromuscular stimulator for short-distance ambulation by certain thoracic-level spinal-cord-injured paraplegics, *Surg. Neurol.* 50 (3) (1998) 202–207.
- [14] M.S. Nash, P.L. Jacobs, B.M. Montalvo, K.J. Klose, R.S. Guest, B.M. Needham- Shropshire, Evaluation of a training program for persons with SCI paraplegia using the Parastep 1 ambulation system: part 5. Lower extremity blood flow and hyperemic responses to occlusion are augmented by ambulation training, *Arch. Phys. Med. Rehabil.* 78 (8) (1997) 808–814.

- [15] R. Brissot, P. Gallien, M.P. Le Bot, A. Beaubras, D. Laisne, J. Beillot, et al., Clinical experience with functional electrical stimulation-assisted gait with Parastep in spinal cord-injured patients, *Spine* 25 (4) (2000) 501–508.
- [16] B. Smith, Z. Tang, M. Johnson, S. Pourmehdi, M. Gazdik, J. Buckett, et al., An externally powered, multichannel, implantable stimulator-telemeter for control of paralyzed muscle, *IEEE Trans. Rehabil. Eng.* 45 (4) (1998) 463–475.
- [17] R.J. Triolo, S.N. Bailey, M.E. Miller, L. Rohde, J. Anderson, J.A. Davis, et al., Longitudinal performance of a surgically implanted neuroprosthesis for lower extremity exercise, standing, and transfers after spinal cord injury, *Arch. Phys. Med. Rehabil.* 93 (5) (2012) 896–904.
- [18] E.B. Marsolais, R. Kobetic, G. Polando, K. Ferguson, S. Tashman, R. Gaudio, et al., The Case Western Reserve University hybrid gait orthosis, *J. Spinal Cord Med.* 23 (2) (2000) 100–108.
- [19] S. Hirokawa, M. Grimm, T. Le, M. Solomonow, R.V. Baratta, H. Shoji, et al., Energy consumption in paraplegic ambulation using the reciprocating gait orthosis and electrical stimulation of the thigh muscles, *Arch. Phys. Med. Rehabil.* 71 (9) (1990) 687–694.
- [20] M. Lyles, J. Munday, Report on the evaluation of the Vannini-Rizzoli stabilizing limb orthosis, *J. Rehabil. Res. Dev.* 29 (2) (1992) 77–104.
- [21] R. Mikelberg, S. Reid, Spinal cord lesions and lower extremity bracing: an overview and follow-up study, *Paraplegia* 19 (6) (1981) 379–385.
- [22] J.W. Middleton, J.D. Yeo, L. Blanch, V. Vare, K. Peterson, K. Brigden, Clinical evaluation of a new orthosis, the ‘Walkabout’, for restoration of functional standing and short distance mobility in spinal paralysed individuals, *Spinal Cord* 35 (9) (1997) 574–579.
- [23] R. Douglas, P.F. Larson, R. D’Ambrosia, R.E. McCall, The LSU reciprocating gait orthosis, *Orthopedics* 6 (1983) 834–839.
- [24] L.A. Harvey, G.M. Davis, M.B. Smith, S. Engel, Energy expenditure during gait using the Walkabout and Isocentric Reciprocating Gait orthoses in persons with paraplegia, *Arch. Phys. Med. Rehabil.* 79 (8) (1998) 945–949.
- [25] L.E. Miller, A.K. Zimmerman, W.G. Herbert, Clinical effectiveness and safety of powered exoskeleton-assisted walking in patients with spinal cord injury: systematic review with meta-analysis, *Med. Devices (Auckl)* 22 (9) (2016) 455–466.
- [26] R. Lapointe, Y. Lajoie, O. Serresse, H. Barbeau, Functional community ambulation requirements in incomplete spinal cord injured subjects, *Spinal Cord* 39 (6) (2001) 327–335.
- [27] M. Solomonow, R. Baratta, S. Hirokawa, N. Rightor, W. Walker, P. Beaudette, et al., The RGO generation II: muscle stimulation powered orthosis as a practical walking system for thoracic paraplegics, *Orthopedics* 12 (10) (1989) 1309–1315.
- [28] E. Isakov, R. Douglas, P. Berns, Ambulation using the reciprocating gait orthosis and functional electrical stimulation, *Paraplegia* 30 (4) (1992) 239–245.
- [29] R. Kobetic, E.B. Marsolais, R.J. Triolo, D.T. Davy, R. Gaudio, S. Tashman, Development of a hybrid gait orthosis: a case report, *J. Spinal Cord Med.* 26 (3) (2003) 254–258.
- [30] M. Solomonow, E. Aguilar, E. Reisin, R.V. Baratta, R. Best, T. Coetze, et al., Reciprocating gait orthosis powered with electrical muscle stimulation (RGO II). Part I: performance evaluation of 70 paraplegic patients, *Orthopedics* 20 (4) (1997) 315–324.
- [31] R. Kobetic, C.S. To, J.R. Schnellenberger, M.L. Audu, T.C. Bulea, R. Gaudio, et al., Development of hybrid orthosis for standing, walking, and stair climbing after spinal cord injury, *J. Rehabil. Res. Dev.* 46 (3) (2009) 447–462.
- [32] C. To, R. Kobetic, T.C. Bulea, M.L. Audu, J. Schnellenberger, G.C. Pinault, et al., Sensor-based hip control with a hybrid neuroprosthesis for walking in paraplegia, *J. Rehabil. Res. Dev.* 51 (2) (2014) 229–244.

- [33] C. To, R. Kobetic, T.C. Bulea, M.L. Audu, J.R. Schnellenberger, G. Pinault, et al., Sensor-based stance control with orthosis and functional neuromuscular stimulation for walking after spinal cord injury, *J. Prosthet. Orthot.* 24 (3) (2012) 124–132.
- [34] C.S. To, R. Kobetic, T. Bulea, M. Audu, J. Schnellenberger, G. Pinault, et al., Stance control knee mechanism for lower extremity support in a hybrid neuroprosthesis, *J. Rehabil. Res. Dev.* 48 (7) (2011) 839–850.
- [35] T.C. Bulea, R. Kobetic, M.L. Audu, J.R. Schnellenberger, G. Pinault, R.J. Triolo, Stance phase knee flexion improves stimulation driven walking after spinal cord injury, *J. Neuroeng. Rehabil.* 10 (68) (2013).
- [36] T.C. Bulea, R. Kobetic, M.L. Audu, J.R. Schnellenberger, R.J. Triolo, Finite state control of a variable impedance hybrid neuroprosthesis for locomotion after paralysis, *IEEE Trans. Neural. Syst. Rehabil. Eng.* 21 (1) (2013) 141–151.
- [37] T.C. Bulea, R. Kobetic, C.S. To, M. Audu, J. Schnellenberger, R.J. Triolo, A variable impedance knee mechanism for controlled stance flexion during pathological gait, *IEEE/ASME Trans. Mechatronics* 17 (5) (2012) 822–832.
- [38] T.C. Bulea, R. Kobetic, M.S. Audu, J.R. Schnellenberger, G. Pinault, R.J. Triolo, Forward stair descent with a hybrid neuroprosthesis after paralysis: a single case study demonstrating feasibility, *J. Rehabil. Res. Dev.* 51 (7) (2014) 1077–1094.
- [39] S.R. Chang, R. Kobetic, R.J. Triolo, Understanding stand-to-sit maneuver: implications for motor system neuroprostheses after paralysis, *J. Rehabil. Res. Dev.* 51 (9) (2014) 1339–1352.
- [40] S.R. Chang, M.J. Nandor, R. Kobetic, K.M. Foglyano, R.D. Quinn, R.J. Triolo, Improving stand-to-sit maneuver for individuals with spinal cord injury, *J. Neuroeng. Rehabil.* 13 (2016) 27.
- [41] S.R. Chang, M.J. Nandor, L. Li, R. Kobetic, K.M. Foglyano, J.R. Schnellenberger, et al., A muscle-driven approach to restore stepping with an exoskeleton for individuals with paraplegia, *J. Neuroeng. Rehabil.* 14 (1) (2017) 48.
- [42] A. Esquenazi, M. Talaty, A. Jayaraman, Powered exoskeletons for walking assistance in persons with central nervous system injuries: a narrative review, *PMR* 9 (1) (2017) 46–62.
- [43] K.H. Ha, S.A. Murray, M. Goldfarb, An approach for the cooperative control of FES with a powered exoskeleton during level walking for persons with paraplegia, *IEEE Trans. Neural. Syst. Rehabil. Eng.* 24 (4) (2016) 455–466.
- [44] P. Gad, Y. Gerasimenko, S. Zdunowski, A. Turner, D. Sayenko, D.C. Lu, et al., Weight bearing over-ground stepping in an exoskeleton with non-invasive spinal cord neuromodulation after motor complete paraplegia, *Front. Neurosci.* 8 (11) (2017) 333.
- [45] A.J. Del-Ama, A. Gil-Agudo, J.L. Pons, J.C. Moreno, Hybrid FES-robot cooperative control of ambulatory gait rehabilitation exoskeleton, *J. Neuroeng. Rehabil.* 11 (2014) 27.
- [46] A.J. Del-Ama, A. Gil-Agudo, J.L. Pons, J.C. Moreno, Hybrid gait training with an overground robot for people with incomplete spinal cord injury: a pilot study, *Front. Hum. Neurosci.* 8 (298) (2014) 1–10.
- [47] J. Perry, M. Garrett, J. Gronley, S. Mulroy, Classification of walking handicap in the stroke population, *Stroke* 26 (6) (1995) 982–989.
- [48] C.S. Robinett, M.A. Vondran, Functional ambulation velocity and distance requirements in rural and urban communities, *Clin. Rep. Phys. Ther.* 68 (9) (1988) 1371–1373.
- [49] P. Winchester, J.J. Carollo, R. Habasevich, Physiologic costs of reciprocal gait in FES assisted walking, *Paraplegia* 32 (10) (1994) 680–686.
- [50] R.L. Waters, B.R. Lunsford, Energy cost of paraplegic locomotion, *J. Bone Joint Surg. Am.* 67 (8) (1985) 1245–1250.
- [51] A. Yang, P. Asselin, S. Knezevic, S. Kornfeld, A.M. Spungen, Assessment of in-hospital walking velocity and level of assistance in a powered exoskeleton in persons with spinal cord injury, *Topics Spinal Cord Inj. Rehabil.* 21 (2) (2015) 100–109.

- [52] A. Esquenazi, M. Talaty, A. Packel, M. Saulino, The ReWalk powered exoskeleton to restore ambulatory function to individuals with thoracic-level motor-complete spinal cord injury, *Am. J. Phys. Med. Rehabil.* 91 (11) (2012) 911–921.
- [53] A. Asselin, S. Knezevic, S. Kornfeld, C. Cirigliaro, I. Agranova-Breyter, W.A. Bauman, et al., Heart rate and oxygen demand of powered exoskeleton-assisted walking in persons with paraplegia, *J. Rehabil. Res. Dev.* 52 (2) (2015) 147–158.
- [54] V.L. Roger, A.S. Go, D.M. Lloyd-Jones, R.J. Adams, J.D. Berry, T.M. Brown, et al., Executive summary: heart disease and stroke statistics - 2011 update, *Circulation* 123 (2011) 459–463.
- [55] P. Dilokthornsakul, R.J. Valuck, K.V. Nair, J.R. Corboy, R.R. Allen, J.D. Campbell, Multiple sclerosis prevalence in the United States commercially insured population, *Neurology* 86 (11) (2016) 1014–1021.
- [56] N.G. LaRocca, Impact of walking impairment in multiple sclerosis: perspectives of patients and care partners, *Patient* 4 (3) (2011) 189–201.
- [57] N.S. Makowski, R. Kobetic, L.M. Lombard, K.M. Foglyano, G. Pinault, S.M. Selkirk, et al., Improving walking with an implanted neuroprosthesis for hip, knee, and ankle control after stroke, *Am. J. Phys. Med. Rehabil.* 95 (12) (2016) 880–888.
- [58] S.M. Selkirk, R. Kobetic, L.M. Lombardo, G. Pinault, R.J. Triolo, Feasibility of restoring walking in multiple sclerosis with multichannel implanted electrical stimulation, *Am. J. Phys. Med. Rehabil.* 96 (9) (2017) e170–e172.
- [59] D.R. Louie, J.J. Eng, Powered robotic exoskeletons in post-stroke rehabilitation of gait: a scoping review, *J. Neuroeng. Rehabil.* 13 (1) (2016) 53.
- [60] A.J. Kozlowski, M. Fabian, D. Lad, A.D. Delgado, Feasibility and safety of a powered exoskeleton for assisted walking for persons with multiple sclerosis: a single-group preliminary study, *Arch. Phys. Med. Rehabil.* 98 (7) (2017) 1300–1307.
- [61] M. Bortole, A. Venkatkrishnan, Z. Fangshi, J.C. Moreno, G.E. Francisco, J.L. Pons, et al., The H₂ robotic exoskeleton for gait rehabilitation after stroke: early findings from a clinical study, *J. Neuroeng. Rehabil.* 12 (2015) 54.
- [62] B. Phillips, H. Zhao, Predictors of assistive technology abandonment, *Assist. Technol.* 5 (1) (1993) 36–45.

HYBRID WEARABLE ROBOTIC EXOSKELETONS FOR HUMAN WALKING

18

Juan C. Moreno¹, Samer Mohammed², Nitin Sharma³ and Antonio J. del-Ama⁴

¹Cajal Institute (CSIC), Madrid, Spain ²University of Paris-Est, Créteil (UPEC), Paris, France ³University of Pittsburgh, Pittsburgh, PA, United States ⁴National Hospital for Paraplegics (SESCAM), Toledo, Spain

18.1 INTRODUCTION

Impairment of the gait function is among the usual consequences of a neurological pathology. Currently, therapies for rehabilitation of the walking function are based on the application of basic concepts: promotion of neural plasticity, strengthening of the remaining muscles, and learning of motor compensation strategies [1], all mediated through the combination of various types of therapeutic exercises and devices adapted to the patient's progression [2]. Among the treatment devices it is common to find neuromuscular stimulation (NMES) in isometric conditions, designed to strengthen the muscles, counteract muscular atrophy, and mitigate spasticity. Another application of the NMES is the generation of joint movements. Since Krajl's pioneering works, a multitude of systems, applications, and protocols for the functional compensation of movement have been developed, called motor neuro-prosthetics (MNP) [3]. Although the idea of combining the therapeutic approach of NMES in an MNP is immediate, there are currently no systems that combine both approaches. The main disadvantages presented by MNP are: the nonlinearity of the response of the stimulated muscle, time-dependent, the rapid appearance of muscle fatigue, the relative limitation in the generation of joint torque by NMES, the lack of adaptability of the muscle systems, control of the user's intentions, as well as the lack of evidence to support the superiority of MNP over traditional rehabilitation therapies [4].

In the last decade we have witnessed a growing interest in the use of robotic exoskeletons for rehabilitation or functional compensation of gait. Since the introduction of the first robotic trainers more than 15 years ago, various devices have been introduced, either stationary (robotic training trainers on treadmill) or ambulatory (hereafter ER: robotic exoskeletons). While robotic trainers have been studied extensively [5], there is a growing interest in investigating the potential of ERs for gait rehabilitation. The current scientific evidence in this respect is limited, but it has made it possible to identify several factors that limit its application to the rehabilitation of walking, such as its size and weight, the lack of adaptation of kinematic patterns to the will of the user, and the lack of versatility for ambulation in real environments [6].

The combination of MNP and ER with the aim of mitigating the disadvantages of MNP and ER technologies was proposed several decades ago [7]. The presence of ER allows improving the

control of joint movement generated by the MNP while minimizing and/or compensating the appearance of muscle fatigue, while the control of joint movement by the MNP can reduce the size of the actuators and the batteries while providing physiological benefits due to the stimulation of muscles during walking. This combination has the potential to facilitate the use of the MNP for gait compensation and/or rehabilitation. This type of hybrid technology (Hybrid EXoskeletons, HEX) has been reviewed previously [7], but recent advancements have made it necessary to update the revision taking into account new technological advances and the most recent research on the application of these technologies for gait rehabilitation. It is therefore the objective of this chapter to provide an updated view of HEX technology, review the latest advances in the field, and provide a perspective for future research.

18.2 ADVANCES IN HYBRID WEARABLE TECHNOLOGIES

HEX were defined and classified in Ref. [7] with regards to two complementary criteria: (1) how the MNP is implemented on the HEX, either in an open loop or closed loop, and (2) the mechanical actuation of the ER, either dissipative, semiactive, or active, depending on the ability of the actuator to dissipate and/or add energy to the joint [7]. We have adopted these classification criteria for this chapter since no new data were found that contradicted these criteria.

Since the publication of the first thematic review on HEX several improvements have been presented in the fields of control of functional electrical stimulation (FES) and exoskeletons (hereinafter cooperative control), while mechatronics, neuroprosthetic, and clinical studies have not advanced as much. The group of Kobetic et al. has continued the development of their HEX, incorporating several improvements. First, a controlled damper was implemented in order to support eccentric quadriceps contractions during (1) the stance phase of walking and (2) stair descent, while minimally impeding knee motion during swing [8,9]. This resulted in a reduction of the stimulation duty cycle during stance, as well as allowing to restore forward stair descent at controllable speeds comfortable for the user. In a further improvement, an hydraulic system was added in order to provide energy to the hip and knee joints to support joint movement [10]. It is noteworthy that this series of HEX is the only one designed for functions other than walking assistance, such as climbing stairs and sit-to-stand [8].

A novel hybrid exoskeleton for walking assistance of patients with low-dorsal spinal cord and preserved ability to flex the hip, was presented recently [11]. As noteworthy aspects, Kinesis, the name of the exoskeleton, features a muscle fatigue estimator based on the physical interaction between the patient's leg and the exoskeleton, as well as a stimulation control strategy based on an iterative learning controller, aimed at optimizing stimulation patterns to the motor response of the user. In addition, Kinesis features an impedance controller for the knee joint, allowing to vary exoskeleton stiffness according to muscle fatigue and the user's motor response. Further work evaluated Kinesis with a sample of three incomplete SCI patients over a week of treatment, reporting certain improvements in the patient's gait function [12].

Another new HEX found was SEAHO [13]. It proposes two concepts that are of interest to implement in HEX: (1) stimulation of ankle plantar flexor muscles in order to improve spatiotemporal parameters of gait and (2) introduction of control techniques that accounts for the redundancy

of HEX joint actuation (several muscles and the robotic actuator for the same joint). Among the techniques proposed, this group has explored the use of a synergy-based approach [14], the use of dynamic control allocation using nonlinear model predictive control [15], and a novel approach based on the use of dynamic postural synergies [16]. The synergy-based approach was also explored by Kurokawa et al., proposing monitoring of the M wave to control movement and muscle fatigue [17]. The result of this system is controversial, since only slight improvements were shown in the kinematics of the ankle and hip.

The exoskeleton designed by Vanderbilt University, which was licensed to Parker Hannifin under the trade name of Indego, has the possibility of incorporating muscle stimulation by connecting an electronic module that contains the stimulator, featuring two channels per stimulator [18]. The stimulation control strategy was comprised by an adaptive algorithm, whose results in experiments performed with a volunteer with spinal cord injury showed good control of the joint trajectory, as well as a considerable reduction of the power of the hip and knee electric motors of approximately 20% [18].

A further theoretical approach was proposed by Vallery and Buss for allocation of control signals to FES and the robotic actuator [19] based on a model predictive control. Given a certain trajectory to track by the controller, a model-predictive system predicts the torque reference to be generated by the combined system (NMES and RE). This torque reference is distributed to the stimulator and mechatronic controller based on a spectral analysis of the control command. The basic idea is to feed low-frequency components to the stimulator control, taking advantage of the high bandwidth of the electric motors while the high-frequency components are fed to the motor controller. In this way, each system (NMES and RE) is optimally used with respect to their dynamic characteristics. This approach allows, according to the authors, to optimize HEX in terms of performance, energy consumption, and muscle fatigue [20]. While this approach was, as far as we are aware, not validated, simulations showed that the variable torque distribution did show a significant reduction of control effort of approximately 5%–10%.

18.2.1 MODELING APPROACHES FOR CONTROL

As mentioned earlier, from a control point of view, the major challenges to be faced when using HEX are chiefly related to the accurate estimation of the muscular generated stimulation torques, the muscular fatigue modeling, and solving the force-sharing problem between the NMES and the needed orthotic actuation torque to perform a given task by the RE [7,21]. Another potential challenge is related to the characterization of the main gait events to trigger FES. An example of such gait events is the time interval following the toe-off event and prior to the initial contact event [22,23]. Different solutions have been proposed in the literature to deal with the aforementioned challenges by either using model-based or sensor-based approaches.

As regards the model-based approaches, estimation of the stimulation-based torques has been reported in different studies. For example, the authors of Refs. [24,25] have used a Hill-based model to estimate the FES-generated stimulation torque while taking into account muscular fatigue [26]. However, model-based approaches generally require an accurate identification process, which is often a difficult task due to the rapidly changing muscular dynamics, muscular fatigue, spasticity, as well as variable physiological and environmental factors such as skin impedance, temperature, and electrode placement [27].

On the other hand, sensor-based approaches have been also used in literature. In Reference [28], for example, a force sensor is used to measure the interaction forces and thus estimate the generated stimulation torque. In Ref. [29], force-sensing resistors were placed at the inner side of the orthosis' shank segment to measure the interaction torque and to estimate the muscular fatigue. In Refs. [22,30], to detect toe-off and initial contact gait events, force-sensing switches were placed in the shoe of the affected foot of paretic patients. Alternatively, an inertia measurement unit (IMU) has also been proved to be effective to detect gait events [21,23]. Compared to ground-reaction-force sensors, a significant benefit of using the IMUs is related to their ability to estimate the joint kinematics, which is of great importance for performance assessments, and necessary for feedback controllers. Moreover, the IMUs show better durability in practice. Although sensor-based approaches do not require a model and are not specific with respect to the subject conducting the experiments, torque/force sensor placement remains a challenge for effective control and they are generally expensive, with the need for a prior calibration process [31].

The closed-loop neuroprosthesis control approaches are used in a hybrid context to control either the NMES or the RE device, and have a great impact on the overall performance of any HEX. Ha et al. have developed in Ref. [18] a hybrid FES-exoskeleton method to control a hip-knee joint during the swing phase using the Vanderbilt lower limb exoskeleton. A PID controller is used to track the desired knee joint trajectory. The PID output torque is used as a reference torque for the feedback stimulation controller. The proposed approach does not need any muscle modeling, nor sensing-based approach to estimate the generated stimulation torque. However, it does not ensure an on-line estimation of the generated stimulation torque and may show some weaknesses with respect to model uncertainties. In Ref. [32], an event-based control algorithm for sit-to-stand (STS) motion was developed. A stiffness and damping controller for the H1 exoskeleton is proposed combined with the use of FES during the STS motion. Experiments show a variation of the human/exoskeleton interaction torque along the STS transfer task. Also, iterative learning-based algorithms have shown great performances in avoiding fast muscular fatigue by appropriately adjusting the FES patterns during cyclic movements such as walking [33].

18.3 POTENTIAL FUTURE TECHNOLOGIES

The next generations of hybrid solutions combining NMES and RE may benefit from nontraditional approaches. Soft exoskeletons are emerging to enable lightweight, inherently safe, and unobtrusive actuation, rendering appropriate moments to the human body. On the other hand, motor neuroprostheses via surface electrical stimulation have been produced as complementary actuators for wearable robotic systems. Moreover, recent advances in FES could enable more sustainable stimulation, achieved with electrode matrix arrangements, that could be used to produce movement in individuals with paralysis. So-called soft exoskeletons are lightweight portable systems in which the mass of the actuators is located proximally, allowing for a positive effect on mobility. Most recent technological advances in soft exoskeletons are thought to rely on the human skeletal structure to transmit forces through “soft” materials building the exoskeleton or exosuit. Such materials could have inherent compliance (e.g., based on pneumatic or cable-driven systems) to produce sufficient mechanical assistance to deliver function while reducing or optimizing its energetic cost for

the user. Some open challenges in soft exoskeletons could be compensated if combined with advanced neuroprosthetics. For example, exosuits lack the rigid frames in traditional exoskeletons that are attached to the body and facilitate distributed torque transfer and support to weight bearing, that could be essential for elderly and heavily impaired subjects. Adequate electrical stimulation of muscles crossing human joints could contribute to the net joint stiffness that is essential for mechanical support (e.g., stance phase stabilization).

Compliant soft exoskeletons usually are driven using Bowden cables from remote actuators. From the control point of view, a main challenge is in the large uncertainties in the relative displacements between the human and the robot (transparency), including variable friction losses and particular user characteristics. These drawbacks are addressed by robust control approaches such as sliding mode control, adaptive control, and also with optimization techniques that aim at improving the overall performance of the wearable robotic assistance [34].

Adding the above-mentioned features of soft robots with FES-induced movement in parallel has large potential to enhance user muscle strength and cardiorespiratory fitness. Moreover, FES could contribute to the stimulation of sensory input from the muscle and nerve afferents that may be beneficial for recovery after neural damage. Also, muscle power generated by a motor neuroprosthetic can reduce the energy demand of the robotic wearable system, as has been explored with rigid wearable robot structures (see Section 18.2).

Most advanced selective noninvasive neuroprosthetics have been proposed shaped as electrode arrays in textiles with different structures depending on the location and size of targeted muscles. Having multiple electrical contact points allows for modification of stimulation pattern to enable diverse movements and, very importantly, to prevent rapid muscle fatigue. Delivery of variant stimulation patterns can be achieved through assessment of diverse types of indexes for motion selectivity or fatigue management, and these indexes can be related to the output joint torque [35], motion/posture [36], or even the evoked electrophysiological response [37]. Roughly, management of fatigue has been more relevant for FES therapeutic approaches in which modulation of the electrical stimulation parameters is critical to evoke a repetitive functional response, for example, to realize active reach-to-grasp training with a selective combination of electrode pads [38]. Most developments have been focused on distributed and sequential stimulation of upper limb muscles. Nonetheless, applications for control of the lower limb remain to be explored further, for example, to exploit the potential benefits of selectively exciting different lower limb muscles fibers [35] to optimize muscle force production.

Hybrid-selective soft robots can be envisioned in which advanced closed-loop FES control algorithms could compensate for the high energy cost associated with mechanical actuations while accounting for key challenges in control of surface stimulation.

18.4 CLINICAL AND USABILITY FACTORS

One of the most remarkable deficits found in the field of hybrid exoskeletons is the lack of clinically oriented studies that actually provide meaningful data regarding the main hypothesis claimed by the scientific community working on this field: combining FES with an active exoskeleton provides all the advantages attributed to FES while increasing the time of use of FES due to a

considerable reduction of muscle fatigue [7,39]. Since this hypothesis seems to be supported by the literature related to FES (e.g., [40]) there are underlying open questions on the actual effects of walking therapy delivered with HEX. One of these questions is: What are the physiological effects of providing stimulation during walking for longer periods attained with HEX? FES-related research has shown positive effects on walking speed in incomplete SCI and muscle hypertrophy [41]. On the other hand, there are evidences of histological changes on fiber composition and muscle damage due to electrical stimulation [42]. Furthermore, there is limited evidence that a combined approach of bracing and FES results in little benefit to functional ambulation in paraplegic patients with complete SCI [43]. Therefore, specific research on whether or not the effects of HEX as a therapeutic intervention is beneficial to the patient should be conducted, in order to give a foundation that supports the further development of HEX technology. Furthermore, the HEX approach involves stimulation of the main muscles involved in walking, but there are several more that are actually involved in walking, such as hip flexors, as well as key muscles that help to maintain dynamic balance during walking. Would therefore the application of FES to a reduced number of muscles actually hamper the functional outcome of the patient after weeks of treatment with HEX?

Another open question remains regarding the functional and therapeutic impact of therapeutic HEX-based interventions. In the form of a question: Has the walking therapy provided by HEX superior clinical outcomes than either exoskeleton or FES therapy alone? Some authors claim that the combinational approach of intensive training with appropriate stimulation of afferences during functional training may maximize the therapeutic outcomes [44]. In this sense, HEX is a combinational approach that should be judged taking into account, not only the actual physiological effects on the patient, but the effect on the walking function of the patient, weighting the increased complexity of the hybrid approach with respect to FES- or exoskeleton-only walking therapies.

Another question remains which may be answered with specific clinical experimentation. While it has been demonstrated that muscle fatigue due to FES is actually reduced with the HEX approach, what is the effect on the overall fatigue of the patient? It has been shown that exoskeletal constraints actually increase the metabolic cost of walking in healthy volunteers [45] compared with nonassisted walking. Regarding FES, there is limited evidence of a reduction in energy demand that supports the use of bracing and FES for ambulation in paraplegic patients with complete SCI [43]. The use of a HEX approach should be investigated regarding the impact on user effort, that is, not only tolerable by the subject, but also regarding the functional and therapeutic outcomes compared with FES- or exoskeleton-only approaches.

18.5 CASE STUDY

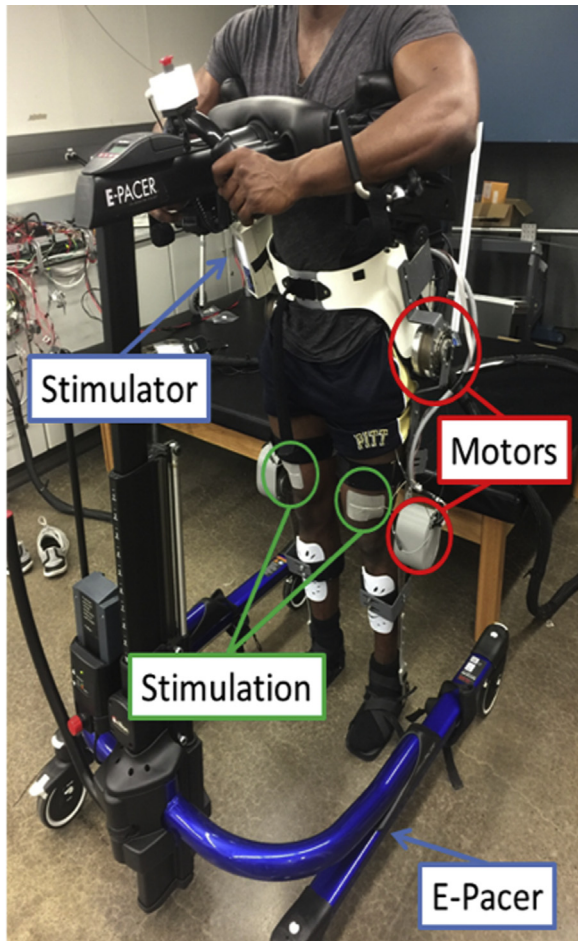
In the following case study, a general framework to coordinate FES of multiple gait-governing muscles with electric motors is presented. A muscle synergy inspired control framework is used to as the controller for achieving the walking function. The controller is motivated mainly to address the actuator redundancy due to the combined use of FES and a powered exoskeleton. More details on the controller derivation and the experimental results can be found in Ref. [16]. In this case study, we briefly present the controller and the experimental results.

The controller uses dynamic postural synergies between FES of the muscles and the electric motors that were artificially generated through dynamic optimizations. These synergies, when activated, mimic flexor and extensor synergies during walking. The synergies were used in the feedforward path of the control system. A dynamic surface control technique [46], modified with a delay compensation term [47,48], is used as the feedback controller to address model uncertainty, the cascaded muscle activation dynamics, and electromechanical delay (EMD). To address muscle fatigue, the stimulation levels in the feedforward path were gradually increased based on a model-based fatigue estimate. The synergy-based controller was demonstrated experimentally on an able-bodied subject and a person with an incomplete SCI.

The hybrid neuroprosthesis testbed, shown in Fig. 18.1, can be broken down into four primary components: an adjustable orthosis, electric motors, a stimulation unit, and an assistive support device. The orthosis is designed to be adjustable to comfortably fit a wide variety of body types while maintaining the alignment of the joints between the orthosis and subject. Custom motor mount brackets were fabricated to attach the electric motors at the joints of the orthosis. The electric motors (Harmonic Drive [49]) at the hip joints can generate a maximum torque of 50 Nm. The knee electric motors were EC90 brushless motors [50] combined with a Harmonic Gear CSD-25-100-2UH [49]. The knee motor can generate a maximum torque of 56 Nm. These electric motors were chosen to be able to generate all of the required torque, if necessary. The testbed only uses electric motors at the hip joints because it is difficult to stimulate hip flexors and extensors, as these muscles are not easily accessible using surface electrodes. The knee joint uses a combination of electric motors and FES of the knee flexors and extensors. A RehaStim eight-channel stimulator [50] was used to generate the current modulated biphasic pulse trains used to elicit muscle contractions. A set of transcutaneous electrodes was placed on the quadriceps and hamstring muscle groups. The current modulated pulse train with a frequency of 35 Hz and a 400- μ s pulse width is used for all experiments. An E-Pacer [51] was used as an assistive support device for the experiments to help the subjects maintain their balance and propel themselves forward. A real-time target machine [52] and xPC target toolbox [53] were used to interface with the different sensors and motor drivers and implement the controller in real-time at 1 kHz. The control algorithms were coded in Simulink [53] and used Simulink's real-time toolbox [53] running on a Windows machine (Intel Xeon 3.10 GHz processor).

The hybrid neuroprosthesis is controlled using two of the adaptive synergy controllers with delay compensation working in tandem to produce gait, one for each leg. The Finite State Machine, shown in Fig. 18.2, is used to determine which trajectories and synergy activations of the gait sequence are used; that is, either half right step (State 1), full left step (State 2), or full right step (State 3). In between the active states; States 1–3, the standby state (State 0) is activated by default, in which the motors at the joints hold their positions and the synergy activations are set to zero. When a leg is activated in a state, it becomes the swing leg and its counterpart becomes the stance leg. When a leg becomes the stance leg the controller only uses feedback to track the stance hip trajectory and hold the position of the knee joint. The progression of the FSM is determined by the progression button, in which the first time it is pressed State 1 is activated, then each time it is pressed after that the even transitions activate State 2 and the odd transitions activate State 3. In addition to the progression button, there is a safety button which turns off all inputs when pressed.

The overall control system was experimentally demonstrated on an able-bodied subject (male; 27 years old; height: 1.80 m; weight: 90 kg) and a person with an incomplete SCI (male; 41 years

**FIGURE 18.1**

The walking hybrid neuroprosthesis and the gait support device used in the experimental demonstration of the synergy-based control system. This system uses an electric motor at the hip and knee joints of each leg and FES of the hamstrings and quadriceps muscle group of each leg.

N.A. Alibeji, N.A. Kirsch, N. Sharma, A muscle synergy-inspired adaptive control scheme for a hybrid walking neuroprosthesis, Front. Bioeng. Biotechnol. 3 (2015) 203; Publisher Frontiers; Permitted reuse under creative commons license.

old; height: 1.70 m; weight: 70 kg; injury: T10 AIS A). For these experiments it was assumed that the behaviors of the right and left legs were similar, therefore, both States 2 and 3 used the same synergies and activations. The optimizations to compute the synergies, their activations, and the optimal joint angle trajectories were performed using the subject's height and weight. The model used the muscle parameters reported in Ref. [25] for an able-bodied subject and person with SCI.

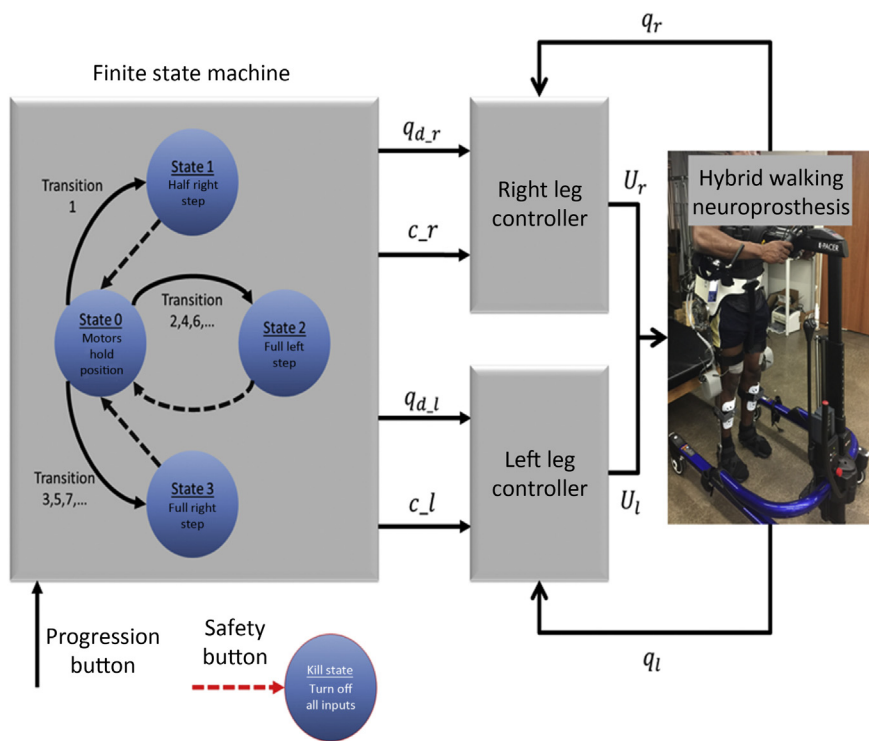


FIGURE 18.2

The Finite State Machine determines the desired trajectories and synergy activations based on what state is activated; either half right step, full left step, or full right step. Then two controllers are used, one for each leg, which work in tandem to produce gait.

Prior to any experimentation, an approval from the Institutional Review Board at the University of Pittsburgh was obtained. The consent procedure for human participants was written and informed. During the experiments, the subject was instructed to relax and refrain from voluntarily interfering with the hybrid exoskeleton. The estimates of the EMD, activation time constants, and fatigue/recovery rates were estimated in system identification experiments in a leg extension machine and assumed to be the same for both legs. The progression and safety buttons were operated by a separate user and were used to control the FSM.

To demonstrate the efficacy of the synergy-based controller for a hybrid neuroprosthesis and to compare the difference in power consumption between a hybrid actuation strategy versus only using electric motors, two different cases were implemented on the subjects. In the first case, the extended adaptive synergy-based controller with dynamic postural synergies was used to distribute the control effort to the hybrid actuation structure, FES, and motors. For the second case, to emulate a powered exoskeleton, only motors were used in the testbed and a Robust Integral of the Sign of the Error (RISE) controller [54] was used to govern the input to the motors. Each experimental trial was run for six steps.

18.5.1 RESULTS

The experimental results from the subject with the incomplete SCI are shown in Figs. 18.3–18.7. The tracking performance for both the right and left hip and the knee joints is shown in Fig. 18.3. Fig. 18.4 shows a sequence of frames from the video footage illustrating the gait produced using the control system.

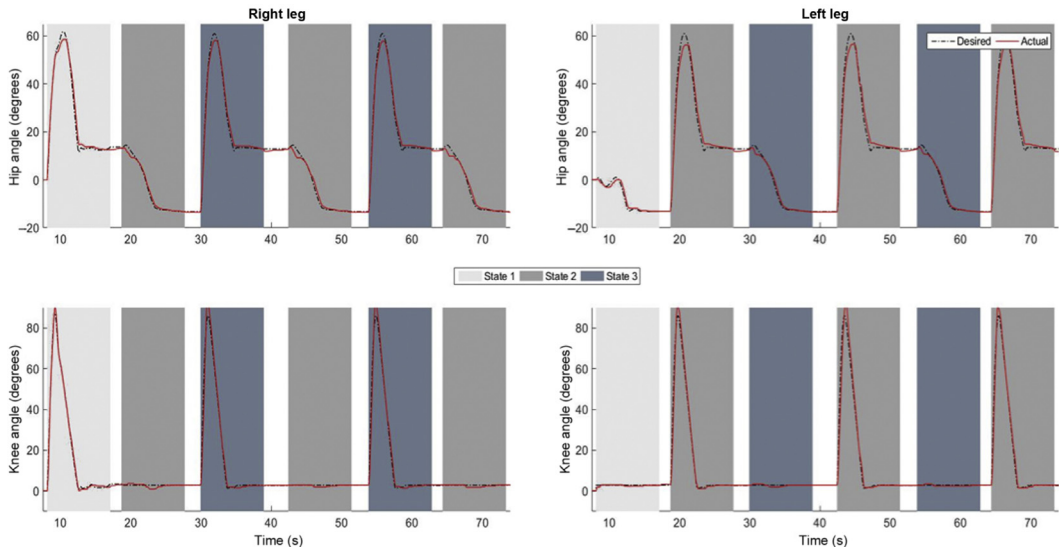


FIGURE 18.3

The desired and actual joint angles of the right and left hip and knee joints resulting from using the developed synergy-based control system in conjunction with the FSM on an able-bodied subject. The shaded regions indicate which state of the FSM is active at that time.

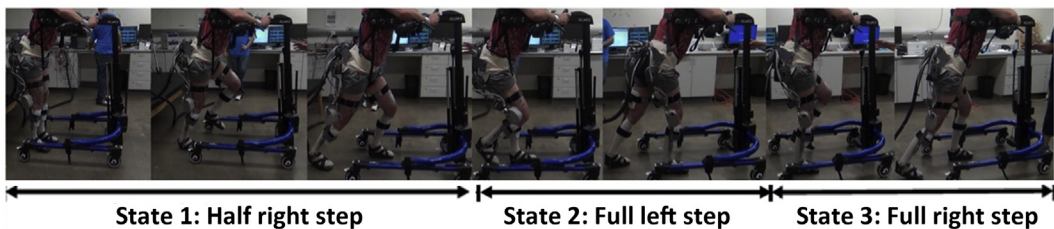


FIGURE 18.4

A sequence of photos illustrating the gait produce during the experiments.

N.A. Alibeji, N.A. Kirsch, N. Sharma, A muscle synergy-inspired adaptive control scheme for a hybrid walking neuroprosthesis, *Front. Bioeng. Biotechnol.* 3 (2015) 203; Publisher Frontiers; Permitted reuse under creative commons license.

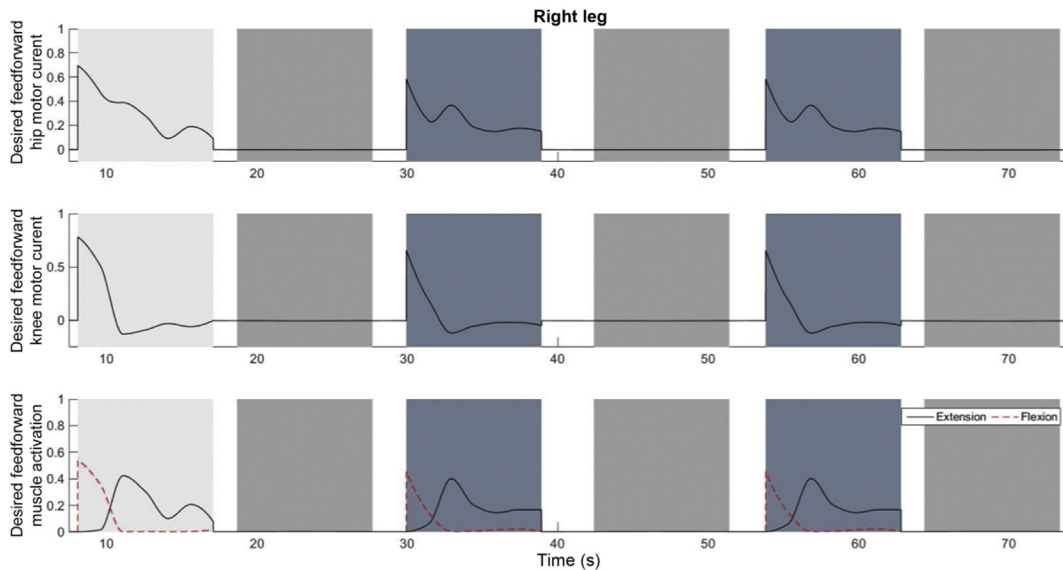


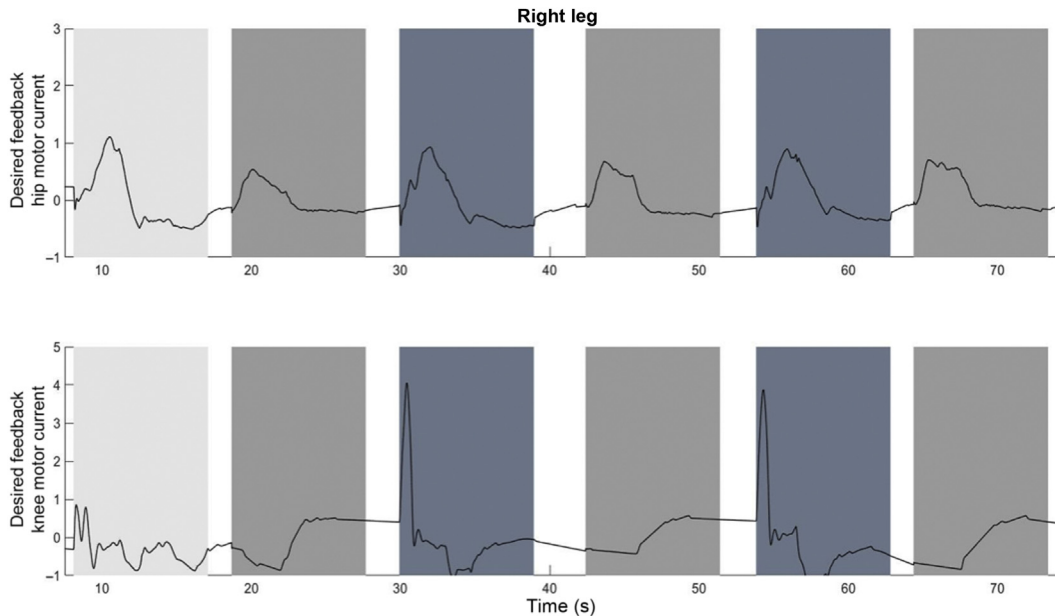
FIGURE 18.5

The desired feedforward component for all of the system inputs. This component is generated from the dynamic postural synergies and their activation after adaptation and with the scaling up from the fatigue estimate and the scaling factor control gain.

N. Kirsch, N. Alibeji, L. Fisher, C. Gregory, N. Sharma, *A semi-active hybrid neuroprosthesis for restoring lower limb function in paraplegics*, in: 2014 36th Annual International Conference of the IEEE Engineering in Medicine and Biology Society, EMBC 2014, 2014, vol. 2014, pp. 2557–2560; Publisher Frontiers; Permitted reuse under creative commons license.

The root mean squared errors (RMSEs) and root mean squared voltages (RMSVs) for the hip and knee joints for the right leg of both the able-bodied subject and the subject with the incomplete SCI are presented in [Table 18.1](#). From the results it can be seen that not only did the synergy-based controller result in better tracking performance, but it did so while consuming less energy compared to the RISE controller. In addition, the hybrid neuroprosthesis testbed, when using the synergy-based controller, also includes therapeutic health benefits due to the use of FES.

The desired feedforward component that includes synergies between FES and the powered exoskeleton, and desired feedback component can be seen in [Figs. 18.5 and 18.6](#). The actual input signals for all eight inputs of the system are shown in [Fig. 18.7](#). It can be observed that when a leg takes the role of the stance leg, the synergy activation is zero. This results in zero stimulation and zero desired feedforward motor activation. Hence, only feedback control of the motors was used to lock the knee joint of the stance leg. From the inputs, it can be seen that the stimulation is well-timed for each step, that is, the flexors are activated first to produce the withdrawal reflex and then the knee extensors are activated to fully extend the swing leg.

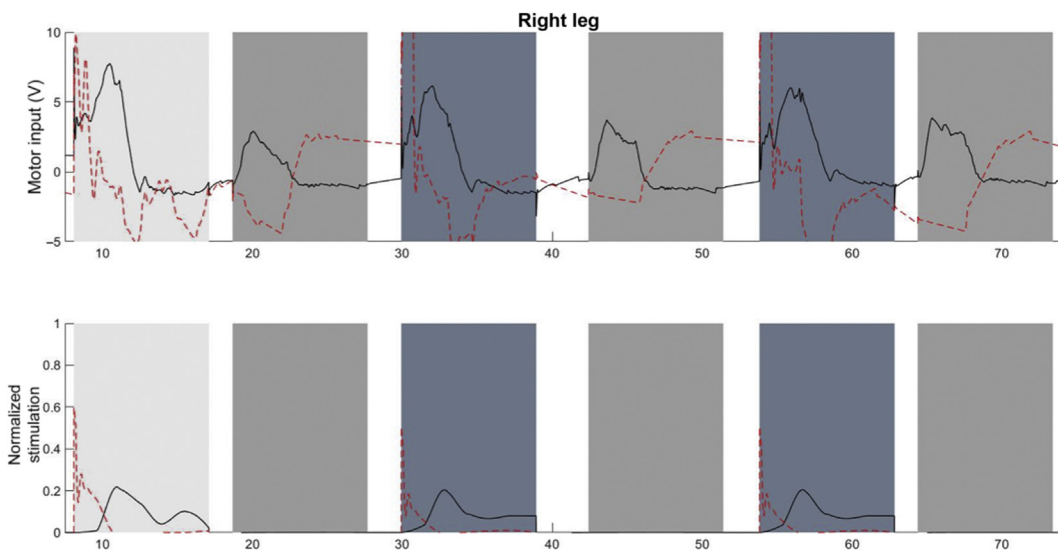
**FIGURE 18.6**

The desired feedback component which is only applied to the four motors at the hip and knee joints of each leg. It can be observed that the majority of the effort occurs during the swing phase of each leg.

N. Kirsch, N. Alibeji, L. Fisher, C. Gregory, N. Sharma, A semi-active hybrid neuroprosthesis for restoring lower limb function in paraplegics, in: 2014 36th Annual International Conference of the IEEE Engineering in Medicine and Biology Society, EMBC 2014, 2014, vol. 2014, pp. 2557–2560; Publisher Frontiers; Permitted reuse under creative commons license.

18.5.2 DISCUSSION

In this case study, a synergy-based control system is used to distribute the control effort to the multiple actuators of a walking hybrid neuroprosthesis. This approach is inspired from the human motor control concept of muscle synergies. In most studies, muscle synergies are proposed as a basis employed during human motor control and found by decomposing recorded EMG signals (collected from multiple muscles) to extract muscle synergies. Unlike these studies, in this case study flexor and extensor synergies are designed, using dynamic optimizations, to be used as a basis for the control system for the walking hybrid neuroprosthesis. This synergy design approach, using optimizations to distribute the control effort among the available actuators, offers multiple advantages and convenience such as allowing for the incorporation of external inputs, that is, electric motors and FES. Another benefit for this method of designing dynamic postural synergies is the ease of adding additional restrictions on the synergies, that is, no co-activation or no negative stimulation. Based on the synergy principle, fewer control signals are used to control multiple actuators in a hybrid neuroprosthesis, therefore the use of synergies will not only solve the actuator redundancy problem similarly to how the body is hypothesized to do so, but it will do it in a more computationally efficient way. To further ensure the effectiveness of the closed-loop synergy-based

**FIGURE 18.7**

The inputs to all of the system inputs, including feedback and feedforward, for this experimental trial. Note that there is no stimulation occurring during the stance phase of each leg.

N. Kirsch, N. Alibeji, L. Fisher, C. Gregory, N. Sharma, A semi-active hybrid neuroprosthesis for restoring lower limb function in paraplegics, in: 2014 36th Annual International Conference of the IEEE Engineering in Medicine and Biology Society, EMBC 2014, 2014, vol. 2014, pp. 2557–2560; Publisher Frontiers; Permitted reuse under creative commons license.

Table 18.1 The Root Mean Squared of the Input Voltage to the Motors

		Synergy-Based Controller		RISE	
Subject	Joint	RMSE (degrees)	RMSV (V)	RMSE (degrees)	RMSV (V)
Incomplete SCI	Right hip	1.35	2.25	1.68	2.49
	Right knee	1.68	3.10	3.52	3.36
Able-bodied	Right hip	1.56	3.22	2.70	3.40
	Right knee	0.92	2.50	3.03	3.70

Note that the synergy-based controller uses less motor input, which means less power consumption and results in better tracking performance.

control system Lyapunov-based control design approaches were used to overcome challenges, such as EMD, actuator dynamics, and muscle fatigue. Therefore, this class of synergy-based controllers is also robust to EMD and compensates for activation dynamics and muscle fatigue. More details on the synergy-inspired control design and Lyapunov-based control design for FES or the hybrid neuroprosthesis can be found in Refs. [13–17,30,38].

18.5.3 CASE STUDY CONCLUSION

In this case study, the adaptive synergy-based controller is developed and experimentally tested on an able-bodied subject and a person with an incomplete SCI using a walking hybrid neuroprosthesis. This control system used flexor and extensor synergies to reproduce the key dynamic postures; the withdrawal reflex and knee extension, which have been shown to be able to reproduce gait. Dynamic optimizations were then used to compute the optimal synergies' activation to produce a half step and full step. A finite state machine was developed to switch between the trajectories and synergy activations depending on three states; half right step, full right step, and full left step. The control system then used two of the synergy-based controllers, one for each leg, working in tandem to reproduce gait. The experiment was conducted on an able-bodied subject and a person with an incomplete SCI. The overall control system showed the ability to recreate gait using the hybrid neuroprosthesis and the gait assistive device.

18.6 CHALLENGES AND FUTURE DIRECTIONS

Although there have been some advances since the last revision, the HEX are still at a very early stage of development, in which the basic design criteria have not yet been established. Meanwhile advancements in the design of controllers for optimizing the cooperation between MNP and the ER [11,14,16,19], and clear criteria for the combination of both technologies are still missing. The real integration (or cooperation) of the MNP and the ER within a single controller that exploits not only the characteristics of each system, for example, as proposed in Refs. [11,14,16], but also the characteristics obtained by the simultaneous operation of both systems, should be considered in order to advance knowledge of the benefits of hybrid wearable robots and their effects on humans with lower limb impairments.

To achieve an optimal implementation of the control of an HEX it is also necessary to advance in the control of artificial muscle stimulation. To date, the most extended conceptual approach for implementation in a HEX is to maximize the contribution of stimulation, compensating the movement and/or fatigue through the ER [13,16,19]. However, recent advances in asynchronous stimulation are showing good results in the reduction of muscle fatigue [34], and hence its application in hybrid systems should be considered.

On the other hand, the capacity of adaptation and personalization of the HEX to the user must also be considered. As is the case with ERs, it is necessary to adapt the physical interface with the HEX: 3D printing methods for custom production of exoskeleton fixation parts or advanced algorithms for compliant control of the HEX by the user could improve the usability of these systems. On the other hand, as discussed in Section 18.3, innovations in the domain of soft exoskeletons [35] can also be applied, providing and optimizing the way to combine the MNP and the ER.

A clear future area in which effort must be made is clinical experimentation. As stated above, there are open important clinical questions that can only be answered with specific, clinical-oriented experimentation.

18.7 CONCLUSION

This chapter has presented an overview of the technology pertaining to the combination of MNP and ER, defined as HEX, focusing on the latest advances in the field. Furthermore, insights into adjacent technologies that can provide further advancements in the field of HEX technology have been discussed. Promising advancements have been made in cooperative control, such as the use of MPC and a synergy-based approach, but their actual superiority with respect to the solely MNP-ER combination, as well as the potential benefits provided to the target population, are needed. In addition, bringing the latest technologies developed in the field of wearable soft-robots, asynchronous and multichannel stimulation and customization would also further improve the performance of HEX.

We have noticed a lack of studies with clinical orientation aimed at providing clinically meaningful data on the effects of HEX on walking compensation and/or rehabilitation on the patient population. Most of the revised systems have been only validated from a technical point of view and with a very limited number of end-users involved. Gathering clinical evidence on the clinical, physiological, and functional effects of the therapy delivered with HEX would provide data to contrast the main hypothesis that has traditionally supported the development of HEX, providing strong foundations to further dynamizing, or abandon, research in the field of HEX. Although advancements must be made, the technology is mature enough to conduct clinical experimentation to unveil the potential impact of HEX on end-users.

REFERENCES

- [1] A. Curt, H.J.A. Van Hedel, D. Klaus, V. Dietz, Recovery from a spinal cord injury: significance of compensation, neural plasticity, and repair, *J. Neurotrauma* 25 (6) (2008) 677–685.
- [2] S. Rossignol, A. Frigon, Recovery of locomotion after spinal cord injury: some facts and mechanisms, *Annu. Rev. Neurosci.* 34 (1) (2011) 413–440.
- [3] P.H. Peckham, J.S. Knutson, Functional electrical stimulation for neuromuscular applications, *Annu. Rev. Biomed. Eng.* 7 (1) (2005) 327–360.
- [4] G.P. Braz, M. Russold, G.M. Davis, Functional electrical stimulation control of standing and stepping after spinal cord injury: a review of technical characteristics, *Neuromodulation* 12 (3) (2009) 180–190.
- [5] V. Dietz, Body weight supported gait training: from laboratory to clinical setting, *Brain Res. Bull.* 76 (5) (2008) 459–463.
- [6] J.L. Contreras-Vidal, N.A. Bhagat, J. Brantley, J.G. Cruz-Garza, Y. He, Q. Manley, et al., Powered exoskeletons for bipedal locomotion after spinal cord injury, *J. Neural. Eng.* 13 (3) (2016).
- [7] A.J. del-Ama, A.D. Koutsou, J.C. Moreno, A. De-los-Reyes, N. Gil-Agudo, J.L. Pons, Review of hybrid exoskeletons to restore gait following spinal cord injury, *J. Rehabil. Res. Dev.* 49 (4) (2012) 497.
- [8] T.C. Bulea, R. Kobetic, M.L. Audu, R.J. Triolo, Stance controlled knee flexion improves stimulation driven walking after spinal cord injury, *J. Neuroeng. Rehabil.* 10 (1) (2013) 68.
- [9] T.C. Bulea, R. Kobetic, M.L. Audu, J.R. Schnellenberger, G. Pinault, R.J. Triolo, Forward stair descent with hybrid neuroprosthesis after paralysis: single case study demonstrating feasibility, *J. Rehabil. Res. Dev.* 51 (7) (2014) 1077–1094.

- [10] K.M. Foglyano, R. Kobetic, C.S. To, T.C. Bulea, J.R. Schnellenberger, M.L. Audu, et al., Feasibility of a hydraulic power assist system for use in hybrid neuroprostheses, *Appl. Bionics Biomech.* 2015 (2015) 1–8.
- [11] A.J. del Ama, J.C. Moreno, Á. Gil-Agudo, J.L. Pons, Hybrid FES-robot cooperative control of ambulatory gait rehabilitation exoskeleton for spinal cord injured users, *Biosyst. Biorobot.* 1 (1) (2013) 155–159.
- [12] A.J. Del-Ama, Á. Gil-Agudo, J.L. Pons, J.C. Moreno, Hybrid gait training with an overground robot for people with incomplete spinal cord injury: a pilot study, *Front. Hum. Neurosci.* 8 (2014) 298. no. May.
- [13] N. Kirsch, N. Alibeji, L. Fisher, C. Gregory, N. Sharma, A semi-active hybrid neuroprosthesis for restoring lower limb function in paraplegics, in: 2014 36th Annual International Conference of the IEEE Engineering in Medicine and Biology Society, EMBC 2014, 2014, vol. 2014, pp. 2557–2560.
- [14] N.A. Alibeji, N.A. Kirsch, N. Sharma, A muscle synergy-inspired adaptive control scheme for a hybrid walking neuroprosthesis, *Front. Bioeng. Biotechnol.* 3 (2015) 203.
- [15] N.A. Kirsch, X. Bao, N.A. Alibeji, B.E. Dicianno, N. Sharma, Model-based dynamic control allocation in a hybrid neuroprosthesis, *IEEE. Trans. Neural. Syst. Rehabil. Eng.* 26 (1) (2018) 224–232.
- [16] N.A. Alibeji, V. Molazadeh, B.E. Dicianno, N. Sharma, A control scheme that uses dynamic postural synergies to coordinate a hybrid walking neuroprosthesis: theory and experiments, *Front. Neurosci.* 12 (2018) 1–15. no. APR.
- [17] N. Kurokawa, N. Yamamoto, Y. Tagawa, T. Yamamoto, H. Kuno, Development of hybrid FES walking assistive system – feasibility study, in: 2012 International Conference on Advanced Mechatronic Systems, 2012, pp. 93–97.
- [18] K.H. Ha, S.A. Murray, M. Goldfarb, An approach for the cooperative control of FES with a powered exoskeleton during level walking for persons with paraplegia, *IEEE. Trans. Neural. Syst. Rehabil. Eng.* 24 (4) (2016) 455–466.
- [19] H. Vallery, T. Stützle, M. Buss, D. Abel, et al., Control of a hybrid motor prosthesis for the knee joint, in: Proceedings IFAC World Congress, International Federation of Automatic Control, 2005.
- [20] H. Vallery, M. Buss, Towards a hybrid motor neural prosthesis for gait rehabilitation: a project description, *J. Autom. Control* 15 (2005).
- [21] J. McCamley, M. Donati, E. Grimpampi, C. Mazzà, An enhanced estimate of initial contact and final contact instants of time using lower trunk inertial sensor data, *Gait. Posture* 36 (2) (2012) 316–318.
- [22] G.M. Lyons, T. Sinkjaer, J.H. Burridge, D.J. Wilcox, A review of portable FES-based neural orthoses for the correction of drop foot, *IEEE. Trans. Neural. Syst. Rehabil. Eng.* 10 (4) (2002) 260–279.
- [23] T. Seel, S. Schäperkötter, M. Valtin, C. Werner, T. Schauer, Design and control of an adaptive peroneal stimulator with inertial sensor-based gait phase detection, *18th Annu. Int. FES Soc. Conf* (2013) 177–180.
- [24] N. Alibeji, N. Kirsch, N. Sharma, An adaptive low-dimensional control to compensate for actuator redundancy and FES-induced muscle fatigue in a hybrid neuroprosthesis, *Control. Eng. Pract.* 59 (2017) 204–219.
- [25] D. Popović, R.B. Stein, N. Oğuztöreli, M. Lebiedowska, S. Jonić, Optimal control of walking with functional electrical stimulation: a computer simulation study, *IEEE. Trans. Rehabil. Eng.* 7 (1) (1999) 69–79.
- [26] R. Riener, J. Quintern, G. Schmidt, Biomechanical model of the human knee evaluated by neuromuscular stimulation, *J. Biomech.* 29 (9) (1996) 1157–1167.
- [27] O. Brend, C. Freeman, M. French, Multiple-model adaptive control of functional electrical stimulation, *IEEE Trans. Control Syst. Technol* 23 (5) (2015) 1901–1913.
- [28] Y. Stauffer, Y. Allemand, M. Bouri, J. Fournier, R. Clavel, P. Metrailler, et al., The WalkTrainer--a new generation of walking reeducation device combining orthoses and muscle stimulation, *IEEE. Trans. Neural. Syst. Rehabil. Eng.* 17 (1) (2009) 38–45.

- [29] Y. Ren, D. Zhang, FEXO Knee: a rehabilitation device for knee joint combining functional electrical stimulation with a compliant exoskeleton, in: 5th IEEE RAS/EMBS International Conference on Biomedical Robotics and Biomechatronics, 2014, pp. 683–688.
- [30] H. Weingarden, H. Ring, Functional electrical stimulation-induced neural changes and recovery after stroke, *Eura. Medicophys.* 42 (2) (2006) 87–90.
- [31] W. Huo, S. Mohammed, Y. Amirat, Observer-based active impedance control of a knee-joint assistive orthosis, in: 2015 IEEE International Conference on Rehabilitation Robotics (ICORR), 2015, pp. 313–318.
- [32] V. Rajasekaran, M. Vinagre, J. Aranda, Event-based control for sit-to-stand transition using a wearable exoskeleton, in: 2017 International Conference on Rehabilitation Robotics (ICORR), 2017, pp. 400–405.
- [33] P. Müller, C. Balligand, T. Seel, T. Schauer, Iterative learning control and system identification of the antagonistic knee muscle complex during gait using functional electrical stimulation, *IFAC-Papers Online* 50 (1) (2017) 8786–8791.
- [34] Y. Ding, M. Kim, S. Kuindersma, C.J. Walsh, Human-in-the-loop optimization of hip assistance with a soft exosuit during walking, *Sci. Robot.* 3 (15) (2018). eaar5438.
- [35] D.G. Sayenko, R. Nguyen, M.R. Popovic, K. Masani, Reducing muscle fatigue during transcutaneous neuromuscular electrical stimulation by spatially and sequentially distributing electrical stimulation sources, *Eur. J. Appl. Physiol.* 114 (4) (2014) 793–804.
- [36] T. Exell, C. Freeman, K. Meadmore, A.-M. Hughes, E. Hallewell, J. Burridge, Optimisation of hand posture stimulation using an electrode array and iterative learning control, *J. Autom. Control* 21 (1) (2013) 1–5.
- [37] C. De Marchis, T. Santos Monteiro, C. Simon-Martinez, S. Conforto, A. Gharabaghi, Multi-contact functional electrical stimulation for hand opening: electrophysiologically driven identification of the optimal stimulation site, *J Neuroeng Rehabil.* 13 (22) (2016) <https://10.1186/s12984-016-0129-6>.
- [38] X. Tu, H. Han, J. Huang, J. Li, C. Su, X. Jiang, et al., Upper limb rehabilitation robot powered by PAMs cooperates with FES arrays to realize reach-to-grasp trainings, *J. Healthc. Eng.* 2017 (2017) 1282934.
- [39] F. Anaya, P. Thangavel, H. Yu, Hybrid FES–robotic gait rehabilitation technologies: a review on mechanical design, actuation, and control strategies, *Int. J. Intell. Rob. Appl.* 2 (2018) 1–28.
- [40] E.J. Nightingale, J. Raymond, J.W. Middleton, J. Crosbie, G.M. Davis, Benefits of FES gait in a spinal cord injured population, *Spinal Cord* 45 (10) (2007) 646–657.
- [41] R.C. Wade, A.S. Gorgey, Skeletal muscle conditioning may be an effective rehabilitation intervention preceding functional electrical stimulation cycling, *Neural Regen. Res.* 11 (8) (2016) 1232–1233.
- [42] A.L. Mackey, J. Bojsen-Møller, K. Qvortrup, H. Langberg, C. Suetta, K.K. Kallikoski, et al., Evidence of skeletal muscle damage following electrically stimulated isometric muscle contractions in humans, *J. Appl. Physiol.* 105 (5) (2008) 1620–1627.
- [43] T. Lam, D.L. Wolfe, J.J. Eng, A. Domingo, T. Lam, D.L. Wolfe, et al., Lower limb following SCI, Veersson 4. Vancouver, <www.scireproject.com>, 2012.
- [44] B.H. Dobkin, P.W. Duncan, Should body weight-supported treadmill training and robotic-assistive steppers for locomotor training trot back to the starting gate? *Neurorehabil. Neural. Repair.* 26 (4) (2012) 308–317.
- [45] S.R. Chang, R. Kobetic, R.J. Triolo, Effect of exoskeletal joint constraint and passive resistance on metabolic energy expenditure: implications for walking in paraplegia, *PLoS One* 12 (8) (2017). p. e0183125.
- [46] N. Alibeji, N. Kirsch, B.E. Dicianno, N. Sharma, A modified dynamic surface controller for delayed neuromuscular electrical stimulation, *IEEE/ASME Trans. Mechatronics.* 22 (4) (2017) 1755–1764.
- [47] N. Alibeji, N. Kirsch, S. Farrokhi, N. Sharma, Further results on predictor-based control of neuromuscular electrical stimulation, *IEEE. Trans. Neural. Syst. Rehabil. Eng.* 23 (6) (2015) 1095–1105.

- [48] N. Sharma, C.M. Gregory, W.E. Dixon, Predictor-based compensation for electromechanical delay during neuromuscular electrical stimulation, *IEEE Trans. Neural. Syst. Rehabil. Eng.* 19 (6) (2011) 601–611.
- [49] Maxon, EC 90 Flat Brushless Motor Specification Page. https://www.maxongroup.com/medias/sys_master/8825435389982.pdf.
- [50] Hasomed GmnbH website, <https://www.hasomed.de/de/home.html>
- [51] Rifton, E-Pacer (Tranfer and Mobility Device) website, <https://www.rifton.com/products/gait-trainers/e-pacer>.
- [52] S. GmbH, <https://www.speedgoat.com>.
- [53] The MathWorks Inc., <https://www.mathworks.com>.
- [54] P.M. Patre, W. MacKunis, K. Kaiser, W.E. Dixon, Asymptotic tracking for uncertain dynamic systems via a multilayer neural network feedforward and RISE feedback control structure, *IEEE Trans. Automat. Control* 53 (9) (2008) 2180–2185.

FURTHER READING

A.J. del-Ama, Á. Gil-Agudo, J.L. Pons, J.C. Moreno, Hybrid FES-robot cooperative control of ambulatory gait rehabilitation exoskeleton, *J. Neuroeng. Rehabil.* 11 (2014) 27.

UPPER LIMB ACTIVE PROSTHETIC SYSTEMS—OVERVIEW

19

Claudio Castellini

Institute of Robotics and Mechatronics, DLR – German Aerospace Center, Wessling, Germany

19.1 INTRODUCTION/MOTIVATION

The world around us is shaped to be operated by *hands* and *arms*: our homes, our workplaces, the means of everyday transportation, etc. For this reason, the loss of an upper limb is a tragedy, leading to a severe impairment in daily-living operational functionality as well as to psychological damage. Given the current state of the art in upper limb prosthetics in general (not just in active prosthetics), such a loss is irreversible. The impact of upper limb loss in our modern, ever-safer societies is less dramatic than that of other severely disabling conditions, for example, diabetes, stroke, and neurodegenerative conditions, or even if compared to *lower* limb loss—in 2010 about 1900 traumatic upper limb amputations per year in Europe were reported, maintaining an estimated total population of 94,000 upper limb amputees [1]. Still, if considered on a case-by-case basis, the loss of an upper limb has devastating consequences: the amputated person cannot operate any longer most of her usual daily appliances, leading to a dramatic lowering in the quality of life; living without a hand or the arm irreparably changes the looks and affective interaction of the amputated person, leading to social rejection, self-pity, and usually severe psychological consequences [2]. The fact that an amputation is definitive has led to the classification of prosthetics, as a subdiscipline of robotics, in *assistive robotics* rather than in rehabilitation robotics: an amputation is definitive and the amputated person needs an assistive device rather than a rehabilitative one, which should become the amputee's companion for life.

To partially recover the lost functions, man has for a long time devised a range of devices to be worn in place of the lost limbs and aiming at restoring the impairment to the best extent possible; but, especially in the case of the upper limb, the level of functional restoration has in general been poor, and we can safely say that it still is. Even neglecting other aspects of the problem, at most three degrees of activation (motor- or cable-driven joints)¹ can be simultaneously controlled, and in the standard case, not in a “natural” fashion [3]—the patient must learn to enforce a sometimes complicated sequence of muscle impulses to switch the control among the motors. Also for this reason, many amputees have preferred in the past, and still do prefer, to wear cosmetic prostheses,

¹Whereas in most relevant literature one refers in this case to the “degrees of freedom” of a device, we prefer to use the term “degree of activation” or even “motor,” since the two concepts do not match and usually a user’s control is applied to movement/force/torque, that is on motors (usually in a coordinated way), not on degrees of freedom.

that is, passive arms/hands with the only capabilities to partially restore the patient's looks and, possibly, to hold an object while the remaining limb operates on it; or even, *to wear nothing at all during daily life*. Rejection rates of upper limb active prostheses are high [4]: what can research and technology in this field *concretely* offer them, that cannot be done using an old-fashioned device or even a cosmetic one?

Only in the past 30 years have some branches of applied science and engineering really come together to try to advance the state of the art in active upper limb prosthetics [5]. But, as we will shortly see, today this problem remains no easy business, mainly, in our opinion, for one general reason: *research in upper limb prosthetics is holistic*, that is, it must be solved at all levels (e.g., dexterity, functionality, control, biocompatibility, man–machine symbiosis) at the same time, and solving only one subproblem will not usually lead to an established, acceptable, widely spread global solution. Decisive steps forward in upper limb prosthetics can be achieved only by involving the mechatronic engineer, the control theorist, the machine learning expert, the physiatrist, the certified orthotist/prosthetist and so on, all at the same time, or at least during the same process, their activity tightly integrated, and tailored for each single patient. Moreover, upper limb prosthetic solutions must be tested on the end-users, on-line, from the start; this requires that research laboratories cooperate with rehabilitation companies, facilities, hospitals, and so on, and involves knowledge of the psychological aspects of human–machine interaction, coadaptation and embodiment, the design of user interfaces, and functional assessment. It is a paradigmatically interdisciplinary problem, a feature that contemporary research facilities are usually in trouble implementing [2].

Before delving into the state of the art of active prostheses, two remarks must be clearly put out. First, one should draw a clear line between *academic* and *commercial* upper limb prosthetic hardware. There is a plethora of academic prototypes that have been, or are being, developed in university laboratories; we will not consider them in detail here, mainly because of the limited space, but all in all, note that the vast majority of such prototypes *do not* turn into commercial applications at the end of their life-cycle as research devices, and actually are never used for more than a few experiments. (There are remarkable exceptions to this; for example, the *Azzurra* hand, a commercial product stemming from the *Cyberhand* project [6] which, though not being certified as a prosthesis, is widely used as an academic prototype.) Without disregarding the related experiments, we believe that upper limb prosthetics is one of the highest forms of applied research: those solutions which do not find their way were probably not suited to really be prosthetic hardware, or are not yet ready to be, or do not match the current state of the art, or more simply have willingly not been turned into certified devices.

Second, in this chapter we will focus on *active* upper limb prostheses and first give a bird's eye view of early research, then we will try to paint a coarse picture of the state of the art in this field; but we will *not* refer to cosmetic and body-powered prostheses. This does not mean that the issue should be in general neglected: body-powered upper limb prostheses constitute an active field of research (see, e.g., Ref. [7]), and it has even been advocated that they are nowadays the most convenient solution [8]—an opinion we largely share. As opposed to a *self-powered* or *active* upper limb prosthesis, a *body-powered* one is generally operated via a cable whose tension is controlled by flexing/extending one's shoulders; although this way only one degree of activation can be controlled, for example, opening and closing a terminal device suited for gripping objects, body-powered prostheses are reliable, since they do not depend on any (semi-)autonomous artificial system whatsoever, and provide force feedback to the subject thanks to the tension exerted, and corresponding resistance felt, at the shoulder girdle. In many respects

they are still superior to active ones, not least because they cost a fraction of the price, which constitutes a further challenge for the researchers. The outcomes of the ARM competition within the *Cybathlon* challenge in 2016 are there to remind the assistive robotics community that the road ahead is still long: in both subsections the prosthetic arms “race” was won by athletes wearing body-powered prostheses [8,9] with one degree of activation only, a sad but instructive tuition for all of us.

19.2 THE PAST

While body-powered upper limb prostheses have been in use for centuries (if not, undocumented, since mankind has been able to use tools), the history of such devices begins soon after the Second World War [3], when small, light, and powerful motors were becoming available. At the same time, “myoelectric” control, that is, control enforced via the activation of muscle remnants, was conceived, thanks to surface electromyography (sEMG) [10–12]. This technique was already in use as a diagnostic tool to detect abnormalities in the activation of muscles, possibly leading to early discovery of neurodegenerative conditions. Indeed, the contraction of muscles generates an oscillating electrical field, whose magnitude hovers around 10–100 mV, which can be detected by silver-chloride electrodes (sensors). A significant alteration of its characteristics might denote abnormalities in the neural signals; on the other hand, the contraction of *healthy* muscles generates specific sEMG signal patterns, whose low-pass rectified version relates monotonically to the torque the muscle applies to a joint. In short, the envelope of sEMG can be used to *detect the intention to move* when applied to voluntary muscles.

After an amputation, the muscle stumps are usually surgically connected to the bone stump and, after the wound has healed, a good deal of remaining muscular activity can clearly be noticed in the remnant of the upper limb—this is evident even by palpation. Voluntary contractions of the imaginary limb² result therefore in quite specific isometric contractions in the stump, which sEMG is still able to detect [10,12]. The initial idea was a simple one: to identify at least two *loci* of maximum, independent muscular activity on the stump surface of a patient, and to accordingly use two sEMG sensors to detect such activity. Typically, for instance, trans-radial amputees can usually independently, voluntarily contract the remains of the *m. flexor digitorum superficialis* and *m. extensor digitorum superficialis* by trying to flex/extend the imaginary wrist. The two resulting sEMG signals are then used to operate the motor of a one-degree-of-activation hand prosthesis—usually opening and closing a gripper [13].

Thanks to an extremely well engineered, highly integrated sensor/socket/gripper solution, developed, tested, and improved to perfection over decades, prosthetic companies such as, for example, *Ottobock* and *Liberating Technologies* have been able to deliver a modular, complete solution to the clinics, de facto setting the commercial standard of active upper limb prostheses. Two sEMG sensors are housed in a semirigid plastic/carbon fiber socket, exactly at the loci of maximal remaining activity the physiatrist has identified, and the magnitude of the two signals is directly mapped onto the opening/closing velocity of a gripper and/or a wrist or elbow motorized joint. Velocity

²We hereby use the term *imaginary limb* rather than *phantom limb* since the phantom limb is usually cramped and, in general, cannot be activated by the amputees. The imaginary limb is informally defined as the missing limb “as it would move were it still present.”

roughly maps to force at the end-effector when in contact with an object, which actually enforces smooth force/torque control of the prosthesis. Moreover, it is reported that amputees fitted with such a prosthetic device can still get force and motion feedback by listening to the noise produced by the motor as it closes around the object to be gripped. Therefore this solution provides both *proportional* force/velocity control and a simple form of physiological feedback; given that the remnant loci of activity have been carefully targeted, it also offers a quite high reliability [4,14]. On the other hand, its commercial price, as well as the time and price of servicing, constitute a severe disadvantage with respect to a body-powered prosthesis, which can usually be self-serviced and costs much less. The debate between two-sensor sEMG-based myoelectric control and body-powered devices is ongoing.

Control over more than one motor though, in turn controlling up to three degrees of freedom, has been enforced using the same hardware but defining some sort of sEMG “language” of cocontraction impulses, through which the patient can switch the proportional control among the motors [2,3]. Typical cases are control over hand opening/closing *and* wrist rotation in the case of trans-radial amputations, and over elbow flexion (no wrist control in this case) for trans-humeral patients. The user must briefly cocontract the two muscle remnants chosen, that is, push *both* sEMG sensors at the same time past a preset threshold, to obtain proportional control over one of the motors; each motor can usually be then controlled in a round-robin fashion. Smart as this control schema looks like, and notwithstanding its widespread usage in clinics, it clearly poses a relevant cognitive burden on the user, is more complicated than what a “natural” form of control would be, and can lead to unacceptable delays in emergency situations [15–17]. Such forms of control arose in the 1950s (e.g., a very early example is discussed in Reference [18]) and it is reported that the idea could even date back to not long after the Second World War (see Ref. [19] and references therein). In Philipson et al. [20] for instance, several examples of well-crafted two-sensor approaches can be found, and even a partition of a two-dimensional input space which somehow resembles a linear classifier.

More or less at this time the usage of more than two sensors and more sophisticated techniques to understand the user’s desire to move/act in a certain way (*intent detection*) was devised. In Ref. [21] it is claimed that the major hurdles to radical improvements in the design of prosthetic arms were an insufficient quality of sEMG signal processing (i.e., intent detection) and lack of light, fast, strong prosthetic hardware; it is approximately since the year 2000, however, that the academic interest in upper limb prosthetics has exploded [5]. This coincides with parallel progress in all areas of research concerning upper limb prosthetics: the miniaturization of sEMG sensors and the introduction of new kinds of sensors; ever-better motors requiring less and less power, to be embedded in an arm/hand system; ever-growing computational capabilities for signal processing and pattern matching, to be embedded on a prosthetic device; last but not least, an increasing awareness of the problems caused by the physical interface to the patient (the so-called *socket*).

19.3 THE PRESENT

19.3.1 DESIGN OF PROSTHETIC DEVICES

In the domain of hardware, the de facto standard active hand prosthesis is probably the *SensorHand Speed* by Ottobock [22], an extremely well engineered one-motor velocity-controlled gripper,

usually activated via two sEMG sensors the way we have described above. The whole system has proved to be reliable and affordable and it can be furthermore coupled with a wrist “rotator,” to be controlled using the switching procedure. This way, in total two independent degrees of freedom are offered to trans-radial amputees.

In an effort to augment the dexterity of a prosthetic hand, that is, informally defined, the number of motors it sports and therefore the number of movements it can enforce, researchers have tried to keep the control as simple as possible, actually exactly as it was before, but also to endow the device with a greater ability. A very interesting trend in this sense is that of exploiting underactuation and environmental constraints to build a prosthetic hand which, still using one motor only, can adapt to the surfaces of the environment, especially conforming to the shape of an object to be grasped. The *SoftHand* [9,23,24] and the *Hannes Hand*³ are the latest developments in this subfield. Both hands work via one actuator only and, it is claimed, can enforce up to 90% of the functionalities lost by the hand amputee. Moreover, at least the SoftHand works according to the principle of muscle synergies [25,26].

As far as the other way is concerned, namely to build a device with more motors, therefore requiring a finer, more complex control (see Section 19.3.2 for more on this issue), at least two breakthroughs have happened with respect to the typical one-degree-of-freedom devices since 2008. The first is the appearance on the clinical market of multifingered prosthetic hands such as, for example, Ottobock’s *Michelangelo*, Touch Bionics’s *i-LIMB Revolution*, and RSL Steeper’s *BeBionic*, with up to six independent motors, usually one for flexion of each finger and possibly one additional one for rotation of the thumb, or two different grasp configurations actuated using two motors and a gear change mechanism. From an exquisitely practical point of view, right now such devices lack proper controllability by the patient and their usefulness with respect to one-motor grippers or even body-powered prostheses is under question, especially given the associated buying and servicing costs. Nevertheless, they clearly show that more dexterity *can* be achieved even in the realm of prosthetic hardware, and to a commercial strength indeed.

The second breakthrough in prosthetic hardware design is represented by the main outcomes of the Revolutionizing Prosthetics program by DARPA (see, e.g., Ref. [27]), namely the *Modular Prosthetic Limb* (MPL) and its commercial counterpart, the *Luke Arm* [28]. The Luke Arm has been designed to be adaptable to most upper limb amputations (trans-radial, trans-humeral, at the shoulder level), and has one motor for each main degree of motion of the human arm—actually, 10 motors in the most complex configuration: two motors for the shoulder, two for the humeral rotation and elbow flexion, two at the wrist, and four in the hand; the hand in particular is gifted with a flexible and rotational thumb, as well as with the flexion of the index and other (combined) fingers. The weight of the full-arm configuration is less than 5 kg. As opposed to this, the MPL has 17 motors to control 26 degrees of freedom, and is equipped with a high number of sensors (torque, position, contact, current, accelerometers). While the MPL is still an academic testbed and is not available for clinical use, its clinical testing is underway [29]; the Luke Arm has recently been certified as a medical device, and while its pricing and conditions of use are, at the time of writing, still unknown, the device can be bought from the manufacturer’s website.

³The Hannes Hand has appeared, at the time of writing, only in the news—see, for instance, <https://www.cnet.com/news/robotic-prosthetic-hand-hannes-lighter-cheaper-grabbier>, accessed May 2019.

According to a recent survey we already cited [3] however, active prosthetic devices are not yet widespread around the world, and definitely not routinely fitted in clinics. Active prosthetic hands/wrists are endowed with two to four degrees of activation (actually six in the hand only for the *i-LIMB*), whereas some degrees of freedom are passively operated by mechanical design, that is, they must be activated by the user using a counteracting surface or the intact limb. The weight of such devices ranges in the few hundreds of grams (570 in the worse case). Active prosthetic elbows can weigh up to a kilogram (see again Ref. [3]).

19.3.2 CONTROL

Complex devices call for dexterous control, all the more reason for prosthetic control. Although, as already mentioned, the clinical standard still uses two sEMG sensors to control one or two motors, giant (academic) steps have been made in the past 20 years as far as “natural” control is concerned. The main trend in active prosthetics is to employ some form of machine learning, specifically called *pattern recognition* in the medical community, to directly interpret the user’s intent to enforce a specific movement [30,31]. The issue that we have grouped here under the umbrella term *control* really consists of several different strands and subproblems: designing the ideal socket/implantation to connect the patient to a set of sensors; defining the number and kind of sensors and the required electronics; designing a suitable machine learning method to interpret the signals as reliably as possible. Each of these subproblems has proved to be extremely difficult *in practice*, despite the initial claims of success.

In the first place, implantation technology is still in its infancy—osseointegration [32] allows, for instance, a prosthetic device to be directly implanted in the user’s stump and exceptionally low rates of post-operation infection have been reported so far; this technique also allows for the direct implantation of sEMG sensors within the stump, improving the signal-to-noise ratio and lowering the muscular cross-talk [33], via minimally invasive surgery or, in the near future, injection [34]. Still, large-scale testing of these methods has yet to appear, to the best of our knowledge. As opposed to that, the traditional device connecting a patient to an upper limb prosthetic device, the *socket*, presents, too, a series of difficult tasks to be carried out [35]. First of all it must be totally bio-compatible; second, it must ensure a perfect housing for the sensors, allowing for good conditioning of their signals, maintaining the contact with the user’s skin/body at all times notwithstanding movement (both *external* and *internal*, meaning relative movement of the body and the socket itself), physical effort, skin irritation, and sweat. No techniques for the automated design of a socket are in sight, although 3D laser scanning is nowadays almost a commercial reality; also, it is hard to say what the best arrangement for the sensors should be, given the *loci* of maximal residual activity on the user’s body. We believe that in this specific case it is paramount to design the device around the patient; but this concept seems still to elude the scientific community, or at least, we are unaware of any attempt to integrate the design process into the research environment dealing with control.

Notice that noninvasive, nonsurgical techniques to gather signals from the subject’s body are still preferred over invasive ones for obvious medical and psychological reasons; but until the mid-2000s this left very little hope of any sensible function restoration to victims of more severe amputations, such as shoulder-level and trans-humeral. With the introduction of targeted muscle reinnervation (TMR) however [36], things have radically changed: patients who have undergone

successful TMR surgery can produce activation patterns corresponding to actions whose musculature has been completely removed, for example, for elbow flexion in trans-humeral. In this case, such an activation corresponds to the activation of a re-innervated set of motor units, which can be still recorded by surface techniques [3].

Given that a uniform, safe, and effective way of connecting sensors and prosthetic devices is still not universally agreed upon, it is also interesting to note, however, that a good deal of research has been spent in determining *what sensors to use*. This subtopic of upper limb prosthetics has indeed produced a plethora of fascinating ideas (see, e.g., Refs. [5,37,38]), but sEMG remains the clinical standard. To what degree it can be integrated into, replaced by, or aided by other forms of sensing muscular activation, is still unclear. The most active field of research, to mention just one, is probably that of pressure sensing, either in its low-resolution (force myography) or high-resolution (tactile myography) variant [39–41]. The technique is promising, probably robust to muscular fatigue and sweat and it enjoys higher stability across time, but its practical applications are still lacking. Other techniques (ultrasound, mechanomyography, near-infrared spectroscopy, electrical impedance tomography, and so on) are still at the level of laboratory testing.

Last but not least, what is probably the most academically fruitful research field: the application of machine learning methods to biological sensors aimed at controlling an upper limb prosthetic devices. The number of scientific articles published in this field is high [5], while the practical results are definitely still not satisfactory. This is mainly due to the inherently probabilistic nature of a control system based upon machine learning. In Ref. [8] it is claimed that, in order to achieve a sensible level of reliability, any form of upper limb control system should reach an accuracy *in excess of six-sigma* in classification *in a practical setting* (whereas no such estimation is given for regression), which is still very far from the state of the art; any comparison of machine learning methods we are aware of is either performed in highly controlled conditions (i.e., in a laboratory) or reports accuracy values of up to 95%. Literally all possible machine learning methods, signals and features, linearity/nonlinearity of the models and training methods have been tried.

The most interesting paradigm shift is probably the introduction of the concept of simultaneous and proportional control, that is, the ability for the subject to modulate the activation of each single motor of the prosthetic device, at the same time and independently, or at least in a physiologically plausibly coordinated fashion [42]. It is a silent assumption that only by having a number of machine learning methods running in parallel this kind of control can be achieved; namely, using each machine to control a motor or a synergistic activation, and having built all models in such a way that muscle activation corresponding to a specific *intended* action will cause the prosthetic device to enact exactly that action—hence, the term *natural* control [15]. Simultaneous and proportional control is advocated nowadays as the main avenue to be pursued [3,5,17,43].

And still, notwithstanding this remarkable scientific production, there is only one company in the world, at the time of writing, selling a commercial solution which uses pattern matching, namely, Coapt LLC with its flagship product, the *Complete Control* system [44], which employs a simple but effective machine learning classification method and a fast data-gathering/calibration procedure based upon on–off goal-directed physiological stimuli. Complete Control uses eight sEMG sensors and can control opening/closing of the hand, flexion of the elbow, and one motor of the wrist.

19.3.3 AMPUTATIONS AND PATIENTS

Academic research in upper limb active prostheses is, in our opinion, still poorly patient-centered and very system-centered—no wonder, given that it is mostly performed in engineering laboratories. This is very likely one of the most important factors causing, in the very end, dissatisfaction and abandonment of prosthetic devices, and needs to be countered by putting the patient at the center—that means at least that a standardized procedure to treat upper limb amputees immediately after the trauma, or soon after the wound has healed and the user is awaiting to receive a prosthetic device, should be defined and accepted by all research facilities working in the field. Also, we miss a standardized functional assessment protocol *including the machine learning system* in the evaluation of the learning progress [45]. The closest approximation to that is the ACMC [46], explicitly conceived to test the functional recovery of upper limb amputees using a myoelectric prosthesis, but not taking into account the changes in the control system itself. In fact, the signals produced by upper limb amputated persons while learning to use upper limb active prostheses *change over time* [47–49]—a standard learning process, much like what happens while learning to use, for example, a new motorbike. In Ref. [43] it has even been clearly demonstrated that quasi-random muscle activation patterns can be learned, retained, and recalled after weeks, if those patterns were associated to a well-defined task. At the same time, since modern myocontrol is adaptive (based upon machine learning), *reciprocal* adaptation is expected to appear and in fact has already been observed (see, e.g., Ref. [49]). This form of synchronous change in time (coadaptation) should be fostered and exploited. It is probably not coincidental, that the Complete Control system allows for “recalibration” whenever required by the subject, thus improving the reliability and stability of the system. Actually, the performance of such a system can degrade over time (and indeed it will) because of several factors, in the first place those which make the sEMG signal quite nonstationary (sweat, fatigue, and so on) but, also, due to intervening novel environmental conditions or body postural changes. Anything which changes the muscular pattern corresponding to a definite action, for example, flexing the elbow, with respect to those gathered during the initial calibration, calls for recalibration or, even better, gathering of new data. This idea is enforced using incremental learning [50,51], which leads to interaction between the user and the machine learning system.

Table 19.1 The Three Main Subproblems of Myocontrol, and Their Perspectives, According to Fougner et al. [15]

Intent Interpretation Preprocessing	Single Function (One Motor) Single EMG feature On–off	Sequential Dual Function Multiple EMG feature Ramp function	State Machine Multimodal Multilevel	Classification (Mutually Exclusive) Proportional	Simultaneous Multifunction
→ Time/research progress/commercial diffusion					
<i>Adapted from Figure 2 in A. Fougner, Ø. Stavdahl, P.J. Kyberd, Y.G. Losier and P.A. Parker, Control of upper-limb prostheses: terminology and proportional myoelectric control - a review, IEEE Trans. Neural Syst. Rehabil. Eng. 20 (2012) 663–677.</i>					

19.4 THE FUTURE: A SHORT NOTE

At the time of writing (2019), the commercial diffusion of active upper limb prostheses either (1) having more than two motors (degrees of control/degrees of activation), and/or (2) being controlled through more than two sensors, and/or (3) being adaptively controlled using machine learning is

Table 19.2 Seven Subproblems in Upper Limb Prosthetics, and Related Challenges/Ideas/Perspectives to be Addressed in the Upcoming Years, for the Benefit of Active Upper Limb Prostheses Users

	Current	Short Term	Mid-Term	Long Term
Socket technology	Different for each patient and in each country; no standard mechanization	3D scanning; assessment of loci of residual activity; CAD design of socket	Semimechanized procedure becomes standard in the clinics	Completely automatic socket design, tailored to each patient
Prosthetic hardware	Electric motors; few or no sensors; up to 10 DoFs	Impedance control; sensors + closed-loop (position/velocity) control	3D printing to industrial strength; low-cost upper limb prosthetics	Tendon-driven activation; semisoft materials; human-likeness (?)
Sensors	Two sEMG sensors with sequential control; eight sEMG sensors with pattern recognition (CoApt)	Validation of novel sensors (tactile, ultrasound, etc.); sensors embedded in bio-compatible silicon	Targeted array of multimodal sensors and built-in miniaturized electronics	Sensor array built contextually with the socket
Proportionality	Present in traditional two-sensors control but only for one DoF at a time	Proportional control over some motors	Proportional coordinated control over all motors	Usage of (novel) muscle synergies to yield physiologically plausible coordinated control
Simultaneous control	None	Simultaneous control over a subset of the motors of the device	Simultaneous control over all motors of the device	
Coadaptation	Scarce evidence; assessment of signal change in the subject	Precise, qualitative, and quantitative assessment of parallel change of subject and control system	Correlation of functional improvement and coadaptation	Structured, standardized quantitative assessment of coadaptation, performed semiautomatically
Functional assessment	ACMC [46] is the only protocol targeting myocontrol—no focus on the control system	Protocols including the characteristics of the myocontrol system	Assessment with both user and control system in the loop	

Time/research progress/commercial diffusion →

Notice that the “Current” column only considers commercial solutions; academic prototypes should be more understood as grouped in the “Short term” column.

still scarce. CoApt LLC's Complete Control is the only case of ML-based adaptive control which is finding a way into the clinical market.⁴ Obviously the applied research performed in the past 30 years can and should do more, and, although some parts of it are ready to be deployed in clinics today, they still have not appeared.

Lastly, we propose an overview of what we deem the forthcoming steps in active upper limb research. Consider Table 19.1, which graphically depicted the state of the art in myocontrol alone, for active upper limb prosthetics in 2011. According to the authors of this remarkable survey, progress in myocontrol has happened/was happening mainly along three independent directions of research (subproblems), namely toward a “proportional activation profile,” that is, allowing for continuous velocity or torque control; toward multimodal “preprocessing,” that is, employing more diverse biological sensors and possibly environmental information, too; and lastly, toward simultaneous, multifunction (multiactivation) intent interpretation.

We take up from their work and hereby extend Table 19.1 to our personal view of active upper limb prosthetics overall—the result is visible in Table 19.2. We identify the progress that has happened in 7 years along the subproblems of Table 19.1, and we add four more, in order to complete the picture.

REFERENCES

- [1] S. Micera, J. Carpaneto, S. Raspopovic, Control of hand prostheses using peripheral information, *IEEE Rev. Biomed. Eng.* 3 (2010) 48–68.
- [2] D. Edeer, C.W. Martin, Upper limb prostheses – a review of the literature with a focus on myoelectric hands, in: WorksafeBC Evidence-Based Practice Group, 2001.
- [3] I. Vujaklija, D. Farina, O. Aszmann, New developments in prosthetic arm systems, *Orthop. Res. Rev.* 8 (2016) 31–39.
- [4] B. Peerdeman, D. Boere, H. Witteveen, R.H. Veld, H. Hermens, S. Stramigioli, et al., Myoelectric forearm prostheses: state of the art from a user-centered perspective, *J. Rehabil. Res. Dev.* 48 (2011) 719–738.
- [5] C. Castellini, P. Artermiadis, M. Wininger, A. Ajoudani, M. Alimusaj, A. Bicchi, et al., Proceedings of the first workshop on Peripheral Machine Interfaces: going beyond traditional surface electromyography, *Front. Neurorobot.* 8 (2014).
- [6] M. Carrozza, G. Cappiello, S. Micera, B.B. Edin, L. Beccai, C. Cipriani, Design of a cybernetic hand for perception and action, *Biol. Cybern.* 95 (6) (2006) 629–644.
- [7] G. Smit, R. Bongers, C. Sluis, D. Plettenburg, Efficiency of voluntary opening hand and hook prosthetic devices: 24 years of development? *J. Rehabil. Res. Dev.* 49 (2012) 523–534.
- [8] W. Schweitzer, M.J. Thali, D. Egger, Case-study of a user-driven prosthetic arm design: bionic hand versus customized body-powered technology in a highly demanding work environment, *J. Neuroeng. Rehabil.* 15 (2018).
- [9] S.B. Godfrey, M. Rossi, C. Piazza, M.G. Catalano, M. Bianchi, G. Grioli, et al., The SoftHand at the CYBATHLON: a user's experience, *J. Neuroeng. Rehabil.* 14 (2017).
- [10] R. Merletti, P.A. Parker, *Electromyography: Physiology, Engineering, and Noninvasive Applications*, vol. 11, Wiley-IEEE Press, 2004.

⁴At the time of going to press, Ottobock has just released a new commercial pattern recognition system, called *Myo Plus*. No statistics about it are yet available as far as we know.

- [11] R. Merletti, A. Botter, C. Cescon, M.A. Minetto, T.M.M. Vieira, Advances in surface EMG: recent progress in clinical research applications, *Crit. Rev. Biomed. Eng.* 38 (2011) 347–379.
- [12] R. Merletti, A. Botter, A. Troiano, E. Merlo, M.A. Minetto, Technology and instrumentation for detection and conditioning of the surface electromyographic signal: state of the art, *Clin. Biomech.* 24 (2009) 122–134.
- [13] M. Zecca, S. Micera, M.C. Carrozza, P. Dario, Control of multifunctional prosthetic hands by processing the electromyographic signal, *Crit. Rev. Biomed. Eng.* 30 (2002) 459–485.
- [14] R.N. Scott, P.A. Parker, Myoelectric prostheses: state of the art, *J. Med. Eng. Technol.* 12 (1988) 143–151.
- [15] A. Fougnier, Ø. Stavdahl, P.J. Kyberd, Y.G. Losier, P.A. Parker, Control of upper-limb prostheses: terminology and proportional myoelectric control - a review, *IEEE Trans. Neural Syst. Rehabil. Eng.* 20 (2012) 663–677.
- [16] N. Jiang, S. Dosen, K.-R. Müller, D. Farina, Myoelectric control of artificial limbs - is there a need to change focus? *IEEE Signal Process. Mag.* 29 (2012) 148–152.
- [17] D. Farina, N. Jiang, H. Rehbaum, A. Holobar, B. Graimann, H. Dietl, et al., The extraction of neural information from surface EMG for the control of upper-limb prostheses: emerging avenues and challenges, *IEEE Trans. Neural. Syst. Rehabil. Eng.* 22 (2014) 797–809.
- [18] C.K. Battye, A. Nightengale, J. Whillis, The use of myo-electric current in the operation of prostheses, *J. Bone Joint. Surg. B* 37 (1955) 506–510.
- [19] A.H. Bottomley, Myoelectric control of powered prostheses, *J. Bone Joint. Surg. B* 47 (1965) 411–415.
- [20] L. Philipson, D.S. Childress, J. Strysik, Digital approaches to myoelectric state control of prostheses, *Bull. Prosthet. Res.* 18 (1981) 3–11.
- [21] S.G. Meek, J.E. Wood, S.C. Jacobsen, Model-Based, multi-muscle EMG control of upper-extremity prostheses, in: J.M. Winters, S.L. Woo (Eds.), *Multiple Muscle Systems: Biomechanics and Movement Organization*, Springer, New York, 1990, pp. 360–376.
- [22] Myoelectric Speed hands by Ottobock SE & Co. KGaA, 2019. [Online]. Available from: <https://www.ottobockus.com/prosthetics/upper-limb-prosthetics/solution-overview/myoelectric-devices-speedhands/index.html>.
- [23] A. Bicchi, M. Gabiccini, M. Santello, Modelling natural and artificial hands with synergies, *Philos. Trans. R. Soc. Lond. B. Biol. Sci.* 366 (2011) 3153–3161.
- [24] M.G. Catalano, G. Grioli, A. Serio, E. Farnioli, C. Piazza, A. Bicchi, Adaptive synergies for a humanoid robot hand, in: *Humanoid Robots (Humanoids)*, 2012 12th IEEE-RAS International Conference on, 2012.
- [25] M. Santello, M. Bianchi, M. Gabiccini, E. Ricciardi, G. Salvietti, D. Prattichizzo, et al., Hand synergies: integration of robotics and neuroscience for understanding the control of biological and artificial hands, *Phys. Life Rev.* 17 (2016) 1–23.
- [26] M. Santello, M. Bianchi, M. Gabiccini, E. Ricciardi, G. Salvietti, D. Prattichizzo, et al., Towards a synergy framework across neuroscience and robotics: lessons learned and open questions. Reply to comments on: “Hand synergies: integration of robotics and neuroscience for understanding the control of biological and artificial hands”, *Phys. Life Rev.* 17 (2016) 54–60.
- [27] G. Hotson, D.P. McMullen, M.S. Fifer, M.S. Johannes, K.D. Katyal, M.P. Para, et al., Individual finger control of a modular prosthetic limb using high-density electrocorticography in a human subject, *J. Neural. Eng.* 13 (2) (2016) 026017.
- [28] The LUKE Arm by Mobius Bionics, 2019. [Online]. Available from: <http://www.mobiusbionics.com/>.
- [29] B.N. Perry, C.W. Moran, R.S. Armiger, P.F. Pasquina, J.W. Vandersea, J.W. Tsao, Initial clinical evaluation of the modular prosthetic limb, *Front. Neurol.* 9 (2018) 153.
- [30] D.S. González, C. Castellini, A realistic implementation of ultrasound imaging as a human-machine interface for upper-limb amputees, *Front. Neurorobot.* 7 (2013).

- [31] P. Beckerle, G. Salvietti, R. Ünal, D. Prattichizzo, S. Rossi, C. Castellini, et al., A human-robot interaction perspective on assistive and rehabilitation robotics, *Front. Neurorobot.* 11 (2017).
- [32] M. Ortiz-Catalan, Neuroengineering: deciphering neural drive, *Nat. Biomed. Eng.* 1 (2017).
- [33] E. Mastinu, P. Doguet, Y. Botquin, B. Håkansson, M. Ortiz-Catalan, Embedded system for prosthetic control using implanted neuromuscular interfaces accessed via an osseointegrated implant, *IEEE Trans. Biomed. Cir. Syst.* 11 (2017) 867–877.
- [34] R. F. f Weir, P.R. Troyk, G.A. DeMichele, D.A. Kerns, J.F. Schorsch, H. Maas, Implantable myoelectric sensors (IMESs) for intramuscular electromyogram recording, *IEEE. Trans. Biomed. Eng.* 56 (1) (2009) 159–171.
- [35] C. Lake, The evolution of upper-limb prosthetic socket design, *J. Prosthet. Orthot.* 20 (2008) 85–92.
- [36] T. Kuiken, Targeted reinnervation for improved prosthetic function, *Phys. Med. Rehabil. Clin. N. Am.* 17 (1) (2006) 1–13.
- [37] J. Lobo-Prat, P.N. Kooren, A. Stienen, J.L. Herder, B. Koopman, P.H. Veltink, Non-invasive control interfaces for intention detection in active movement-assistive devices, *J. Neuroeng. Rehabil.* 11 (2014) 168.
- [38] Y. Fang, N. Hettiarachchi, D. Zhou, H. Liu, Multi-modal sensing techniques for interfacing hand prostheses: a review, *IEEE. Sens. J.* 15 (2015) 6065–6076.
- [39] M. Wininger, N. Kim, W. Craelius, Pressure signature of forearm as predictor of grip force, *J. Rehabil. Res. Dev.* 45 (2008) 883–892.
- [40] E. Cho, R. Chen, L.-K. Merhi, Z. Xiao, B. Pousett, C. Menon, Force myography to control robotic upper extremity prostheses: a feasibility study, *Front. Bioeng. Biotechnol.* 4 (2016) 18.
- [41] C. Castellini, R. Kõiva, C. Pasluosta, C. Viegas, B.M. Eskofier, Tactile myography: an off-line assessment on able-bodied subjects and one upper-limb amputee, *MDPI Technol.* 6 (2018) 38.
- [42] N. Jiang, K. Englehart, P. Parker, Extracting simultaneous and proportional neural control information for multiple degree of freedom prostheses from the surface electromyographic signal, *IEEE Trans. Biomed. Eng.* 56 (4) (2009) 1070–1080.
- [43] M. Ison, P. Artermiadis, The role of muscle synergies in myoelectric control: trends and challenges for simultaneous multifunction control, *J. Neural. Eng.* 11 (2014).
- [44] Complete Control by CoApt, LLC, 2019. [Online]. Available from: <https://www.coaptengineering.com>.
- [45] C. Castellini, R.M. Bongers, M. Nowak, C.K. Sluis, Upper-limb prosthetic myocontrol: two recommendations, *Front. Neurosci.* 9 (2015).
- [46] H.Y. Lindner, A. Langius-Eklöf, L.M. Hermansson, Test-retest reliability and rater agreements of Assessment of Capacity for Myoelectric Control version 2.0, *J. Rehabil. Res. Dev.* 51 (2014) 635–644.
- [47] M.A. Powell, N.V. Thakor, A training strategy for learning pattern recognition control for myoelectric prostheses, *J. Prosthet. Orthot.* 25 (2013) 30–41.
- [48] G. Borghini, P. Aricò, G. Di Flumeri, N. Sciaraffa, A. Colosimo, M.-T. Herrero, et al., A new perspective for the training assessment: machine learning-based neurometric for augmented user's evaluation, *Front. Neurosci.* 11 (2017) 325.
- [49] J.M. Hahne, M. Markovic, D. Farina, User adaptation in myoelectric man-machine interfaces, *Sci. Rep.* 7 (2017).
- [50] P.M. Pilarski, M.R. Dawson, T. Degris, F. Fahimi, J.P. Carey, R.S. Sutton, Online human training of a myoelectric prosthesis controller via actor-critic reinforcement learning, in: 2011 IEEE International Conference on Rehabilitation Robotics (ICORR), 2011.
- [51] I. Strazzulla, M. Nowak, M. Controzzi, C. Cipriani, C. Castellini, Online bimanual manipulation using surface electromyography and incremental learning, *IEEE. Trans. Neural. Syst. Rehabil. Eng.* 25 (2017) 227–234.

DESIGN PRINCIPLES OF A LIGHT, WEARABLE UPPER LIMB INTERFACE FOR PROSTHETICS AND TELEOPERATION

20

Claudio Castellini

Institute of Robotics and Mechatronics, DLR – German Aerospace Center, Wessling, Germany

20.1 WEARABLE INTERFACES FOR WEARABLE ROBOTS

According to Peter Cariiani, *all technology is prosthesis* (see the commentaries to Ref. [1], p. 267), in the sense that whatever artefact mankind has ever built, it has built it in order to *augment in some way its own performances*. Examples are plenty: the invention and application of the wheel, which enabled our fellows of the Stone Age to carry objects that were unthinkably heavy; the invention of the printing press and its diffusion on a large scale, which enabled us all to read the classics; widespread usage of the steam engine, which has increased 100-fold the speed of traveling and transportation; and so on and so forth. However, irrespective of what exactly was invented, each new artefact has called forth for a specific user interface (*human–machine interface*, HMI from now on) to be designed—from the handles of the humble wheelbarrow to the pinch-and-zoom glass screen of modern smartphones.

Being able to properly control a tool is as important as the tool itself, maybe even more so, and control is enforced through an HMI. Unsurprisingly then, this concept is extremely wide, diverse, and complex: everything we do in our daily life has to do with (a series of specific) HMIs. Today, we operate electromechanical appliances at all times at home, at work, during our free time, while driving, shopping, walking, preparing dinner, etc., and in each case we need to be supported by a *dexterous* and *intuitive* HMI: by *dexterous* we mean that the HMI must enable *full control* over the device; and *intuitive* means that it must be *easy to understand and operate*, quickly and safely allowing the user to take the aforementioned full control.

The ideal HMI requires little training to let the human functional augmentation enforced by the device be enjoyed by the user to its full extent. It is, to use again Peter Cariiani's metaphor, a seamless, transparent, effective connection to a prosthesis—after a while, the user forgets about it and happily uses the device as if it were a part of his own body [2,3]—this phenomenon affects both nondisabled persons in their everyday living as well as patients with musculoskeletal degeneration, amputees, and their phantom limbs, their pain, and sensations, stroke survivors in their rehabilitation process; in Ref. [4], for instance, the effects of tactile (touch) feedback on the perception of their own limbs by amputees is discussed. The rubber hand effect is a similar phenomenon easily

elicited in perfectly healthy subjects [5]. Think about driving one's own car: while driving, can we not say that to some extent *the body of the car becomes a transparent extension of our own bodies?* It is no surprise then, that a lot of research effort has gone into the HMIs devoted to human–robot interaction. A robot is a complex artefact which must sometimes operate in hostile, unstructured environments, and it must be controlled to the best extent possible through a symbiosis, a coupling between man and machine—sometimes even leading to embodiment of a robotic artifact, exactly defined as the feeling that a robot has become a part of the user's own body.

Following up the previous contributions in this book dealing with wearable hardware/wearable robots, in this chapter we talk about some HMIs which are specifically conceived and designed to control wearable robots, specifically for disabled persons such as upper limb amputees, and specifically enforcing coadaptation of man and machine using biological signals. Such HMIs pose to the researcher and the engineer a set of challenges on top of the standard ones—they must be light-weight, low power, robust to signal variability and to the diversity of human interaction with the environment; moreover, most of these interfaces are to be used by persons whose bodily functions are hindered when not almost totally absent, which, if possible, makes their design even harder.

We will first try to highlight the current problems associated with these HMIs, then discuss the pitfalls in which the scientific community is still getting entangled and does not yet clearly know how to overcome, and finally give a set of suggestions/guidelines/design principles on how to sensibly enforce a tight human–machine interaction using them.

20.2 CURRENT PROBLEMS

Let us for the moment restrain to upper limb prosthetics. Upper limb prostheses are possibly the quintessential wearable artefacts: not only *must* they be actually worn to be of any usefulness whatsoever, but they must be unobtrusive, biocompatible, and at the same time they must allow for delicate tasks such as those of daily living (extreme precision) as well as for heavy work in hard weather, in stress conditions, or for long times [6]. Wearing an upper limb prosthesis for 8–12 hours a day must in no way lead to, for example, skin irritation and eczema, body posture alteration, nerve compression, and musculoskeletal impairments related to fatigue. Physical discomfort and mid-term nerve strain or tilted gait are widely reported among the problems associated with active upper limb prostheses [7–9]. Rejection rates still appear to affect one third to 80% of all prosthetic users worldwide [9–11], to the extent that—some authors claim—body-powered arms and grippers are still better than mechatronic arms and hands [6,12]. The main critique is that there is as yet very little a mechatronic arm/hand system (myoprosthesis) can do, that cannot be done using a body-powered device (that is, a mechanical arm operated using a cable harnessed around the shoulders); actually, too little to justify the cost, weight, heat production, and long maintenance times required by these devices. The results of the Cybathlon ARM competition 2016 seem to point in this direction, too [6].

But let us for the sake of the argument assume that we could have at our disposal the ideal, modular, mechatronic arm/hand system: easily adapted to the degree of amputation (trans-radial/trans-humeral amputation, shoulder disarticulation), weighing like a human upper limb, having a similar payload and enough motors/motion capability/strength to restore, say, 95% of the

functionalities lost after an upper limb amputation, both in daily-living activities and during hard work. How would we let a human subject properly control this device?

The answer generally provided by the scientific community (and there is no other one in sight, to the best of our knowledge) is that several different kinds of signals—actually, as many and as diverse as possible—should be used to detect the intended action/movement/application of force/muscle activation [13]. Such representative signals are to be gathered from the subject's body, possibly noninvasively or minimally invasively; then, as directly and naturally as possible, they must be “turned” into those prosthetic control commands required to enact the desired movement/action/activation. Simple as it sounds, this is a so-far by and large unsolved problem [14]. We identify three large areas in the design of an upper limb HMI where the state of the art at the time of writing is still insufficient, namely: the sensors and the signals they provide, their physical interface to the human body; and the control/intent detection system itself.

20.2.1 SENSORS AND BODILY SIGNALS

In mammals, torques and forces at the skeletal joints and, in the very end, movement, are produced via the (voluntary, graded, simultaneous, coordinated) activation of muscles; it is therefore quite an obvious choice, when aiming to detect the intention to move or act with one's arm and hand, to employ sensors able to estimate such activation, either directly connecting to the nerves responsible for motion and sensation in the arm [15] or by exploiting the muscles themselves as amplifiers of the neural signals [16]. We focus on the latter alternative, since the first is still in its infancy mainly due to the technological difficulty associated with a proper, informative, long-lasting and biocompatible connection to nerves. Since the 1950s, the reference method to estimate muscle activity has been surface electromyography (sEMG) [17–19], used to control opening and closing of prosthetic one-degree-of-motion grippers such as, for example, the *SensorHand Speed* by Ottobock [20]. sEMG exploits the depolarization waves traveling along the muscle fibers during muscle activation to estimate the percentage of maximum voluntary contraction currently being enforced [21]; notwithstanding the low intensity of such electrical fields (in the order of magnitude of 10 mV), the cross-talk among adjacent fibers, the attenuation due to fat tissue, and the noise due, among other factors, to muscle fiber recruitment, it turns out that well-engineered sEMG sensors can effectively detect the activation of large surface muscles, or of their remnants after a traumatic event such as an amputation. In practice, in the case, for example, of trans-radial amputees, a physiatrist would spot at least two *loci* of residual *independent, stable, and repeatable* voluntary muscle activity on the patient's stump, and design a housing for such sensors inside a semirigid *socket*, such that the sensors remain in place as precisely as possible. The subject must then learn to activate such muscles (usually, the *m. flexor digitorum superficialis* and the *m. extensor digitorum superficialis*) to operate the opening and closing of the prosthetic gripper. More complex schemata using cocontraction to switch among motors can be used to also control, for example, a wrist rotator.

As early as 1969 though [22], in an attempt to control more than one motor or to enforce more than one movement (opening/closing), researchers have tried to apply *pattern recognition* to an array of more than two sensors. On one hand, this idea has produced the unwanted side-effect that much research has concentrated on improving the recognition method rather than on its practical application—the result is a *corpus* of scientific publications showing improvements of a few percent in offline analysis, with hardly any practical application [14]; whereas, it is now widely

recognized (see, e.g., Refs. [23,24]) that offline classification performance of machine learning methods, as well as performance obtained in highly controlled laboratory conditions, does not generalize to online usefulness. On the other hand, using many sEMG sensors simultaneously has proved to be easy in principle but extremely hard in practice, mainly due to well-known problems associated with sEMG. Such problems would hardly matter when two sensors only are used, and on large superficial muscles, but turn into formidable hurdles in this more complex case: sEMG is extremely sensitive to sensor displacement and detachment from the skin; it can hardly gather the activity of deep muscles due to distance, cross-talk, and fat tissue, in which stumps are usually rich; and even muscular fatigue will significantly change it whenever it kicks in, which unfortunately is usually the case given the weight of prosthetic devices [21]. On top of this, the electronics required for a proper conditioning of many sEMG sensors, with a bandwidth of 15–500 Hz, can be problematic both in terms of computational power, electrical power consumption and—major problem!—weight and heat issues. (The recent advancement proposed in Ref. [25] looks extremely promising in this sense.) Attempts in this sense have appeared in the scientific literature (e.g., [26,27]) and actually, in the case of patients who have undergone targeted muscle reinnervation [28–31], this is still the only possible solution and its drawbacks must somehow be coped with.

The problems associated with sEMG are also being countered, and to some extent solved, although not in clinical practice so far, by employing more invasive forms of sensing—requiring minimal surgery to be implanted in the body. Osseointegration [32] is being tried for trans-radial and trans-humeral amputees as a radical form of man–machine integration: in this case a prosthesis is directly affixed on the stump using a titanium pin housed in the bone stump. This technique solves all sEMG drawbacks due to displacement, cross-talk, and sweat: during the implantation of the pin, intramuscular (nonsurface!) EMG sensors can be fit within the remnants of the stump muscles; cabling occurs *through* the pin itself. The advantages are a higher signal-to-noise ratio than in the surface case and minimal cross-talk due to a careful insertion of the sensors. But even if osseointegration is not planned, bio-compatible miniature EMG sensors can be implanted in the user’s muscle remnants and left inside for an indefinite amount of time; in this case, an electromagnetic induction coil, wrapped around the stump, both supplies power to the sensors and receives their signals [33,34].

On the other hand it has been advocated (e.g., in Refs. [10,13,14]) that novel kinds of sensors be devised, tested, and applied in practice. A plethora of new ways to gather muscle activation has flourished in the academic laboratories: listening to the sound produced by contracting muscles (mechanomyography) [35,36]; using ultrasound imaging or linear sensing to detect the displacement induced by the contraction in the deep structures of the body (sonomyography) [37–40]; using the injection of light or small electrical currents to do the same job (near-infrared spectroscopy, photoplethysmography, electrical impedance tomography); using pressure sensors to detect the deformation induced at the surface of the stump by the contraction (force- or tactilemyography) [41–43]; and even using computer vision to detect such deformation by just looking at the stump (optical myography) [44]. Each novel technique promises a different way to overcome the limitations of sEMG but at the same time introduces new problems and pitfalls: pressure sensing, for instance, is by and large insensitive to sweat and fatigue, but is sensitive to artefacts induced by movement and bumping; ultrasound and similar tomography techniques are usually extremely sensitive to relative motion of sensors and stump, although they provide useful information on the activation and induced motion of deep body structures, usually inaccessible to their surface

counterparts. Optical recognition is probably the most noninvasive technique but, like standard computer vision, it is affected by changes in illumination, position, orientation, and distance. (A thorough review of alternative muscle activation detection techniques can be found in Ref. [45]). To these limitations it must be added that each kind of sensor needs proper signal conditioning, in turn requiring dedicated electronics, which in turn, once again, means power consumption, weight, and heat.

On a slightly different note, inertial sensing and the use of data related to acceleration have gained quite a lot of attention lately [46] and are now being explored as one of the further ways to enhance intent detection: coupling these data through a smart integration/filtering schema, one can reasonably reconstruct the *kinematics* of (the remnants of) the upper limb (relative position, for instance, of the shoulder, upper arm, and lower arm), which is a potentially very useful source of information, since some tasks in daily living are typically performed while enacting a very specific arm/hand configuration. (The Modular Prosthetic Limb [47] in its commercial incarnation, the *Luke Arm*, can even be controlled using inertial sensors placed in the user's shoes [48]!) Properly estimating this configuration can constitute a substantial prior to the prediction of a desired set of actions, namely those involved in a specific task (academic attempts at using such priors appear in, e.g., Refs. [49,50]). For instance, while trying to open a jar by unscrewing the lid, the hands are placed one above the other, one of them holding the jar laterally/cylindrically, while the other one grabs the lid with a circular grasp. This information can be used, for example, to select a subset of the grasping actions available to the control system, thereby improving its recognition rate. A great advantage of these sensors is that they are nowadays cheap, efficient, and extremely light, even when coupled with a wireless transmitter; the popular *Myo* sEMG bracelet by Thalmic Labs (no longer in production) already contains an accelerometer and an inertial measurement unit (IMU).

On the other hand, their usage is limited by the unavoidable integration errors which accumulate through time and appear in the tracking as a drifting behavior. A smart recurrent recalibration schema and/or adaptation by the subject can mitigate this problem. Notice that the usage of an accelerometer and IMU data is already advocated in the 2011 survey [10]. Also, at the time of writing, commercial components which seem to be virtually drift-free have appeared on the market [51].

In general no silver bullet has been found yet: the limitations of sEMG are well known to the community, but no-one knows what novel sensors could replace it, or be proficiently coupled with it, to really get a better understanding of the intended muscle activations. Possibly, force and tactile sensing are the frontrunner (see, e.g., Refs. [42,43,52]).

20.2.2 THE PHYSICAL INTERFACE: PROPERLY HOUSING THE SENSORS

Any HMI of the kind we have described above must be wearable, almost by definition (some of the computation could be devoted to another wearable device, e.g., a smartphone). Additionally, in case the mechatronic device to be controlled is a prosthesis, it must be worn at all times during its usage. This places a non-negligible burden on the user, where *burden* is meant in its literal sense—weight added for the user's body to carry around. Permanently adding weight on a body can have many detrimental consequences—postural problems, nerve and muscle strain, skin edema and rash—for this reason, the design of the physical interface/attachment, the socket, of a prosthesis to the body is an extremely important part of the prosthetic design *tout court*, highly tailored on the user and specifically on the type of amputation (more generally, on the type of disability) [53].

On top of this, sockets for upper limb disabilities must enable the user to achieve the largest possible range of motion, in the ideal case equal to the range enjoyed by the lost limb—especially for shoulder disarticulations this can be highly problematic (see, e.g., Ref. [54] and references therein). Also, sockets must be easy to don and doff, and the performance of the prosthetic system should remain comparably good irrespective of donning and doffing.

In our case, the socket additionally houses the sensors. Traditional sEMG sensors, as well as essentially all sensors being tried in the academic environment, must remain as much as possible in the same spot of the body of the user irrespective of donning/doffing (avoid electrode displacement) and stay in contact with the skin—a detached sensor will yield a signal artefact and confuse the control system (sensor lift-off). Of course, embedded sensors add weight to the socket, as does their power supply and the cabling; and, as mentioned above, some sensors suffer from specific changes in the morphology of the body and from physiological issues. Unfortunately, the added weight calls in the end for more muscular effort, which has the precise effect of eliciting fatigue and changing the muscle configuration. Due to all these reasons, designing a good socket remains more of a highly skilled craft than a science [53,55], and can significantly increase the overall cost of the prosthetic fit.

20.2.3 SIGNAL PROCESSING, MACHINE LEARNING, ADAPTATION

As long as two sEMG sensors are used, a simple form of proportional control has been enforced in the past: the amplitude of the rectified signal is used to operate both ways one motor of the prosthesis. More motors can be controlled by enforcing a coded sequence of activation impulses, for instance cocontraction (simultaneous activation) of the flexor and extensor would signal the desire to switch from controlling the gripper to controlling the elbow [56]. On the other hand, machine learning methods, typically called *pattern recognition* in the medical/rehabilitation field, have been applied whenever more motors needed to be controlled, and/or whenever a relatively larger number of sensors and signals was available [14]. sEMG patterns have been classified in all possible ways, in the hope of detecting what the subject wants to do and accordingly control the prosthesis. Whereas in the beginning this approach seemed highly promising, it was soon discovered that it would rarely work in practice: although extremely high classification rates were obtained while analyzing offline sEMG data collected while one or more subjects were enforcing grasping patterns (usually in highly controlled laboratory conditions), this would not correspond to any practically applicable control system [23,24]. The only success story so far is represented by CoApt Engineering’s *Complete Control* system [57], which employs up to eight sEMG sensors and an entry-level classification method to actuate three motors (wrist, elbow, and hand) [58]. In fact, to the best of our knowledge, the overwhelming majority of machine learning/pattern recognition systems tried out in the literature are *classifiers*, which ironically gives up on proportional control of force and velocity, which is enjoyed by the traditional two-sensors schema. For this reason, in the 2000s, the idea of using simultaneous and proportional control was introduced [59,60], leading to natural enforcement of the user’s intent (intent detection).

All in all however, even if we are restricted to the machine learning method, that is without considering the quality of the signals and of the socket, it has been remarked that (1) the variety of situations to be encountered in the real world while operating a self-powered prosthesis in daily living is overwhelming with respect to the typical initial calibration [61]; at the same time, (2) the

classification accuracy which *true* prosthetic usage requires is way higher than any value so far achieved in controlled conditions [6].

On top of this, any machine learning method designed for practical usage should be compact enough to be run on a microcontroller, or at least on a portable device such as a smartphone; also, calibration times cannot exceed a reasonable threshold, due to the expectation of the subject being able to seamlessly and quickly use the device at all times.

For these reasons, incremental and/or bounded approaches have lately been preferred [62,63]. Incremental approaches also have the advantage of engaging the user in an interactive loop, which potentially induces coadaptation leading to an ever-better symbiosis with the prosthetic device [1,64]. These remarks also justify the success obtained by the Complete Control system: the actions controlled by the system are enforced by independent groups of muscles (hand, wrist, elbow), resulting in highly separable and repeatable patterns, even given the small number of sensors. On top of that, the “recalibration” procedure allowed for by Complete Control allows to somehow counter the nonstationarity of sEMG. To some extent, this looks like the need for periodical recalibration of IMU and accelerometer sensors. As long as recalibration is fast and does not need to happen too often, it is fine and the system is practically usable. It seems that so far the simplest solution is the winning one, at least from a commercial point of view [65,66].

20.3 DESIGN GUIDELINES FOR A WEARABLE UPPER LIMB INTERFACE

Let us then try to imagine how the ideal HMI would look. Although we hereby focus on upper limb *prosthetics*, most of what we say here also applies to other applications for such an HMI: for instance, a robotic arm/hand system teleoperated by intact (i.e., nonamputated) human subjects [67], either in an assistive or industrial scenario; or an *app* on a consumer smartphone, through which to control one’s own self-driving car, smart home, and appliances, an avatar in virtual or augmented reality, and so on. We claim that prosthetics are among the hardest applications for such an HMI, meaning that if it works in this case it will probably also work in many other cases. (See also the final remarks to this chapter.) Therefore at the time of writing and to the best of our knowledge, the most advanced complete, certified prosthetic arm is the Modular Prosthetic Limb (MPL), developed at the Johns Hopkins University [47], now in its initial clinical evaluation [68]. Upper limb amputations constitute a wide range of different disabilities, mainly depending on the level of amputation (trans-radial, trans-humeral, shoulder); the MPL was designed modularly, in order to be adapted to the type of amputation. What would the ideal HMI for the MPL look like?

20.3.1 CURRENT PITFALLS

At the beginning of this chapter we called for two main characteristics of the ideal HMI: dexterity and intuitiveness. Matching these two requirements with the overview of the state of the art presented in the previous section, we can identify the following pitfalls that currently hinder the way toward the ideal HMI:

- *Nonsystematic design of sockets.* Physically connecting the sensors, the electronics, and the prosthetic device to the subject’s body is still a manual craft, largely varying in quality across

countries and even rehabilitation facilities within the same country. Three-dimensional (3D) laser scanning, the use of professional CAD design, and 3D printing, could be useful tools toward mechanization/standardization of the procedure to build sockets—including precise tailoring of the socket to the needs of the patient and to the device to be used.

- *Too little knowledge about sensing.* What kind of sensors are better suited to detect which kind of activity; what features to extract from each data stream; and how to combine the sensors, both in hardware and in software; these factors are still, in practice, unknown.
- *Too few sensors and/or insufficient targeting of the stump.* Irrespective of the kind of sensors and their combination, *more* sensors are very likely to be required to build a control system at the ideal level of dexterity of an HMI. To this aim, we should either enforce higher spatial resolution, that is, many smaller sensors uniformly placed on the user's body, and/or better targeting of the *loci* of activity the control system is interested in recognizing. (Targeted muscle reinnervation is a remarkable step in this direction.)
- *Weight, power consumption, biocompatibility, appearance.* The whole system must be worn for a long time without causing postural and/or skin problems; therefore it must be ergonomic and lightweight, produce as little heat as possible, consume as little power as possible, enforce biocompatibility and resilience to body shape changes and sweating, and last but not least it must look human in order to be socially acceptable. These aspects are frequently mentioned passim, neglected, or even omitted from the scientific research—the integration of all these requirements constitutes a *formidable interdisciplinary challenge*, whereas research teams often tend to concentrate on other aspects [6].
- *Nonnatural control.* Back to the remark we made at the very beginning of this chapter, *control is as important as the tool to be controlled*. Now, controlling the ideal upper limb prosthesis is a complicated task; therefore (1) *natural myocontrol* must be provided (simultaneous, proportional, incremental), and (2) the control system as a whole must work through an effective *graphical* user interface—much like what the Android or iOS operating systems are to smartphones. The functionalities offered by contemporary smartphones are extremely complicated in principle; nevertheless, such operating systems turn learning to use such devices into a simple, intuitive, exciting experience. So should be the “operating system”/GUI of a dexterous prosthetic device.
- Last but not least, *lack of coadaptation*. A prosthesis should in the end become an intimate object, a part of the user's body, which, given the current state-of-the-art, is impossible. The ideal HMI is so fast, precise, responsive, and intuitive that it provides the user with a strong feeling of immersion since the start; if the device responds quickly enough, the immersion can be so strong that the user will introject the device as well as the control system itself, embodying the system.

This issue is strongly coupled with the

- *lack of sensory feedback*, which is a so-far much less explored field than that of intent detection (feedforward signal processing versus feedback signal interpretation leading to sensory substitution) [69]. The ideal HMI is actually a *bidirectional* HMI (bHMI).

20.3.2 IMPLEMENTATION AND TESTING

Implementing a bHMI which overcomes the above-mentioned problems implies several design requirements. We hereby divide these into two categories: *patient-specific* and *nonpatient-specific*.

Patient-specific requirements are those constraints imposed on the bHMI which arise from the user's needs and desires. Given the level of amputation, the condition of the stump, and the general psychophysical condition, and given the available prosthetic device, the design of the ideal bHMI goes through the following steps:

- Identifying the remaining muscle activity and matching it with the degrees of activation (motors) offered by the prosthesis; in the presence of TMR, the use of the sensorimotor reinnervation map is paramount;
- Choosing a set of sensors adequate to detect the remaining activity as best as possible, and to control all possible degrees of motion of the prosthesis;
- Choosing the optimal placement of the sensors and accordingly designing the socket—this step must by all means take into account the musculoskeletal condition of the user.

Nonpatient-specific requirements are, moreover:

- To embed the computation (that is, the required electronics) inside the socket/prosthesis complex; or at least, that the computing machinery be unobtrusively wearable, for example, on a smartphone or a tablet;
- To keep the system as light and low power as possible; a reasonable estimation is weighing less than 400 g including the battery and lasting at least 8 hours;
- To provide natural, simultaneous, and proportional control over all degrees of motion of the prosthesis;
- To provide an incremental machine learning system as the core control component, in turn providing on-demand model updates and corrections; and lastly,
- To provide an intuitive user interface to manage the interaction.

20.3.3 FINAL REMARK: NOT JUST PROSTHETICS

We believe that a bHMI such as the one outlined above also has a range of less dramatic, but not less interesting and useful, applications. Training an amputated person to use such a system entails inducing this person to produce “ever-better” signals, enforcing clearer patterns in the course of time. Given the lack of sensorimotor feedback caused by an amputation, or even worse, the presence of a strong phantom feeling which potentially contradicts the motor intention, this learning process is usually long and, in some cases, even painful. Therefore applying these guidelines to “simpler” applications should be possible with a reasonable effort; here are a few directions in which the strong requirements on upper limb prosthetics can be lifted, in each case leading to a new realm of possibilities for the ideal bHMI.

1. *Amputated persons could use the bHMI to control an avatar in virtual reality/augmented reality (VR/AR) instead of in real tasks—they would literally see their missing limb back in action, with potentially astounding psychological effects.* VR/AR has two advantages with respect to prosthetics: first, the unlimited range of possibilities for the experimenter to build worlds exactly targeted at a specific objective to be enforced by the system—serious games to reduce phantom-limb pain, a mechatronic simulation of the prosthesis the patient is waiting to receive, and so on. Second, the lack of haptic interaction with the virtual world: the weight added to the musculoskeletal system while grasping, carrying, and manipulating an object in “real reality”

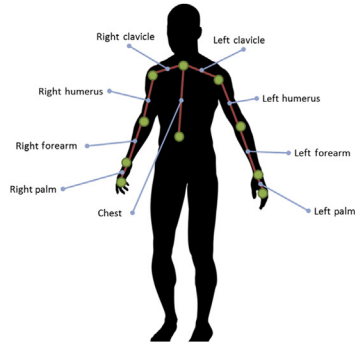


FIGURE 20.1

(Left) Sketch of a bidirectional HMI consisting of an intent-detection/sensory feedback bracelet with embedded IMU on the user's forearm or stump (3), two further IMUs on the user's back and upper arm (1, 2), a Bluetooth transmitter (1) and a battery (1). (Center) Abstract schema of a possible placement of parts of the interface. (Right) A prototype of such an interface, currently in use at the author's laboratory.

Claudio Castellini and Marek Sierotowicz with permission.

will significantly alter the user's muscle configuration, leading to instability in machine-learning-based control methods. In VR/AR this problem does not exist, leading to a simplified interaction with the virtual world. (Note that the lack of haptics is deemed to be the main drawback of VR/AR, but here it can be exploited for a good reason.)

2. *Intact subjects could use the bHMI better than amputated/disabled persons* (although, see, e.g., Ref. [43] for a somewhat contradictory example). In the case of able-bodied people designing the physical attachment is simpler, and the healthy sensorimotor feedback helps to produce exactly the required signals. Therefore the bHMI could proficiently be used to have intact users teleoperate their avatars in VR/AR, or an arm/hand system in a remote location. Interfaces such as this could not enforce the same *precision* a standard HMI does—picture position control using sEMG versus magnetic or optical motion tracking of an arm, or even simply the usage of a joystick—still they can enforce a more natural control, leaving the hands of the subject free to operate (i.e., no sensors/markers on the fingers, nor a glove) and be light, a very desirable characteristic when operating, for example, in space.

As an example, Fig. 20.1 is our personal view of one such ideal bHMI, one which would work for both able-bodied and trans-radially amputated persons, both in VR/AR and in reality, both while using an upper-limb active prosthesis and a tele-operated arm/hand system. The interface consists of three submodules: an intent-detection/sensory feedback bracelet with embedded IMU placed on the forearm, and two more IMUs placed on the user's back and upper arm. Intent detection happens using, for example, sEMG, force, or tactile sensors embedded in the bracelet; sensory feedback is enforced via electro-cutaneous stimulation [69]; and thanks to the three IMUs the kinematics of the arm/hand can be reconstructed. A standard transmitter, for instance via Bluetooth, embedded in one of the submodules, makes the bHMI completely wireless, giving the user maximum freedom of movement. The total weight of such an interface is estimated in a few hundred grams including one or more batteries. All required computation can be run on a portable device such as, for example, a smartphone, or, most likely, even on a microcontroller embedded in one of the submodules.

ACKNOWLEDGMENT

I would like to thank Mr. Marek Sierotowicz of the DLR for providing parts of Fig. 20.1. These parts appear in his M.Sc. thesis, as yet unpublished.

REFERENCES

- [1] M. Nowak, C. Castellini, C. Massironi, Applying radical constructivism to machine learning: a pilot study in assistive robotics, *Constr. Foundat.* 13 (2018) 250–262.
- [2] M.J. Giummarra, S.J. Gibson, N. Georgiou-Karistianis, J.L. Bradshaw, Mechanisms underlying embodiment, disembodiment and loss of embodiment, *Neurosci. Biobehav. Rev.* 32 (2008) 143–160.
- [3] B. Lenggenhager, A. Carolyn, J. Giummarra Melita, Phantom limbs: pain, embodiment, and scientific advances in integrative therapies, *Wiley Interdiscip. Rev. Cognit. Sci.* 5 (2014) 221–231.
- [4] P.D. Marasco, K. Kim, J.E. Colgate, M.A. Peshkin, T.A. Kuiken, Robotic touch shifts perception of embodiment to a prosthesis in targeted reinnervation amputees, *Brain* 134 (2011) 747–758.

- [5] M. Botvinick, J. Cohen, Rubber hands “feel” touch that eyes see, *Nature* 391 (1998) 756.
- [6] W. Schweitzer, M.J. Thali, D. Egger, Case-study of a user-driven prosthetic arm design: bionic hand versus customized body-powered technology in a highly demanding work environment, *J. Neuroeng. Rehabil.* 15 (2018).
- [7] S. Micera, J. Carpaneto, S. Raspovic, Control of hand prostheses using peripheral information, *IEEE Rev. Biomed. Eng.* 3 (2010) 48–68.
- [8] B. Peerdeman, D. Boere, H. Witteveen, R.H. in ’t Veld, H. Hermens, S. Stramigioli, et al., Myoelectric forearm prostheses: state of the art from a user-centered perspective, *J. Rehabil. Res. Dev.* 48 (2011) 719–738.
- [9] S.M. Engdahl, B.P. Christie, B. Kelly, A. Davis, C.A. Chestek, D.H. Gates, Surveying the interest of individuals with upper limb loss in novel prosthetic control techniques, *J. Neuroeng. Rehabil.* 12 (2015) 53.
- [10] A. Fougnier, Ø. Stavdahl, P.J. Kyberd, Y.G. Losier, P.A. Parker, Control of upper-limb prostheses: terminology and proportional myoelectric control — a review, *IEEE Trans. Neur. Syst. Rehabil. Eng.* 20 (2012) 663–677.
- [11] R.N. Scott, P.A. Parker, Myoelectric prostheses: state of the art, *J. Med. Eng. Technol.* 12 (1988) 143–151.
- [12] G. Smit, R. Bongers, C. Sluis, D. Plettenburg, Efficiency of voluntary opening hand and hook prosthetic devices: 24 years of development? *J. Rehabil. Res. Dev.* 49 (2012) 523–534.
- [13] N. Jiang, S. Dosen, K.-R. Müller, D. Farina, Myoelectric control of artificial limbs - is there a need to change focus? *IEEE Signal Process. Mag.* 29 (2012) 148–152.
- [14] C. Castellini, P. Artermiadis, M. Wininger, A. Ajoudani, M. Alimusaj, A. Bicchi, et al., Proceedings of the first workshop on Peripheral Machine Interfaces: going beyond traditional surface electromyography, *Front. Neurorobot.* 8 (2014).
- [15] S. Raspovic, M. Capogrosso, F.M. Petrini, M. Bonizzato, J. Rigosa, G. Di Pino, et al., Restoring natural sensory feedback in real-time bidirectional hand prostheses, *Sci. Translat. Med.* 6 (222) (2014) 222ra19.
- [16] D. Farina, I. Vujaklija, M. Sartori, T. Kapelner, F. Negro, N. Jiang, et al., Man/machine interface based on the discharge timings of spinal motor neurons after targeted muscle reinnervation, *Nat. Biomed. Eng.* 1 (2017).
- [17] R. Merletti, P.A. Parker, *Electromyography: Physiology, Engineering, and Noninvasive Applications*, vol. 11, Wiley-IEEE Press, 2004.
- [18] R. Merletti, A. Botter, C. Cescon, M.A. Minetto, T.M.M. Vieira, Advances in surface EMG: recent progress in clinical research applications, *Crit. Rev. Biomed. Eng.* 38 (2011) 347–379.
- [19] R. Merletti, A. Botter, A. Troiano, E. Merlo, M.A. Minetto, Technology and instrumentation for detection and conditioning of the surface electromyographic signal: state of the art, *Clin. Biomech.* 24 (2009) 122–134.
- [20] Myoelectric Speed hands by Ottobock SE & Co. KGaA, 2019. [Online]. Available from: <https://www.ottobockus.com/prosthetics/upper-limb-prosthetics/solution-overview/myoelectric-devices-speedhands/index.html>.
- [21] M. Zecca, S. Micera, M.C. Carrozza, P. Dario, Control of multifunctional prosthetic hands by processing the electromyographic signal, *Crit. Rev. Biomed. Eng.* 30 (2002) 459–485.
- [22] D.A. Childress, A myoelectric three-state controller using rate sensitivity, in: *Proceedings 8th ICMBE*, Chicago, IL, 1969.
- [23] M. Ortiz-Catalan, F. Rouhani, R. Bränemark, B. Håkansson, Offline accuracy: a potentially misleading metric in myoelectric pattern recognition for prosthetic control, in: *2015 37th Annual International Conference of the IEEE Engineering in Medicine and Biology Society (EMBC)*, 2015.
- [24] N. Jiang, I. Vujaklija, H. Rehbaum, B. Graumann, D. Farina, Is accurate mapping of EMG signals on kinematics needed for precise online myoelectric control? *IEEE Trans. Neural. Syst. Rehabil. Eng.* 22 (2013) 549–558.

- [25] G.L. Cerone, A. Botter, M. Gazzoni, A modular, smart, and wearable system for high density sEMG detection, *IEEE Trans. Biomed. Eng.* (2019).
- [26] M. Ison, I. Vujaklija, B. Whitsell, D. Farina, P. Artermiadis, High-density electromyography and motor skill learning for robust long-term control of a 7-DoF robot arm, *IEEE. Trans. Neural. Syst. Rehabil. Eng.* 24 (2016) 424–433.
- [27] S. Muceli, N. Jiang, D. Farina, Extracting signals robust to electrode number and shift for online simultaneous and proportional myoelectric control by factorization algorithms, in: *Neural Systems and Rehabilitation Engineering*, IEEE Transactions, 2013.
- [28] T. Kuiken, Targeted reinnervation for improved prosthetic function, *Phys. Med. Rehabil. Clin. N. Am.* 17 (2006) 1–13.
- [29] T.A. Kuiken, L.A. Miller, R.D. Lipschutz, B.A. Lock, K. Stubblefield, P.D. Marasco, et al., Targeted reinnervation for enhanced prosthetic arm function in a woman with a proximal amputation: a case study, *Lancet* 369 (2007) 371–380.
- [30] G. Li, A.E. Schultz, T.A. Kuiken, Quantifying pattern recognition-based myoelectric control of multi-functional transradial prostheses, *IEEE. Trans. Neural. Syst. Rehabil. Eng.* 18 (2010) 185–192. 4.
- [31] L.J. Hargrove, B.A. Lock, A.M. Simon, Pattern recognition control outperforms conventional myoelectric control in upper limb patients with targeted muscle reinnervation, in: 2013 35th Annual International Conference of the IEEE Engineering in Medicine and Biology Society (EMBC), 2013.
- [32] E. Mastinu, P. Doguet, Y. Botquin, B. Håkansson, M. Ortiz-Catalan, Embedded system for prosthetic control using implanted neuromuscular interfaces accessed via an osseointegrated implant, *IEEE Trans. Biomed. Circ. Syst.* 11 (2017) 867–877.
- [33] T.R. Farrell, R.F. Weir, A comparison of the effects of electrode implantation and targeting on pattern classification accuracy for prosthesis control, *IEEE Trans. Biomed. Eng.* 55 (2008) 2198–2211.
- [34] W.R.F.P.R. Troyk, G.A. DeMichele, D.A. Kerns, J.F. Schorsch, H. Maas, Implantable Myoelectric sensors (IMESs) for intramuscular electromyogram recording, *IEEE. Trans. Biomed. Eng* 56 (2009) 159–171.
- [35] C. Orizio, Surface mechanomyogram, in: R. Merletti, P. Parker (Eds.), *Electromyography: Physiology, Engineering, and Noninvasive Applications*, Wiley-IEEE Press, 2004, pp. 305–322.
- [36] Z.F. Yang, D.K. Kumar, S.P. Arjunan, Mechanomyogram for identifying muscle activity and fatigue, in: *Engineering in Medicine and Biology Society*, 2009. EMBC 2009. Annual International Conference of the IEEE, 2009.
- [37] J.I.N.G.-Y.I. Guo, Y.O.N.G.-P.I.N.G. Zheng, L.P.J. Kenney, A. Bowen, D. Howard, J.J. Canderle, A comparative evaluation of sonomyography, electromyography, force, and wrist angle in a discrete tracking task, *Ultrasound Med. Biol.* 37 (2011) 884–891.
- [38] C. Castellini, in: P. Artermiadis (Ed.), *Neuro-Robotics: From Brain Machine Interfaces to Rehabilitation Robotics*, Springer, Netherlands, 2014, pp. 37–58.
- [39] Y. Li, K. He, X. Sun, H. Liu, Human-machine interface based on multi-channel single-element ultrasound transducers: a preliminary study, in: 2016 IEEE 18th International Conference on e-Health Networking, Applications and Services (Healthcom), 2016.
- [40] S. Sikdar, H. Rangwala, E.B. Eastlake, I.A. Hunt, A.J. Nelson, J. Devanathan, et al., Novel method for predicting dexterous individual finger movements by imaging muscle activity using a wearable ultrasonic system, *Neur. Syst. Rehabil. Eng. IEEE Trans.* 22 (2014) 69–76.
- [41] M. Wininger, N. Kim, W. Craelius, Pressure signature of forearm as predictor of grip force, *J. Rehabil. Res. Dev.* 45 (2008) 883–892.
- [42] E. Cho, R. Chen, L.-K. Merhi, Z. Xiao, B. Pousett, C. Menon, Force myography to control robotic upper extremity prostheses: a feasibility study, *Front. Bioeng. Biotechnol.* 4 (2016) 18.
- [43] C. Castellini, R. Kõiva, C. Pasluosta, C. Viegas, B.M. Eskofier, Tactile myography: an off-line assessment on able-bodied subjects and one upper-limb amputee, *MDPI Technol.* 6 (2018) 38.

- [44] C. Nissler, N. Mouriki, C. Castellini, Optical myography: detecting finger movements by looking at the forearm, *Front. Neurorobot.* 10 (2016).
- [45] Y. Fang, N. Hettiarachchi, D. Zhou, H. Liu, Multi-modal sensing techniques for interfacing hand prostheses: a review, *IEEE. Sens. J.* 15 (2015) 6065–6076.
- [46] A. Krasoulis, I. Kyranou, M.S. Erden, K. Nazarpour, S. Vijayakumar, Improved prosthetic hand control with concurrent use of myoelectric and inertial measurements, *J. Neuroeng. Rehabil.* 14 (2017) 71.
- [47] G. Hotson, D.P. McMullen, M.S. Fifer, M.S. Johannes, K.D. Katyal, M.P. Para, et al., Individual finger control of a modular prosthetic limb using high-density electrocorticography in a human subject, *J. Neural. Eng* 13 (2016) 026017.
- [48] The LUKE Arm by Mobius Bionics, 2019. [Online]. Available from: <http://www.mobiusbionics.com/>.
- [49] K.J.K. Minas, V. Liarokapis, P. Artermiadis, in: P. Artermiadis (Ed.), *Neuro-Robotics: From Brain Machine Interfaces to Rehabilitation Robotics*, vol. 2, Springer, Netherlands, 2014, pp. 3–36.
- [50] G. Patel, M. Nowak, C. Castellini, Exploiting knowledge composition to improve real-life hand prosthetic control, *IEEE. Trans. Neural. Syst. Rehabil. Eng* 25 (2017) 967–975.
- [51] BNO055 inertial measurement unit by Bosch, 2019. [Online]. Available from: https://www.bosch-sensortec.com/bst/products/all_products/bno055.
- [52] A. Radmand, E. Scheme, K. Englehart, High-density force myography: a possible alternative for upper-limb prosthetic control, *J. Rehabil. Res. Dev* 53 (2016) 443–456.
- [53] C. Lake, The evolution of upper-limb prosthetic socket design, *J. Prosthet. Orthot.* 20 (2008) 85–92.
- [54] Ovadia, M. Askari, Upper extremity amputations and prosthetics, *Semin. Plast. Surg.* 29 (2015) 55–61.
- [55] R.D. Alley, T.W. Williams, M.J. Albuquerque, D.E. Altobelli, Prosthetic sockets stabilized by alternating areas of tissue compression and release, *J. Rehabil. Res. Dev.* 48 (2011) 679–696.
- [56] D.S. Childress, R.F. Weir, Upper-limb prosthetics: control of limb prostheses, in: H.K. Bowler, J.W. Michael (Eds.), *Atlas of Limb Prosthetics: Surgical, Prosthetic, and Rehabilitation Principles*, second ed, C. V. Mosby, 1992.
- [57] Complete Control by CoApt, LLC, 2019. [Online]. Available from: <https://www.coaptengineering.com>.
- [58] A.M. Simon, B.A. Lock, K.A. Stubblefield, Patient training for functional use of pattern recognition-controlled prostheses, *J. Prosthet. Orthot.* 24 (2012) 56–64.
- [59] N. Jiang, K. Englehart, P. Parker, Extracting simultaneous and proportional neural control information for multiple degree of freedom prostheses from the surface electromyographic signal, *IEEE Trans. Biomed. Eng.* 56 (2009) 1070–1080.
- [60] A.J. Young, L.H. Smith, E.J. Rouse, L.J. Hargrove, A new hierarchical approach for simultaneous control of multi-joint powered prostheses, in: 2012 4th IEEE RAS EMBS International Conference on Biomedical Robotics and Biomechatronics (BioRob), 2012.
- [61] C. Castellini, in: M. Bianchi, A. Moscatelli (Eds.), *Human and Robot Hands: Sensorimotor Synergies to Bridge the Gap Between Neuroscience and Robotics*, Springer International Publishing, 2016, pp. 171–193.
- [62] P.M. Pilarski, M.R. Dawson, T. Degris, F. Fahimi, J.P. Carey, R.S. Sutton, Online human training of a myoelectric prosthesis controller via actor-critic reinforcement learning, in: 2011 IEEE International Conference on Rehabilitation Robotics (ICORR), 2011.
- [63] I. Strazzulla, M. Nowak, M. Controzzi, C. Cipriani, C. Castellini, Online bimanual manipulation using surface electromyography and incremental learning, *IEEE. Trans. Neural. Syst. Rehabil. Eng.* 25 (2017) 227–234.
- [64] J.M. Hahne, M. Markovic, D. Farina, User adaptation in myoelectric man-machine interfaces, *Sci. Rep.* 7 (2017).

- [65] J.W. Sensinger, B.A. Lock, T.A. Kuiken, Adaptive pattern recognition of myoelectric signals: exploration of conceptual framework and practical algorithms, *IEEE Trans. Neural. Syst. Rehabil. Eng.* 17 (2009) 270–278.
- [66] A.M. Simon, L.J. Hargrove, B.A. Lock, T.A. Kuiken, Target Achievement Control Test: evaluating real-time myoelectric pattern-recognition control of multifunctional upper-limb prostheses, *J. Rehabil. Res. Dev.* 48 (2011) 619–627.
- [67] A. Gijsberts, R. Bohra, D. Sierra González, A. Werner, M. Nowak, B. Caputo, et al., Stable myoelectric control of a hand prosthesis using non-linear incremental learning, *Front. Neurorobot.* 8 (2014).
- [68] B.N. Perry, C.W. Moran, R.S. Armiger, P.F. Pasquina, J.W. Vandersea, J.W. Tsao, Initial clinical evaluation of the modular prosthetic limb, *Front. Neurol.* 9 (2018) 153.
- [69] M. Štrbac, M. Belić, M. Isaković, V. Kojić, G. Bijelić, I. Popović, et al., Integrated and flexible multi-channel interface for electrotactile stimulation, *J. Neural. Eng.* 13 (2016) 046014.

THE MODULAR PROSTHETIC LIMB

21

Matthew S. Johannes¹, Eric L. Faulring², Kapil D. Katyal¹, Matthew P. Para¹, John B. Helder¹, Alexander Makhlin¹, Tom Moyer², Daniel Wahl², James Solberg², Steve Clark², Robert S. Armiger¹, Travis Lontz², Kathryn Geberth², Courtney W. Moran¹, Brock A. Wester¹, Thomas Van Doren² and Julio J. Santos-Munne²

¹The Johns Hopkins University Applied Physics Laboratory, Laurel, MD, United States

²HDT Global, Solon, OH, United States

21.1 INTRODUCTION AND OVERVIEW

21.1.1 BACKGROUND

In 2005, the Defense Advanced Research Projects Agency (DARPA) selected the Johns Hopkins University Applied Physics Laboratory (JHU/APL) as one of two primary participants to execute the Revolutionizing Prosthetics program.¹ Our mission was to replicate the functionality of the human arm and hand through a neurally integrated prosthetic system to a level of complexity and capability never before realized. Neurally integrated implied leveraging emerging technologies for bidirectional man–machine interaction through implantable cortical or peripheral nerve electrodes [2,3]. The vision was to create a prosthetic arm system that sought to match the dexterity, size, weight, strength, speed, and sensory capabilities of the natural arm. To that end a large set of challenging requirements were established (Table 21.1), which flowed down to key specifications for the subsystems. The overall goal was to meet as many of these challenging requirements as possible subject to engineering and technological feasibility in an anthropomorphic form factor. To reduce risk at each iteration, a phased approach was adopted for the design iterations. APL—while a large institution with far-reaching capabilities and resources—realized at the outset that a large multiinstitutional and international team of domain experts with diverse skill sets across industry, government, and academia was necessary to ensure success. Here we highlight and overview the design and development of the Modular Prosthetic Limb (MPL), covering its historical evolution and design, highlight details of the current system, and briefly describe select applications of the technology.

At the program start, given the nature of the challenging requirements set and vision for neural integration there was a possibility that the program goal might not be realized due to technical infeasibility and modern engineering constraints. In order to create a fully anthropomorphic prosthetic device coupled with lofty goals for full closed loop cortical control reaching levels beyond

¹The other institution was Deka Integrated Solutions Corp. which developed the Luke Arm [1].

Table 21.1 Select Challenging High-Level Requirements Influencing the MPL Design

Performance and Function	Environmental, Sustainability, and Reliability
Weigh less than 3.9 kg (8.6 lbs.)	Survive rain up to 4 in. per hour
Match human limb inertial properties	Survive blowing dust and sand per MIL-810
Provide 81.3 Nm of torque at elbow	Survive 3 ft. drop
Provide 13.6 Nm of torque at wrist flex/extend	Function after patient fall on prosthetic
Hand cylindrical grasp strength of 311 N	24 h of operation on a single charge
Unloaded joint speeds of 120 degrees per second	Wearable up to 18 h with no ill effects
Full hand and arm articulation capabilities	Production cost of \$50,000
All actuated joint torque sensing	Maintenance cost of \$500 per year or less
All revolute joint position/velocity sensing	Shoulder, elbow, and wrist quick releases
Fingertip force sensing of 0–5 N, 0.1 N resolution	MTBF of 3000 h
Fingertip spatial touch discrimination of 2 mm	MTBM of 1500 h
Accommodate all amputation levels from shoulder to wrist disarticulation	MTTR of 2 h
Natural swing kinematics during running	Chronically implantable neural interface components

all efforts to date, the APL team assembled a collaborative international multiinstitutional team. APL assumed the role of lead institution and developer, seeking experts in the fields of clinical prosthetics, prosthetic device manufacturing, electromechanical system design, implantable neural device and electrode manufacturing, sensors, actuators, materials science, neurosurgery, and neuroscience to round out technical proficiencies and fill development gaps. The ~50 primary participating institutions in the Revolutionizing Prosthetics Program coordinated by APL are highlighted in [Table 21.2](#), which highlights the breadth of expertise that contributed to the various prototype prosthetic designs, technological capabilities, and clinical experiments.

21.1.2 EARLY DEVELOPMENT: PROTOTYPES AND PHASES

A component of DARPA's vision early in the program was to not assume that any singular technology or approach would be sufficient to meet program goals. The entire team was very much interested in leveraging novel and cutting-edge research technologies and approaches to see if they could be adopted to produce revolutionary prosthetic limb capabilities. This was driven in part by open questions as to the feasibility of reaching program goals given conventional prosthetic technologies. A key overarching challenge was to create a prosthetic limb that met the mass target but achieved the strength requirements. This required actuation technologies that were very efficient and had high specific torque density (Nm/kg). To this end, numerous members of our team were experts in novel actuation technologies that could be brought to the development process for an advanced, neurally integrated prosthetic limb. The scope was broad, but a few of these technologies beyond traditional electromechanical actuation approaches included mesofluidic [\[4\]](#), pneumatic driven by liquid propellants [\[5\]](#), electroactive polymers [\[6\]](#), and continuously variable transmissions

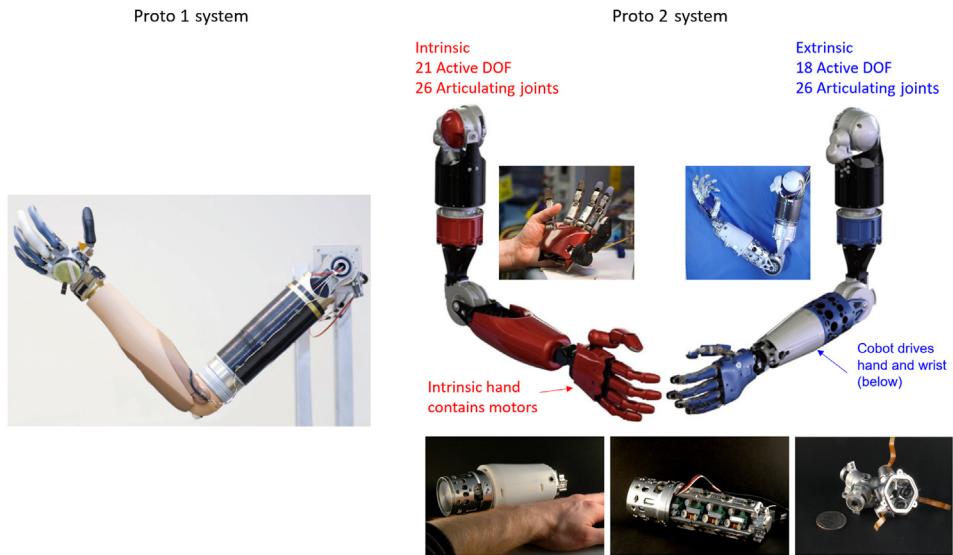
Table 21.2 APL's Collaborating Institutions in the Revolutionizing Prosthetics Program

The Alfred E. Mann Foundation	Arizona State University
BioStar Group	Blackrock Microsystems
Booz Allen Hamilton	Chicago Physical Therapists LLC
The California Institute of Technology	The Defense Advanced Research Projects Agency
Duke University	Flexsys Incorporated
Fraunhofer Society	HDT Global
Illinois Institute of Technology	The Johns Hopkins University
The Johns Hopkins Medical Institute	Harvey Mudd College
IDEO	Kinea Design
National Institute of Aerospace	Martin Bionics
The National Aeronautics and Space Administration	The National Rehabilitation Hospital
New World Associates	Northwestern University
Oak Ridge National Laboratories	Orthocare Innovations
Otto Bock	Punch Communications
Ripple LLC	Rockwell Scientific
The Rehabilitation Institute of Chicago	Rutgers University
Science and Technology Associates	Scott Sabolich Prosthetics and Research
Scuola Superiore Sant'Anna	Space and Naval Warfare Systems Command
Stanford University	Sigenics Incorporated
Umea University	The University of California Irvine
The University of Chicago	The University of Michigan
The University of New Brunswick	The University of Pittsburgh
The University of Rochester	The University of Southern California
The University of Texas Health Science Center	The University of Utah
Vanderbilt University	Van Doren Designs LLC
Walter Reed National Military Medical Center	

(CVTs) [7]. Given that there were many candidate technologies and approaches to consider going forward, a three-phase effort for the program was executed, which resulted in five total revisions of the prosthetic system. At the end of each phase, mature and proven technologies were selected for further refinement going forward. The three phases are discussed in brief below while additional detailed information can be found in Ref. [8].

21.1.2.1 Phase 1

The early phase 1 effort focused on realizing an initial prototype system that leveraged a combination of commercial off the shelf (COTS) prosthetic components married with low-risk capabilities to realize a seven active DoF prosthetic system (Proto 1, Fig. 21.1, left) by the end of the first year (December 2006). The system was eventually clinically tested using surface electromyography on a patient who had undergone targeted muscle reinnervation [9]. Proto 1 leveraged some COTS components such as active wrist rotation, elbow flexion/extension (F/E), and humeral rotation found in the AxonArm (Ottobock) coupled with a passive shoulder abduction/adduction (A/A) joint, which

**FIGURE 21.1**

Phase 1 limb systems. (Left) Proto 1 leveraged a combination of COTS available solutions as well as emergent and specifically designed capabilities. (Right) The two Prototype 2 systems varied in the location of hand actuators. The Intrinsic system (red) had actuation located within the hand, while the Extrinsic system (blue) had all actuators located in the forearm where finger and wrist joints were tendon driven. Detailed images of a CVT for actuation of the extrinsic Proto 2 system.

JHU/APL and HDT.

was a variant of the Liberating Technologies Inc. Locking Shoulder Joint. These were combined with a custom-designed active shoulder and wrist F/E drives as well as an early prototype version of the Michelangelo hand under development by Ottobock, which could realize two grasps patterns (lateral and power) with actuators in the palm and thumb. Additionally in phase 1, there were specific research investigations and experiments seeking to provide data and results necessary to inform critical down-selections and gating decision processes for candidate technologies going forward for subsequent systems. In particular, the development of the Prototype 2 systems (Fig. 21.1, right) completed in December 2007 narrowed down actuation approaches to identify electromechanical actuation as the primary methodology going forward over more exotic approaches due to factors such as efficiency, packaging, maturity, safety, and reliability. The two separate prototype limb systems, one intrinsically actuated (motors within the hand) and the other extrinsically actuated (a CVT [7] in the forearm driving tendons to the wrist and fingers) shared a common upper arm design with active three-DoF shoulder and elbow. Both systems had different active three-DoF wrist designs. The intrinsically actuated system had an active three-DoF thumb, four active two-DoF (one-DoF underactuated) fingers, active index, ring, and little finger A/A, and a passive middle A/A. The extrinsically actuated system had an active four-DoF thumb, four active one-DoF (two-DoF underactuated) fingers, and active index, ring, and little finger A/A. These two prototype

systems were meant to push the boundaries of the possible, considering a wearable, self-contained electromechanically actuated prosthetic limb system.

21.1.2.2 Phase 2

The phase 2 effort spanned primarily from January 2008 to December 2009. At the outset of phase 2, a major architectural decision was necessary from an actuation standpoint between the Proto 2 systems. The primary driving factors in choosing all intrinsically actuated design for the Modular Prosthetic Limb system was for patient accommodation, namely being able to accommodate transradial and longer residual limb lengths, which accounts for a large portion of the amputee population ranging from 62% to 85% in studies with larger patient populations ($N > 200$) [10]. An extrinsically actuated hand would make accommodating this patient population infeasible and/or impractical. A key feature of the MPL system as a result of this decision was modularity, which allowed for accommodating amputees from shoulder to wrist disarticulations. A major focus of this effort was to further refine technologies to optimize for creating very torque dense and efficient actuation. This required customized motors, gearboxes, motor controllers, sensors, processors, and structural components that were very tightly integrated. Cost was typically not a major consideration, as the technological extent of the possible was a primary driver. At the end of phase 2, the first version of the MPL was built and tested (Fig. 21.2, left). Additionally, there was much progress in supporting technology areas such as cosmetic coverings, implantable neural devices, body attachment capabilities, virtual integration and testing, as well as neuroscience research on neural motor control and sensory feedback (Fig. 21.2, right). Given the breadth of technologies to be developed and integrated, a substantial systems engineering effort proceeded in lock step with the

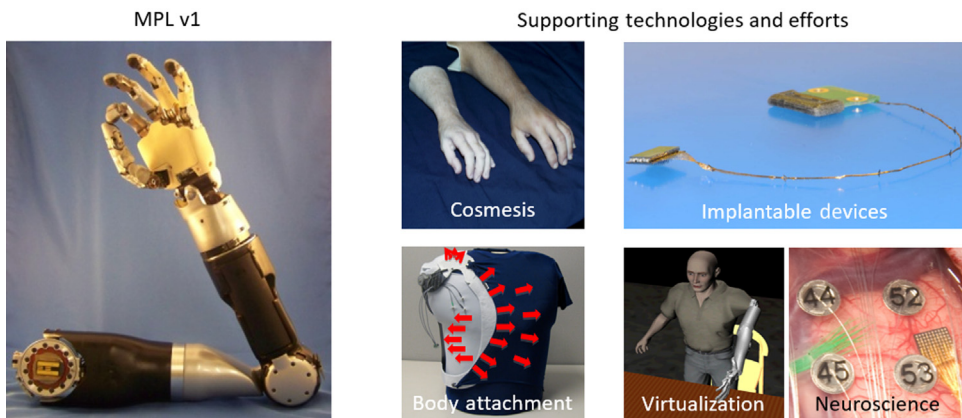


FIGURE 21.2

The MPL v1 System (left) was the first fully built system within the program based upon the final selected architecture characteristics, actuation technologies, and form factor. Numerous supporting technologies were also part of the phase 2 effort (right).

technology design and development, including detailed interface definition and capture, requirements generation and traceability, design history documentation, and system-wide configuration management.

21.1.2.3 Phase 3

Since its start in June of 2010, the phase 3 effort is still an active project. Earlier parts of the phase 3 effort were primarily focused on a number of key areas to position the MPL system to be ready for and used in clinical experimentation to perform closed loop cortical control ([Section 21.4](#)). Coming out of phase 2, the MPL wrist was nonfunctional and the thumb had performance issues related to reliability and gearbox efficiency that required design revisions. Additionally the entire system needed design revisions focusing on assembly, reliability, and maintainability to produce a system suitable for clinical applications. Specifically the development of tools such as front end and diagnostic interfaces (VulcanX and OCU, [Section 21.3.1](#)) allowed for a simplified system operation. The team also refined low- and high-level controls, optimized performance to minimize latency, maximized feedback bandwidth, and tuned system performance for application-specific use cases. The team also executed major improvements to the virtual representation of the MPL system, the Virtual Integration Environment ([Section 21.3.3](#)), to allow for clinical system integration, testing, and development in the absence of actual MPL hardware. Major clinical initiatives related to amputee patient testing as well as closed-loop cortical control with a variety of neural interface devices for both neural recording and stimulating were executed. As a precursor to human clinical activities, efforts were undertaken using animal models to control and receive feedback from MPL systems to prove out efficacy of neural integration [[11,12](#)]. In the scope of the phase 3 effort, there were two major revisions of the MPL system, version 2 (qty 5) and version 3 (qty 4), that were built, tested, and utilized in clinical applications ([Fig. 21.3](#)). The major focus of a large portion of this chapter is on the details and key characteristics of the current MPL system, v3. Additional details on the scope of the phase 3 effort can be found in Ref. [[13](#)].



FIGURE 21.3

MPL systems developed in the scope of the phase 3 effort. MPL v2.0 (left) and MPL v3.0 (right).

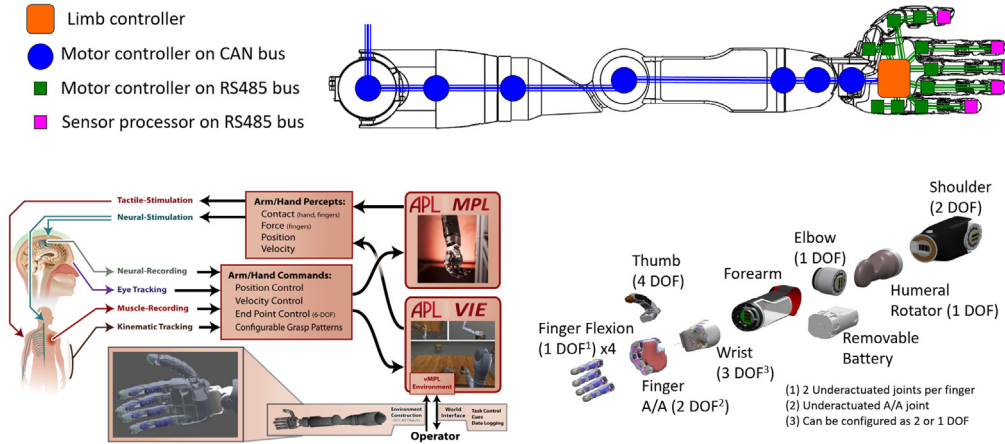


FIGURE 21.4

MPL architecture overview highlighting the communications bus, central processing and low-level controller locations, active and passive degrees of freedom, modularity, and data flow between a user and virtual and physical systems.

JHU/APL and HDT.

21.1.3 MPL ARCHITECTURE OVERVIEW, CAPABILITIES, AND FEATURES

The overall MPL architecture is highlighted in Fig. 21.4. The MPL system as a whole has 17 controllable actuators that drive 26 articulated joints in a variety of underactuated methods. One of the defining characteristics of the MPL is its modularity, which as mentioned previously not only accommodates varying user amputation levels, but also adds an element of maintainability not found in more integrated system designs (e.g., tendon-based actuation). The ability to swap, interchange, and reconfigure components is highly desirable from a serviceability and maintainability standpoint. The MPL has one primary processor, the limb controller (LC), which is the arbitrator of all information coming in and out of the MPL. It coordinates data flow between low-level motor controllers and sensor processing nodes. The low-level controllers and processors are responsible for receiving incoming commands, commutating joint motors, and outputting joint state and sensor feedback. The LC is located in the palm, which is an important and critical feature as it allows the MPL to accommodate even the longest of amputees at the wrist disarticulation level. Various input sources ranging from user intent through wearable and implanted sensors to commands coming from preprogrammed or automated trajectories can be sent into the system. Concurrently, feedback information such as position, velocity, discrete contact, and interaction force can be sent to the user-based stimulating electrodes or implants, surface tactile elements, or higher level control systems for autonomous trajectory planning and control.

From a performance standpoint, the current version of the MPL and associated specifications (Table 21.3) come close to achieving DARPA's vision for an advanced neurally integrated prosthetic system. One of the consequences of the intrinsic actuation architecture, however, is that heavier components are located more distally, which can lead to nonanthropomorphic weight

Table 21.3 Select MPL v3 Performance Specifications

Select MPL Specifications		
Parameter	Value	Units
Articulated joints	26	
Motors (DoF)	17	
Onboard motor controllers	17	
Mass of hand and wrist	2.9	lbs
Mass of upper arm with battery	7.4	lbs
Payload capacity (wrist active)	15	lbs
Cylindrical grasp force	70	lbf
Two-jaw pinch force	15	lbf
Three-jaw chuck pinch force	25	lbf
Lateral key pinch force	25	lbf
Upper arm and wrist joint speed	120	deg/s
Finger joint speed	> 360	deg/s
Hand open or close time	300	ms
Communications	CAN (MPL direct), UDP (VulcanX)	
JHU/APL and HDT.		

distribution. The whole limb system weighs 10.5 lbs (4.7 kg) with a battery, which is two pounds heavier than the weight target. It should be noted that the system has not yet been optimized for weight but rather for performance. In general, features such as maximum joint speed were traded off for strength, which is more apparent in the larger joints of the upper arm. Hand joint speeds and grasp forces tend to approach those of human capability. Currently the application areas for the MPL are in research and limited clinical use settings, some of which will be touched upon later ([Section 21.4](#)). In order to realize the human-like movement capability and torque efficient design in the MPL required very tight integration across all components, which meant that virtually all subsystems are primarily made from customized parts and components. A direct result is large build costs for low-quantity systems that currently eclipse costs of market prosthetic offerings. Transition efforts and engagements are underway, but future revisions with an eye on suitability for the prosthetic marketplace will ultimately have to make hard tradeoffs between size, weight, strength, speed, controlled and underactuated joint articulations, and manufacturability in quantity.

21.2 MPL DETAILED DESCRIPTION

The following sections cover a description of the MPL system in detail. The progression for each section moves from proximal to distal with respect to human anatomy, starting at the shoulder and moving down to the hand. After a description of the actuated joints and associated software details are covered, details regarding the sensor systems as well as other auxiliary

subsystems are provided, including those for human attachment and higher level control when used as a wearable robot.

21.2.1 UPPER ARM AND WRIST DESIGN

The upper arm (UA) and wrist consist of seven actuated drives, each controlling a DoF that corresponds to human upper arm and wrist movement. These are described in detail in the following section.

21.2.1.1 Upper arm

There were challenging goals to be met in order to achieve the performance requirements for the upper arm to match human performance. The goals for the upper arm were to:

1. Provide near-human levels of strength and speed;
2. Maintain the kinematics of a human arm (including the location of the axes of motion) with four DoFs;
3. Maintain the form factor of a human arm;
4. Be modular to accommodate different levels of amputation;
5. Provide a lightweight design;
6. Contain the system battery.

As shown in Fig. 21.5 the upper arm consists of four detachable modules:

- Two DoFs, shoulder with abduction/adduction and flex/extend actuators;



FIGURE 21.5

MPL v3 upper arm assembly highlighting the modularity and the common connector between modules.

HDT.

- One DoF, humeral rotator actuator;
- One DoF, elbow flex/extend actuator;
- Forearm with battery dock.

The upper arm can be used without the shoulder, humeral rotator, and elbow modules as required by the amputation level of the user. If the elbow module is not used a different battery pack and enclosure is required, and is typically located within a belt-pack or strapped to the user's humerus. The full assembly as shown in Fig. 21.5 weighs 6.9 lbs (3.1 kg) without the battery and is capable of lifting in excess of 44 lbs (20 kg).

To provide near-human strength and speed for the upper arm, a custom 60-Nm, 120 degrees per second actuator was developed (see Figs. 21.6 and 21.7). The key design parameters for this actuator were:

1. 60-Nm peak torque;
2. 120 degrees per second peak speed;
3. Compact enough to fit in the human arm profile;
4. Light weight;
5. High energy efficiency to minimize battery mass;
6. Breakaway features that minimize loads on users in the event of a fall or impact to the arm;
7. 250 degrees range of motion minimum.

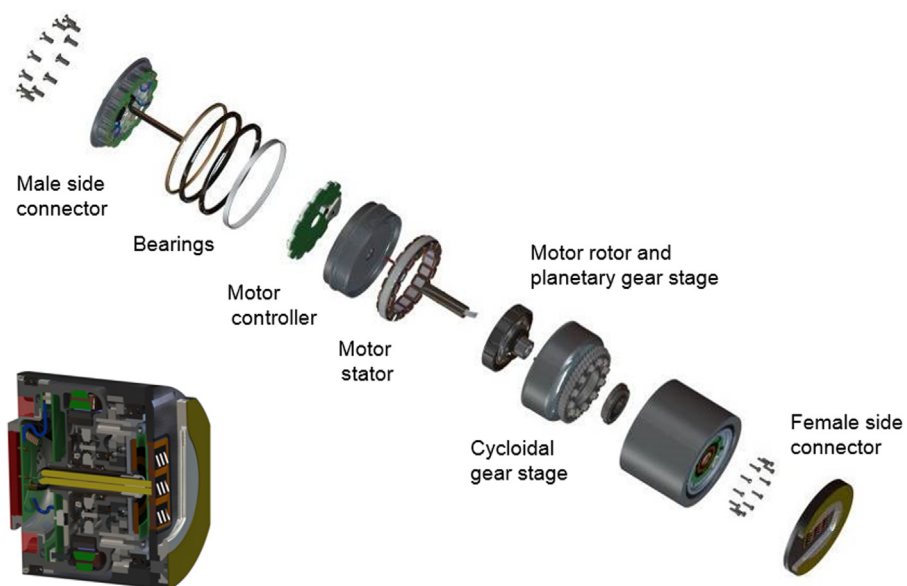


FIGURE 21.6

Exploded view of the 60-Nm actuator used in the upper arm.

HDT.

**FIGURE 21.7**

BLDC motor and two gear stages for the 60-Nm actuator used in the upper arm.

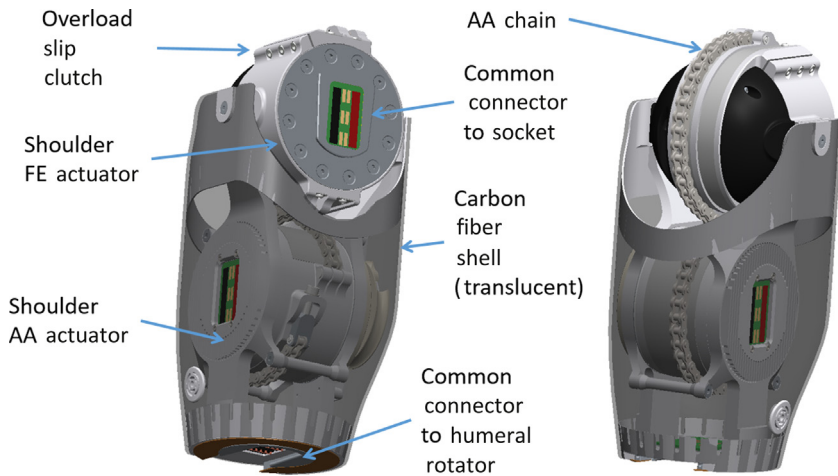
HDT.

The architecture chosen for the actuator was a tightly integrated unit with

- Brushless DC (BLDC) motor;
- Two-stage gear train (see Fig. 21.7)
 - First stage: 3.1:1 friction planetary to minimize noise
 - Second stage: 50:1 dual-lobed toothed cycloidal;
- Integral motor controller;
- Integral output torque sensor using strain gauges and a co-located strain gauge amplifier;
- Absolute position sensor on output;
- Thin-section ball bearings and seals;
- Through-axis wiring;
- Common connectors on both ends (male on one side and female on the other).

An exploded view of the actuator is shown in Fig. 21.6. The cylindrical actuator weighs ~ 1 lb (~ 450 g) and is 2.63 in (67.0 mm) in diameter by 2 in (51.8 mm) long including the common connector.

The two DoF shoulder module (Fig. 21.8) uses one 60-Nm actuator to directly drive the flex/extend motion and one 60-Nm actuator that drives chains to create the abduction/adduction motion. There is an adjustable slip clutch on the flex/extend axis, and the pins that hold the chain ends are designed to fail under unsafe loads. An aluminum frame holds the actuators into a hand-built, multi-layer carbon fiber shell.

**FIGURE 21.8**

Shoulder module consisting of flex/extend and abduction/adduction drives.

HDT.

The humeral rotator module (Fig. 21.9) uses a single 60-Nm actuator in a multilayer carbon fiber shell. The elbow module (Fig. 21.10) uses a single 60-Nm actuator that is held in a carbon fiber shell by a slip clutch. The battery compartment and wrist interface are described in later sections.

Each upper arm drive on the MPL includes a large motor controller (LMC), which is an embedded PCB capable of communicating with the LC and drives the brushless DC (BLDC) motor in response to a set of high-level control commands. At the heart of the LMC is an ARM Cortex M3 processor, which runs the embedded control algorithms, and interacts with the suite of modules and sensors shown in Fig. 21.11.

The LMC computer board (Fig. 21.12) is also connected to a variety of peripheral boards within the drive, which directly manage the power distribution/filtering, absolute position sensing, and strain gauge amplification/measurement. Communication with the LC is managed over CANbus, a message-based, multidrop networking interface initially developed for the automotive industry.

The LMC hardware is an example of the highly customized engineering development required to simultaneously produce human power and at a human scale. Equivalently capable COTS motor controllers are up to several orders of magnitude heavier and larger, while still lacking the required mechanical integration, and critical functionality such as strain measurement support. The LMC design also served as the basis for the wrist motor controller (WMC), described in Section 21.2.1.2.

21.2.1.2 Wrist

The overarching goal for the wrist design was to make it as short (in length along the forearm) as feasible, such that it could be used by the largest patient population as previously discussed. Secondary to this consideration, the thickness of the forearm constrained the axial length of a radial/ulnar deviator drive and the diameter of flexion and rotation drives. Third, it was decided for

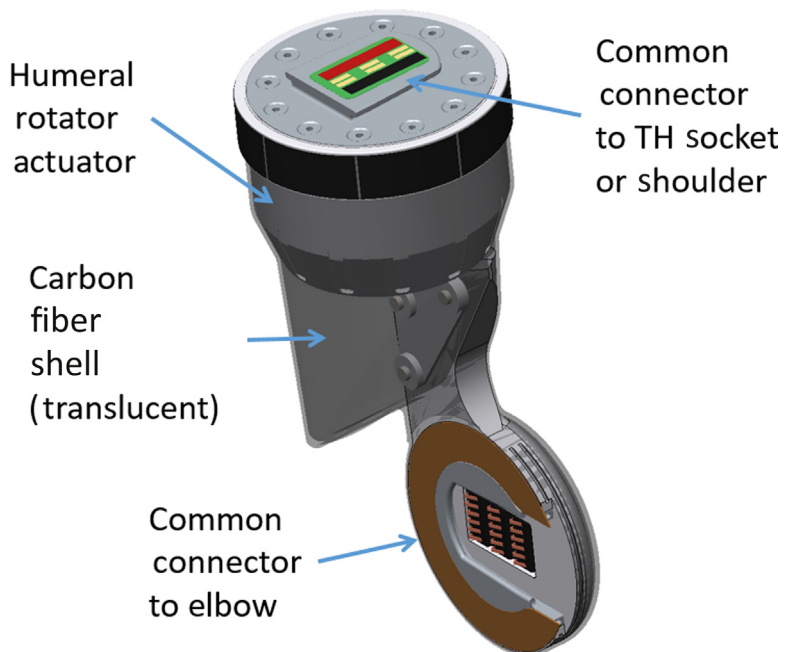


FIGURE 21.9

Humeral rotator.

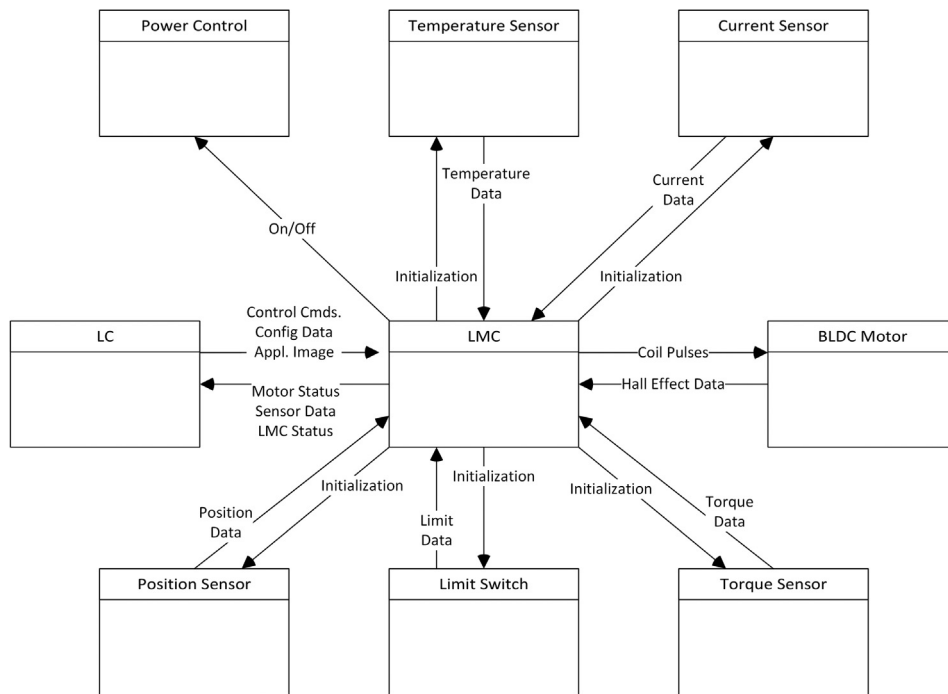
HDT.



FIGURE 21.10

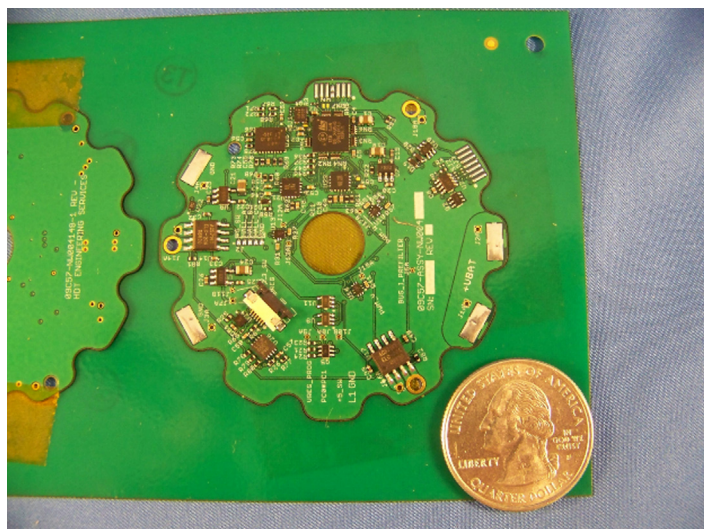
Elbow module.

JHU/APL and HDT.

**FIGURE 21.11**

Flow diagram of the LMC's interaction with other MPL system modules.

JHU/APL.

**FIGURE 21.12**

The large motor controller.

HDT.

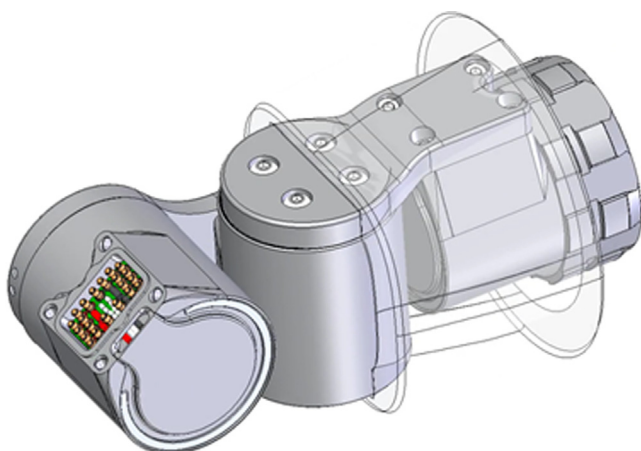


FIGURE 21.13

The wrist consists of three identical drives for flexion, deviation and rotation, or any combination thereof via a use of configuration-specific brackets. A polyurethane shell fits around the rotator and deviator, and the flexor fits mostly within the volume of the palm. At the proximal end an adapter accommodates the quick-release mechanism at the end of the forearm.

HDT.

economic reasons, that all three actuators should be identical, even if packaging became slightly less than optimal, resulting in a bracket between two drives rather than a monolithic housing for a pair of drives. In addition, the actuator should be suitable for bracketing not only into combination of less than three DoFs, depending on cost/weight and preferences of patient and prosthetist, but also into left- and right-handed configurations (Fig. 21.13).

The baseline requirements for minimum useful active flexion torque migrated from 4 Nm to near 8 Nm during the program, some of this dedicated to lifting the hand (which is heavier than anthropomorphic) and some due to having to operate through a cosmetic glove. In addition, it was a requirement that the joint lock at up to 13.6 Nm while consuming no power. Since program practice was to use a factor of safety (FS) of 3.0 on a routine load and an FS of 1.5 on quantifiable shock loads (catching a patient's fall, or an impact of the arm at full speed with an object), 13.6 Nm became a 41 Nm on-axis and off-axis durability requirement for all three wrist joints (since they were to be the same for economic reasons). The scenario of a patient *catching a fall* with outstretched arms drove a requirement for a 1500 N heel-of-palm strike up the wrist and forearm. It was also desirable for the wrist rotator to have infinite rotation, so all (identical) wrist joints have a slip ring group for power and data. The wrist joint consisted of a 4:1 planetary followed by a 76:1 cycloidal reduction, for a total reduction of 304:1. The torque-speed curve was carefully sloped to provide a balance between stall torque and high speed. The motor's rotor inertia was carefully specified to match that of the hand interacting with a 2–3 lbs (0.9–1.4 kg) object in order to assure stable load lowering and admittance control despite backlash. The wrist incorporated a tuned "drag" seal (i.e., tuned friction) on an early stage in the reduction in order to provide zero-power load-holding, this approach avoided having to integrate a roller-clutch mechanism. Although this

approach increased power consumption when moving it kept the system from back-driving at up to the 13.6 Nm load hold, without getting in the way of admittance control. The construction of the wrist involves exotic/specialty materials and very complex machining operations. Strain gage-based torque sensing is integrated into each joint output. Analog hall sensors permit sinusoidal commutation of the motor. The drive is oil-filled to evacuate heat generated by a custom frameless brushless DC motor. The gears and bearings are custom, with ring gears tightly integrated into the structure.

The third iteration of the WMC electronics focused on dramatically reducing the space claim and more intimate integration with the mechanical system of the wrist drive. This version of the power electronics shrunk down to require just a single side of the PCB roughly 1.2 in (30 mm) in diameter from a two board stack in previous versions. The other side of the PCB was dedicated to the brush blocks required for the continuous rotation requirements in the latest version of the wrist. A picture of an assembled board is shown in [Fig. 21.14](#).

Part of the strategy for reducing the overall size of the drive was more intimate integration of electronics with mechanical parts. For example, the motor controller PCB acts as a mechanical shim and the spring pins located around the periphery of the board serve the double duty of pre-loading the brush blocks against the trace board as well as electrical connection for the motor phases and MCU programming pins. Due to the tolerance stackup considerations of the mechanical assembly some of the board features such as located holes, outline routing, and copper registration required manufacturing tolerances well beyond the capabilities of a typical board house. Another example of a high degree of integration is the position sensors. The position-sensing approach

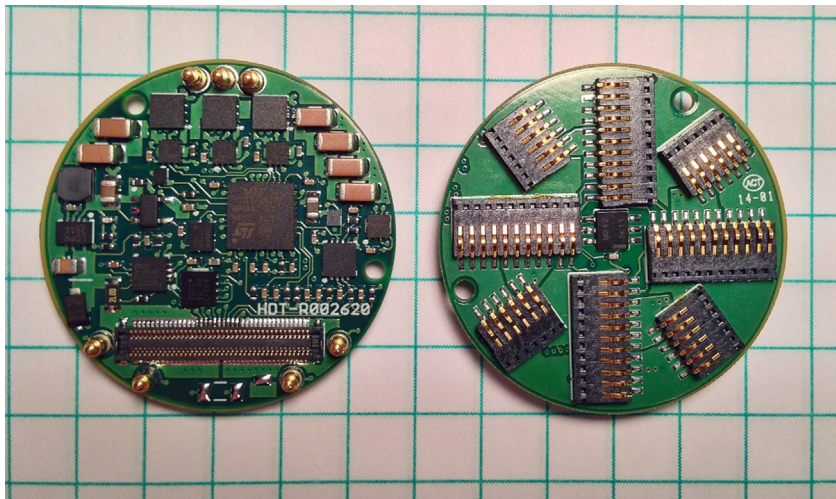
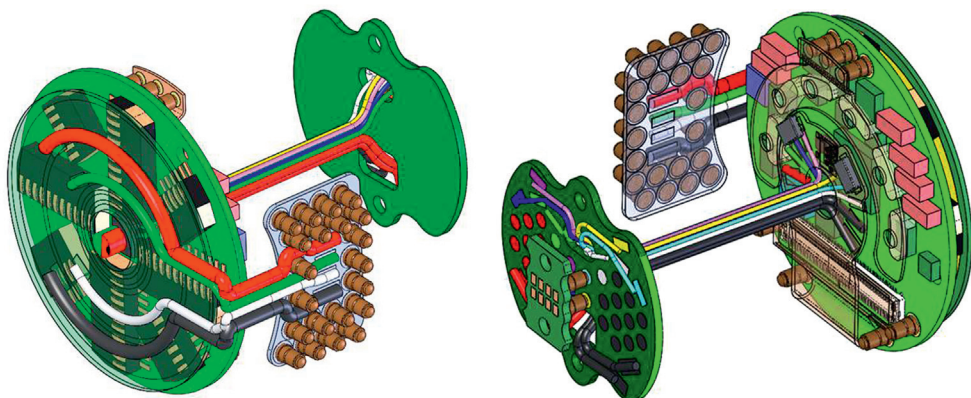


FIGURE 21.14

The wrist motor controller.

HDT.

**FIGURE 21.15**

Wrist electronics board topology.

HDT.

chosen for the wrist was through magnetic field effects. The actuator output position sensor is located in the center of the back side of the board where it senses the field of a small magnet attached to the back cover of the drive. The motor rotor position is measured by sensing the rotating magnetic field which fringes out from the air gap between the motor rotor magnets and the lamination stack. Two analog Hall effect sensors are positioned in quadrature on a flex board which attaches to the motor controller through the main connector (Fig. 21.15). This approach allowed the team to do away with a larger magnetic ring sensor used in the previous design.

The board has the following features and benefits:

- High efficiency, smooth brushless motor control via field-oriented control (FOC) algorithms;
- Motor current estimation based on rotor velocity and bus voltage rather than direct current measurement saves board space by replacing electronic components with algorithms;
- 6 A continuous, 10 A peak phase current capabilities;
- Board-mounted magnetic output position sensor enables better overall system integration;
- Thermal motor power de-rating based on direct measurement of motor winding temperature;
- Direct joint power consumption sensing (current, voltage) can be used for limb-wide power scheduling;
- Capable of very low-power operation via direct control of all on-board sensors/circuitry power including microcontroller's own external oscillator. Wake up based on CAN bus traffic is supported;
- Use of push-pins and slip-rings enables the modularity of the wrist actuator;
- Additional connectors to facilitate assembly and serviceability.

Some of the space savings also came from removing some of the previously used components and replacing them with software. For example, the phase current sensing circuitry was removed and replaced with software algorithms that used the motor model and bus current sensing in order

to estimate the phase currents. Careful selection of components further reduced the number of power supply components to only two. An overview depiction of the wrist electronics including the WMC is shown in [Fig. 21.15](#).

21.2.1.3 Battery and wrist quick release

The objective for the battery was to fit as much energy as possible into the smallest space while adding the least mass possible. Space was reserved for the battery in the carbon fiber shell of the forearm. The MPL battery ([Fig. 21.16](#)) needed to be mounted as far distal as possible to fit with the modularity construct of the arm. It was desirable for a battery to fit into a left or right arm, be user swappable, and have a dock for recharging. The need for power density pointed to lithium batteries. More energy storage was possible using flat cells than cylindrical ones that packed with wasted space. Hobby batteries were available in the size and voltage required, but their packaging did not lend well to swapping or safety, so a case design was necessary.

This case needed a thin wall, and had to incorporate retaining features, a power switch, and a battery protection circuit. The complexity of the features and short lead times led to the selection of SLS nylon as the case material. It allowed for complex geometry and the nylon was well suited for snap-fit plastic features. The design of the case was closely tied to the development of the circuit card for the battery management system (BMS) and control electronics, as such it was a codevelopment effort between mechanical designers and electrical engineers. These battery assemblies needed to fit into the existing forearm volumetric allowance and be oriented toward the body midline ([Fig. 21.17](#)). This satisfies the requirement that a patient be able to insert and remove the battery from the receptacle with one hand and minimal force.



FIGURE 21.16

MPL battery case showing split shell, retaining clips, and integral recessed power button.

HDT.

**FIGURE 21.17**

Right forearm, battery socket, and battery.

HDT.

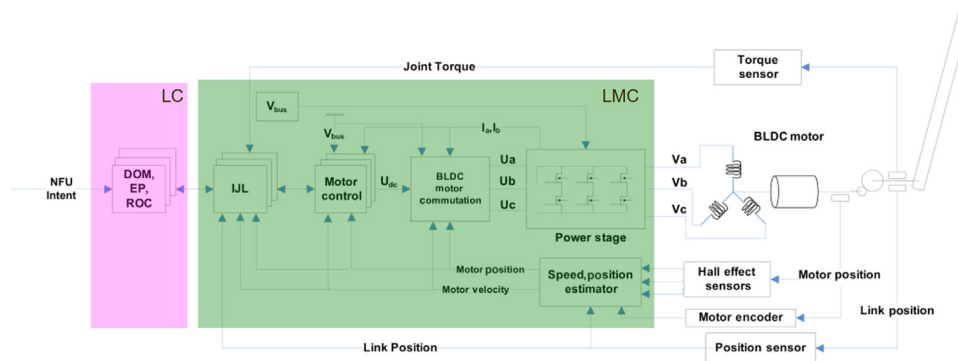
The MPL uses lithium polymer batteries (6 cells, 22.2 V nominal, 30C 2200 mAh) that are wired using custom safety circuitry to prevent accidental discharge and operation if the cells are imbalanced. Battery life is highly dependent on usage. In the “ready state,” the MPL in trans-humeral configuration (elbow, wrist, hand) can run for approximately 5 hours. With heavy continuous use, the battery can be expended in as little as 2 hours depending on the activity. The user is notified of low power conditions via vibrations and the removable battery can be replaced in seconds with a spare. Recharging is accomplished using a commercial battery balance charger combined with a custom charging cradle. The balance recharging process takes approximately 90 minutes, allowing near-continuous operation with two batteries (one active and in-use, the other recharging). Additionally, this system allows remote wireless charge monitoring via a web-app ([Section 21.3.4](#)).

Similar to the battery pack, the requirement of the wrist quick-release mechanism was to allow disengaging the wrist/hand from the rest of the limb with a single hand ([Fig. 21.18](#)). This is useful for unsafe situations if the wearer needed to be able to remove the hand from the arm, even if it were locked in a grip around a stationary or moving object. It also needed to have a precise slip fit and minimum axial length. The team settled on a system leveraging spring-loaded radial teeth which engage a groove in the outside diameter at the base of the wrist rotator. The wrist rotator plugs into the forearm with a simple axial push, which makes mechanical and electrical contact together. The hand is released by twisting an external ring on the forearm. That retracts the teeth and allows the hand to slide free.

**FIGURE 21.18**

Quick-disconnect between the battery compartment of the forearm and the wrist rotator.

HDT.

**FIGURE 21.19**

Block diagram highlighting the data flow and functionality between elements of the upper arm control software.

JHU/APL and HDT.

21.2.1.4 Upper arm software

Each joint in the upper arm and wrist is equipped with its own processor and embedded firmware, capable of interpreting high-level commands from the LC and executing the desired motion profile. This is accomplished through the three main steps as shown in Fig. 21.19 below, which are individual joint/link (I JL), motor controller, and BLDC motor commutation.

The I JL algorithm is responsible for integrating various LC commands into a cohesive set of control variables. Depending on the high-level system mode, the LC may send position, velocity, and/or torque commands and separately issue apparent inertia, stiffness, and damping parameters.

The IJL algorithm runs a simulated second-order impedance loop in real-time, then synchronizes the output with the position and velocity commands to produce the control variables. The motor controller block represents a series of nested proportional, integral, derivative (PID) controllers, each of which is tasked with closing the loop around a specific drive variable. The outermost loop takes in the desired and measured position, and produces a velocity command (with respect to the drive's position and velocity limits). Next, the middle PID controller closes its loop around the velocity command, producing a desired motor current. Depending on the hardware package, a final set of loops may be used to control the direct and quadrature motor current. The BLDC motor commutation routine supports both traditional FOC and a modified approach which uses open-loop current estimates based on motor properties and sensor measurements, eliminating the need for separate phase current sensors and reducing the overall size of the electronics package.

21.2.2 HAND DESIGN

The hand of the MPL system consists of 10 actuated drives and 19 articulating joints. There is one actuator in each finger controlling an additional two underactuated degrees of freedom for three total revolute joints per finger. In the palm tucked behind the LC are two finger A/A drives, one for the index finger and another for the ring/little fingers connected via a linkage for an additional underactuated DoF. Finally, there is an actuated four-DoF thumb that allows the MPL to assume a plurality of grasps and provide for an anthropomorphic movement quality. These components are described in detail in the following sections.

21.2.3 FINGERS

The driving requirements for the fingers (Fig. 21.20) were to have the strength of a 95th percentile male, but a form factor suited for a 50th percentile female palm. The finger design needed to have

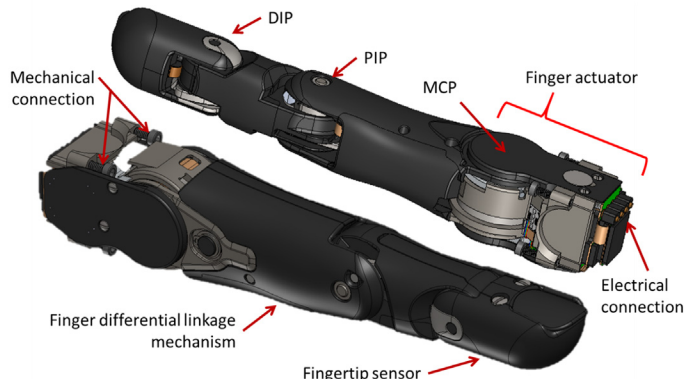


FIGURE 21.20

The MPL finger mechanism.

a significant fraction of anthropomorphic speed and dexterity matching or approaching that of a human finger, integrate tactile sensors, accommodate a cosmetic covering, and incorporate compliance within the mechanism both for shock protection and also as a series-elastic element to enable the finger to handle objects with a light touch.

The dexterity requirement coupled with a desire to minimize weight and complexity drove the development of a one-motor finger (1MF) with behaviors similar to a finger with two independently controllable degrees of freedom. This was done by the invention of a novel differential linkage mechanism [14]. The difficulty in controlling three finger joints with a single motor is that there is usually a tradeoff between tip-pinch behavior and grasping behavior. It is possible to couple all three joints with a kinematic linkage that *appears* to behave similarly to a human finger—except that the finger will not curl well around an object to make a secure grip. It is also possible to couple all three joints differentially. This is common with cable mechanisms. That kind of finger curls well around objects, but often cannot hold a stable tip pinch. The 1MF linkages invented and developed for the MPL hand are able to do both things well. Contact with the fingertip—or anywhere distal to a location called the “focal point”—does not produce curling. The joint positions stay stable for good fingertip manipulation. Contact anywhere proximal to that, such as on the medial or proximal phalange, produces curling behavior that brings objects into a stable grasp.

The unique behavior of the 1MF linkage can be best described by referring to Fig. 21.21, where:

A illustrates how a palmar force encountered distal to the focal point while the motor is moving results in a predictable three-joint simultaneous curling without buckling behavior;

B illustrates how a palmar force encountered proximal to the focal point while the motor is moving results in a conformal grasping behavior. In other words, the MCP joint stops moving while the PIP and DIP joints continue to curl until they are themselves obstructed;

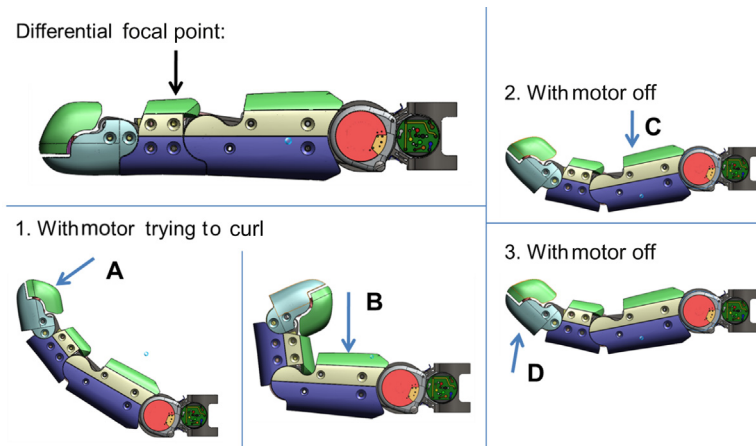


FIGURE 21.21

Description of novel hybrid fixed-linkage/differential that allows the one-motor finger to exhibit both pinching and conformal grasping behaviors, previously only achievable with a two-motor or tendon-based finger.

HDT.

C and D illustrate how the finger buckles when a palmar force is applied proximal or distal to the focal point while the motor is off; very similar behavior to that of the human finger.

The finger actuator located near the MCP axis delivers torque through a differential linkage to both the MCP joint and the pairing of the PIP and DIP joints. The PIP and DIP joints are themselves coupled geometrically. The position of one joint fully determines the position of the other. The differential allows PIP and DIP to continue curling or conforming to an object whenever the MCP joint is blocked by that object. A second “PIP-stop” linkage dictates when in the stroke of the MCP’s flexion the PIP and DIP joints are allowed to start moving. This secondary linkage also dictates at all times a minimum amount of PIP-DIP curling given the position of the MCP joint. We termed this “predictable” three-joint curling, and it serves well for automated tip-pinch grasps in opposition with the thumb where we do not want mechanism friction or cosmetic covering affecting the differential between MCP and PIP-DIP. Over time, the program established the optimal tuning of these linkages:

- The onset of PIP/DIP curling (changed from MCP 0° to MCP 10°);
- The ratio of PIP/DIP to MCP curling (changed from 1.1 to 0.9);
- The focal point of differential (shifted more proximal—to be mid-way along the distal phalange).

The consequence of this pair of linkages within the finger is that it is just as dense as if it had a second motor, but has significantly less weight and expense. The dense linkage mechanism forces the designer to use exotic alloys for linkage members such as M2 dowel pins and 18Ni 350 ksi maraging steel links. Even then, in order to keep the lever arms maximal so that loads are small, no room exists for pin-joint bushings except for coatings. Some additional key considerations of the finger linkage design are as follows:

1. Integration of tactile sensors meant:
 - a. The finger needed to accommodate a service loop for communication and power bus down the length of the finger;
 - b. The distal phalange was reserved in its entirety for the fingertip tactile sensor;
 - c. The palmar surface of each finger, to some appreciable depth, was reserved for PVDF sensors embedded in a soft durometer urethane overmold.
2. The strength of a 95% male means resisting a 67 N (15 lbf) tip-pinch force generated by the thumb. We designed for a safety-factor of 3, which means the finger is robust to a fingertip force of 200 N (45 lbf), even though the finger actuator can only actively generate a 32 N (7 lbf) force [i.e., from 2.7 Nm (21 lb-in) drive torque at the MCP joint].
3. The series-elastic element took the form of a custom spring engineered into the linkage within the proximal phalange. This series-elasticity serves to soften the touch of the finger in dynamic situations, whereas admittance control (motor motion in response to measured joint torque) alters the finger’s impedance to static forces.
4. An overarching concern during the design of the knuckles was to anticipate the behavior of the cosmetic covering (cosmesis). In other words, design it such that it did not promote cosmesis wear or pinching/tearing.

5. In addition to the fingertip pinch force cases, the finger was also designed for a 600 N (134 lbf) *stab/poke* scenario, as well as a 67 N (14 lbf) lateral pinch case (i.e., thumb pinching against the side of the index finger).

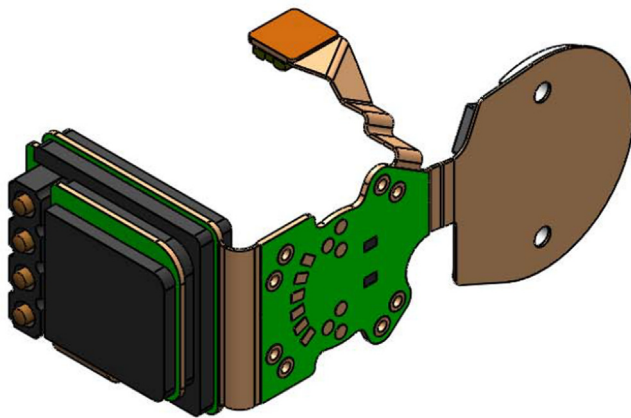
Given the strength requirements, numerous linkage elements, and sensor integration and wiring to each phalange, very little room was available for the structure/shape of each phalange. Monolithic phalanges from 7068-T6 Aluminum, with convex lateral and dorsal surfaces, and concave accommodations for a polyurethane over-mold on the palmar surfaces permitted the greatest volume dedicated to palmar pads and sensors.

For driving the finger linkages, there is a custom motor, gearbox, sensors, and motor controller at the finger base, commonly called the metacarpophalangeal (MCP) drive. The primary mechanical power producing elements is a custom frameless brushless DC motor, which is common among the actuators of the hand. The motor feeds a 6.5:1 spur gear reduction followed by a 60:1 eccentric (cycloidal) reduction for a total 390:1 reduction. Through the reduction a combination of plain polymer and customized steel rolling element bearings are chosen carefully to optimize dynamic life, overload robustness, and overall gearbox efficiency. While just 20 mm in diameter, the output stage is robust to 24 Nm (212 in-lbf) impacts without damage. The actuator housing is instrumented with custom strain gage coupons placed on a machined flexure to measure MCP joint torque. The actuator has two concentric channels of custom magnetic position sensing—one which measures movement of the proximal phalange (MCP) and a second which measures its output. Given these two measurements and knowledge of the finger linkage position, the behavior of the differential between MCP and the PIP-DIP can be determined. One channel is a magneto-resistive sensor on-axis looking at a diametrically magnetized cylinder magnet, while another channel is a pair of analog halls in quadrature looking at an axially magnetized ring.

The small motor controller (SMC) electronics were developed to fit within a highly space-constrained environment to meet the mechanical requirements of the finger, thumb, and A/A joints to drive the custom frameless BLDC motor of the MCP drive. The core electronics are the same between variants, with the main changes to accommodate the different volumetric allotment requirements and signal pinouts to accommodate signal routing. Nominally, the units are capable of delivering 8 W continuously and a 90 W peak to the custom-wound motors. Communications are provided by a half-duplex RS-485 bus using a 9-bit protocol and up to three devices per bus. The finger SMC variant interfaced to the palm using pogo pins captivated in a plastic housing to ensure planarity, improve rigidity, and improve force distribution during insertion and extraction cycles ([Fig. 21.22](#)). The thumb and finger A/A variant incorporated a larger pair of connectors to support the additional downstream power loads, which the 1MF does not require, as well as installation diversity to reduce the variant count.

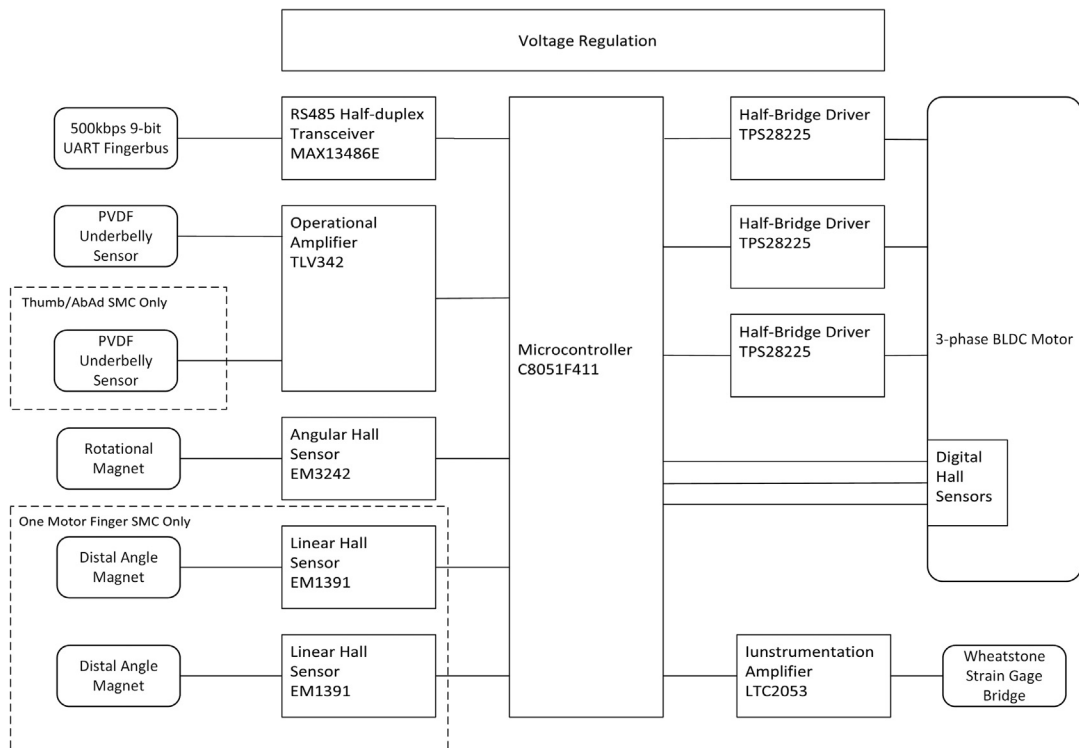
Both SMC designs (thumb depicted later) use rigid-flex construction that deviates from the standard practice of terminating the polyimide overlays in the rigid sections for a rigid prepreg material. The tight bend radii of the flex regions and high via count near these regions inhibited a clean transition zone. The solid continuous layer prevents interlayer shorting when bent to the required curvature.

A block diagram of the hardware architecture is shown in [Fig. 21.23](#). The onboard 8051 microcontroller provides the full software stack: from communications to sensor acquisition to motor commutation. The system initializes to an absolute position using the previously described angular

**FIGURE 21.22**

1MF SMC when folded around the mechanical assembly housing the motor (not shown).

JHU/APL.

**FIGURE 21.23**

SMC Electronics hardware block diagram.

JHU/APL.

Hall effect sensor and continues to monitor this signal to correct for positional drift. High-resolution positional control is based on the Hall effect sensors at the motor rotor level. At low speeds, traditional six-step commutation is performed, but to improve the commutation efficiency, a model of the motor is incorporated in the software to estimate its rotor position so sinusoidal commutation can be performed at higher angular velocities. This bimodal scheme proved effective enough for the higher level control schemes at the system level that the additional hardware required for conventional sinusoidal commutation was not required. As previously described, the IMF has a compliant mechanical linkage that can curl the distal linkage. This outer linkage angle can be determined by a mathematical transform of the linear Hall sensors and angular Hall sensor. Additionally, impedance control to dynamically adjust finger compliance is performed by closing the loop around the strain gauge value amplified by the on-board chopper-stabilized instrumentation amplifier.

21.2.3.1 Thumb

The driving requirement for the thumb was that it include four independently actuated DoFs, abduction/adduction and three parallel flexion axes, such that the thumb had adequate dexterity to *tip-pinch* each of the four fingers, and to perform a lateral *key* pinch (i.e., when the thumb pinches the side of the index finger). A further constraint of the thumb subassembly was that the *knuckle-to-knuckle* distance not be longer than 28.5 mm (~1 in.), in order to be able to package three parallel flexion actuators and maintain an anthropomorphic form factor, while leaving room for a finger-tip sensor ([Fig. 21.24](#)).

Over the course of the program, for risk reduction reasons, two finger/thumb actuator designs were incorporated. The *cycloidal joint* was used for each of four fingers as it was better suited there, but its diameter was prohibitive for a four-joint thumb. [The finger *cycloidal* drive system had 20 mm (~3/4") diameter output stage versus 15 mm (~5/8") diameter for the thumb *planetary* drive]. Despite the differences, both drive systems utilized the same custom motor, this was important as it was desired to maintain a common architecture and electrical interface for all finger joints. Ultimately the *planetary* thumb joint was used for the three thumb flexion joints, the thumb abduction/adduction, and the two finger abduction/adduction drives housed in the palm; for a total of six locations within the hand. Therefore, a single actuator needed to have mechanical and electrical mounting and connectorization provisions to work for six different applications within the hand.

The *planetary* thumb joint controller, the thumb SMC, is architecturally similar to the finger SMC as discussed previously. As shown in [Fig. 21.25](#), the thumb SMC is mechanically interleaved with the mechanical structure directly (capacitors, mounting features), indirectly (connector placement to minimize bus impedance and accommodate service loops), and with the motor-phase leads physically bypassing the controller. The design of the motor's electrical interface is such that routing is made feasible. Intimate understanding of rigid flex tolerances was required for optimization within the mechanical assembly.

The gear reduction of the thumb joint is a 4.75:1 spur gear reduction from the motor to the planetary system input. The three-stage planetary consisted of two 5:1 stages with four planets each, followed by a 3:1 stage with eight planets for a total reduction of 356:1. The distal three joints (i.e., the three parallel axes joints) of the thumb, which are not part of the core palm assembly and are more vulnerable to damage, are replaceable via a quick connection with no soldering required. Unlike the fingers, the thumb's proximal joints needed to be compatible with left- and right-handed

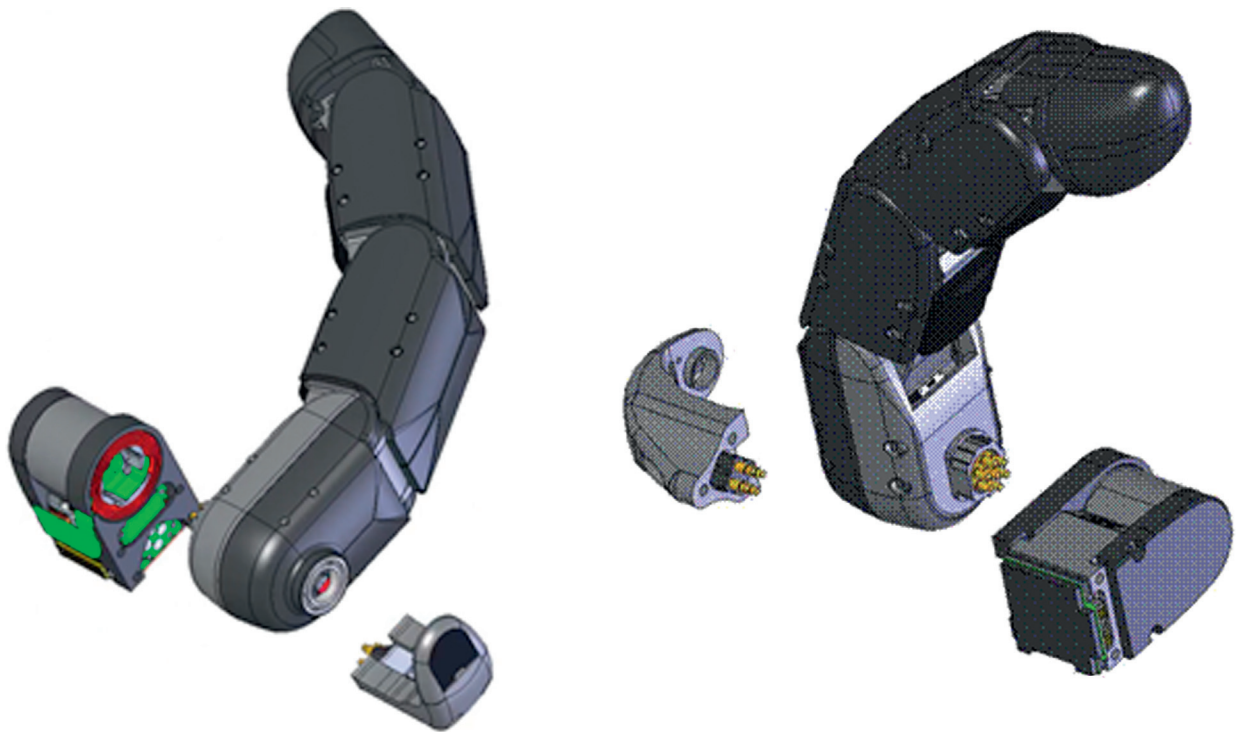
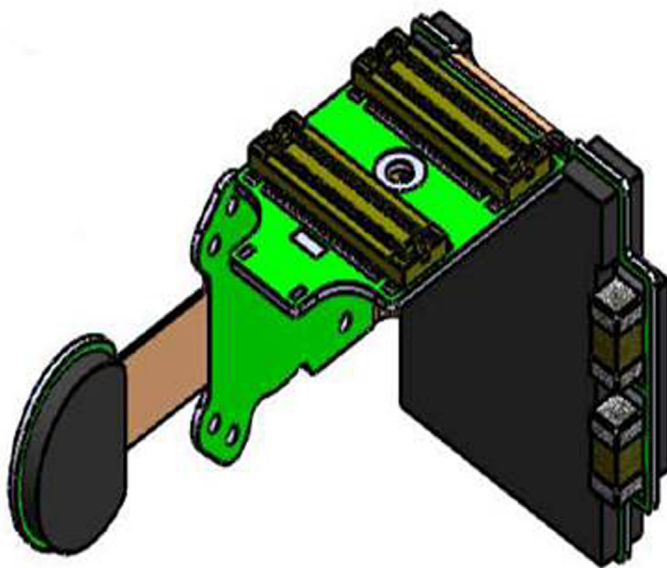


FIGURE 21.24

The thumb consists of three flexion joints and a thumb tip sensor that are a single replaceable element living outside the palm. The abduction/adduction drive lives within the palm and a bracket allows easy replacing of the flexion joints.

HDT.

**FIGURE 21.25**

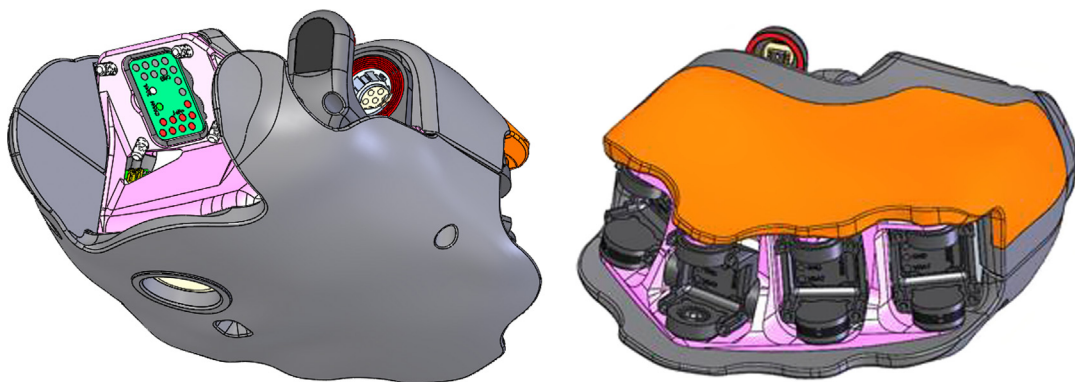
Thumb SMC when folded around the mechanical assembly housing the motor (not shown).

JHU/APL.

configurations. This was achieved without the need for custom parts other than the palm structure and flex circuits within the palm. The thumb's power and communication bus electrical design required a custom left- and right-handed compatible clock-spring behaving flexible board service loop in order to pass the required electrical signals across the thumb's abduction/adduction joint. Similar to the fingers, a rolling bubble flexible board service loop was used on the thumb to pass electrical signals across its flexion joints.

21.2.3.2 Palm and finger abduction/adduction

The palm is best described as a system of systems as it houses the MPL's LC, actuators to abduct/adduct the fingers, tactile sensors, a signal distribution network, and other components such as linkages, LEDs, and buttons. It is a structural member relating the wrist to the fingers and thumb. It is at the middle of 20 kg (44 lbs) lifts, and survives a 1500 N (337 lbf) palm-heel strike during a fall. There is engineered compliance/shock where the finger receptacles are mounted to the palm for MCP flexion and twist about the length of finger as well as for abduction/adduction. The palm contains the finger abduction/adduction actuators and thumb abduction/adduction actuator. These are copies of the thumb flexion actuators (i.e., the planetary drive) having the same variant of the SMC, with the exception of linkages that connect to the finger sockets. These drives have integrated torque sensing in order to monitor the finger's abduction/adduction torques. The palm houses the LC, which coordinates the control of the entire 17-actuator limb system (i.e., hand/wrist/arm system) and coordinates communication to higher level systems (described in Section 21.3.1) of 17

**FIGURE 21.26**

The palm has bolted solderless quick connections to the thumb, wrist, and fingers. A soft overmolded region on the palmar surface contains tactile sensor regions.

HDT.

axes of joint data and numerous other channels of tactile sensor data. The palm distributes communication and power buses from the wrist to the four fingers, the thumb base, two finger abduction/adduction drives, as well as the palmar and dorsal coverings of the palm (Fig. 21.26). Finally, it is relied upon for thermal dissipation from numerous heat sources, user notification via LEDs, user interaction through a dorsally located button, contains tactile sensors on the palmar surface, accommodates serviceability through quick disconnects at the finger and thumb, and provides convenient access to internal components.

The space for the palm functions is very limited. The wrist flexor is positioned as distal as possible (more distal than anthropomorphic). Conversely, fingers with integrated torque sensors, motor, and controller as well as electromechanical quick-connect for serviceability consume significant space proximal (within the palm) to an anthropomorphically placed MCP axis. Finally, since the same length finger is used at ring–middle–index positions (the little finger is ~18 mm shorter), index and ring were placed quite proximal. An endoskeleton/exoskeleton approach was adopted to permit serviceability (Fig. 21.27). Polyurethane covers provided little structure (no bending moments transmitted from fingers to wrist, etc.) aside from conveying normal forces directly to the endoskeleton. The covers provided shape and a surface for tactile sensor integration. In order to be optimal, the endoskeleton palm structure needed to be a single monolithic piece of aluminum with strength where needed, attachment points where needed, and clear volumes for service loops and room for the abduction/adduction linkages to sweep.

One challenge in the design and manufacture of the palm was simply geometry. In an effort to develop: (1) an underactuated (less degrees-of-freedom than a person) system that can perform a multitude of grasps as similarly as a human, as effectively as possible, (2) accommodate artificial constraints due to packaging and economics related to finger lengths, A/A drives, and flexible service loops, the geometry of the palm endoskeleton became quite complex. It contains multiple compound angles between fingers, the thumb, abduction/adduction drives, and

**FIGURE 21.27**

The assembled palm (left), with monolithic endoskeleton and the exoskeleton coverings of the palm subassembly (right).

internal components. The power and communications are distributed through six flexible circuits that are unique for a right and left palm. The palm structure and these loops are the only components with left–right variation in the MPL system. These loops are distinct for each finger, finger A/A drives, and the thumb. All of the palm service loops, and those internal to the thumb, share the same board–board connection pinout for economy and facilitate the testing/debugging of the hardware.

The LC electronics were developed to act as the central controller of the entire system. The location of the LC in the palm imposed significant volume restrictions and processor selection difficulty to achieve the required level of computation. To meet this necessary computational density for a general processing system, a component with a package-on-package (PoP) option available in suitable quantities was required. This downselection process culminated in the OMAP3503 by Texas Instruments. A flash-based FPGA was added alongside the processor to support seven 9-bit UART busses to communicate with the fingers and thumb, as well as support for the controller area network (CAN) to communicate with the LMCs located in the wrist and arm. Early revisions were custom OMAP3503 circuit boards, but due to reliability, cost of manufacture, and new market options, a system-on-module (SOM) using the same processor was selected for later units. This increased the overall volumetric requirements, in particular the height, but greatly increased reliability and reduced the overall cost.

This revised LC system was comprised of a three-board stack-up (Fig. 21.28): a passive interconnect board to route power and communications; a mainboard to provide the communications transceivers, power regulation, and FPGA; and the SOM. Heatsinking of the SOM processor was provided by a copper strap to the surrounding frame and also served as protection beneath the polymeric palm exoskeleton.

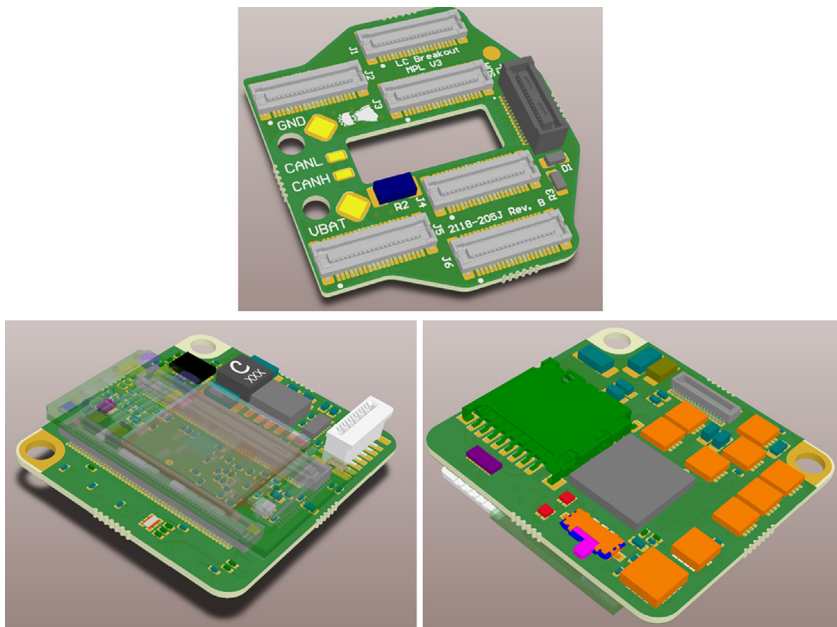


FIGURE 21.28

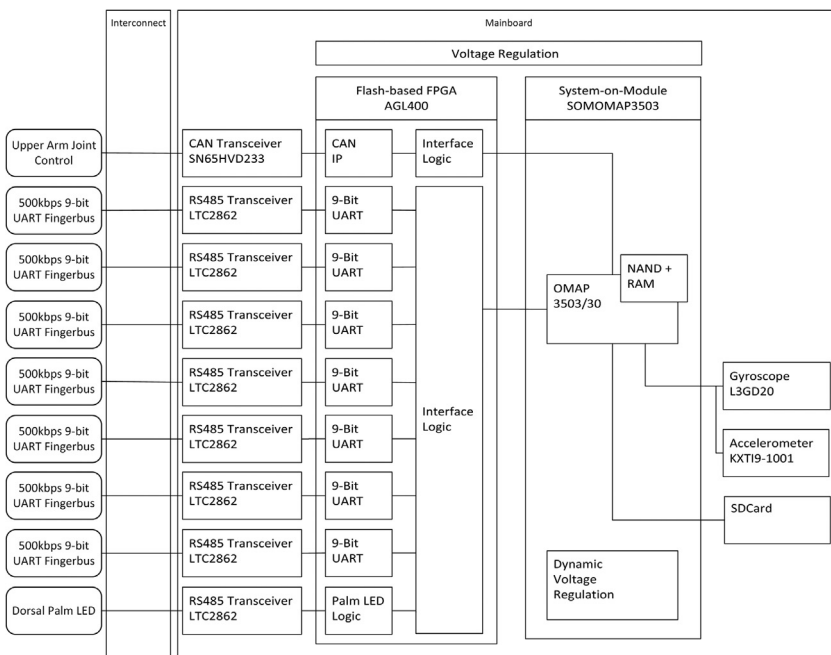
Limb controller breakout interconnect board (top) and mainboard with SOM (bottom).

JHU/APL.

A block diagram of the LC hardware architecture is shown in Fig. 21.29. The FPGA firmware was composed of the controller area network MAC and the bank of UARTs to communicate with each fingerbus in parallel. One transceiver also served as the driver to the bicolor LED visible on the dorsal side of the palm. As mentioned previously, the flexible service loops to each finger were different between the left-hand and right-hand models and across palm generations, which was solved with minimal software impact by remapping inside the FPGA to the intended comms endpoint. To communicate with all these various endpoints, the hardware utilized high-speed multi-channel buffered serial ports (McBSP) of the OMAP3503 as unidirectional pipes. The CAN interface used two McBSPs, one for receive and one for transmit. The bank of UARTs were similarly configured. These ports could then be used by the software to dispatch messages rapidly in parallel and wait for all the messages to asynchronously respond. These decisions freed up clock cycles for computation instead of managing data flows.

21.2.3.3 Hand software

The LC software was designed to support multiple communication interfaces, emphasize hardware abstraction to the extent possible, while minimizing interrupt latencies. The software was written on top of the QNX operating system which was specifically selected because of the hard real-time operating system support compared to various other Linux distributions available at design

**FIGURE 21.29**

Limb controller electronic hardware block diagram.

JHU/APL.

conceptualization. The main components of the LC include hand communication, arm communication, execution of control algorithms, safety monitoring, configuration, and reprogramming. Hand communication was primarily supported by sending 9-bit UART commands across an RS-485 bus. This differential bus supports communications to seven simultaneous busses with three nodes on each bus. Each hand node [SMC or fingertip sensor node (FTSN)] communicated at 200 Hz including control commands and telemetry reporting. Arm communication was primarily across the CAN bus. The LC provided hand state information, received telemetry data from upper arm and wrist controllers, and sent control commands all at 50 Hz. Whole arm control algorithms were first developed in Simulink and transferred to the embedded system using the Matlab Real Time Workshop framework. The algorithms provided closed-loop position, velocity, and impedance control for each actuated degree of freedom in the system. In addition, the limb can operate in a variety of endpoint control configurations including endpoint position, velocity, impedance control as well as signals reduced order control (ROC) where individual motors can be grouped together for lower DoF control signal, which is particularly useful for grasp sequences. Finally, the LC was designed for patient safety first by incorporating several self-monitoring and diagnostics capabilities including loss of communications, over temperature, and current monitoring and reporting. In addition, all firmware configuration and reprogramming support was provided by the LC software.

The SMC software was primarily designed to provide closed-loop position control and sinusoidal commutation to a three-phase, brushless DC motor with Hall effect sensing. Other responsibilities were to read and report sensor data from a variety of sensors in the hand including strain gages measuring force on the finger, piezoelectric contact sensors measuring high-speed tactile events, and potentiometers for absolute position sensing. The SMC software was written for the Silicon Labs 8051 family of processors. The software used a combination of C and Assembly routines for fast math operations including fixed-point multiply and divide to account for the lack of a math coprocessor. The SMC software receives high-level control commands from the LC at a rate of 200 Hz while running an internal position and velocity controller at 600 Hz. The SMC software also samples sensor data at 600 Hz using a 12-bit ADC. The SMC packages and sends this telemetry data to the LC at 200 Hz. In order to provide sinusoidal commutation of the motor, a HW interrupt is generated at every rotor Hall edge transition. At every Hall edge, the SW computes the velocity of the rotor using a motor cycle window. In between Hall edges, the SW computes motor velocity to provide an estimate of the rotor position. This estimated rotor position is then used to provide sinusoidal commutation to the motor.

21.2.3.4 MPL sensors

A primary focus for the MPL system was to contain a variety of sensor modalities to provide for adequate data in an attempt to try to meet the lofty and near-impossible goal for matching human-level sensory perception in the hand. This is reflected in the degree of integration and tedious design that went into the sensors of the MPL system, which still are a long way from fully replicating the sensation present in the human hand. Fig. 21.30 highlights all the sensing elements in the MPL system, some of which have been touched upon previously. In general, each actuated joint in the MPL system has position, velocity, torque, and internal temperature feedback. Underactuated joints have direct position sensing or have deterministic kinematic relationships to allow for position and velocity calculation. In this section we present a detailed focus on the fingertip level sensors.

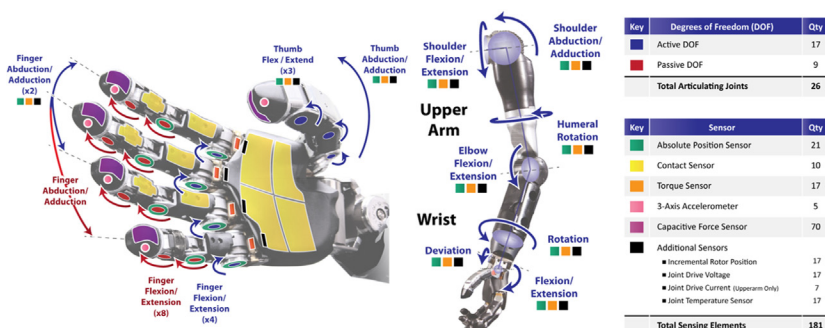


FIGURE 21.30

Sensor elements found in the MPL system.

**FIGURE 21.31**

The v1 FTS: (left) thumb-tip flexure, fingertip flexure (right), and fully assembled fingertip sensor (center).

HDT.

The human fingertip is likely the most sensitive skin area in the animal world, capable of discriminating between a smooth surface and one with 13 nm-deep features [15]. One could argue that fingertip sensing facilitated the evolution of human intelligence by enabling precision manipulation of tools, including utensils for creating drawings and written communication. In modern society, tactile feedback is as critical as ever, and for prosthetic users it represents a large technological gap in capability that affects not only performance but may also impact user acceptance.

21.2.3.5 Fingertip sensor v1

The v1 fingertip sensor (FTS, Fig. 21.31) provides the means of sensing force, vibration, heat flux, and four discreet contact sensors and is used for characterizing and identifying surfaces and objects in contact with the fingertips of the MPL. Each FTS is a self-contained modular unit that houses all required sensors and electronics in the form of the distal finger phalanx. Sensor signal conditioning is handled by locally embedded electronics which convey preprocessed sensor information to the LC.

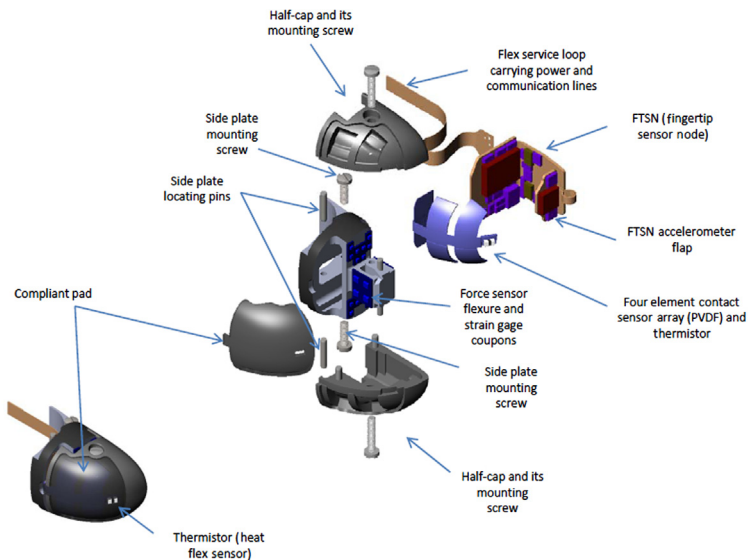
The FTS is designed to be a modular and replaceable unit that can be installed on the 1MF, 2MF (deprecated design), and thumb. There is a slight difference between the sensor used on the thumb to that on the fingers. The thumb-tip sensor has a longer and larger diameter cap and one integral side plate. In addition, the thumb-tip sensor lacks contact and heat flux sensors. An exploded view of the fingertip sensor is shown in Fig. 21.32.

21.2.3.6 Force sensing

Fingertip force sensing is implemented by means of a flexure instrumented with strain gages. Low-frequency force feedback provided by the fingertip sensors can be used for force control of the MPL with the human in the loop as well as local hand grasp (i.e., antislip) control. Dynamic force signatures generated during haptic exploration by the MPL can be used to characterize surface textures. The fingertip senses three axes of force applied anywhere on the fingertip cap that comprises roughly one half of the distal portion of the phalanx.

21.2.3.7 Contact sensing

Contact sensing is implemented by means of an array of polyvinylidene fluoride (PVDF) elements arranged on the underside of the finger pad. Although PVDF material has only a transient response to a persistent stimulus, its use is appropriate in the context of motion-based tactile sensors because

**FIGURE 21.32**

Exploded view of the v1 fingertip sensor.

HDT.

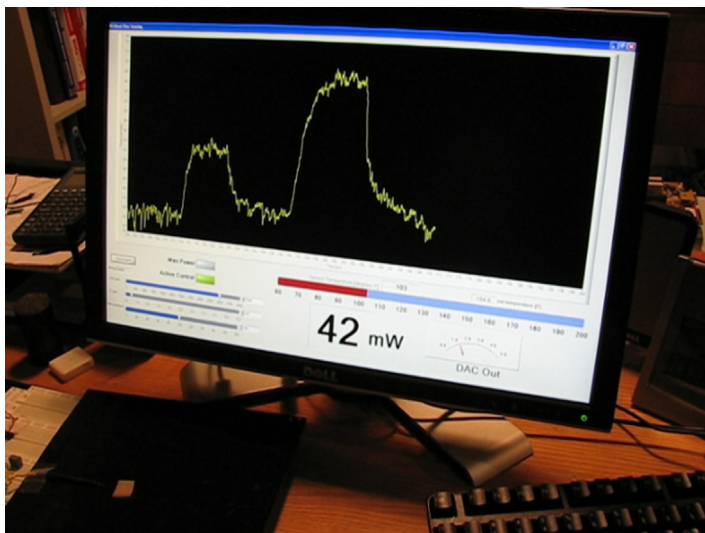
of the transient nature of the stimulus. In that respect the response of the PVDF material resembles the fast reacting Pacinian mechanoreceptors in the native skin responsible for tactile sensation. The PVDF sensors are mechanically durable, have a wide bandwidth response, and are self-powered. A group of PVDF elements overlaid on top of the cap is used as a contact sensor array. The output of the array is conveyed either by the haptic system or through neural integration to resolve closely spaced surface features such as Braille cells or to localize applied forces.

21.2.3.8 Vibration sensing

Vibration is sensed by a dedicated three-axes accelerometer. This information is primarily used by the haptic system to enable the MPL wearer to recognize surface textures. This capability is also leveraged to assist with a slip detection algorithm for autonomous grasping.

21.2.3.9 Heat flux sensing

Metal is perceived as being colder to the touch than wood when both are at room temperature. This is the result of human skin sensing the rate of heat flow rather than absolute temperature. Thus, it is desirable for the MPL fingertip to sense the heat flux between itself and its environment. The heat flux sensor consists of a self-heating thermistor, whose resistance varies proportionally to its temperature. To measure heat flux, the excitation voltage applied to the sensor is regulated to achieve a constant above-environment temperature. The required voltage needed to maintain this temperature is a measure of the I^2R heat loss to the environment. To measure temperature, a constant current is passed through the resistor, the resulting voltage is a measure of its temperature.

**FIGURE 21.33**

Demonstration of sensing materials of different thermal impedances. Free air is perceived most like a thermal insulator, requiring only 42 mW of heat to maintain the thermistor's set temperature of 104°F. Aluminum most readily conducted heat from the sensor.

HDT.

Note that while the thermistor can heat itself and its environment, it cannot actively cool down. Therefore when the environment temperature exceeds the temperature of the thermistor, it can no longer function as a heat flux sensor. In this situation, the thermistor can only act as a temperature sensor. Fig. 21.33 shows the results of a trade study that investigated the suitability of heat flux sensing for successfully discriminating between commonly encountered materials.

21.2.3.10 FTS electronics

The FTS electronics resides in the distal end of each finger on the MPL and contains the circuits enabling it to measure three axes of force and acceleration/vibration as well as total heat flux. Additionally, the FTS flexible circuit board includes an array of touch sensors for closely spaced feature discrimination (Fig. 21.34). The FTS node (FTSN) is a printed circuit board consisting of a microcontroller (MC), a low drop-out linear regulator power supply (LDO), a three-axis accelerometer, a three-axis strain beam assembly, a three-channel bridge signal conditioner with analog to digital converter (ADC), a PVDF touch sensor array, a touch sensor signal conditioner with a buffer, and a thermistor-based heat flux sensor. Additionally, there are solder tab connections for the PVDF array, strain beam assemblies, and a debug/programming port. From a hardware and software standpoint, the FTSN is very similar to the SMC electrical hardware as discussed previously

21.2.3.11 Fingertip sensor v2

For the second major iteration of the fingertip sensor, there was motivation to increase the tactile spatial resolution and reduce complexity and cost, while not foregoing salient capabilities. The strain-gage load cell and the four-element contact-sensing array were replaced with a 14-element haptic contact array. Each element is a compliant capacitor patch on the palmar surface of the fingertip. A specialized embedded microprocessor interprets the deformation of each capacitor patch as a local applied force. Fig. 21.35 shows an exploded view of the v2 fingertip sensor. The upper-right corner calls out the three functional layers of the multielement capacitive sensor. Glued to the finger core is a flexible PCB, which has (1) the electrical components (including a three-axes accelerometer) located under the fingernail, (2) the fixed half of each capacitive patch that is actively driven by the microprocessor, and (3) the communication and power “tail” connecting to the finger bus. A neoprene dielectric layer covers the capacitive patch portion of the flex PCB. The neoprene was specifically selected for its high compliance and compressibility, which enables both high sensitivity and minimal mechanical coupling to neighboring patches. A copper grounding plane over the neoprene is the other half of each capacitor patch whose distance to the flex PCB changes with applied pressure and changes the capacitive coupling measured by the embedded microprocessor. The entire sensor is then overmolded with urethane (50 A), which is the layer that interacts with the world. A fingerprint-type feature was designed into the urethane overmold in order to better excite the accelerometer when the fingertip is used to explore different surface textures.

Photos of the new fingertip sensor are shown in Fig. 21.36. The embedded electronics can be seen in the left photo. The right photo shows an assembled fingertip. A similar motion/vibration-

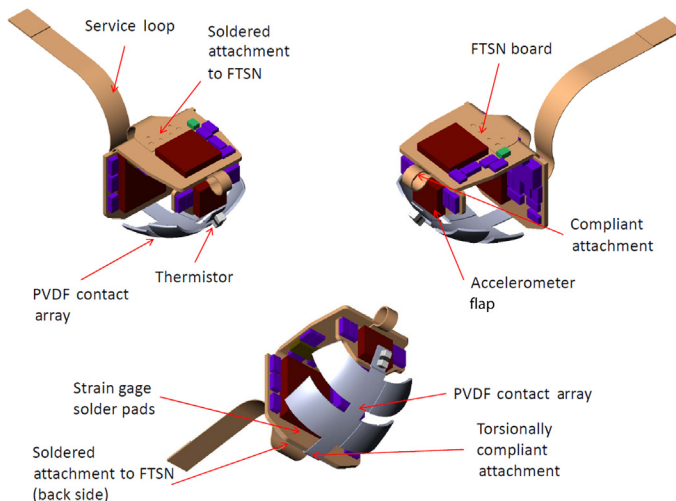
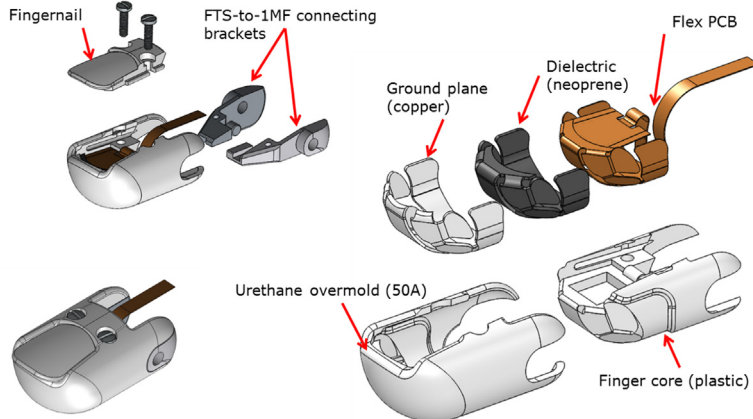


FIGURE 21.34

FTSN board (a fingertip sensor version with a touch sensor array is shown).

HDT.

**FIGURE 21.35**

Exploded view of the v2 fingertip sensor and its components.

HDT.

**FIGURE 21.36**

The v2 fingertip sensor. Fingernail removed showing the FTSN electrical hardware (left) and fully assembled unit (right).

HDT.

sensing system (accelerometer with fingerprint) was propagated to the new fingertip, while heat-flux sensing was removed. The thumb-tip sensor has a similar design, albeit larger.

21.2.4 AUXILIARY SUBSYSTEMS

21.2.4.1 *The neural fusion unit*

The original neural fusion unit (NFU) was derived from the LC, but with fewer RS485 transceivers and an 802.11 g WiFi transceiver added (Fig. 21.37). It could stream user intent and feedback data wirelessly to a computer for system configuration, training, and analytics. Eventually, the goal was to move PC-based algorithms and controls to the device itself. However, the bespoke nature of the

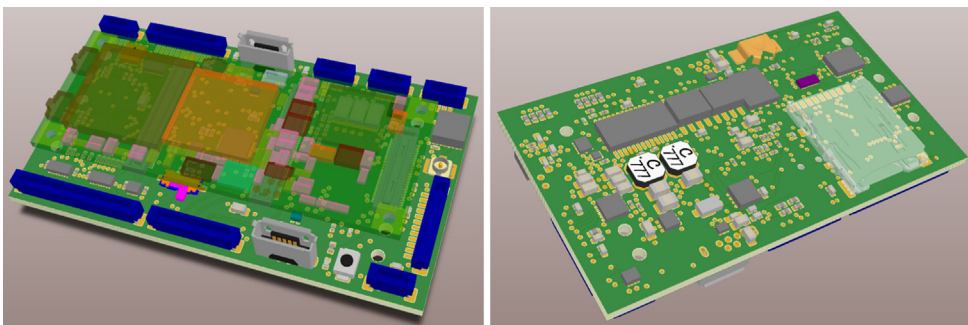


FIGURE 21.37

NFUv2 front and back images. The board is 2.2 in (55.8 mm) by 1.25 in (31.7 mm) in a horizontal plane. Stack height is 0.754 in (19.2 mm).

JHU/APL.

QNX operating system, inefficient WiFi chipset, system integration issues, and insufficient processing capabilities necessitated an update, which would become NFU v2. The real-time requirements of the NFU operating system were relaxed after having controlled the system successfully for years over WiFi connections to an external PC, which opened up the potential to using Linux as the core OS. After performing a market study for a SOM incorporating a newer processor with a volumetric footprint approaching the SOM used in the LC, a quad-core iMX6 was selected. The new SOM selection provided a bevy of additional enhancements, not previously considered in the original NFU. It provided dual controller area network interfaces which meant independent limb systems could be operated concurrently from a single central controller, thereby improving bilateral coordination and simplifying remote interfaces. The new wireless access chip included Bluetooth, which allowed direct connections to third-party low-cost electromyographic (EMG) input systems, such as the Myoband. To support improved logging of utilization data, a real-time clock and inertial measurement unit (IMU) sensors were added that were accessible to the software.

The NFU runs an embedded linux system running Ubuntu 16.10 as an operating system. This allows the flexibility of dynamically updating software modules and integrating new components and subsystems with relative ease. The NFU software includes the following modules: (1) a limb interface process, which predominantly handles CAN bus communication and state control; (2) an external device IO module which handles the interface with patient bidirectional biointerface components (e.g., wireless EMG, haptic feedback devices), and (3) a software instantiation of the virtual integration environment (VIE) which processes all signals, runs machine learning algorithms for extracting user intent, commands the limb system to move, and processes feedback delivered to the user. All software processes communicate with each other using User Datagram Protocol (UDP) which allows myriad software languages to be used across the platform (e.g., C, C++, python, etc.) according to the speed versus flexibility needs. Commands within the VIE are processed at a rate of 50 Hz (20 ms loop) which matches the native MPL CANbus communication rate. This also allows asynchronous communications with external devices (e.g., mobile devices) as needed.

21.2.4.2 Body attachment

The ability for an amputee to use the MPL as an extension of his or her body requires an effective body attachment strategy. The MPL was first integrated with traditional socket-based attachment mechanisms with a custom-designed electromechanical interface plate that enabled use by all levels of upper limb amputation from wrist to shoulder; a transhumeral example is shown in Fig. 21.38. The socket-based system shown in the figure houses embedded surface EMG hardware [the Conventional Prosthetic Controls Headstage (CPCH), deprecated design] and an early version of the NFU that provided signal acquisition and delivery of feedback for closed-loop sensory motor control of the limb including novel elements like fabric electrodes and flexible interface options. But socket systems can be problematic for the user, creating skin irritation and unreliable fit as the body changes throughout the day, which may lead to rejection and abandonment [16].

Advancements in surgical procedures like osseointegration (Fig. 21.39) provide an option for direct skeletal connection of the MPL to the user that result in consistent mechanical attachment



FIGURE 21.38

Example MPL v2 socket-based attachment strategy for a transhumeral patient. The NFU sits in a small compartment adjacent to the elbow drive.

JHU/APL.

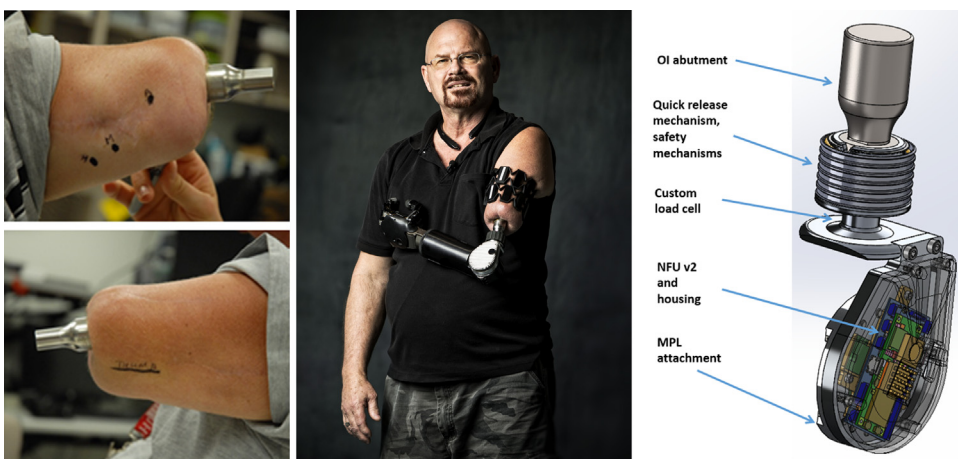


FIGURE 21.39

Transhumeral patient with osseointegrated implant for MPL attachment. Implant abutment (left). The same patient operating an MPL v3 system (center). The NFU v2 housing is next to the elbow and below the OI quick release mechanism. Model of the OI quick release mechanism (right).

JHU/APL.

[17–19]. Custom mechanical attachment hardware was developed to facilitate this body attachment method. The custom hardware includes real-time force monitoring at the level of the implant abutment as well as one-handed quick connect and disconnect of the MPL by the user. The challenge for restoring electrical control lost upon elimination of physical interface real estate for housing surface EMG electrodes previously located in the socket is resolved with a wireless sEMG control band. This band is an adaptation of an off-the-shelf device controller by Thalamic Labs called the Myo. The Myo provides eight channels of surface EMG control per band and multiple bands can be used. The combination of direct body attachment with osseointegration and wireless sEMG control represents the most advanced user interface seen with the MPL to date. We touch upon select clinical efforts with amputees in [Section 21.4](#).

21.3 HIGH-LEVEL CONTROLS AND SYSTEM INTERFACING

21.3.1 HIGH-LEVEL CONTROLS

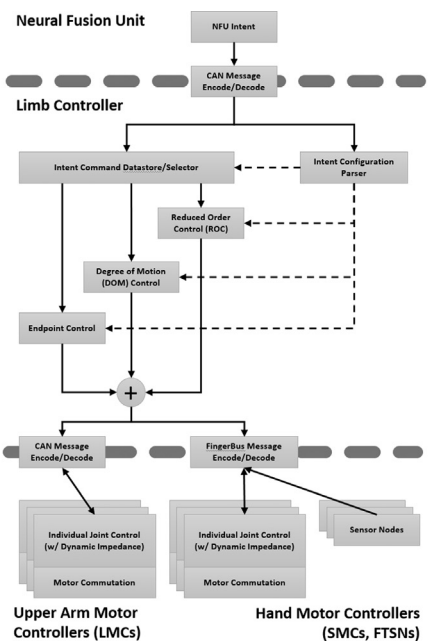
The MPL control architecture was designed to allow the user to operate the limb in multiple modalities as well as allow for smooth transitions to avoid introducing discontinuous behavior. The system consists of IJL controllers that are responsible for a low-level impedance algorithm that takes position, velocity, and torque feedback and controls the actuator to emulate a desired impedance relationship in order for the system to exhibit more natural human-like motion. In essence, the algorithm behaves as a configurable mass-spring-damper system. [Fig. 21.40](#) describes the control message architecture. High-level control data are sent down from the NFU at a fixed 50 Hz rate. Configuration data are only sent when the desired control modality changes and supports smooth transitions between modes.

There are three high-level modalities that are fused to form IJL commands:

1. Endpoint control—allows the patient to control the position and orientation of the palm in Cartesian space;
2. Degree of motion control—allows the patient to separately control the motion of each individual joint, provided they have enough input channels;
3. Reduced order control—allows the patient to use a single-input channel to control multiple joints simultaneously.

Using the combination of desired high-level commands from the patient and feedback from the physical system, the control algorithms produce low-level actuator commands to achieve the desired system behavior. The control message format encompasses a wide range of command types that the patient can use to interact with the prosthetic limb. For instance, individual joints or degrees of freedom can be commanded with a desired velocity, position, or torque. Alternatively, a virtual coordinate system is attached to the palm of the MPL hand, and Cartesian space commands can be issued to move to a fixed position/orientation in space or to move/rotate at a specified velocity. Patients that are unable to easily control individual joints due to a lack of input channels may instead issue grasp commands as well as control smooth transitions between different grasps. Additional parameters can be adjusted within all control modes to modulate the impedance of

- The limb controller performs the high-level controls:
 - DOM control
 - Endpoint control
 - Reduced-order control
 - Patient safety
 - Current allocation & limiting
 - Dynamic impedance for hand joints
- The motor controllers perform lower-level controls:
 - High-rate impedance loops
 - High-rate motion tracking
 - Motor commutation

**FIGURE 21.40**

High-level controls block diagram for the MPL.

selected joints. Such impedance modulation, for example, allows the limb to better mimic the compliance of a human limb.

21.3.2 VULCANX AND THE OCU

VulcanX serves as a common interface with both the physical MPL, and the virtual MPL (vMPL), allowing both commands from the user and percepts from the system to be received, interpreted, and relayed from a single location. This layer of abstraction with the entire system ensured a consistent interface for the user to send commands and receive percepts as the MPL and vMPL were developed and capabilities or features added or updated, or if the MPL or vMPL were swapped for one another in various testing scenarios. VulcanX utilizes UDP message streaming to ensure cross-platform compatibility, versatility in the networking setup, and distribution of functional roles of computing and testing systems, as well as easy stopping, starting, or swapping in and out of command sources or command destinations.

The operator control unit (OCU) provides a direct interface to monitor configuration settings in the MPL LC. This enables reading and modification of hardware and signal processing parameters for limb calibration and performance tweaking. Additionally, the user can set specific parameters and settings for hardware configurations depending on patient setup and preferences. The OCU is the primary interface for system debugging and diagnostics.

21.3.3 THE VIE AND THE VMPL

The Virtual Integration Environment (VIE, Fig. 21.41) is a software emulation of the modular prosthetic limb (MPL) with shared communication interfaces. It is designed as an integration and training tool for clinical research in the fields of upper extremity prosthetics and rehabilitation. The VIE system [20] is a flexible software environment that is dynamic and scalable enough to be run from server systems down to an embedded system on module architectures (e.g., Raspberry Pi). The VIE provides both a 3D graphical visualization and physical simulation of the MPL including the 26 articulating joints and 17 independently controllable virtual motors operating and interacting within a virtual world. The VIE simulates physical object interactions with the virtual MPL (vMPL), including contact, grasping, and fingertip force, and allows grasping, transporting, and repositioning of objects. Limb data and virtual sensor percepts are generated through control of the vMPL, from object interactions to event handling within the environment. Data and percepts are available to the clinical operator through defined interfaces that are shared between the physical and virtual MPL systems. The VIE has been developed as a framework allowing creation of multiple virtual scenarios that facilitate clinical training, real-time operation of the vMPL, and offline data analysis. Because of its versatility and portability, the VIE is well suited to support the development of closed-loop experimental systems for both motor control and sensory feedback, which establishes a basis for eventual clinical use of a physical MPL system. In the case of end-user operation of the MPL on amputees, the signal processing and command aspects of the VIE are run using the open-source Python variant [21,22].

The vMPL is a simulator for the MPL system to support both control system development and evaluation, and clinical testing for both motor control and sensory feedback. The vMPL was constructed in the Unity3d gaming engine, which provides a visualization of an emulated MPL system with textured meshes and physics engine elements that include hinge joints and motors, springs, dampers, and surface colliders. The game engine environment allows for simulated physical object interactions, permitting the vMPL to pick up and manipulate objects in the scene, as well as the emulated data streaming of joint, contact, and fingertip sensors normally found in the physical MPL system. Development within the Unity3d environment allows for the rapid construction of immersive training scenarios, integration with third-party technologies such as kinematic tracking sensors, and quick deployment to virtual reality and augmented reality platforms to support a number of use cases and training setups.

21.3.4 WEB INTERFACE

Typically the operation of the MPL system runs in a “closed-loop” operation mode with the user only “thinking” about movements and the device responding. Specifically the process involves the following steps: the system acquires biological signals from the user related to intention to move the arm, the system then processes these signals using machine learning algorithms to generate a command signal to the prosthetic, actuation commands are then sent to the individual MPL motors to allow manipulation. In parallel, as the MPL interacts with the environment, sensor data are acquired, processed, and actuated in the reverse process to allow the user to “feel” from the prosthetic arm [23]. At times, however, the user may want to recalibrate the machine learning algorithm, change various settings such as speed and stiffness of the MPL, or change the active

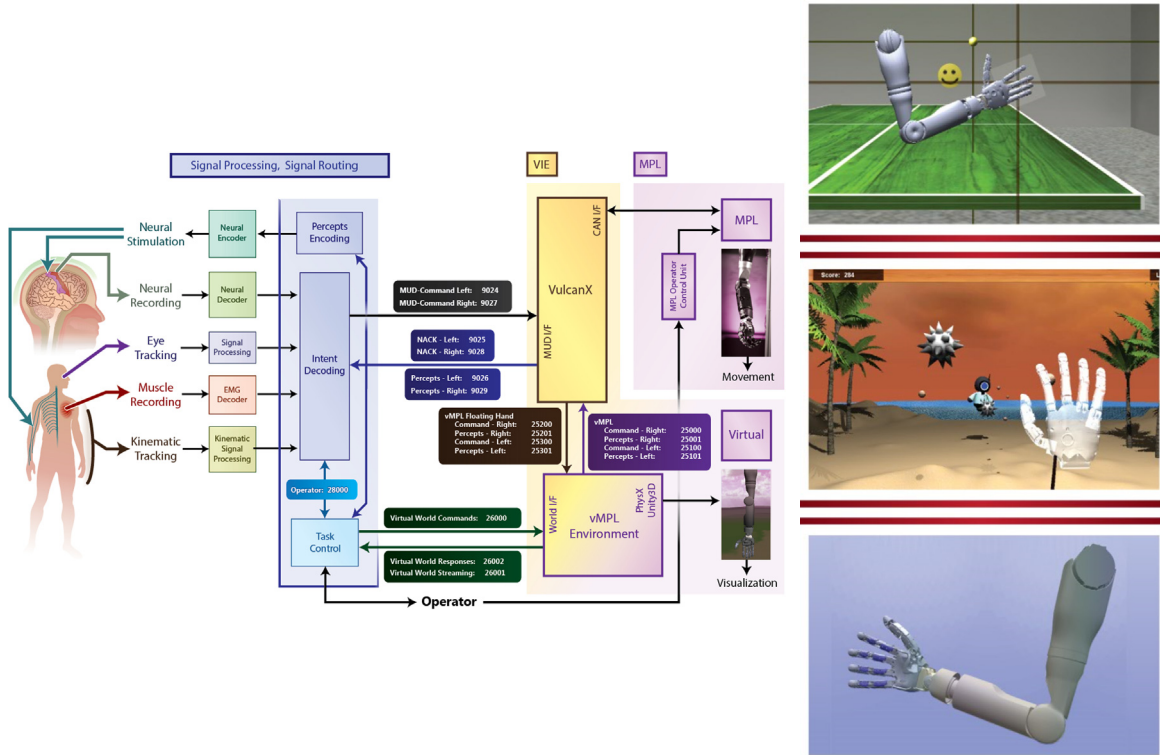


FIGURE 21.41

High-level VIE architecture (left) and example vMPL scenarios (right).

JHU/APL.

grasping modes of the arm. For these purposes, a mobile web application was developed such that the user can adjust these parameters using any web browser or smartphone (Fig. 21.42).

The mobile application is hosted by an embedded server running on the MPL NFU. Once connected to the password-protected local wireless network (WiFi ad hoc network mode), any device with a browser can access the javascript-enabled webpage to interface with and configure the system. Operation of the mobile WebApp can be performed by the end user assuming they have the ability to operate a computer or smartphone (e.g., unilateral amputation or voice control), or the interface can be operated by a separate user (e.g., physical therapist, prosthetist, or caregiver). The user can swipe the images to select various trainable motions of the arm, view system status and battery details, configure parameters, and complete control assessments which monitor and log the level of proficiency of user control. One such assessment is the Target Achievement Control (TAC) test [24], which has been adapted from published work in order to create a variant that can run on a smartphone. This assessment presents the user with a desired position configuration of the arm and logs the time and path taken by the user to achieve the position using volitional control.

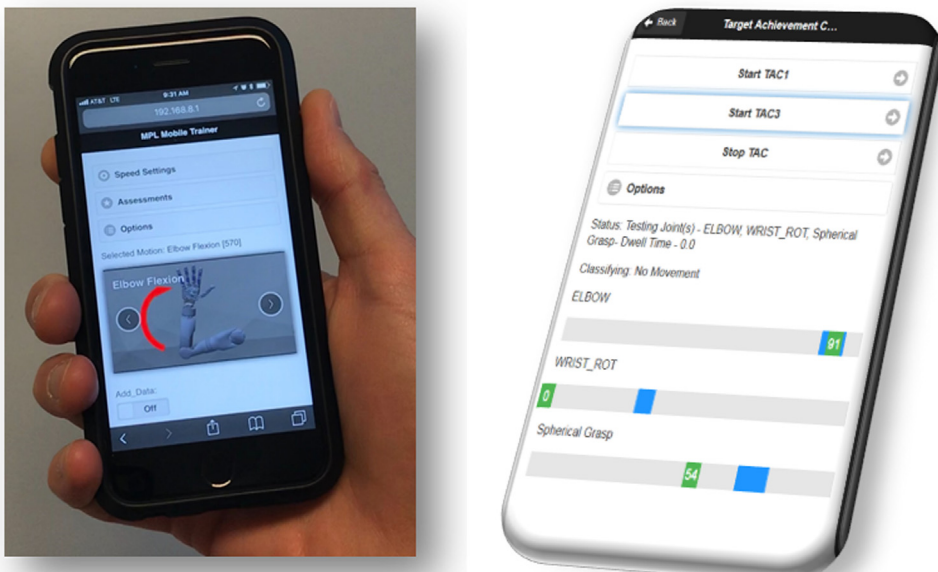


FIGURE 21.42

Mobile WebApp interface for calibrating and configuring the MPL system (left). Mobile WebApp page dedicated to assessing user control proficiency (right).

21.4 SELECT MPL APPLICATIONS AND USES

21.4.1 CORTICAL CONTROL AND FEEDBACK

As noted in the introduction, a primary goal of the program was to use the MPL in the creation of a neurally integrated prosthetic system. APL teamed with key clinical collaborators at the University of Pittsburgh Medical Center (UPMC) [25], Caltech [26], and the University of Chicago in an effort to achieve this end. The individuals that qualified for the procedure were those with upper spinal cord injuries or neurodegenerative disorders typically resulting in quadriplegia. The first patient to use the MPL in a cortical control scenario had two microelectrode arrays [27] implanted in her motor cortex (M1). Leveraging advancements in motor decoding, the patient was able to achieve a level of control of the MPL system at very life-like and naturalistic levels, achieving a self-feeding task [28]. The patient was very quickly able to reach a high degree of control at seven dimensions, which included six-DoF endpoint control over the MPL (Cartesian position and rotation of the palm) and one grasp pattern (typically a spherical or power grasp) [29], peaking out at 10 dimensional control, adding in four unique hand-shaping components [30]. This level of control established a new performance benchmark for neurally integrated prosthetics.

The second patient implanted at UPMC (Fig. 21.43, right) had two implants both in motor cortex and somatosensory cortex (S1) to close the sensory feedback loop. This individual progressed to a level of motor control commensurate with patient one for a period of time at seven-dimensional control, but was unable to replicate 10-dimensional control. Regardless, the primary focus of patient #2's clinical activities was to prove out the efficacy and usefulness of direct cortical microstimulation using a neural prosthesis [31]. Given the placement of the implant and overlapping coverage of the receptive field (palm and index finger), patient 2 achieved painless sensation representation through microstimulation of S1 described as warm, pressure, electrical, and touch-like.



FIGURE 21.43

UPMC SCI patient #1 controlling the MPL for a self-feeding task (left). Pitt SCI patient #2 undergoing a sensory stimulation experiment using direct neural stimulation driven by physical interaction with the MPL.

UPMC.

The patient at Caltech had two implants similar to UPMC patient #1 for motor decoding. A primary difference was implant location, as this patient had their implants in their posterior parietal cortex (PPC) [32,33]. Due to a number of factors the patient had difficulty achieving a high degree of direct dimensional control over the MPL. To circumvent this challenge we leveraged internally developed approaches classified as hybrid BCI [34] in order to leverage the goal-oriented information coming from PPC with autonomous robot manipulation planning [26,35]. This allowed the patient to execute functional activities of daily living (ADL) such as drinking [36].

21.4.2 AMPUTEES

The MPL has been used in a research context by a variety of end-users with varying levels of amputations including wrist disarticulation, trans-radial, trans-humeral, and shoulder disarticulation levels (Fig. 21.44). This includes users with both unilateral [37] and bilateral amputation [38], congenital versus acquired limb deficiency, users with and without targeted muscle reinnervation surgery [9], and users with osseointegration [39,40]. It is very much the nature of the modular system to be adapted and configured to any level of amputation. In all cases for amputee end-users the control has been based upon pattern recognition-based machine learning. The system is trained on biological signals (EMG) acquired while mentally visualizing creating those motions with their missing arm. As the user imagines creating these motions, the pattern of EMG activity is recorded and labeled with the desired motion. Signal features (mean absolute value, curve length, zero crossings, and slope sign changes) are extracted from the EMG signal and these training examples are used to train a linear discriminant analysis classifier [41]. Users train each of the arm joints in each direction (e.g., elbow flex, elbow extend, wrist pronate, wrist supinate, etc.). However, for the hand, coordinated “grasps” are trained. Any hand configuration can be trained in the system using reduced order control which generates a motion by identifying several key frames and then interpolating the motion between. As an example, to train a precision grasp with the thumb and forefinger,



FIGURE 21.44

Full bilateral shoulder level control of the MPL with 42 total degrees of freedom (left). Dexterous and intuitive control enabled by targeted muscle reinnervation and osseointegrated body attachment implant (right).

first the middle, ring, and little finger are fully flexed and the thumb is positioned in opposition to the forefinger. This grasp prehension is saved as a key frame in addition to the full open position. Finally, the fully closed fine pinch position is saved. The user has to only think about and visualize closing the hand in a particular hand conformation and the prosthetic will smoothly transition through each state. At any point the process can be stopped, reversed, and continued as needed to perform the desired manipulation. Users can customize and define their own grasps for both functional grasping patterns such as “power grasp,” “fine pinch grasp,” “key grasp,” as well as expressive hand conformations such as “peace,” “OK,” “hang loose,” etc.

Dozens of users have evaluated the MPL in a clinical setting. Recent research studies however, have taken the MPL system into more everyday environments in a “take-home” setting, allowing users to take full advantage of the dexterous function of the MPL (Fig. 21.44, right). One user leverages the flexibility of the MPL to do everything from cooking to household chores to gardening using a roto-tiller to playing the piano with individual fingers [42,43].

21.4.3 ROBO SALLY

As a very capable wearable robotic system, there is tremendous opportunity to leverage the capabilities of the MPL system for humanoid robot applications. Over the last 10 plus years, APL has been leveraging MPL technology through internal research and development activities to realize a semihumanoid robotic system named Robo Sally [44,45] (Fig. 21.45). In general, the forms of Robo Sally have been comprised of a number of key subsystems including ground-based mobility with sensing, torso articulation, bilateral MPL systems, computing, power, sensorized head (pan and tilt), comms, and power. Robo Sally has been leveraged for executing research-level activities focused on demonstrating the usefulness of a bimanual manipulation system to replicate human capabilities to keep humans out of harm’s way in hazardous environments such as disaster response, space, explosive ordnance disposal, and nuclear facility operations.



FIGURE 21.45

The JHU/APL bimanual mobile manipulation system Robo Sally (left) which leverages MPL systems (right). A nested marsupial system consisting of Robo Sally, a small UAV, and a micro-UGV (right).

JHU/APL.

We typically focus research into control modalities ranging from direct teleoperation [44] to varying degrees of autonomous operations [46], including multirobot teaming to explore unknown spaces [47–49].

21.5 CONCLUSION

We currently live in an exciting time where the technological lines between robotics, artificial intelligence, and medical science continue to overlap and become ever more intertwined. The Revolutionizing Prosthetics Program has helped push technology further toward an age where wearable robotic systems are being further integrated with the processing capabilities, dexterous movement intent, and sensory pathways of the human brain. The MPL is a state-of-the-art example of a dexterous wearable robotic system that has helped define the realm of possibilities in restoring the functional dexterity and sensory feedback capabilities of the human arm and hand. Here we have covered the design and functional capabilities of the MPL system in its entirety. Through the now 14 years and counting, the Revolutionizing Prosthetics team has created and developed technologies with the singular goal of realizing a neurally integrated prosthetic system. Our mission continues to be focused on restoration of functional capabilities for humans who have lost hand or arm function through amputation, impairment, injury, or congenital conditions. We have successfully demonstrated this vision through a number of clinical activities with collaborating institutions with amputees and spinal cord injury patients. As we execute our mission, we continually seek to further understand and overcome technological limitations and take full advantage of evolving opportunities to create and define capabilities to restore lost human functionality.

ACKNOWLEDGMENTS

Throughout the course of the RP program there have been too many individual contributors to name in entirety here, but the authors give thanks to all who touched the development and applications of the MPL. Special thanks to principal DARPA and APL leadership on the program throughout the years from Geoff Ling, Justin Sanchez, Stuart Harshbarger, John Bigelow, Alan Ravitz, and Mike McLoughlin. Additionally, a special thanks to Ezra Johnson for his key role in the design of the MPL system, Aseem Raval for software development, and John Roycroft, Jared Wormley, and Chris Dohopolski for supporting and maintaining MPL systems. This work has been supported by the Space and Naval Warfare Systems Command under Contracts N66001-10-C-4056 and N66001-06-C-8005. Any opinions, findings and conclusions, or recommendations expressed in this material are those of the authors and do not necessarily reflect the views of DARPA or Space and Naval Warfare Systems Command.

REFERENCES

- [1] L. Resnik, S.L. Klinger, K. Etter, The DEKA arm: its features, functionality, and evolution during the Veterans Affairs Study to optimize the DEKA arm, *Prosthet. Orthot. Int.* (2013).

- [2] R.A. Miranda, et al., DARPA-funded efforts in the development of novel brain–computer interface technologies, *J. Neurosci. Methods* 244 (Apr. 2015) 52–67.
- [3] R.A. Andersen, E.J. Hwang, G.H. Mulliken, Cognitive neural prosthetics, *Annu. Rev. Psychol.* 61 (1) (2010) 169–190.
- [4] L.J. Love, R.F. Lind, J.F. Jansen, Mesofluidic actuation for articulated finger and hand prosthetics, in: 2009 IEEE/RSJ International Conference on Intelligent Robots and Systems, 2009, pp. 2586–2591.
- [5] K.B. Fite, T.J. Withrow, K.W. Wait, M. Goldfarb, A gas-actuated anthropomorphic transhumeral prosthesis, in: IEEE International Conference on Robotics and Automation 2007, pp. 3748–3754.
- [6] W. Kaal, S. Herold, Electroactive polymer actuators in dynamic applications, *IEEE/ASME Trans. Mechatron.* 16 (1) (Feb. 2011) 24–32.
- [7] E.L. Faulring, J.E. Colgate, M.A. Peshkin, A high performance 6-DOF haptic Cobot, in: Proceedings ICRA'04. 2004 IEEE International Conference on Robotics and Automation, IEEE, 2004, pp. 1980–1985, vol. 2.
- [8] M.S. Johannes, J.D. Bigelow, J.M. Burck, S.D. Harshbarger, M.V. Kozlowski, T. Van Doren, An overview of the developmental process for the modular prosthetic limb, *Johns Hopkins APL Tech. Digest* 30 (3) (2011) 207–216.
- [9] T.A. Kuiken, et al., Targeted muscle reinnervation for real-time myoelectric control of multifunction artificial arms, *JAMA* 301 (6) (2009) 619–628.
- [10] F. Cordella, et al., Literature review on needs of upper limb prosthesis users, *Front. Neurosci.* 10 (2016).
- [11] M. Velliste, S. Perel, M.C. Spalding, A.S. Whitford, A.B. Schwartz, Cortical control of a prosthetic arm for self-feeding, *Nature* 453 (7198) (2008) 1098–1101.
- [12] J.A. Berg, et al., Behavioral demonstration of a somatosensory neuroprosthesis, *IEEE. Trans. Neural. Syst. Rehabil. Eng.* 21 (3) (2013) 500–507.
- [13] A.D. Ravitz, et al., Revolutionizing prosthetics - phase 3, *Johns Hopkins APL Tech. Digest* 31 (4) (2013) 366–376.
- [14] T. Moyer, E.L. Faulring, J.J. Santos-Munne, One motor finger mechanism, 8,470,051 B2, June 25, 2103.
- [15] L. Skedung, M. Arvidsson, J.Y. Chung, C.M. Stafford, B. Berglund, M.W. Rutland, Feeling small: exploring the tactile perception limits, *Sci. Rep.* 3 (2013).
- [16] E.A. Biddiss, T.T. Chau, Upper limb prosthesis use and abandonment: a survey of the last 25 years, *Prosthet. Orthot. Int.* 31 (3) (2007) 236–257.
- [17] R.T. Bothe, L.E. Beaton, H.A. Davenport, Reaction of bone to multiple metallic implants, *Surg. Gynecol. Obstetr.* 71 (1940) 598–601.
- [18] G.S. Leventhal, Titanium, a metal for surgery, *J. Bone Joint Surg. Am.* 33-A (2) (1951) 473–474.
- [19] P.I. Branemark, Osseointegration and its experimental background, *J. Prosthet. Dent.* 50 (3) (1983) 12.
- [20] R.S. Armiger, et al., A real-time virtual integration environment for neuroprosthetics and rehabilitation, *Johns Hopkins APL Tech. Digest* 30 (3) (2011) 198–206.
- [21] R.S. Armiger, MiniVIE. [Online]. Available from: <https://bitbucket.org/rarmiger/minivie>.
- [22] W. Haris, J. Lesho, A. Chi, R. Armiger, Low-cost pattern recognition based multi-digit myoelectric hand prosthesis, in: Presented at the American Academy of Orthotists & Prosthetists 43rd Academy Annual Meeting & Scientific Symposium, 2017.
- [23] A. Chi, C.W. Moran, R.S. Armiger, The JHU/APL modular prosthetic limb: first case study experience with integrated sensory feedbackon a transhumeral amputee with targeted muscle reinnervation, in: Presented at the American Academy of Orthotists & Prosthetists 40th Academy Annual Meeting & Scientific Symposium, 2014.
- [24] A.M. Simon, L.J. Hargrove, B.A. Lock, T.A. Kuiken, The target achievement control test: evaluating real-time myoelectric pattern recognition control of a multifunctional upper-limb prosthesis, *JRRD* 48 (2011) 619–628.

- [25] J.L. Collinger, et al., Collaborative approach in the development of high-performance brain-computer interfaces for a neuroprosthetic arm: translation from animal models to human control: the multidisciplinary team behind an advanced BCI, *Clin. Transl. Sci.* (2013).
- [26] K.D. Katyal, et al., A collaborative BCI approach to autonomous control of a prosthetic limb system, in: 2014 IEEE International Conference on Systems, Man and Cybernetics (SMC), 2014, pp. 1479–1482.
- [27] K.E. Jones, P.K. Campbell, R.A. Normann, A glass/silicon composite intracortical electrode array, *Ann. Biomed. Eng.* 20 (4) (1992) 423–437.
- [28] C.B.S. News, Breakthrough: robotic limbs moved by the mind. [Online]. Available <https://www.youtube.com/watch?v=Z3a5u6djGnE>.
- [29] J.L. Collinger, et al., High-performance neuroprosthetic control by an individual with tetraplegia, *The Lancet* 381 (9866) (2013) 557–564.
- [30] B. Wodlinger, J.E. Downey, E.C. Tyler-Kabara, A.B. Schwartz, M.L. Boninger, J.L. Collinger, Ten-dimensional anthropomorphic arm control in a human brain – machine interface: difficulties, solutions, and limitations, *J. Neural. Eng.* 12 (1) (2015) 016011.
- [31] S.N. Flesher, et al., Intracortical microstimulation of human somatosensory cortex, *Sci. Translat. Med.* 8 (361) (2016), pp. 361ra141–361ra141.
- [32] T. Aflalo, et al., Decoding motor imagery from the posterior parietal cortex of a tetraplegic human, *Science* 348 (6237) (2015) 906–910.
- [33] C. Klaes, et al., Hand shape representations in the human posterior parietal cortex, *J. Neurosci.* 35 (46) (2015) 15466–15476.
- [34] R. Leeb, J. d R. Millán, Introduction to devices, applications and users: towards practical BCIs based on shared control techniques, in: B.Z. Allison, S. Dunne, R. Leeb, J.D.R. Millán, A. Nijholt (Eds.), *Towards Practical Brain-Computer Interfaces*, Springer, Berlin Heidelberg, 2013, pp. 107–129.
- [35] K.D. Katyal, et al., HARMONIE: a multimodal control framework for human assistive robotics, in: Neural Engineering (NER), 2013 6th International IEEE/EMBS Conference on, 2013, pp. 1274–1278.
- [36] Caltech, HARMONIE success HD 2. [Online]. Available from: <https://www.youtube.com/watch?v=3RUIzAsM5dM>.
- [37] B.N. Perry, C.W. Moran, R.S. Armiger, P.F. Pasquina, J.W. Vandersea, J.W. Tsao, Initial clinical evaluation of the modular prosthetic limb, *Front. Neurol.* 9 (2018).
- [38] The Johns Hopkins University Applied Physics Laboratory, Amputee Makes History with APL's Modular Prosthetic Limb. [Online]. Available from: <https://youtu.be/9NOncx2jU0Q>.
- [39] L.M. Carroll, M.S. Johannes, R.S. Armiger, Development of an osseointegration interface for a dexterous prosthetic limb, in: Presented at the 7th International Conference: Advances in Orthopaedic Osseointegration, San Francisco, CA, 2017.
- [40] L.M. Carroll, M.S. Johannes, C.W. Moran, R.S. Armiger, Comparison of pattern recognition control with a socket and with an osseointegration implant: a case report, in: Presented at the 7th International Conference: Advances in Orthopaedic Osseointegration, San Francisco, CA, 2017.
- [41] L.J. Hargrove, G. Li, K.B. Englehart, B.S. Hudgins, Principal components analysis preprocessing for improved classification accuracies in pattern-recognition-based myoelectric control, *IEEE Trans. Biomed. Eng.* 56 (5) (2009) 1407–1414.
- [42] Quartz Media, Living with a mind-controlled robot arm. [Online]. Available from: <https://www.youtube.com/watch?v=xKUn0-Bhb7U>.
- [43] Quartz Media, Playing piano with a mind-controlled robotic arm. [Online]. Available from: <https://www.youtube.com/watch?v=DP677IA DEA>.
- [44] M.S. Johannes, R.S. Armiger, M.J. Zeher, M.V. Kozlowski, J.D. Bigelow, S.D. Harshbarger, Human capabilities projection: dexterous robotic telemanipulation with haptic feedback, *Johns Hopkins APL Tech. Dig.* 31 (4) (2013) 315–324.

- [45] JHU/APL, Bimanual Dexterous Robotic Platform (Robo Sally). [Online]. Available from: <https://www.youtube.com/watch?v=elZU29F4Bbc>.
- [46] K.D. Katyal, et al., Approaches to robotic teleoperation in a disaster scenario: from supervised autonomy to direct control, in: 2014 IEEE/RSJ International Conference on Intelligent Robots and Systems (IROS 2014), 2014, pp. 1874–1881.
- [47] J. Moore, et al., Nested marsupial robotic system for search and sampling in increasingly constrained environments, in: 2016 IEEE International Conference on Systems, Man, and Cybernetics (SMC), 2016, pp. 002279–002286.
- [48] JHU/APL, Intelligent Co-robots: Demonstration. [Online]. Available from: <https://www.youtube.com/watch?v=Hvh20ySwgPw&t>.
- [49] JHU/APL, Intelligent Systems: Autonomous Marsupial Robot Teams. [Online]. Available from: <https://www.youtube.com/watch?v=7Gz7yjYqEEM&t>.

SENSING AND CONTROL FOR PROSTHETIC HANDS IN CLINICAL AND RESEARCH APPLICATIONS

22

Luke E. Osborn¹, Mark M. Iskarous¹ and Nitish V. Thakor^{1,2,3}

¹*Department of Biomedical Engineering, Johns Hopkins School of Medicine, Baltimore, MD, United States*

²*Department of Electrical and Computer Engineering, Johns Hopkins University, Baltimore, MD, United States*

³*Singapore Institute for Neurotechnology, National University of Singapore, Singapore, Singapore*

22.1 INTRODUCTION

From gross movements to object grasping and fine manipulation our arms and hands play an obviously valuable role in our daily lives. The movement of our hands, combined with our sophisticated sense of touch, enables us to seamlessly interact with our environment. The loss of a limb presents a difficult challenge in that much of the basic functionality we rely on as humans is no longer available in the same way. The use of prosthetic hands has proven to be a viable option for replacing a lost or missing hand.

The technology and functionality of upper limb prostheses have seen notable progress since the 2010s, specifically in control of the device as well as sensory feedback. Two of the most important factors for creating an effective prosthesis are in making the control of the device intuitive and natural and in creating a naturalistic and usable form of sensory feedback to the user. Given that our hands are highly functional organs essential to our daily lives, and that hand function relies heavily on the sense of touch, it is crucial for an upper limb prosthesis to help replace some of the lost sensory components in addition to providing a way of grasping and manipulating objects.

Rudimentary prosthetic hands have been documented as early as the 200s BC and have slowly improved from passive iron devices to movable joints to body-powered hooks to myoelectrically controlled hands [1]. For an overview of prosthetic hand history, see Ref. [1]. Today, technological advancements have made more realistic and functional upper limb prostheses a reality. For example, the modular prosthetic limb (MPL) developed by the Johns Hopkins University Applied Physics Laboratory (JHU/APL) has 26 controllable degrees of freedom (DoFs) and over 100 sensors [2].

The focus of this chapter is on prosthetic hands that are powered through physiological signals, such as electromyography (EMG), electrocorticography (ECoG), electroencephalography (EEG), or even neuron spikes. However, it should be noted that body-powered prostheses have also improved and are still a common prosthesis solution for upper limb amputees [3] and continue to be researched [4]. At this point, it is worth noting that prosthetic arms can be used by amputees as

well as people living with congenital limb deficiencies or paralysis. For the purpose of this chapter, we discuss research and clinical applications of prosthetic hands for amputee users. A myoelectric prosthesis is controlled using EMG signals from the residual limb of an amputee, but EEG and ECoG signals from the brain can also be used to control a prosthesis. There are several examples of prosthetic hand control using EEG [5], ECoG [6], and even neuron spikes [7,8], but perhaps the most common way to control a prosthetic hand in clinical and real-world settings is using EMG signals. This is due to several factors including the noninvasive nature of measuring surface EMG as well as the currently available commercial prosthetic hands that are capable of fine movements, which are developed to interface with EMG signals.

Regardless of the input control signal, many of the same techniques such as movement decoding and sensory feedback are used to create functional and effective prostheses for clinical and research applications. Research has led to improvements in the mechanical design and dexterity of prosthetic limbs [2], signal processing techniques for movement decoding [9], biomimetic sensors for capturing information during prosthesis use [10–12], and providing sensory feedback to elicit sensations of movement [13], touch [14], and even pain [12].

Prosthesis fit and comfort are of paramount importance to users [15] and are leading reasons for the relatively high abandonment rates (estimated at 23% in 2007) of upper limb prostheses [16]. Users cite poor fit and heat or perspiration as contributors to this discomfort [15], but clinical efforts have led to developments in novel prosthetic socket technology to address these issues and provide better upper limb prosthesis fit [17], while research has also been done on creating an adaptive socket that creates uniform loading on the residual limb during prosthesis use [18].

Although fit and comfort are fundamental components of a prosthetic limb, this chapter focuses on the control and sensing aspects for clinical and research applications. In fact, there are numerous other areas related to upper limb prostheses and brain–computer interfaces in general that are not discussed in this chapter. However, we refer interested readers to more thorough reviews on neural interfaces [19], integrated neural circuits and amplifiers [20], and micro- and nanoelectrodes for neural recordings [21]. For a more general overview of neural prostheses, including upper limb devices, see Ref. [22].

For the remainder of this chapter, we discuss methods for both control and sensing of prosthetic hands. To make a truly human-like and effective prosthesis, there needs to be robust and intuitive forward control as well as natural and reliable sensory feedback, which are complementary in nature. Forward control is dictated by the quality of the movement decoding and signal quality, whereas the feedback relies heavily on the capabilities of the sensors and is useful for both the user and the prosthesis. Sensory feedback is necessary because it completes the loop by informing the user on what the prosthesis is touching or where it is in space, which are crucial components for creating a lifelike and functional prosthetic limb. In the following sections, we will provide examples of progress in these areas. We will address both the current state-of-the-art technologies for clinical and research applications and the future directions of prosthetic hands.

22.2 PROSTHESIS CONTROL

Cosmetic, body-powered, and myoelectric devices are the most common prostheses, each making up roughly one third of devices used [23]. In this section we focus on electronically powered

prosthetic hands because they present interesting control challenges. Multiarticulated prosthetic hands can be controlled by a range of physiological signals, but there are several challenges that researchers and users face when decoding intended movements, such as effects from limb position and electrode contact.

22.2.1 MOVEMENT SIGNALS

Electrical activity produced within the nervous system initiates movement. This activity is generated in the cortex and is sent through the spinal cord to the peripheral nerves and finally to the muscles which then causes muscle contractions and ultimately limb movement. For a prosthetic hand, the electrical activity that results from volitional movement is captured and sent to a controller that classifies the intended movement and outputs the correct commands to the prosthesis to drive movement. The common modalities for recording electrical activity due to intended movement from the brain are *electroencephalography* (EEG) (Fig. 22.1A), *electrocorticography* (ECoG), and *action potentials*. Electrical activity from muscle movement can also be recorded from the peripheral nervous system with *electromyography* (EMG) (Fig. 22.1B), which is the most common technique for controlling upper limb prostheses in research and clinical applications, as it is noninvasive and relatively easy to set up.

EEG signals, obtained noninvasively through the scalp, have been used for controlling multiple DoFs of a hand [5], but EEG is generally considered a poor choice for prosthesis control because of complications with the electrode–scalp interface during head movement as well as the low-pass filtering effect on signals. A more invasive approach for recording neural signals from the brain may be needed to obtain greater signal-to-noise ratio. For instance, ECoG, in which electrodes are placed directly on the surface of the brain, gives the opportunity to capture the signals and interactions in wide regions of the brain and its motor and sensory cortices. ECoG signals have been shown to decode individual finger movements [24,25] as well as three DoFs in a prosthetic arm [6]. Alternatively, highly specific signals can be obtained when action potentials are recorded from microelectrode arrays directly from the cortex. These action potentials have also been shown to enable decoding of reaching and grasping in a prosthetic arm [8]. As a completely different

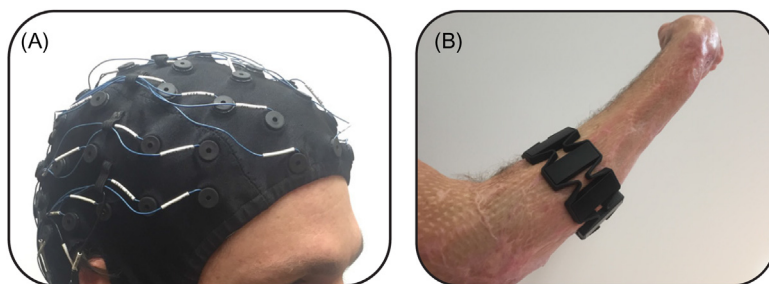


FIGURE 22.1

(A) Noninvasive electrode cap for measuring EEG signals and (B) an electrode cuff for capturing EMG signals from the surface of the arm of an amputee. EEG and EMG, along with other physiological signals such as ECoG and neuron spikes, can be used to capture volitional movement commands and decoded for prosthesis control.

alternative, action potentials can also be recorded in the peripheral nervous system for prosthesis control as well [26]. For a more thorough discussion on the relative merits of using neural signals used for decoding movement intent and controlling a prosthesis, see Ref. [27].

Cortical and peripheral signals require delicate and usually invasive neural interfaces. For complex and dexterous prostheses in real-world applications, these decoding and control signals are still difficult to record, decode, and manipulate. Surface EMG signals can be obtained noninvasively and have served very well as a practical input signal for today's commercial prostheses. EMG signals are easy to acquire and do not require a significant setup period. EMG can be recorded invasively using implanted electrodes to measure intramuscular activity; however, this approach has not become as common. A thorough discussion of EMG and its use in controlling prosthetic hands can be found in Ref. [28].

There are several challenges with movement decoding using physiological signals. One is that machine learning methods rely on incoming signals to be similar to signals acquired during training. However, signals may change over time with fatigue or other factors that negatively influence the signal stability. For instance, positional changes of the limb in space can reduce EMG signal similarity [29] and loading effects on the prosthesis can also degrade classification performance [30]. Considering the practicality, and higher prevalence of EMG signal-based prostheses and their applicability to active users, the next section focuses on decoding intended movements from myoelectric signals.

22.2.2 MOVEMENT DECODING

The emerging method for controlling a prosthetic hand is pattern recognition. The idea being that when natural movements are made by an amputee, they elicit unique and reproducible neural signal patterns (Fig. 22.2A). Those signals are recorded and decoded into different intended hand or limb movements. The signals are then transformed into features, which are then mapped to corresponding hand movements using pattern recognition techniques (Fig. 22.2B). Various machine learning techniques such as Kalman filters [26,31], linear regression [32], neural networks [33], maximum likelihood estimation [34], and linear discriminant analysis [35] can be utilized to estimate intended hand movements based on the neural signals. These methods can be used regardless of the neural signal being used to decode intended movements.

In general, movement decoding techniques have been continuously improved over the past several years [28,36,37] and results have shown that training is a major factor in improving prosthesis control [38]. Recently, linear regression techniques with surface EMG signals have enabled simultaneous DoF and proportional prosthesis control, which improves functionality during activities of daily living [32]. Another emerging trend is the use of high-density EMG signals to create images of EMG activity for predicting hand movements [39].

Effects from activities of daily living, such as limb position, loading, and changes in electrode contact, can all degrade decoding performance. It is difficult to predict all of these adverse effects, which presents a challenge while training the classifiers. As a result, researchers will continue to develop more robust methods to overcome these challenges. To test the efficacy of movement decoding, prosthesis users often perform some standardized experiments. Some of these clinically validated methods include the target achievement control (TAC) test, which provides prosthesis users with targets such as a particular hand grip and position that they have to achieve [40].

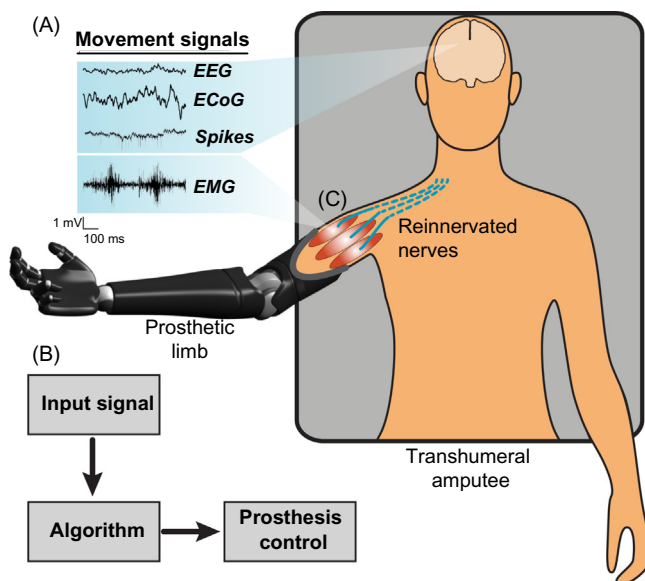


FIGURE 22.2

(A) Prostheses control can be achieved through motor commands generated through EEG, ECoG, neuron spiking, or EMG signals. Each signal contains different qualities, such as frequency band and amplitude, but all can carry information regarding movement intentions. (B) For pattern recognition, the neural signals are used as an input to a machine learning algorithm to classify the desired movement. Outputs from the algorithm are used to drive the movement of the prosthesis. (C) In TMR, residual nerves that once directly controlled limb movements are placed in healthy muscle, which act as bio-amplifiers for signals from the motor nerves.

The Southampton Hand Assessment Procedure (SHAP) was developed to test a range of different prosthetic hand grasps to manipulate objects that are commonly encountered during the day, such as moving a jar or opening a door handle [41]. These tasks, along with others such as the Clothespin Task [42], help validate movement decoding and machine learning strategies for prosthesis control.

22.2.3 TARGETED MUSCLE REINNERVATION AND OSSEointegration

TMR is a surgical technique where the nerves from an amputated limb are placed into healthy muscles to act as bio-amplifiers, making movement signals stronger and easier to measure [43,44] (Fig. 22.2C). TMR has greatly improved the ability for prosthesis users to achieve a wider range of grips and patterns while controlling their limb [45].

A relatively new method known as osseointegration (OI) has also been shown to address several common issues such as prosthesis loading and position effects [46,47]. In osseointegration, the prosthesis attaches directly to the body through a metal link that is inserted directly into the bone in the residual limb of an amputee. This intimate human–machine interface alleviates several issues such as loading effects that cause changes to surface EMG signals while also improving the

mobility and range of motion of the prosthesis [46]. Clinical research shows that the osseointegrated implant can sustain loading during normal use and no incidents were reported as a result of overloading [47]. Some patients were reported as being overprotective of their prosthesis and did not load it as much as others; however failure of the OI implant is seen as unlikely given that it is capable of sustaining larger loads than the bone itself [47].

22.2.4 STATE OF THE ART

Researchers are beginning to take advantage of new surgical techniques like TMR to develop enhanced decoding strategies [9] and achieve greater dexterity [45] for further improving prosthesis control. Another developing area is in designing control strategies that enable both simultaneous and proportional prosthesis control. Typically, users can only control one DoF of their prosthesis at a time. Recently, researchers have shown promising results with simultaneous and proportional control in two [32] and five DoFs [26]. Challenges that will continue to be addressed include environmental effects such as limb position and loading. Researchers will undoubtedly turn toward more sophisticated machine learning techniques to resolve these issues.

22.3 SENSORS FOR PROSTHETIC HANDS

Sensory feedback is also an important part for prosthetic hands. Traditionally, prosthesis users relied on visual and auditory information to monitor their prosthesis during manipulation. With the recent advancements in providing sensory feedback to users, researchers have shown that we can now complete the feedback loop by providing natural sensations back to amputees so they can actually feel with their prosthesis.

22.3.1 SENSING IN BIOLOGY

Before giving details on sensors used in hand prostheses, it is useful to take a brief look at the sensing capabilities of intact hands. Prosthetic hands replace lost or missing hands, so it makes sense that these devices should aim to mimic the functionality and behavior of their biological counterparts. In healthy skin, we have receptors and complex feedback loops to convey interoceptive, such as proprioception, and exteroceptive, such as pressure, temperature, and pain, perceptions. Mechanoreceptors are the primary means of our ability to perceive touch, and they are classified as either slowly adapting (SA) [Merkel cells (SA1) and Ruffini endings (SA2)] or rapidly adapting [Meissner (RA1) and Pacinian corpuscles (RA2)]. SA mechanoreceptors respond to sustained loads, whereas RAs respond primarily to the transient periods of tactile loading [48].

While mechanoreceptors provide information on touch, nociceptors (free nerve endings) in the skin are responsible for conveying noxious (painful) mechanical sensations [49]. A_δ- and C-low-threshold mechanoreceptors (LTMRs) are primarily responsible for conveying sensations of temperature and it is thought that SA2 receptors, which respond to things like skin stretch, work in conjunction with muscle spindles to provide sensations of proprioception [48].

Biological sensory receptors and pathways provide insight into the necessary components required for making sophisticated prosthetic hands that can provide meaningful, relevant, and natural sensations back to the user.

22.3.2 SENSING DEVICES

Currently, sensors for prosthetic hands capture information about force, pressure, torque, or hand movement. Various types of sensors are used to measure these modalities. For a review of tactile sensing technologies see Ref. [50] and for a more in-depth discussion about the fabrication, signal processing, and applications of tactile sensing systems see Ref. [51].

22.3.2.1 Piezoresistive

Piezoresistive materials change resistance due to mechanical strain and are effective for measuring static forces. In the case of sensors on a prosthetic hand, the mechanical strain is due to physical contact with the environment. The piezoresistors are usually made from thick film resistors [52], textiles [12,53,54] (Fig. 22.3A), carbon nanotubes (CNTs) [58], or silicon microelectromechanical systems (MEMSs) [59]. Piezoresistive sensors are simple and low-cost but have high manufacturing variance [50]. These force sensors have been used on the fingertips of prostheses to improve grasping and prevent object slip [11,52].

22.3.2.2 Piezoelectric

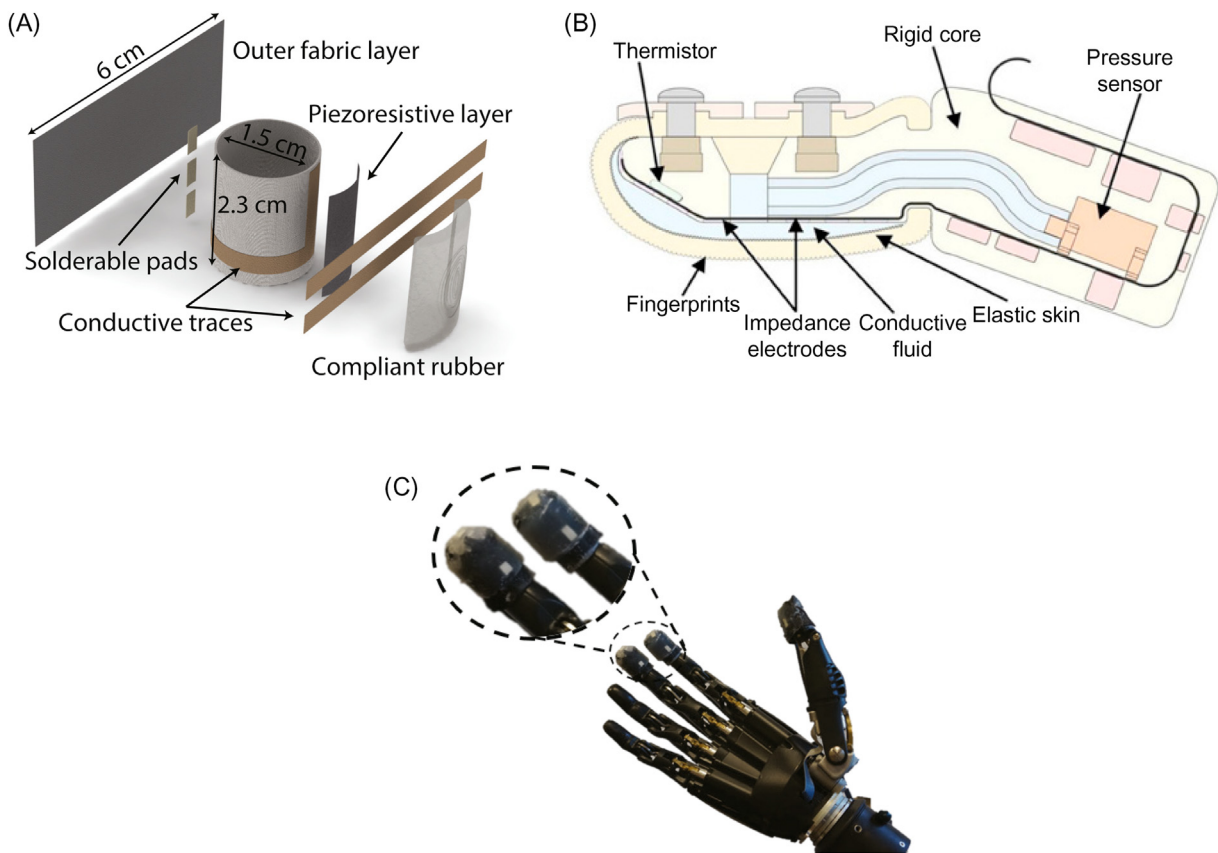
Piezoelectric materials generate electrical charge due to mechanical strain and are effective for measuring dynamic (high-frequency) forces. Piezoelectric sensors are commonly made from polyvinylidene fluoride (PVDF) [60] or lead-zirconate-titanate (PZT) pastes [52] and have high sensitivity and frequency response but poor spatial resolution [50]. Inspired by the mechanoreceptors of the skin, Liu et al. [58] created a double-layer tactile sensor using piezoelectric and piezoresistive materials for the top (dynamic forces) and bottom layers (static forces), respectively.

22.3.2.3 Capacitive

Capacitive sensors respond to mechanical forces resulting from changes in capacitor geometry due to force on the capacitive plates. They are usually made with MEMS technology and have high sensitivity and spatial resolution but can be susceptible to cross-talk noise [50]. Liang et al. [61] designed a 4×4 capacitive three-axis force sensor array using four capacitors, square electrodes, and a polydimethylsiloxane (PDMS) bump for each sensor fabricated with a MEMS-polymer process.

22.3.2.4 Pressure

Tactile pressure can also be measured through changes in sensor material or even fluid. For example, the BioTAC tactile sensor (Fig. 22.3B) measures a change in impedance of its electrode array in response to force on the fingertip, which changes the pressure of the internal fluid. The BioTAC has been used to characterize object compliance [56] and to identify textures [55]. It has also been used to enable grasping of fragile objects [57].

**FIGURE 22.3**

Examples of sensors for prosthetic hands. (A) Piezoresistive textiles can be used for detecting forces during grasping with a prosthetic hand, 2016 IEEE. (B) The BioTac fingertip sensor. Changes in fluid impedance enable fine discrimination of textures [55], detecting object compliance [56], and grasping fragile objects [57]. (C) To maximize utility, sensors are most often placed on the fingertips of the prosthesis. During object grasping and manipulation, the prosthesis fingertips are generally in contact with the target object making them an ideal location for sensing elements. 2016 IEEE.

(A) Reprinted, with permission, from L. Osborn, R. Kaliki, A. Soares, N. Thakor, Neuromimetic event-based detection for closed-loop tactile feedback control of upper limb prostheses, *IEEE Trans. Hapt.* 9 (2) (2016) 196–206. doi:10.1109/TOH.2016.2564965; (B) Reprinted from Z. Su, J. Fishel, G. Loeb, Use of tactile feedback to control exploratory movements to characterize object compliance, *Front. Neurosci.* 6 (7) (2012). doi:10.3389/fnbot.2012.00007 under the CC-BY license. (C) Reprinted, with permission, from L. Osborn, R. Kaliki, A. Soares, N. Thakor, Neuromimetic event-based detection for closed-loop tactile feedback control of upper limb prostheses, *IEEE Trans. Hapt.* 9 (2) (2016) 196–206. doi:10.1109/TOH.2016.2564965.

22.3.2.5 Optical

Optical tactile sensors work by measuring changes in light transmitted from optical cables onto a surface. These sensors have high spatial resolution and wide sensing range but can be bulky [50]. Ahmadi et al. [62] developed a beam-type optical fiber sensor which can measure distributed tactile information and was demonstrated for palpation in minimally invasive robotic surgery.

22.3.2.6 Magnetic

Magnetic tactile sensors typically operate by measuring the change in magnetic field intensity due to the Hall effect or through characterizing the change in electromagnetic induction due to applied forces. Magnetic sensors are highly sensitive but have poor reliability [50]. Alfadhel and Kosel [63] designed an array of nanocomposite cilia which cause a change in their magnetic fields when deflected by an external force.

22.3.2.7 Thermistor

A thermistor is a thermally sensitive resistor. Thermistors have a significant and linear relationship with temperature that allows for consistent temperature characterization. They are simple and easy to manufacture using a silicon process. A thermistor-based temperature sensor has been integrated into a variety of sensors such as the BioTAC [56], force and slip sensors [52], and a malleable electronic skin [64].

22.3.2.8 Inertial

Inertial measurement units (IMU) are composed of accelerometers, gyroscopes, and magnetometers which measure linear acceleration, angular velocity, and magnetic field strength (to orient with respect to the Earth's axes), respectively. For hand prostheses, these sensors capture information about hand movement, position, and torque. Bennett and Goldfarb [65] used IMUs to control the wrist rotation of a prosthesis. Krasoulis et al. [66] used them to improve hand control. Finally, Li et al. [67] used bending sensors to get information about finger position, while the IMU was used to obtain wrist location and orientation.

When it comes to perceiving touch with sensors like those described in this section, many are placed on or near the fingertips of the prosthetic hand (Fig. 22.3C). The fingers are the ideal place for detecting touch, whereas inertial sensors may be placed in other areas, such as the back of the hand or on the wrist, to track movement.

22.3.3 STATE OF THE ART

More recently, there has been progress in materials science to create more sophisticated sensing modalities and electronic skins (e-skins). For prosthetic hands, an e-skin is ideal because the sensors are embodied in flexible or compliant materials. The ability to capture sensory information, such as touch and proprioception, is only part of an e-skin, as there are other factors that have been developed such as flexibility, compliance, self-healing, and other skin-like characteristics. Researchers have used advanced materials to create stretchable sensors [68], microstructured ferroelectric skins with pressure and temperature sensing [69], compliant prosthetic fingers that use

stretchable waveguides to detect pressure [70], compliant and wireless e-skins [71], and healable and malleable e-skin [64].

Pressure and flexion sensors have also been developed that can both electrically and mechanically heal themselves [72]. Entire pneumatic robots have also been shown to self-heal [73]. Ultraflexible organic electronics have also been constructed into skin-like material [74], and even biomimetic temperature-sensitive layers [75]. More relevant to prosthetic hands has been the development of e-skins with sensors that behave like actual mechanoreceptors. Spiking like outputs from a pressure sensor were created by ring oscillators and used to directly stimulate neurons in the somatosensory cortex of a mouse [10]. More recently, an artificial afferent was created using flexible organic electronics to mimic the function of a sensory nerve. The sensor converted pressure into action potentials, also using ring oscillators, which were then used to stimulate the motor nerves in a cockroach to create a reflex arc that actuates muscles based on measured pressure [76].

Biomimetic designs have also been implemented to capture the layering aspects of receptors in the skin [12,53]. A multilayered e-dermis was developed with superficial sensing elements modeled after nociceptors and a deeper layer of mechanoreceptor behaving sensing elements [12]. For a more thorough discussion of flexible electronics, advanced materials for sensors, and e-skins, see Ref. [77]. These recent technological advancements in sensors and materials are promising in that they will hopefully be translated into sensors and e-skins placed directly on prosthetic hands for functional testing.

22.4 SENSORY FEEDBACK

There have been several efforts to provide realistic and meaningful sensory feedback to upper limb amputees. Touch is a complicated, multifaceted sensation that works in harmony with muscle movements to enable highly sophisticated manipulation tasks and tactile perceptions. One of the challenges to providing sensory feedback is not only capturing comprehensive touch information through sensors but also in providing that information back to a user, effectively closing the loop (Fig. 22.4). Some of the most significant advancements in upper limb prostheses in the past several years have come in the form of sensory feedback to amputees. Sensory feedback can be provided by stimulating the peripheral nerves or even the somatosensory cortex directly. For peripheral nerve stimulation, relevant sensory feedback can be achieved by using noninvasive approaches, such as transcutaneous electrical nerve stimulation (TENS), or using electrodes implanted directly into the nerves. The median, ulnar, and radial nerves are common targets when providing sensory feedback due to their coverage of the hand.

22.4.1 TACTILE

For clarity, we refer to tactile as a sensation that can include perceptions of force, pressure, vibration, or texture. Groundbreaking results show the ability to provide sensory activation and sensations of pressure in the thumb, index finger, and little finger of the phantom hand of an amputee using implanted stimulating electrodes [14]. Through tactile perceptions, prosthesis users with implanted stimulating electrodes in their median and ulnar nerves have been shown to differentiate

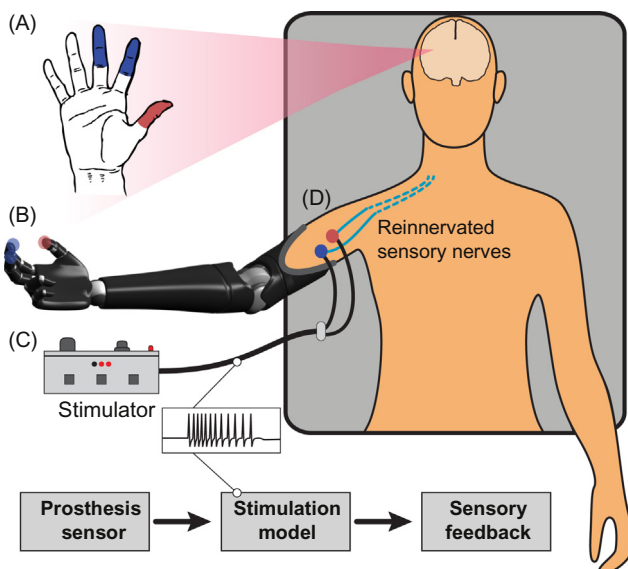


FIGURE 22.4

Sensory feedback is a vital part for creating a lifelike prosthesis. (A) Tactile sensations can be perceived in the phantom hand of amputees. (B) Sensors on the prosthesis capture touch information and (C) send information back to the user through a stimulator. Stimulation models transform the sensor information into potentially natural and relevant sensory information in the form of electrical stimulation. (D) Stimulation of reinnervated sensory nerves provides the tactile perceptions in the phantom hand.

between object stiffness [14], perform fine motor movements such as pulling a stem off a cherry [78], and improve performance in functional tasks [79] and activities of daily living [46].

Touch sensations have been mapped in the phantom hand in several different studies, and each case varies in terms of the coverage obtained. Stimulation from multiple microelectrode arrays implanted in the median and ulnar nerves was shown to provide several percepts in one study [78] (Fig. 22.5A) and over 100 percepts in another study [26] (Fig. 22.5B). Implanted stimulating electrodes are able to target smaller nerve fascicles, as opposed to the larger nerve bundles likely activated using noninvasive approaches. Stimulation through implanted electrodes has the potential to provide more localized and a greater variety of tactile percepts in the phantom hand [26,78] compared to more general coverage through noninvasive approaches [12,80,81].

Natural tactile sensations in the phantom hand have also been provided by noninvasively electrically stimulating the peripheral nerves [12,80,82] (Fig. 22.5C). Despite not having direct contact with the peripheral nerve, electrical stimulation dissipates through the skin and, if positioned correctly, can reach and activate the underlying peripheral nerve bundles. Targeting the underlying nerves through the skin can be a difficult process, but targeted sensory reinnervation (TSR), a surgical technique that intentionally separates sensory nerves during surgery, can be used to enable larger spatial coverage of tactile feedback in the phantom hand [83,84]. It was shown that subjects who had undergone TSR had a capacity to perceive sensations of grating that were similar to able-

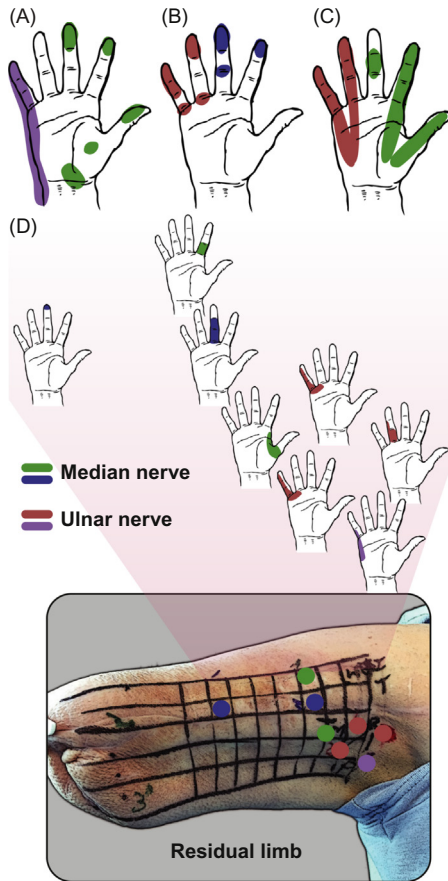


FIGURE 22.5

Sensory mapping of the phantom hand can provide information on the types of sensations perceived by the amputee. (A) Tactile perceptions are generally perceived in parts of the phantom hand that were once innervated by the median and ulnar nerves. (B) In general, sensory mapping varies in each case. For implanted stimulating electrodes, perceptions seem to be localized to smaller areas. This sensory map shows the general coverage of sensory feedback provided to amputees through electrodes implanted in the median and ulnar nerves. Individual percepts were localized to smaller regions within the larger areas. (C) Noninvasive stimulation of median and ulnar nerves can also provide tactile sensations and each stimulation site generally covers larger areas of the phantom hand. (D) In a subject with TSR, the sensory nerves are separated and organized such that noninvasive stimulation tends to elicit more localized tactile sensations in the phantom hand. 2017 IEEE.

(A) Results adapted from D.W. Tan, M.A. Schiefer, M.W. Keith, J.R. Anderson, J. Tyler, D.J. Tyler, *A neural interface provides long-term stable natural touch perception*, *Sci. Translat. Med.* 6 (257) (2014) 257ra138. doi:10.1126/scitranslmed.3008669.

(B) Results adapted from S. Wendelken, D.M. Page, T. Davis, H.A.C. Wark, D.T. Kluger, C. Duncan, et al., *Restoration of motor control and proprioceptive and cutaneous sensation in humans with prior upper-limb amputation via multiple utah slanted electrode arrays (useas) implanted in residual peripheral arm nerves*, *J. Neuroeng. Rehabil.* 14 (1) (2017) 121. doi:10.1186/s12984-017-0320-4.

(C) Results adapted from E. D'Anna, F.M. Petrini, F. Artoni, I. Popovic, I. Simanic, S. Raspopovic, et al., *A somatotopic bidirectional hand prosthesis with transcutaneous electrical nerve stimulation based sensory feedback*, *Sci. Rep.* 7 (1) (2017) 10930. doi:10.1038/s41598-017-11306-w.

(D) Reprinted, with permission, from L. Osborn, M. Fifer, C. Moran, J. Betthauser, R. Armiger, R. Kaliki, et al., *Targeted transcutaneous electrical nerve stimulation for phantom limb sensory feedback*, in: *IEEE Biomedical Circuits and Systems (BioCAS)*, 2017, pp. 1–4. doi:10.1109/BIOCAS.2017.8325200.

bodied subjects; however, the ability of TSR subjects to identify and localize points of contact was slightly lower than in the controls [85]. It was also shown that at least eight unique sites of the phantom hand could be activated by using targeted TENS with a TSR patient [81] (Fig. 22.5D).

Tactile sensations play a role in helping us differentiate textures. Researchers were able to give sensations of texture roughness by using direct nerve stimulation in an upper limb amputee [86]. The stimulation provided to the user was based on SA mechanoreceptor mechanics by using an Izhikevich neuron model [87]. Textures, each with a different surface roughness, were presented to the amputee subject who then relied on the perceived tactile sensations from the stimulation to identify which textures were more rough. This particular study used an interesting approach where it based the nerve stimulation for sensory feedback on actual mechanics of receptors that, although no longer present, are responsible for our perceived tactile sensations. Because the peripheral nerves are still intact, the neural pathways to the brain are preserved, even after amputation. Because of this preservation, the nerve stimulation was patterned in a way to replicate the output of a healthy mechanoreceptor based on the output of the sensor on the prosthetic hand's fingertip.

Although less common, it is possible to also produce tactile sensations through stimulation at the cortical level, in the somatosensory cortex [88]. This approach is a valid solution for prosthesis users who have a spinal cord injury and do not have intact peripheral nerve and spinal cord pathways for transmitting neural information.

Providing tactile feedback in upper limb prostheses is still in its infancy, and yet has seen tremendous progress in a matter of several years. As sensory feedback to users becomes more common, it is important to monitor the ability to provide meaningful information throughout the day even during physically demanding activities of daily living, like exercise or working with tools. Throughout the day or due to the physical nature of activities of daily living, the noninvasive stimulating electrodes can shift or even peel off the skin, which affects the electrical path to the targeted nerves. Researchers developed a control strategy that monitors the impedance of noninvasive stimulating electrodes to continuously provide the correct levels of sensory feedback even during physically demanding activities of daily living [89].

Now that technology has enabled tactile feedback to prosthesis users, researchers have begun to explore additional touch perceptions that can be naturally conveyed through nerve stimulation.

22.4.2 PAIN

In addition to tactile sensations, pain has also been conveyed in the form of sensory feedback to an amputee. Although undesirable, pain provides valuable information for protecting the body. Typically, a prosthetic hand has no sense of pain from grasping an object, let alone the user. By implementing an autonomous pain reflex to mimic in the prosthesis, researchers showed that the prosthesis can identify and react to painful stimuli in a lifelike fashion [12]. The nerve stimulation signal was produced using a neuromorphic framework, the same as in Ref. [86], except that in this case both mechanoreceptors and nociceptors were modeled to provide these sensations.

22.4.3 PROPRIOCEPTION

One of the major forms of feedback in closed-loop manipulation with a hand is proprioception. It helps guide hand movement and complements touch feedback in that it allows an individual to create

a more comprehensive understanding and representation of any movements or object manipulation. Touch information gives the context of an object's features, such as surface roughness and material stiffness, while proprioceptive information helps convey object size and shape while also tracking the position of the hand. By knowing the current position of the hand through proprioception, an individual can send motor commands to make fine movements without the need for visual feedback. This type of comprehensive proprioceptive and tactile feedback is lacking in prosthetic hands.

Using implanted microelectrode arrays in the median and ulnar nerves of amputees, researchers have also identified several instances of proprioceptive feedback. One amputee was able to perceive 17 different proprioceptive sensations (i.e., finger or hand movements in the phantom hand) while another amputee was only able to perceive one sensation [26]. It is unclear which afferent nerve fibers were being stimulated within the median and ulnar nerves to create these sensations, but the location of the stimulating electrode seemed to play a major role in eliciting proprioceptive sensations.

Illusory movements, sensations that the phantom hand is moving, can also be caused by vibratory feedback on the skin of amputees who have undergone TMR [13]. In multiple subjects, vibration of the proximal reinnervated muscles elicited an illusion of hand movement, such as finger and wrist extension and flexion. This kinesthetic illusion was shown to improve movement control of their myoelectric prosthesis [13]. Although the vibration was applied to muscles, there was a perceived sensation of limb movement, which indicates the important relationship between muscle activity and sensory feedback to produce the sense of proprioception. Research has shown that proprioceptive percepts can be provided by stimulating sites in both sensory nerves and muscles, and it is most likely a combination of providing feedback to both sensory and motor neurons that will elicit more natural sensations of proprioception. The combined stimulation of muscles and sensory nerves for proprioceptive feedback makes sense considering that SA2 mechanoreceptors provide information on skin stretch while muscle spindles convey information on limb position, which together make up our ability to localize our limb position in space without the need for visual feedback.

22.4.4 STATE OF THE ART

The types of sensory feedback conveyed from a prosthetic hand to its user are still limited in that they do not fully encompass the complex nature of our sensations of touch. There is a continuous push to make prosthetic hands more life-like, and that requires sensory capabilities that enable a user to better utilize and embody their device. It is likely that future research will attempt to provide sensations of temperature, more sophisticated forms of proprioception, and combinations of other sensations back to prosthesis users. For realistic sensations to be re-created artificially, we should consider how biology produces those sensations to begin with. This leads to the use of neuromorphic systems, which aim to mimic aspects of healthy nervous system architecture, by using digital spikes, akin to neural action potentials, to convey information. Previous work has demonstrated the ability to provide real-time neuromorphic tactile feedback to prostheses for local feedback to improve grasping [90]. Researchers have also used a neuromorphic SA mechanoreceptor model for enabling an amputee to discriminate between textures [86] as well as differentiating between innocuous touch and pain by using neuromorphic models of mechanoreceptors and nociceptors [12]. The idea is that by using neuromorphic models, essentially modeling healthy receptor behavior as a way to stimulate peripheral nerves, more natural sensations can be produced because

the stimulation is based on actual biological behavior. The limitation with this approach is that we are not yet able to stimulate individual sensory nerve fibers due to their small size. Thus, using a neuromorphic model to provide sensory feedback has not reached its full potential yet. At this point, the nerve stimulation is representative of the activity of a population of receptors, which can then be used to stimulate a nerve fascicle or bundle. However, researchers have already developed extremely sophisticated models that very accurately predict and replicate actual mechanoreceptor behavior. Using physiological data from afferents in nonhuman primates, SA1, RA1, and RA2 receptors have been modeled, with millisecond precision [91].

A major part of providing sensory information from a prosthetic hand back to the user is understanding how that feedback is perceived by the user. Researchers are using traditional psychophysical experiments to quantify sensory perceptions and identify how different parameters influence perceptions of intensity [92]. Furthermore, an amputee is able to adapt to sensations in the phantom hand, such as a repeated tapping, in a similar way as someone adapts to sensations in an intact limb [93]. Differences in stimulating electrode (invasive vs. noninvasive) are also a question worth considering in terms of how sensations change. Implanted stimulating electrodes to elicit sensory feedback are more stable than noninvasive approaches since they consistently stimulate the same regions after implantation [26,88]; however, noninvasive feedback has been shown to be stable over a period of at least a year but requires manual electrode placement each time [12]. Combined with understanding user perception of feedback, researchers have looked at how feedback influences the neural signals of an amputee [80], which could also be used to help better understand the quality of sensory perceptions from nerve stimulation. The effect of the stimulation on neural signals may offer an insight into how information is processed in the somatosensory cortex after an amputation or spinal cord injury. This effect will help continue to push knowledge for improving not only prostheses but brain-machine interfaces in general.

TSR surgery has already enhanced the ability of researchers to provide sensory feedback to the peripheral nerves of amputees. There is often natural regrowth of peripheral nerves in an amputated limb, but this growth is somewhat arbitrary in that the nerve fibers may end up close to the surface of the skin, in the soft tissue, or deeper within the arm. With TSR, surgeons intentionally separate the afferent nerve fascicles and place them so that their growth into the soft tissue will make it easier for providing sensory feedback.

Another surgical technique, the agonist–antagonist myoneural interface (AMI), connects muscle tendons in series to provide intuitive proprioceptive information to the user, which will undoubtedly improve prosthesis control [94]. The AMI has been validated in lower limb amputees [95] and will likely make its way to upper limb amputees in the near future. Even though stimulating electrodes will be necessary for providing touch information back to an amputee, it is feasible that surgical techniques could make it possible for sensations of proprioception to be retained through an AMI or similar approach.

22.5 FUTURE DIRECTIONS

All components of prosthetic hands, from sensors to the socket to improved control and functional outcome measures, will undoubtedly improve in the coming years. As technology improves, there will continue to be a push to make next-generation prostheses a reality.

22.5.1 PROSTHETIC SOCKETS

Although not discussed in this chapter, the physical interface of the prosthetic socket and the user is of critical importance. Research on the clinical side has led to improved socket material and design [17], but socket fit and comfort are still a major issue and a leading cause of device abandonment. In the case of myoelectric prostheses, electrode contact is important and shifts in socket position and loading can affect the underlying EMG signal. Thus, improving prosthesis fit and comfort are critical areas that will hopefully see improvements in the near future.

22.5.2 PROSTHESIS CONTROL

Notably, there are numerous challenges that remain to be addressed by control strategies, such as effects from limb position and loading as well as electrode shift. Efforts have been made to eliminate some of these problems by measuring from muscles directly using either implanted electrodes or intramuscular EMG recordings, which interface with the muscle directly, to improve prosthesis control [96]. Both neural signal recording techniques and signal processing methods will need to improve to get around these external factors that degrade prosthesis functionality. One potential step will be to utilize a high-density grid of EMG electrodes for capturing a more complete representation of muscle activity for movement decoding [39]. Another area of progress will be in simultaneous and proportional control of multiple DoFs. Researchers have already shown promising results using positional proportional control to move individual fingers and joints [26], which will undoubtedly become a more common goal for prosthesis control strategies.

As control strategies become more robust, there has been discussion on the need for improved and more comprehensive functional outcome measures specifically for upper limb prosthesis users. As mentioned previously, the SHAP and TAC tests are commonly used and clinically validated, for evaluating the ability of a user to control his or her prosthesis for activities of daily living. The SHAP test offers a variety of objects, each requiring a different grip and movement. As the control of prostheses continues to improve, there is an interest in having standardized functional outcome measures that encompass a larger range of activities, especially ones that require limb movement such as moving objects overhead or across the body.

22.5.3 AUGMENTED REALITY TRAINING

We will likely see an increase in new technology being used for prosthetic limbs. One example is the use of augmented reality technology to enable training for prosthesis use. Many upper limb amputees go through an extended period of time before receiving a prosthesis. There is a period of time before, and even after, receiving a prosthesis that could be utilized to train for prosthesis control. While augmented reality is beginning to emerge in the consumer electronics market, it offers a unique platform to enable potential prosthesis users to practice with an “actual” device in their native environment without the need to visit a research or clinical lab.

22.5.4 SENSORS AND E-SKINS

The sensor hardware in prosthetic hands has already begun to shift toward using more lifelike e-skins. The sensors themselves will continue to reduce in size and increase in resolution, enabling finer details

of touch to be captured. More importantly, sensors will likely begin combining various components and sensing modalities into single devices for use on a prosthesis. For instance, piezoresistive elements can be used to capture tactile information, thermal sensors to measure temperature, and IMUs to track position. Combining other sensing modalities is also more common. For example, researchers have used visual information [97] and combined neuromorphic visual and tactile information [98] to improve grasping. A missing component in current prosthetic hand sensors is the ability to self-heal. Just like healthy skin that repairs itself over time, an e-skin with self-healing properties that is capable of detecting pain and then repairing the damage will bring prosthetic hands to an even more advanced state. Researchers have demonstrated the feasibility of such a material, so it will only be a matter of time before these self-healing devices become a ubiquitous part of prosthetic hand sensors.

22.5.5 SENSORY FEEDBACK

In parallel with advances in sensor materials will be improvements in sensory feedback techniques. There is a developing trend of using more biomimetic approaches to provide stimulation, such as the neuron models developed in Ref. [91] or the Izhikevich model used in Refs. [86] and [12]. However, a limiting factor of providing sensory information is in the stimulating hardware itself. Advances in electrode material will eventually enable better resolution and specificity for stimulating peripheral nerves, but there will still be the hurdle of understanding how to provide the correct stimulation patterns to elicit natural and meaningful sensations. This will require extensive psychophysics and sensory mapping to fully understand the breadth and richness of the sensory feedback. The number of percepts used in sensory feedback will continue to grow. Currently, it has been shown that sensations of pressure, gratings and vibrations, texture, pain, and hand movement can be provided. Perceptions of temperature, skin stretch, and hand position will be valuable additions to further enhance sensory feedback.

22.6 CONCLUSION

In this area of research it is important to remember that innovation and progress are tied not only to developments in technology but also to the needs of the user. With the overarching goal being to achieve a prosthetic arm that can perfectly mimic an intact limb in both control and sensory feedback, there are many steps that remain to get there. The focus should be on improving functionality in the daily lives of individuals living with limb differences or paralysis.

ACKNOWLEDGMENT

Unless otherwise specified, images reproduced from open access sources are done so under the Creative Commons Attribution 3.0 license.

ABBREVIATIONS

AMI agonist–antagonist myoneural interface
CNT carbon nanotube

- DoF** degree of freedom
ECoG electrocorticography
EEG electroencephalography
EMG electromyography
IMU inertial measurement unit
MEMS microelectromechanical systems
OI osseointegration
PDMS polydimethylsiloxane
PVDF polyvinylidene fluoride
PZT lead-zirconate-titanate
SHAP Southampton Hand Assessment Procedure
TAC target achievement control
TENS transcutaneous electrical nerve stimulation
TMR/TSR targeted muscle/sensory reinnervation

REFERENCES

- [1] K.J. Zuo, J.L. Olson, The evolution of functional hand replacement: from iron prostheses to hand transplantation, *Plast. Surg.* 22 (1) (2014) 44–51. Available from: <https://doi.org/10.1177/22955031402200111>.
- [2] M. Johannes, J. Bigelow, J. Burck, S. Harshbarger, M. Kozlowski, T.V. Doren, An overview of the development process for the modular prosthetic limb, *JHU APL Tech. Digest* 30 (3) (2011) 207–216.
- [3] S.L. Carey, D.J. Lura, M.J. Highsmith, Differences in myoelectric and body-powered upperlimb prostheses: systematic literature review, *J. Rehabil. Res. Dev.* 52 (3) (2015) 247–262. Available from: <https://doi.org/10.1682/JRRD.2014.08.0192>.
- [4] L.H.B. Huinink, H. Bouwsema, D.H. Plettenburg, C.K. van der Sluis, R.M. Bongers, Learning to use a body-powered prosthesis: changes in functionality and kinematics, *J. Neuroeng. Rehabil.* 13 (1) (2016) 90. Available from: <https://doi.org/10.1186/s12984-016-0197-7>.
- [5] T.J. Bradberry, R.J. Gentili, J.L. Contreras-Vidal, Reconstructing three-dimensional hand movements from noninvasive electroencephalographic signals, *J. Neurosci.* 30 (9) (2010) 3432–3437. Available from: <https://doi.org/10.1523/JNEUROSCI.6107-09.2010>.
- [6] D.T. Bundy, M. Pahwa, N. Szrama, E.C. Leuthardt, Decoding three-dimensional reaching movements using electrocorticographic signals in humans, *J. Neural. Eng.* 13 (2) (2016) 026021. Available from: <https://doi.org/10.1088/1741-2560/13/2/026021>.
- [7] M. Velliste, S. Perel, M.C. Spalding, A.S. Whitford, A.B. Schwartz, Cortical control of a prosthetic arm for self-feeding, *Nature* 453 (7198) (2008) 1098–1101. Available from: <https://doi.org/10.1038/nature06996>.
- [8] L.R. Hochberg, D. Bacher, B. Jarosiewicz, N.Y. Masse, J.D. Simeral, J. Vogel, et al., Reach and grasp by people with tetraplegia using a neurally controlled robotic arm, *Nature* 485 (2012) 372–375. Available from: <https://doi.org/10.1038/nature11076>.
- [9] D. Farina, I. Vujaklija, M. Sartori, T. Kapelner, F. Negro, N. Jiang, et al., Man/machine interface based on the discharge timings of spinal motor neurons after targeted muscle reinnervation, *Nat. Biomed. Eng.* 1 (2017) 0025. Available from: <https://doi.org/10.1038/s41551-016-0025>.
- [10] B.C.K. Tee, A. Chortos, A. Berndt, A.K. Nguyen, A. Tom, A. McGuire, et al., A skin-inspired organic digital mechanoreceptor, *Science* 350 (6258) (2015) 313–316. Available from: <https://doi.org/10.1126/science.aaa9306>.

- [11] L. Osborn, R. Kaliki, A. Soares, N. Thakor, Neuromimetic event-based detection for closed-loop tactile feedback control of upper limb prostheses, *IEEE Trans. Hapt.* 9 (2) (2016) 196–206. Available from: <https://doi.org/10.1109/TOH.2016.2564965>.
- [12] L.E. Osborn, A. Dragomir, J.L. Betthauser, C.L. Hunt, H.H. Nguyen, R.R. Kaliki, et al., Prosthesis with neuromorphic multilayered e-dermis perceives touch and pain, *Sci. Robot.* 3 (19) (2018) eaat3818. Available from: <https://doi.org/10.1126/scirobotics.aat3818>.
- [13] P.D. Marasco, J.S. Hebert, J.W. Sensinger, C.E. Shell, J.S. Schofield, Z.C. Thumser, et al., Illusory movement perception improves motor control for prosthetic hands, *Sci. Translat. Med.* 10 (432) (2018) eaa06990. Available from: <https://doi.org/10.1126/scitranslmed.eaa06990>.
- [14] S. Raspopovic, M. Capogrosso, F.M. Petrini, M. Bonizzato, J. Rigosa, G.D. Pino, et al., Restoring natural sensory feedback in real-time bidirectional hand prostheses, *Sci. Translat. Med.* 6 (222) (2014) 222ra19. Available from: <https://doi.org/10.1126/scitranslmed.3006820>.
- [15] E. Biddiss, D. Beaton, T. Chau, Consumer design priorities for upper limb prosthetics, *Disabil. Rehabil. Assistive Technol.* 2 (6) (2007) 346–357. Available from: <https://doi.org/10.1080/17483100701714733>.
- [16] E.A. Biddiss, T.T. Chau, Upper limb prosthesis use and abandonment: a survey of the last 25 years, *Prosthet. Orthot. Int.* 31 (3) (2007) 236–257. Available from: <https://doi.org/10.1080/03093640600994581>.
- [17] R.D. Alley, T.W. Williams 3rd, M.J. Albuquerque, D.E. Altobelli, Prosthetic sockets stabilized by alternating areas of tissue compression and release, *J. Rehabil. Res. Dev.* 48 (6) (2011) 679–696. Available from: <https://doi.org/10.1682/JRRD.2009.12.0197>.
- [18] D. Candrea, A. Sharma, L. Osborn, Y. Gu, N. Thakor, An adaptable prosthetic socket: regulating independent air bladders through closed-loop control, in: *IEEE International Symposium on Circuits and Systems (ISCAS)*, 2017, pp. 1–4. <https://doi.org/10.1109/ISCAS.2017.8050727>.
- [19] E. Greenwald, M. Masters, N. Thakor, Implantable neurotechnologies: bidirectional neural interfaces—applications and vlsi circuit implementations, *Med. Biol. Eng. Comp.* 54 (1) (2016) 1–17. Available from: <https://doi.org/10.1007/s11517-015-1429-x>.
- [20] K. Ng, E. Greenwald, Y.P. Xu, N. Thakor, Implantable neurotechnologies: a review of integrated circuit neural amplifiers, *Med. Biol. Eng. Comp.* 54 (1) (2016) 45–62. Available from: <https://doi.org/10.1007/s11517-015-1431-3>.
- [21] A. Patil, N. Thakor, Implantable neurotechnologies: a review of micro- and nanoelectrodes for neural recording, *Med. Biol. Eng. Comp.* 54 (1) (2016) 23–44. Available from: <https://doi.org/10.1007/s11517-015-1430-4>.
- [22] L.E. Osborn, J.L. Betthauser, N.V. Thakor, Neural prostheses, in: J.G. Webster (Ed.), *Wiley Encyclopedia of Electrical and Electronics Engineering*, John Wiley & Sons, 2019, pp. 1–20. Available from: <http://dx.doi.org/10.1002/047134608X.W1424.pub2>.
- [23] K. Østlie, I.M. Lesjø, R.J. Franklin, B. Garfelt, O.H. Skjeldal, P. Magnus, Prosthesis use in adult acquired major upper-limb amputees: patterns of wear, prosthetic skills and the actual use of prostheses in activities of daily life, *Disabil. Rehabil. Assistive Technol.* 7 (6) (2012) 479–493. Available from: <https://doi.org/10.3109/17483107.2011.653296>.
- [24] S. Acharya, M.S. Fifer, H.L. Benz, N.E. Crone, N.V. Thakor, Electrocorticographic amplitude predicts finger positions during slow grasping motions of the hand, *J. Neural. Eng.* 7 (4) (2010) 046002. Available from: <https://doi.org/10.1088/1741-2560/7/4/046002>.
- [25] G. Hotson, D.P. McMullen, M.S. Fifer, M.S. Johannes, K.D. Katyal, M.P. Para, et al., Individual finger control of a modular prosthetic limb using high-density electrocorticography in a human subject, *J. Neural. Eng.* 13 (2) (2016) 026017. Available from: <https://doi.org/10.1088/1741-2560/13/2/026017>.
- [26] S. Wendelken, D.M. Page, T. Davis, H.A.C. Wark, D.T. Kluger, C. Duncan, et al., Restoration of motor control and proprioceptive and cutaneous sensation in humans with prior upper-limb amputation via

- multiple utah slanted electrode arrays (useas) implanted in residual peripheral arm nerves, *J. Neuroeng. Rehabil.* 14 (1) (2017) 121. Available from: <https://doi.org/10.1186/s12984-017-0320-4>.
- [27] N.V. Thakor, Translating the brain-machine interface, *Sci. Translat. Med.* 5 (210) (2013) 210ps17. Available from: <https://doi.org/10.1126/scitranslmed.3007303>.
- [28] E. Scheme, K. Englehart, Electromyogram pattern recognition for control of powered upper-limb prostheses: state of the art and challenges for clinical use, *J. Rehabil. Res. Dev.* 48 (6) (2011) 643–659. Available from: <https://doi.org/10.1682/JRRD.2010.09.0177>.
- [29] A. Fougner, E. Scheme, A.D.C. Chan, K. Englehart, Ø. Stavdahl, Resolving the limb position effect in myoelectric pattern recognition, *IEEE Trans. Neural. Syst. Rehabil. Eng.* 19 (6) (2011) 644–651. Available from: <https://doi.org/10.1109/TNSRE.2011.2163529>.
- [30] C. Cipriani, R. Sassu, M. Controzzi, M.C. Carrozza, Influence of the weight actions of the hand prosthesis on the performance of pattern recognition based myoelectric control: preliminary study, in: International Conference of the IEEE Engineering in Medicine and Biology Society, 2011, pp. 1620–1623. <https://doi.org/10.1109/IEMBS.2011.6090468>.
- [31] V. Gilja, P. Nuyujukian, C.A. Chestek, J.P. Cunningham, M.Y. Byron, J.M. Fan, et al., A high-performance neural prosthesis enabled by control algorithm design, *Nat. Neurosci.* 15 (12) (2012) 1752–1757. Available from: <https://doi.org/10.1038/nn.3265>.
- [32] J.M. Hahne, M.A. Schweisfurth, M. Koppe, D. Farina, Simultaneous control of multiple functions of bionic hand prostheses: performance and robustness in end users, *Sci. Robot.* 3 (19) (2018) eaat3630. Available from: <https://doi.org/10.1126/scirobotics.aat3630>.
- [33] T. Tsuji, R.O. Fukuda, M. Kaneko, K. Ito, Pattern classification of time-series emg signals using neural networks, *Int. J. Adapt. Control Signal Process* 14 (8) (2000) 829–848. Available from: [https://doi.org/10.1002/1099-1115\(200012\)14:83.0.CO;2-L](https://doi.org/10.1002/1099-1115(200012)14:83.0.CO;2-L).
- [34] H.C. Shin, V. Aggarwal, S. Acharya, M.H. Schieber, N.V. Thakor, Neural decoding of finger movements using skellam-based maximum-likelihood decoding, *IEEE Trans. Biomed. Eng.* 57 (3) (2010) 754–760. Available from: <https://doi.org/10.1109/TBME.2009.2020791>.
- [35] L.J. Hargrove, E.J. Scheme, K.B. Englehart, B.S. Hudgins, Multiple binary classifications via linear discriminant analysis for improved controllability of a powered prosthesis, *IEEE Trans. Neural. Syst. Rehabil. Eng.* 18 (1) (2010) 49–57. Available from: <https://doi.org/10.1109/TNSRE.2009.2039590>.
- [36] K. Englehart, B. Hudgins, A robust, real-time control scheme for multifunction myoelectric control, *IEEE Trans. Biomed. Eng.* 50 (7) (2003) 848–854. Available from: <https://doi.org/10.1109/TBME.2003.813539>.
- [37] J. Betthauser, C. Hunt, L. Osborn, M. Masters, G. Lévay, R. Kaliki, et al., Limb position tolerant pattern recognition for myoelectric prosthesis control with adaptive sparse representations from extreme learning, *IEEE Trans. Biomed. Eng.* 65 (4) (2018) 770–778. Available from: <https://doi.org/10.1109/TBME.2017.2719400>.
- [38] M.A. Powell, R.R. Kaliki, N.V. Thakor, User training for pattern recognition-based myoelectric prostheses: improving phantom limb movement consistency and distinguishability, *IEEE Trans. Neural. Syst. Rehabil. Eng.* 22 (3) (2014) 522–532. Available from: <https://doi.org/10.1109/TNSRE.2013.2279737>.
- [39] W. Geng, Y. Du, W. Jin, W. Wei, Y. Hu, J. Li, Gesture recognition by instantaneous surface emg images, *Sci. Rep.* 6 (2016) 36571. Available from: <https://doi.org/10.1038/srep36571>.
- [40] A.M. Simon, L.J. Hargrove, B.A. Lock, T.A. Kuiken, The target achievement control test: evaluating real-time myoelectric pattern recognition control of a multifunctional upper-limb prosthesis, *J. Rehabil. Res. Dev.* 48 (6) (2011) 619–628. Available from: <https://doi.org/10.1682/JRRD.2010.08.0149>.
- [41] P.J. Kyberd, A. Murgia, M. Gasson, T. Tjerks, C. Metcalf, P.H. Chappell, et al., Case studies to demonstrate the range of applications of the southampton hand assessment procedure, *Brit. J. Occupat. Therapy* 72 (5) (2009) 212–218. Available from: <https://doi.org/10.1177/030802260907200506>.

- [42] P. Kyberd, A. Hussaini, G. Maillet, Characterisation of the clothespin relocation test as a functional assessment tool, *J. Rehabil. Assistive Technol. Eng.* 5 (2018). Available from: <https://doi.org/10.1177/2055668317750810>.
- [43] T.A. Kuiken, L.A. Miller, R.D. Lipschutz, B.A. Lock, K. Stubblefield, P.D. Marasco, et al., Targeted reinnervation for enhanced prosthetic arm function in a woman with a proximal amputation: a case study, *Lancet* 369 (9559) (2007) 371–380. Available from: [https://doi.org/10.1016/S0140-6736\(07\)60193-7](https://doi.org/10.1016/S0140-6736(07)60193-7).
- [44] T.A. Kuiken, G. Li, B.A. Lock, R.D. Lipschutz, L.A. Miller, K.A. Stubblefield, et al., Targeted muscle reinnervation for real-time myoelectric control of multifunction artificial arms, *J. Am. Med. Assoc.* 301 (6) (2009) 619–628. Available from: <https://doi.org/10.1001/jama.2009.116>.
- [45] L.J. Hargrove, L.A. Miller, K. Turner, T.A. Kuiken, Myoelectric pattern recognition out-performs direct control for transhumeral amputees with targeted muscle reinnervation: a randomized clinical trial, *Sci. Rep.* 7 (2017) 1. Available from: <https://doi.org/10.1038/s41598-017-14386-w>.
- [46] M. Ortiz-Catalan, B. Håkansson, R. Bränemark, An osseointegrated human-machine gateway for long-term sensory feedback and motor control of artificial limbs, *Sci. Translat. Med.* 6 (257) (2014) 257re6. Available from: <https://doi.org/10.1126/scitranslmed.3008933>.
- [47] P. Stenlund, K. Kulbacka-Ortiz, S. Jönsson, R. Bränemark, Loads on transhumeral amputees using osseointegrated prostheses, *Ann. Biomed. Eng.* (2019) 1–9. Available from: <https://doi.org/10.1007/s10439-019-02244-x>.
- [48] V.E. Abraira, D.D. Ginty, The sensory neurons of touch, *Neuron* 79 (4) (2013) 618–639. Available from: <https://doi.org/10.1016/j.neuron.2013.07.051>.
- [49] A.E. Dubin, A. Patapoutian, Nociceptors: the sensors of the pain pathway, *J. Clin. Invest.* 120 (11) (2010) 3760–3772. Available from: <https://doi.org/10.1172/JCI42843>.
- [50] C. Chi, X. Sun, N. Xue, T. Li, C. Liu, Recent progress in technologies for tactile sensors, *Sensors* 18 (4) (2018) 948. Available from: <https://doi.org/10.3390/s18040948>.
- [51] Z. Liang, G. Chang, Z.J. Wang, E. Cretu, L. Xiaoou, Novel tactile sensor technology and smart tactile sensing systems: a review, *Sensors* (14248220) 17 (11) (2017) 1–24. Available from: <https://doi.org/10.3390/s17112653>.
- [52] A. Cranny, D.P.J. Cotton, P.H. Chappell, S.P. Beeby, N.M. White, Thick-film force and slip sensors for a prosthetic hand, *Sensors Actuators A: Phys.* 123–124 (0) (2005) 162–171. Available from: <https://doi.org/10.1016/j.sna.2005.02.015>.
- [53] L. Osborn, H. Nguyen, J. Betthauser, R. Kaliki, N. Thakor, Biologically inspired multi-layered synthetic skin for tactile feedback in prosthetic limbs, in: IEEE Engineering in Medicine and Biology Society (EMBC), 2016, pp. 4622–4625. <https://doi.org/10.1109/EMBC.2016.7591757>.
- [54] L. Osborn, W.W. Lee, R. Kaliki, N.V. Thakor, Tactile feedback in upper limb prosthetic devices using flexible textile force sensors, in: 5th IEEE RAS & EMBS International Conference on Biomedical Robotics and Biomechatronics (BioRob), 2014, pp. 114–119. <https://doi.org/10.1109/BIOROB.2014.6913762>.
- [55] J. Fishel, G. Loeb, Bayesian exploration for intelligent identification of textures, *Front. Neurorobot.* 6 (2012) 4. Available from: <https://doi.org/10.3389/fnbot.2012.00004>.
- [56] Z. Su, J. Fishel, G. Loeb, Use of tactile feedback to control exploratory movements to characterize object compliance, *Front. Neurosci.* 6 (7) (2012). Available from: <https://doi.org/10.3389/fnbot.2012.00007>.
- [57] B. Matulevich, G.E. Loeb, J.A. Fishel, Utility of contact detection reflexes in prosthetic hand control, in: IEEE/RSJ International Conference on Intelligent Robots and Systems (IROS), 2013, pp. 4741–4746. <https://doi.org/10.1109/IROS.2013.6697039>.
- [58] W. Liu, D. He, Y. Ruan, X. Ruan, X. Fu, C. Stefanini, Preliminary study on piezoresistive and piezoelectric properties of a double-layer soft material for tactile sensing, *Mater. Sci.* 21 (2) (2015) 238–243. Available from: <https://doi.org/10.5755/j01.ms.21.2.6454>.

- [59] R. Kilaru, Z. Çelik Butler, D.P. Butler, I.E. Gönenli, Nicr mems tactile sensors embedded in polyimide toward smart skin, *J. Microelectromech. Syst.* 22 (2) (2013) 349–355. Available from: <https://doi.org/10.1109/JMEMS.2012.2222867>.
- [60] P. Yu, W. Liu, C. Gu, X. Cheng, X. Fu, Flexible piezoelectric tactile sensor array for dynamic three-axis force measurement, *Sensors* 16 (6) (2016). Available from: <https://doi.org/10.3390/s16060819>.
- [61] G. Liang, Y. Wang, D. Mei, K. Xi, Z. Chen, Flexible capacitive tactile sensor array with truncated pyramids as dielectric layer for three-axis force measurement, *J. Micro-electromechan. Syst.* 24 (5) (2015) 1510–1519. Available from: <https://doi.org/10.1109/JMEMS.2015.2418095>.
- [62] R. Ahmadi, M. Packirisamy, J. Dargahi, R. Cecere, Discretely loaded beam-type optical fiber tactile sensor for tissue manipulation and palpation in minimally invasive robotic surgery, *IEEE. Sens. J.* 12 (1) (2012) 22–32. Available from: <https://doi.org/10.1109/JSEN.2011.2113394>.
- [63] A. Alfadhel, J. Kosel, Magnetic nanocomposite cilia tactile sensor, *Adv. Mater.* 27 (47) (2015) 7888–7892. Available from: <https://doi.org/10.1002/adma.201504015>.
- [64] Z. Zou, C. Zhu, Y. Li, X. Lei, W. Zhang, J. Xiao, Rehealable, fully recyclable, and malleable electronic skin enabled by dynamic covalent thermoset nanocomposite, *Sci. Adv.* 4 (2) (2018) eaaoq0508. Available from: <https://doi.org/10.1126/sciadv.aaoq0508>.
- [65] D.A. Bennett, M. Goldfarb, Imu-based wrist rotation control of a transradial myoelectric prosthesis, *IEEE. Trans. Neural. Syst. Rehabil. Eng.* 26 (2) (2018) 419–427. Available from: <https://doi.org/10.1109/TNSRE.2017.2682642>.
- [66] A. Krasoulis, I. Kyranou, M.S. Erden, K. Nazarpour, S. Vijayakumar, Improved prosthetic hand control with concurrent use of myoelectric and inertial measurements, *J. Neuro Eng. Rehabil. (JNER)* 14 (2017) 1–14. Available from: <https://doi.org/10.1186/s12984-017-0284-4>.
- [67] X. Li, R. Wen, Z. Shen, Z. Wang, K.D.K. Luk, Y. Hu, A wearable detector for simultaneous finger joint motion measurement, *IEEE Trans. Biomed. Circ. Syst.* 12 (3) (2018) 644–654. Available from: <https://doi.org/10.1109/TBCAS.2018.2810182>.
- [68] J. Kim, M. Lee, H.J. Shim, R. Ghaffari, H.R. Cho, D. Son, et al., Stretchable silicon nanoribbon electronics for skin prosthesis, *Nat. Commun.* 5 (2014) 5747. Available from: <https://doi.org/10.1038/ncomms6747>.
- [69] J. Park, M. Kim, Y. Lee, H.S. Lee, H. Ko, Fingertip skin–inspired microstructured ferroelectric skins discriminate static/dynamic pressure and temperature stimuli, *Sci. Adv.* 1 (9) (2015). Available from: <https://doi.org/10.1126/sciadv.1500661>.
- [70] H. Zhao, K. O’Brien, S. Li, R.F. Shepherd, Optoelectronically innervated soft prosthetic hand via stretchable optical waveguides, *Sci. Robot.* 1 (1) (2016) eaai7529. Available from: <https://doi.org/10.1126/scirobotics.aai7529>.
- [71] J. Byun, Y. Lee, J. Yoon, B. Lee, E. Oh, S. Chung, et al., Electronic skins for soft, compact, reversible assembly of wirelessly activated fully soft robots, *Sci. Robot.* 3 (18) (2018) eaas9020. Available from: <https://doi.org/10.1126/scirobotics.aas9020>.
- [72] B.C. Tee, C. Wang, R. Allen, Z. Bao, An electrically and mechanically self-healing composite with pressure- and flexion-sensitive properties for electronic skin applications, *Nat. Nanotechnol.* 7 (12) (2012) 825–832. Available from: <https://doi.org/10.1038/nnano.2012.192>.
- [73] S. Terryn, J. Brancart, D. Lefeber, G. Van Assche, B. Vanderborght, Self-healing soft pneumatic robots, *Sci. Robot.* 2 (9) (2017) eaan4268. Available from: <https://doi.org/10.1126/scirobotics.aan4268>.
- [74] T. Yokota, P. Zalar, M. Kaltenbrunner, H. Jinno, N. Matsuhisa, H. Kitanosako, et al., Ultraflexible organic photonic skin, *Sci. Adv.* 2 (4) (2016) e1501856. Available from: <https://doi.org/10.1126/sciadv.1501856>.
- [75] R. Di Giacomo, L. Bonanomi, V. Costanza, B. Maresca, C. Daraio, Biomimetic temperature-sensing layer for artificial skins, *Sci. Robot.* 2 (3) (2017) eaai9251. Available from: <https://doi.org/10.1126/scirobotics.aai9251>.

- [76] Y. Kim, A. Chortos, W. Xu, Y. Liu, J.Y. Oh, D. Son, et al., A bioinspired flexible organic artificial afferent nerve, *Science* 360 (6392) (2018) 998–1003. Available from: <https://doi.org/10.1126/science.aao0098>.
- [77] A. Chortos, J. Liu, Z. Bao, Pursuing prosthetic electronic skin, *Nat. Mater.* 15 (9) (2016) 937–950. Available from: <https://doi.org/10.1038/nmat4671>.
- [78] D.W. Tan, M.A. Schiefer, M.W. Keith, J.R. Anderson, J. Tyler, D.J. Tyler, A neural interface provides long-term stable natural touch perception, *Sci. Translat. Med.* 6 (257) (2014) 257ra138. Available from: <https://doi.org/10.1126/scitranslmed.3008669>.
- [79] M. Schiefer, D. Tan, S.M. Sidek, D.J. Tyler, Sensory feedback by peripheral nerve stimulation improves task performance in individuals with upper limb loss using a myoelectric prosthesis, *J. Neural. Eng.* 13 (1) (2015) 016001. Available from: <https://doi.org/10.1088/1741-2560/13/1/016001>.
- [80] E. D'Anna, F.M. Petrini, F. Artoni, I. Popovic, I. Simanić, S. Raspopovic, et al., A somatotopic bidirectional hand prosthesis with transcutaneous electrical nerve stimulation based sensory feedback, *Sci. Rep.* 7 (1) (2017) 10930. Available from: <https://doi.org/10.1038/s41598-017-11306-w>.
- [81] L. Osborn, M. Fifer, C. Moran, J. Betthauser, R. Armiger, R. Kaliki, et al., Targeted transcutaneous electrical nerve stimulation for phantom limb sensory feedback, in: IEEE Biomedical Circuits and Systems (BioCAS), 2017, pp. 1–4. <https://doi.org/10.1109/BIOCAS.2017.8325200>.
- [82] H. Shin, Z. Watkins, H.H. Huang, Y. Zhu, X. Hu, Evoked haptic sensations in the hand via non-invasive proximal nerve stimulation, *J. Neural. Eng.* 15 (4) (2018) 046005. Available from: <https://doi.org/10.1088/1741-2552/aabd5d>.
- [83] T.A. Kuiken, P.D. Marasco, B.A. Lock, R.N. Harden, J.P.A. Dewald, Redirection of cutaneous sensation from the hand to the chest skin of human amputees with targeted reinnervation, *Proc. Natl. Acad. Sci.* 104 (50) (2007) 20061–20066. Available from: <https://doi.org/10.1073/pnas.0706525104>.
- [84] J.S. Hebert, J.L. Olson, M.J. Morhart, M.R. Dawson, P.D. Marasco, T.A. Kuiken, et al., Novel targeted sensory reinnervation technique to restore functional hand sensation after transhumeral amputation, *IEEE. Trans. Neural. Syst. Rehabil. Eng.* 22 (4) (2014) 765–773. Available from: <https://doi.org/10.1109/TNSRE.2013.2294907>.
- [85] P.D. Marasco, A.E. Schultz, T.A. Kuiken, Sensory capacity of reinnervated skin after redirection of amputated upper limb nerves to the chest, *Brain* 132 (6) (2009) 1441–1448. Available from: <https://doi.org/10.1093/brain/awp082>.
- [86] C.M. Oddo, S. Raspopovic, F. Artoni, A. Mazzoni, G. Spigler, F. Petrini, et al., Intraneuronal stimulation elicits discrimination of textural features by artificial fingertip in intact and amputee humans, *eLife* 5 (2016) e09148. Available from: <https://doi.org/10.7554/eLife.09148>.
- [87] E.M. Izhikevich, Simple model of spiking neurons, *IEEE Trans. Neur. Net.* 14 (6) (2003) 1569–1572. Available from: <https://doi.org/10.1109/TNN.2003.820440>.
- [88] S.N. Flesher, J.L. Collinger, S.T. Foldes, J.M. Weiss, J.E. Downey, E.C. Tyler-Kabara, et al., Intracortical microstimulation of human somatosensory cortex, *Sci. Translat. Med.* 8 (361) (2016) 361ra141. Available from: <https://doi.org/10.1126/scitranslmed.aaf8083>.
- [89] A. Akhtar, J. Sombeck, B. Boyce, T. Bretl, Controlling sensation intensity for electrotactile stimulation in human-machine interfaces, *Sci. Robot.* 3 (17) (2018) eaap9770. Available from: <https://doi.org/10.1126/scirobotics.aap9770>.
- [90] L. Osborn, H. Nguyen, R. Kaliki, N. Thakor, Prosthesis grip force modulation using neuromorphic tactile sensing, in: Myoelectric Controls Symposium (MEC), 2017, pp. 188–191.
- [91] H.P. Saal, B.P. Delhaye, B.C. Rayhaun, S.J. Bensmaia, Simulating tactile signals from the whole hand with millisecond precision, *Proc. Natl. Acad. Sci.* (2017). Available from: <https://doi.org/10.1073/pnas.1704856114>.

- [92] E.L. Graczyk, M.A. Schiefer, H.P. Saal, B.P. Delhaye, S.J. Bensmaia, D.J. Tyler, The neural basis of perceived intensity in natural and artificial touch, *Sci. Translat. Med.* 8 (362) (2016) 362ra142. Available from: <https://doi.org/10.1126/scitranslmed.aaf5187>.
- [93] E.L. Graczyk, B.P. Delhaye, M.A. Schiefer, S.J. Bensmaia, D.J. Tyler, Sensory adaptation to electrical stimulation of the somatosensory nerves, *J. Neural. Eng.* 15 (4) (2018) 046002. Available from: <https://doi.org/10.1088/1741-2552/aab790>.
- [94] S.S. Srinivasan, M.J. Carty, P.W. Calvaresi, T.R. Clites, B.E. Maimon, C.R. Taylor, et al., On prosthetic control: a regenerative agonist-antagonist myoneural interface, *Sci. Robot.* 2 (6) (2017) eaan2971. Available from: <https://doi.org/10.1126/scirobotics.aan2971>.
- [95] T.R. Clites, M.J. Carty, J.B. Ullauri, M.E. Carney, L.M. Mooney, J.-F. Duval, et al., Proprioception from a neurally controlled lower-extremity prosthesis, *Sci. Translat. Med.* 10 (443) (2018) eaap8373. Available from: <https://doi.org/10.1126/scitranslmed.aap8373>.
- [96] L.H. Smith, T.A. Kuiken, L.J. Hargrove, Real-time simultaneous and proportional myoelectric control using intramuscular emg, *J. Neural. Eng.* 11 (6) (2014) 066013. Available from: <https://doi.org/10.1088/1741-2560/11/6/066013>.
- [97] G. Ghazaei, A. Alameer, P. Degenaar, G. Morgan, K. Nazarpour, Deep learning-based artificial vision for grasp classification in myoelectric hands, *J. Neural. Eng.* 14 (3) (2017) 036025. Available from: <https://doi.org/10.1088/1741-2552/aa6802>.
- [98] M. Hays, L. Osborn, R. Ghosh, M. Iskarous, C. Hunt, N.V. Thakor, Neuromorphic vision and tactile fusion for upper limb prosthesis control, in: 2019 9th International IEEE/EMBS Conference on Neural Engineering (NER), 2019, pp. 981–984. <https://doi.org/10.1109/NER.2019.8716890>.

LOWER LIMB ACTIVE PROSTHETIC SYSTEMS—OVERVIEW

23

Alexandra S. Voloshina and Steven H. Collins

Department of Mechanical Engineering, Stanford University, Stanford, CA, United States

23.1 INTRODUCTION

Changes in lower limb mechanics, sensory feedback, and power output associated with lower limb loss have substantial impacts on the gait biomechanics and energetics of individuals with amputations. During unimpaired level ground walking, the ankle produces significant net positive ankle power throughout the stride [1,2], with other locomotor tasks, such as walking up slopes, relying on additional net positive power output at the knee [3]. As a result, lower limb amputation and the associated loss of ankle and knee power production is linked to slower self-selected walking speeds and increased energy expenditure [4]. People with transtibial and transfemoral amputation expend up to 30% and 60% more metabolic energy, respectively [4,5], when compared to unimpaired individuals walking at the same speed. Similarly, the preferred walking speed of individuals with amputation can be 10%–65% slower than the average walking speed of unaffected individuals, depending on the level of amputation and the walking surface [4,6].

Individuals with lower limb amputation often adapt compensatory gait strategies that can lead to significant changes in gait dynamics, joint loading and work, and muscle activity in the affected and unaffected limbs. For example, unilateral below-knee prosthesis users tend to favor their unaffected limb [7,8], which often endures greater joint forces, moments, and stress during daily activity [9–11]. The hip joint on the contralateral limb can produce up to three times more work than the hip joint of an unimpaired individual, likely as compensation for lack of power production of conventional passive prostheses [1,12]. The affected limb generally exhibits significantly lower knee moments when compared to the contralateral limb or to individuals without impairment [11]. In addition, affected limb knee flexor and extensor muscles can exhibit higher co-contraction levels [13], a strategy commonly adapted to stabilize the joint in uncertain conditions (e.g., [14–16]). Such marked gait asymmetry and joint loading can lead to chronic health issues, such as premature joint degeneration, early-onset osteoarthritis, and joint pain [7].

Slower walking speeds, increases in muscle co-contraction, and changes in gait symmetry can also be indicators of compromised balance [15,17,18]. About half of all individuals with amputation experience at least one fall a year, usually during walking. Of these individuals, 75% fall at

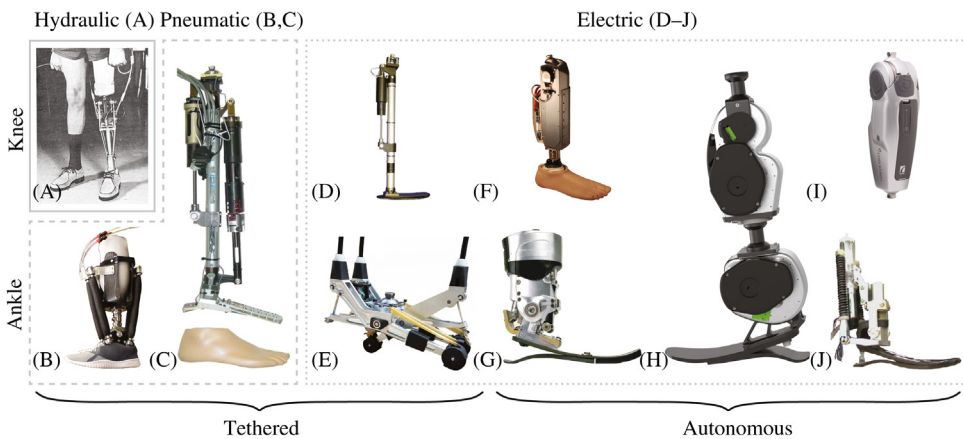
least twice, and 10% experience at least one fall that results in serious injury requiring medical treatment [19]. About half of individuals with lower limb amputation report a fear of falling and 60% list inability to walk on natural surfaces, such as wooded areas or fields, as a major limitation. As the causes of these limitations, about 50% of affected individuals cite an inability to adequately sense the walking surface, 40% an inability to walk without a stabilizing gait aid, and 30% difficulty in controlling their prosthesis [20]. Gait asymmetry, changes in joint loading often leading to pain, and elevated risk of falling and other injuries severely reduce mobility and overall quality of life of individuals with amputation.

23.2 BACKGROUND

Most currently available commercial prostheses rely on elastic elements, such as carbon-fiber plates or mechanical springs, to absorb and return energy passively [21,22]. Such energy storage and return devices cannot actively generate power, unlike biological lower limb muscles which produce up to 80% of the mechanical work per step [23–25]. More so, these devices can only be mechanically adjusted and lack the ability to actively adapt to the user or changes in the environment. Even partial actuation in prosthetic devices appears to benefit user performance. Several semiactive devices, which do not generate net positive power but allow for controlled damping or transition between gait modes, have led to improved user balance and stability by actively adjusting joint angles based on gait type [26,27]. Effective control of fully actuated devices could address the current limitations of prosthetic devices even further, potentially improving balance, comfort, and gait symmetry in individuals with lower limb amputation.

Development of active lower limb prosthetic devices began to gain traction in the late 1970s, with the introduction of a tethered, hydraulically powered knee prosthesis [28] (Fig. 23.1A). This system demonstrated the feasibility of active prostheses to generate prescribed movement at the desired times in the gait cycle. Although no biomechanical user data were collected, individuals with amputation tended to prefer the active device with simple control paradigms to their prescribed passive knees. Evaluation of devices that followed (e.g., Fig. 23.1F) revealed that an active knee prosthesis could produce kinematics and power output similar to intact limbs and lead to a more kinematically symmetric gait [33], with one such device produced commercially (Fig. 23.1I). In turn, different control architectures could accommodate walking on sloped terrain (implemented in devices similar to Fig. 23.1C,D), while still maintaining the trajectories of an unaffected joint [38].

Previous research has also suggested that active ankle power modulation could have significant gait benefits. For example, active inversion/eversion assistance implemented on an experimental ankle prosthesis (similar to Fig. 23.1E) reduced the metabolic cost of walking without significantly affecting gait mechanics or the perception of comfort [39]. This suggests that energy economy is correlated with the active need to correct body dynamics on a step-to-step basis, and that active devices can improve performance even if overall mechanics remain unchanged. The effects of active ankle push-off work on energy expenditure are less clear. One commercially available device (based on Fig. 23.1G) has been shown to lead to energetic reductions of up to 8% [34,40], as well as increased walking speeds [41,42], in users with transtibial amputation during walking on level

**FIGURE 23.1**

Selected autonomous and tethered active ankle and knee prosthetic devices. With the exception of (E) and (J), all devices are actuated only in the sagittal plane. Solid, dashed, and dotted outlines indicate hydraulic, pneumatic, and electrical devices, respectively. (A) The first active knee prosthesis with echo control [28], (B) ankle prosthesis with pneumatic artificial muscles and myoelectric control from North Carolina State University, based on [29] (image courtesy of S. Huang), (C) Pneumatic cylinder actuated ankle and knee prosthesis controlled by an impedance-based strategy, similar to [30] (image courtesy of M. Goldfarb), (D) Prosthetic knee joint with passive ankle and impedance-based control [31] (image courtesy of M. Goldfarb), (E) Ankle prosthesis emulator with three individually actuated digits for frontal and sagittal plane actuation [32] (image courtesy of V. Chiu), (F) Variable impedance knee prosthesis [33] (image courtesy of E. Martinez-Villalpando), (G) Bionic ankle foot prosthesis that served as the basis for the BiOM [34], and consequently the Ottobock Empower (image courtesy of A. Grabowski), (H) The Open-source Robotic Leg, a scalable and customizable knee and ankle prosthesis system intended as an easily accessible platform for research testing [35] (image courtesy of E. Rouse), (I) The Össur Power Knee, the only commercially available powered knee prosthesis to date [36] (image courtesy of Össur), (J) The SPARKy 2 ankle prosthesis that allows for fore-aft and medio-lateral control of the joint [37] (image courtesy of T. Sugar).

ground, when compared to their prescribed device. In contrast, using a tethered prosthesis to increase prosthesis mechanical work in isolation has not been found to affect energy expenditure [43]. Differences in outcomes could be due to variation in other prosthesis characteristics, rather than the addition of active power itself, including control features that might affect balance. To facilitate well-controlled comparisons of prosthesis function outside the laboratory, the Open-source Robotic Leg Prosthesis (Fig. 23.1H), an active ankle and/or knee prosthetic device, is currently being developed for laboratory applications [35]. The standalone device can be configured both mechanically and in software, allowing for evaluation of a range of configurations with just one device.

Differences in user response to active assistance may also be due to the difficulties of hand tuning control parameters for each individual. For example, even minor changes in timing and magnitude can have substantial effects on energy expenditure [44–46]. More accurate control optimization strategies could allow devices to be more effectively tuned to each user and have

already shown promising results in improving performance of exoskeleton assistive devices (e.g., [47,48]). Similarly, devices relying on more direct control from the user, for example by using muscle activation signals to control the device (as in Fig. 23.1B), could lead to reductions in energetic cost [29].

The biomechanical response of people with amputation to active devices is promising, but very few active prostheses are currently on the market. Further advances in energetically efficient actuators (like those used for Fig. 23.1J), controllers capable of adapting to the user and the environment, and accessible platforms for prosthetic research, could significantly increase the availability of powered prostheses to affected individuals. This could improve balance, reduce falls and other injuries, redistribute joint loading, and decrease the severity of premature joint generation and other mobility restrictions.

23.3 SYSTEMS

Building lower limb prosthetic devices that can emulate the behavior of natural joints is a long-standing goal of researchers aiming to enhance mobility for people with amputations. Effective prosthetic devices would need to generate sufficient torque while still being relatively lightweight, adapt to a variety of terrains and locomotion tasks, and effectively interface with the user. For comparison, for an 86-kg individual, the ankle can provide up to 450 W peak power and 150 Nm of peak torque [23], with an ankle/shank mass of less than 5 kg [1]. Prosthetic devices must be even lighter, depending on the weight of the residual limb post amputation, while still providing comparable energetic outputs. Effective device controllers would provide intuitive integration with the user and an ability to conform to day-to-day activities. Finally, proper socket fit is critical for user comfort and effective attachment of the device. Although not discussed in this chapter, socket fit and design is one of the most valued features of a prosthesis [49], and requires further development. Active prosthetic devices have only been a research focus since the 1970s, yet significant progress in advancing this technology has been made. These advances, in both autonomous and research-oriented devices, are discussed in the following sections.

23.3.1 MECHANICAL CONFIGURATION AND ACTUATION APPROACHES

To be most effective, active lower limb prosthetic devices may need to provide torque and power outputs similar to the capabilities of the biological leg. Electric actuators are well suited for these purposes and have been previously implemented in research and commercial prosthetic devices. Pneumatic actuators can also generate a range of behaviors necessary for human gait but generally require off-board air compressors, thus limiting their use primarily to research. Several hydraulically powered devices have also been proposed, although hydraulic actuators are mainly used for controlled damping and are not discussed in detail in this chapter. Finally, tethered systems that place actuation components off-board are crucial in advancing the development of prosthetic devices, as they provide the ability to test a wide range of control ideas without the need for building new hardware. The trade-offs in benefits and limitations of several mechanical configurations and actuation approaches are discussed further.

23.3.1.1 Remote actuation

As lower limb prosthetic device designs move towards smart, actuated systems, there are still many aspects of device control and human–robot interaction that remain unclear. Testing new control and actuation approaches often requires building new hardware for evaluation, which is both expensive and time consuming. For this reason, several testbed, tethered prosthesis systems move control and/or power components from the wearable device and place them off-board. This allows for the worn system to remain lightweight and low-profile, while still maintaining the ability to produce forces and torques similar to those seen in biological joints. In addition, tethered devices are generally tested within a laboratory or clinical setting, which provides access to lab-based equipment and a means to test approaches which would otherwise be infeasible. For example, one tethered ankle prosthesis used ground reaction forces from an instrumented treadmill to identify center of mass sway and to control inversion/eversion torques generated by the device [39]. Implementing such a control architecture would be more challenging in a standalone device, which would need a separate, independent system of detecting ground reaction forces. Tethered devices are more conducive to long-term studies in a controlled environment, which lead to insights into gait mechanics and control of individuals with lower limb amputation.

Tethered prostheses have been powered by hydraulic, pneumatic, and electric actuators, with the transmission often relying on flexible tubes or cables so as to not restrict user movements. Hydraulic and pneumatic approaches are well-suited for off-board actuation, as they can be connected to external pumps or compressors via flexible tubing. The first active prosthesis systems relied on an off-board hydraulic pump and computing hardware to drive an artificial knee joint with an on-board hydraulic cylinder [28] (Fig. 23.1A). The setup served as a proof of concept that active devices could lead to gait patterns similar to unimpaired gait. It was later adapted to test other control architectures, such as using myoelectric activity to dictate knee damping magnitude [50], or enforcing unimpaired gait kinematics to remove vaulting during stance [51]. Similar tethered pneumatic systems also place cylinders directly on the device, while an air compressor and computing hardware remain off-board. Such research prototypes have helped demonstrate, for example, that direct proportional myoelectric control can effectively control ankle torque [29], and that adaptable ankle stiffness may improve gait in individuals with lower limb amputation [52].

Recent advances in electrically powered tethered testbeds provide a way of exploring an even broader range of prosthesis design and control approaches. A typical system consists of powerful off-board motors and control hardware, connected to a robotic ankle prosthesis, or end-effector, by means of Bowden cables and flexible tethers [53,54]. High-torque, low-inertia electrical motors generate device peak torques and powers up to 50% higher than seen in the biological ankle, while more easily tracking fast-changing torque profiles when compared to pneumatic and hydraulic systems of comparable weight. This approach also significantly reduces the worn mass and profile of the prosthesis since, unlike in tethered pneumatic and hydraulic systems, no part of the actuator is placed on the leg. In turn, this allows for the development of tethered prostheses with more degrees of freedom. To date, end-effectors developed for this testbed include devices with one, two, or three degrees of freedom (Fig. 23.1E), which allow for plantarflexion, inversion/eversion, and center of pressure control by actuating various components of the device [32,53,54].

23.3.1.2 Pneumatic actuators

Pneumatic artificial muscles, a type of compliant pneumatic actuator, have been used for actuation of prosthetic devices. One of the more common pneumatic muscles, the McKibben artificial muscle, consists of a cylindrical inner rubber bladder, enclosed in a braided sheath [55]. As the inner bladder inflates, it shortens, expands radially, and produces a pulling force between the two actuator end-points. Adding a damper in parallel with the pneumatic actuator drives actuator performance to more closely emulate the force–velocity dynamics of biological muscle–tendon units [56,57]. Furthermore, folding the membrane of the actuator in on itself in a cylindrical shape along its central axis, akin to accordion bellows, reduces hysteresis by mitigating material strain during inflation [55,58,59]. This leads to more predictable dynamics of the actuator, reduces actuator failure rates, allows for simpler control strategies that do not need to take into account actuator deformation, and yields a position error of less than 2% [60]. In all, pneumatic artificial muscles have the advantage of being extremely lightweight and compliant, with the capability of generating high peak torques and variable stiffness spring-like behavior similar to biological muscle [55,61].

Like biological muscle, pneumatic actuator muscles only provide pulling forces and often need to be arranged in an antagonistic configuration for prosthetic devices. This is exemplified by several designs of prosthetic ankles, which consist of a one degree of freedom ankle joint attached to a commercially available foot. The muscles are then attached to the front and back of the foot and to protrusions either on the socket or the pylon of the device (e.g., [29,62], Fig. 23.1B). A similar arrangement was also demonstrated in a pneumatic knee prosthesis, where two artificial muscles produced bidirectional motion about the knee joint while the ankle joint remained passive [63].

Pneumatic cylinder actuators offer certain trade-offs compared to soft pneumatic muscles. One of the main benefits of pneumatic cylinders is their ability to generate force in both directions. This force is independent of actuator displacement and simplifies control by mitigating the need to compensate for actuator dynamics [55]. Pneumatic cylinders can also operate at much higher pressure and thereby produce larger forces than soft pneumatic actuators. However, all pneumatic devices need to consider the trade-off between pressure, area, and flow rate. Greater force production can be achieved by increasing pressure or actuator cross area, but both approaches introduce some drawbacks. For example, increasing pressure is more likely to lead to mechanical failures, while increasing the cylinder size results in higher flow rates and power loss across valves. The importance of these trade-offs is apparent in a powered ankle and knee prosthesis that relied on two double-acting pneumatic cylinders to actuate the joints [30]. The particular configuration limited the maximum size of the actuators, in turn reducing the maximum torque that could be produced as well. As a result, only 76% of the maximum biological ankle torque was achieved, since a larger actuator would impede the range of motion of the prosthesis. Nonetheless, the device was able to produce ankle and knee kinematics comparable to nonimpaired gait, and provided significant assistance to the user.

Pneumatic actuators offer certain benefits but several drawbacks exist. For one, air compressors tend to be heavy and inefficient, so pneumatic systems are rarely untethered. Efforts to develop portable pneumatic actuation systems, for example by using monopropellants [64,65], could address this limitation in the future. Another drawback is that pneumatic artificial muscles expand significantly when inflated and are not suited for low-profile applications. Finally, pneumatic actuators are often loud, making them impractical for standalone prostheses.

23.3.1.3 Electric actuators

Electric motors are the most common actuators in active prosthetic devices, especially for autonomous devices. However, heavier, larger motors are generally required to produce the peak and average power demonstrated by human joints during gait [66]. In addition, most electric motors achieve peak power at high speeds, which is not always conducive to generating appropriate prosthesis behavior [66]. Transmissions with high gear reductions can address this issue, but also introduce high impedance when the system is unpowered. More complex transmissions involving springs or clutches can improve torque control or allow energy capture and return, at the cost of added mass and size.

Several knee prostheses have been developed that rely on ball screw systems to translate rotary motion into linear motion. One such setup was able to demonstrate power profiles comparable to biological knees during slow walking [31] (Fig. 23.1D). Although tethered, it was estimated that the device could provide power for an 85-kg user to walk for up to 5 km on a small battery pack. The knee joint of another autonomous knee and ankle device relied on a similar setup, but with the ball screw assembly attached to a slider crank mechanism that actuated the joint (based on Ref. [30]) [67]. Although such configurations can generate the required power outputs for level walking, they cannot take advantage of the passive dynamics of the leg or other energy storage and return mechanisms, leading to considerable power consumption [68]. The only commercially available powered knee device to date, the Össur Power Knee, is similarly actuated [36].

Adding passive compliance to the transmission system can provide additional benefits. Springs placed in parallel to the actuator can reduce actuator torque and power requirements, particularly when the desired behavior of the motor is spring-like and not antagonistic to the elastic element. A mechanical spring in parallel with a ball screw mechanism of a joint, for example, can supplement motor torque and reduce actuator energy use [67]. Springs instead placed in series with the actuator can help regulate and maintain joint torque and protect against damage due to impact (for example, at heel-strike) [69], although this makes the control of joint angle and speed more difficult. A range of devices utilize this series elastic actuator (SEA) approach to improve performance. One such autonomous knee device used two antagonistically placed SEAs to emulate the elasticity and damping characteristics of a biological knee [33,68] (Fig. 23.1F). The only commercially available ankle prosthesis to provide active power, the BiOM (now the Ottobock Empower), incorporates both series and parallel elastic elements [70–72]. A rotary SEA helps with the control of joint torque, while the parallel spring allows for a lower gear ratio and, consequently, faster joint movement. The prosthesis is similar in weight to an intact limb (Fig. 23.1G), provides adequate power and torque output to the user, and was even demonstrated to lead to reductions in user energy expenditure when compared to passive devices [34,70].

However, SEA components have drawbacks, such as increased prosthesis weight and reduced control bandwidth. Elastic components can also be used with locking mechanisms to improve energy storage and release during the gait cycle [73], or with systems that transfer energy from the knee to the ankle joint [74], both of which can improve device performance. The previously mentioned Open-source Robotic Leg Prosthesis can be configured to include series elasticity of variable stiffness to facilitate research on a wide range of prosthesis designs [35]. Series elasticity can be added to both the ankle and knee joints of the device, which rely on an electric motor coupled to a multistage belt-drive transmission for torque generation. The configuration results in a relatively low transmission ratio, usually associated with smaller mass and improved force control.

23.3.2 CONTROL APPROACHES

One of the main challenges of developing active prostheses is identifying controllers that can reliably improve performance during a given locomotor task. Walking follows a cyclical pattern and imitating this behavior mathematically is an attractive option. Feedforward control may be sufficient for certain cyclic tasks but does not allow for human input or significant variability in the gait cycle. To provide reactive control and handle a greater variety of tasks, some prosthesis controllers incorporate varying levels of online feedback from the user in order to drive the device or direct state transitions.

23.3.2.1 Gait pattern generator control

Prosthesis joint torque or angle dynamics are often prescribed as predefined functions of some state of the system. Such gait pattern generators can be time-dependent or based on measures such as joint angle and velocity, user muscle activity, or gait phase. One of the earlier active knee prostheses relied on this approach by “echoing” leg dynamics of the contralateral side. Angle trajectories from the intact side were recorded and scaled, and played back on the prosthesis half a gait cycle later [75]. Participants adapted to the system quickly during steady-state walking, although such enforcement of biological knee trajectories did not improve user hip dynamics [76]. Furthermore, since the angle trajectory profile was defined through instrumentation of the sound-leg, this control approach enforces a control lag and can only be used to control devices for individuals with unilateral amputation, and limits human–device interaction.

Referencing predefined joint dynamics with respect to time or gait phase can mitigate time delay concerns and allow for prostheses to behave independently from the contralateral limb. The Spring Ankle with Regenerative Kinetics (SPARKy) prosthesis, for example, was controlled by expressing able-bodied ankle moments as a time-dependent function [37,77–79]. The configuration of the device was such that a low-power motor could regulate the loading of an in-series spring that then recoiled to provide positive power later in the step [80,81]. Torque generation started at heel-contact, with the motor moving the spring through a predetermined pattern configured to assist in steady-state gait. Alternatively, the phase of one or more variables can be used to define the desired prosthesis torque. One such approach utilized thigh angle as the phase variable to effectively generate more diverse cyclic, as well as discrete motions in a knee prosthesis [82]. The gait cycle was divided into several segments, as determined by foot contact, with the phase of the thigh angle mapping to various desired torque profiles for each segment. This control approach naturally scaled to gaits at different speeds, nonsteady-state tasks such as crossing obstacles, and even backwards walking. Furthermore, the control approach could then be adapted for more intuitive tuning of the desired knee trajectories by using a control interface that allowed clinicians to adjust certain sections of the ankle and knee angle trajectories [83]. A similar approach mapped the states of the residual limb to reference states of the missing knee joint using statistical regression of data from unimpaired gait. In other words, the prosthetic knee was driven relative to residual hip motion, based on the hip–knee relationship seen in unimpaired gait. This allowed for successful generation of locomotion with near physiological gait patterns, as well as for stair ascent and descent.

Gait patterns can also be successfully mimicked using mathematical models, rather than mapping to predefined states. For example, a model can characterize joint behavior as a simulated spring and damper, with different parameterizations for different phases of the gait cycle (e.g.,

[30]). Such impedance-based control approaches only generate net power when switching between the gait phases, but can produce joint dynamics similar to unimpaired walking and generate the torques and power required for even, sloped, and uneven terrain walking [30,38,84]. Alternatively, some models generate gait patterns using biologically inspired approaches. One such neuromuscular model, comprising a human ankle-foot complex with Hill-type muscle dynamics, received prosthesis angle and angular velocity as inputs and generated the desired ankle torque command [85]. Without additional sensing of the walking surface, the system was able to successfully adapt to changes in ground slope. When modified to include muscle length and velocity terms, it could also demonstrate adaptation to walking speed [86]. A similar approach has been demonstrated in a powered prosthetic knee [87]. Adding history-dependent muscle properties, such as a winding-spring system mimicking the role of titin in muscle [88], can produce variable speed walking and stair ascent without explicit changes to model parameters [89]. It is important to note that the presented controllers rely on an estimation of gait dynamics, which may be limiting in real-world, unpredictable environments.

23.3.2.2 EMG-based control

Active prosthesis control generated from electromyographic (EMG) signals can potentially provide intuitive, volitional control of the device. However, electromyography signals obtained from muscles in the residual limb vary in quality and availability between users [90], and EMG electrodes are either invasive or prone to noise and movement artifacts. This makes EMG control approaches challenging to develop, with early myoelectric controllers primarily relying on EMG signals to produce knee-lock during stance (e.g., [91,92]). Some adaptations have used EMG to modulate joint impedance, for example, by employing flexor and extensor thigh muscle activity to determine the damping magnitude of a knee prosthesis [50,93], without generating any active work.

Although residual limb muscle recruitment patterns tend to be highly variable between individuals, they tend to be consistent from stride to stride and suitable for certain types of feedforward control of prosthetic devices [90]. As a result, several active devices have utilized direct myoelectric control. One knee prosthesis relied on a weighted summation of residual thigh flexor and extensor muscles to define prosthesis joint stiffness and set point [94]. With this approach, a participant with a transfemoral amputation could control the device during steady-state walking, although knee dynamics significantly differed from unimpaired gait. Further addition of a state-dependent damping term to the myoelectric torque controller allowed participants to ascend and descend stairs [95]. Ankle prostheses controlled directly with myoelectric signals have also been developed. In one pneumatically powered device, artificial plantarflexor muscle pressure was directly regulated by filtering and rectifying residual limb gastrocnemius muscle activity [29]. With less than an hour of training, a participant with a transtibial amputation was able to control the device and produce functional gait. Muscle pattern adaptation was further improved by adding visual feedback, leading to increased ankle power and ankle positive work during walking [96].

More often, EMG-based control for active prostheses is used alongside additional control paradigms, such as gait pattern generators (see Section 23.3.2.1), in order to avoid relying on direct EMG control. To control a virtual ankle joint angle, one approach used a flexor and extensor muscle model that used EMG signals from the residual limb gastrocnemius, soleus, and tibialis anterior muscles to determine the model's force–velocity characteristics [97]. Similarly, EMG signals from the residual limb have been used as input to a Hill-type muscle model of ankle behavior [98].

A powered ankle prosthesis was controlled using a finite-state machine, with ankle torque gain at late stance selectively driven by the model. This control architecture allowed one participant with a unilateral transtibial amputation to modulate net ankle work and peak ankle power.

23.3.2.3 Motion intent detection control

Natural transitions are seamless and intuitive, without requiring distinct actions (e.g., pressing a button) from the user. Since prosthetic devices are often governed by multiple finite-state controllers designed for different gait phases, intent recognition algorithms are necessary to differentiate and transition between these controllers. One such algorithm relied on a probabilistic model to successfully differentiate between standing, sitting, and walking on a powered ankle and knee prosthesis, based on measurements of knee, ankle, and socket kinematics and forces experienced at the foot [99]. After training the model using approximately 60 trials of prerecorded walking and standing data from an individual with a transfemoral amputation, the model generated a database that could classify a range of activity modes during prosthesis use. The classification approach resulted in reliable mode-recognition and could be adapted to include other locomotion modes, although longer training periods would likely be required. Electromyography has also been successfully used for motion intent recognition [100], in contrast to being used to directly control the device as described in Section 23.3.2.1. In combination with ground reaction force data, electromyography is more informative in identifying user intent than just prosthesis kinematics. In fact, pattern recognition algorithms applied to muscle activation signals from lower limb muscles have been shown to identify up to seven gait modes for users with transfemoral amputation, with classification error rates between 4% and 15% [101]. In practice, a feedforward neural network was able to accurately dictate transitions between walking on level ground and stair ascent/descent for an ankle prosthesis, using residual limb gastrocnemius and tibialis anterior muscle signals [72]. Similarly, a quadratic discriminant analysis classifier, using residual limb hamstring and quadriceps muscle signals, reliably identified flexion and extension modes with less than 5 minutes of training data [102]. Residual limb thigh muscle activity can even be used to identify intent of both knee and ankle flexion and extension during nonweight-bearing activities in individuals with transfemoral amputation [103]. A linear discriminant analysis classifier recognized knee and ankle motion with approximately 90% accuracy using signals from nine residual limb muscles located in the thigh. Finally, developments in targeted muscle reinnervation in individuals with lower limb amputation are showing promise in helping identify user intent [104]. During the amputation surgery of one patient, nerve branches previously used to control the ankle joint were redirected to innervate two hamstring muscles. After recovery, the patient was able to volitionally contract the hamstring muscles when intending to move the ankle joint. Using pattern recognition algorithms, EMG signals from the hamstrings could provide robust, intuitive transitions between multiple gait modes in a prosthetic ankle with less than a 2% error rate. However, people usually take several thousand steps per day, meaning that even a 99.9% success rate in identifying gait modes could lead to several falls a day, depending on the consequences of a classification error. Near-zero error rates or robust error recovery would be required to develop a reliable, usable device.

23.3.2.4 Tuning control parameters

Currently available active prostheses show only modest improvements in energy expenditure and balance during walking on level ground, when compared to passive systems (e.g., [34,42]). This is

possibly due to active prosthetic devices typically being controlled using actuation profiles similar to those of unaffected individuals, although optimal assistance likely varies between users and from unimpaired mechanics [105]. Tuning the device to each user could address this issue but conventional prosthetic device fittings are typically based on subjective clinical evaluations [106,107], which may be ineffective for tuning more complex active devices. In addition, user dynamics fluctuate with time in response to adaptation and increased exposure to an active device [108,109], making effective control parameters for each individual difficult to identify. Methods for automatically identifying optimal user-specific characteristics could improve the effectiveness of active prosthetic limbs, especially for devices with balance-enhancing control.

Several control optimization algorithms have been effective in improving human performance by systematically adapting assistive exoskeleton control parameters. One such approach relied on a gradient descent technique [110] to successfully optimize the onset time of assistive ankle torque, with the goal of minimizing user energy expenditure [109]. Unlike gradient descent optimization, which is susceptible to noise and does not scale well with more complex controllers, strategies such as the Covariance Matrix Adaptation Evolution Strategy (CMA-ES) and Bayesian optimizations are potentially better suited for optimizing a larger number of control parameters in noisy conditions. CMA-ES, in particular, was tested on individuals walking with an ankle exoskeleton providing unilateral assistive plantarflexion torque as defined by four parameters, and led to optimized assistance that reduced energy expenditure between 14.2% and 41.5%, and 24% on average [47]. Such reductions in metabolic cost due to an assistive device are the largest reported to date, and are a several-fold improvement over hand-tuned controllers [111], even outperforming devices that provide assistance to multiple joints (e.g., [112]). Bayesian optimization does not require multiple parameter evaluations like CMA-ES and is specifically well suited for optimizing noisy and changing systems, but becomes computationally impractical when attempting to tune many parameters simultaneously. When used to optimize step frequency with the goal of minimizing energetic cost, Bayesian optimization required significantly less time compared to the gradient descent approach [113].

Although the above-described optimization strategies have been tested on unassisted walking or walking with an exoskeleton assistive device, it is possible that they will also be effective in optimizing prosthesis control. Assistance profiles would need to be redefined for prosthetic devices, however, since common torque profiles may no longer be suitable for individuals with amputation. Nonetheless, with some changes to the optimization strategy and device controllers, human-in-the-loop optimization strategies have the potential to advance the development of user-specific active prosthesis control.

23.4 CONCLUSIONS AND FUTURE DIRECTIONS

Significant progress has been made in the last several decades to advance active prosthetic devices, yet many engineering challenges still remain. For example, autonomous devices are often cumbersome, with restricted maximum torques and battery life. Further development of efficient, energy-dense power sources, as well as light and powerful actuators, is crucial for effective active prostheses. Current prosthetic controllers are also rarely individualized to each user, and struggle with

effectively adapting to changes in user biomechanics or the environment. Developments in online control optimization and intent recognition are promising for addressing these limitations, especially given that persons with amputation may benefit from assistance different from the biological profiles of unimpaired gait. Still, full human–prosthesis integration is limited by the difficulty of closing the feedback loop between user and device. For example, introducing agonist–antagonist muscle interaction can improve controllability of a two degrees-of-freedom electrically powered ankle prosthesis [114]. During transtibial amputation surgery for several individuals, lateral gastrocnemius and tibialis anterior residual muscles were surgically connected. When one muscle contracted, the other elongated, thus providing sensory feedback to the nervous system. This setup, tested on one participant, showed promise in generating more natural and intuitive behaviors when compared to conventional devices. Furthermore, interfacing with the peripheral nerves in the residual limb through electrode implant is promising for controlling upper limb prostheses (e.g., [115]). Still, methods for administering feedback to the user from lower limb prosthetic devices are underdeveloped. This likely restricts user ability to take full advantage of an active prosthesis, making it challenging to determine optimal assistance approaches. As a result, proper feedback pathways, to both human and device, need to be explored in future research in order to improve our understanding of the needs of prosthesis users.

Another factor that significantly affects the usability and efficacy of prosthetic devices is the mechanical interface between the prosthesis and user. Most prostheses connect to the residual limb of the user through a socket, which can significantly affect the load transmission, stability, and control of the device [116]. However, proper socket fit is difficult to achieve and is one of the primary concerns of prosthesis users, many of whom frequently experience discomfort and chronic skin problems [49]. Osseointegration, or the direct attachment of a prosthetic device to the residual bone of the patient, is one way to circumvent the use of prosthetic sockets. Long-term studies show that individuals with an osseointegrated prosthesis demonstrate significant improvements in walking ability and overall quality of life [117]. However, this surgical approach is still uncommon and can cause complications, meaning that further development of comfortable and reliable prosthetic sockets is likely necessary.

With the number of people with amputations expected to quadruple in the US alone by the year 2050 due to increasing rates of obesity and diabetes [118], active prosthesis development is becoming increasingly prevalent in research and industry. Given the technological advances made in a relatively short time, active prosthetic devices hold great promise for restoring natural function to individuals with lower limb amputation in the near future.

REFERENCES

- [1] D.A. Winter, Biomechanics and motor control of human gait: normal, elderly and pathological, *Waterloo Biomechanics*, 1991.
- [2] A. Hof, B. Geelen, J. Van den Berg, Calf muscle moment, work and efficiency in level walking; role of series elasticity, *J. Biomech.* 16 (7) (1983) 523–537.
- [3] R. Riener, M. Rabuffetti, C. Frigo, Joint powers in stair climbing at different slopes, in: *Engineering in Medicine and Biology*, 1999. 21st Annual Conference and the 1999 Annual Fall Meeting of the

- Biomedical Engineering Society, BMES/EMBS Conference, 1999. Proceedings of the First Joint, vol. 1, IEEE, 1999, p. 530.
- [4] R. Waters, J. Perry, D. Antonelli, H. Hislop, Energy cost of walking of amputees: the influence of level of amputation, *J. Bone Joint Surg.* 58 (1) (1976) 42–46.
 - [5] L. Hak, J.H. van Dieën, P. van der Wurff, M.R. Prins, A. Mert, P.J. Beek, et al., Walking in an unstable environment: strategies used by transtibial amputees to prevent falling during gait, *Arch. Phys. Med. Rehabil.* 94 (11) (2013) 2186–2193.
 - [6] J. Paysant, C. Beyaert, A.-M. Datié, N. Martinet, J.-M. André, Influence of terrain on metabolic and temporal gait characteristics of unilateral transtibial amputees, *J. Rehabil. Res. Dev.* 43 (2) (2006).
 - [7] R. Gailey, K. Allen, J. Castles, J. Kucharik, M. Roeder, Review of secondary physical conditions associated with lower-limb amputation and long-term prosthesis use, *J. Rehabil. Res. Dev.* 45 (1) (2008).
 - [8] S.J. Mattes, P.E. Martin, T.D. Royer, Walking symmetry and energy cost in persons with unilateral transtibial amputations: matching prosthetic and intact limb inertial properties, *Arch. Phys. Med. Rehabil.* 81 (5) (2000) 561–568.
 - [9] E.D. Lemaire, F.R. Fisher, Osteoarthritis and elderly amputee gait, *Arch. Phys. Med. Rehabil.* 75 (10) (1994) 1094–1099.
 - [10] R.D. Snyder, C.M. Powers, C. Fountain, J. Perry, The effect of five prosthetic feet on the gait and loading of the sound limb in dysvascular below-knee amputees, *J. Rehabil. Res. Dev.* 32 (1995) 309–315.
 - [11] D.J. Sanderson, P.E. Martin, Lower extremity kinematic and kinetic adaptations in unilateral below-knee amputees during walking, *Gait. Posture* 6 (2) (1997) 126–136.
 - [12] R.E. Seroussi, A. Gitter, J.M. Czerniecki, K. Weaver, Mechanical work adaptations of above-knee amputee ambulation, *Arch. Phys. Med. Rehabil.* 77 (11) (1996) 1209–1214.
 - [13] C.M. Powers, S. Rao, J. Perry, Knee kinetics in trans-tibial amputee gait, *Gait. Posture* 8 (1) (1998) 1–7.
 - [14] A.S. Voloshina, A.D. Kuo, M.A. Daley, D.P. Ferris, Biomechanics and energetics of walking on uneven terrain, *J. Exp. Biol.* (2013) 3963–3970.
 - [15] G. Cappellini, Y.P. Ivanenko, N. Dominici, R.E. Poppele, F. Lacquaniti, Motor patterns during walking on a slippery walkway, *J. Neurophysiol.* 103 (2) (2009) 746–760.
 - [16] D.S. Marigold, A.E. Patla, Adapting locomotion to different surface compliances: neuromuscular responses and changes in movement dynamics, *J. Neurophysiol.* 94 (3) (2005) 1733–1750.
 - [17] C. Wade, M.S. Redfern, R.O. Andres, S.P. Breloff, Joint kinetics and muscle activity while walking on ballast, *Hum. Factors* 52 (5) (2010) 560–573.
 - [18] D.H. Gates, J.B. Dingwell, S.J. Scott, E.H. Sinitski, J.M. Wilken, Gait characteristics of individuals with transtibial amputations walking on a destabilizing rock surface, *Gait. Posture* 36 (1) (2012) 33–39.
 - [19] W.C. Miller, A.B. Deathe, M. Speechley, J. Koval, The influence of falling, fear of falling, and balance confidence on prosthetic mobility and social activity among individuals with a lower extremity amputation, *Arch. Phys. Med. Rehabil.* 82 (9) (2001) 1238–1244.
 - [20] K. Hagberg, R. Bråmark, Consequences of non-vascular trans-femoral amputation: a survey of quality of life, prosthetic use and problems, *Prosthet. Orthot. Int.* 25 (3) (2001) 186–194.
 - [21] B.J. Hafner, J.E. Sanders, J.M. Czerniecki, J. Fergason, Transtibial energy-storage-and-return prosthetic devices: a review of energy concepts and a proposed nomenclature, *J. Rehabil. Res. Dev.* 39 (1) (2002) 1–12.
 - [22] N.P. Fey, G.K. Klute, R.R. Neptune, The influence of energy storage and return foot stiffness on walking mechanics and muscle activity in below-knee amputees, *Clin. Biomechan.* 26 (10) (2011) 1025–1032.
 - [23] D.A. Winter, Energy generation and absorption at the ankle and knee during fast, natural, and slow cadences, *Clin. Orthop. Relat. Res.* 175 (1983) 147–154.

- [24] C.H. Soo, J.M. Donelan, Mechanics and energetics of step-to-step transitions isolated from human walking, *J. Exp. Biol.* 213 (24) (2010) 4265–4271.
- [25] P. DeVita, J. Helseth, T. Hortobagyi, Muscles do more positive than negative work in human locomotion, *J. Exp. Biol.* 210 (19) (2007) 3361–3373.
- [26] K. Kaufman, J. Levine, R. Brey, B. Iverson, S. McCrady, D. Padgett, et al., Gait and balance of transfemoral amputees using passive mechanical and microprocessor-controlled prosthetic knees, *Gait. Posture* 26 (4) (2007) 489–493.
- [27] J.L. Johansson, D.M. Sherrill, P.O. Riley, P. Bonato, H. Herr, A clinical comparison of variable-damping and mechanically passive prosthetic knee devices, *Am. J. Phys. Med. Rehabil.* 84 (8) (2005) 563–575.
- [28] W.C. Flowers, R.W. Mann, An electrohydraulic knee-torque controller for a prosthesis simulator, *J. Biomech. Eng.* 99 (1) (1977) 3–8.
- [29] S. Huang, J.P. Wensman, D.P. Ferris, An experimental powered lower limb prosthesis using proportional myoelectric control, *J. Med. Device* 8 (2) (2014) 024501.
- [30] F. Sup, A. Bohara, M. Goldfarb, Design and control of a powered transfemoral prosthesis, *Int. J. Robot. Res.* 27 (2) (2008) 263–273.
- [31] K. Fite, J. Mitchell, F. Sup, M. Goldfarb, Design and control of an electrically powered knee prosthesis, in: Rehabilitation Robotics, 2007. IEEE 10th International Conference on, IEEE, 2007, pp. 902–905.
- [32] V. Chiu, A. Voloshina, S. Collins, An ankle-foot prosthesis emulator capable of modulating center of pressure, *IEEE Trans. Biomed. Eng.* (2019).
- [33] E.C. Martinez-Villalpando, J. Weber, G. Elliott, H. Herr, Design of an agonist-antagonist active knee prosthesis, in: Biomedical Robotics and Biomechatronics, 2008. BioRob 2008. 2nd IEEE RAS & EMBS International Conference on, IEEE, 2008, pp. 529–534.
- [34] H.M. Herr, A.M. Grabowski, Bionic ankle–foot prosthesis normalizes walking gait for persons with leg amputation, in: Proceedings of the Royal Society of London B: Biological Sciences, 2012, rspb20111194.
- [35] A.F. Azocar, L.M. Mooney, L.J. Hargrove, E.J. Rouse, Design and characterization of an open-source robotic leg prosthesis, in: 2018 7th IEEE International Conference on Biomedical Robotics and Biomechatronics (Biorob), IEEE, 2018, pp. 111–118.
- [36] S. Bédard, P.-O. Roy, Actuated leg prosthesis for above-knee amputees, US Patent 8,231,687, July 31, 2012.
- [37] R.D. Bellman, M.A. Holgate, T.G. Sugar, Sparky 3: design of an active robotic ankle prosthesis with two actuated degrees of freedom using regenerative kinetics, in: 2008 2nd IEEE RAS & EMBS International Conference on Biomedical Robotics and Biomechatronics, IEEE, 2008, pp. 511–516.
- [38] F. Sup, H.A. Varol, M. Goldfarb, Upslope walking with a powered knee and ankle prosthesis: initial results with an amputee subject, *IEEE. Trans. Neural. Syst. Rehabil. Eng.* 19 (1) (2011) 71–78.
- [39] M. Kim, S.H. Collins, Step-to-step ankle inversion/eversion torque modulation can reduce effort associated with balance, *Front. Neurorobot.* 11 (2017) 62.
- [40] E. Russell Esposito, J.M. Aldridge Whitehead, J.M. Wilken, Step-to-step transition work during level and inclined walking using passive and powered ankle–foot prostheses, *Prosthet. Orthot. Int.* 40 (3) (2016) 311–319.
- [41] A.E. Ferris, J.M. Aldridge, C.A. Rábago, J.M. Wilken, et al., Evaluation of a powered ankle-foot prosthetic system during walking, *Arch. Phys. Med. Rehabil.* 93 (11) (2012) 1911–1918.
- [42] D.H. Gates, J.M. Aldridge, J.M. Wilken, Kinematic comparison of walking on uneven ground using powered and unpowered prostheses, *Clin. Biomechan.* 28 (4) (2013) 467–472.
- [43] R.E. Quesada, J.M. Caputo, S.H. Collins, Increasing ankle push-off work with a powered prosthesis does not necessarily reduce metabolic rate for transtibial amputees, *J. Biomech.* 49 (14) (2016) 3452–3459.

- [44] K.A. Ingraham, H. Choi, E.S. Gardiner, C.D. Remy, D.H. Gates, Choosing appropriate prosthetic ankle work to reduce the metabolic cost of individuals with transtibial amputation, *Sci. Rep.* 8 (1) (2018) 15303.
- [45] P. Malcolm, R.E. Quesada, J.M. Caputo, S.H. Collins, The influence of push-off timing in a robotic ankle-foot prosthesis on the energetics and mechanics of walking, *J. Neuroeng. Rehabil.* 12 (1) (2015) 21.
- [46] A.D. Kuo, Energetics of actively powered locomotion using the simplest walking model, *J. Biomech. Eng.* 124 (1) (2002) 113–120.
- [47] J. Zhang, P. Fiers, K.A. Witte, R.W. Jackson, K.L. Poggensee, C.G. Atkeson, et al., Human-in-the-loop optimization of exoskeleton assistance during walking, *Science* 356 (6344) (2017) 1280–1284.
- [48] M. Kim, Y. Ding, C. Liu, J. Kim, S. Lee, N. Karavas, et al., Human-in-the-loop bayesian optimization of a tethered soft exosuit for assisting hip extension, in: International Symposium on Wearable Robotics, Springer, 2018, pp. 142–146.
- [49] M.W. Legro, G. Reiber, M. del Aguila, M.J. Ajax, D.A. Boone, J.A. Larsen, et al., Issues of importance reported by persons with lower limb amputations and prostheses, *J. Rehabil. Res. Dev.* 36 (3) (1999) 155–163.
- [50] M. Donath, Proportional emg control for above knee prostheses, Ph.D. thesis, Massachusetts Institute of Technology, 1974.
- [51] D. Grimes, W.C. Flowers, M. Donath, Feasibility of an active control scheme for above knee prostheses, *J. Biomech. Eng.* 99 (4) (1977) 215–221.
- [52] R. Versluys, P. Beyl, M. Van Damme, A. Desomer, R. Van Ham, D. Lefebvre, Prosthetic feet: state-of-the-art review and the importance of mimicking human ankle–foot biomechanics, *Disabil. Rehabil. Assistive Technol.* 4 (2) (2009) 65–75.
- [53] J.M. Caputo, S.H. Collins, A universal ankle–foot prosthesis emulator for human locomotion experiments, *J. Biomech. Eng.* 136 (3) (2014) 035002.
- [54] S.H. Collins, M. Kim, T. Chen, T. Chen, An ankle-foot prosthesis emulator with control of plantarflexion and inversion-eversion torque, in: Robotics and Automation (ICRA), 2015 IEEE International Conference on, IEEE, 2015, pp. 1210–1216.
- [55] F. Daerden, D. Lefebvre, Pneumatic artificial muscles: actuators for robotics and automation, *Eur. J. Mech. Environ. Eng.* 47 (1) (2002) 11–21.
- [56] G.K. Klute, J.M. Czerniecki, B. Hannaford, McKibben artificial muscles: pneumatic actuators with biomechanical intelligence, in: Advanced Intelligent Mechatronics, 1999. Proceedings. 1999 IEEE/ASME International Conference on, IEEE, 1999, pp. 221–226.
- [57] G. Klute, J. Czerniecki, B. Hannaford, Muscle-like pneumatic actuators for below-knee prostheses, in: New Actuators, 7th International Conference on, 2000, pp. 289–292.
- [58] F. Daerden, Conception and realization of pleated pneumatic artificial muscles and their use as compliant actuation elements, Ph.D. thesis, Vrije Universiteit Brussel, Belgium, 1999.
- [59] F. Daerden, D. Lefebvre, The concept and design of pleated pneumatic artificial muscles, *Int. J. Fluid Power* 2 (3) (2001) 41–50.
- [60] C.-P. Chou, B. Hannaford, Measurement and modeling of mckibben pneumatic artificial muscles, *IEEE Trans. Rob. Autom.* 12 (1) (1996) 90–102.
- [61] B. Hannaford, J. Winters, Actuator properties and movement control: biological and technological models, *Multiple Muscle Systems*, Springer, 1990, pp. 101–120.
- [62] R. Versluys, A. Desomer, G. Lenaerts, M. Van Damme, P. Beyl, G. Van der Perre, et al., A pneumatically powered below-knee prosthesis: design specifications and first experiments with an amputee, in: Biomedical Robotics and Biomechatronics, 2008. BioRob 2008. 2nd IEEE RAS & EMBS International Conference on, IEEE, 2008, pp. 372–377.

- [63] G. Waycaster, S.-K. Wu, X. Shen, Design and control of a pneumatic artificial muscle actuated above-knee prosthesis, *J. Med. Device* 5 (3) (2011) 031003.
- [64] K.B. Fite, M. Goldfarb, Design and energetic characterization of a proportional-injector monopropellant-powered actuator, *IEEE/ASME Trans. Mechatron.* 11 (2) (2006) 196–204.
- [65] X. Shen, D. Christ, Design and control of chemomuscle: a liquid-propellant-powered muscle actuation system, *J. Dyn. Syst. Meas. Control.* 133 (2) (2011) 021006.
- [66] H.M. Herr, R.D. Kornbluh, New horizons for orthotic and prosthetic technology: artificial muscle for ambulation, in: Smart Structures and Materials 2004: Electroactive Polymer Actuators and Devices (EAPAD), Vol. 5385, International Society for Optics and Photonics, 2004, pp. 1–10.
- [67] F. Sup, H.A. Varol, J. Mitchell, T.J. Withrow, M. Goldfarb, Self-contained powered knee and ankle prosthesis: initial evaluation on a transfemoral amputee, in: Rehabilitation Robotics, 2009. ICORR 2009. IEEE International Conference on, IEEE, 2009, pp. 638–644.
- [68] E.C. Martinez-Villalpando, H. Herr, Agonist-antagonist active knee prosthesis: a preliminary study in level-ground walking, *J. Rehabil. Res. Dev.* 46 (3) (2009).
- [69] G.A. Pratt, M.M. Williamson, Series elastic actuators, in: Intelligent Robots and Systems 95. ‘Human Robot Interaction and Cooperative Robots’, Proceedings. 1995 IEEE/RSJ International Conference on, vol. 1, IEEE, 1995, pp. 399–406.
- [70] S.K. Au, J. Weber, H. Herr, Powered ankle–foot prosthesis improves walking metabolic economy, *IEEE Trans. Robot.* 25 (1) (2009) 51–66.
- [71] S.K. Au, H. Herr, J. Weber, E.C. Martinez-Villalpando, Powered ankle-foot prosthesis for the improvement of amputee ambulation, in: Engineering in Medicine and Biology Society, 2007. EMBS 2007. 29th Annual International Conference of the IEEE, IEEE, 2007, pp. 3020–3026.
- [72] S. Au, M. Berniker, H. Herr, Powered ankle-foot prosthesis to assist level-ground and stair-descent gaits, *Neur. Netw.* 21 (4) (2008) 654–666.
- [73] P. Cherelle, V. Grosu, M. Cestari, B. Vanderborght, D. Lefeber, The amp-foot 3, new generation propulsive prosthetic feet with explosive motion characteristics: design and validation, *Biomed. Eng. Online.* 15 (3) (2016) 145.
- [74] J. Geeroms, L. Flynn, R. Jimenez-Fabian, B. Vanderborght, D. Lefeber, Ankle-knee prosthesis with powered ankle and energy transfer for cyberlegs α-prototype, in: Rehabilitation Robotics (ICORR), 2013 IEEE 13th International Conference on, IEEE, 2013, pp. 1–6.
- [75] D.L. Grimes, An active multi-mode above knee prosthesis controller, Ph.D. thesis, Massachusetts Institute of Technology, 1979.
- [76] J.L. Stein, W.C. Flowers, Stance phase control of above-knee prostheses: knee control versus sach foot design, *J. Biomech.* 20 (1) (1987) 19–28.
- [77] J.K. Hitt, R. Bellman, M. Holgate, T.G. Sugar, K.W. Hollander, The sparky (spring ankle with regenerative kinetics) project: design and analysis of a robotic transtibial prosthesis with regenerative kinetics, in: ASME 2007 International Design Engineering Technical Conferences and Computers and Information in Engineering Conference, American Society of Mechanical Engineers, 2007, pp. 1587–1596.
- [78] J. Hitt, T. Sugar, M. Holgate, R. Bellman, K. Hollander, Robotic transtibial prosthesis with biomechanical energy regeneration, *Ind. Robot Int. J.* 36 (5) (2009) 441–447.
- [79] J.K. Hitt, T.G. Sugar, M. Holgate, R. Bellman, An active foot-ankle prosthesis with biomechanical energy regeneration, *J. Med. Device* 4 (1) (2010) 011003.
- [80] K.W. Hollander, T.G. Sugar, D.E. Herring, Adjustable robotic tendon using a ‘jack spring’/spl trade, in: Rehabilitation robotics, 2005. ICORR 2005. 9th International Conference on, IEEE, 2005, pp. 113–118.
- [81] K.W. Hollander, R. Ilg, T.G. Sugar, D. Herring, An efficient robotic tendon for gait assistance, *J. Biomech. Eng.* 128 (5) (2006) 788–791.

- [82] S. Rezazadeh, D. Quintero, N. Divekar, R.D. Gregg, A phase variable approach to volitional control of powered knee-ankle prostheses, in: 2018 IEEE/RSJ International Conference on Intelligent Robots and Systems (IROS), IEEE, 2018, pp. 2292–2298.
- [83] D. Quintero, E. Reznick, D.J. Lambert, S. Rezazadeh, L. Gray, R.D. Gregg, Intuitive clinician control interface for a powered knee-ankle prosthesis: a case study, *IEEE J. Transl. Eng. Health Med.* 6 (2018) 1–9.
- [84] A.H. Shultz, M. Goldfarb, A unified controller for walking on even and uneven terrain with a powered ankle prosthesis, *IEEE Trans. Neural. Syst. Rehabil. Eng.* (2018).
- [85] M.F. Eilenberg, H. Geyer, H. Herr, Control of a powered ankle–foot prosthesis based on a neuromuscular model, *IEEE Trans. Neural. Syst. Rehabil. Eng.* 18 (2) (2010) 164–173.
- [86] J. Markowitz, P. Krishnaswamy, M.F. Eilenberg, K. Endo, C. Barnhart, H. Herr, Speed adaptation in a powered transtibial prosthesis controlled with a neuromuscular model, *Philosophical Transactions of the Royal Society of London B: Biological Sciences* 366 (1570) (2011) 1621–1631.
- [87] N. Thatte, H. Geyer, Toward balance recovery with leg prostheses using neuromuscular model control, *IEEE Trans. Biomed. Eng.* 63 (5) (2015) 904–913.
- [88] K.C. Nishikawa, J.A. Monroy, T.E. Uyeno, S.H. Yeo, D.K. Pai, S.L. Lindstedt, Is titin a ‘winding filament’? a new twist on muscle contraction, *Proc. Biol. Sci.* 279 (1730) (2011) 981–990.
- [89] U. Tahir, A.L. Hessel, E.R. Lockwood, J.T. Tester, Z. Han, D.J. Rivera, et al., Case study: a bio-inspired control algorithm for a robotic foot-ankle prosthesis provides adaptive control of level walking and stair ascent, *Front. Robot. AI* 5 (2018) 36.
- [90] S. Huang, D.P. Ferris, Muscle activation patterns during walking from transtibial amputees recorded within the residual limb-prosthetic interface, *J. Neuroeng. Rehabil.* 9 (1) (2012) 55.
- [91] G. Horn, Electro-control: am emg-controlled a/k prosthesis, *Med. Biol. Eng.* 10 (1) (1972) 61–73.
- [92] S. Saxena, P. Mukhopadhyay, Emg operated electronic artificial-leg controller, *Med. Biol. Eng. Comput.* 15 (5) (1977) 553–557.
- [93] W. Dyck, S. Onyshko, D. Hobson, D. Winter, A. Quanbury, A voluntarily controlled electrohydraulic above-knee prosthesis, *Bull. Prosthet. Res.* (1975) 169–186.
- [94] C.D. Hoover, G.D. Fulk, K.B. Fite, The design and initial experimental validation of an active myoelectric transfemoral prosthesis, *J. Med. Device* 6 (1) (2012) 011005.
- [95] C.D. Hoover, G.D. Fulk, K.B. Fite, Stair ascent with a powered transfemoral prosthesis under direct myoelectric control, *IEEE/ASME Trans. Mechatron.* 18 (3) (2013) 1191–1200.
- [96] S. Huang, J.P. Wensman, D.P. Ferris, Locomotor adaptation by transtibial amputees walking with an experimental powered prosthesis under continuous myoelectric control, *IEEE Trans. Neural. Syst. Rehabil. Eng.* 24 (5) (2016) 573–581.
- [97] S.K. Au, P. Bonato, H. Herr, An emg-position controlled system for an active ankle-foot prosthesis: an initial experimental study, in: Rehabilitation Robotics, 2005. ICORR 2005. 9th International Conference on, IEEE, 2005, pp. 375–379.
- [98] J. Wang, O.A. Kannape, H.M. Herr, Proportional emg control of ankle plantar flexion in a powered transtibial prosthesis, in: Rehabilitation Robotics (ICORR), 2013 IEEE International Conference on, IEEE, 2013, pp. 1–5.
- [99] H.A. Varol, F. Sup, M. Goldfarb, Multiclass real-time intent recognition of a powered lower limb prosthesis, *IEEE Trans. Biomed. Eng.* 57 (3) (2010) 542–551.
- [100] F. Zhang, H. Huang, Source selection for real-time user intent recognition toward volitional control of artificial legs, *IEEE J. Biomed. Health Informat.* 17 (5) (2013) 907–914.
- [101] H. Huang, T.A. Kuiken, R.D. Lipschutz, et al., A strategy for identifying locomotion modes using surface electromyography, *IEEE Trans. Biomed. Eng.* 56 (1) (2009) 65–73.
- [102] K.H. Ha, H.A. Varol, M. Goldfarb, Volitional control of a prosthetic knee using surface electromyography, *IEEE Trans. Biomed. Eng.* 58 (1) (2011) 144–151.

- [103] L.J. Hargrove, A.M. Simon, R. Lipschutz, S.B. Finucane, T.A. Kuiken, Non-weight-bearing neural control of a powered transfemoral prosthesis, *J. Neuroeng. Rehabil.* 10 (1) (2013) 62.
- [104] L.J. Hargrove, A.M. Simon, A.J. Young, R.D. Lipschutz, S.B. Finucane, D.G. Smith, et al., Robotic leg control with emg decoding in an amputee with nerve transfers, *N. Engl. J. Med.* 369 (13) (2013) 1237–1242.
- [105] J.R. Koller, D.A. Jacobs, D.P. Ferris, C.D. Remy, Learning to walk with an adaptive gain proportional myoelectric controller for a robotic ankle exoskeleton, *J. Neuroeng. Rehabil.* 12 (1) (2015) 97.
- [106] H. Herr, Exoskeletons and orthoses: classification, design challenges and future directions, *J. Neuroeng. Rehabil.* 6 (1) (2009) 21.
- [107] C.J. Hofstad, H. van der Linde, J. van Limbeek, K. Postema, Prescription of prosthetic ankle-foot mechanisms after lower limb amputation, Wiley Online Library, 2004.
- [108] J.C. Selinger, S.M. O'Connor, J.D. Wong, J.M. Donelan, Humans can continuously optimize energetic cost during walking, *Curr. Biol.* 25 (18) (2015) 2452–2456.
- [109] J.R. Koller, D.H. Gates, D.P. Ferris, C.D. Remy, Body-in-the-loop optimization of assistive robotic devices: a validation study., in: *Robotics: Science and Systems*, 2016, pp. 1–10.
- [110] W. Felt, J.C. Selinger, J.M. Donelan, C.D. Remy, Body-in-the-loop: optimizing device parameters using measures of instantaneous energetic cost, *PLoS One* 10 (8) (2015) e0135342.
- [111] R.W. Jackson, S.H. Collins, An experimental comparison of the relative benefits of work and torque assistance in ankle exoskeletons, *J. Appl. Physiol.* 119 (5) (2015) 541–557.
- [112] A.T. Asbeck, S.M. De Rossi, K.G. Holt, C.J. Walsh, A biologically inspired soft exosuit for walking assistance, *Int. J. Robot. Res.* 34 (6) (2015) 744–762.
- [113] M. Kim, Y. Ding, P. Malcolm, J. Speeckaert, C.J. Siviy, C.J. Walsh, et al., Human-in-the-loop bayesian optimization of wearable device parameters, *PLoS One* 12 (9) (2017) e0184054.
- [114] T.R. Clites, M.J. Carty, J.B. Ullauri, M.E. Carney, L.M. Mooney, J.-F. Duval, et al., Proprioception from a neurally controlled lower-extremity prosthesis, *Sci. Translat. Med.* 10 (443) (2018) eaap8373.
- [115] G.S. Dhillon, K.W. Horch, Direct neural sensory feedback and control of a prosthetic arm, *IEEE Trans. Neural. Syst. Rehabil. Eng.* 13 (4) (2005) 468–472.
- [116] A.F. Mak, M. Zhang, D.A. Boone, State-of-the-art research in lower-limb prosthetic biomechanics-socket interface: a review, *J. Rehabil. Res. Dev.* 38 (2) (2001) 161–174.
- [117] H. Van de Meent, M.T. Hopman, J.P. Frölke, Walking ability and quality of life in subjects with transfemoral amputation: a comparison of osseointegration with socket prostheses, *Arch. Phys. Med. Rehabil.* 94 (11) (2013) 2174–2178.
- [118] K. Ziegler-Graham, E.J. MacKenzie, P.L. Ephraim, T.G. Travison, R. Brookmeyer, Estimating the prevalence of limb loss in the united states: 2005 to 2050, *Arch. Phys. Med. Rehabil.* 89 (3) (2008) 422–429.

CONTROLLING A POWERED TRANSFEMORAL PROSTHETIC LEG USING A UNIFIED PHASE VARIABLE

24

Dario J. Villarreal¹ and Robert D. Gregg²

¹*Electrical and Computer Engineering Department, Mechanical Engineering Department, Southern Methodist University, University Park, TX, United States* ²*Electrical Engineering and Computer Science, University of Michigan, Ann Arbor, MI, United States*

Estimates indicate that by 2050 the United States will incur a twofold increase in the incidence of amputation and stroke, due largely to the prevalence of vascular disease. Amputees suffer from a slower, less stable, and less efficient gait than able-bodied persons. Developing methods to control powered prosthetic legs in a simple, efficient, and customizable manner could help current and future amputees ambulate more efficiently. The current methodology used to control powered prosthetic legs sees the gait cycle as a process consisting of discrete states (e.g., heel strike, load acceptance, toe off, preswing, mid-swing, etc.). Thus, current powered prosthetic legs synchronize to their wearer by transitioning between a finite number of states based on switching rules. This approach is limited as state machine control strategies end up dictating the walking speed and response of the robotic leg rather than the amputee. Novel approaches from the biped robotic field have led to new ways of visualizing the gait cycle. The gait cycle is seen and controlled as a continuous periodic process synchronized by a phase variable rather than a sequence of discrete events.

A key feature describing the synchrony of multijoint patterns during locomotion is the phase of gait. In a periodic process, such as the gait cycle, phase is a scalar quantity representing the location on the periodic orbit of multijoint kinematics. Specifically, if this quantity is given at a particular point in time then it is possible to determine the entire configuration of the system along the nominal periodic orbit. Due to the complexity and the vast amount of degrees of freedom involved in locomotion, it is difficult to compute and sketch a multidimensional representation of the gait cycle's phase. Various models (e.g., CPGs [1,2], coupled oscillators [3–5], and adaptive oscillators [6]) have different ways of representing the phase of the gait cycle (i.e., the overall synchronization of the leg joint patterns), often depending on the entire system state or extended states in higher dimensional dynamics. To address this challenge, it has been proposed that a single mechanical variable, a “phase variable,” could provide a robust representation of gait cycle phase [7–9].

A phase variable is a mechanical signal that changes monotonically, that is, it strictly increases or decreases, over time and therefore is able to parameterize a rhythmic process. Given the phase variable at a specific time, the specific state of the process can be determined as well as its next

movement. In a gait cycle, a phase variable can be used to control the progression of leg joint trajectories. Current biped robots are able to achieve stable locomotion by synchronizing their locomotion using a phase variable to parameterize their lower limb kinematics through the gait cycle [9–12]. This concept has been translated to the rehabilitation field and has been used to control powered prosthetic legs [8,13,14]. This methodology provides robustness to the controller since it makes it time-independent. In addition, if the phase variable is chosen correctly, then the desired joint kinematics would match the subject’s location in the gait cycle, even during nonsteady gait [7]. Phase variables for human gait analysis have been proposed primarily from the perspective of biomimicry. Biomechanical signals involved in key reflex pathways [15] may be closely related to the phase of human gait. In particular, the neuroscience literature suggests that muscle afferents acting at the hip joint are essential to controlling the more distal joints of the leg (e.g., knee and ankle) in mammalian locomotion [16]. This evidence motivated Villarreal and Gregg [17] to consider the progression of the hip angle as a potential phase variable to represent gait due to its physiological importance in synchronizing joints across the gait cycle. However, because the hip angle has a piecewise monotonic trajectory the map from this phase variable to joint angles loses uniqueness across the stance and swing periods of each leg. Recent work aiming to unify the control of the gait cycle for powered prosthetic legs requires a unified and monotonic phase variable capable of parameterizing joint patterns across the entire gait cycle [18].

There are challenges associated with using a phase variable to control a nonlinear plant, such as a powered prosthetic leg or biped robot. For instance, the controller can only access the limited information provided by the on-board sensor of the wearable robot to calculate a phase variable. This assumption is made to avoid instrumenting and upsetting the user. Another challenge is properly defining a phase variable given the limited sensor information. An ill-defined phase variable can lower the relative degree of the system. Finally, the need for a continuous rhythmic motion to calculate a phase variable is unrealistic in human users since people perform multiple activities that involve walking and stopping.

24.1 BACKGROUND

We denote the time integral of the configuration vector $q(t)$ as $\tilde{q} \triangleq \int_0^t q(\tau)d\tau$. In addition, we define the partial derivative of a function $h(\cdot)$ with respect to a vector $z(t)$ to be $H_z \triangleq \frac{\partial h}{\partial z} = \nabla_z h$.

Without loss of generality and following the Euler–Lagrange equation, the equations of motion of any mechanical system can be represented by

$$M(q) \ddot{q} + C(q, \dot{q})\dot{q} + N(q) = B\mathbf{u}.$$

The matrices M , C , and N represent the mass/inertia forces, Coriolis forces, and gravitational forces of the system, respectively. The vector \mathbf{u} represents the inputs to the system, and we assume the dimension of \mathbf{u} equals the dimension of q for the sake of this chapter. These inputs are torques or forces acting on the configuration vector through the mapping B . If we were to compute the value of the acceleration terms from this equation in order to represent these dynamics as a system of differential equations, then it would yield the following equation

$$\ddot{q} = M(q)^{-1}B\mathbf{u} - M(q)^{-1}[C(q, \dot{q})\dot{q} + N(q)].$$

where $M(q)^{-1}$ exists for any well-defined mechanical system [19]. For simplicity we express this highly nonlinear equation as $\ddot{q} = F(q, \dot{q}) + G(q)\mathbf{u}$.

Let $x_1 = q$ and $x_2 = \dot{q}$ define the state of the corresponding nonlinear dynamical system such that

$$\begin{aligned}\dot{x}_1 &= x_2 \\ \dot{x}_2 &= F(x_1, x_2) + G(x_1)\mathbf{u} \\ y &= x_1 - h^d(\varphi(x_1)) = h(q)\end{aligned}\tag{24.1}$$

where y is defined as an output function to be regulated by the input \mathbf{u} . Notice that y is dependent only on the configuration vector (q) of the system and not on velocity terms. The function $h^d(\cdot)$, known as a virtual constraint, represents a desired kinematic trajectory we want to enforce as a function of the phase variable (φ). In other words, we want to constrain the movement of the mechanical system to a specific trajectory that is evaluated as the phase variable progresses. The goal of a phase-based controller is to derive a control law that drives the error between the measured joint angles (q) and the virtual constraint function ($h^d(\varphi)$) to zero.

By taking twice the time derivative of the output function we get the following equations:

$$\begin{aligned}\dot{y} &= H_q\dot{q} \\ \ddot{y} &= \dot{H}_q\dot{q} + H_{q\dot{q}} \\ &= \dot{H}_q\dot{q} + H_q(F(q, \dot{q}) + G(q)\mathbf{u}).\end{aligned}\tag{24.2}$$

This system is said to have relative degree 2 (i.e., $r = 2$) because we had to differentiate the output function (y) twice before the input of our system (\mathbf{u}) appeared. Since the original system is second order ($n = 2$) and the number of outputs equals the number of inputs, all states of the system can be controlled by the input \mathbf{u} (i.e., there are no “internal” dynamics when $n - r = 0$) [20]. Using feedback linearization, the control law

$$\mathbf{u} = [H_q G(q)]^{-1}(\mathbf{v} - [H_q \dot{q} + H_q F(q, \dot{q})])\tag{24.3}$$

enforces the system to follow the virtual constraint, as long as $[H_q G(q)]^{-1}$ exists, when a feedback PD controller is implemented (i.e., $\mathbf{v} = -K_p y - K_d \dot{y}$, where $K_p > 0$ and $K_d > 0$). If the model of the system is not well defined, then implementing just the feedback PD control law \mathbf{v} will also enforce the virtual constraints. Notice that if the input of the system appeared in the first time derivative of our output function, then the relative degree of the system would have decreased (i.e., $r = 1$). This occurs when the output is a function of velocities, that is, $y = h(q, \dot{q})$, which limits input v to its proportional control term and implies that internal dynamics will remain [21].

A phase variable that does not lower the relative degree of the system has been used in the past to control biped robots, but it is not suitable for amputee subjects. Biped robots use a phase variable compatible with real-time controllers since it is simply a function of the configuration vector and not of velocities of the system. However, the measurements of both leg joints of the robot are needed in order to compute this phase variable. This is due to the fact that in biped robots each step is parameterized independently rather than a complete gait cycle (i.e., this phase variable does not unify stance and swing). In contrast to biped robots, the sensor placement in powered prosthetic legs is limited to the prosthesis itself. This encourages using integral terms to compute a unified phase variable (i.e., the integral term helps differentiate between stance and swing hip motions). Limiting the sensor placement to the robotic leg avoids nuisances for the subject by not having to wear extra

hardware on their sound leg. In this chapter, we propose a unified phase variable algorithm capable of correctly parameterizing the joint kinematics of the gait cycle during rhythmic tasks for control in powered prosthetic legs and their measurements are limited to sensors on-board the device.

24.2 PHASE VARIABLE ALGORITHM

24.2.1 REAL-TIME PHASE VARIABLE ALGORITHM FOR CONTROL APPLICATIONS

The algorithm structure is mainly composed of two subsystems: (1) a piecewise (PW) phase variable algorithm and (2) a unified phase variable algorithm ($\hat{\Phi}$) (Fig. 24.1). The default output of the phase variable algorithm is the PW phase variable. This variable is used when the subject is at rest or during a nonsteady gait. When the algorithm detects the subject is walking steadily, then the output of the algorithm transitions to the unified phase variable. The algorithm detects a steady walking condition by measuring rhythmic patterns on the hip position and velocity measurements. The transition between phase variables (i.e., PW to unified) does not happen until the measurement of both phase variables agree. This particular condition avoids undesired jumps in the phase variable value. In other words, once the algorithm detects the person is walking, the transition happens only when the unified phase variable crosses the PW phase variable. This generally takes a few strides. When the subject stops walking, the algorithm switches back to the PW phase variable.

24.2.1.1 Piecewise phase variable algorithm (PW)

A diagram of the PW phase variable algorithm is presented in Fig. 24.2. The PW phase variable is a function of the global hip angle (Θ_h). The PW phase variable is divided into stance and swing regions depending on a binary contact sensor under the shoe. A high value on the sensor measurement denotes stance (i.e., the subject's foot is in contact with the ground) whereas a low value denotes swing. In order to calculate a piecewise phase variable that is between the values of 0 and 1 (i.e., corresponding to 0% and 100% of the gait cycle), the hip angle needs to be normalized to a

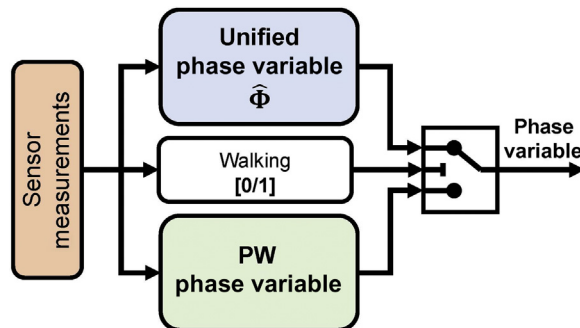


FIGURE 24.1

Diagram of the overall algorithm. Walking is function with a Boolean output that determines if the subject is in rhythmic locomotion [1] or nonrhythmic locomotion [0].

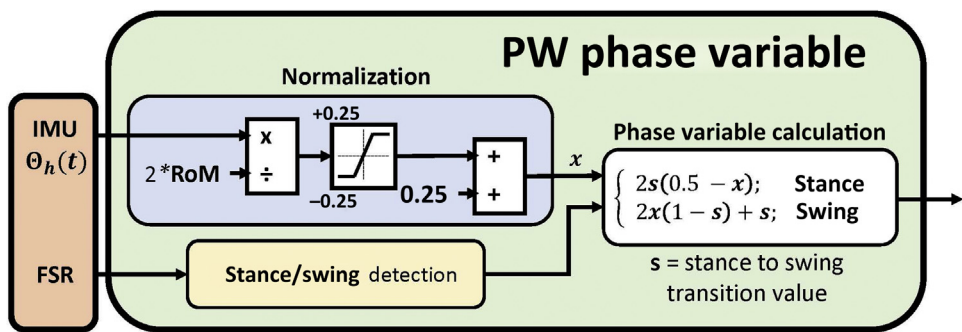
**FIGURE 24.2**

Diagram of the piecewise phase variable algorithm. The variable s denotes the transition between stance and swing during locomotion (at a normal walking speed $s = 0.62$ according to Ref. [22]). The variable x represents the global hip angle $\Theta_h(t)$ after normalization and saturation.

predefined range of motion. In particular, stance is normalized between $[0, s]$ and swing between $(s, 1]$ in an independent manner, $s \in (0, 1)$ denotes the desired phase value transition between stance and swing. This implies that we need to normalize the hip angle to twice a predefined range of motion ($2 \cdot \text{RoM}$). The normalized hip motion is saturated if its value is greater than 0.25 or smaller than -0.25 (corresponding to a hip motion outside the predefined normalized RoM). A constant offset value of 0.25 is added to the normalized hip angle in order to compute a PW phase variable that starts at zero. The PW phase variable is then calculated by

$$\begin{cases} 2s(0.5 - x), & \text{stance} \\ 2x(1 - s) + s, & \text{swing} \end{cases} \quad (24.4)$$

where x represents the hip angle after normalization and saturation. Stance is given a phase variable range of $[0, 0.62]$ whereas swing is given the range of $(0.62, 1]$ [22].

Normalizing the PW phase variable using the RoM of the hip angle introduces a new challenge to the algorithm as humans typically walk with a varying RoM. The RoM value for normalization was selected to be fairly small (corresponding to short steps) in order to avoid instantaneous jumps of the phase variable value between stance and swing. However, a small RoM results in phase variable saturation whenever a subject increases his/her RoM (corresponding to longer steps). It was decided that, for the safety of the hardware and its user in future amputee experiments, a saturation in the phase variable was preferred over instantaneous jumps, since the latter could introduce high-frequency accelerations to the joint actuators. Moreover, longer steps are more typical during steady walking, which will be performed by the unified phase variable algorithm.

24.2.1.2 Unified phase variable algorithm ($\hat{\Phi}$)

This phase variable is computed exploiting the fact that the motion of the global hip angle (Θ_h) is correlated to a cosine-like trajectory during human locomotion. We compute the phase variable PHI as $\Phi = \arctan2(\omega\dot{\Theta}_h, \Theta_h)$, where we have defined $\dot{\Theta}_h \triangleq \int_0^t \Theta_h(\tau)d\tau$ and ω is the walking frequency of a person. The variable Φ yields a monotonic, bounded, and linear phase variable. The

implication of using the integral of a state of our dynamical system in this phase variable calculation is that we extend the order of our system plus one (i.e., $\bar{n} = n + 1$). We notice that the input of the dynamical system (\mathbf{u}) appears at the second time derivative of the output function $y = g(\Phi(q, \dot{q})) = h(q, \dot{q})$, where $h = g \circ \Phi$. In other words,

$$\begin{aligned}\dot{y} &= H_q \dot{q} + H_{\dot{q}} q \\ \ddot{y} &= \dot{H}_q \dot{q} + H_{\dot{q}} \dot{q} + \dot{H}_{\dot{q}} q + H_q \dot{q} \\ &= \dot{H}_q \dot{q} + H_{\dot{q}} \dot{q} + \dot{H}_{\dot{q}} q + H_q(F(q, \dot{q}) + G(q)\mathbf{u}).\end{aligned}$$

Using this phase variable for control still yields internal dynamics (i.e., $\bar{n} - r = 3 - 2 = 1$) but the relative degree of the system is two. However, this allows us to use a PD control for trajectory tracking.

A diagram of the real-time algorithm used to compute the unified phase variable can be seen in Fig. 24.3. The unified and normalized phase variable for real-time application is calculated as

$$\Phi(t) = \frac{\text{atan2}(k\tilde{\Theta}_h, \Theta_h) + \pi}{2\pi}, \quad (24.5)$$

where atan2 is the four-quadrant inverse tangent function. The variable k is a scaling factor that increases the linearity of the phase variable [7]. It is calculated every gait cycle as

$$k = \frac{|\max(\Theta_h) - \min(\Theta_h)|}{|\max(\tilde{\Theta}_h) - \min(\Theta_h)|}.$$

The global maximum and minimum hip angle and hip integral need to be known prior to the phase variable computation. These values are stored during the current gait cycle and the scale factor is computed and applied to the calculation of the phase variable at the end of the stride. It should be noted that in contrast to the PW phase variable, the unified phase variable does not have problems with normalization since by construction it is always between the range of $[0, 2\pi)$ due to the atan2 function. Thus, there are no saturations or instantaneous jumps occurring in the unified phase variable due to a wrong normalization value.

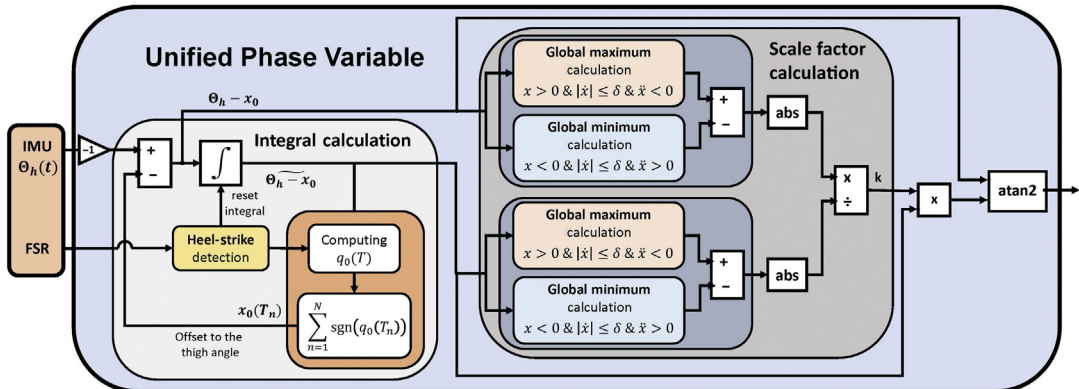


FIGURE 24.3

Diagram of the unified phase variable algorithm.

The integral of the hip angle gets reset at heel strike every gait cycle in order to avoid drift. Furthermore, at every heel strike event the algorithm uses the information from previous strides to compute a correction term for the integral. For linearity of the unified phase variable, the sinusoidal trajectory from the integral of the global hip angle should start and end at zero for each gait cycle (given the cyclic nature of the global hip angle [7]). However, due to the variability of human locomotion the integral might not end at exactly zero. If the value of the integral at the end of the gait cycle is different than zero, then it means the area under the curve of the hip angle is greater or less in the positive side versus the negative side. This issue could potentially introduce a phase shift to the phase variable. One solution to this problem would be to shift the hip angle measurement every stride by $q_0(T) = \tilde{\Theta}_h(T)/T$. Ideally this adjustment term in the hip angle measurement would allow us to reach a perfect phase estimation over time. Nonetheless, in practice the best adaptation was to gradually adjust the signal of the hip angle every gait cycle. The adapted unified and normalized phase variable is finally computed as

$$\hat{\phi}(t) = \frac{\text{atan}2\left(\hat{k}\tilde{\Theta}, \dot{\Theta}\right) + \pi}{2\pi}, \quad (24.6)$$

where the gradual adjustment per stride is defined by

$$x_0(T_N) = \sum_{n=1}^N \text{sgn}(q_0(T_n)), \quad (24.7)$$

and the adjusted global hip angle by $\hat{\Theta} = \Theta_h - x_0(T_n)$. The variable \hat{k} is calculated as in Eq. (24.6) but taking into account the adjusted global hip angle and its integral.

Computing a phase variable that is linear with respect to time helps achieve proper behavior of the controller for a powered prosthetic leg. The virtual constraints define joint angles as polynomial functions of a perfectly linear phase variable. Thus, nonlinear regions in the phase trajectory will cause excessively slow or fast progression through the joint patterns [18].

24.3 CONTROLLING A TRANSFEMORAL POWERED PROSTHETIC LEG USING A PHASE VARIABLE

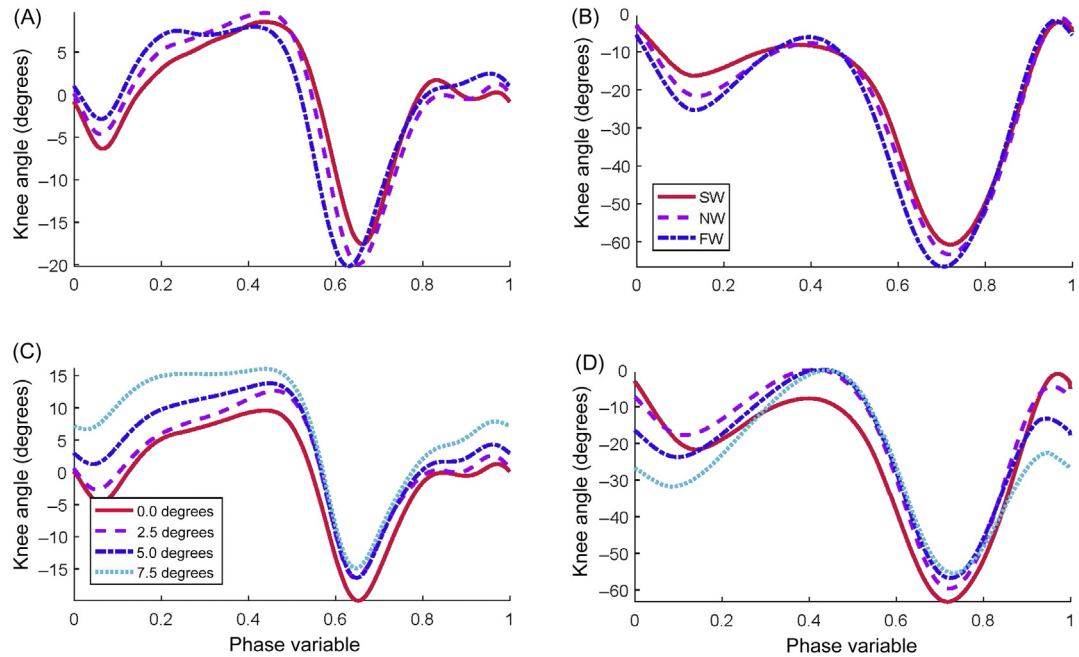
24.3.1 CONTROL LAW

The objective of the phase-based controller is to enforce specific able-bodied kinematic trajectories through the knee and ankle motors of the powered prosthetic leg. These trajectories are encoded by a virtual constraint of the form of Fourier polynomial functions of the unified phase variable [18]. Simply put, we want to drive the error between the virtual constraint function and the joint measurement to zero:

$$y_i = q_i - h_i^d(\varphi) \quad (24.8)$$

where q_i is the measured angular position of joint i (i = knee or ankle), h_i^d is the desired joint trajectory (i.e., virtual constraint) as a function of a phase variable φ , and y_i is the output function.

In biped robots a common way to enforce these virtual constraint functions is by using partial (i.e., input–output) feedback linearization [9–11,23,24]. Due to the complexity of accurately

**FIGURE 24.4**

The reference ankle (A) and knee (B) trajectories as functions of the phase variable for different walking speeds (SW, slow walking; NW, normal walking; FW, fast walking) (C) and inclines (D) based on able-bodied data from [25]. These phase-based trajectories are the virtual constraints enforced by the prosthetic control system.

measuring the interaction forces between the human and the prosthetic leg it may not be appropriate to use partial feedback linearization when controlling a powered prosthetic leg. Instead, a model-free torque control method is used to enforce the virtual constraints, specifically output PD control [8,18].

The PD controller implemented in the powered prosthetic leg has the following form:

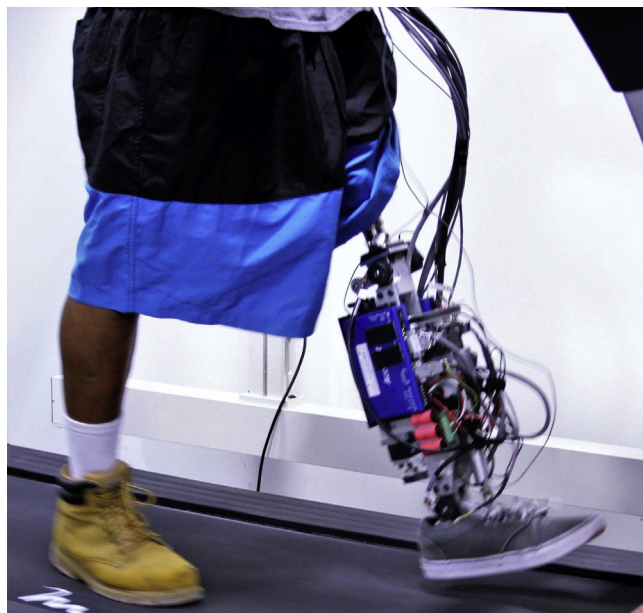
$$v_i = -K_{pi}y_i - K_{di}\dot{y}_i \quad (24.9)$$

where $K_{pi} > 0$ and $K_{di} > 0$ are the proportional and derivative gains, respectively.

Fig. 24.4 shows the desired knee and ankle joint trajectories (i.e., virtual constraints) as a function of phase. These are the knee and ankle joint trajectories that were commanded at each particular locomotion task. These virtual constraints represent the average knee and ankle kinematics of an able-bodied person walking at each locomotion task [25].

24.3.2 HARDWARE SETUP

The design requirements of the powered prosthetic leg were based on the joint kinematics and kinetics of able-bodied walking [26]. The knee and ankle joints were designed for a maximum

**FIGURE 24.5**

The powered prosthetic leg being worn by a transfemoral amputee during an experiment.

torque of 40 and 120 Nm, respectively, based on a user weight of 75 kg. A linear ball screw actuator acting as a four bar linkage actuated each joint. An off-board microcontroller received signals from onboard sensors and transmitted commands to onboard motor drivers through a cable. At the joints, a high-resolution optical encoder was mounted on the output shaft to measure joint angular position for feedback. More details and specifications about the actuation, embedded systems, and sensors used in the powered prosthetic leg can be found in Refs. [27,28]. Fig. 24.5 shows the powered prosthetic leg being worn by an amputee subject.

24.3.3 EXPERIMENTAL PROTOCOL

The experimental protocol was reviewed and approved by the Institutional Review Board (IRB) at the University of Texas at Dallas. The powered knee and ankle prosthetic leg, using the phase variable algorithm, was tested in a total of three nonexpert transfemoral amputee subjects (i.e., they had never used a powered prosthetic leg). Before experiments took place, the prosthetic leg was worn by an able-bodied subject wearing a bypass adapter [27,28] and the gains were tuned for comfortable walking. This was achieved by tuning the gains to a point where the system was more compliant as it was noticed that stronger gains were uncomfortable during walking.

The experimental setup with amputees began by attaching the IMU to the top of the robotic leg's knee joint. A force-sensitive resistor sensor (FSR—FlexiForce A401, Tekscan Inc., Massachusetts, USA) was placed inside the pyramid adapter of the prosthetic foot to measure

stance and swing. Once the IMU was in place, the cables were connected and the powered prosthetic leg was powered on. Amputee subjects were given time to adapt and acclimate to the powered prosthetic leg in overground walking between handrails.

Once the subjects were acclimated to the robotic leg, a trial was tested and recorded of the subjects walking overground. During this trial subjects were asked to walk the length of the handrails, stop, turn around, and start again during 60 seconds. Given that the overground trial involved a lot of nonrhythmic motions (i.e., starting and stopping), the phase variable algorithm output was predominantly the PW phase variable. This is related to the fact that the overground trial required more voluntary control from the subject's perspective as they were not able to reach a steady and rhythmic locomotion.

After the overground trial was completed, subjects were asked to step onto a treadmill for the next trials. Once on the treadmill, subjects were provided a safety harness and walked at a comfortable speed until acclimated. Subjects were asked to select their preferred slow (SW), normal (NW), and fast (FW) walking speed at level ground. Each walking speed condition was tested and recorded during a trial lasting no longer than 60 seconds. Then, subjects were asked to walk at three different inclines (e.g., 2.5, 5, and 7.5 degrees) at their preselected normal walking speed. A trial no longer than 60 seconds was recorded for each incline condition. Note that across all trials the control gains and the phase variable algorithm were not modified. However, for each trial a predefined virtual constraint function, representing the average kinematic trajectories of an able-bodied subject across that particular task, was selected according to the locomotion task being tested. During treadmill trials the phase variable algorithm used predominantly the unified phase variable since a steady and rhythmic locomotion was achieved.

Finally, subjects were asked to walk for two variable virtual constraints trials. In the first variable trial, subjects were asked to walk at level ground while the treadmill changed speeds from SW to FW. A logic switch was implemented that measured the cadence of the subject and selected the virtual constraints (Fig. 24.4) corresponding to each walking speed. In the second variable trial, subjects were asked to walk at a constant walking speed while the incline of the treadmill changed between 0 and 7.5 degrees. During this trial, the virtual constraints were selected manually as the subject progressed through the inclines used in the trial.

Outlier gait cycles were removed for each trial. An outlier gait cycle was defined as a gait cycle where the phase variable was greater or less than \pm three standard deviations away from the average phase variable for that particular trial. Note that the average and standard deviation of the phase variable had to be computed for each trial prior to the outlier detection algorithm. If an outlier gait cycle was detected, then that particular gait was discarded from our results. Removing outlier gait cycles from the trials was justified by the fact that the three amputee subjects were inexperienced powered prosthetic leg users and did not have much training. Thus, the hip angle trajectories of the amputee subjects during locomotion had more variability than the experienced able-bodied subject in the experiment of Quintero et al. [27,28]. A total of 27.46% of all trials across all amputee subjects were removed as outliers.

24.3.4 RESULTS FROM AMPUTEE EXPERIMENTS

Note that it becomes difficult to average the results of the controller for all subjects given they did not have the same preferred walking speeds across trials. Thus, we show the performance of the

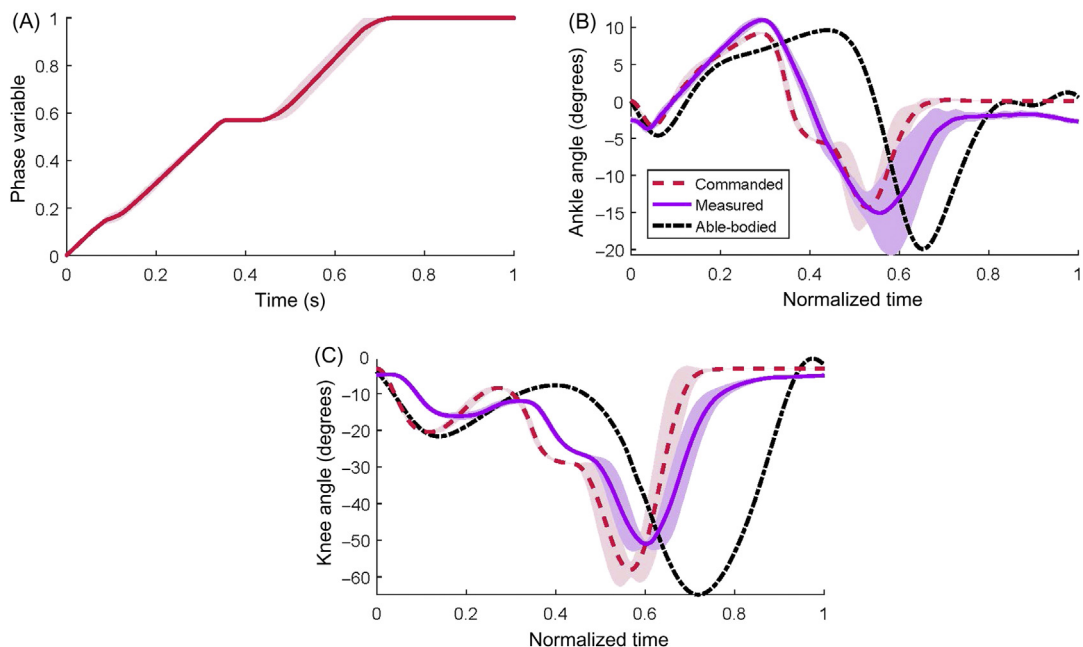
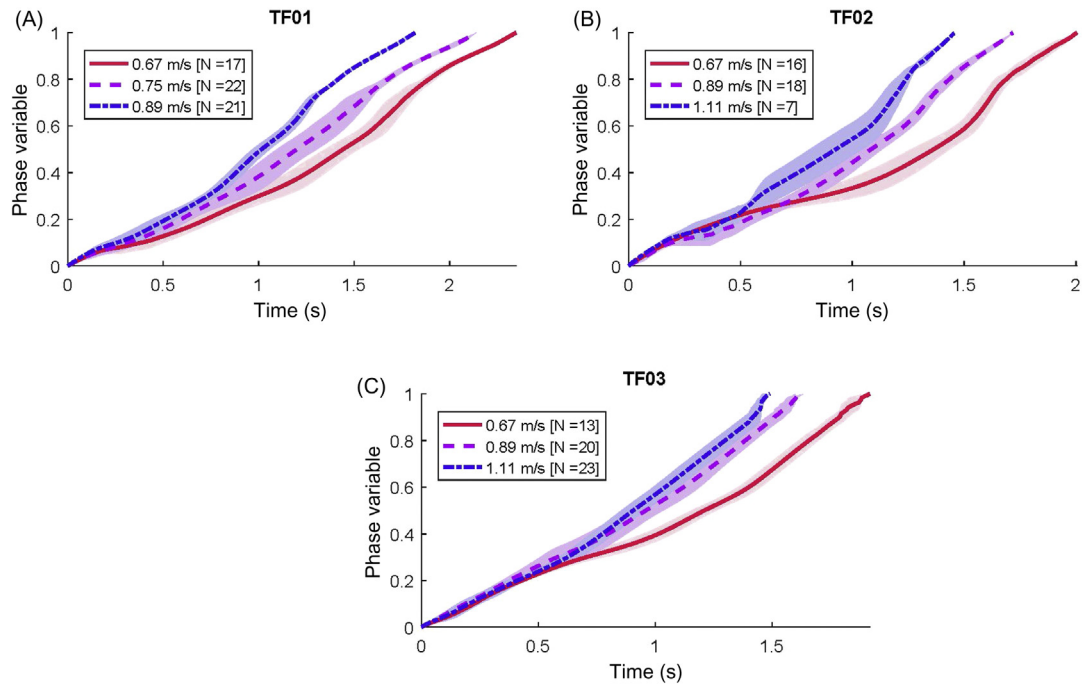


FIGURE 24.6

The average output of the PW phase variable algorithm for TF03 is shown for the overground trial (A) ($N = 9$). The resulting commanded and measured joint trajectories (mean ± 1 std) of the ankle (B) and knee (C) are shown as a function of normalized time. The black dashed line represents the average joint angle trajectory of an able-bodied subject [25]. These able-bodied kinematics were enforced over phase.

controller for representative subjects in the results section. Fig. 24.6 shows the results of the overground trial for TF03, during which the PW phase variable output was predominant. This is due to the fact that the subject remained in a nonsteady locomotion state when walking the short length of the parallel bars. The commanded and measured knee and ankle trajectories are shown over normalized time in Fig. 24.6. Overall, using the PW phase variable the subject was able to walk comfortably overground and the controller produced fairly normative joint kinematics but with some differences in timing from rhythmic able-bodied data.

During treadmill trials the phase variable algorithm took no more than three strides to transition between the PW and the unified phase variable (Section 24.2.1). Fig. 24.7 shows the average output of the unified phase variable for each amputee subject across each different walking speed condition. It can be seen that the phase variable remains linear across the entire gait cycle, where the slope with respect to time is different for each walking speed. This shows that the phase variable captures the speed of the amputee's gait. Fig. 24.8 also shows the average phase variable output across different incline conditions for each subject. The phase variable adapts to each incline and remains linear across the entire gait cycle. Note that the variability on the phase variable demonstrates the effect of variability of the user's hip motion, which subsequently causes variation in the prosthetic joint kinematics.

**FIGURE 24.7**

The output of the phase variable algorithm is shown for three different amputee subjects [TF01 (A), TF02 (B), and TF03 (C)] across three different self-selected speeds. The variable N represents the number of strides used in the calculation of mean \pm 1 std for each walking speed condition.

[Fig. 24.9](#) shows the commanded and measured knee and ankle trajectories for the NW trial over normalized time and phase for a representative subject (TF03). It can be seen that over phase the measured trajectories have a slight phase delay with respect to the commanded joint trajectories (i.e., the virtual constraints). This was a consequence of tuning the control gains to achieve more compliant and comfortable behavior on the robotic leg (Section 24.3.3). Increased tracking error was the tradeoff for user comfort. As a comparison to level ground walking, [Fig. 24.10](#) shows the knee and ankle commanded and measured joint trajectories for a representative subject (TF03) at the 5 degrees incline trial over normalized time and phase.

It can be seen from [Figs. 24.9 and 24.10](#) that over phase the commanded trajectories have no variance and the measured joint kinematics have small variations. This is due to the virtual constraints of the controller being parameterized over the phase variable. On the other hand, over normalized time it can be seen that there is more variability in the commanded and measured joint kinematics. This variability comes from the variance in the user's hip motion which in turn affected the phase variable over time. It is important to note that, over time, the measured joint trajectories do resemble the kinematics of an able-bodied subject during locomotion. In conclusion, the prosthetic leg exhibited able-bodied behavior as the amputee subject walked at different speeds and inclines.

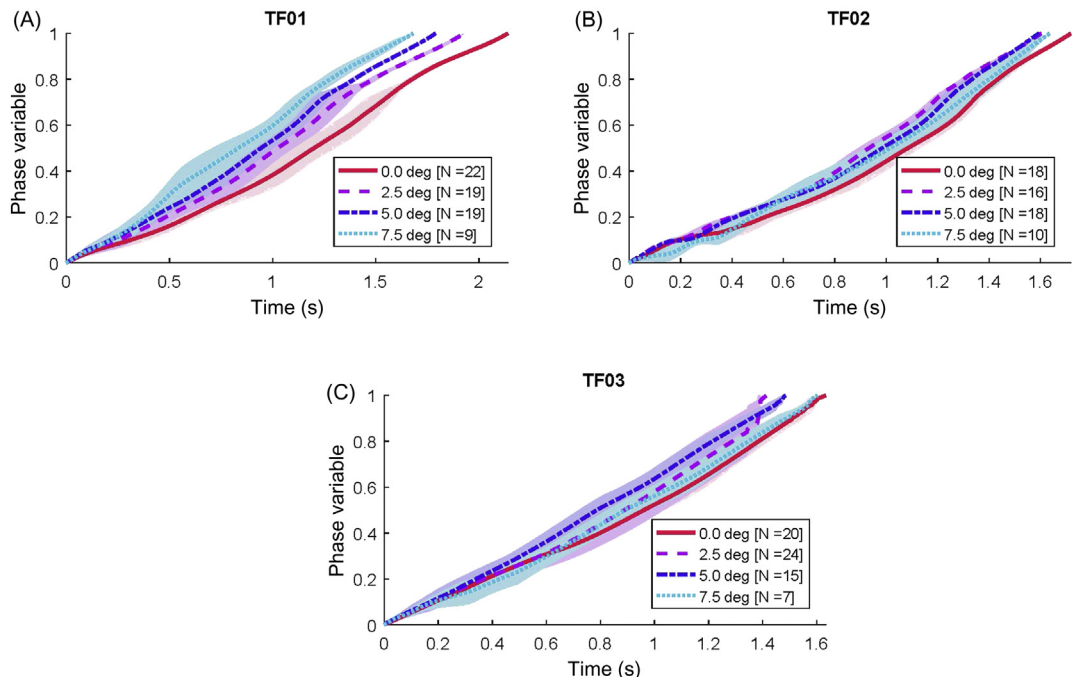
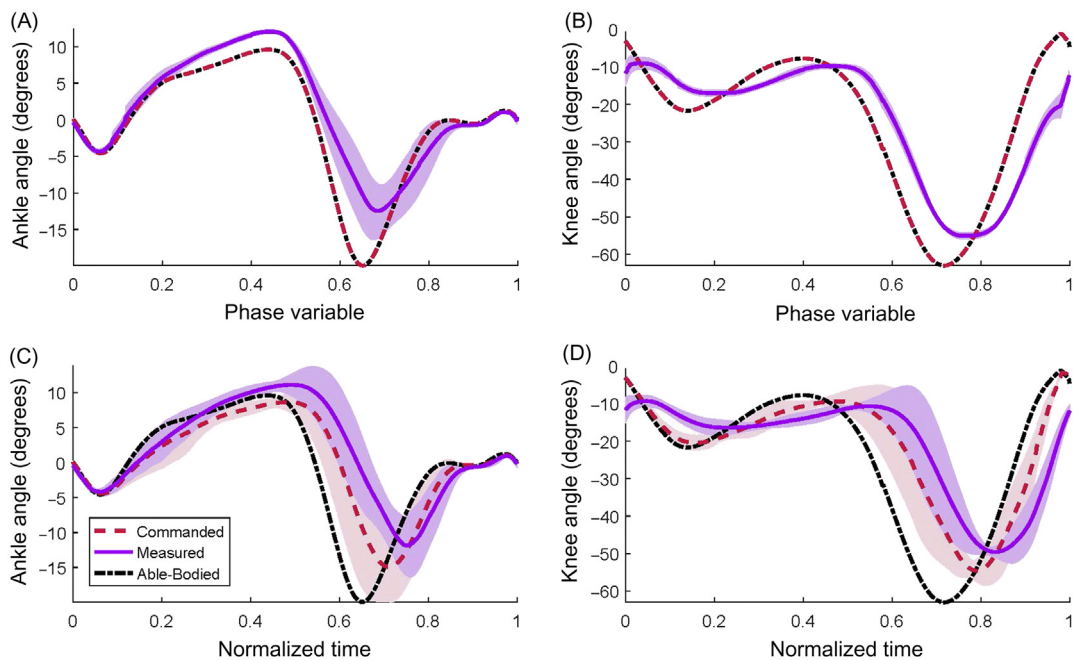


FIGURE 24.8

The output of the phase variable algorithm is shown for three different amputee subjects [TF01 (A), TF02 (B), and TF03 (C)] across four different ground incline conditions (bottom). The variable N represents the number of strides used in the calculation of mean ± 1 std for each incline condition.

Across the variable trials (i.e., changing the virtual constraints for different walking speeds and inclines during a trial), the amputee subject was able to walk while the virtual constraints were changed. Figs. 24.11 and 24.12 show the average phase variable across these trials for a representative subject (TF02). The phase variable algorithm was able to adapt to environmental and kinematic changes occurring during each trial (i.e., different treadmill speeds and inclines). Figs. 24.11 and 24.12 also show the commanded and measured joint trajectories as a function of phase during these trials. Note that compared to previous trials, during which the virtual constraint was not changed, these trials produced visible variability in the commanded trajectory. This is in fact due to changing the commanded virtual constraints during the trial. A closer analysis on the average total work done by the powered prosthetic leg in TF03 per stride (i.e., the integral of total joint power over a stride) informed us that both parameterizations yield a net work close to zero as in able-bodied locomotion (i.e., $PW = 0.077 \pm 0.057$ J/kg and unified = 0.007 ± 0.167 J/kg) (Fig. 24.13). This shows that the synergy between the positive ankle work and the negative knee work in the powered prosthetic leg complemented each other during a stride. In fact, the knee and ankle work done by the robotic leg during the unified phase variable parameterization was closer to the work done by the leg of an able-bodied subject [25]. In Fig. 24.13 it can be seen that the instantaneous power of

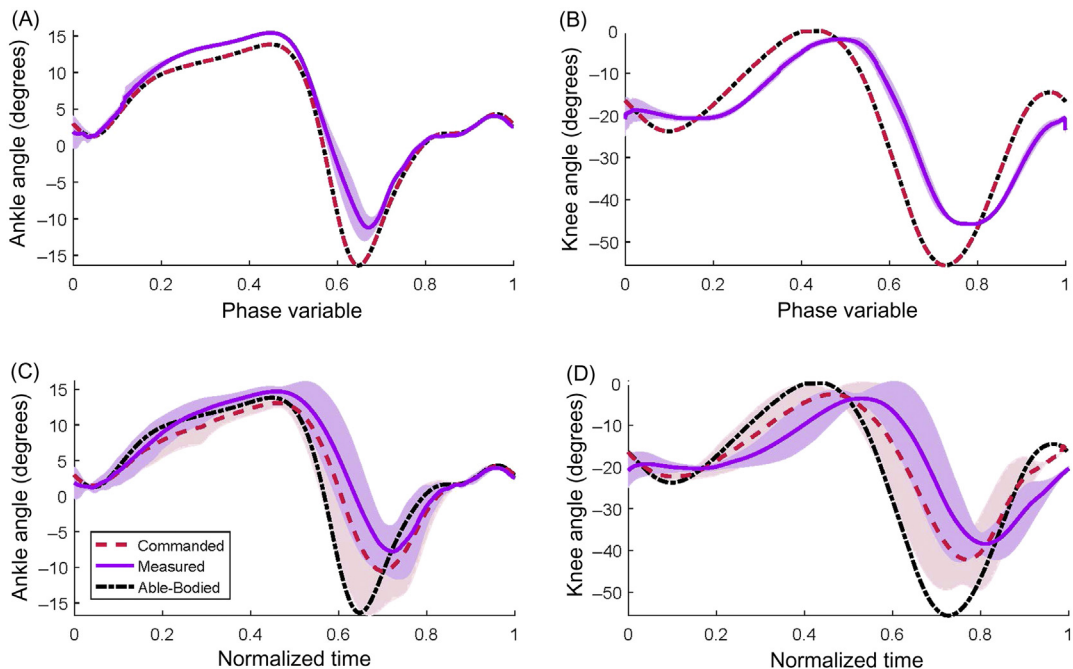
**FIGURE 24.9**

The ankle and knee commanded and measured joint kinematics for TF03 are shown as a function of unified phase variable (A, B) and normalized time (C, D) for the NW trial ($N = 20$). The black dashed line represents the average joint angle kinematics of an able-bodied subject [25].

the robotic leg joints between overground and treadmill NW trials follow a similar trend to able-bodied leg joint power curves, and ankle pushoff power is delivered at the appropriate phase of the gait cycle.

24.3.5 DISCUSSION OF AMPUTEE EXPERIMENTS

One of the main characteristics of a normal and healthy gait is achieving symmetry between leg motion. This also translates to biped robots where assumptions in the symmetry between steps are key to the stability of the robot during locomotion [9]. Pathological gaits are often detected by the lack of symmetry and coordination between the movements of the legs [22]. This behavior is present as well during amputee locomotion [29] and could be due to the mistrust involved in wearing an artificial leg. During our experiments it was noticed that the phase variable algorithm had some difficulties adapting to asymmetric gaits as it was designed taking into account symmetric able-bodied kinematics. The problem arises when parameters calculated from the information of previous asymmetric gait cycles get input into the current phase variable calculation (Section 24.2.1). In order to avoid this issue it was essential for the subjects to relearn how to walk symmetrically and trust the powered prosthetic leg during the acclimation period. After a short acclimation period,

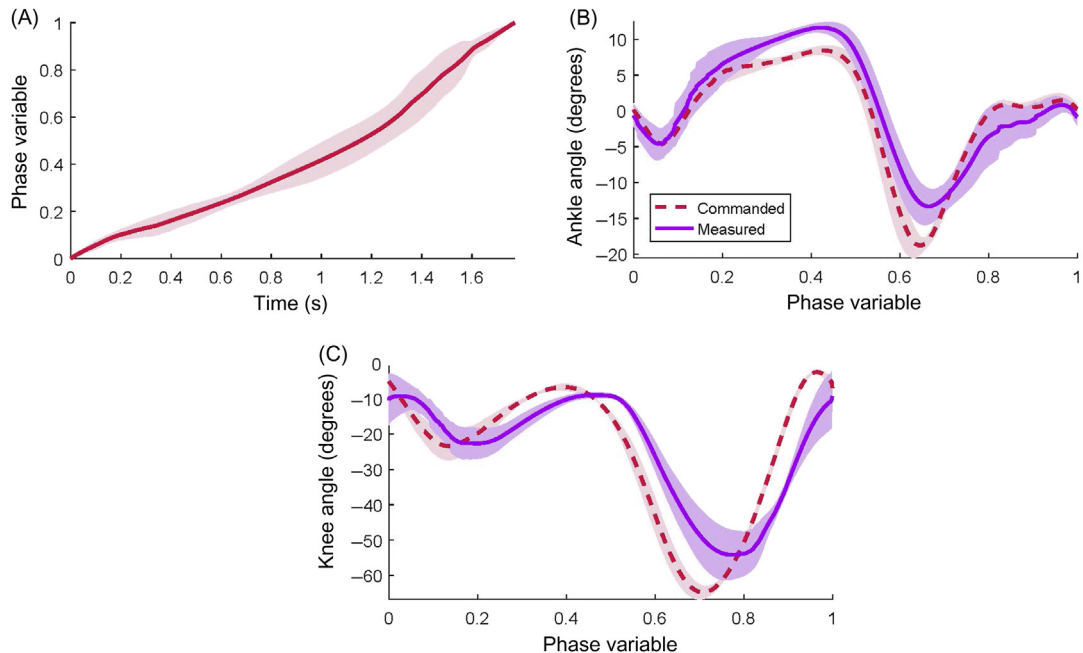
**FIGURE 24.10**

The ankle and knee commanded and measured joint kinematics for TF03 are shown as a function of unified phase variable (A, B) and normalized time (C, D) for the 5 degrees incline trial ($N = 15$). The black dashed line represents the average joint angle kinematics of an able-bodied subject [25].

subjects were able to walk symmetrically most of the time and thus the phase variable algorithm behaved as designed.

The phase variable algorithm was able to adapt to all locomotion tasks once the subject learned to walk symmetrically. Across all locomotion tasks tested on a treadmill (i.e., different walking speeds and inclines) the unified phase variable algorithm adapted and computed a monotonic linear unified phase variable. The mass/inertia of the prosthetic leg and compliant socket interactions did not alter the sinusoidal property of the thigh motion. The monotonic and boundedness properties of the phase variable would not be altered as long as the thigh motion of the subject traces a cosine-like trajectory during the gait cycle. To our knowledge, this is the first time that it has been shown that a phase variable algorithm can synchronize the joints of a powered prosthetic leg across various ranges of speeds and inclines. However, a phase variable algorithm that is invariant to locomotion tasks does not necessarily translate to a controller that is invariant to tasks.

Even though the phase variable algorithm was able to adapt to all locomotion tasks tested, the joint trajectories enforced by the controller (i.e., the virtual constraints) were changed across different locomotion tasks. A simple classifier based on cadence automatically transitioned between the virtual constraints for each speed. However, in comparison to measuring walking speeds, inclines are more difficult to estimate with the current on-board sensors of the prosthetic leg. Thus, the

**FIGURE 24.11**

The phase variable (A) is shown for the variable speed trial (TF02). The ankle (B) and knee (C) commanded and measured joint trajectories as a function of phase are shown with one standard deviation away from the mean.

virtual constraints used during the variable incline trial had to be manually selected (Fig. 24.12). It is also possible to model the desired joint kinematics as continuous functions of walking speed and slope so the controller does not have to rely on state-machine logic [26]. The phase variable algorithm can give the amputee intuitive control over the robotic leg for whatever virtual constraints are used.

The piecewise and unified phase variable algorithms gave the subject a more intuitive and natural control over the powered prosthetic leg. The PW phase variable algorithm allowed subjects to perform volitional and nonrhythmic movements such as swinging the leg back and forth [30], stepping forward and back, and walking backwards [31]. To our knowledge, this is the first time it has been reported that a phase-based control algorithm used in a powered prosthetic leg was used to walk backward without any modification. During the acclimation period for overground walking, the phase variable algorithm more often than not remained in piecewise mode (Fig. 24.6). This helped the subject trust the robotic leg and become acquainted with the feeling of using a powered prosthetic leg during a nonrhythmic gait. During treadmill trials, the PW algorithm transitioned into the unified phase variable after a couple of strides. The piecewise phase variable algorithm gives the subject voluntary control over the powered prosthetic leg during nonrhythmic motions while the unified phase variable algorithm provides a synchronized gait cycle during rhythmic walking (i.e., dynamic walking). Even though the phase variable algorithm allowed amputees to

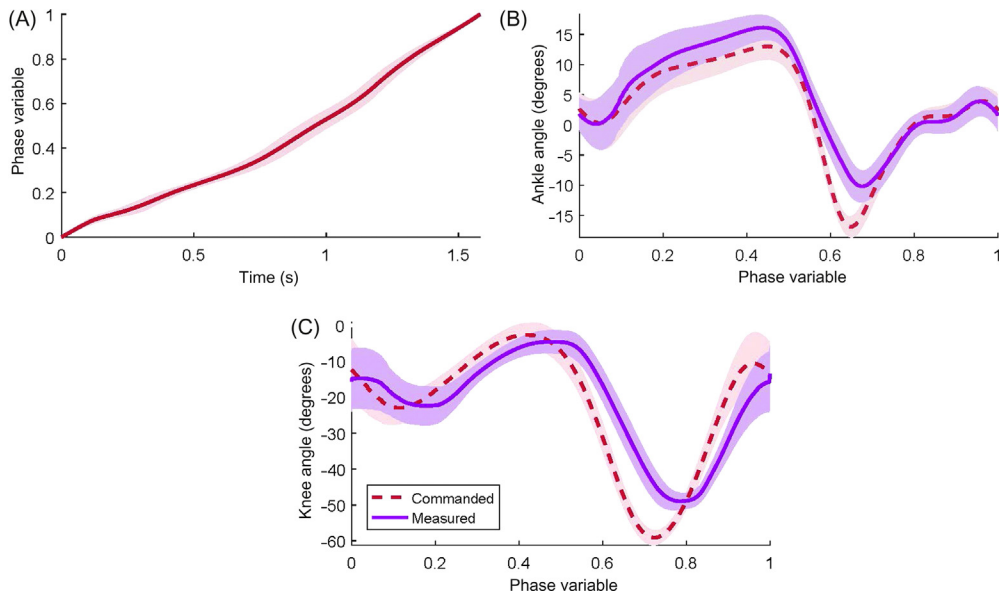


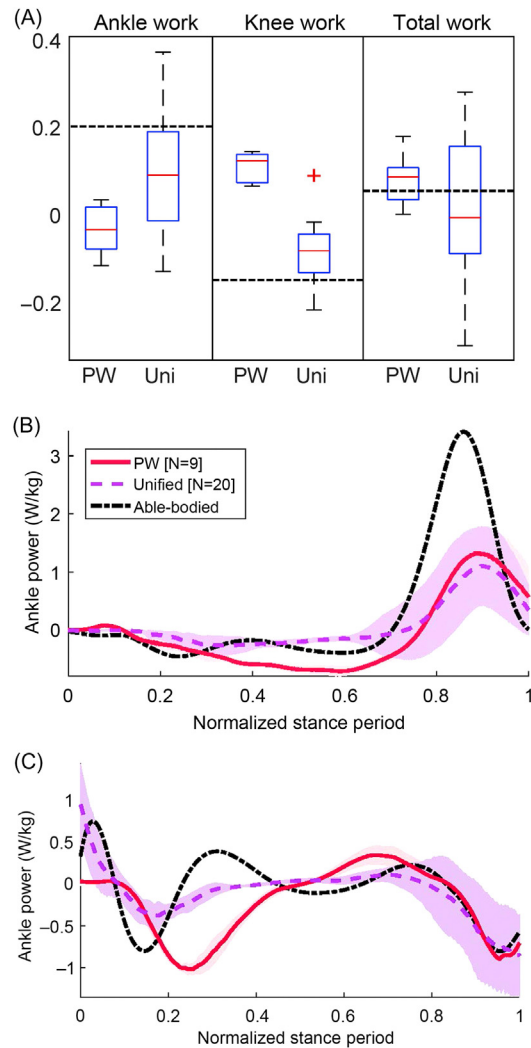
FIGURE 24.12

The phase variable (A) is shown for the variable incline trial (TF02). The ankle (B) and knee (C) commanded and measured joint trajectories as a function of phase are shown with one standard deviation away from the mean.

walk steadily during experiments, there are still open questions related to the overall mathematical stability of the system.

The choice of virtual constraints has an impact on the overall stability of the system. Achieving stable locomotion is a major concern for researchers in the area of biped robots [9]. Choosing the appropriate set of virtual constraints play a major role in determining the convergence to a stable limit cycle as well as the region of stability around it [9]. However, due to the unpredicted dynamics that are introduced to the system, once a human is in the loop, a rigorous metric for stability cannot be defined in the mathematical sense [32]. For our application, the choice of virtual constraints was inspired by the natural motion that occurs during human locomotion. It is intuitive to think that if we want to provide able-bodied locomotion to a transfemoral amputee wearing the powered prosthetic leg, then the virtual constraints would need to be encoded with the kinematics of an able-bodied subject. Given the lack of a rigorous mathematical definition of stability in this particular application we must rely on the expertise of clinicians that are trained to differentiate between stable and unstable gaits. Currently, researchers are developing a software platform that would allow clinicians to customize virtual constraints for each of their amputee patients [27,28]. This would enable the clinician and the amputee to interact until the most stable and comfortable gait is achieved. One of our biggest motivations behind the development of this phase-based controller was to reduce the amount of time and work needed for the clinician to tune the controller before an amputee could start walking.

The experiments show that the phase-based control architecture could allow powered prosthetic legs to behave as plug-and-play devices. Our experimental procedure was kept relatively short

**FIGURE 24.13**

The normalized ankle, knee, and total work done by the powered prosthetic leg during the overground (PW) and treadmill NW (Uni) trials for TF03 is shown in (A). The normalized ankle (B) and knee (C) power of the powered prosthetic leg is shown during piecewise and unified phase variable conditions across a normalized stance period. The black dash-and-dot line represents the average power of an able-bodied subject from Ref. [25].

thanks to the adaptability of the phase variable algorithm and the phase-based control architecture. While it has been reported that the tuning and calibration process in other controllers used in powered prosthetic legs can take hours across multiple clinical sessions [33], the calibration process in our control architecture was kept relatively short (<20 minutes). The gains in the controller were

tuned days prior to the experiment with an able-bodied subject wearing a bypass adapter [27,28,34], and the same gains were used across all trials with the amputee subject reported in this chapter. The control architecture only uses on-board sensors to measure phase and requires no major tuning across walking speeds, which makes it highly viable for clinical applications.

REFERENCES

- [1] R.J. Vogelstein, R. Etienne-Cummings, N.V. Thakor, A.H. Cohen, Phase-dependent effects of spinal cord stimulation on locomotor activity, *IEEE Trans. Neur. Syst. Rehabil. Eng.* 14 (3) (2006) 257–265.
- [2] F. Dzeladini, J. van den Kieboom, A. Ijspeert, The contribution of a central pattern generator in a reflex-based neuromuscular model, *Frontiers in Human Neuroscience*, 8, no. June, pp. 1–18, 2014, [Online]. Available from: [http://www.frontiersin.org/Human\(_Neuroscience\)/10.3389/fnhum.2014.00371/abstract](http://www.frontiersin.org/Human(_Neuroscience)/10.3389/fnhum.2014.00371/abstract)
- [3] A. Taghvaei, S.A. Hutchinson, P.G. Mehta, A coupled oscillators-based control architecture for locomotory gaits, in: 53rd IEEE Conference on Decision and Control, 2014, pp. 3487–3492, [Online]. Available from: [http://ieeexplore.ieee.org/lpdocs/epic03\(wrapper.htm?arnumber=7039930](http://ieeexplore.ieee.org/lpdocs/epic03(wrapper.htm?arnumber=7039930).
- [4] A.K. Tilton, E.T. Hsiao-Wecksler, P.G. Mehta, Filtering with rhythms: application to estimation of gait cycle, in: American Control Conference, 2012, pp. 3433–3438.
- [5] S. Revzen, J.M. Guckenheimer, Estimating the phase of synchronized oscillators, *Phys. Rev. E - Statist. Nonlinear, Soft Matter Phys.* 78 (5) (2008) 1–12.
- [6] R. Ronsse, N. Vitiello, T. Lenzi, J. van den Kieboom, M.C. Carrozza, A.J. Ijspeert, Human – robot synchrony: flexible assistance using adaptive oscillators, *IEEE Trans. Biomed. Eng.* 58 (4) (2011) 1001–1012 [Online]. Available from: [http://ieeexplore.ieee.org/lpdocs/epic03\(wrapper.htm?arnumber=5609195](http://ieeexplore.ieee.org/lpdocs/epic03(wrapper.htm?arnumber=5609195).
- [7] D.J. Villarreal, H.A. Poonawala, R.D. Gregg, A robust parameterization of human gait patterns across phase-shifting perturbations, *IEEE. Trans. Neural. Syst. Rehabil. Eng.* 4320 (c) (2016) 1 [Online]. Available from: Available from: <http://ieeexplore.ieee.org/document/7469796/>.
- [8] R.D. Gregg, J.W. Sensinger, Towards biomimetic virtual constraint control of a powered prosthetic leg, *IEEE Trans. Control Syst. Technol.* 22 (1) (2014) 246–254.
- [9] E.R. Westervelt, J.W. Grizzle, C. Chevallereau, J.H. Choi, B. Morris, *Feedback Control of Dynamic Bipedal Robot Locomotion*, CRC Press, Boca Raton, FL, 2007.
- [10] K. Akbari Hamed, B.G. Buss, J.W. Grizzle, Continuous-time controllers for stabilizing periodic orbits of hybrid systems: application to an underactuated 3D bipedal robot, in: 53rd IEEE Conference on Decision and Control, dec 2014, pp. 1507–1513, [Online]. Available from: [http://ieeexplore.ieee.org/lpdocs/epic03\(wrapper.htm?arnumber=7039613](http://ieeexplore.ieee.org/lpdocs/epic03(wrapper.htm?arnumber=7039613).
- [11] B.G. Buss, A. Ramezani, K.A. Hamed, B.A. Griffin, K.S. Galloway, J.W. Grizzle, Preliminary walking experiments with underactuated 3d bipedal robot marlo, in: 2014 IEEE/RSJ International Conference on Intelligent Robots and Systems, Sept 2014, pp. 2529–2536.
- [12] A.E. Martin, D.C. Post, J.P. Schmiedeler, The effects of foot geometric properties on the gait of planar bipeds walking under HZD-based control, *Int. J. Robot. Res.* 33 (12) (2014) 1530–1543 [Online]. Available from: Available from: <http://ijr.sagepub.com/cgi/doi/10.1177/0278364914532391>.
- [13] R.D. Gregg, T. Lenzi, L.J. Hargrove, J.W. Sensinger, Virtual constraint control of a powered prosthetic leg : from simulation to experiments with transfemoral amputees, *IEEE Trans. Robot.* 30 (6) (2014) 1455–1471.
- [14] R.D. Gregg, T. Lenzi, N.P. Fey, L.J. Hargrove, J.W. Sensinger, Experimental effective shape control of a powered transfemoral prosthesis, *IEEE Int. Conf. Rehabil. Robot.* (2013).

- [15] S. Song, H. Geyer, A neural circuitry that emphasizes spinal feed back generates diverse behaviours of human locomotion, *J. Physiol.* 593 (16) (2015) 3493–3511 [Online]. Available from: <<http://doi.wiley.com/10.1113/JP270228>>.
- [16] S. Rossignol, R. Dubuc, J.P. Gossard, **Dynamic sensorimotor interactions in locomotion**, *Physiol. Rev.* 86 (1) (2006) 89–154.
- [17] D.J. Villarreal, R.D. Gregg, A survey of phase variable candidates of human locomotion, in: 2014 36th Annual International Conference of the IEEE Engineering in Medicine and Biology Society. IEEE, Aug 2014, pp. 4017–4021.
- [18] D. Quintero, A.E. Martin, R.D. Gregg, Toward unified control of a powered prosthetic leg: A simulation study, *IEEE Trans. Control Syst. Technol.* (2017) 1–8.
- [19] M.W. Spong, S. Hutchinson, M. Vidyasagar, **Robot Modeling and Control**, John Wiley & Sons, Inc, Hoboken, NJ, 2006.
- [20] H.K. Khalil, **Nonlinear Control**, Pearson, London, 2014.
- [21] A. Isidori, **Nonlinear Control Systems**, Springer, New York, 1995.
- [22] J. Perry, J.M. Burnfield, L.M. Cabico, *Gait Analysis: Normal and Pathological Function*. Thorofare, NJ: SLACK, 2010.
- [23] K. Sreenath, H.-W. Park, I. Poulakakis, J.W. Grizzle, A compliant hybrid zero dynamics controller for stable, efficient and fast bipedal walking on MABEL, *Int. J. Robot. Res.* 30 (9) (2011) 170–1193.
- [24] K.A. Hamed, B.G. Buss, J.W. Grizzle, Continuous-time controllers for stabilizing periodic orbits of hybrid systems: application to an underactuated 3D bipedal robot, in: 53rd IEEE Conference of Decision and Control, 2014.
- [25] D. Winter, **Biomechanics and Motor Control of Human Movement**, J. Wiley and Sons, Hoboken, NJ, 2009.
- [26] K. Embry, D.J. Villarreal, R.D. Gregg, A unified parameterization of human gait across ambulation modes, in: 2016 38th Annual International Conference of the IEEE Engineering in Medicine and Biology Society (EMBC), 2016.
- [27] D. Quintero, D.J. Villarreal, R.D. Gregg, preliminary experiments with a unified controller for a powered knee-ankle prosthetic leg across walking speeds, *IEEE Int. Conf. Intell. Robots Syst.* (2016).
- [28] D. Quintero, D.J. Villarreal, D.J. Lambert, S. Kapp, R.D. Gregg, Continuous-phase control of a powered knee-ankle prosthesis: Amputee experiments across speeds and inclines, *IEEE Trans. Robot.* 34 (3) (2018) 686–701.
- [29] D.G. Smith, J.W. Michael, J.H. Bowker, **Atlas of Amputations and Limb Deficiencies**, Amer Academy of Orthopaedic, 2004.
- [30] D. Quintero, D.J. Villarreal, R.D. Gregg, First amputee experiment with unified phase-based control of a powered knee-ankle prosthesis. [Online]. Available from: <https://www.youtube.com/watch?v=NjHT9LjZuVw>, 2016
- [31] D. Quintero, D. Villarreal, R.D. Gregg, Amputee subject walking backwards on utd powered prosthetic leg. [Online]. Available from: <https://www.youtube.com/watch?v=WiaaQ0bXzMw>, 2017
- [32] A.E. Martin, R.D. Gregg, Stable, robust hybrid zero dynamics control of powered lower-limb prostheses, *IEEE Transactions on Automatic Control* PP (99) (2017), pp. 1–1.
- [33] A.M. Simon, K.A. Ingraham, N.P. Fey, S.B. Finucane, R.D. Lipschutz, A.J. Young, et al., Configuring a powered knee and ankle prosthesis for transfemoral amputees within five specific ambulation modes, *PLoS One* 9 (6) (2014).
- [34] D. Quintero, D.J. Villarreal, R.D. Gregg, Fast walking up to 3 miles/hr on the utd powered knee-ankle prosthesis. [Online]. Available from: <https://www.youtube.com/watch?v=f3NyxRoesOY>, 2016.

Index

Note: Page numbers followed by “*f*” and “*t*” refer to figures and tables, respectively.

A

- A/A. *See* Abduction and adduction (A/A)
AAN control. *See* Assist-as-needed control (AAN control)
AAPM&R. *See* American Academy of Physical Medicine and Rehabilitation (AAPM&R)
Abduction and adduction (A/A), 150, 194, 395–397
ABLE device, 9, 208–210
axis kinematics, 54*f*, 55*f*
completion of ABLE 7D, 54–62
 axial displacement law of parallel structure, 58*f*
 CAD view, 57*f*
 computed grooves, 60*f*, 61*f*
 first prototype, 64*f*
 forearm articulated structure allowing pronosupination, 57*f*
 forearm–wrist design, 54–60
 joints kinematics, 63*f*
 new shoulder with nonorthogonal joints and simple bearing, 60–62
 translation magnitude for biomechanical dimensions, 58*f*
 wrist U-joint articulation and SCS drives with cable routing, 61*f*
first ABLE 4D, 52–53, 53*f*
 main specifications, 56*t*
SCS mechanism, 45–52
ABS. *See* Acrylonitrile butadiene styrene (ABS)
AC synovial joint. *See* Acromioclavicular synovial joint (AC synovial joint)
Accuracy test, 81
Achilles exoskeleton, 255
Acromioclavicular synovial joint (AC synovial joint), 106–107
Acrylonitrile butadiene styrene (ABS), 181
ACT^{3D} robotic system. *See* Arm Coordination Training 3-D robotic system (ACT^{3D} robotic system)
Action potentials, 447
Active assistive motion, 34–35
 results of, 39–41
Active prosthesis
 control, 477
 systems, 473
Active prosthetic devices, 472
Active upper limb prostheses, 366–367
Activities of daily living (ADLs), 8, 81, 114, 161, 439
Actuation
 for hand exoskeleton systems, 154–155
 of lower limb exoskeletons, 221–222
 systems, 232–234
 for upper limb exoskeleton systems, 4–8
Actuators, 155
 electric, 475
 forearm pronosupination, 56, 59*f*
 hydraulic, 5
 pancake coil brushless DC, 98
 pneumatic, 5, 155, 207–208, 474
 series elastic actuators (SEAs), 2, 5, 13, 67–68, 155, 207–208, 475
Adaptation of sEMG sensors, 382–383
Adaptive law, 143
Adaptive synergy-based controller, 360
ADC. *See* Analog to digital converter (ADC)
Adjustment-free biomimetic clavicle, 117–118
ADLs. *See* Activities of daily living (ADLs)
Admittance control, 8, 77–79. *See also* Direct torque control
 evaluation, 80–81, 83–84
 control bandwidth, 84
 transparency, 83
Advanced selective noninvasive neuroprosthetics, 351
Advanced Skill Assessment, 320
Adverse events (AEs), 311–312, 322
AFO braces. *See* Ankle–foot–orthosis braces (AFO braces)
Agonist–antagonist myoneural interface (AMI), 459
AIST, 9
ALEX Exoskeleton, 67
American Academy of Physical Medicine and Rehabilitation (AAPM&R), 321
AMI. *See* Agonist–antagonist myoneural interface (AMI)
Amputation(s), 365, 381–383
 and patients, 372
Amputees, 439–440, 459
 experiments, 500–505
 results from, 496–500
Analog to digital converter (ADC), 428
Angle dynamics, 476
Ankle and knee prosthetic devices, autonomous and tethered active, 471*f*
Ankle exoskeletons
 CMU, 261–262
 end-effector designed for low forces and safety, 258–260
Ankle joint trajectories, 494, 494*f*
Ankle–foot–orthosis braces (AFO braces), 315, 336
Anthropomorphic
 exoskeleton, 106–107
 form factor, 393, 418
 shoulder actuation, 110
AREA, 200, 200*f*

- Arm assessment, 116
- Arm Coordination Training 3-D robotic system (ACT^{3D} robotic system), 11
- Arm exoskeletons with multi-DOF hand modules, 161
- ARM Guide. *See* Assisted Rehabilitation and Measurement Guide (ARM Guide)
- ARMin
- I prototypes, 107
 - II prototypes, 107
 - III prototypes, 12, 107
- Articulating legs, 318
- Articulation, 106–107
- Artificial reversibility, 47–48
- Assist-as-needed control (AAN control), 8, 216
- Assisted Rehabilitation and Measurement Guide (ARM Guide), 10
- Assistive devices, 329
- active movement-assistive devices, 7
 - exoskeleton, 471–472
 - primary, 314–315
 - wearable, 68
- Assistive exoskeletons, 207–215. *See also* Rehabilitation exoskeletons
- AUSTIN, 209_t, 215
 - Ekso, 209_t, 218, 303–304, 339–340
 - eLEGS, 209_t
 - HAL, 9, 209_t, 302–304, 306, 339
 - Mina, 209_t, 214, 246–247
 - MindWalker, 209_t, 215
 - ReWalk, 209_t, 214, 246–247, 255, 317–320, 339
 - REX, 209_t, 215, 339
 - RGO, 209_t, 210–212, 336
 - Robin H1, 209_t, 214
 - WPAL, 209_t, 214–215
- Assistive hand exoskeletons, 158–160
- by Brown et al., 158–159
 - by In et al., 159
 - ExoGlove, 159
 - HX hand exoskeleton, 160
 - by Kadowaki et al., 159
 - by Lucas et al., 159
 - OFX, 159
 - by Polygerinos et al., 160
 - by Secciani et al., 160
- Assistive lower limb exoskeletons, 207, 214–215
- Assistive performance, 84–86
- Assistive robotics, 365
- Assistive upper limb exoskeletons, 8–9
- ABLE, 9
 - AIST, 9
 - HAL, 9
 - MULOS, 9
 - MyoPro, 9
 - SUEFUL-7, 9
- Assistive walking
- burden of SCI, 312–314
 - current treatment options, 314–316
 - functional electric stimulation, 315–316
 - leg braces, 315
 - standing frames and standing mobility devices, 316
 - wheelchairs, 314–315
 - economic impact, 328–331
 - challenges of exoskeletons, 329
 - exosuits, 329
 - ReStoreexosuit design, 330–331, 330_f
 - rationale for exoskeletons, 316
 - ReWalk product summary, 317–320
 - safety and efficacy profile
 - exoskeleton-assisted walking simulating normal physiological effects, 322–325
 - patient selection, 320–321
 - safe ambulatory function and patient tolerance, 321–322
- ATX, 163
- Augmentation
- augmented reality training, 460
 - exoskeleton, 207–208, 213_t, 217–221
 - assistance applied on users, 219–221
 - assistance directly applied to tasks, 218–219
 - hand exoskeletons, 165–167
 - Hasegawa et al., 166
 - Matheson et al., 167
 - RoboGlove, 167
 - Shields et al., 166
 - Skil Mate, 166
 - Tadano et al., 167
 - lower limb exoskeleton, 6–7
 - actuation of, 221–222
 - assistive exoskeletons, 208–215, 209_t
 - augmentation exoskeletons, 213_t, 217–221
 - control, 269–271
 - exoskeleton emulator testbeds, 251–254
 - future for, 222
 - making strides in future, 271–272
 - mechanical design of onboard components, 255–269
 - rehabilitation exoskeletons, 211_t, 215–217
 - untethered systems, 254–255
 - upper limb exoskeletons, 14–15
 - EksoVest from Ekso Bionics, 15
 - SARCOS Guardian GT system, 15
 - SARCOS Guardian XO, 15
 - ShoulderX from SuitX, 15
- AUSTIN, 215
- Auxiliary subsystems
- body attachment, 432–433
 - NFU, 430–431
- Azzurra hand, 366
- A δ -and C-low-threshold mechanoreceptors (LTMRs), 450

B

- Back case, 177–178
- Backdrivability, 46–48
- Backpack of WalkON Suit, 235
- Ball screw, 49–51, 56
- Bandwidth test, 81
- Base-to-distal topology exoskeletons, 154, 193–194
- Basic Skill Assessment, 320
- Battery and wrist quick release, 410–411, 410 f
right forearm, battery socket, and battery, 411 f
- Battery management system (BMS), 410
- Bayesian optimizations, 479
- BeBionic*, 369
- Bending stress of beam, 138
- bHMI. *See* Bidirectional HMI (bHMI)
- Bi-Manu-Track system, 11
- Biarticular mechanism, 234
- Bidirectional HMI (bHMI), 384, 386 f
- Bidirectional man–machine interaction, 393
- Bilateral Lower Limb Exoskeleton Emulator (BiLLEE), 268
- Bilateral shoulder designs, 111
- Bio-compatible miniature EMG sensors, 380
- Bidex System 4 Pro, 1
- Biological sensors, 371, 374
- BiOM, 475
- Biomechanical signals, 487–488
- Biomechanics, 1, 68–69
- Biomimetic designs, 454
- BioMot, 214
- Biosignal control, 8, 158
- BioTac fingertip sensor, 449 f , 451
- Biped robots, 493–494
- Bladder management, 326
- BLDC motor. *See* Brushless direct current motor (BLDC motor)
- BLEEX, 218, 221–222
- Blister generation method, 276
verification experiments for obtaining inherently safe region against
analysis for safety verification test, 279–280
experiments, 278–279
procedure, 276–277, 277 f
- Block-and-tackle torque amplifier mechanism, 48, 49 f
- BLUE SABINO
concept, 112–113
upper limb exoskeleton, 14
- Bluetooth, 430–431
- BMD. *See* Bone mineral density (BMD)
- BMS. *See* Battery management system (BMS)
- Body attachment, 432–433
- Body Weight-Supported Treadmill Training system (BWSTT system), 215–217
- Body-powered device, 378

Body-powered upper limb prostheses, 367

Bone mineral density (BMD), 208–210

BONES, 12

Bowden cable, 72, 155

Brain–computer interface, 446

Brain–machine interface, 16, 305 t , 459

BRAVO hand exoskeleton, 164

Brushless direct current motor (BLDC motor), 234, 403–404

Brute force algorithm, 194

“BTS SMART-suite” motion capture system, 183–185

BWSTT system. *See* Body Weight-Supported Treadmill Training system (BWSTT system)

C

- Cable-Actuated Dexterous Exoskeleton for Neuro-rehabilitation-7 (CADEN-7), 14, 67–68, 95
- CADEN-7. *See* Cable-Actuated Dexterous Exoskeleton for Neuro-rehabilitation-7 (CADEN-7)
- CAN. *See* Controller area network (CAN)
- Capacitive sensors, 451
- CAPIO (dual-arm exoskeleton), 16
- Capstan drive mechanism, 45, 48, 50 f
- Carbon fiber, 267, 470
- Carbon nanotubes (CNTs), 451
- Cardiovascular disease (CVD), 316
- Carnegie Mellon University (CMU), 257
ankle exoskeleton, 261–262
evolution, 268–269
control of any CMU emulator, 271
- Carpometacarpal joint (CMC joint), 150, 194
- Cartesian errors, 37, 38 f , 39 f
- Center of gravity (CoG), 240–241
- Center of mass (COM), 214, 290, 293 f
- Center of pressure (COP), 214, 290
- Chronic pain, 326
- Circular-prismatic joints, 153–154
- Classifiers, 382
- Clavicular link design, 124
- Clavicular translations, 126–128
- Claw-type single DOF hand, 98
- Clinical evidence, 305–308
early-stage feasibility and case studies, 307–308
randomized controlled trials, 308
- Closed-loop
neuroprosthesis control approaches, 350
operation mode, 435–437
synergy-based control system, 358–360
- CMA-ES. *See* Covariance Matrix Adaptation Evolution Strategy (CMA-ES)
- CMC joint. *See* Carpometacarpal joint (CMC joint)
- CMU. *See* Carnegie Mellon University (CMU)
- CNTs. *See* Carbon nanotubes (CNTs)
- Cochrane analysis, 305–306

- CoG. *See* Center of gravity (CoG)
- Collocated admittance control, 78, 79f
- COM. *See* Center of mass (COM)
- Commercial off the shelf components (COTS components), 395–397
- Communicator, 317–318
- Complete control system, 371, 373–374, 382
- Compliant topology exoskeletons, 154
- Compliant transmissions, 156
- Computer-aided drafting model, 122
- Computer Numerical Control (CNC) machining, 267
- Contact sensing, 426–427
- Continuous passive motion (CPM), 157
- Continuum robotic devices, 67
- Control, 7–8, 384
- algorithms, 99
 - bandwidth, 84
 - design, 28–35, 34f, 76–79
 - active assistive motion, 34–35
 - admittance control, 77–79
 - design of ISOTSMC, 30–34
 - direct torque control, 76–77
 - estimation of state of system, 28–29
 - uncertain estimation, 28
 - gains, 80
 - for hand exoskeleton systems, 157–158
 - law, 489, 493–494
 - optimization algorithms, 479
 - system of WalkON Suit
 - main functions, 240–244
 - processes of overall control system, 238–240
 - techniques, 348–349
 - unit of WalkON Suit, 235
- Controller area network (CAN), 422
- Conventional manual wheelchairs, 314–315
- Conventional powered exoskeletons, 336–337
- Conventional Prosthetic Controls Headstage (CPCH), 432
- Conventional SMC, 24
- COP. *See* Center of pressure (COP); Projection of COM (COP)
- Coriolis forces, 488–489
- Cortical control and feedback, 438–439
- Cortical signals, 447
- COTS components. *See* Commercial off the shelf components (COTS components)
- Covariance Matrix Adaptation Evolution Strategy (CMA-ES), 479
- CPCH. *See* Conventional Prosthetic Controls Headstage (CPCH)
- CPM. *See* Continuous passive motion (CPM)
- cRIO-9038 device, 235
- Crutches of WalkON Suit, 235
- Cuff motion reproduction, optimization for, 282–285
- Curving motion under limited DoF, 295–296
- motions required in daily living environment, 295
- natural curving motion and DoF, 295
- observation of compensation motion of DoF restriction, 296
- use of wearable robots, 297
- CVD. *See* Cardiovascular disease (CVD)
- Cyathlon, 366–367
- analysis, 246–247
 - Cyathlon 2016, 246
- Cyberhand* project, 366
- CYBERLEGs Alpha-Prototype, 221
- Cycloidal joint, 418
- D**
- Damped least squares (DLS), 34–35
- Damping mechanism, 339
- DARPA. *See* Defense Advanced Research Projects Agency (DARPA)
- Data analysis techniques, 222
- De facto standard active hand prosthesis, 368–369
- Defense Advanced Research Projects Agency (DARPA), 393
- Degree of activation, 365–367
- Degrees of freedom (DoFs), 2–4, 67, 91–92, 106, 133–134, 149, 194, 210–212, 287, 365–366, 445, 447–448
- control signal, 423–424
 - curving motion under limited, 295–296
 - 3-DOF shoulder, 110–111
 - 5-DOF
 - knee exoskeleton, 263
 - shoulder, 110–111
 - 6-DOF
 - CAD view of force feedback, 52f
 - endpoint control, 438
 - Virtuose 6D master arm, 45, 46f
 - shoulder exoskeleton with 2-DOF, 133–135
 - trajectories of 1-DOF finger mechanism joints, 179, 180f
- Demographics, 312
- Department of Industrial Engineering of the University of Florence (DIEF), 179, 180f
- Design
- for additive manufacturing, 269
 - for ergonomics, 183–184
 - lower-limb exoskeletons, 251
 - process of exoskeleton parts, 181f
 - of soft exosuit, 71–72
 - of WalkON Suit, 233f
- Design score*, 198–203
- Desired motion intention (DMI), 24–25
- Device control, 473
- DexoHand, 165
- Dexterity, 383–384
- Dexterous HMI, 377
- DGO. *See* Driven gait orthosis (DGO)

DIEF. *See* Department of Industrial Engineering of the University of Florence (DIEF)
 Digit mechanism, 193–194
 Dinamixel SDK library, 144–145
 DIP joint. *See* Distal interphalangeal joint (DIP joint)
 Direct torque control, 76–77
 evaluation, 79–83
 transparency, 80–83
 full-state feedback controller, 77, 78f
 optimal observer for estimation of joint torque, 76–77
 Displacement histograms, 122
 Distal anchor point, 72
 Distal interphalangeal joint (DIP joint), 150, 194
 DLS. *See* Damped least squares (DLS)
 DME. *See* Durable medical equipment (DME)
 DMI. *See* Desired motion intention (DMI)
 DoFs. *See* Degrees of freedom (DoFs)
 Driven gait orthosis (DGO), 216
 DSKM. *See* Dual-state knee mechanism (DSKM)
 Dual four-bar mechanism
 preliminary modeling, 118–120
 proof-of-concept mockup, 122–124
 Dual-arm training, 100
 Dual-state knee mechanism (DSKM), 338
 Durable medical equipment (DME), 320–321
 Dynamic control allocation, 348–349
 Dynamic postural synergies, 358–360
 Dynamic surface control technique, 353
 Dynamometers, 1

E

E-pacer, 353
 E-skins. *See* Electronic skins (E-skins)
 EAW. *See* Exoskeleton-assisted walking (EAW)
 “Echoing” leg dynamics, 476
 ECeG. *See* Electrocorticography (ECeG)
 Ecole de TechnologieSuprieure—Motion Assistive Robotic-exoskeleton for Superior Extremity (ETS-MARSE), 13, 25, 35–36
 dynamics, 25–27
 reference frames, 26f
 workspace of ETS-MARSE exoskeleton robot, 26t
 EEG. *See* Electroencephalography (EEG)
 Ekso, 303–304, 305f
 Eksovest from Ekso bionics, 15
 Elastomers, 68
 Elbow
 flexion, 7
 module, 404, 405f
 Elbow exosuit. *See* Soft exosuit
 Electric actuators, 472, 475
 Electric motors, 4–5, 154–155, 475
 Electrical activity, 157, 447

Electrocorticography (ECeG), 445–448, 449f
 Electroencephalography (EEG), 2, 7, 157, 445–447
 noninvasive electrode cap, 447f
 signals, 447–448, 449f
 Electromechanical delay (EMD), 353
 Electromyography (EMG), 7, 85, 157, 186, 288, 445–447, 478. *See also* Surface electromyography (sEMG)
 EMG-based control strategy, 477–478
 input systems, 430–431
 sensors, 266
 signals, 219, 439–440, 448, 449f, 477–478
 Electronic and control system, 143–145
 Electronic skins (E-skins), 453–454, 460–461
 Electrooculogram (EOG), 158
 Embedded sensors, 382
 EMD. *See* Electromechanical delay (EMD)
 Emergency, 244
 EMG. *See* Electromyography (EMG)
 EMY
 balance exoskeletons, 53
 dual-arm exoskeleton, 16
 End-effector
 end-effector–based systems, 105–106
 positions, 80, 80f
 robots, 11
 Energy
 economy, 470–471
 expenditure, 324
 sources, 222
 EOG. *See* Electrooculogram (EOG)
 Ergonomics, 183–185
 electronics and control architecture, 184
 mechanical design, 183–184
 testing and discussion, 185
 ESA. *See* European Space Agency (ESA)
 Ethylene-vinyl acetate (EVA), 72
 Euler angles, 134
 Euler–Lagrange equation, 488
 European Space Agency (ESA), 15
 EVA. *See* Ethylene-vinyl acetate (EVA)
 EVA gloves. *See* Extravehicular activity gloves (EVA gloves)
 Even neuron spikes, 445–446
 Event-based control algorithm, 350
 EXARM, 15
 EXO-UL series, 14
 EXO-UL1, 14, 92–94, 93f
 EXO-UL3, 14, 94–95, 95f
 EXO-UL7, 14, 95–96, 96f, 113–114, 113f
 EXO-UL8, 14, 96–99, 97f
 design approach, 113–114, 113f
 mechanism, actuation, and sensing, 98–99
 system architecture, 96–97
 ExoGlove, 159
 Exorn, 13

- Exoskeleton-assisted walking (EAW), 321–325
 simulation of normal physiological effects, 322–325
 energy expenditure, 324
 gait speed, 324–325
 ground reaction force, 325
 impact on QoL, 325
- Exoskeleton(s), 1, 45, 52–53, 67, 133, 207, 251, 318
 challenges, 329
 clavicle design and assembly, 124
 descriptions, 69–72
 emulator testbeds, 251–254
 emulator pros and cons, 252–254
 off-board components, 254
- exoskeleton–based systems, 105–106
- experimental setup, 79–81
- models, 73–76
- rationale for, 316
- results, 81–86
- robot development, 25, 91
- shoulder background, 106–111
 bilateral *vs.* unilateral shoulder designs, 111
 3-DOF *vs.* 5-DOF shoulder, 110–111
 state-of-the-art, 106–110
- systems, 92–99
- technologies, 301
 by construction, 304t
 control schemes for exoskeletons, 305t
 early designs, 301
 exoskeleton awakening, 302
 exoskeletons in development, 302–303
 FDA-approved devices, 303–304
 first prototypes (1961–73), 301–302
 new exoskeleton renaissance, 302
 by power source, 304t
 types, 303t
 users, 311–312
- Exosuits, 329
- Extravehicular activity gloves (EVA gloves), 166
- F**
- F/E. *See* Flexion and extension (F/E)
- Fabric material, 68
- Fall risk
 contact with environmental object
 motion in daily living environment and risk of collision, 292–295
 observation of reaction motion, 293–295
 during gait using wearable robot, 286–297
 mismatch between motion of wearable robot and wearer
 experimental setup, 289
 factors causing mismatch and risks, 288–289
 MALO, 290f
 methods detecting wearer’s intention, 288–292
- observation of reaction motion, 290–292
- Fast TSMC, 24
- Fast walking (FW), 496
- FDA. *See* Food and Drug Administration (FDA)
- Feedback linearization, 489
- FES. *See* Functional electrical stimulation (FES)
- Field programmable gate array (FPGA), 35–36
- Field-oriented control algorithms (FOC algorithms), 409
- Fine pinch grasp, 439–440
- Finger(s), 413–430
 contact sensing, 426–427
 cycloidal drive system, 418
 fingertip sensor v2, 429–430, 430f
 force sensing, 426
 hand software, 423–425
 heat flux sensing, 427–428
 hybrid fixed-linkage/differential, 414f
 mechanism, 177–178, 178f, 196
 MPL sensors, 425–426, 425f
 palm and finger abduction/adduction, 420–423, 421f
 thumb, 418–420, 419f
 vibration sensing, 427
- Fingertip sensor (FTS)
 electronics, 428
 v1, 426, 426f, 427f
 v2, 429–430, 430f
- Fingertip sensor node (FTSN), 423–424, 428
 board, 429f
- Finite State Machine, 353, 355f
- Finite time convergence, 31
 of sliding surface, 34
- Five-degrees of freedom (5-DOF)
 knee exoskeleton, 263
 shoulder, 110–111
- FIW. *See* Forward inflection walking (FIW)
- Flash-based FPGA, 422
- Flexible PCB, 429
- Flexion and extension (F/E), 150, 194, 395–397
- FMA. *See* Fugl-Meyer Assessment (FMA)
- FNS. *See* Functional neuromuscular stimulation (FNS)
- FOC algorithms. *See* Field-oriented control algorithms (FOC algorithms)
- Focal point, 414
- Food and Drug Administration (FDA), 303–304
- Force
 amplifier, 133
 control, 87
 force-based strategies, 158
 force-sensing resistors, 350
 myography, 371
 reflecting hand controller, 45, 48
 sensing, 426
 sensor, 350
 feedback, 35–36

torque
 control, 7
 sensors, 6–7, 98–99, 156–157

Forearm pronosupination actuator, 56, 59f

Forward inflection walking (FIW), 240–241, 246–247.
See also Exoskeleton-assisted walking (EAW)

Four-bar mechanism for remote positioning, 118. *See also*
 Dual four-bar mechanism

Fourier polynomial functions, 493

FPGA. *See* Field programmable gate array (FPGA)

Fractional order, 24

Frame design, 260–261

Free body diagrams, 255–256

Free motion, 23–24

FTS. *See* Fingertip sensor (FTS)

FTSN. *See* Fingertip sensor node (FTSN)

Fugl-Meyer Assessment (FMA), 99–100

Full-state feedback. *See also* Sensory feedback
 controller, 77, 78f
 joint torque–based interaction control, 76

Functional electrical stimulation (FES), 217, 315–316

Functional neuromuscular stimulation (FNS), 335–336
 powered exoskeletons and, 339–340

FW. *See* Fast walking (FW)

G

Gain scheduling method, 243–244

Gait, 336
 asymmetry, 469–470
 function impairment, 347
 patterns, 476–477
 generator control, 476–477
 restoration technologies, 337
 speed, 324–325
 stability, 238

Gait cycle (GC), 287, 487–488
 outlier, 496

GaitMaster, 215–216

GAITRite mat, 309

GC. *See* Gait cycle (GC)

General Electric, 302

Gentle/G system, 161–162

GENTLE/s system, 11

Glenohumeral joint (GH joint), 106–107

Global Lipschitz function, 27

Gloreha Sinfonia soft exoskeleton glove, 164

Graphical user interface (GUI), 188–190, 384

Gravitational forces, 488–489

Gravity compensation methods, 120

Ground reaction force sensors
 (GRF sensors), 214, 322–325

Gruebler’s equation, 118–119

GUI. *See* Graphical user interface (GUI)

H

H&E staining. *See* Hematoxylin and eosin staining (H&E staining)

HAL. *See* Hybrid assistive limb (HAL)

Hall sensor, 28–29

Hand design, 413

Hand disabilities
 ergonomics improvements, 183–185
 kinematic
 analysis and synthesis, 177–179
 chain assessment, 179–182
 portable tailor-made exoskeleton for, 177
 user-based actuation strategy, 185–190

Hand exoskeleton systems, 149–158, 151f, 193
 actuation, 154–155
 assistive hand exoskeletons, 158–160
 augmentation hand exoskeletons, 165–167
 control, 157–158
 mechanism, 150–154
 degrees of freedom, 150–152
 topology, 153–154

other exoskeletons
 by Fontana et al., 168
 by Jo et al., 168
 Rutgers Master II-New Design force-feedback glove, 168
 SKK Hand Master, 168
 by Stergiopoulos et al., 168

rehabilitation hand exoskeletons, 160–165
 sensing method, 156–157
 transmission, 155–156

Hand software, 423–425

Hand-Wrist Assisting Robotic Device (HWARD), 161

HandCARE, 149

HANDEXOS, 162

HandSOME, 149

Hannes Hand, 369

Haptic devices, 15, 133

HapticMASTER robot, 11

HapticWalker, 215–216

Harmonic drive (HD), 71

HARMONY dual upper-limb exoskeleton, 107–110

Harvard Biodesign Lab, 255

Harvard soft exoskeleton, 302–303

HC. *See* Heel contact (HC)

HD. *See* Harmonic drive (HD)

Heart rate (HR), 324

Heat flux sensing, 427–428

Heel contact (HC), 287

Heel strike, 220

HELIOS software, 35–36

Hematoxylin and eosin staining (H&E staining), 276–277

Hercule Slim exoskeletons, 53

Hertz theory, 279

- HEX. *See* Hybrid EXoskeletons (HEX)
- HEXORR, 163
- HEXOSYS-I, 164
- High-activity switching gain, 24
- High-level controls, 433–434, 434f
- Hill-based model, 349
- Hill-type muscle model of ankle behavior, 477–478
- Hip
- angle, 492–493
 - joint on contralateral limb, 469
- Hip-knee-ankle-foot orthosis (HKAFO), 336
- HMI. *See* Human Machine Interface (HMI)
- HNP. *See* Hybrid neuromprosthesis (HNP)
- Hooke's law, 137
- HR. *See* Heart rate (HR)
- HS-5495BH High-Torque Servo from Hitec, 184
- HUMAC NORM, 1
- Human augmentation, 5, 68–69
- Human digits modeling, 194–195
- Human locomotion, 491–493, 503
- Human Machine Interface (HMI), 94, 377
- Human–exoskeleton interaction, 222
- Human–prosthesis integration, 479–480
- Human–robot interaction, 67, 76, 177, 377–378
- Humeral rotator module, 404, 405f
- HWARD. *See* Hand-Wrist Assisting Robotic Device (HWARD)
- HX hand exoskeleton, 160
- Hybrid assistive limb (HAL), 9, 219, 302–304
- Hybrid EXoskeletons (HEX), 347–348, 351–352, 360
- state-of-the-art systems for restoration of walking, 337–342
 - technologies to restore walking, 335–337
- Hybrid neuromechanical systems, 337
- Hybrid neuromprosthesis (HNP), 337–339, 353
- testbed, 353, 357
- Hybrid technology, 347–348
- Hybrid wearable robotic exoskeletons
- advances in hybrid wearable technologies, 348–350
 - case study, 352–360
 - inputs to all of system inputs, 359f
 - results, 356–357
 - root mean squared of input voltage, 359t
 - sequence of photos, 356f
 - synergy-based control system, 358–360
 - challenges and future directions, 360–361
 - clinical and usability factors, 351–352
 - modeling approaches for control, 349–350
 - potential future technologies, 350–351
- Hybrid-selective soft robots, 351
- Hydraulic
- actuators, 5, 472
 - damping mechanism, 339
- I**
- i-LIMB Revolution, 369
- Ideal HMI, 383–384
- IFT. *See* Iterative feedback tuning (IFT)
- iHandRehab, 163
- IJL. *See* Individual joint/link (IJL)
- Illusory movements, 458
- Imaginary limb, 367–368
- Impedance control, 7, 216, 476–477
- Implantation
- microelectrode arrays, 458
 - powered exoskeletons and implanted FNS, 340
 - technology, 370
- IMU. *See* Inertial measurement unit (IMU)
- In-shoe pressure-mapping system, 325
- Incremental learning, 372
- Incremental machine learning, 385
- Indego, 303–304, 305f
- Individual joint/link (IJL), 412
- Inertia matrix, 27
- Inertial measurement unit (IMU), 214, 235–236, 350, 381, 430–431, 453
- Injury, 23
- InMotionArm. *See* Interactive Motion Technologies (InMotionArm)
- Institutional Review Board (IRB), 495
- Integral second-order terminal sliding mode controller (ISOTSMC), 24–25, 27–28
- design, 30–34
- IntelliArm, 12
- Intent detection, 368, 387
- Interaction forces, 69
- Interactive machine learning, 372
- Interactive Motion Technologies (InMotionArm), 10
- International space station (ISS), 15
- Interphalangeal joint (IP joint), 150, 194
- Intramuscular EMG sensors, 380
- Intuitive HMI, 377
- Intuitiveness, 383–384
- IOTA. *See* Isolated Orthosis for Thumb Actuation (IOTA)
- IP joint. *See* Interphalangeal joint (IP joint)
- iPAM system, 11
- IRB. *See* Institutional Review Board (IRB)
- ISO. *See* Isotropy (ISO)
- ISO 13482 standard, 275
- ISO/technical report (ISO/TR), 275
- ISO/TR. *See* ISO/technical report (ISO/TR)
- Isolated Orthosis for Thumb Actuation (IOTA), 163
- Isotropy (ISO), 198–199
- ISOTSMC. *See* Integral second-order terminal sliding mode controller (ISOTSMC)
- ISS. *See* International space station (ISS)

Iterative feedback tuning (IFT), 283, 286
 Iterative learning-based algorithms, 350
 Izhikevich neuron model, 457

J

Jacobian of robot, 140
 Johns Hopkins University Applied Physics Laboratory (JHU/APL), 393, 445
 Joint
 contracture, 236–238
 design, 262–263
 joint-torque control law, 77
 motions, 106
 trajectory generation, 240–241

K

KAF powered exoskeleton. *See* Knee–ankle–foot powered exoskeleton (KAF powered exoskeleton)
 KAFO braces. *See* Knee–ankle–foot–orthosis braces (KAFO braces)
 Kalman filters, 448
 Keeogo, 302–303
 Key grasp, 439–440
 KINARM robotic system, 11–12
 Kinematic
 analysis and synthesis, 177–179
 chain assessment, 179–182
 electronics and control architecture, 182
 mechanical design, 181–182
 testing and discussion, 182
 model, 139
 optimization strategy, 194
 Kinesis, 340, 348
 Kinesthetic illusion, 458
 Kinetic energy of system, 140
 “Kinovea” software, 181–184
 Kirchhoff’s voltage law, 144
 Knee exoskeletons, 258, 271
 end-effector utilizes hard stops, 257
 Knee joint
 contracture, 236–237
 trajectories, 494, 494f
 Knee–ankle–foot powered exoskeleton (KAF powered exoskeleton), 340
 Knee–ankle–foot–orthosis braces (KAFO braces), 237–238, 307–308, 315, 336
 Kutzbach criterion, 118–119

L

L-Exos, 12
LabVIEW interface, 35–36
 Lagrangian equation, 141
 Large motor controller (LMC), 404, 406f. *See also* Small motor controller (SMC)
 LC. *See* Limb controller (LC)
 LDO. *See* Linear regulator power supply (LDO)
 Lead-zirconate-titanate pastes (PZT pastes), 451
 Leg braces, 315
 Levenberg–Marquardt stabilization, 34–35
 Limb controller (LC), 399
 breakout interconnect board, 423f
 electronics, 422
 software, 423–424
 Linear control, 142
 Linear discriminant analysis, 448
 Linear regression, 448
 Linear regulator power supply (LDO), 428
 Linear torque amplification, challenge of, 45–52
 Link length evaluation, 201–203
 Lithium polymer batteries, 411
 LMC. *See* Large motor controller (LMC)
 Load-carrying quasi-passive lower limb exoskeleton, 219
 Locomotion, 251, 258, 487
 amputee, 500–501
 human, 503
 leg, 217
 mode, 240
 nonsteady-state, 271–272, 496–497
 recovery of, 311
 tasks, 472
 Logic switch, 496
 LokoHelp, 215–216
 Lokomat, 302, 305–306
 Low-level motor driver, 79
 Lower limb amputation, 469
 individuals with, 469
 Lower limb exoskeletons, 207
 actuation of, 221–222
 assistive exoskeletons, 208–215, 209f
 augmentation exoskeletons, 213t, 217–221
 assistance applied on users, 256–260
 assistance directly applied to tasks, 255–256
 control, 269–271
 of any CMU emulator, 271
 development, 208f
 exoskeleton emulator testbeds, 251–254
 future for, 222
 making strides in future, 271–272
 mechanical design of onboard components, 255–269
 ankle exoskeleton end-effector designed for low forces and safety, 258–260
 Carnegie Mellon University’s ankle exoskeleton, 261–262
 5-degree-of-freedom knee exoskeleton, 263
 frame design, 260–261
 Joint design, 262–263

- Lower limb exoskeletons (*Continued*)

knee exoskeleton end-effector utilizes hard stops, 257

loading analysis, 255–256

materials and manufacturing, 267–269

physical interfaces, 256–260

safety stops, 256–257

sensing, 264–266

series elasticity for improved torque tracking, 266

straps, 257–258

rehabilitation exoskeletons, 211_t, 215–217

 rehabilitation with weight support, 215–216

 rehabilitation without weight support, 217

untethered systems, 254–255
- Lower limb orthoses, 336
- Lower limb prosthetic devices, 470–472

 future directions, 479–480

 systems, 472–479

 control approaches, 476–479

 mechanical configuration and actuation approaches, 472–475
- LTMRs. *See* A_δ-and C-low-threshold mechanoreceptors (LTMRs)
- Luke Arm, 369, 381
- Lyapunov function, 30–33, 141–142
- Lyapunov stability, 141
- Lyapunov-based control design approaches, 358–360
- M**
- m. extensor digitorum superficialis*, 367, 379
- m. flexor digitorum superficialis*, 367, 379
- MA23 (electric servomanipulator), 45, 48
- Machine learning, 372, 382–383, 448
- MagEnc V3.0 Low Rev, 184
- Magnetic tactile sensors, 453
- MALO. *See* Motor-Actuated Lower-limb Orthosis (MALO)
- Man-Amplifier Project, 301–302
- Maryland-Georgetown-Army exoskeleton (MGA)

 exoskeleton, 12, 107
- Mass/inertia forces, 488–489
- Master device, 133
- Master/slave system, 8, 157–158
- Matched axe exoskeletons, 153
- Matlab Real Time Workshop, 423–424
- MATLAB Simulink, 144
- Maximum likelihood estimation, 448
- Maxon DC brushed motors, 98
- MC. *See* Microcontroller (MC)
- McBSP. *See* Multichannel buffered serial ports (McBSP)
- McKibben artificial muscle, 474
- MCP joint. *See* Metacarpophalangeal joint (MCP joint)
- MCS. *See* Mental Health Component Summary (MCS)
- Mechanical reversibility/irreversibility, 46–48, 48_t
- Mechanical springs, 470
- Mechanical torque amplification on servomanipulators, 48–52
- Mechanism design, 1, 149–150
- Mechanism isotropy, 198–199
- Mechanism optimization, 181–182
- Mechanomyography, 380–381
- Mechanoreceptors, 450
- MEDARM function. *See* Motorized Exoskeleton Device for Advanced Rehabilitation of Motor function (MEDARM function)
- Meissner corpuscles, 450
- MEMSs. *See* Microelectromechanical systems (MEMSs)
- Mental Health Component Summary (MCS), 308
- Merkel cells, 450
- Metacarpophalangeal joint (MCP joint), 150, 178, 194, 416
- MGA exoskeleton. *See* Maryland-Georgetown-Army exoskeleton (MGA exoskeleton)
- Michelangelo hand, 369, 395–397
- Microcontroller (MC), 428
- Microelectromechanical systems (MEMSs), 451
- MIME robotic system, 11
- MindWalker, 214–215
- Mini DisplayPort of cRIO-9038, 235
- Minimum Jerk Trajectories (MJT), 81
- MIT Anklebot, 252
- MIT-MANUS, 10
- MJT. *See* Minimum Jerk Trajectories (MJT)
- MNP. *See* Motor neuro-prosthetics (MNP)
- Mobile WebApp interface, 437, 437_f
- Mobility equation, 118–119
- Model-based approaches, 349
- Modeling, 99–100

 approaches for control, 349–350

 human digits, 194–195

 shoulder exoskeleton, 139–141

 3R planar mechanisms, 197
- Modified Ashworth scale, 327
- Modified Denavit–Hartenberg Parameters, 25, 27_t
- Modular prosthetic limb (MPL), 369, 381, 383, 393, 400–433, 445
- APL’s collaborating institutions in the revolutionizing prosthetics program, 395_t
- application selection and uses

 amputees, 439–440

 cortical control and feedback, 438–439

 Robo Sally, 440–441
- architecture overview, capabilities, and features, 399–400, 399_f

 selection of MPL v3 performance specifications, 400_t

 auxiliary subsystems, 430–433

 battery and wrist quick release, 410–411, 410_f

 challenging high-level requirements influencing design, 394_f

- early development, 394–398
MPL v1 System, 397*f*
 Phase 1, 395–397, 396*f*
 Phase 2, 397–398
 Phase 3, 398
 fingers, 413–430
 full bilateral shoulder level control, 439*f*
 hand design, 413
 high-level controls, 433–434, 434*f*
 Humeral rotator, 405*f*
 LMC interaction with other MPL system modules, 406*f*
 UA, 401–404
 upper arm software, 412–413
 v2 socket-based attachment strategy, 432*f*
 VIE, 435
 vMPL, 435, 436*f*
 VulcanX and OCU, 434
 web interface, 435–437
 wrist
 design, 401, 404–410
 electronics board topology, 409*f*
 motor controller, 408*f*
- Motion
 control algorithms, 242
 intent detection control, 477–478
 shoulder range of motion requirements estimation, 114–116, 122
 tracking, 387
- Motor
 control, 1, 435
 loop, 339
 neural, 397–398
 cortex, 438
 neuroprostheses, 350–351
- Motor neuro-prosthetics (MNP), 347
- Motor-Actuated Lower-limb Orthosis (MALO), 289, 290*f*
- Motorized Exoskeleton Device for Advanced Rehabilitation of Motor function (MEDARM function), 13
 6-DOF exoskeleton, 107
- Motorized exoskeletons, 339–340
- Motorized upper limb orthotic system (MULOS), 9
- Movement
 decoding, 446, 448–449
 signals, 447–448
- MPL. *See* Modular prosthetic limb (MPL)
- MS. *See* Multiple sclerosis (MS)
- MULOS. *See* Motorized upper limb orthotic system (MULOS)
- Multarticulated prosthetic hands, 446–447
- Multichannel buffered serial ports (McBSP), 423
- Multilayered e-dermis, 454
- Multiple joints model, 74–75
- Multiple sclerosis (MS), 303–304, 329, 342
- Muscle
 fatigue estimator, 348
 muscle-first approach, 340
 synergy inspired control framework, 352
 weakness, 91
- Myo, 432–433
 Myoband, 430–431
 “Myoelectric” control, 367
 Myomo e100 NeuroRobotic System, 1–2
- MyoPro systems, 1–2, 9
- Myoprocessor, 94
- MyoWare Muscle Sensors, 186
- N**
- Natural control, 370–371
 Natural curving motion and required degree of freedom, 295
 Natural myocontrol, 384
 Natural tactile sensations, 455–457
 Natural transitions, 478
 NeReBot, 10
 Neural control, 143
 Neural fusion unit (NFU), 430–431
 Neural networks, 143, 448
 Neural signal recording techniques, 460
 Neural stimulation technology, 335–336, 339
 NEUROExos, 67–68
 Neuromechanical systems, 67–68
 Neuromorphic systems, 337
 Neuromuscular stimulation (NMES), 347
 Neuron spiking, 449*f*
 Neurorehabilitaion, 12
 New exoskeleton renaissance, 302
 NFU. *See* Neural fusion unit (NFU)
 NI-PXI 8081 controller card, 35–36
 NMES. *See* Neuromuscular stimulation (NMES)
 Noninvasive feedback, 459
 Nonlinear control techniques, 24
 Nonlinear dynamical system, 489
 Nonlinear model, 142
 Nonnatural control, 384
 Nonpatient-specific requirements, 385
 Nonsingular TSMC, 24
 Normal walking (NW), 496
 NRS. *See* Numeric rating scale (NRS)
 nth-order differentiator, 28–29
 Numeric rating scale (NRS), 327
 NW. *See* Normal walking (NW)
- O**
- O/R. *See* Opposition and reposition (O/R)
- OCU. *See* Operator control unit (OCU)
- Off-board components, 254
- OFX. *See* Open Fingerpad eXoskeleton (OFX)

- OI. *See* Osseointegration (OI)
- One-degrees of freedom (1-DOF)
- One-motor finger (1MF), 414
 SMC, 417f
- Open Fingerpad eXoskeleton (OFX), 159
- Operator control unit (OCU), 398, 434
- Opioids, 313
- Opposition and reposition (O/R), 150, 194
- Optical myography, 380–381
- Optical recognition, 380–381
- Optical tactile sensors, 453
- Optimal kinematic design of link lengths of hand exoskeleton exoskeleton topology, 195–197
link length evaluation, 201–203
method, 194–200
modeling
 human digits, 194–195
 3R planar mechanisms, 197
optimization algorithm, 197–200
physical prototype evaluation, 201
prototype workspace evaluation, 203
simulation results, 200
- Optimal observer for estimation of joint torque, 76–77
- Optimization
algorithm, 197–200
for cuff motion reproduction, 282–285
- Orthoses, 336
- Osseointegration (OI), 380, 449–450
- Other exoskeletons
for upper limb exoskeletons
 CAPIO, 16
 EMY, 16
 EXARM, 15
 SAM, 16
 SARCOS Dextrous Arm, 16
 SARCOS Master Arm, 16
 X-Arm-2, 16
- Ottobock Empower. *See* BiOM
- Outlier gait cycles, 496
- Overconstrained mechanism, 119–120
- P**
- Pacinian corpuscles, 450
- Package-on-package (PoP), 422
- Palm and finger abduction/adduction, 420–423, 421f
- PAM. *See* Pelvic Assist Manipulator (PAM)
- Pancake coil brushless DC actuators, 98
- Parallel remote inclusion of shoulder mobility (PRISM), 111
 BLUE SABINO concept, 112–113
conceptual design of remote biomimetic shoulder module, 116–120
- EXO-UL8 design approach, 113–114
- exoskeleton shoulder background, 106–111
final design, 126–128
gravity compensation methods, 120
methods, 111–120
rehabilitation robotics, 105–106
results, 120–128
shoulder range of motion requirements estimation, 114–116
- Parallelogram mechanisms, 153–154
- Paraplegia, SCIs result in, 335
- Paraplegics, powered exoskeleton for, 231
- Parkinson’s disease, 329
- PARM. *See* Pneumatic artificial rubber muscles (PARM)
- Partial feedback linearization, 493–494
- Passive assistive motion, results of, 37
- Passive motion, 157
- Passive physical therapy, 23–24
- Pathological gaits, 500–501
- Patient selection, 320–321
- Patient tolerance, 321–322
- “Patient-cooperative” strategy, 216
- Patient-specific requirements, 385
- Pattern
 matching, 371
 recognition, 370, 379–380, 382
 algorithms, 478
- PD controller, 494
- PDMS. *See* Polydimethylsiloxane (PDMS)
- Pelvic Assist Manipulator (PAM), 215–216
- Pelvic band, 318
- Penn scale to assess spasticity and global impression of change (PGIC), 327
- PEPSCI. *See* Powered exoskeletons in persons with SCI (PEPSCI)
- Peripheral signals, 447
- Personal care robots, 275
- PGIC. *See* Penn scale to assess spasticity and global impression of change (PGIC)
- PGO. *See* Powered gait orthosis (PGO)
- Phantom hand, 458
 sensory mapping of, 456f
- Phantom limb, 367–368
- Phase variable, 487–490. *See also* Transfemoral powered prosthetic leg control
algorithm, 490–493, 501
 output, 498f
transfemoral powered prosthetic leg control using, 493–505
 for variable incline trial, 503f
 for variable speed trial, 502f
- pHRI. *See* Physical human–robot interaction (pHRI)
- Physical assistant robot safety
 contact safety, 275–286
 curving motion under limited DoF, 295–296
 fall risk during gait using wearable robot, 286–297

- V&V test procedure, 276
- Physical human–robot interaction (pHRI), 1
- Physical MPL, 434
- Physical prototype evaluation, 201
- Physical stress hazards, 275–276
- Physical therapy, 23
- Physiotherapy, 133
- PID controllers. *See* Proportional, integral, derivative controllers (PID controllers)
- Piecewise phase variable algorithm (PW phase variable algorithm), 490–491, 491f, 502–503
- Piezoelectric materials, 451
- Piezoresistive materials, 451
- textiles, 449f
- Pilot, 236–237
- PIP joint. *See* Proximal interphalangeal joint (PIP joint)
- “PIP-stop” linkage, 415
- Pitch, 134
- Planetary thumb joint, 418
- Plantarflexion, 342
- Plug-and-play devices, 503–505
- Pneumatic actuators, 5, 155, 207–208, 474
- cylinders, 474
- actuators, 474
- robots, 454
- Pneumatic artificial rubber muscles (PARM), 167
- Point-in-polygon algorithm, 188
- Polydimethylsiloxane (PDMS), 451
- Polyurethane covers, 421
- Polyvinylidene fluoride (PVDF), 426–427, 451
- PoP. *See* Package-on-package (PoP)
- Portable devices, 69
- Position
- position-sensing approach, 408–409
 - position/velocity control, 7
 - sensors, 6, 98–99, 156
- Posterior parietal cortex (PPC), 439
- Potential energy of robot, 140–141
- Power
- grasp, 439–440
 - transmission approaches, 6
- Powered exoskeletons, 301–302, 314, 336–337
- CoG in, 240–241
- and functional neuromuscular stimulation, 339–340
- and implanted functional neuromuscular stimulation, 340
- for paraplegics, 231
- race in Cybathlon 2016, 231
- safety and usability of, 237–238
- WalkON Suit, 247–248
- Powered exoskeletons in persons with SCI (PEPSCI), 308
- Powered gait orthosis (PGO), 324
- Powered prosthetic legs, 487, 495f. *See also* Transfemoral powered prosthetic leg control
- PPC. *See* Posterior parietal cortex (PPC)
- Predefined joint dynamics, 476
- “Predictable” three-joint curling, 415
- Pressure and flexion sensors, 454
- PRISM. *See* Parallel remote inclusion of shoulder mobility (PRISM)
- Projection of COM (COP), 220
- Pronosupination (PS), 110
- Proof-of-concept wood mockup, 122, 124f
- Proportional, integral, derivative controllers (PID controllers), 142, 144–145, 350, 412–413
- Proportional force/velocity control, 367–368
- Proprioception, 457–458
- Prosthesis
- control, 446–450, 449f, 460
 - movement decoding, 448–449
 - movement signals, 447–448
 - state of the art, 450
 - TMR and OI, 449–450
 - development, 480
 - fit and comfort, 446
 - joint torque, 476
- Prosthetic(s)
- arm system, 393
 - hands, 445
 - augmented reality training, 460
 - multiarticulated, 446–447
 - prosthesis control, 446–450, 449f, 460
 - prosthetic sockets, 460
 - rudimentary, 445
 - sensors and e-skins, 460–461
 - sensors for, 450–454, 452f
 - sensory feedback, 454–459, 455f, 461
 - one-degree-of-motion grippers, 379
 - sockets, 460
- Prototype workspace evaluation, 203
- Proximal interphalangeal joint (PIP joint), 150, 194
- PS. *See* Pronosupination (PS)
- PVDF. *See* Polyvinylidene fluoride (PVDF)
- PW phase variable algorithm. *See* Piecewise phase variable algorithm (PW phase variable algorithm)
- PZT pastes. *See* Lead-zirconate-titanate pastes (PZT pastes)
- Q**
- Qt4 development environment, 144
- Quality of life (QoL), 311, 313
- EAW impact on, 325
- Quasi-TDE, 24–25
- “Quasianthropomorphic” kinematics, 168

R

Race simulation training, 246

Radial base function neural network, 143

Radio frequency identification (RFID), 159

Randomized controlled trials, 306, 308

Range of motion (ROM), 107, 163, 182, 236–237, 287

Rapidly adapting, 450

Raspberry Pi, 435

Raytheon XOS, 219

Reaction motion against trigger for falling, 287–288

Real-time

- phase variable algorithm for control applications, 490–493, 490f

- PW phase variable algorithm, 490–491, 491f
- unified phase variable algorithm, 490–493, 492f

risk assessment and management, 243

target machine, 353

Recalibration, 372

- procedure, 383

Reciprocal adaptation, 372

Reciprocating gait orthosis (RGO), 210–212, 336

Recovery

- of locomotion, 311

- of walking function, 314

Recupera-Reha system, 13–14

Reduced order control (ROC), 423–424

Redundancy

- redundant linkage topology, 154

- resolution, 99

Reference trajectory, 81

Reha-Digit, 149

Rehab-Exos, 67, 69–71, 70f, 73–75

- mechanical design, 70–71

- multiple joints model, 74–75

- single joint model, 73, 73f

Rehabilitation, 1–2, 149–150

- field, 487–488

- robotics, 105–106

- clinical evidence, 305–308

- exoskeleton technologies, 301–304

- future, 309

- of walking, 347

Rehabilitation exoskeletons, 207, 211t, 215–217

- rehabilitation with weight support, 215–216

- rehabilitation without weight support, 217

Rehabilitation hand exoskeletons, 160–165

- by Abdallah et al., 165

- by Agarwal et al., 164

- by Arata et al., 163

- ATX, 163

- BRAVO hand exoskeleton, 164

- DexoHand, 165

- by Ferguson et al., 165

Gentle/G, 161–162

HANDEXOS, 162

HEXORR, 163

HEXOSYS-I, 164

HWARD, 161

iHandRehab, 163

IOTA, 163

by Kawasaki et al., 162

by Rahman et al., 163

Sinfonia, 164

by Tong et al., 162

by Wege et al., 162

by Zhang et al., 164

Rehabilitation robots, 23. *See also* Wearable robots

characterization of system rehabilitation, 25–27

comparative study, 37–39

control

- design, 28–35

- inputs, 38f, 40f

controller parameters, 37t

ethics statement, 42

experiment setup, 35–36

experimental architecture with humans, 36f

results

- of active assistive motion, 39–41

- of passive assistive motion, 37

torque input of active rehabilitation task, 41f

workspace

- tracking of robot, 40f

- trajectories of robot, 39f

Rehabilitation upper limb exoskeletons, 10–14

ACT^{3D} robotic system, 11

ARM Guide, 10

ARMin III, 12

Bi-Manu-Track system, 11

BONES, 12

ETS-MARSE, 13

EXO-UL series, 14

Exorn, 13

GENTLE/s system, 11

IntelliArm, 12

iPAM system, 11

KINARM, 11–12

L-Exos, 12

MEDARM function, 13

MGA exoskeleton, 12

MIME, 11

MIT-MANUS, 10

NeReBot, 10

Recupera-Reha system, 13–14

RehaBot, 13

ReoGo therapy system, 11

RUPERT IV, 13

SRE, 13

- RehaBot, 13
- RehaStim eight-channel stimulator, 353
- Remote actuation, 473
- Remote biomimetic shoulder module
- adjustment-free biomimetic clavicle, 117–118
 - conceptual design of, 116–120
 - dual four-bar mechanism preliminary modeling, 118–120
 - four-bar mechanism for remote positioning, 118
- Remote control communicator, 317–318, 317*f*
- ReoGo therapy system, 11
- Restorative springs, 156
- ReStore exosuit design, 330–331, 330*f*
- Restore walking
- current state-of-the-art systems for, 337–342
 - ease of use and cosmesis, 341–342
 - HNP, 337–339
 - need for speed, 340–341
 - other applications of hybrid systems, 342
 - powered exoskeletons and FNS, 339–340
 - powered exoskeletons and implanted FNS, 340
 - function, 311
 - technologies to, 335–337
 - FNS systems, 335–336
 - lower limb orthoses, 336
 - powered exoskeletons, 336–337
- Reversibility, 46–47, 48*t*
- Reversibilization, 47–48
- Review, 1, 115, 149, 305–306, 308, 322, 324, 326, 348, 380–381, 469
- Revolutionizing Prosthetics program, 369, 393–394
- Revolutions per minute (RPM), 234
- ReWalk, 214, 303–304
- device, 255
 - personal system, 311
 - product summary, 317–320
 - communicator, 317–318
 - components and specifications, 317
 - exoskeleton, 318
 - levels of patient training, 320
 - system configuration, 318
 - video links, 318–319
 - waist pack, 318, 319*f*
- REX (lower limb exoskeleton), 215
- RexRehab, 303–304
- RFID. *See* Radio frequency identification (RFID)
- RGO. *See* Reciprocating gait orthosis (RGO)
- Rheometer, 276–277
- Rigid exoskeleton, 70–71
- Rigid links robotic solutions, 68–69
- Rigid wearable robots, 69
- Ring oscillators, 454
- RISE controller. *See* Robust Integral of Sign of Error controller (RISE controller)
- Risk management strategies in WalkON Suit, 234
- RMSE. *See* Root mean square error (RMSE)
- RMSVs. *See* Root mean squared voltages (RMSVs)
- Robin H1, 214
- Robo Sally, 440–441
- RoboGlove, 167
- Robot(s), 377–378
- with compliant joints connecting rigid links, 67
 - transparency, 23–24
- Robotic Upper Extremity Repetitive Trainer IV (RUPERT IV), 13
- Robotic(s), 105
- assistance strategies, 23–24
 - exoskeletons in rehabilitation, 315, 347
 - clinical evidence, 305–308
 - future, 309
 - technologies, 301–304
- leg prosthesis, 470–471
- manipulators, 91
- systems control, 269–271
- Robust control approaches, 351
- Robust Integral of Sign of Error controller (RISE controller), 355
- ROC. *See* Reduced order control (ROC)
- ROM. *See* Range of motion (ROM)
- Root mean square error (RMSE), 81, 83, 357
- Root mean squared voltages (RMSVs), 357
- RPM. *See* Revolutions per minute (RPM)
- Rubber hand effect, 377–378
- Rudimentary prosthetic hands, 445
- Ruffini endings, 450
- RUPERT IV. *See* Robotic Upper Extremity Repetitive Trainer IV (RUPERT IV)
- Rutgers Master II-New Design force-feedback glove, 168

S

- SA. *See* Slowly adapting (SA)
- SAEs. *See* Serious adverse events (SAEs)
- Safe ambulatory function, 321–322
- Safe mode, 238–240
- Safety verification test, analysis for, 279–280
- Salford Rehabilitation Exoskeleton (SRE), 13
- SAM. *See* Sensoric Arm Master (SAM)
- SARCOS Dextrous Arm (SARCOS DA), 16
- SARCOS series, 1–2
- SARCOS Guardian GT system, 15
 - SARCOS Guardian XO exoskeleton, 15
 - SARCOS Master Arm, 16
- Savox SH-0254 servomotors, 182
- SC synovial joint. *See* Sternoclavicular synovial joint (SC synovial joint)
- Scapulohumeral rhythm, 107
- Scapulothoracic joint (ST joint), 106–107
- SCI. *See* Spinal cord injury (SCI)

- SCOPE. *See* Spinal Cord Outcomes Partnership Endeavor (SCOPE)
- Screw-and-cable-system (SCS), 45
- actuator basic principle, 50f
 - backdrivability, 46–48
 - mechanical
 - reversibility/irreversibility, 46–48
 - torque amplification on servomanipulators, 48–52
 - mechanism, 45–52
 - torque transfer
 - linearity, 46–48
 - of SCS and filtering effect, 51f
- SCRIPT device, 149
- SCS. *See* Screw-and-cable-system (SCS)
- SEA. *See* Series elastic actuators (SEA)
- Second-order robust exact differentiator, 28–29
- Second-order sliding mode controller (SOSMC), 24
- Second-order terminal sliding mode control (SOTSMC), 24
- Self-contained HNP, 339
- Self-locking, 46–47
- Self-powered upper limb prostheses, 366–367
- sEMG. *See* Surface electromyography (sEMG)
- Semiactive devices, 470
- Sensing method, 6–7, 264–266
- for hand exoskeleton systems, 156–157
- Sensor(s), 460–461
- and bodily signals, 379–381
 - for prosthetic hands, 450–454, 452f
 - sensing devices, 451–453
 - sensing in biology, 450–451
 - state of the art, 453–454
 - sensor-based approaches, 350
 - system of WalkON Suit, 235–236
 - encoders, 236f
- SensorHand Speed*, 379
- Sensoric Arm Master (SAM), 16
- Sensory feedback, 387, 446, 454–459, 455f, 461. *See also* Full-state feedback
- pain, 457
 - proprioception, 457–458
 - state of the art, 458–459
 - tactile sensations, 454–457
- Series elastic actuators (SEA), 2, 5, 13, 67–68, 155, 207–208, 475
- Series elasticity for improving torque tracking, 266
- Serious adverse events (SAEs), 321
- Service robots, 275
- Servomanipulators, mechanical torque amplification on, 48–52
- Servomotors, 144
- SF-36 (patient-reported measure of health status), 327
- SHAP. *See* Southampton Hand Assessment Procedure (SHAP)
- Shoulder
- complex, 106–107, 108f
- exoskeleton, 136f
- with 2 degrees of freedom, 133–135
 - control for exoskeleton, 141–143
 - design, 135–139
 - electronic and control system, 143–145
 - experimental results, 145–147
 - on human, 137f
 - modeling, 139–141
- range of motion requirements estimation, 114–116, 122
- ShoulderX from SuitX, 15
- Shut-down mode, 240
- Signal processing, 382–383
- Simply roll, 134
- Simulink, 353
- Sinfonia, 164
- Single joint model, 73, 73f
- Sit-to-stand motion (STS motion), 350
- Six-degrees of freedom (6-DOF)
 - CAD view of force feedback, 52f
 - endpoint control, 438
 - Virtuose 6D master arm, 45, 46f
- Skil Mate, 166
- Skin abrasion, 275
- SKK Hand Master, 168
- Sliding mode control(ler) (SMC), 24, 142–143
- Sliding surface, 142
- Slow walking (SW), 496
- Slowly adapting (SA), 450
- SMA. *See* Spinal Muscular Atrophy (SMA)
- Small motor controller (SMC), 416, 423–424. *See also* Large motor controller (LMC)
 - electronics hardware block diagram, 417f
 - software, 425
 - thumb, 418, 420f
- Smart recurrent recalibration schema, 381
- Smart Shoes system, 236
- SMC. *See* Sliding mode control(ler) (SMC); Small motor controller (SMC)
- Socket, 368, 382
- Soft exoskeletons, 222, 350–351
- Soft exosuit, 70–72, 75–76. *See also* WalkON Suit
 - for assistance of elbow joint, 72f
 - design, 71–72
 - planar model of tendon routing, 75f
 - for shoulder, 68
- Soft materials, 68
- Soft robotics, 67
- Soft wearable robots, 69
- SoftHand*, 369
- SolidWorks model, 122, 124f
- SOM. *See* System-on-module (SOM)
- Somatosensory cortex, 438
- Sonomyography, 380–381
- SOSMC. *See* Second-order sliding mode controller (SOSMC)

- SOTSMC. *See* Second-order terminal sliding mode control (SOTSMC)
- Southampton Hand Assessment Procedure (SHAP), 448–449
- SPARKy prosthesis. *See* Spring Ankle with Regenerative Kinetics prosthesis (SPARKy prosthesis)
- Spasticity, 326–327
- Spherical joints in robotics, 133–134
- Spinal cord injury (SCI), 208–210, 231, 303–304, 307, 311, 328, 335
burden of, 312–314
- Spinal Cord Outcomes Partnership Endeavor (SCOPE), 306
- Spinal Muscular Atrophy (SMA), 179
- Spring Ankle with Regenerative Kinetics prosthesis (SPARKy prosthesis), 476
- Spring(s), 475
spring-based gravity compensation, 124–126
- Spur gear torque amplification, 48, 49^f
- SRE. *See* Salford Rehabilitation Exoskeleton (SRE)
- ST joint. *See* Scapulothoracic joint (ST joint)
- Stand-to-sit maneuver (STS maneuver), 339
- “Stand-up and sit-down” motion, 285
- Standardized functional assessment protocol, 372
- Standing
frames, 316
mobility devices, 316
- Starship Troopers* (1959), 301
- Start-up mode, 238
- State of system estimation, 28–29
- Sternoclavicular synovial joint (SC synovial joint), 106–107
- Stimulation
control strategy, 349
stimulation-based torque estimation, 349
- Straps, 257–258
- Stress on end fibers in curved beams, 138
- Stroke, 10, 91, 308, 329, 342
- STS maneuver. *See* Stand-to-sit maneuver (STS maneuver)
- STS motion. *See* Sit-to-stand motion (STS motion)
- Stub/poke scenario, 416
- SUEFUL-7, 9
- Supermodified V3.0 for RC-servos, 184
- Surface electromyography (sEMG), 2, 94, 96, 157, 367–368, 370, 395–397. *See also* Electromyography (EMG)
electrodes, 94
sensors, 379–380, 382
signals, 448
- Surrogate skin, 276
for safety validation application, 285
- SW. *See* Slow walking (SW)
- Synergy
analysis, 99–100
synergy-based control system, 358–360
synergy-based controller, 353
- System rehabilitation
characterization of, 25–27
- dynamics of ETS-MARSE robot, 25–27
exoskeleton robot development, 25
problem statement, 27
- System-on-module (SOM), 422
- T**
- TAC test. *See* Target achievement control test (TAC test)
- Tactile myography, 371
- Tactile pressure, 451–452
- Tactile sensations, 454–457
- Target achievement control test (TAC test), 437, 448–449
- Targeted muscle reinnervation (TMR), 370–371, 384, 449–450
- Targeted sensory reinnervation (TSR), 455–457
surgery, 459
- TDE. *See* Time delay estimation (TDE)
- TEDEA 1040, 94–95
- Teleoperation, 15
current problems, 378–383
design guidelines for, 383–387
wearable interfaces for wearable robots, 377–378
- Tendon driven wearable gloves, 156
- TENS. *See* Transcutaneous electrical nerve stimulation (TENS)
- Terminal sliding mode control (TSMC), 24
- Tethered prosthesis systems, 473
- Tethered systems, 472
- Textures, 457
- Thermistor, 453
- THKAFO. *See* Trunk-hip-knee-ankle-foot orthosis (THKAFO)
- Three-degrees of freedom shoulder (3-DOF shoulder), 110–111
- Three-dimension (3D)
laser scanning, 383–384
printing methods, 267–268, 360
- Three-finger multi-DOF hand, 98
- Three-linkage mechanism, 195
- 3R planar mechanisms, 196
modeling, 197
- Thumb, 418–420, 419^f
- Time
derivative, 32
time-based control, 271
- Time delay estimation (TDE), 24–25
- TMR. *See* Targeted muscle reinnervation (TMR)
- Torque transfer
comparative torque transfer diagram for reversible and irreversible mechanism, 47^f
linearity, 46–48
- Touch, 453
sensations, 455
- Tracking error, 141–142, 498
- Training for pilot, 244–246

- Trajectory tracking, 145
- Transcutaneous electrical nerve stimulation (TENS), 454
- Transfemoral powered prosthetic leg control
- ampuete experiments
 - discussion of, 500–505
 - results from, 496–500
 - control law, 493–494
 - experimental protocol, 495–496
 - hardware setup, 494–495
- Transformation matrix, 140
- Transmission
- for hand exoskeleton systems, 155–156
 - Bowden cable, 155
 - compliant transmissions, 156
 - direct drive, gear, or linkage, 155
 - restorative springs, 156
 - tendon driven, 156
 - for upper limb exoskeleton systems, 5–6
 - cable-driven, 6
 - direct drive, gear, or linkage, 5–6
- Transparency, 45–46, 54, 80–83
- test, 79
 - transparent mechanism, 47
- Treadmill-based exoskeletons, 305–306
- Trunk-hip-knee-ankle-foot orthosis (THKAFO), 336–337
- TSMC. *See* Terminal sliding mode control (TSMC)
- TSR. *See* Targeted sensory reinnervation (TSR)
- Tuning control parameters, 478–479
- 12-camera VICON motion capture system, 114
- Two-degrees of freedom (2-DOF)
- shoulder exoskeleton with, 133–135
- U**
- UA. *See* Upper arm (UA)
- UDP. *See* User datagram protocol (UDP)
- UMs. *See* Unwanted movements (UMs)
- Uncertain estimation, 28
- Underactuation, 106, 369
- Unified phase variable algorithms, 490–493, 492*f*, 502–503
- Unilateral below-knee prosthesis users, 469
- Unilateral shoulder designs, 111
- Unimpaired level ground walking, 469
- University of Pittsburgh Medical Center (UPMC), 438, 438*f*
- Untethered HNP prototype, 339
- Untethered systems, 254–255
- Unwanted movements (UMs), 186–188
- Updated law, 143
- UPMC. *See* University of Pittsburgh Medical Center (UPMC)
- Upper arm (UA), 401–404
- software, 412–413
- Upper limb active prosthetics, 365
- amputations and patients, 372
 - control, 370–371
 - design of prosthetic devices, 368–370
- future, 373–374
- mainsubproblems of myocontrol, and perspectives, 372*t*
 - sevensubproblems in upper limb prosthetics, 373*t*
 - past, 367–368
- Upper limb exoskeleton systems, 1–8, 4*f*, 92, 133. *See also*
- Hand exoskeleton systems
 - actuation
 - control, 7–8
 - electric motors, 4–5
 - sensing method, 6–7
 - transmission, 5–6
 - assistive, 8–9
 - ABLE, 9
 - AIST, 9
 - HAL, 9
 - MULOS, 9
 - MYOPRO, 9
 - SUEFUL-7, 9
 - augmentation, 14–15
 - EksoVest from Ekso Bionics, 15
 - SARCOS Guardian GT system, 15
 - SARCOS Guardian XO, 15
 - ShoulderX from SuitX, 15
 - mechanism, 3–4
 - other exoskeletons
 - CAPIO, 16
 - EMY, 16
 - EXARM, 15
 - SAM, 16
 - SARCOS Dextrous Arm, 16
 - SARCOS Master Arm, 16
 - X-Arm-2, 16
 - rehabilitation, 10–14
 - ACT^{3D}, 11
 - ARM Guide, 10
 - ARMin III, 12
 - Bi-Manu-Track, 11
 - BONES, 12
 - ETS-MARSE, 13
 - Exorn, 13
 - EXO-UL series, 14
 - GENTLE/s, 11
 - IntelliArm, 12
 - iPAM system, 11
 - KINARM, 11–12
 - L-EXOS, 12
 - MEDARM, 13
 - MGA, 12
 - MIME, 11
 - MIT-MANUS, 10
 - NeReBot, 10
 - Recupera-Reha system, 13–14
 - RehaBot, 13
 - ReoGo Therapy System, 11
 - RUPERT IV, 13

SRE, 13
 Upper limb prostheses, 378, 445
 kinematics of, 381
 Urinary tract infections (UTIs), 325
 User datagram protocol (UDP), 431, 434
 User-based actuation strategy, 185–190
 electronic components and control architecture, 186–190
 mechanical design, 186
 testing and discussion, 190
 UTIs. *See* Urinary tract infections (UTIs)

V

V&V. *See* Verification and validation (V&V)
 v1 fingertip sensor (v1 FTS), 426, 426f, 427f
 VA. *See* Veteran Administration (VA)
 Vanderbilt Lower Limb Exoskeleton, 217
 Variable constraint hip mechanism (VCHM), 337–338
 Variable impedance knee mechanism (VIKM), 338–339
 Variable trials, 499–500
 VCHM. *See* Variable constraint hip mechanism (VCHM)
 VE. *See* Virtual environment (VE)
 Verification and validation (V&V), 275
 test procedure, 276
 validation test method for wound risk, 280–285
 verification experiments
 analysis for safety verification test, 279–280
 experiments, 278–279
 procedure, 276–277, 277f
 Vertical ground reaction forces (vGRFs), 325
 Veteran Administration (VA), 321, 329
 vGRFs. *See* Vertical ground reaction forces (vGRFs)
 Vibration sensing, 427
 VIE. *See* Virtual integration environment (VIE)
 VIKM. *See* Variable impedance knee mechanism (VIKM)
 Virtual constraints, 489, 493–494, 498, 503
 Virtual environment (VE), 24–25
 Virtual integration environment (VIE), 398, 431, 435
 Virtual MPL (vMPL), 434–435
 Virtual reality (VR), 1–2, 96–97, 100
 Virtual reality/augmented reality (VR/AR), 385–387
 vMPL. *See* Virtual MPL (vMPL)
 VR. *See* Virtual reality (VR)
 VR/AR. *See* Virtual reality/augmented reality (VR/AR)
 VulcanX, 398, 434

W

Waist pack, 318, 319f
 Walking Improvement for SCI with Exoskeleton trial (WISE trial), 306
 WalkON Suit, 231. *See also* Soft exosuit
 control system, 238–244
 after Cybathlon, 247–248
 design, 233f
 actuation systems, 232–234

configuration, 232
 control unit and backpack, 235
 crutches, 235
 mechanical specification, 234t
 robotic legs, 234
 user display, 235
 evaluation, 246–247
 Cybathlon 2016, 246–247
 training, 244–246
 human factors, 236–238
 KAFO, 237–238
 pilot, 236–237
 pilot wearing, 232f
 sensor system, 235–236
 Wearable Power-Assist Locomotor (WPAL), 214–215
 Wearable robots, 207, 275, 286. *See also* Rehabilitation robots
 fall risk during gait using, 286–297
 reaction motion against trigger for falling, 287–288
 wearable robots installation in society, 286
 wearable interfaces for, 377–378
 Wearable upper limb interface. *See also* Hybrid wearable
 robotic exoskeletons
 current problems, 378–383
 physical interface, 381–382
 sensors and bodily signals, 379–381
 signal processing, machine learning, adaptation,
 382–383
 design guidelines for, 383–387
 bHMI, 385–387, 386f
 current pitfalls, 383–384
 implementation and testing, 384–385
 for wearable robots, 377–378
 Web interface, 435–437
 Weight support, rehabilitation with, 215–216
 Wheelchairs, 314–315
 WHO. *See* World Health Organization (WHO)
 WISE trial. *See* Walking Improvement for SCI with
 Exoskeleton trial (WISE trial)
 WMC. *See* Wrist motor controller (WMC)
 World Health Organization (WHO), 312–313
 Wound risk, validation test method for, 280–285
 WPAL. *See* Wearable Power-Assist Locomotor (WPAL)
 Wrist
 design, 401, 404–410
 flexor, 421
 Wrist motor controller (WMC), 404

X

X-Arm-2, 16
 XCoM, 215
 xPC target toolbox, 353

Y

Yaw, 134

Wearable Robotics

Systems and Applications

Edited by

Jacob Rosen

Peter Walker Ferguson

Wearable Robotics: Systems and Applications provides a comprehensive overview of the entire field of wearable robotics including active orthotics (exoskeleton) and active prosthetics for the upper and lower limb. In its two major sections including Systems and Applications, wearable robotics systems are described from both the engineering perspectives as well as the systems' application in medicine and industry. Systems and applications are presented at various levels of the development cycle including systems which are still under active research and development, and systems that are under preliminary or full clinical trials as well as commercialized products.

This book is a valuable resource for anyone working in this field, such as researchers and industry professionals, and also useful in teaching.

Key Features

- An entry point to the world of wearable robotics, the content ranges from fundamentals, through to systems and then to application
- Provides a comprehensive overview of the entire field with both engineering and medical perspectives
- Helps you to design and develop wearable robotics for healthcare quickly and efficiently

About the editors

Jacob Rosen is a professor of medical robotics at the Department of Mechanical and Aerospace Engineering with joint appointments with the Department Surgery and the Department of Bioengineering, University of California, Los Angeles (UCLA). His research interests focus on medical robotics, biorobotics, human centered robotics, surgical robotics, wearable robotics, rehabilitation robotics, neural control, and human-machine interface. He developed several key systems in the field of medical robotics, such as the Blue and the Red Dragon for minimally invasive surgical skill evaluation that is commercialized by Simulab as the "Edge"; Raven, a surgical robotic system for telesurgery, is commercialized by Applied Dexterity as an open-source research platform; several generations of upper- and lower-limb exoskeletons; and most recently the Exo-UL8—a dual arm wearable robotic system. He is a co-author of more than 100 manuscripts in the field of medical robotics and a co-author and co-editor of two books. Dr. Rosen has brought his real-world experience to leading and editing this book and included contributions from worldwide experts.

Peter Walker Ferguson is a doctoral student in mechanical engineering with an emphasis on design, robotics, and manufacturing at the University of California, Los Angeles (UCLA). He holds a lecturer position in the electrical engineering department of Loyola Marymount University (LMU). He graduated from the LMU honors program in 2012 with a B.S. in electrical engineering and obtained a M.S. degree in mechanical engineering from UCLA in 2017. His research interests lie in the areas of wearable robotics, rehabilitation robotics, medical robotics, dynamics, and mechanical/electrical design. His thesis work focuses on the development and application of a robotic hand exoskeleton for stroke rehabilitation.



ACADEMIC PRESS

An imprint of Elsevier

elsevier.com/books-and-journals

ISBN 978-0-12-814659-0



9 780128 146590